

Cleared: January 20th, 1976
Clearing Authority: Air Force Wright Aeronautical Laboratories

FOREWORD

This report describes work accomplished under Contract AF33(657)-11461, Exhibit "C" entitled, "Fracture Toughness and Tear Tests." This program was performed by a joint venture organization of The Boeing Company and North American Aviation, Incorporated.

Mr. D. L. Posner of North American Aviation was program manager, and Mr. L. T. Goodman of Boeing was assistant program manager. The Boeing Company had prime responsibility for the work accomplished under Exhibit "C" and technical direction of the program was carried out by Mr. D. R. Donaldson of The Boeing Company and Mr. J. W. Ellis of North American Aviation. Mr. R. A. Davis of Boeing was principal project leader of the program and Mr. L. Bakow of North American Aviation was assistant project leader.

Significant contributions to this project were made by the following personnel at Boeing: Mr. T. Kane, Structures Laboratory; Mr. R. Kurtak, Structures Laboratory; Mr. W. Larson, Structures Laboratory; Mr. J. C. McMillan, Metals Technology; Mr. H. Myers, Structures Laboratory; Mr. J. P. Przybylinski, Structures Research; Mr. S. H. Smith, Fail-Safe Research; and Mr. W. Swift, Structures Laboratory. Significant contributions to this project were made by the following personnel at North American Aviation: Mr. R. Farwell, Metallic Materials Laboratory; Mr. K. Kono, Metallic Materials Laboratory; Mr. G. R. Martin, Metallic Materials Laboratory; Mr. W. D. Rittenhouse, Structures Laboratory; and Mr. J. Walker, Structures Laboratory.

The program was administered under the direction of the Aeronautical Systems Division, United States Air Force, by Mr. C. L. Harmsworth, Project Engineer. The contract time period covered by this final summary report is July 1, 1963 to June 30, 1964.

CONVERSION OF CRACK GROWTH RATE DATA FROM ML-TDR-64-238 "FRACTURE TOUGHNESS AND TEAR TESTS" TO STANDARD da/dN vs ΔK

TERMINOLOGY:

$D2ADN(i)$ = $d2A/dN$, total crack growth rate from TDR-238, inch/cycle
 $K(i)$ = stress intensity factor at maximum stress, $ksi \cdot inch^{0.5}$
 $DADN(j)$ = standard crack growth rate, inch/cycle
 $\Delta K(j)$ = stress intensity factor range, $K_{max} - K_{min}$, $ksi \cdot inch^{0.5}$

FORMULA:

$DADN(j) = D2ADN(i)/2.0$
 $\Delta K(j) = K(i) \cdot (1-R)$

see program: LTV-APG, Jefferson Site, Building 220, VAX system.
user\$bauer:[bauer.matprop]CNVRT_TDR238.FOR
program listing on next page.

Contrails

```
c*****
c                                CNVRT_TDR23B.FOR
c      Take d2A/dN vs Kmax data taken from report ML-TDR-64-238 and
c      convert it to standard dA/dN vs dK data.
c
c 900827 Mark K. Bauer                                LTV Aircraft Products
c*****
      IMPLICIT NONE
      REAL      R, dK1(1000), dK2(1000), DADN1(1000), DADN2(1000)
      INTEGER    I, Imax
      CHARACTER*80 FileIn, FileOut, Date1
c*****
c      FileIn = 'INPUT.DAT'      I A raw listing of the d(2A)/d(N) vs Kmax
c      R      = 0.60             I The input file's R ratio.
c      CALL Date(Date1)
c      FileOut = 'OUTPUT.DAT'
c*****
      CLOSE(1)
      OPEN( 1, FILE=FileIn, FORM='FORMATTED', STATUS='OLD', READONLY)
      REWIND(1)

      CLOSE(2)
      OPEN(2, FILE=FileOut, FORM='FORMATTED', STATUS='NEW',
+        CARRIAGECONTROL='LIST', RECL=132)
c*****
c      READ INPUT FILE      Reading paired-datasets
c
      I = 1
200  READ( 1, *,ERR=200,END=400) DADN2(I), DK2(I)
      WRITE(*, '(I10,F10.2,E10.2)') I, DADN2(I), DK2(I)
      I = I + 1
      GO TO 200
c*****
c      CONVERT DATA TO STANDARD dA/dN vs dK
c
400  Imax = I - 1
      WRITE(*,*) ' '
      WRITE(*,*) ' Total number = ', Imax

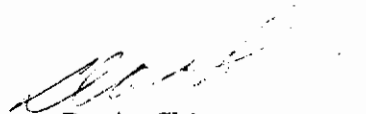
      DO I=1,Imax
        DADN1(I) = (DADN2(I)/2.0) * 1.0E-6
        DK1(I)   = DK2(I)*(1-R)
      ENDDO
c*****
c      WRITE NEW DATA TO OUTPUT FILE
c
      WRITE(2, *)
      WRITE(2, *) '*****'
      WRITE(2, *) ' CODE:      '//FileOut
      WRITE(2, *) ' REVISED:   '//Date1
      WRITE(2, *) ' TEMPERATURE: 75.0 F'
      WRITE(2, *) ' KUNIT:      ksi*inch**0.5'
      WRITE(2, *) ' AUNIT:      inch/cycle'
      WRITE(2,610) ' RRATIO:', R
      WRITE(2, *) ' FREQUENCY:   120.0 CPM'
      WRITE(2, *) ' THICKNESS:   0.025 inch'
      WRITE(2, *) ' ORIENT:      '
      WRITE(2, *) ' SOURCE:     ML-TDR-64-238 "Fracture Toughness and Tear Tests" 1964 '
      WRITE(2, *) '
      WRITE(2, *) '          ksi*inch**0.5 inch/cycle '
      WRITE(2, *) ' -----'
      DO I=1,Imax
        WRITE(2,620) DK1(I), DADN1(I)
      ENDDO
610  FORMAT(1X,A,T17,F10.3)
620  FORMAT(T6,F15.2,T25,1PG8.2)
      END
```

(this page was previously blank)

ABSTRACT

Fracture and fatigue crack propagation testing of five sheet alloys being considered for commercial supersonic transport applications has been carried out. The five alloys tested were titanium 8Al-1Mo-1V (duplex annealed), stainless steel AM350 (SCT 850), nickel alloy Inconel 718 (CRA), titanium 6Al-4V (mill annealed), and stainless steel PH 14-8Mo (SRH 1050). Both 8 x 24-inch and 24 x 72-inch centrally fatigued cracked panels were used in these evaluations. Crack propagation data were gathered at room temperature during the fatigue cracking of panels. Fracture tests were made over the temperature range of -110 to 650°F for both the longitudinal and transverse grain directions and for material thicknesses up to 0.200 inch for the titanium alloys and 0.125 inch for the other alloys. The variables of crack length, stress rate, and heat variation were also examined. In addition, the effect of exposure for 1000 hours at 650°F under a stress of 25 ksi for the titanium alloys and 40 ksi for the other alloys was determined. Comparisons were made among the alloys, based on a principal sheet thickness of 0.025 inch for the steel and nickel alloys and 0.050 inch for the titanium alloys. These comparisons showed that the two titanium alloys displayed the best overall fracture toughness properties when the density of the alloys is taken into account.

This technical documentary report has been reviewed and is approved.



D. A. Shinn
Chief, Materials Information Branch
Materials Application Division
AF Materials Laboratory

Contrails

TABLE OF CONTENTS

Section	Page
1. INTRODUCTION	1
2. SUMMARY	3
3. FRACTURE MECHANICS TECHNOLOGY APPLIED TO SHEET MATERIAL EVALUATION	7
Background	7
Griffith-Irwin Theory of Crack Instability	7
Centrally-Cracked Panel Stress Intensity Factor	11
Stress Intensity Factor Concept of Fatigue Crack Propagation	19
4. OUTLINE OF TEST PROGRAM	23
Statement of Problem and Approach	23
Material	24
Testing Plan	24
5. PROCEDURE	31
Materials	31
Specimen Fabrication	31
Heat Treatment	32
Center Notching	32
Tensile Testing	32
Test Equipment	32
Fatigue Cracking	35
Fracture Testing	40
Exposure Testing	43
Coordination Testing	43
Fractographic Studies	44
6. RESULTS AND DISCUSSION	45
General	45
Ti 8Al-1Mo-1V	47
AM 350 Stainless Steel	88
Inco 718 Nickel Alloy	126
Ti 6Al-4V	163
PH 14-8Mo Stainless Steel	204
Coordination Testing	247
7. COMPARISON OF ALLOYS	253
Fatigue Crack Growth	253
Fracture Properties	255

TABLE OF CONTENTS (continued)

Section	Page
8. CONCLUSIONS	263
Crack Propagation Tests	263
Fracture Tests	264
9. RECOMMENDATIONS	265
10. REFERENCES	267
Appendix	
I INVESTIGATION OF TECHNIQUES FOR DETECTION OF "POP-IN"	271
Introduction	271
Discussion	271
II HIGH-SPEED PHOTOGRAPHY STUDIES	285
Introduction	285
Test Equipment and Procedure	285
Data Reduction Technique	286
Test Results	288
III FRACTURE SURFACE MEASUREMENTS	331

LIST OF ILLUSTRATIONS

Figure		Page
1	Comparison of Crack Growth Rate for All Alloys, Density Considered	4
2	Fracture Toughness/Density Summary for All Alloys	5
3	Gross Fracture Stress/Density Summary for All Alloys	5
4	Griffith Plate Configuration	9
5	Stress Acting on an Element of Material Near a Crack Front	9
6	Centrally Cracked Panel Configuration with Infinite and Finite Widths	13
7	Comparison of Polynomial and Tangent Geometry Correction Factors	18
8	Fatigue Crack Growth Rate Data Correlation Technique	20
9	Test Specimen Configurations	26
10	Three Hydraulic Equipped Loading Towers	34
11	Electronic Components in Servo-Controlled Loading System	36
12	Load Control Console and Recording Oscillograph	37
13	Hydraulic Loading System Diagram for 200 KIP Tower	38
14	Fatigue Cracking in 300 KIP Tower	39
15	Fatigue Cracking in IV-12 Equipment	41
16	Steel Buckling Restraints Used During Testing	42
17	Photomicrographs of Ti 8Al-1Mo-1V Showing Thickness Variation, Heat 3457	49
18	Photomicrographs of Ti 8Al-1Mo-1V, Heats 4535, 3454 and 3457	50
19	Crack Growth Data for Ti 8Al-1Mo-1V, Heat D4535	53
20	Crack Growth Data for Ti 8Al-1Mo-1V, Heat D4535	53
21	Crack Growth Data for Ti 8Al-1Mo-IV, Heat D4535	54

LIST OF ILLUSTRATIONS (continued)

Figure		Page
22	Crack Growth Data for Ti 8Al-1Mo-1V, Heat D3454	54
23	Crack Growth Data for Ti 8Al-1Mo-1V, Heat D3454	55
24	Crack Growth Data for Ti 8Al-1Mo-1V, Heat D3457	55
25	Crack Growth Data for Ti 8Al-1Mo-1V, Heat D3457	56
26	Crack Growth Data for Ti 8Al-1Mo-1V, Heat D3457	57
27	Crack Growth Data for Ti 8Al-1Mo-1V, Heat D3457	57
28	Crack Growth Data for Ti 8Al-1Mo-1V, Heat D3457	58
29	Crack Growth Data for Ti 8Al-1Mo-1V, Heat D3457	58
30	Crack Growth Data for Exposed Ti 8Al-1Mo-1V Panels, Heat D3457	59
31	Crack Growth Rate Data for Ti 8Al-1Mo-1V, Heat 4535	60
32	Crack Growth Rate Data for Ti 8Al-1Mo-1V, Heat 4535	60
33	Crack Growth Rate Data for Ti 8Al-1Mo-1V, Heat 4535	61
34	Crack Growth Rate Data for Ti 8Al-1Mo-1V, Heat 4535	61
35	Crack Growth Rate Data for Ti 8Al-1Mo-1V, Heat 3454	62
36	Crack Growth Rate Data for Ti 8Al-1Mo-1V, Heat 3454	62
37	Crack Growth Rate Data for Ti 8Al-1Mo-1V, Heat 3457	63
38	Crack Growth Rate Data for Ti 8Al-1Mo-1V, Heat 3457	63
39	Crack Growth Rate Data for Ti 8Al-1Mo-1V, Heat 3457	64
40	Crack Growth Rate Data for Ti 8Al-1Mo-1V, Heats 3454, 3457 and 4535	65
41	Comparison of Exposed and Unexposed Crack Growth Rates for Ti 8Al-1Mo-1V, Heat 3457	65
42	Comparison of Exposed and Unexposed Crack Growth Rates for Ti 8Al-1Mo-1V, Heat 3457	66

LIST OF ILLUSTRATIONS (continued)

Figure		Page
43	Comparison of Exposed and Unexposed Crack Growth Rates for Ti 8Al-1Mo-1V, Heat 3457	66
44	Effect of Test Temperature on K_{IC} for Ti 8Al-1Mo-1V	72
45	Effect of Test Temperature on Residual Strength for Ti 8Al-1Mo-1V	72
46	Residual Strength vs Damage for 8 x 24 inch Ti 8Al-1Mo-1V Panels, Heats D4535, D3454 and D3457	73
47	Variation of K_{IC} with Grain Direction for Ti 8Al-1Mo-1V	74
48	Variation of Residual Strength with Grain Direction for Ti 8Al-1Mo-1V	74
49	Residual Strength vs Damage for 24 x 72 inch Ti 8Al-1Mo-1V Panels, Heats D4535 and D3454	75
50	Variation of K_{IC} with Thickness for Ti 8Al-1Mo-1V	76
51	Variation of Residual Strength with Thickness for Ti 8Al-1Mo-1V	76
52	Variation of K_{IC} with Temperature, Crack Length and Grain Direction for Ti 8Al-1Mo-1V	78
53	Variation of K_{IC} with Temperature, Crack Length, Thickness and Grain Direction for Ti 8Al-1Mo-1V	79
54	Residual Strength vs Damage for 24 x 72 inch Ti 8Al-1Mo-1V Panels, Heat D3457	80
55	Residual Strength vs Damage for 24 x 72 inch Ti 8Al-1Mo-1V Panels, Heats D4535, D3454 and D3457	81
56	The Effect of Stress Rate on K_{IC} for Ti 8Al-1Mo-1V	82
57	Comparison of Exposed and Unexposed K_{IC} Values for Ti 8Al-1Mo-1V	82
58	Fractographic Study of Ti 8Al-1Mo-1V Specimen DA21	84
59	Fractographic Study of Ti 8Al-1Mo-1V Specimen DA62	85
60	Fractographic Study of Ti 8Al-1Mo-1V Specimen DA64	86

LIST OF ILLUSTRATIONS (continued)

Figure		Page
61	Macrograph of Specimen DA66 Showing Fracture Mode Transition	87
62	Photomicrographs of AM 350 Showing Thickness Variation, Heat 19020	91
63	Photomicrographs of AM 350, Heats 19207, 55538 and 19020	92
64	Photomicrograph Showing Segregation in AM 350, Heat 19020	93
65	Crack Growth Data for AM 350, Heat 19207	98
66	Crack Growth Data for AM 350, Heat 19207	98
67	Crack Growth Data for AM 350, Heat 55538	99
68	Crack Growth Data for AM 350, Heat 19020	99
69	Crack Growth Data for AM 350, Heat 19020	100
70	Crack Growth Data for AM 350, Heat 19020	100
71	Crack Growth Data for AM 350, Heat 55538	101
72	Crack Growth Data for AM 350, Heats 19020, 19207 and 55538	101
73	Crack Growth Data for AM 350, Heat 19020	102
74	Crack Growth Data for AM 350, Heat 19020	102
75	Crack Growth Data for Exposed AM 350 Panels, Heat 19020	103
76	Crack Growth Rate Data for AM 350 (SCT 850) Heat 19207	103
77	Crack Growth Rate Data for AM 350 (SCT 850) Heat 19207	104
78	Crack Growth Rate Data for AM 350, Heat 19207	104
79	Crack Growth Rate Data for AM 350, Heat 55538	105
80	Crack Growth Rate Data for AM 350, Heat 55538	105
81	Crack Growth Rate Data for AM 350, Heat 19020	106
82	Crack Growth Rate Data for AM 350, Heat 19020	106

LIST OF ILLUSTRATIONS (continued)

Figure		Page
83	Crack Growth Rate Data for AM 350, Heat 19020	107
84	Comparison of Exposed and Unexposed Crack Growth Rates for AM 350, Heat 19020	108
85	Comparison of Exposed and Unexposed Crack Growth Rates for AM 350, Heat 19020	108
86	Comparison of Exposed and Unexposed Crack Growth Rates for AM 350, Heat 19020	109
87	Crack Growth Rate Data for AM 350, Heats 19020, 19207 and 55538	109
88	Effect of Test Temperature on K_{IC} for AM 350	114
89	Effect of Test Temperature on Residual Strength for AM 350	114
90	Variation of K_{IC} with Grain Direction for AM 350	116
91	Variation of Residual Strength with Grain Direction for AM 350	116
92	Variation of K_{IC} with Thickness for AM 350	117
93	Variation of Residual Strength with Thickness for AM 350	117
94	Variation of K_{IC} with Temperature, Crack Length and Grain Direction for AM 350	118
95	Variation of K_{IC} , Crack Length, Thickness and Grain Direction for AM 350, Heat 19020	119
96	Residual Strength vs Damage for 24 x 72 inch Am 350 Panels, Heats 19207, 55538 and 19020	120
97	Residual Strength vs Damage for 24 x 72 inch AM 350 Panels, Heat 19020	121
98	The Effect of Stress Rate on K_{IC} for AM 350	122
99	Comparison of Exposed and Unexposed K_{IC} Values for AM 350	123
100	Fractographic Study of AM 350 Specimen DB74	125
101	Photomicrographs of Inco 718, Heats 6713, 6905 and 6902	128
102	Photomicrographs of Inco 718 Showing Thickness Variation, Heat 6902	129

LIST OF ILLUSTRATIONS (continued)

Figure		Page
103	Crack Growth Data for Inco 718, Heat 6713	133
104	Crack Growth Data for Inco 718, Heats 6713 and 6902	133
105	Crack Growth Data for Inco 718, Heat 6713	134
106	Crack Growth Data for Inco 718, Heat 6905	134
107	Crack Growth Data for Inco 718, Heats 6905 and 6902	135
108	Crack Growth Data for Inco 718, Heat 6902	135
109	Crack Growth Data for Inco 718, Heat 6902	136
110	Crack Growth Data for Inco 718, Heats 6713 and 6902	136
111	Crack Growth Data for Inco 718, Heats 6713, 6905 and 6902	137
112	Crack Growth Data for Inco 718, Heat 6902	137
113	Crack Growth Data for Inco 718, Heat 6902	138
114	Crack Growth Data for Inco 718, Heat 6902	138
115	Crack Growth Data for Exposed Inco 718 Panels, Heat 6902	139
116	Crack Growth Rate Data for Inco 718, Heat 6713	140
117	Crack Growth Rate Data for Inco 718, Heat 6713	140
118	Crack Growth Rate Data for Inco 718, Heat 6905	141
119	Crack Growth Rate Data for Inco 718, Heat 6905	141
120	Crack Growth Rate Data for Inco 718, Heat 6902	142
121	Crack Growth Rate Data for Inco 718, Heat 6902	142
122	Crack Growth Rate Data for Inco 718, Heat 6902	143
123	Comparison of Exposed and Unexposed Crack Growth Rates For Inco 718, Heat 6902	143
124	Comparison of Exposed and Unexposed Crack Growth Rates for Inco 718, Heat 6902	144

LIST OF ILLUSTRATIONS (continued)

Figure		Page
125	Comparison of Exposed and Unexposed Crack Growth Rates for Inco 718, Heat 6902	144
126	Crack Growth Rate Data for Inco 718, Heats 6713, 6902 and 6905	146
127	Effect of Test Temperature on K_C for Inco 718	151
128	Effect of Test Temperature on Residual Strength for Inco 718	151
129	Variation of K_C with Grain Direction for Inco 718	152
130	Variation of Residual Strength with Grain Direction for Inco 718	152
131	Variation of K_C with Thickness for Inco 718	153
132	Variation of Residual Strength with Thickness for Inco 718	153
133	Variation of K_C with Temperature, Crack Length and Grain Direction for Inco 718	154
134	Variation of K_C with Temperature, Crack Length, Thickness and Grain Direction for Inco 718	155
135	Variation of K_C with Temperature, Crack Length and Grain Direction for Inco 718	156
136	Residual Strength vs Damage for 24 x 72 inch Inco 718 Panels, Heat 6902	157
137	Residual Strength vs Damage for 8 x 24 inch Inco 718 Panels, Heats 6713, 6905 and 6902	158
138	Residual Strength vs Damage for 24 x 72 inch Inco 718 Panels, Heats 6713, 6905 and 6902	159
139	The Effect of Stress Rate on K_C for Inco 718	161
140	Comparison of Exposed and Unexposed K_C Values for Inco 718	161
141	Fractographic Study of Inco 718 Specimen DC74	162
142	Photomicrographs of Ti 6Al-4V Showing Thickness Variation, Heat 4949	168
143	Photomicrographs of Ti 6Al-4V, Heat 5257	169

LIST OF ILLUSTRATIONS (continued)

Figure		Page
144	Crack Growth Data for Ti 6Al-4V, Heats D5257 and D4949	169
145	Crack Growth Data for Ti 6Al-4V, Heat D5257	170
146	Crack Growth Data for Ti 6Al-4V, Heat D5257	171
147	Crack Growth Data for Ti 6Al-4V, Heats D5257 and D4949	171
148	Crack Growth Data for Ti 6Al-4V, Heat D4949	172
149	Crack Growth Data for Ti 6Al-4V, Heat D4949	172
150	Crack Growth Data for Ti 6Al-4V, Heat D5256	173
151	Crack Growth Data for Ti 6Al-4V, Heat D4949	173
152	Crack Growth Data for Ti 6Al-4V, Heat D5256	174
153	Crack Growth Data for Ti 6Al-4V, Heat D4949	175
154	Crack Growth Data for Ti 6Al-4V, Heats D5257 and D5256	176
155	Crack Growth Data for Ti 6Al-4V, Heat D4949	177
156	Crack Growth Data for Ti 6Al-4V, Heat D4949	178
157	Crack Growth Data for Ti 6Al-4V, Heat D4949	179
158	Crack Growth Rate Data for Ti 6Al-4V, Heat D5257	181
159	Crack Growth Rate Data for Ti 6Al-4V, Heat D5257	181
160	Crack Growth Rate Data for Ti 6Al-4V, Heat D5257	182
161	Crack Growth Rate Data for Ti 6Al-4V, Heat D5256	182
162	Crack Growth Rate Data for Ti 6Al-4V, Heat D5256	183
163	Crack Growth Rate Data for Ti 6Al-4V, Heat D4949	183
164	Crack Growth Rate Data for Ti 6Al-4V, Heat D4949	184
165	Crack Growth Rate Data for Ti 6Al-4V, Heat D4949	184
166	Crack Growth Rate Data for Ti 6Al-4V, Heat D4949	185
167	Crack Growth Rate Data for Ti 6Al-4V, Heat D4949	185

LIST OF ILLUSTRATIONS (continued)

Figure		Page
168	Crack Growth Rate Data for Ti 6Al-4V, Heat D4949	186
169	Crack Growth Rate Data for Ti 6Al-4V, Heat D4949	186
170	Crack Growth Rate Data for Ti 6Al-4V, Heat D4949	187
171	Crack Growth Rate Data for Ti 6Al-4V, Heats D5257, D5256 and D4949	187
172	Effect of Test Temperature on K_C for Ti 6Al-4V	192
173	Effect of Test Temperature on Residual Strength for Ti 6Al-4V	192
174	Residual Strength vs Damage for 24 x 72 inch Ti 6Al-4V Panel, Heats D5257, D5256 and D4949	193
175	Residual Strength vs Damage for 24 x 72 inch Ti 6Al-4V Panel, Heat D4949	194
176	Variation of K_C with Grain Direction for Ti 6Al-4V	195
177	Variation of Residual Strength with Grain Direction for Ti 6Al-4V	195
178	Variation of K_C with Thickness for Ti 6Al-4V	196
179	Variation of Residual Strength with Thickness for Ti 6Al-4V, Heat D4949	196
180	Variation of K_C with Temperature, Crack Length and Grain Direction for Ti 6Al-4V	197
181	Variation of K_C with Temperature, Crack Length, Thickness and Grain Direction for Ti 6Al-4V	199
182	The Effect of Stress Rate on K_C for Ti 6Al-4V, Heats 5257, 5256 and 4949	201
183	Comparison of Exposed and Unexposed K_C Values for Ti 6Al-4V, Heat 4949	201
184	Fractographic Study of Ti 6Al-4V Specimen DD21	202
185	Fractographic Study of Ti 6Al-4V Specimen DD74	203
186	Photomicrographs of PH 14-8Mo, Heat 33347	206
187	Photomicrographs of PH 14-8Mo with Unacceptable Heat Treat Response	207

LIST OF ILLUSTRATIONS (continued)

Figure		Page
188	Photomicrographs of PH 14-8Mo that was Re-Heat Treated	208
189	Crack Growth Data for PH 14-8Mo, Heat 43208 and 33347	212
190	Crack Growth Data for PH 14-8Mo, Heat 43208	213
191	Crack Growth Data for PH 14-8Mo, Heat 43208	214
192	Crack Growth Data for PH 14-8Mo, Heats 43208 and 33570	215
193	Crack Growth Data for PH 14-8Mo, Heat 33570	215
194	Crack Growth Data for PH 14-8Mo, Heat 33347	216
195	Crack Growth Data for PH 14-8Mo, Heat 33347	216
196	Crack Growth Data for PH 14-8Mo, Heats 33347 and 33570	217
197	Crack Growth Data for PH 14-8Mo, Heats 33347 and 33570	217
198	Crack Growth Data for PH 14-8Mo, Heat 33347	218
199	Crack Growth Data for PH 14-8Mo, Heat 33347	219
200	Crack Growth to Fracture Data for PH 14-8Mo, Heat 43208	219
201	Crack Growth Data for PH 14-8Mo, Heat 43208	220
202	Crack Growth Rate Data for PH 14-8Mo, Heat 43208	222
203	Crack Growth Rate Data for PH 14-8Mo, Heat 43208	222
204	Crack Growth Rate Data for PH 14-8Mo, Heat 43208	223
205	Crack Growth Rate Data for PH 14-8Mo, Heat 33570	223
206	Crack Growth Rate Data for PH 14-8Mo, Heat 33570	224
207	Crack Growth Rate Data for PH 14-8Mo, Heat 33347	224
208	Crack Growth Rate Data for PH 14-8Mo, Heat 33347	225
209	Crack Growth Rate Data for PH 14-8Mo, Heats 33347 and 33570	225
210	Crack Growth Rate Data for PH 14-8Mo, Heats 33347 and 33570	226

LIST OF ILLUSTRATIONS (continued)

Figure		Page
211	Crack Growth Rate Data for PH 14-8Mo, Heat 33347	226
212	Crack Growth Rate Data for PH 14-8Mo, Heat 33347	227
213	Crack Growth Rate Data for PH 14-8Mo, Heat 43208	227
214	Comparison of Exposed and Unexposed Crack Growth Rates for PH 14-8Mo, Heat 33347	228
215	Comparison of Exposed and Unexposed Crack Growth Rates for PH 14-8Mo, Heat 33347	228
216	Comparison of Exposed and Unexposed Crack Growth Rates for PH 14-8Mo, Heat 33347	229
217	Crack Growth Rate Data for PH 14-8Mo, Heats 33347, 33570 and 43208	229
218	Effect of Test Temperature on K_C for PH 14-8Mo	235
219	Effect of Test Temperature on Residual Strength for PH 14-8Mo	235
220	Residual Strength vs Damage for 24 x 72 inch PH 14-8Mo Panels, Heats 33347 and 33570	236
221	Residual Strength vs Damage for 24 x 72 inch PH 14-8Mo Panels, Heats 43208, 33347 and 33570	237
222	Variation of K_C with Grain Direction with PH 14-8Mo	238
223	Variation of Residual Strength with Grain Direction for PH 14-8Mo	238
224	Variation of K_C with Thickness for PH 14-8Mo	239
225	Variation of Residual Strength with Thickness for PH 14-8Mo	239
226	Variation of K_C with Temperature, Crack Length and Grain Direction for PH 14-8Mo	240
227	Variation of K_C with Temperature, Crack Length, Thickness and Grain Direction for PH 14-8Mo	241
228	Variation of K_C with Temperature, Crack Length and Grain Direction for PH 14-8Mo	242
229	The Effect of Stress Rate on K_C for PH 14-8Mo	244

LIST OF ILLUSTRATIONS (continued)

Figure		Page
230	Comparison of Exposed and Unexposed K_C Values for PH 14-8Mo	244
231	Fractographic Study of PH 14-8Mo Specimen DE21	245
232	Fractographic Study of PH 14-8Mo Specimen DE74	246
233	Coordination Testing Crack Growth Data for Ti 6Al-4V	247
234	Coordination Testing Crack Growth Rate Data for Ti 6Al-4V	248
235	Coordination Testing Residual Strength and Damage Comparison for Ti 8Al-1Mo-1V Panels	250
236	Coordination Testing Residual Strength and Stress Rate Relationship for Ti 8Al-1Mo-1V	251
237	Comparison of Crack Growth Rate for all Alloys, Density Not Considered	253
238	Comparison of Crack Growth Rate for all Alloys, Density Considered	254
239	Variation of Residual Strength with Temperature for all Alloys	255
240	Variation of Fracture Toughness/Density Ratio with Temperature for all Alloys	257
241	Variation of Fracture Toughness with Temperature for all Alloys	258
242	Alloy Comparison for K_C , Temperature and Thickness for 8 x 24 inch Panels	260
243	Alloy Comparison for K_C , Temperature and Thickness for 24 x 72 inch Panels	261
244	Test Setup with Extensometer and 4 x 16 inch 7075-T6 Panel	273
245	Compliance and Strain Gage Plot for Test Number 1	274
246	Compliance and Strain Gage Plot for Test Number 2	275
247	Compliance and Strain Gage Plot for Test Number 3	276
248	Compliance and Strain Gage Plot for Test Number 4	278
249	Test Setup for High-Speed Photography Equipment	279

LIST OF ILLUSTRATIONS (continued)

Figure		Page
250	Typical Strain Output Plot from a Test of an 8 x 24 inch Exhibit C Specimen	280
251	Plane-Strain Fracture Toughness Based on Initiation of Slow Crack Growth for Ti 6Al-4V	283
252	Timing and Ramp Start Pulse Circuits	287
253	Various Frames Showing Crack Growth of a 8 x 24 inch Ti 6Al-4V Specimen	289
254	Various Frames Showing Crack Growth of a 24 x 72 inch Ti 6Al-4V Specimen	290
255	Static Crack Growth for Ti 8Al-1Mo-1V Specimen DA19	291
256	Static Crack Growth for Ti 8Al-1Mo-1V Specimen DA75	292
257	Static Crack Growth for Ti 8Al-1Mo-1V Specimen DA76	293
258	Static Crack Growth for Ti 8Al-1Mo-1V Specimen DA77	294
259	Static Crack Growth for AM 350 Specimen DB19	295
260	Static Crack Growth for AM 350 Specimen DB75	296
261	Static Crack Growth for AM 350 Specimen DB76	297
262	Static Crack Growth for AM 350 Specimen DB77	298
263	Static Crack Growth for Inco 718 Specimen DC19	299
264	Static Crack Growth for Inco 718 Specimen DC75	300
265	Static Crack Growth for Inco 718 Specimen DC77	301
266	Static Crack Growth for Inco 718 Specimen DC78	302
267	Static Crack Growth for Ti 6Al-4V Specimen DD3	303
268	Static Crack Growth for Ti 6Al-4V Specimen DD4	304
269	Static Crack Growth for Ti 6Al-4V Specimen DD5	305
270	Static Crack Growth for Ti 6Al-4V Specimen DD6	305
271	Static Crack Growth for Ti 6Al-4V Specimen DD19	306

LIST OF ILLUSTRATIONS (continued)

Figure		Page
272	Static Crack Growth for Ti 6Al-4V Specimen DD20	307
273	Static Crack Growth for Ti 6Al-4V Specimen DD22	308
274	Static Crack Growth for Ti 6Al-4V Specimen DD23	308
275	Static Crack Growth for Ti 6Al-4V Specimen DD24	309
276	Static Crack Growth for Ti 6Al-4V Specimen DD25	309
277	Static Crack Growth for Ti 6Al-4V Specimen DD36	310
278	Static Crack Growth for Ti 6Al-4V Specimen DD38	310
279	Static Crack Growth for Ti 6Al-4V Specimen DD42	311
280	Static Crack Growth for Ti 6Al-4V Specimen DD52	311
281	Static Crack Growth for Ti 6Al-4V Specimen DD54	312
282	Static Crack Growth for Ti 6Al-4V Specimen DD56	313
283	Static Crack Growth for Ti 6Al-4V Specimen DD70	313
284	Static Crack Growth for Ti 6Al-4V Specimen DD74	314
285	Static Crack Growth for Ti 6Al-4V Specimen DD75	315
286	Static Crack Growth for Ti 6Al-4V Specimen DD76	316
287	Static Crack Growth for Ti 6Al-4V Specimen DD77	317
288	Static Crack Growth for Ti 6Al-4V Specimen DD78	318
289	Static Crack Growth for PH 14-8Mo Specimen DE4	319
290	Static Crack Growth for PH 14-8Mo Specimen DE5	320
291	Static Crack Growth for PH 14-8Mo Specimen DE19	320
292	Static Crack Growth for PH 14-8Mo Specimen DE22	321
293	Static Crack Growth for PH 14-8Mo Specimen DE23	321
294	Static Crack Growth for PH 14-8Mo Specimen DE24	322
295	Static Crack Growth for PH 14-8Mo Specimen DE36	323

LIST OF ILLUSTRATIONS (continued)

Figure		Page
296	Static Crack Growth for PH 14-8Mo Specimen DE39	324
297	Static Crack Growth for PH 14-8Mo Specimen DE71	325
298	Static Crack Growth for PH 14-8Mo Specimen DE75	326
299	Static Crack Growth for PH 14-8Mo Specimen DE76	327
300	Static Crack Growth for PH 14-8Mo Specimen DE77	327
301	Static Crack Growth for PH 14-8Mo Specimen DE78	328

Contrails

LIST OF TABLES

Table		Page
1	Summary of Alloys and Conditions Being Evaluated	25
2	Detailed Testing Outline for All Fracture Panels	27
3	Outline of Crack Propagation Variables Studied	29
4	Summary of Alloy Heats Purchased for Testing	31
5	Heat Treatment Procedures for AM 350, PH 14-8Mo and Inco 718	33
6	Vendor Certified Chemical Analysis for Ti 8Al-1Mo-1V (Weight Percent)	48
7	Tensile Test Data for Ti 8Al-1Mo-1V	52
8	Fracture Toughness Data for 24 x 72-inch Panels of Ti-8Al-1Mo-1V	68
9	Fracture Toughness Data for 8 x 24-inch Panels of Ti 8Al-1Mo-1V	70
10	Room Temperature Plane Strain Fracture Toughness Estimates for Ti 8Al-1Mo-1V	89
11	Vendor Certified Chemical Analysis for AM 350 (Weight Percent)	89
12	Tensile Test Data for AM 350	95
13	Fracture Toughness Data for 24 x 72-inch Panels of Am 350	110
14	Fracture Toughness Data for 8 x 24-inch Panels of Am 350	112
15	Vendor Certified Chemical Analysis for Inco 718 (Weight Percent)	126
16	Tensile Test Data for Inco 718	130
17	Fracture Toughness Data for 24 x 72-inch Panels of Inco 718	147
18	Fracture Toughness Data for 8 x 24-inch Panels of Inco 718	149
19	Vendor Certified Chemical Analysis for Ti 6Al-4V (Weight Percent)	164
20	Tensile Test Data for Ti 6Al-4V	166

LIST OF TABLES (continued)

Table		Page
21	Fracture Toughness Data for 24 x 72-inch Panels of Ti 6Al-4V (Mill Anneal)	188
22	Fracture Toughness Data for 8 x 24-inch Panels of Ti 6Al-4V	190
23	Vendor Certified Chemical Analysis for PH 14-8Mo (Weight Percent)	204
24	Tensile Properties of PH 14-8Mo, Heats 43208 and 33570	210
25	Tensile Test Data for PH 14-8Mo	
26	Fracture Toughness Data for 24 x 72-inch Panels of PH 14-8Mo	230
27	Fracture Toughness Data for 8 x 24-inch Panels of PH 14-8Mo	232
28	Coordination Testing Fracture Toughness Data for 8 x 24-inch Ti 6Al-4V Panels	249
29	Coordination Testing Specimen and Test Data for Ti 8Al-1Mo-1V	249
30	Rating of Residual Strength at Temperatures for All Alloys	256
31	Rating of Fracture Toughness/Density at Temperature for All Alloys	256
32	Values of K_{ICN} from Initiation of Slow Crack Growth Revealed by High-Speed Photography for Ti 6Al-4V	282
33	Summary of Fracture Toughness Calculations Based on High-Speed Photography Crack Length Measurements	329
34	Post Fracture Crack Length Measurements for 24 x 72-inch Panels for All Alloys	332

LIST OF SYMBOLS

K_{ICN}	Nominal Plane Strain Critical Stress Intensity Factor (ksi $\sqrt{\text{inches}}$)
K_{IC}	Plane Strain Critical Stress Intensity Factor (ksi $\sqrt{\text{inches}}$)
K_C^*	Plane Stress Critical Stress Intensity Factor Based on Critical Crack Length from High Speed Photography (ksi $\sqrt{\text{inches}}$)
K_C	Plane Stress Critical Stress Intensity Factor (ksi $\sqrt{\text{inches}}$)
K_{CN}	Nominal Critical Stress Intensity Factor Based on $2a_o$ (ksi $\sqrt{\text{inches}}$)
G_C	Plane Stress Fracture Toughness or Strain Energy Release Rate (in.-lbs./in. ²)
G_{IC}	Plane Strain Fracture Toughness or Strain Energy Release Rate (in.-lbs./in. ²)
$2a$	Total Crack Length (inches)
$2a_i$	Internal Total Fatigue Crack Length (inches)
$2a_o$	Final Surface Fatigue Crack Length (inches)
$2a_p$	Internal Total Crack Length Including Plane Strain (inches)
$2b$ or W	Panel Width (inches)
t	Panel Thickness (inches)
a or a_2	Greenspan Geometry Correction Factor = $\frac{\sqrt{4 + 2(\frac{a}{b})^4}}{2 - (\frac{a}{b})^2 - (\frac{a}{b})^4}$
a_1	Tangent Finite Width Correction Factor = $\left[\frac{2b}{\pi a} \tan \frac{\pi a}{2b} \right]^{1/2}$
$\Delta 2a/\Delta N$	Crack Growth Rate (microinches per cycle)
T	Transverse Grain Direction
L	Longitudinal Grain Direction
R	Ratio of Minimum Stress to Maximum Stress
N_T	Total Number of Cycles
N	Net Number of Cycles
N_D	Number of Cycles to Initiate Fatigue Crack

LIST OF SYMBOLS (continued)

E	Young's Modulus (psi)
ksi	Thousands of Pounds per Square Inch
psi	Pounds per Square Inch
lbs.	Pounds
σ_M	Maximum Gross Area Stress (psi or ksi)
σ_G	Gross Area Stress (psi or ksi)
σ_N	Net Area Stress (psi or ksi)
$\dot{\sigma}$	Stress Rate Based on Gross Area (psi per second)
F_{tu}	Ultimate Tensile Strength (psi or ksi)
F_{ty} or σ_{yp}	0.2 Percent Yield Strength (psi or ksi)
AC	Air Cooled
FC	Furnace Cooled
GD	Grain Direction
CPM	Cycles per Minute
ρ	Material Density (Pounds per Cubic Inch)
CRA	Cold Rolled and Aged Heat Treatment Condition (Inco 718)
SCT	Subzero Cooled and Tempered Heat Treatment Condition (AM 350)
SRH	Subzero Cooled and Tempered Heat Treatment Condition (PH 14-8Mo)
CRT	Cold Rolled and Tempered Heat Treatment Condition (AM 350)
x, y, z	Rectangular Coordinates
r, θ	Polar Coordinates
$\sigma_x, \sigma_y, \sigma_z$	Normal Stress Components
$\tau_{xy}, \tau_{xz}, \tau_{yz}$	Shear Stress Components
ϵ_z	Normal Strain Components

LIST OF SYMBOLS (continued)

γ_{xz}, γ_{yz}	Shear Strain Components
ν	Poisson's Ratio
K_1, K_2	Symmetric and Skew-Symmetric Stress Intensity Factor Components
Φ	Airy Stress Function
∇	Del Operator
ζ	Complex Variable $\zeta = x + iy$
$Z(\zeta)$	Westergaard Stress Function
K	Opening Mode Stress Intensity Factor - General (ksi $\sqrt{\text{inches}}$)
w	Plastic Zone Width
q_1	$\tan \frac{\pi}{W} \left[a_0 + \frac{K_c^2}{2\pi\sigma_{yp}^2} \right]$

SECTION 1 INTRODUCTION

The purpose of the program was to extend the fracture toughness and crack growth information for sheet alloys under consideration for commercial supersonic transport usage. Preliminary fracture toughness and crack propagation information was developed by the Douglas Aircraft Company under contract AF 33(657)-8545 (Ref. 1).

In the Douglas program an 8 by 24-inch specimen was used to evaluate five candidate materials at a basic sheet thickness of 0.025 inches. The five alloys studied in the Douglas program were Ti 8Al-1Mo-1V (triplex anneal), Ti 6Al-4V (mill anneal), stainless steel AM 350 (SCT and CRT), stainless steel PH 15-7Mo (RH 1100), and the nickel base alloy René 41 (cold rolled and aged).

Between the initiation of the Douglas program and the present program, two new sheet alloys reached developmental production status. One of these, PH 14-8Mo (Ref. 2), a variation of the older precipitation hardening family of stainless steel alloys, was selected for evaluation in this program in place of PH 15-7Mo. The other, Inco 718 (CRA), a weldable nickel base alloy, was selected for evaluation in this program to replace René 41.

In this program the following five sheet alloys are evaluated and tested:

- 1) Ti 8Al-1Mo-1V (Duplex Anneal)
- 2) AM 350 Stainless Steel (SCT 850)
- 3) Inco 718 Nickel Alloy (CRA)
- 4) Ti 6Al-4V (Mill Anneal)
- 5) PH 14-8Mo Stainless Steel (SRH 1050)

Fracture toughness tests on both 8-inch and 24-inch wide centrally notched and fatigue cracked panels were performed. The testing was conducted to study the effect of temperature (-110 to 650°F), grain direction, specimen thickness, fatigue crack length, and stress rate on fracture toughness properties. In addition, the effect of exposure for 1000 hours at 650°F under stress (25 ksi for the titanium alloys and 40 ksi for the others) on the room temperature fracture toughness properties was determined. Three heats of each alloy were evaluated to assess heat-to-heat variation.

The basic material thickness used for comparisons among the alloys was 0.050 inches for the titanium alloys and 0.025 inches for the others. These thicknesses were selected as an approximate average sheet thickness which would be used for fuselage and wing structure for the three basic classes of alloys (titanium, stainless steel and nickel-base). Comparisons among the alloys were made at the highest stress rate (approximately 10^6 psi/sec) since this rate is considered to be representative of the loading rate encountered during aircraft operation.

Manuscript was released by author October, 1964 for publication as a RTD Technical Documentary Report.

The range of thickness studied was 0.025 to 0.200 inches for the titanium alloys and 0.025 to 0.125 inches for the stainless steel and nickel-base alloys.

Since the field of fracture toughness testing and evaluation is an emerging discipline in material studies and component design applications, the philosophy guiding the preparation of this report has been fracture toughness oriented. It is recognized, however, that individuals, companies, and government organizations differ in both the interpretation and application of fracture toughness data. Because of this, the basic fracture toughness data is included in tabular form in sufficient detail for individual interpretation.

In accordance with the fracture toughness concept, the fatigue data gathered during the room temperature fatigue cracking of panels has been presented in terms of the stress intensity factor, K , and crack growth rate. With this method, it is possible to depict the rate of crack propagation of various materials in a graphic manner which can be used for fatigue predictions.

SECTION 2. SUMMARY

Fracture testing of five sheet alloys under consideration for commercial supersonic transport application has been carried out. The five alloys studied were Ti 8Al-1Mo-1V (duplex anneal), stainless steel AM 350 (SCT 850), nickel alloy Inco 718 (CRA), Ti 6Al-4V (mill anneal), and stainless steel PH 14-8Mo (SRH 1050). The basic sheet thicknesses studied were 0.025 inches for the stainless steel and nickel alloys and 0.050 inches for the titanium alloys. These thicknesses were selected to represent the approximate average thicknesses in which each alloy would be used in design.

The variables examined in this program were test temperature, grain direction, thickness, crack length, and stress rate. In addition, the effect on fracture properties of exposure for 1000 hours at 650°F under a stress of 25 ksi for the titanium alloys and 40 ksi for the other alloys was determined. Room temperature fatigue crack propagation data were generated for various stress levels and stress ratios during the cracking of both the 8 x 24-inch and 24 x 72-inch test panels.

A summary of the fatigue crack propagation data is shown in Fig. 1. Here the stress intensity factor K has been divided by the material density to normalize the data among all the alloys. This comparison is made for both longitudinal and transverse tests for thicknesses of 0.025 and 0.050 inches and for stress ratios of 0.20 and 0.05 for each alloy. The conservative boundary of the scatter band for each alloy has been used in this comparison. Although the titanium alloys generally have a higher crack propagation rate than the other alloys for a given stress intensity level, this effect is significantly modified when density is considered. The titanium alloys display better crack propagation characteristics when compared in this manner.

The crack propagation tests show that increasing panel thickness results in a faster propagation rate for the 8Al-1Mo-1V, 6Al-4V, and Inco 718 alloys. No thickness effect was evident for the AM 350 and PH 14-8Mo alloys. For the Ti 8Al-1Mo-1V and 6Al-4V alloys, both longitudinal and transverse grain direction tests showed approximately equal cracking rates. For the AM 350, Inco 718, and the PH 14-8Mo alloys, the transverse grain direction showed a significantly higher crack propagation rate. The 650°F exposure treatment caused no change in crack propagation rate for the AM 350 and Inco 718 alloys. For the titanium and PH 14-8Mo alloys, the 650°F exposure increased the crack propagation rate slightly, with the amount depending on the material thickness.

The fracture test results are summarized in Figs. 2 and 3 for the principal alloy thicknesses for the test temperatures of -110°F, room temperature, 400°F, and 650°F. For this comparison, the grain direction showing the lowest value for that specific alloy is used. This is the transverse grain direction for the AM 350, Inco 718, and PH 14-8Mo alloys. For the titanium alloys, the transverse and longitudinal results are generally similar. Fig. 2 shows the comparison based on the critical stress intensity factor (K_{IC}) approach and Fig. 3 shows the comparison based on a gross fracture stress-density approach (σ_G/ρ). Both methods of comparison show the titanium alloys to have a marked superiority

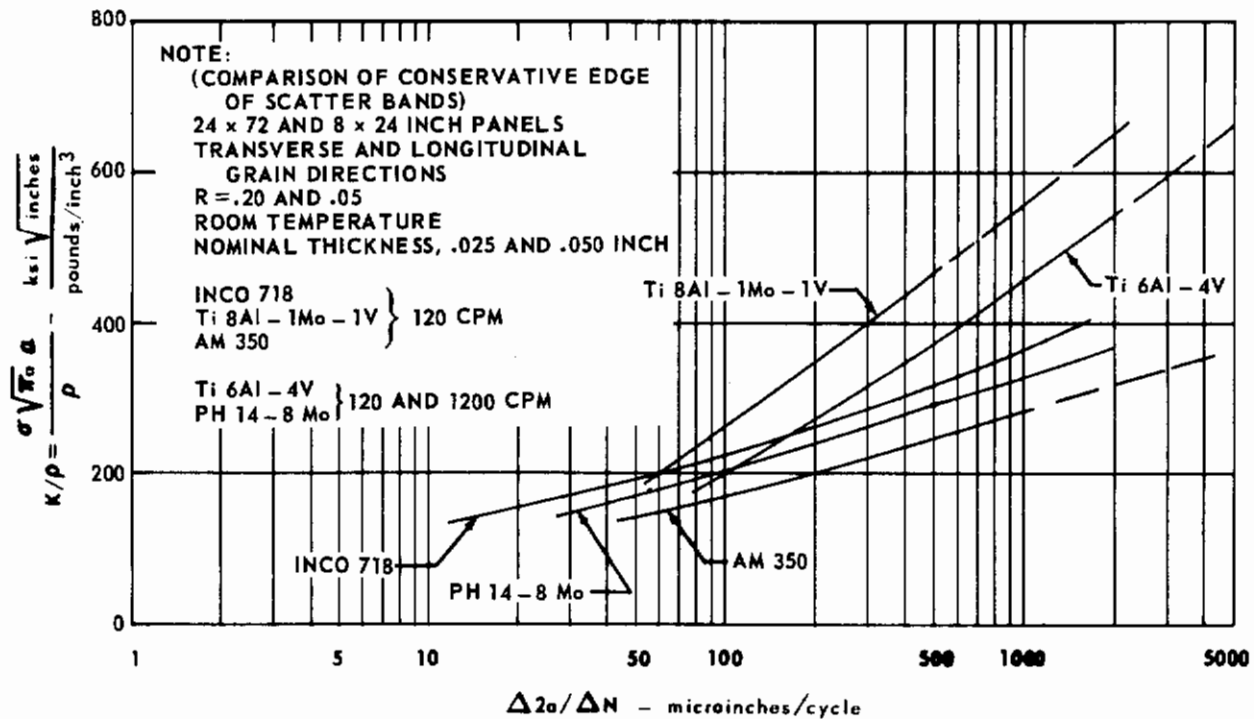


FIG. 1 COMPARISON OF CRACK GROWTH RATE FOR ALL ALLOYS, DENSITY CONSIDERED

over the complete temperature range. Inco 718 and PH 14-8Mo also appear attractive at the low test temperature (-110°F). The AM 350 (SCT 850) alloy exhibits brittle fracture behavior at -110°F.

The detailed variable study showed that fracture properties were essentially the same for both grain directions with the two titanium alloys. This consistency is believed to be due to the cross rolling mill production methods. For the other alloys, transverse fracture properties are significantly lower than the longitudinal properties probably because of continuous mill processing methods.

Fracture toughness and residual strength were found to generally increase with an increase in thickness for the 24 x 72-inch specimen size, while fracture toughness and residual strength trends were dependent on other variables for the 8 x 24-inch specimens. Increasing the stress rate produced an increase in the toughness and residual strength properties with the titanium alloys, had no effect on the AM 350 and Inco 718 alloys, and decreased the fracture properties of the PH 14-8Mo alloy.

Fracture properties of all the alloys were affected to some extent as a result of the 1000-hour, 650°F, and applied stress exposure treatment. The fracture properties of the Ti 8Al-1Mo-1V and Inco 718 were reduced by the exposure; the fracture properties of the Ti 6Al-4V, AM 350, and PH 14-8Mo alloys were increased or reduced by the exposure depending on thickness.

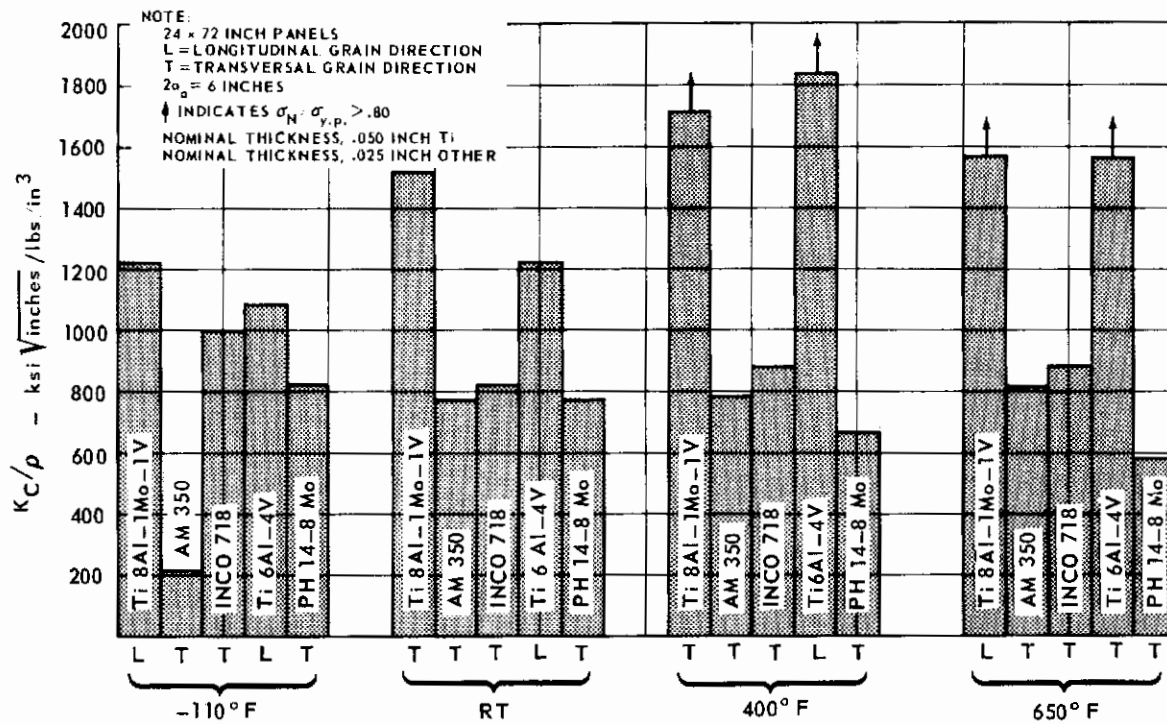


FIG. 2 FRACTURE TOUGHNESS/DENSITY SUMMARY FOR ALL ALLOYS

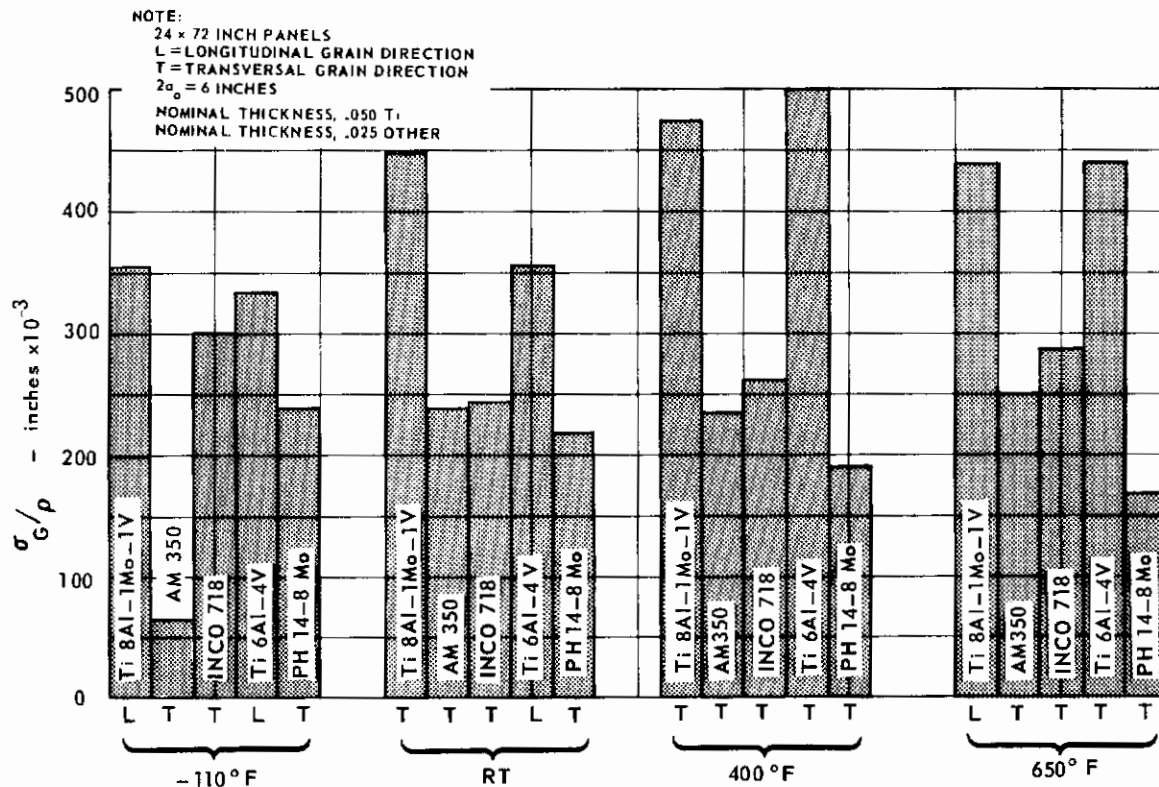


FIG. 3 GROSS FRACTURE STRESS/DENSITY SUMMARY FOR ALL ALLOYS

Contrails

SECTION 3 FRACTURE MECHANICS TECHNOLOGY APPLIED TO SHEET MATERIAL EVALUATION

BACKGROUND

The problem of fatigue crack propagation and resulting crack instability is of primary importance in the design, analysis, and inspection of a fail-safe aircraft structure. Fatigue cracks or other imperfections that occur in an aircraft structure must be contained within the structure without danger of catastrophic failure. The state-of-the-art of fracture mechanics technology allows a means of evaluating the fail-safe capability of aircraft structural sheet materials. This is accomplished through laboratory experimentation of the fatigue crack propagation and fracture toughness characteristics of the structural material under simulated service environment. In utilizing fracture mechanics concepts and existing material data, predictions of service fatigue crack propagation performance are readily obtainable.

The Griffith-Irwin fracture mechanics theory has become the classic approach for treating the mechanics of fatigue crack propagation and crack instability. This theoretical approach is used in this experimental investigation of sinusoidal fatigue crack propagation behavior and plane stress fracture toughness characteristics of the five candidate high-strength sheet materials for supersonic transport application.

The following subsections discuss the basic aspects of fracture mechanics theory as applied in evaluating the sheet materials.

GRIFFITH-IRWIN THEORY OF CRACK INSTABILITY

The Griffith-Irwin Fracture Theory consists of an energy balance concept of the fracture process in the treatment of the crack instability problem. The original fracture theory as developed by Griffith (Ref. 3) is applicable to ideally elastic or brittle solids. An extension of the Griffith-Theory is given by Irwin (Ref. 4, 5, 6) in which additional energy dissipation associated with local crack tip plastic deformation is considered. From these concepts a fracture mechanics approach has evolved for evaluating the brittle fracture characteristics of ductile materials. The theory is applicable in describing the failure modes, as governed by the crack front stress state, that actually occur in cracked structure.

Crack Instability Criterion

Griffith's (Ref. 3) approach to instability of cracks or imperfections in an elastic body is based on the theorem of minimum potential energy. Upon the formation of a crack in an elastic body subjected to boundary forces or stresses, an imbalance of energy occurs resulting in an imbalance of the system. According to the theorem of minimum potential energy, equilibrium is attained by a state of minimum potential energy of the system. The total change in potential energy of the system, due to the formation of the crack, stems from the following sources. First, a decrease in potential energy occurs due to boundary stress displacements and change in strain energy brought about by body deformation. Second, an increase in potential energy occurs due to a characteristic surface energy or surface tension of the material.

Griffith applied the above equilibrium concept by considering a cracked plate of uniform thickness subjected to uniform tension stresses at the plate edges as shown in Fig. 4. This plate configuration is sometimes referred to as the Griffith panel. An equilibrium or crack stability equation is derived by applying the minimum potential energy theorem for equilibrium. Summation of the surface energy and strain energy of the cracked panel results in the total potential energy change, U_T . For the state of plane stress, U_T is:

$$U_T = 4Ta - \frac{\pi \sigma^2 a^2}{E} \quad (1)$$

Where: T is the surface tension, $2a$ is the crack length, σ is the applied tension stress, and E is Young's modulus of elasticity. For equilibrium U_T is a minimum or:

$$\frac{\partial U_T}{\partial a} = 4T - \frac{2\pi \sigma^2 a}{E} = 0 \quad (2)$$

Therefore, the required fracture stress for a given crack length, $2a$, is:

$$\sigma = \left[\frac{2TE}{\pi a} \right]^{1/2} \quad (3)$$

In examining Equation (2), it can be seen that at the onset of rapid fracture or crack instability the strain energy release per unit crack extension is a maximum and is proportional to the dissipation of surface energy per unit crack extension.

An extension of the stability theory discussed above was accomplished by Irwin (Refs. 4, 5, 6) and Orowan (Ref. 7). The extension of the theory considered energy dissipation associated with local plastic deformation at the crack tip. Irwin argued that for a ductile material, the required fracture stress (based on a work rate analysis of the fracture process) is:

$$\sigma = \left[\frac{E(2T + p)}{\pi a} \right]^{1/2} \quad (4)$$

Where p is the energy dissipation per unit of crack extension associated with plastic deformation.

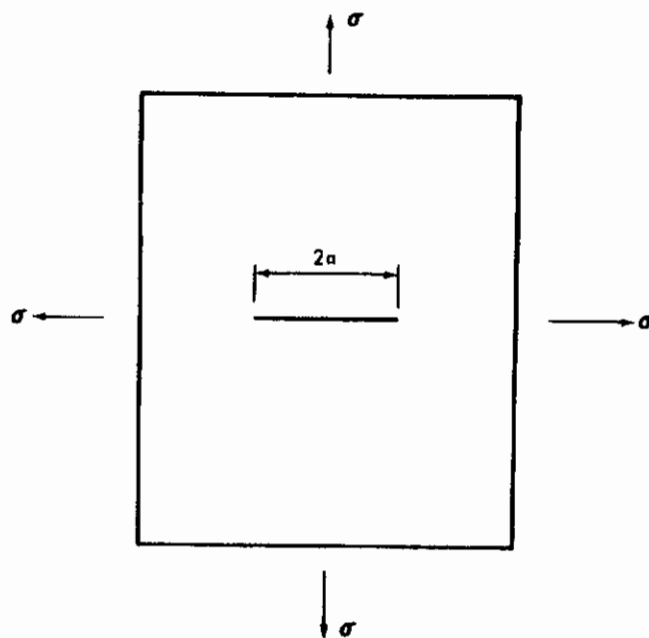


FIG. 4 GRIFFITH PLATE CONFIGURATION

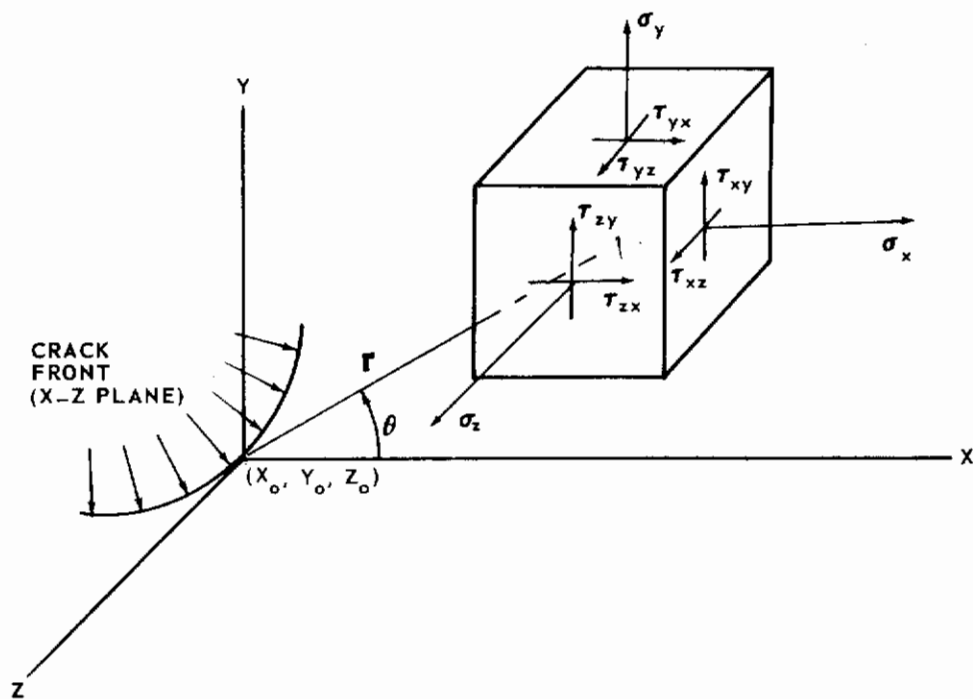


FIG. 5 STRESS ACTING ON AN ELEMENT OF MATERIAL NEAR A CRACK FRONT

The Griffith approach to the crack instability problem emphasized an energy and equilibrium concept of the fracture process. However, a more rigorous analytical approach to crack instability is presented by Irwin (Ref. 8). The approach results in a determination of the crack tip stress field and its relationship to the strain energy release rate at onset of rapid fracture. The following discusses this approach.

Relationship of Crack Tip Stress Field and Crack Instability

The state of stress and strain that exist in the vicinity of a crack tip or crack front governs the mode of fracture that will occur in a cracked structure. In plane problems, the extreme conditions are the state of plane strain and state of plane stress. Irwin (Ref. 8) has shown that stresses acting on an element of material near the crack front, as shown in Fig. 5, can be represented by a factor, K , which is termed the stress intensity factor. The general equations for normal and shear stresses near the crack front for the states of plane stress and plane strain are:

Plane stress state:

$$\sigma_x = \frac{K_1}{\sqrt{2\pi r}} \cos \frac{\theta}{2} \left(1 - \sin \frac{\theta}{2} \sin \frac{3\theta}{2} \right) - \frac{K_2}{\sqrt{2\pi r}} \sin \frac{\theta}{2} \left(2 + \cos \frac{\theta}{2} \cos \frac{3\theta}{2} \right)$$

$$\sigma_y = \frac{K_1}{\sqrt{2\pi r}} \cos \frac{\theta}{2} \left(1 + \sin \frac{\theta}{2} \sin \frac{3\theta}{2} \right) + \frac{K_2}{\sqrt{2\pi r}} \sin \frac{\theta}{2} \cos \frac{3\theta}{2} \cos \frac{\theta}{2}$$

$$\tau_{xy} = \frac{K_1}{\sqrt{2\pi r}} \sin \frac{\theta}{2} \cos \frac{\theta}{2} \cos \frac{3\theta}{2} + \frac{K_2}{\sqrt{2\pi r}} \cos \frac{\theta}{2} \left(1 - \sin \frac{\theta}{2} \sin \frac{3\theta}{2} \right)$$

$$\sigma_z = \tau_{xz} = \tau_{yz} = 0. \quad (5)$$

Plane strain state:

$$\sigma_z = \nu (\sigma_x + \sigma_y)$$

$$\epsilon_z = \gamma_{xz} = \gamma_{yz} = 0.$$

Where γ and θ are polar coordinates (x,y plane) and ν is Poisson's ratio. In addition, K_1 and K_2 are symmetric and skew-symmetric stress intensity factor components relative to applied crack extension loadings (Refs. 9, 10). Essentially, the same form given in Equation (5) for the stress field was derived by Williams (Ref. 11) and Sneddon (Ref. 12). Moreover, the elastic stress equations give a satisfactory description of the crack tip stress field provided the extent of the local plastic zone is small in comparison to the crack dimensions.

Irwin (Refs. 13, 14) has shown that at onset of rapid crack extension the strain energy release rate, G , is related to the critical stress field surrounding the crack tip. For applied loadings, producing opening mode displacement upon crack extension, the relationships for the states of plane stress and plane strain are, respectively:

$$G_C = \frac{K_C^2}{E}$$

and

$$G_{IC} = \frac{(1 - \nu^2) K_{IC}^2}{E} \quad (6)$$

Where G_C and G_{IC} are plane-stress and plane-strain strain-energy release rates and K_C and K_{IC} are plane-stress and plane-strain critical-stress intensity factors.

The above relationship of the stress-field stress intensity factor and strain energy release rate is called the Griffith-Irwin Theory of crack instability. In the literature, the quantities G_C and G_{IC} have often been termed plane stress and plane strain fracture toughness. Moreover, the material quantities are evaluated experimentally through the use of fracture test specimens in which solutions for the stress intensity factor are known.

The fracture test specimen configuration utilized in this sheet material evaluation program is the centrally-cracked panel. The following section discusses the crack tip stress field analysis and resulting solution for the stress intensity factor.

CENTRALLY-CRACKED PANEL STRESS INTENSITY FACTOR

The technique employed in the derivation of the stress intensity factor is based on Westergaard's (Ref. 15) semi-inverse stress function method of linear elastic stress analysis. The panel is considered of infinite width and the appropriate stress function is utilized in deriving an infinite solution for the stress intensity factor. The infinite solution is corrected by considering the panel as a series of colinear cracks. Finally, the size of the crack tip plastic zone is incorporated into the analysis.

Westergaard's Stress Function Method

A differential element of material near the tip of a crack in an infinite plate subjected to a uniform tension stress, σ , is shown in Fig. 6. An Airy stress function, Φ , which solves for the normal and shear stresses acting on the differential element must satisfy the boundary conditions and conditions of equilibrium and compatibility.

From elementary theory of elasticity, the equilibrium equations for a state of plane stress are:

$$\frac{\partial \sigma_x}{\partial x} + \frac{\partial \tau_{xy}}{\partial y} = 0$$

$$\frac{\partial \sigma_y}{\partial y} + \frac{\partial \tau_{xy}}{\partial x} = 0$$

$$\tau_{xy} = \tau_{yx} \quad (7)$$

and the compatibility equation is:

$$\nabla^2 (\sigma_x + \sigma_y) = 0$$

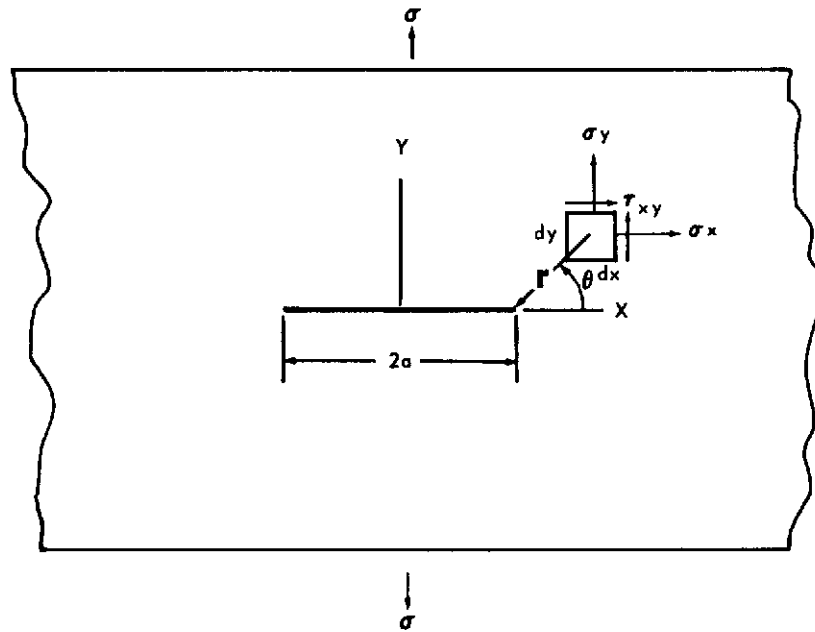
where

$$\nabla^2 = \frac{\partial^2}{\partial x^2} + \frac{\partial^2}{\partial y^2} \quad (8)$$

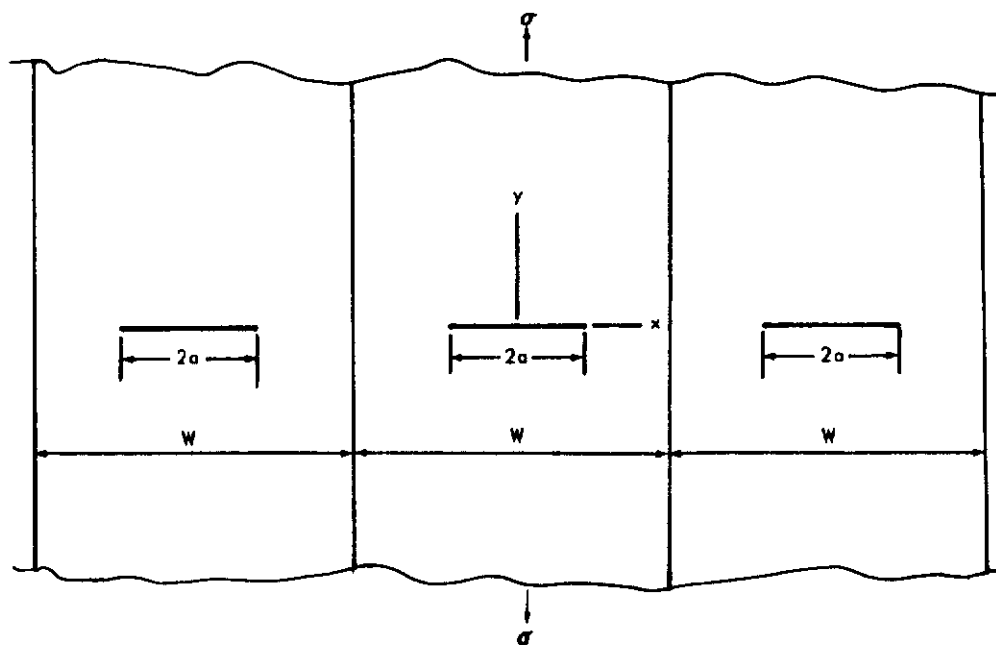
The normal and shear stresses in terms of the Airy stress function are given as:

$$\sigma_x = \frac{\partial^2 \Phi}{\partial y^2} ; \quad \sigma_y = \frac{\partial^2 \Phi}{\partial x^2} ; \quad \tau_{xy} = - \frac{\partial^2 \Phi}{\partial x \partial y} \quad (9)$$

Combining Equations (7), (8) and (9) results in the biharmonic equation:



(A) INFINITE PANEL SUBJECTED TO UNIFORM TENSION



(B) COLLINEAR ARRAY OF CRACKS SUBJECTED TO UNIFORM TENSION

FIG. 6 CENTRALLY-CRACKED PANEL CONFIGURATION WITH INFINITE AND FINITE WIDTHS

$$\nabla^4 \Phi = 0.$$

where

$$\nabla^4 = \frac{\partial^4}{\partial x^4} + 2 \frac{\partial^4}{\partial x^2 \partial y^2} + \frac{\partial^4}{\partial y^4} \quad (10)$$

Westergaard defines the Airy stress function as:

$$\Phi = \text{Re} \bar{Z} + y \text{Im} \bar{Z} \quad (11)$$

where \bar{Z} is an analytic function of the complex variable $\zeta = x + iy$. Furthermore,

$$\bar{Z} = \frac{d\bar{Z}}{d\zeta} ; \quad Z = \frac{dZ}{d\zeta} ; \quad Z' = \frac{dZ}{d\zeta} \quad (12)$$

Incorporating Equation (11) into Equation (9) results in the following stress field equations:

$$\sigma_x = \text{Re} Z - y \text{Im} Z'$$

$$\sigma_y = \text{Re} Z + y \text{Im} Z'$$

$$\tau_{xy} = -y \text{Re} Z' \quad (13)$$

In examining Equation (13), the remaining unknown to the solution of the stress field equations is the Westergaard stress function, $Z(\zeta)$.

Infinite Panel Solution

The stress function, $Z(\zeta)$ which solves the infinite panel given in Fig. 6A is:

$$Z(\zeta) = \sigma \left[1 - \left(\frac{a}{\zeta} \right)^2 \right]^{-\frac{1}{2}} \quad (14)$$

Now, along the x-axis, σ_y from Equation (13) is:

$$\sigma_y = \text{Re}Z = \sigma \left[1 - \left(\frac{a}{x} \right)^2 \right]^{-\frac{1}{2}} \quad (15)$$

From previous discussion, σ_y along the x-axis can also be written in terms of K as given in Equation (5).

$$\sigma_y = \frac{K}{\sqrt{2\pi r}} \quad (16)$$

By equating the results of Equations (15) and (16), K can be written as:

$$K = \sigma \left[\frac{2\pi r x^2}{x^2 - a^2} \right]^{\frac{1}{2}} \quad (17)$$

where $x = a + r$. Since the stress intensity factor is a measure of the stress field in only a local area near the crack tip (i. e., small r) the following limiting process is taken:

$$K = \lim_{r \rightarrow 0} \sigma \left[\frac{2\pi r (a + r)^2}{(a + r)^2 - a^2} \right]^{\frac{1}{2}} \quad (18)$$

which in the limit reduces to:

$$K = \sigma \sqrt{\pi a} \quad (19)$$

Correction Factor for Finite Width Geometry

The solution for the stress intensity factor of Equation (19) is based on the assumption that the centrally-cracked plate is of infinite width. The effect of finite width geometry on the crack tip stress field or stress intensity factor may be analyzed several ways.

One approach is to consider a series of cracks located along the x-axis and equally spaced at a distance W as shown in Fig. 6b. For such a plate subjected to uniform tension stress, σ , the Westergaard stress function is:

$$Z(\xi) = \frac{\sigma \sin \frac{\pi \xi}{W}}{\left[\left(\sin \frac{\pi \xi}{W} \right)^2 - \left(\sin \frac{\pi a}{W} \right)^2 \right]^{1/2}} \quad (20)$$

Utilizing this approach in deriving the infinite plate solution, the following result is obtained.

$$K = \lim_{r \rightarrow 0} \sigma \sin \frac{\pi(a+r)}{W} \left[\frac{2\pi r}{\left(\sin \frac{\pi(a+r)}{W} \right)^2 - \left(\sin \frac{\pi a}{W} \right)^2} \right]^{1/2} \quad (21)$$

which in the limit reduces to:

$$K = \sigma \sqrt{\pi a} \left[\frac{W}{\pi a} \tan \frac{\pi a}{W} \right]^{1/2} \quad (22)$$

Equation (22) can be rewritten as:

$$K = \sigma \sqrt{\pi a} a_1$$

where

$$a_1 = \left[\frac{W}{\pi a} \tan \frac{\pi a}{W} \right]^{1/2} \quad (23)$$

By comparing Equations (19) and (23), the factor a is a stress intensity correction factor for finite width geometry.

In addition, a solution for the correction factor is reported by Greenspan (Ref. 16). For a series of elliptical perforations, analogous to the previous approach, Greenspan's correction factor a_2 is:

$$a_2 = \frac{\left[4 + 2 \left(\frac{2a}{W} \right)^4 \right]^{1/2}}{2 - \left(\frac{2a}{W} \right)^2 - \left(\frac{2a}{W} \right)^4} \quad (24)$$

Fig. 7 shows a comparison of a_1 and a_2 for various $\frac{2a}{W}$. In general, a_1 gives a conservative value when compared to a_2 .

Correction for Crack Tip Plastic Zone

The previous analysis of the stress intensity factor for the centrally cracked panel configuration was based on theory of elasticity techniques. However, local plastic deformation occurs at the crack tip. Therefore, it seems appropriate to examine the extent of the plastic zone.

The plastic zone size is determined by employing a yield criterion and the elastic stress field in the vicinity of the crack tip. The yield criterion utilized is the Henky-Von Mises distortional energy criterion. For a state of plane stress, yielding occurs when:

$$\sigma_x^2 - \sigma_x \sigma_y + \sigma_y^2 + 3 \tau_{xy}^2 = \sigma_{yp}^2 \quad (25)$$

where σ_{yp} is the yield stress as determined by an axial test of the material under consideration. Substitution of Equation (5), for symmetrically applied loadings, into Equation (25) results in:

$$r = \frac{K^2}{2 \pi \sigma_{yp}^2} \cos^2 \frac{\theta}{2} \left[1 + 3 \sin^2 \frac{\theta}{2} \right] \quad (26)$$

The plastic zone width, w , along the x-axis or $\theta = 0$ is:

$$w = \frac{K^2}{2 \pi \sigma_{yp}^2} \quad (27)$$

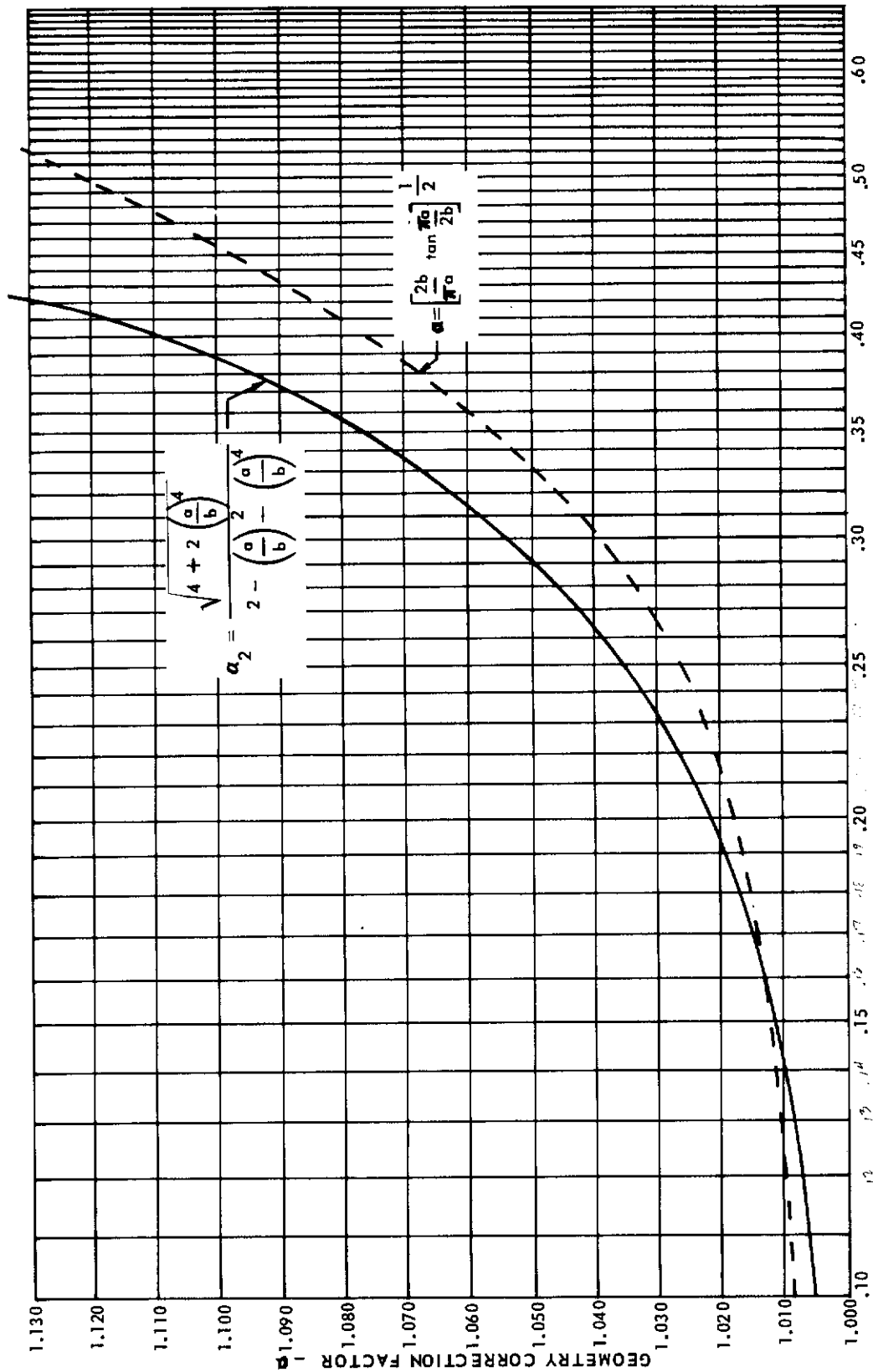


FIG. 7 COMPARISON OF POLYNOMIAL AND TANGENT GEOMETRY CORRECTION FACTORS

This plastic zone width is considered as an effective increase in crack length. Therefore, the stress intensity factor when corrected for the plastic zone size becomes:

$$K = \sigma \left[W \tan \left(\frac{\pi a}{W} + \frac{K^2}{2W\sigma_{yp}^2} \right) \right]^{\frac{1}{2}} \quad (28)$$

The above equation, for the stress intensity factor, is the recommended analytical expression for material evaluation by the ASTM Committee on Fracture Testing of High Strength Materials (Ref. 17). Moreover, the committee recommends that center-cracked panels be so designed for fracture toughness testing so that $\sigma_N \leq 0.8 \sigma_{yp}$, where σ_N is the net-section stress at failure.

STRESS INTENSITY FACTOR CONCEPT OF FATIGUE CRACK PROPAGATION

An analytical approach to the treatment of sinusoidal fatigue crack propagation behavior of airframe sheet materials is presented by Paris, Gomez and Anderson (Ref. 18). Realizing that the stress intensity factor measures the intensity of stress in the region of the crack tip and the plastic zone size, the investigators rationalized that the stress intensity factor controls the rate of fatigue crack propagation. That is, in a loading cycle, the controlling stress intensity parameters are the maximum stress intensity factor and the stress intensity fluctuation.

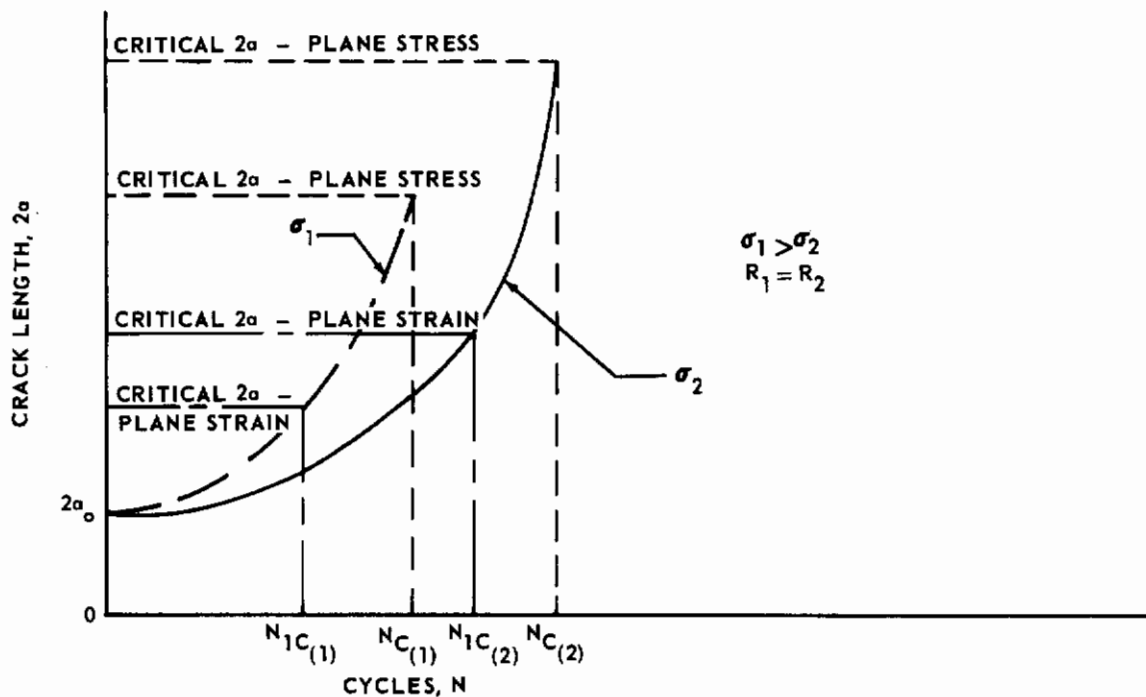
The fluctuation in stress intensity at the crack tip is measured by the ratio, R , defined as:

$$R = \frac{K_{MIN}}{K_{MAX}} \quad (29)$$

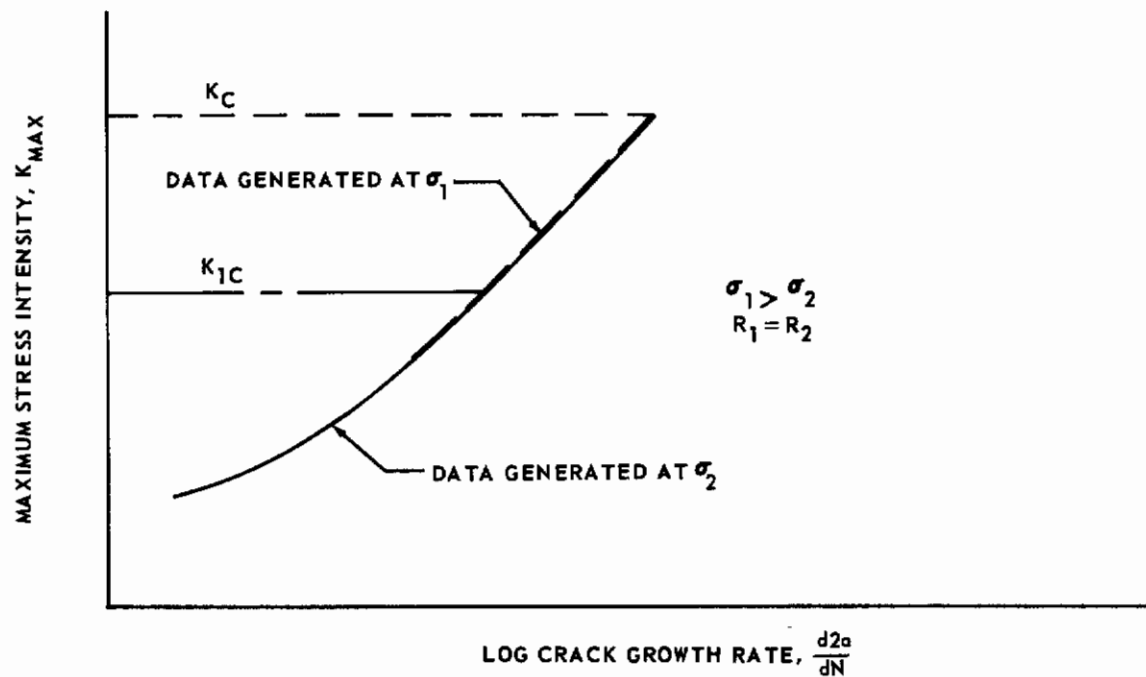
where K_{MIN} and K_{MAX} are respectively, the minimum and maximum stress intensity factors in a loading cycle.

The stress intensity factor concept of fatigue crack propagation is best explained by referring to the schematic diagrams of Fig. 8. It is assumed that the relative experimental crack growth behaviors, from an initial crack length $2a_0$, at maximum constant cyclic stress levels σ_1 and σ_2 with $\sigma_1 > \sigma_2$ are as shown in Fig. 8a. In addition, it is assumed that the R ratios R_1 and R_2 for the cyclic conditions are equivalent. The relative critical crack lengths and cyclic life for plane strain and plane stress fracture modes are as noted. The fracture mode that actually occurs depends upon structure or specimen geometry and material fracture toughness properties.

Now, reduction of the crack growth behaviors of Fig. 8a to maximum stress intensity-crack growth rate behaviors will result in curves as shown schemati-



(a) CRACK GROWTH BEHAVIOR



(b) $K_{MAX} - \frac{d2a}{dN}$ BEHAVIOR

FIG. 8 FATIGUE CRACK GROWTH RATE DATA CORRELATION TECHNIQUE

cally in Fig. 8b. The crack growth rate data generated at σ_1 and σ_2 will coincide since the conditions at the crack tips are identical. That is, the same maximum stress intensity and fluctuation will produce identical crack growth rates. The maximum value of stress intensity is governed by the critical stress intensity factor of the material. Fatigue crack growth data of some airframe materials correlated by the above approach is presented by Donaldson, Anderson, and Paris (Refs. 19 and 20).

The stress intensity factor concept of fatigue crack propagation leads to the following application. The fatigue crack growth behavior, from an initially assumed crack length, can be predicted by numerically integrating stress intensity-crack growth rate data for a given material and fatigue loading conditions. For example, the fatigue crack growth behavior under σ_1 is predicted by integrating stress intensity-crack growth rate data generated under σ_2 . Furthermore, a material comparison of fatigue crack propagation behavior is accomplished by comparing stress intensity-crack growth rate material data plots.

Contrails

SECTION 4 OUTLINE OF TEST PROGRAM

STATEMENT OF PROBLEM AND APPROACH

Obtaining realistic and reliable plane stress fracture toughness and crack propagation design data for the high-strength metals being considered presents a number of problem areas. These may be conveniently grouped into five categories.

- 1) The inclusion of all the important variables in the testing.
- 2) A knowledge of the contemplated service conditions which quantitatively defines the limits of the testing variables.
- 3) The accurate measurement of the reaction or behavior of the test specimen when it is exposed to the test variables.
- 4) The mathematical analysis of the measured behavior of the specimens to quantitatively describe the property being examined.
- 5) The grouping of the test values, or calculated quantities, and the variables into curves which will enhance the practical evaluation and design application.

The first problem area has evolved to the extent that many important variables in the field of structural analysis and structural testing are now recognized. Comparable developments are still seriously lacking in the metallurgical field. The metallurgical shortcomings are exemplified by the wide variations in structure-sensitive properties of materials which have been processed by apparently similar standard techniques and tested in an identical manner. Mill processing and heat treatment data on each of the alloys tested in this program were recorded so that some base line reference point can be established for further delineation of the effects of processing variables on fracture properties.

For the second problem area, in addition to testing over the range of service temperatures, an increasingly realistic approach to the rate of stress application was followed. The fast load rates imposed by large gusts under actual flight conditions were approximated in the testing; this in turn produces more realistic fracture toughness values which for different materials, may be lower or higher than the values obtained under conventional laboratory conditions. In order to simulate actual aircraft structure and to provide consistent data among the various material thicknesses, the test panels were laterally restrained to prevent buckling from occurring during fatigue cracking and during all fracture testing.

The third problem area is epitomized by the difficulties incident to determination of crack dimensions and load. Linear servovalve control programmers were used in conjunction with hydraulic-mechanical systems to achieve the desired accuracy in load values (± 4 percent). High speed photography was used in an attempt to assess the amount of slow crack growth occurring at the low stress rate tests (5×10^3 psi/sec).

The fourth problem area revolves about the theoretical basis for the formulations used in relating loading, dimensional, and material variables in cracked strength

evaluations. Current state-of-the-art formulations were used in making comparisons among materials with ASTM recommendations (Refs. 21, 22 and 23) being used as a guide.

In the fifth problem area, standard graphic methods were utilized to present data in a usable form. In addition, detailed tabular data were presented so that evaluations could be made by other methods of interpretation since there has been considerable confusion caused by failure to report all the testing variables and computational methods in the fracture mechanics field.

MATERIAL

Table 1 lists the five sheet alloys tested in the program along with their heat treatment test condition and the specification tensile property requirements. Three heats of each alloy were evaluated with the basic thickness being 0.050 inches for the titanium alloys and 0.025 inches for the stainless steel and nickel alloys. One large heat of each material was procured in four thicknesses. These thicknesses were 0.025, 0.050, 0.125, and 0.200 inches for the titanium alloys and 0.025, 0.050, 0.093, and 0.125 inches for the stainless steel and nickel alloys.

TESTING PLAN

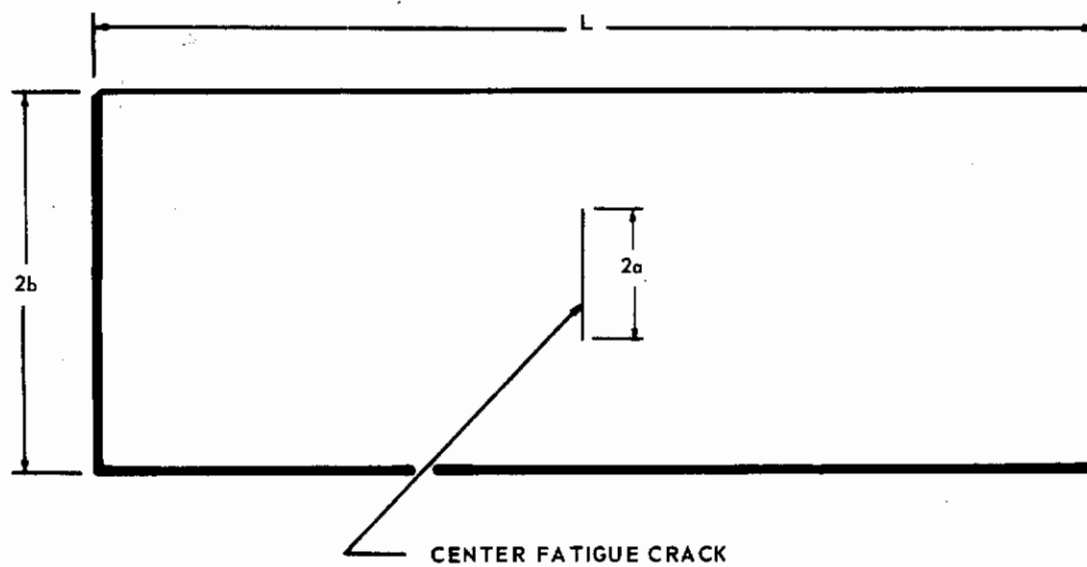
Two fracture toughness specimen configurations were used in this program. The small 8-inch wide by 24-inch long specimen design remained identical to the configuration tested by Douglas under Contract AF33(657)-8543 (Ref. 1) except for a different grip pattern. A large 24-inch wide by 72-inch long specimen was also used. For the 24-inch by 72-inch transverse grain direction specimens extensions were welded to extend the length of the panel from the basic sheet width to 72 inches. Standard sheet tensile specimens were used for tensile property evaluations. Specimen configurations are shown in Fig. 9.

The testing outline for fracture panels is included in Table 2. Panels were center-notched and cyclically loaded to produce a central fatigue crack. The final increment of fatigue cracking was carried out at a stress ratio, R , of 0.20 and at a stress level to produce a final K of approximately 50 ksi $\sqrt{\text{inches}}$ with the titanium alloys and approximately 75 ksi $\sqrt{\text{inches}}$ with the stainless steel and nickel alloys. In this way the crack tip plastic zone size, which is proportional to $(K/\sigma_{yp})^2$, was approximately the same for each alloy. During fracture testing the panels were prevented from buckling with the use of buckling restraints. Six 8 by 24 by 0.025-inch panels of Ti 8Al-1Mo-1V heat D3369 from the Douglas program (Ref. 1) were tested to provide a reference point between the two programs. In addition, three 8 by 24-inch panels of Ti 6Al-4V were tested by each joint venture company to determine testing compatibility between the two companies.

Crack length measurements were made during cycling to obtain crack growth information. Restraints were used during cycling to prevent buckling on nearly all 24 by 72-inch panels and as required on the 8 by 24-inch panels. The

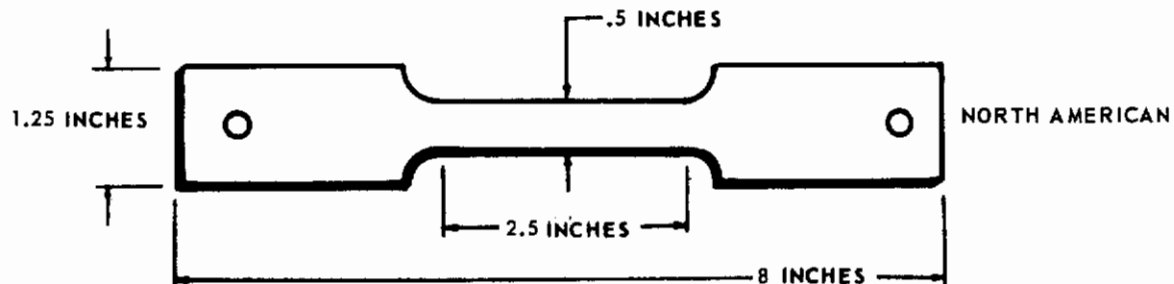
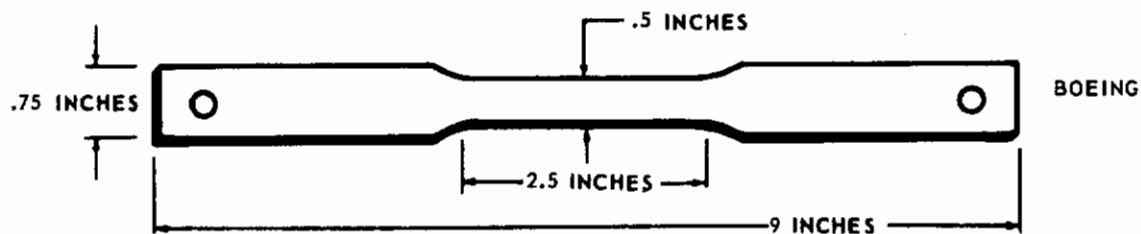
TABLE 1 SUMMARY OF ALLOYS AND CONDITIONS BEING EVALUATED

MATERIAL	HEAT TREATMENT	MINIMUM MECHANICAL PROPERTIES		
		F _{tu} ksi	F _{ty} ksi	ELONG. IN 2"
TITANIUM 8Al-1Mo-IV	1450 °F 8 HRS. FC & 1450 °F 15 MIN. AC DUPLEX ANNEALED	135	125	10%
TITANIUM 6Al-4V	MILL ANNEALED	130	120	8%
AM 350	1710 °F 30 MIN AC, -100 °F 3 HRS. 850 °F 3 HRS. SCT 850	185	150	10%
PH 14-8Mo	1700 °F 1 HR. AC -100 °F 8 HRS. 1050 °F 1 HR. SRH 1050	200	180	5%
INCONEL 718	COLD ROLLED AND AGED 1275 °F 8 HRS., FC 20 °F/HR. TO 1150 °F HOLD 10 HRS. AC	210	190	6%



CONFIGURATION	$2b$	L	$2a$
1	8 INCH	24 INCH	1, 2, 3 INCH
2	24 INCH	72 INCH	3, 6, 10 INCH

FRACTURE PANELS - TWO CONFIGURATIONS



TENSILE SPECIMENS - TWO CONFIGURATIONS

FIG. 9 TEST SPECIMEN CONFIGURATIONS

TABLE 2 DETAILED TESTING OUTLINE FOR ALL FRACTURE PANELS

ALLOY	HEAT NO.	NOMINAL THICKNESS inches	GRAIN DIRECTION	24 INCH WIDE x 72 INCH LONG PANELS						8 INCH WIDE x 24 INCH LONG PANELS										SPECIMEN TOTALS	
				CRACK LENGTH VARIABLE $\bar{a}=10^6$			STRESS RATE (RT) VARIABLE $2a=6$ inches	TEMP VARIABLE $\bar{\sigma}=10^6$, $2a=6$ inches		TEMP VARIABLE $\bar{\sigma}=5 \times 10^3$, $2a=2$ inches		TEMP VARIABLE $\bar{\sigma}=10^6$, $2a=2$ inches		CRACK LENGTH VARIABLE $\bar{a}=10^6$		650° F EXPOSURE 1000 HOURS					
				RT	650° F	3"		6"	10"	3"	6"	10"	3"	6"	10"		3"	6"	10"		
							RT									650° F				RT	650° F
Ti-6Al-4V	D4535	.050	L	1	2	1	2	1	2	2	2	2	2	2	2	2	2	2	15	3	
	D4535	.050	T	2	2	2	2	2	2	2	2	2	2	2	2	2	2	4	3		
	D3454	.050	L	2	2	2	2	2	2	2	2	2	2	2	2	2	2	8	3		
	D3454	.050	T	2	2	2	2	2	2	2	2	2	2	2	2	2	2	4	3		
	D3457	.200	L	1	2	1	2	1	2	1	1	1	1	1	1	1	1	11	9		
	D3457	.200	T	2	2	2	2	2	2	2	2	2	2	2	2	2	2	1	3		
	D3457	.125	L	2	2	2	2	2	2	2	2	2	2	2	2	2	2	4	6		
	D3457	.125	T	2	2	2	2	2	2	2	2	2	2	2	2	2	2	1	5		
	D3457	.050	L	2	2	2	2	2	2	2	2	2	2	2	2	2	2	4	3		
	D3457	.050	T	2	2	2	2	2	2	2	2	2	2	2	2	2	2	4	6		
	D3457	.025	L	2	2	2	2	2	2	2	2	2	2	2	2	2	2	1	1		
	D3457	.025	T	2	2	2	2	2	2	2	2	2	2	2	2	2	2	1	5		
AM 350	19207	.025	L	1	2	1	2	1	2	2	2	2	2	2	2	2	2	16	3		
	19207	.025	T	2	2	2	2	2	2	2	2	2	2	2	2	2	2	4	3		
	55538	.025	L	2	2	2	2	2	2	2	2	2	2	2	2	2	2	6	3		
	55538	.025	T	2	2	2	2	2	2	2	2	2	2	2	2	2	2	3	3		
	19020	.125	L	2	2	1	2	1	2	2	2	2	2	2	2	2	2	12	9		
	19020	.125	T	2	2	2	2	2	2	2	2	2	2	2	2	2	2	2	1		
	19020	.093	L	2	2	2	2	2	2	2	2	2	2	2	2	2	2	4	3		
	19020	.093	T	2	2	2	2	2	2	2	2	2	2	2	2	2	2	4	6		
	19020	.050	L	2	2	2	2	2	2	2	2	2	2	2	2	2	2	4	6		
	19020	.050	T	2	2	2	2	2	2	2	2	2	2	2	2	2	2	1	1		
	19020	.025	L	2	2	2	2	2	2	2	2	2	2	2	2	2	2	4	6		
	19020	.025	T	2	2	2	2	2	2	2	2	2	2	2	2	2	2	1	5		
INCO 718	6713	.025	L	1	2	1	2	1	2	2	2	2	2	2	2	2	2	11	1		
	6713	.025	T	2	2	2	2	2	2	2	2	2	2	2	2	2	2	4	5		
	6905	.025	L	2	2	2	2	2	2	2	2	2	2	2	2	2	2	8	3		
	6905	.025	T	2	2	2	2	2	2	2	2	2	2	2	2	2	2	4	3		
	6902	.125	L	1	2	1	2	1	2	2	2	2	2	2	2	2	2	14	9		
	6902	.125	T	2	2	2	2	2	2	2	2	2	2	2	2	2	2	1	3		
	6902	.093	L	2	2	2	2	2	2	2	2	2	2	2	2	2	2	4	3		
	6902	.093	T	2	2	2	2	2	2	2	2	2	2	2	2	2	2	4	3		
	6902	.050	L	2	2	2	2	2	2	2	2	2	2	2	2	2	2	1	6		
	6902	.050	T	2	2	2	2	2	2	2	2	2	2	2	2	2	2	1	1		
	6902	.025	L	2	2	2	2	2	2	2	2	2	2	2	2	2	2	4	6		
	6902	.025	T	2	2	2	2	2	2	2	2	2	2	2	2	2	2	1	1		

Δ 1 SPECIMEN @ $2a=2$ INCHES
 + 1 SPECIMEN @ $2a=3$ INCHES AND 1 @ $2a=10$ INCHES
 ● 2 SPECIMENS CYCLED TO FAILURE

TABLE 2 DETAILED TESTING OUTLINE FOR ALL FRACTURE PANELS (continued)

ALLOY	24 INCH WIDE x 72 INCH LONG PANELS										8 INCH WIDE x 24 INCH LONG PANELS										SPECIMEN TOTALS								
	HEAT NO.	NOMINAL THICKNESS inches	GRAIN DIRECTION	CRACK LENGTH VARIABLE $\bar{\sigma}=10^6$		STRESS RATE (RT) VARIABLE $2a=6$ inches	TEMP VARIABLE $\bar{\sigma}=10^6$, $2a=6$ inches			TEMP VARIABLE $\bar{\sigma}=5 \times 10^3$, $2a=2$ inches			TEMP VARIABLE $\bar{\sigma}=10^6$, $2a=2$ inches			CRACK LENGTH VARIABLE $\bar{\sigma}=10^6$	650° F EXPOSURE 1000 HOURS												
				RT	650° F		5 x 10 ³	-110° F	RT	400° F	650° F	-110° F	RT	400° F	650° F			1"	3"	1"	3"								
																						3"	6"	10"	3"	6"	10"		
T. 6Al-4V	D5257	.050	L	1	2	1	1	2	1	2																			12
	D5257	.050	T	2	2	2	2	2	2	2																			4
	D5256	.050	L	2	2	2	2	2	2	2																			4
	D5256	.050	T	2	2	2	2	2	2	2																			4
	D4949	.200	L	1	2	1	1	2	1	2	2																		14
	D4949	.200	T																										10
	D4949	.125	L																										1
	D4949	.125	T																										3
	D4949	.050	L																										4
	D4949	.050	T																										4
	D4949	.025	L																										1
	D4949	.025	T																										6
PH 14-Beta	43208	.025	L	1	3	1	2	1	2	2																			12
	43208	.025	T	1	1	1	1	2	1	2																			4
	33570	.025	L	2	2	2	2	2	2	2																			8
	33570	.025	T	2	2	2	2	2	2	2																			4
	33570	.125	L	2	2	1	1	1	1	1																			7
	33347	.125	L	1	1	1	1	1	1	1																			7
	33347	.125	T																										9
	33347	.093	L																										1
	33347	.093	T																										4
	33347	.025	L																										4
	33347	.025	T																										4
	33347	.050	L																										1
33347	.050	T																										6	
TOTALS										TOTALS										24 x 72 inches	8 x 24 inches								

1 SPECIMEN $2a=3$ INCHES
 2 SPECIMEN $2a=3$ INCHES AND $1 \times 2a=10$ INCHES

2 SPECIMENS CYCLED TO FAILURE

TABLE 3 OUTLINE OF CRACK PROPAGATION VARIABLES STUDIED

ALLOY	RANGE OF STRESS LEVELS	RANGE OF STRESS RATIOS	CRACK LENGTHS FOR DATA GATHERING*	
			24" X 72" PANELS (3", 6", & 10" FINAL CRACK LENGTHS)	8" X 24" PANELS (2" FINAL CRACK LENGTHS)
TITANIUM 6 Al-4V & 8 Al-1Mo-1V	40 ksi 30 ksi 25 ksi 20 ksi 12.5 ksi	.05 .10 .20 .60	1" TO 2.50" 2" TO 5.25" 3" TO 9.0"	.5" TO 1.5"
AM 350 PH 14-8Mo & INCO 718	67 ksi 56 ksi 48 ksi 40 ksi 36 ksi 32 ksi 20 ksi	.05 .10 .20 .60	1" TO 2.50" 2" TO 5.25" 3" TO 9.0"	.5" TO 1.5" .5" TO FINAL FRACTURE PH 14-8Mo & INCO 718

*THE FINAL INCREMENT OF CRACK GROWTH WAS CARRIED OUT SO THAT THE FINAL K FOR THE TITANIUM ALLOYS WAS APPROXIMATELY $50 \text{ ksi} \sqrt{\text{in}}$ AND FOR THE STEEL AND NICKEL ALLOYS WAS APPROXIMATELY $75 \text{ ksi} \sqrt{\text{in}}$.

cracking variables studied are outlined in Table 3. The cycling frequency for all the large panels was 120 cpm; for the small panels from 8Al-1Mo-1V, AM 350, and INCO 718, 120 cpm; and for the small panels from 6Al-4V and PH 14-8Mo, 1200 cpm and 120 cpm. Additional testing was performed on some 8 by 24-inch panels to relate the effect of cycling speed on crack growth rate for the 6Al-4V and PH 14-8Mo materials and to provide a basis for comparing the panels tested at both speeds.

Fracture toughness tests were conducted at three stress rates: approximately $5 \times 10^3 \text{ psi/sec.}$, $1 \times 10^5 \text{ psi/sec.}$, and $1 \times 10^6 \text{ psi/sec.}$ The majority of the 8 by 24-inch long panels were evaluated at a single crack length of two inches. Because two of the materials were new and testing was desired which would parallel testing at Douglas, crack lengths of 1 and 3 inches were also examined. The large 24-inch wide panels were evaluated at crack lengths of 3, 6, and 10 inches. All 8 x 24-inch panels tested at the low loading rates were instrumented with strain gages to detect discontinuous loading effects associated with the phenomenon of discontinuous crack growth or "pop-in".

Four testing temperatures were used to provide fracture toughness data to cover the temperature range to be encountered by a Mach 2.4 to Mach 3 transport. These temperatures were -110° F, room temperature, 400° F, and 650° F. Six 8-inch wide unnotched specimens from each alloy were exposed at 650° F for 1000 hours under a sustained stress of 25 ksi for the titanium alloys and 40 ksi for the steel and nickel alloys. After exposure, the specimens were notched and the crack growth rates and fracture toughness values were compared with unexposed specimen data.

Contrails

SECTION 5 PROCEDURE

MATERIALS

The three heats of each material were purchased as shown in Table 4. A complete processing history was requested from each supplier of materials along with certified test reports. Upon receipt of the material, microstructural examinations and room temperature tensile tests were made as quality checks.

TABLE 4 SUMMARY OF ALLOY HEATS PURCHASED FOR TESTING

MATERIAL	HEAT NUMBERS	PRODUCER	PURCHASE SPECIFICATION
Ti 8Al-1Mo-1V (D. ANN)	3454, 3457, 4535	TITANIUM METALS CORPORATION OF AMERICA (TMCA)	TMCA INTERNAL
AM 350 (COND. H)	19020, 19207, 55538	ALLEGHENY LUDLUM STEEL CORPORATION	MIL-S-8840
INCO 718 (CR)	6713, 6902, 6905	HUNTINGTON ALLOY PRODUCTS DIVISION OF THE INTERNATIONAL NICKEL CO. (INCO)	BOEING PRELIMINARY
Ti 6Al-4V (M. ANN)	5256, 5257, 4949	TITANIUM METALS CORPORATION OF AMERICA (TMCA)	NAA LBO 170-113
PH 14-8Mo (COND A)	33347, 33570, 43208	ARMCO STEEL CORPORATION	NAA LBO 160-165

SPECIMEN FABRICATION

For one of the Ti 8Al-1Mo-1V heats, two of the AM 350 heats, and all of the Inco 718 heats, 24 x 72-inch sheets were purchased so that it was not necessary to machine the large fracture panels to size. For heats 4535 and 3454 of the Ti 8Al-1Mo-1V alloy, sheets were purchased in widths of 24 to 48 inches and lengths of 72 to 144 inches. For the Ti 6Al-4V alloy, sheets were purchased in widths of 32 and 48 inches and lengths of 96 inches. For heat 55538 of the AM 350 alloy, sheets were purchased in widths of 36 inches and lengths of 120 inches; and for the PH 14-8Mo alloy, in widths of 36 and 44 inches and lengths of 72 and 96 inches.

Preparation of the large 24 x 72-inch panels from the oversize sheets and all the 8 x 24-inch panels was carried out by shearing and/or milling to the appropriate size. The 24 x 72-inch panels for transverse grain direction tests were fabricated by fusion welding extensions from the same thickness material to the basic material sheet widths. The tungsten inert-gas-shielded process was used for

each alloy; filler wire was not used. All welds were radiographically inspected after welding to ensure that welds were of sound quality. After welding, the AM 350 and PH 14-8Mo welded panels were heat treated along with the unwelded panels. With the two titanium alloys, no heat treatment of the as-welded panels was carried out.

HEAT TREATMENT

A transformation heat treatment of all the AM 350 and PH 14-8Mo alloy panels was carried out to achieve the desired tensile properties. Only an aging cycle was required with the Inco 718 alloy, which was purchased in the cold rolled condition. Heat treatment details for these three alloys are included in Table 5.

CENTER NOTCHING

Hole patterns for grip attachments were drilled in each end of each panel with a drill jig to ensure uniformity among all the panels of any one size. Holes were one-half inch in diameter for the 8 x 24-inch panels and one inch in diameter for the 24 x 72-inch panels. All panels were centrally notched except six 8 x 24-inch transverse grain specimens from each alloy, which were to be exposed under stress at 650°F for 1000 hours.

All titanium 8Al-1Mo-1V, AM 350, and Inco 718 panels were center notched by first drilling a small hole in the center of the panel, then inserting a saw through the hole to rough saw a slot to within 0.20 inches of the desired notch length, and finally extending the slot to finished length with a jewellers' saw. The final cut was 0.005-inch wide. For the titanium 6Al-4V and PH 14-8Mo alloys, center notches were made with an 0.005-inch thick copper-tungsten electrode and an electrical discharge machining method.

For the 8 x 24-inch panels, all starter notches were 0.50 inch in length. For the 24 x 72-inch panels, the starter notch length depended upon the final fatigue crack length. Starter notches were 1.00 inch for 3.00-inch fatigue cracks; 2.00 inches for 6.00-inch fatigue cracks; and 3.00 inches for 10.00-inch fatigue cracks.

TENSILE TESTING

Tensile tests were made in accordance with Federal Test Method, Standard Number 151(a). These tests were made at temperatures of -110°F, room temperature, 400°F, and 650°F to establish the variation of tensile properties with temperature for each of the materials.

TEST EQUIPMENT

The test equipment at both companies is essentially the same; hence, the following descriptions apply to both testing laboratories. Cycling and fracture testing were carried out in servovalve-controlled hydraulic-load-cylinder jigs. Fig. 10 shows the three loading towers used at North American Aviation. Static loading capacities from left to right are 700 kips, 200 kips, and 300 kips. At Boeing, four similar loading towers were used which have static capacities of 125 kips,

TABLE 5 HEAT TREATMENT PROCEDURES FOR AM 350, PH 14-8Mo AND INCO 718

AM 350 CONDITION H	PH14-8Mo CONDITION A	INCO 718 - COLD ROLLED
1. ALKALINE CLEAN AND TURCO PRECOAT.	1. ALKALINE CLEAN AND PRECOAT.	1. 1275°F ± 25°F FOR 8 HOURS.
2. 1710°F ± 15°F FOR 30 MIN.; AC TO 300°-500°F.	2. 1700°F ± 10°F FOR 90 MINUTES; AC TO 300°-500°F.	2. FC 20°/HOUR TO 1150°F ± 25°F.
3. TRANSFER TO 1 1/2 INCH THICK PLATES AND CLAMP BETWEEN PLATES.	3. TRANSFER TO 1 1/2 INCH THICK PLATES AND CLAMP BETWEEN PLATES.	3. 1150°F FOR 10 HOURS; AC.
4. AC TO -100°F WITHIN 1 HOUR.	4. AC TO -100°F WITHIN 1 HOUR.	4. INCO 718 CRA
5. -100°F FOR 4 HOURS. (DRY ICE AND TRICHLOROETHYLENE TANK)	5. -100°F FOR 8 HOURS. (REFRIGERATED TRICHLOROETHYLENE TANK)	
6. AIR WARM TO R.T.	6. AIR WARM TO R.T.	
7. 850°F ± 25°F FOR 3 HOURS; AC.	7. 1050°F ± 10°F FOR 1 HOUR; AC.	
8. REMOVE MATERIAL FROM PLATES.	8. REMOVE MATERIAL FROM PLATES	
9. PICKLE TO REMOVE SCALE.	9. PICKLE TO REMOVE SCALE.	
10. AM 350 SCT 850	10. PH 14-8Mo SRH 1050	

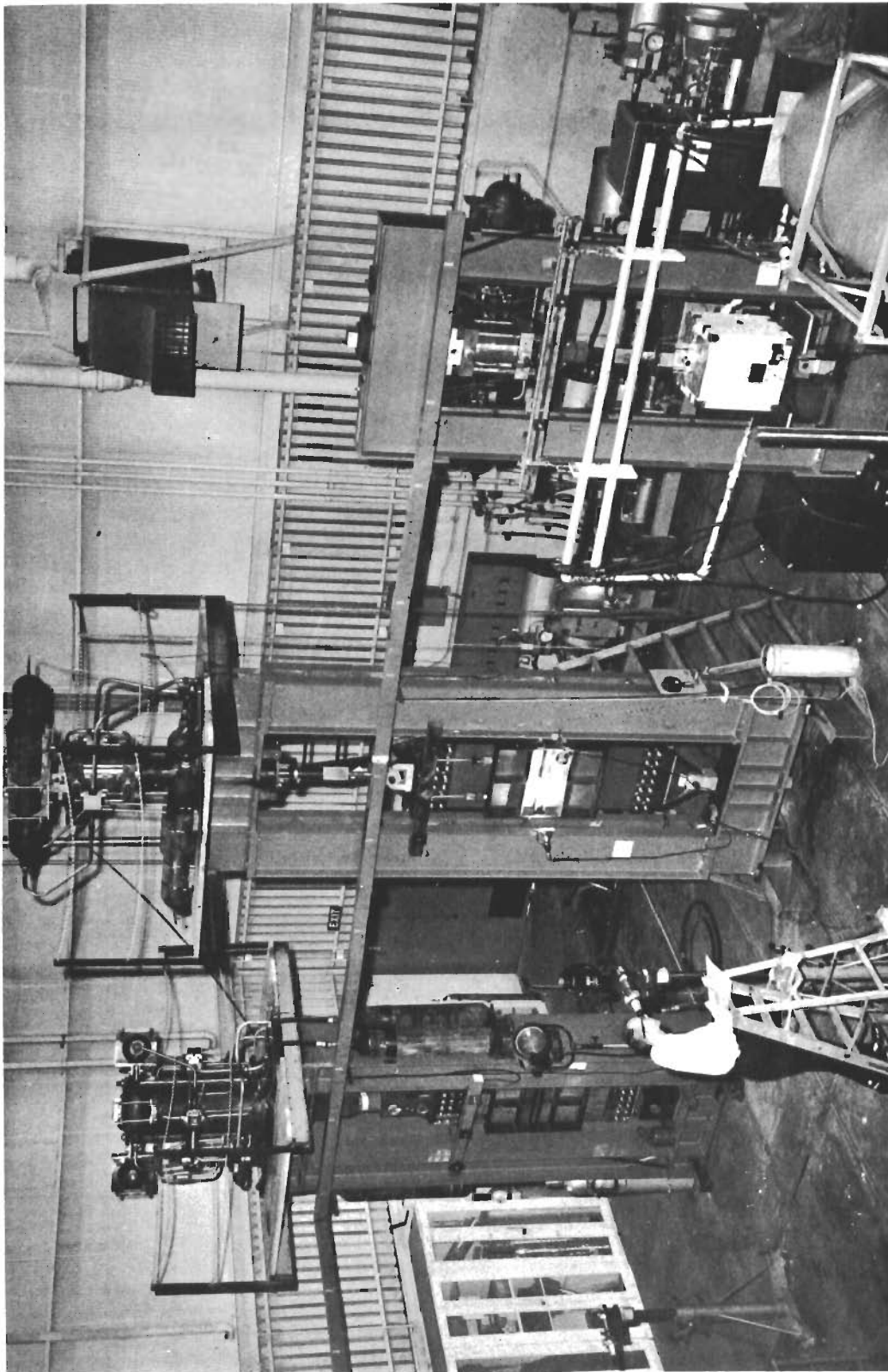


FIG. 10 THREE HYDRAULIC EQUIPPED LOADING TOWERS

250 kips, 300 kips, and 1000 kips. In Fig. 10, the buckling restraints can be seen in position on the specimens in the two towers to the left. The tower at the right has an elevated temperature test in place.

A schematic diagram of the load control system for these towers is shown in Fig. 11. For fatigue cycling, the sine wave generator is programmed into the circuit.

For rapid fracturing at loading rates of 10^5 and 10^6 psi/sec, either the short ramp generator or the battery ramp was used. The short ramp generator circuit was a closed loop or feedback control circuit and had an adjustable time-base from 0.05 to 11 seconds. Also included in the short ramp circuit was an adjustment for setting the load which would occur when the time base setting had elapsed. No adjustment other than that of battery voltage was required for the battery ramp circuit. For fracture testing at loading rates of 5×10^3 psi/sec, the long ramp generator was employed because it had a fixed time base of 60 seconds. Fig. 12 shows the load control console and the load recording oscillograph.

A schematic layout of the hydraulic system for the 200 kip loading tower is shown in Fig. 13. Two Moog servovalves rated at 60 gallons per minute and 5000 psi were used to provide sufficient oil flow during fracture testing to achieve the desired loading rates on the 24 x 72-inch panels of the lowest modulus alloy. A sufficient volume of high-pressure oil was provided by two Greer hydraulic accumulators with a 10-gallon capacity at 3000 psi. The basic changes necessary to the system with the higher capacity loading towers are to increase the accumulator and flow-through oil capacity of the system. For example, the 700 kip system had four 60-gallon-per-minute Moog servovalves, supported by four 10-gallon capacity accumulators rated at 3000 psi, and four 2.5-gallon accumulators rated at 5500 psi.

FATIGUE CRACKING

Pin-ended loading plates, which ensured axial loading, were bolted to the specimen ends in preparing specimens for fatigue cracking. The surface area adjacent to the crack was polished when necessary to improve crack length observations. All 24 x 72-inch panels of the five alloys and all 8 x 24-inch panels of Ti 8Al-1Mo-1V, AM 350, and Inco 718 were cycled at 120 cpm at room temperature to produce fatigue cracks in the hydraulically-equipped loading towers. The 8 x 24-inch panels of Ti 6Al-4V, and PH 14-8Mo were cycled at 1200 cpm at room temperature in a Baldwin-Lima-Hamilton IV-12 fatigue machine.

All 24 x 72-inch panels were restrained from buckling during fatigue cracking. At North American, the steel restraints shown on the test equipment in Fig. 10 were used. At Boeing, both steel restraints and thick plexiglass restraints were used depending on the material thickness. Fig. 14 shows a 24 x 72-inch panel with the plexiglass restraint in place in the 300 kip tower at Boeing. For the thin gages of material (less than 0.125 inch) the plexiglass provided adequate stiffness. For the thicker panels, gross buckling was not evident. The main requirement here of the buckling restraint was to prevent any relative shearing motion across the fatigue crack.

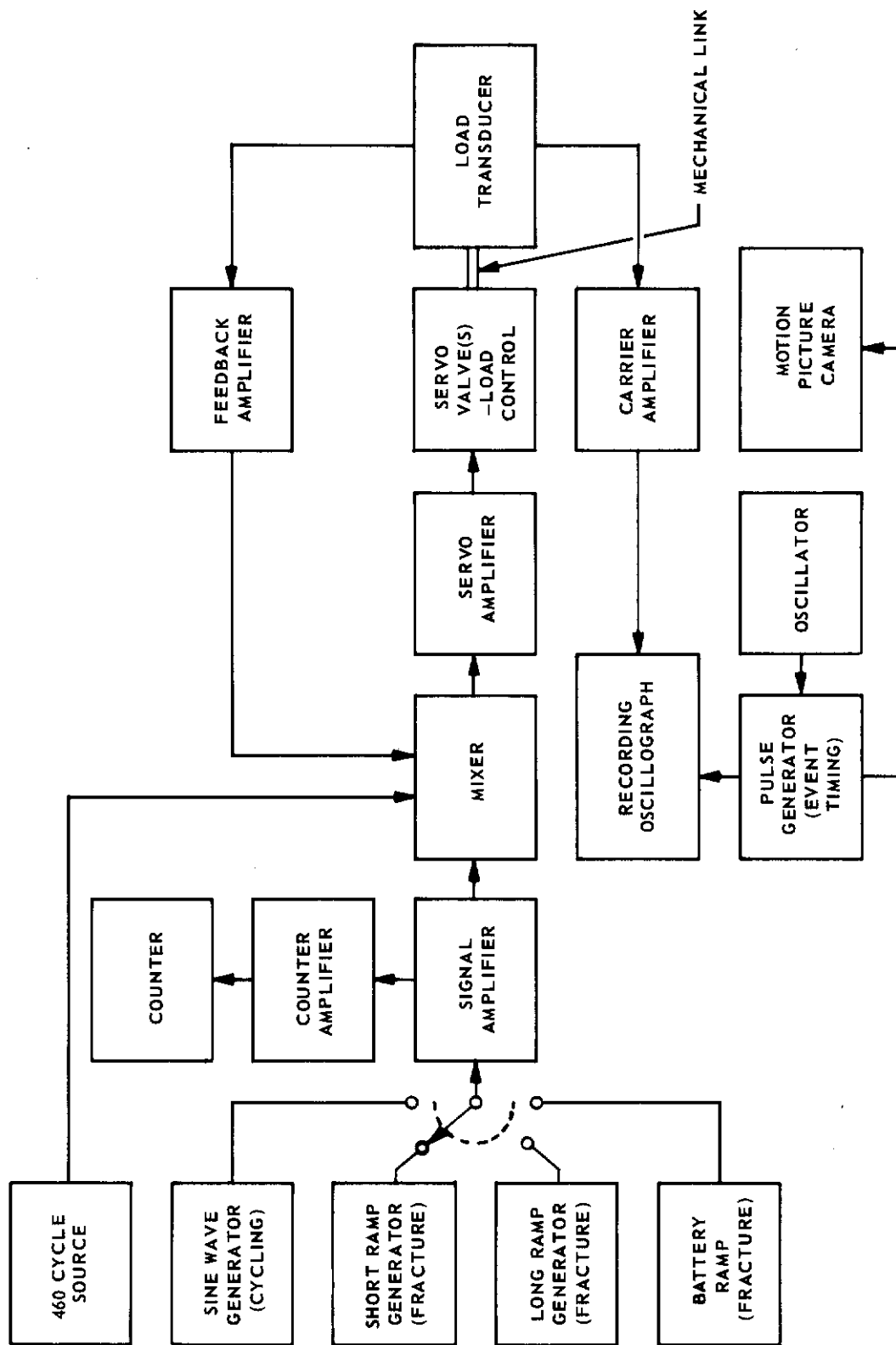


FIG. 11 ELECTRONIC COMPONENTS IN SERVO-CONTROLLED LOADING SYSTEM

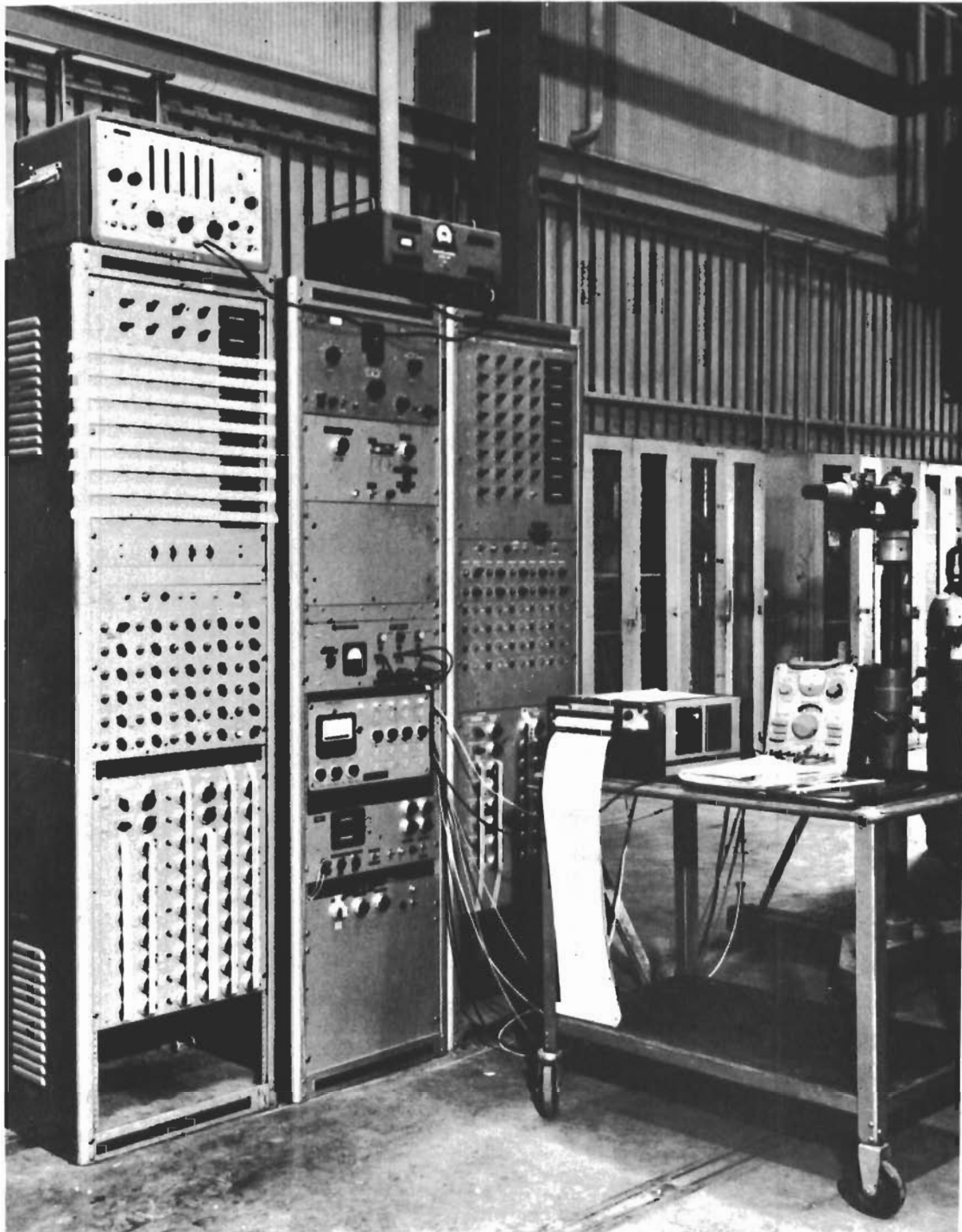


FIG. 12 LOAD CONTROL CONSOLE AND RECORDING OSCILLOGRAPH

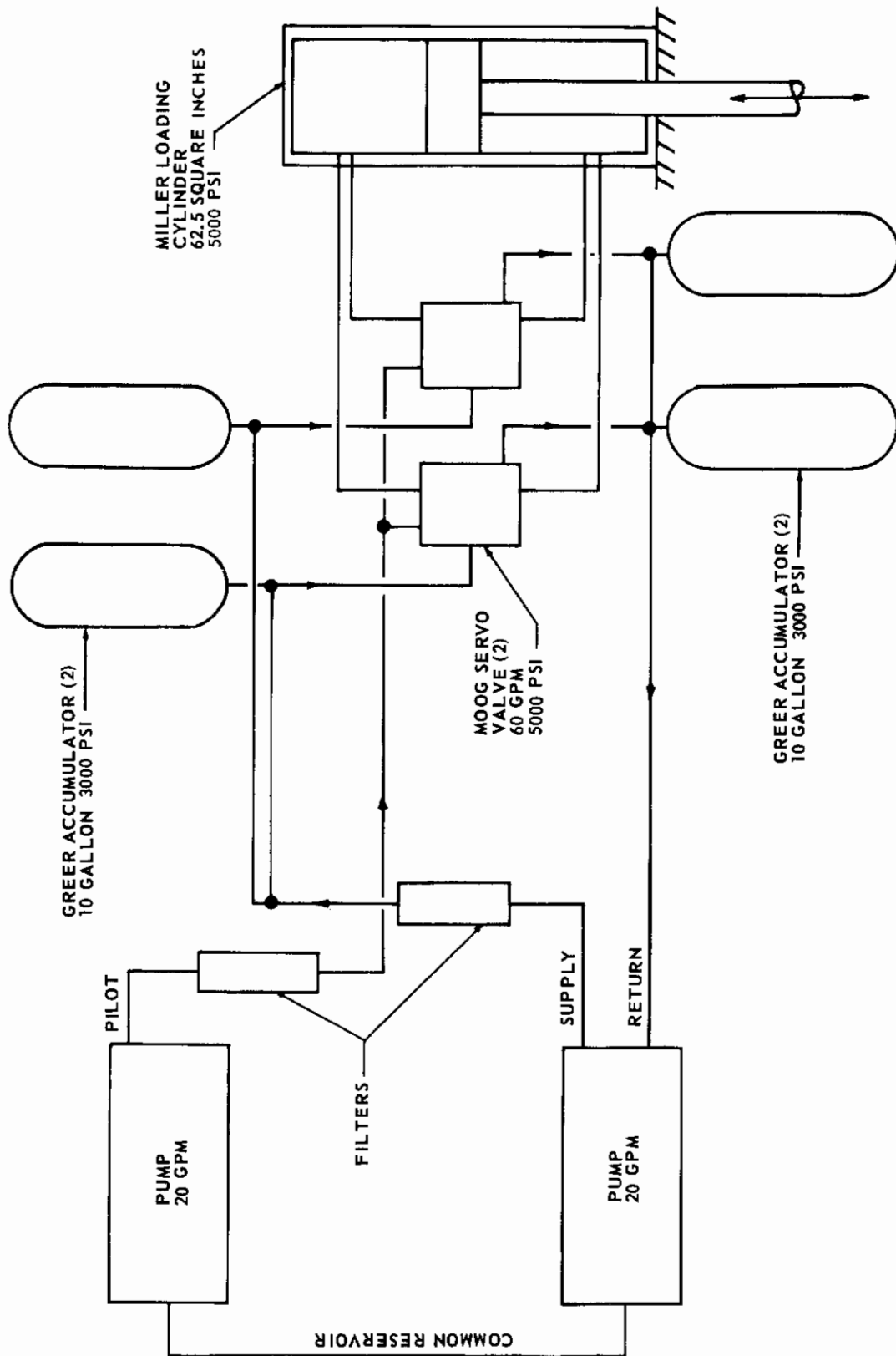


FIG. 13 HYDRAULIC LOADING SYSTEM DIAGRAM FOR 200 KIP TOWER

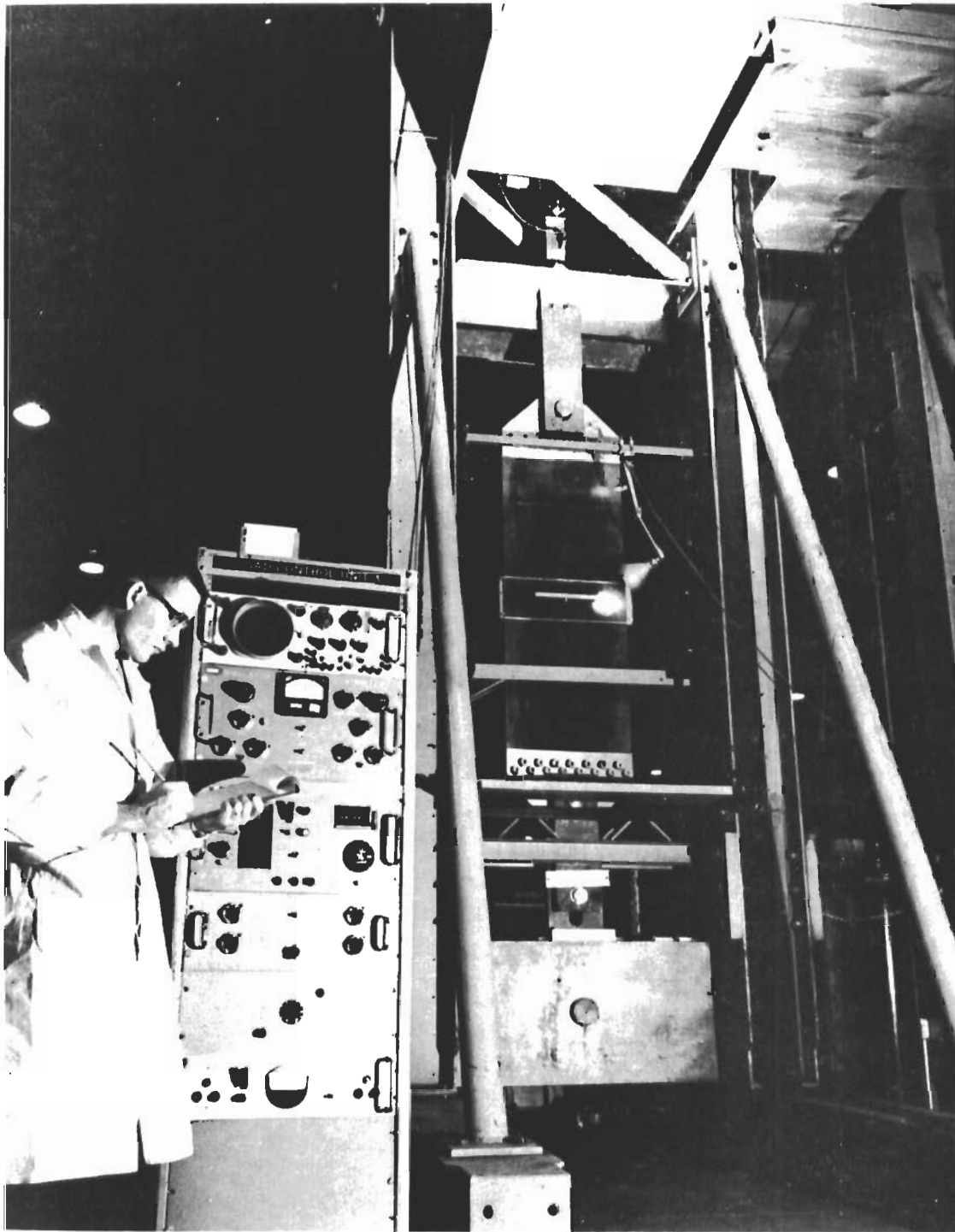


FIG. 14 FATIGUE CRACKING IN 300 KIP TOWER

Buckling restraints were only necessary on the 0.025 and 0.050-inch thick 8 x 24-inch panels. At Boeing, plexiglass restraints were used; at North American, a slotted rubber-backed wood panel was mounted on one surface of the specimen and a hard rubber sheet against the other. The rubber and wood restraint was required basically for vibrational damping at the 1200 cpm frequency.

Crack length measurements were made during cyclic loading with a 20X telescope, a surveyor's transit, or a Gaertner traveling telescope. A machinists' scale with 0.01-inch graduations was attached to the specimen directly above the fatigue crack. Crack growth was recorded by simultaneously observing the scale and each crack tip in turn through the telescope. Cycling was interrupted to make the crack length readings. With the panels cycled at 1200 cpm, a synchronized stroboscopic light was required for clear observation of the crack and readings were taken during cycling. Fig. 15 illustrates the method used with the IV-12 equipment.

FRACTURE TESTING

All panels were statically loaded to fracture in the hydraulic-load-cylinder towers. Steel buckling restraints were used with all panels except as noted in the tabular data for several of the thick panels. Fig. 16 shows the restraints used at North American Aviation. Boeing restraints were of similar design. Tests were carried out at the temperatures and loading rates described in Table 1 in the OUTLINE OF TEST PROGRAM, Section 4. .

All 8 x 24-inch panels tested at the loading rate of 5×10^3 psi/sec were instrumented with two strain gages located adjacent to the fatigue crack tips to detect any local strain discontinuities associated with the phenomenon of "pop-in". Originally, it has been speculated from state-of-the-art information that the "pop-in" phenomenon would provide a method for estimating K_{IC} from plane stress fracture tests. Unfortunately the plane strain fracture toughness value is not so easily attainable. Appendix I includes detailed discussions of "pop-in" studies carried out on this program along with independent contractor studies.

The existence or absence of "slow" crack growth during fracture testing was determined with specimens tested at a loading rate of 5×10^3 psi/sec with high-speed photography. With this technique, a camera capable of film speeds of 400 frames per second was used to photograph the crack extension during loading. Timing marks were put on the film and the loading trace so that the crack length could be correlated with load at the same time. Details of this technique are included in Appendix II.

For the titanium 6Al-4V and PH 14-8Mo alloys, environmental boxes were used for low- and elevated-temperature testing. The environmental boxes were made from 1-inch thick marinite sheet. A cutout was provided in each box for an air blower unit, which was required for mixing and circulating liquid nitrogen used in low-temperature testing. Other holes were provided for hot air tubes used for elevated temperature testing. The environmental boxes were large enough to enclose the buckling restraint bars plus several inches of specimen above and below the buckling restraint bars. Temperature readings at the various thermocouples located within the environmental box were obtained from a Leeds Northrup

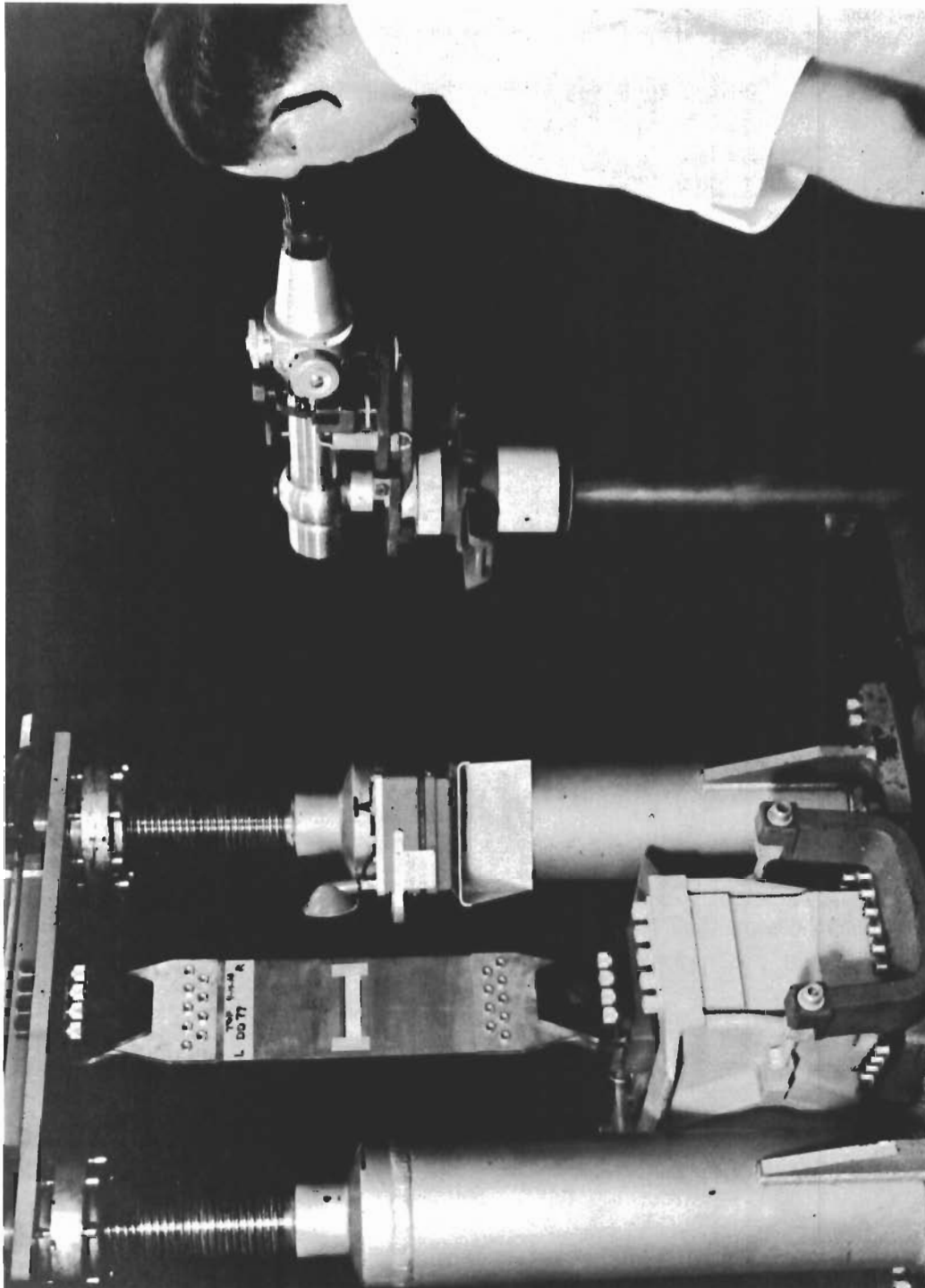
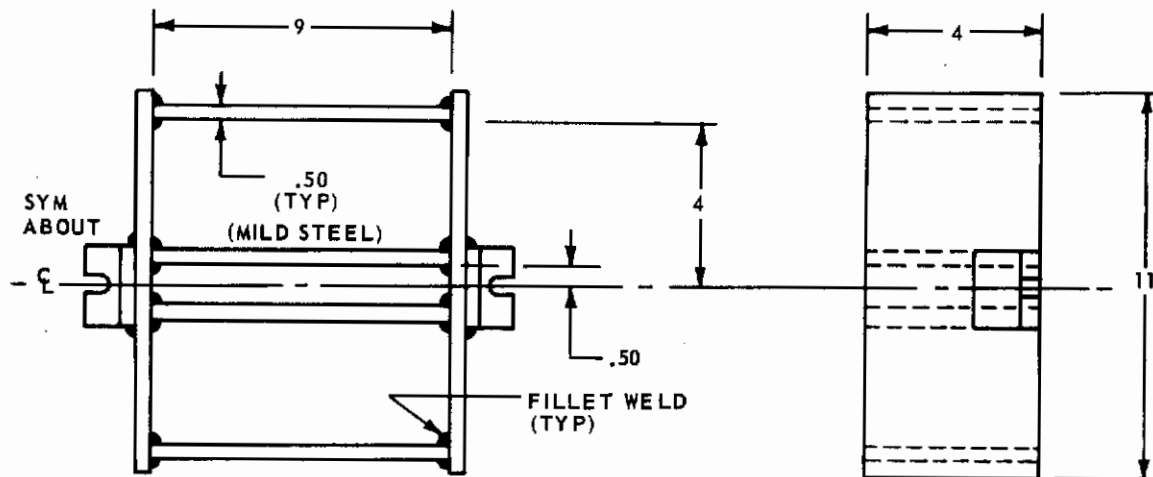
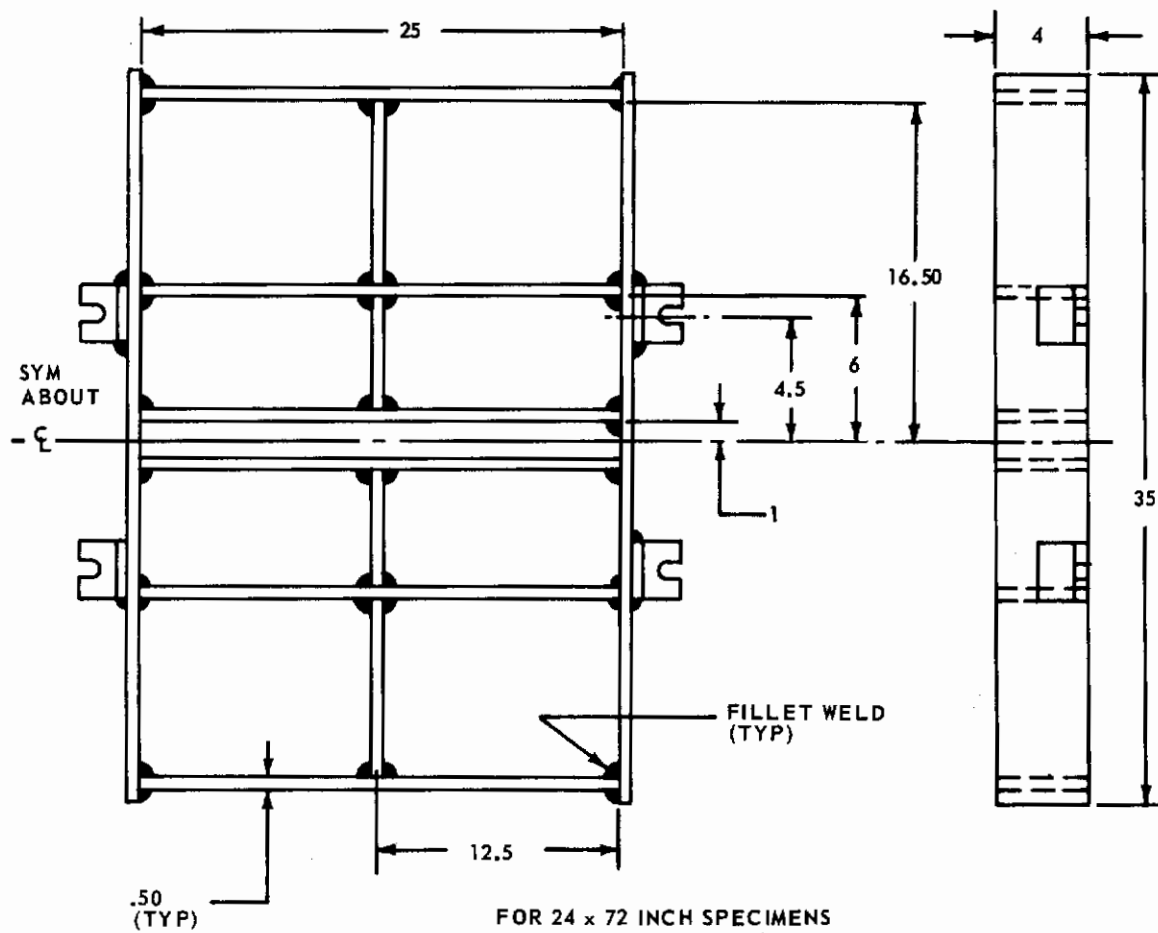


FIG. 15 FATIGUE CRACKING IN IV - 12 EQUIPMENT



FOR 8 x 24 INCH SPECIMENS



FOR 24 x 72 INCH SPECIMENS

FIG. 16 STEEL BUCKLING RESTRAINTS USED DURING TESTING

temperature indicator-controller unit. Three thermocouples were used for surveying the specimen temperature. Other thermocouples were used for measuring the air temperature and the buckling restraint bar temperature.

With the titanium 8Al-1Mo-1V, AM 350, and Inco 718 alloys, the subzero test temperatures of -110°F were attained by cooling gaseous nitrogen with liquid nitrogen and then spraying the gaseous nitrogen through a manifold adjacent to the specimen. The specimen and manifold were enclosed in an insulated box and the test temperature was checked by thermocouples attached to the specimen. For the elevated test temperature of 400°F and 650°F , quartz radiant-heat lamps were used to heat the specimen over an area of one-half panel width on each side of the slot.

EXPOSURE TESTING

Six 8 x 24-inch unnotched transverse panels from each alloy were selected to check for the effects of 1000-hour exposure at 650°F and stress on fracture properties. For the titanium alloys, panel thicknesses were 0.025, 0.050, and 0.200 inches; for the steel and nickel alloys, 0.025, 0.050, and 0.125 inches. The panels were exposed in circulating air creep ovens at stress levels of 25 ksi for the titanium and 40 ksi for steel and nickel alloys. After exposure, the panels were notched, fatigue cracked, and statically fractured. In the Douglas program (Ref. 1) exposure tests were carried out with fatigue cracked panels. As pointed out by Freeman (Ref. 22), a sharp notch present during exposure causes creep relaxation and hence, provides a less severe test condition. For this reason, the unnotched condition was used for all exposure panels.

Tensile tests were made from the exposed panels after fracturing to assess any changes in properties resulting from exposure.

COORDINATION TESTING

A small program was initiated to check agreement between the testing facilities at Boeing and North American Aviation. For this, Boeing and North American each tested three Ti 6Al-4V, 8 x 24-inch specimens made from the transverse grain direction of one 0.050 inch thick sheet of heat D 4949. Test conditions were identical for all specimens. Each specimen was cycled at 120 cpm at a gross stress level of 25 ksi and $R = 0.20$ to grow a 2.00-inch fatigue crack from a 0.50-inch starter notch. Specimens were then fractured at a stress rate of 10^6 psi/sec at room temperature.

A corresponding check was made among Boeing, North American Aviation, and Douglas Testing facilities with one heat of Ti 8Al-1Mo-1V (triplex annealed). Douglas (Ref. 1) had tested 8 x 24 x 0.025-inch transverse panels at a loading rate of 1.67×10^3 psi/sec from this heat and had extra material available. In order to check the testing techniques and also to provide high stress rate data for this heat of material, three 8 x 24 x 0.025-inch panels were tested at a loading rate of approximately 1.67×10^3 psi/sec at North American Aviation and three panels were tested at a loading rate of 10^6 psi/sec at Boeing.

FRACTOGRAPHIC STUDIES

The fracture face from each panel was examined after fracture testing to assess the percent of shear occurring in the rapid fracture zone. Although the ASTM Committee (Ref. 23) recommended that the shear fraction be measured at one to two thicknesses from the specimen edge, this location is not practical with the wide thin panels tested in this program. For this reason, the percent shear from all the panels was determined at a point midway between the final fatigue crack tip and the specimen edge.

Measurements of the internal fatigue crack length at the mid-thickness position and also of any plane strain cracking were made. Electron microscopic examinations were made of several fracture faces from each of the alloys to check characteristics at fatigue, plane strain, and plane stress fracture areas. In this work a two-stage technique was used in preparing replicas for electron microscope examination. The initial plastic replicas were shadowed with germanium and a subsequent vacuum deposit of carbon. The plastic was dissolved in solvent to leave a carbon-germanium shadowed replica. Large areas of the fracture face were replicated and photographs were taken of replicas representative of the various fracture mode areas.

SECTION 6 RESULTS AND DISCUSSION

GENERAL

The various investigations and the test data are presented separately for each alloy. For each alloy, the presentation is made in the following sequence:

- 1) Chemistry and mill processing history
- 2) Microstructure
- 3) Tensile properties
- 4) Fatigue crack propagation
- 5) Residual strength and fracture toughness
- 6) Fractography

All the information is presented using the goals of simplicity and brevity. Several methods of data preparation can be used for presenting and comparing the properties of the alloys tested. The stress intensity parameter concept is the principal method used herein, but all test details are tabulated so data can be prepared and reviewed by other methods.

The fatigue crack propagation data are presented to show crack growth and the rate of crack growth. The fatigue crack growth data are presented by plotting the crack length, $2a$, versus net cycles, N , on linear scales. Net cycles are the cycles of actual crack propagation; i. e., the cycles required to initiate crack growth (dwell cycles) from the starter notch are subtracted from the total cycles (gross cycles). This approach allows the influence of the number of cycles required to initiate fatigue crack growth from notches with variable acuities to be removed from the data. The dwell cycles are determined by plotting the raw crack growth data on a greatly reduced scale; however, even by this method, dwell cycle determination is sometimes elusive. The crack growth curve is the best method for showing total cycle life and the crack growth delay periods that exist between various combinations of stress level and stress ratio. Because comparisons may be made with the data generated under ASD Contract No. AF33(657)-8545 and published in Ref. 1, it should be noted that the fatigue crack growth curves contained therein have not had the dwell cycles subtracted from the gross cycles.

The rate of fatigue crack growth, $\Delta 2a/\Delta N$, is computed from the fatigue crack growth curve and is plotted on a log scale versus the stress intensity factor, K , which is on a linear scale. Such a computation is made by taking two points along the crack growth curve and:

- 1) Calculating an average K , where

$$K = \sigma_G \sqrt{\pi a} \quad a$$

- 2) Calculating an average crack growth rate by dividing the change in crack length by the change in cycles.

Because K is computed by using σ_G , a , and a , the effects of these variables are excluded from the fatigue crack growth rate curve. Plotted in this manner, only variables such as the stress ratio, thickness of material, and cycling fre-

Since: $\Delta K = K_{max} - K_{min}$ where $a_i = a_{i+1}$

$$K_{max} = \sigma_{max} \sqrt{\pi a}$$

$$K_{min} = \sigma_{min} \sqrt{\pi a}$$

$$\Delta K = (\sigma_{max} - \sigma_{min}) \sqrt{\pi a}$$

quency will influence the curve. This type of plot is used in this report to compare fatigue crack propagation characteristics of the materials as influenced by stress ratio, heat, thickness, and alloy variables. This type of data presentation was proposed (Refs. 18 and 20) as a method for unifying crack propagation data.

K has been calculated based on surface crack length determinations and with the polynomial correction factor. No correction has been made to the surface crack length for the yield zone at the crack tips. On the K-rate graphs, the K ordinate is designated with the formal $K = \sigma_G \sqrt{\pi a'} a$.

For the fracture toughness data reported in tabular form in this section, the critical fracture toughness parameter has been calculated in two ways. Computations of the critical fracture toughness parameter have been carried out in two ways so that comparisons can be made with previous K_{CN} and K_C data. One calculation, designated K_{CN} , is referred to as the nominal fracture toughness value. In the Tables, the column for this nominal value is designated by the formula $K_{CN} = \sigma_G \sqrt{\pi a_0'} a$. Here, the surface fatigue crack length is used in the computation with no corrections being made to the expression for "slow" crack extension or crack tip yield zone size. The polynomial expression for the geometry correction factor, a , is used in the calculation. Most of the testing has been carried out at crack-length to panel-widths of 0.25; at this ratio, the difference between the two expressions for finite specimen geometry is less than one percent. The second computation method for the critical fracture toughness parameter is based on ASTM recommended procedures (Ref. 21) and is designated K_C . In this method, $K_C = \sigma_G \sqrt{q_1} W$, where $q_1 = \tan u$ and u includes both the tangent correction factor implicitly and also a correction to the crack length for the yield zone size, e.g.,

$$\mu = \frac{\pi}{W} \left[a_0 + \frac{K_C^2}{2\pi \sigma_{yp}^2} \right]$$

For the K_C calculation, a value of σ_{yp} has been estimated from published data (Refs. 25 and 26) for the appropriate loading rates used during static fracture testing. Although it has been pointed out (Ref. 24) that a 10 percent error in σ_{yp} generally results in an error in the K_C calculation of less than 2 percent, it was felt that the best estimate for the actual σ_{yp} should be used in this case. The ASTM criterion for valid fracture toughness tests is based on the σ_N/σ_{yp} ratio being less than 0.80. A more realistic appraisal of test validity is possible by using the estimated σ_{yp} values at the actual loading rates. The K_C calculation is based on the surface fatigue crack length with a yield zone size correction factor.

Appendix II contains details of high-speed photography studies made with the slower stress rate tests to assess the extent of "slow" crack extension.

Also reported in the tabular data is the ratio of σ_G/F_{tu} which is often referred to as the residual or relative residual strength. In these, the ultimate tensile strength (F_{tu}) is derived from the standard slow strain rate tensile test. No corrections have been made for high strain rate effects. Comparisons carried out in the following subsections are all based on K_C , which includes the σ_{yp} for the particular test loading rate. In some cases the residual strength, based on the standard tensile ultimate strength, is used in making comparisons.

The shear percentage is included in the tables to aid in assessing the fracture toughness values. The percent-of-shear values are reported just as they were measured and have not been rounded off to reflect a measurement accuracy of ± 5 percent.

Instrumentation for the detection of pop-in did not reveal any discontinuous strain effects during testing. It was possible to estimate a K_{IC} value from several thick Ti 8Al-1Mo-1V panels by measuring the change in fracture mode from plane strain to mixed plane strain and plane stress modes on the fatigue portion of the fracture face. These data are reported in the Ti 8Al-1Mo-1V subsection. Estimates of K_{IC} were also made from high speed photography data for Ti 6Al-4V and are included in Appendix I. Computations of the critical fracture toughness parameter have been carried out in two ways so that comparisons can be made with previous K_{CN} and K_C data.

Ti 8Al-1Mo-1V

Chemistry and Mill Processing History

The chemical composition of the three heats of material are shown in Table 6 along with specification ranges. Variation of any one element within its specified range is very small. Mill processing history is included in the following list.

- 1) Forge ingot to sheet bar - final 53% reduction from 1950°F.
- 2) Sheet bar ultrasonically inspected and cropped.
- 3) Rough roll sheet bar to intermediate thickness at 1860°-1880°F.
- 4) Descale, rough roll sheet bar.
- 5) Condition and vacuum anneal at 1350°F.
- 6) Hot roll at 1810°F.
- 7) Resquare and descale sheets.
- 8) Creep flatten anneal at 1450°F and furnace cool.
- 9) Heat to 1450°F for 15 min. Air cool.
- 10) Descale, grind and pickle.

TABLE 6 VENDOR CERTIFIED CHEMICAL ANALYSIS FOR Ti 8Al - 1Mo - 1V
(WEIGHT PERCENT)

HEAT NO.	PRODUCER	C	Ti	Al	Mo	Fe	V	Zr	N	H	O
D 4535	TMCA	.022	BALANCE	7.7	1.0	.09	1.1	.009	.016	.006	.09
D 3454		.023		7.7	1.0	.07	1.0	.006	.012	.003	.08
D 3457		.025		7.9	1.0	.08	1.0	.009	.010	.006	.08
SPEC. { MIN. MAX.		.08		7.35 8.35	.75 1.25	.50	.75 1.25		.05	.0125	

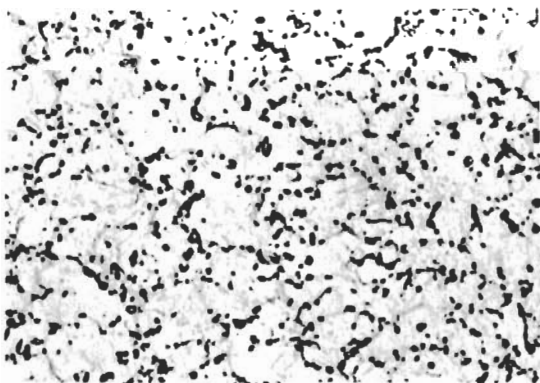
- 11) Longitudinal and transverse tensile and bend tests performed. Hydrogen content determined.
- 12) Inspect, resquare, mark, crate, and ship sheets.

Although the processing details are somewhat brief and do not reflect the actual control details exercised in melting and processing the alloys, they do provide an initial reference point for comparison with any future gross process changes. For example, the present material is rolled on hand mills so that the sheets are cross rolled and longitudinal and transverse properties would be expected to be similar. If a continuous sheet mill such as a Sendzimir were used in the processing, a significant difference between longitudinal and transverse properties would be expected.

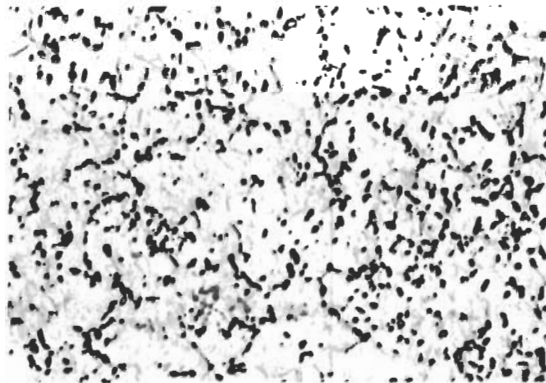
Microstructure

Typical microstructures for the three heats of Ti 8Al-1Mo-1V are shown in Figs. 17 and 18. Fig. 17 shows the variation between the longitudinal and transverse grain directions for the three thicknesses of heat 3457. There is very little directionality noted and most of the alpha grains are small and uniform for all thicknesses. Fig. 18 shows the variation between the longitudinal and transverse grain directions for the 0.050-inch thickness of each of the three heats. Again, the microstructures are typified by a small uniform alpha grain size. The very small grains dispersed throughout the structure are believed to be the retained beta phase.

$t = .025$ INCHES

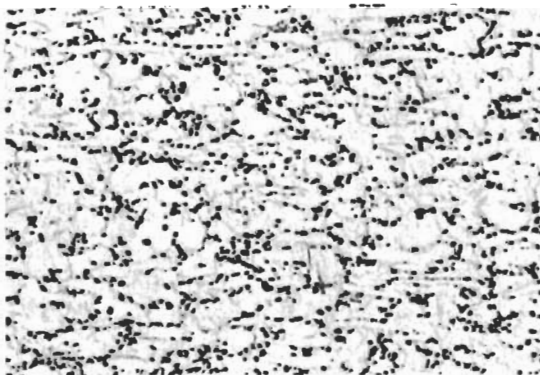


(A) LONGITUDINAL GRAIN (500x)

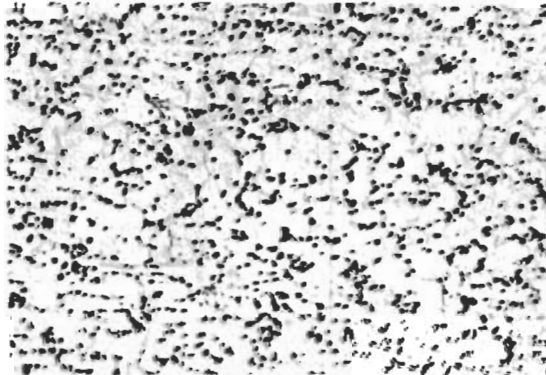


(B) TRANSVERSE GRAIN (500x)

$t = .125$ INCHES

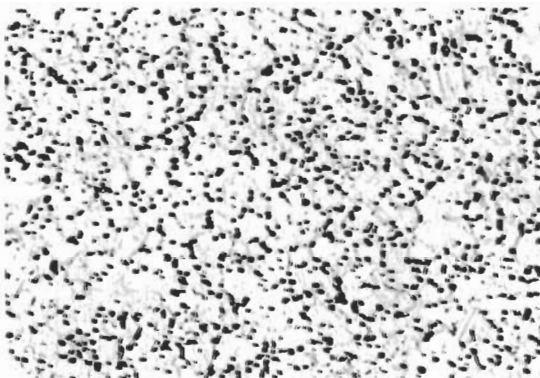


(C) LONGITUDINAL GRAIN (500x)

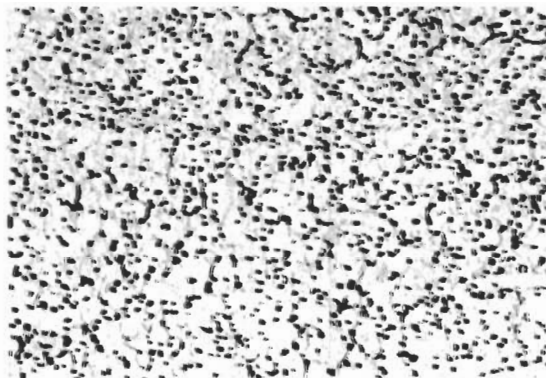


(D) TRANSVERSE GRAIN (500x)

$t = .200$ INCHES



(E) LONGITUDINAL GRAIN (500x)



(F) TRANSVERSE GRAIN (500x)

NOTE: Lactic Acid Etchant

FIG. 17 PHOTOMICROGRAPHS OF Ti 8Al - 1Mo - 1V SHOWING THICKNESS VARIATION,
HEAT 3457

HEAT 4535, $t = .050$ INCHES

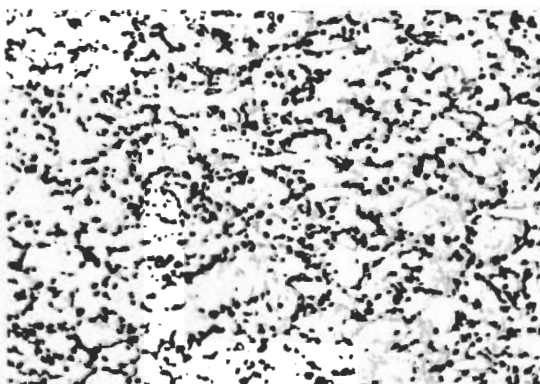


(A) LONGITUDINAL GRAIN (500x)

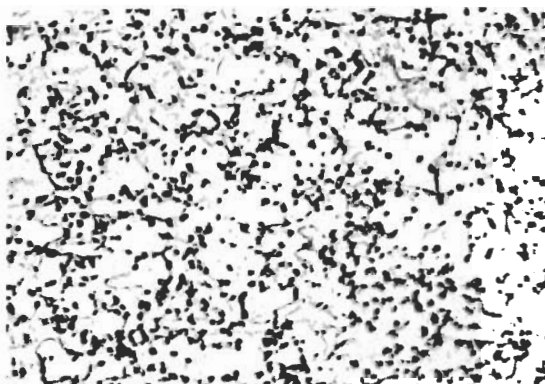


(B) TRANSVERSE GRAIN (500x)

HEAT 3454, $t = .050$ INCHES

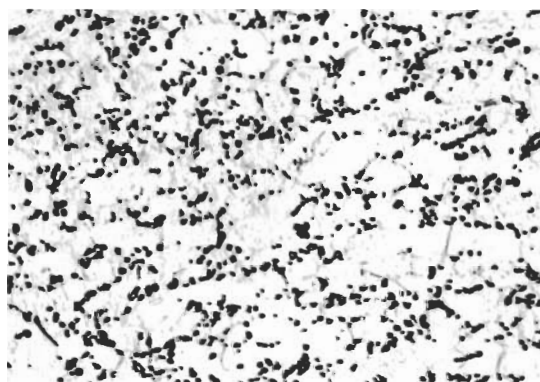


(C) LONGITUDINAL GRAIN (500x)

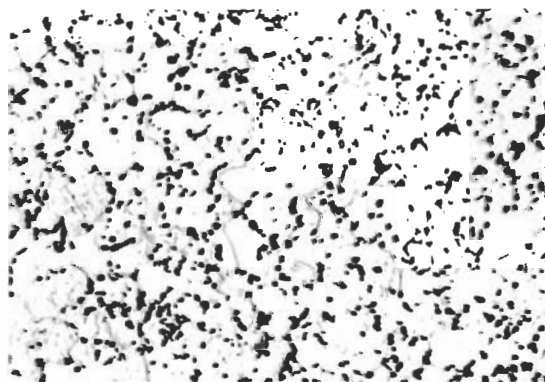


(D) TRANSVERSE GRAIN (500x)

HEAT 3457, $t = .050$ INCHES



(E) LONGITUDINAL GRAIN (500x)



(F) TRANSVERSE GRAIN (500x)

NOTE: Lactic Acid Etchant

FIG. 18 PHOTOMICROGRAPHS OF Ti 8Al - 1Mo - 1V, HEATS 4535, 3454 AND 3457

Tensile Properties

Tensile properties representing the three heats of Ti 8Al-1Mo-1V over the temperature range -110 to 650°F are included in Table 7. The tensile ultimate and tensile yield strength values at room temperature are relatively constant for the three heats and for the four thicknesses of the one large heat. The room temperature elongation values exceed the specification guaranteed value of 10 percent in each case. Tensile yield and ultimate strengths increase markedly at the -110°F test temperature with elongation values showing a small consistent decrease. Transverse and longitudinal results show no significant differences.

Tensile test data from specimens cut from the failed halves of the exposed fracture panels are also included in Table 7. These tensile properties show a small but consistent increase in strength compared with the unexposed tensile data. The gross stress level during static fracture testing of the panels did not exceed 80 ksi, which is below the yield strength, and so the fracture testing should have had no effect on the tensile test data.

Crack Propagation

Crack Growth Data

Crack propagation data are plotted as crack length versus cycles curves for the 24 x 72-inch panels in Figs. 19 through 26 and for the 8 x 24-inch panels in Figs. 27, 28, 29. Fig. 30 includes the crack growth curves for the exposed panels. All data were gathered at room temperature at a cycling frequency of 120 cpm.

As mentioned in Section 4, the final increment of crack growth for each specimen was carried out at $R = 0.20$ and at a stress level to produce a final K of approximately $50 \text{ ksi} \sqrt{\text{in.}}$. Specifically, for the 24 x 72-inch panels, the 3-inch final crack lengths were grown from 2.5 inches at a stress level of 25 ksi; the 6-inch final crack length were grown from 5.25 inches at a stress level of 17.5 ksi; and the 10-inch final crack lengths were grown from 9 inches at a stress level of 12.5 ksi.

A discontinuity is often observed in the crack length-cycles curves at the point of stress level change. As the maximum stress was changed during cycling, crack growth was retarded in dropping from a high stress to a lower stress. This point is best illustrated by specimens DA22 and DA23 in Fig. 22 and specimen DA26 in Fig. 23. In some cases, almost 500,000 cycles (dwell cycles) were required to reinitiate crack growth at the lower stress levels. Once the trend in this behavior had been established, a small jeweler's sawcut was made through the previous yield zone in several specimens so that crack propagation could easily continue (e.g., specimen DA30 Fig. 23).

The reverse effect was observed in changing from a low stress level to a higher stress level; crack growth was accelerated. This trend is illustrated by specimen DA63 in Fig. 25. This phenomenon associated with the change in stress level has been observed in previous testing with different alloys as summarized by Hardrath (Ref. 27).

TABLE 7 TENSILE TEST DATA FOR Ti 8Al-1Mo-1V

HEAT NO.	NOMINAL THICKNESS inches	GRAIN DIRECTION	TEST TEMPERATURE											
			-110° F			R. T. (68 °F)			400° F			650° F		
			F _{tu} (ksi)	F _{ty} (ksi)	** ELONG.	F _{tu} (ksi)	F _{ty} (ksi)	** ELONG.	F _{tu} (ksi)	F _{ty} (ksi)	ELONG.	F _{tu} (ksi)	F _{ty} (ksi)	** ELONG.
D4535	.050	T	169.9	159.3	13.0	139.7	130.7	16.5				104.8	82.5	15.0
		T				140.3	130.7	16.5				105.2	82.7	14.5
		L	162.1	151.3	13.0	139.5	128.4	14.5	115.4	94.5		105.0	79.6	14.5
		L				139.5	128.8	14.5				105.1	80.2	17.5
D3454	.050	T	175.9	162.4	13.5	141.2	130.8	16.0				105.7	85.1	13.0
		T				141.0	131.2	14.0				104.7	84.5	12.0
		L	176.8	164.4	14.5	141.2	128.7	15.5				106.5	83.6	13.5
		L				142.0	129.7	17.5				105.5	83.1	14.0
D3457	.025	T				136.9	123.5	16.5				101.1	77.6	18.0
		T	163.7	146.2	15.5	137.9	124.0	16.5						
		L	164.0	153.0	13.5	140.4	128.2	15.0				104.9	83.5	14.0
		L				141.2	129.1	16.5						
	.050	T	177.0	164.5	13.0	141.6	128.7	14.5	113.8	93.0	13.0	104.8	82.4	11.0
		T				142.4	129.3	14.0						
		L	188.4	165.4	13.0	142.6	129.5	15.0	115.9	93.5	13.0	104.5	82.3	11.5
		L	173.5	159.2	12.0	142.7	129.4	15.0	120.0	97.1	14.0	104.9	83.1	10.5
	.125	T	169.3	157.2	15.0	144.2	133.9	16.0				109.3	89.6	17.0
		T				143.2	133.1	16.5						
		L	162.2	152.5	13.5	138.2	128.5	16.0				103.2	79.9	20.0
		L				138.1	128.0	16.5						
.200	T	159.1	149.6	—	142.1	131.1	14.0	116.1	95.6	18.0	105.5	83.0	18.5	
	T				139.6	128.8	15.5				106.2	83.9	18.5	
	L	161.9	150.9	10.0	137.6	126.3	15.5	111.6	91.7	19.0	101.9	77.9	20.0	
	L	163.4	151.8	11.0	136.2	126.3	16.5	111.5	90.7	18.5	101.8	78.4	20.0	
D3457 *	.025 *	T				144.3	126.3	16.0						
		T				143.9	126.5	15.5						
	.050 *	T				149.1	131.7	13.5						
		T				151.0	133.7	15.0						
	.200 *	T				144.3	129.9	13.5						
		T				143.9	130.0	13.0						

* AFTER EXPOSURE AT 650° F FOR 1000 HOURS AT 25 ksi
** PERCENT IN 2 INCHES

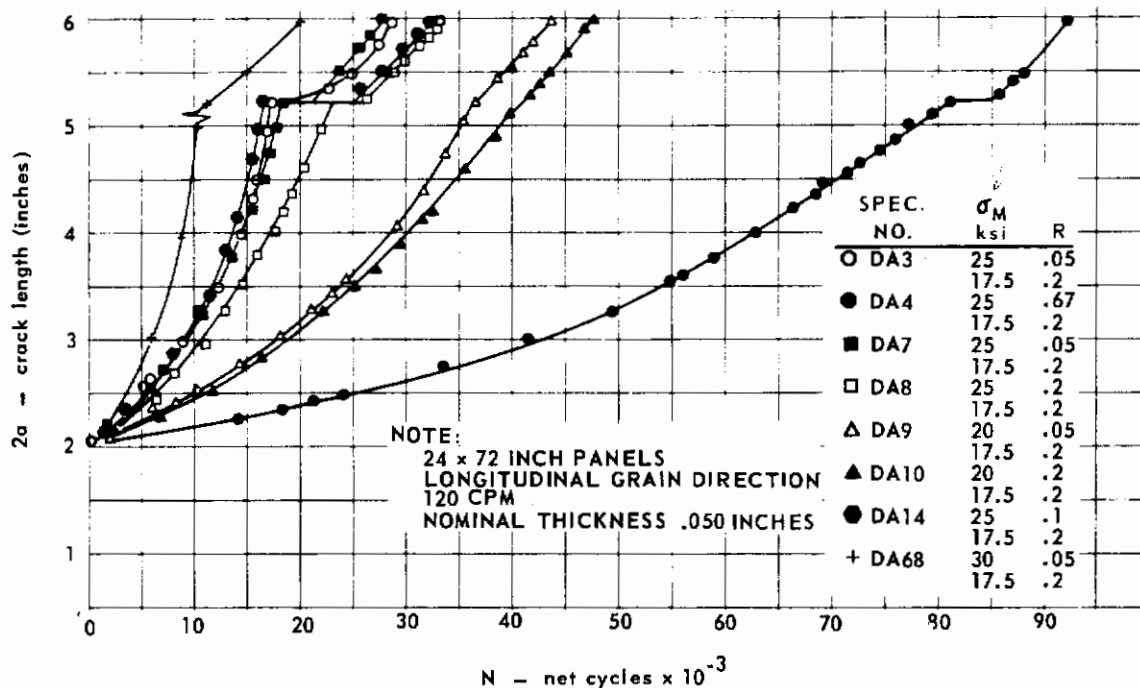


FIG. 19 CRACK GROWTH DATA FOR Ti 8Al-1Mo-1V, HEAT 4535

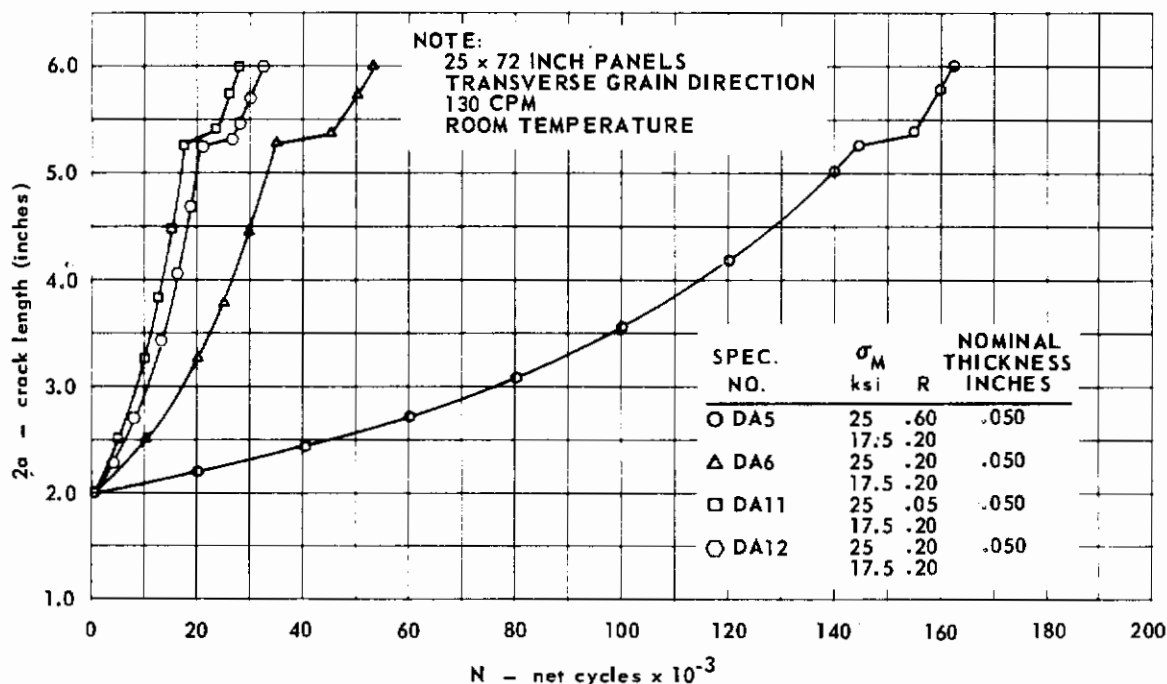


FIG. 20 CRACK GROWTH DATA FOR Ti 8Al-1Mo-1V, HEAT D4535

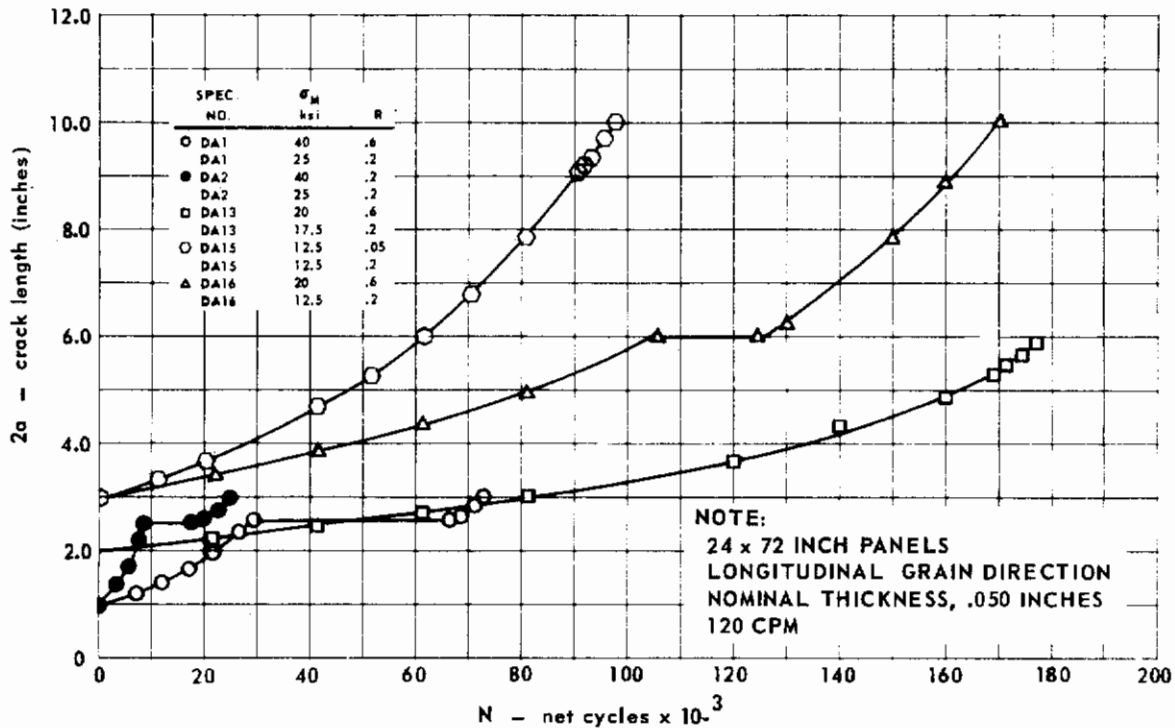


FIG. 21 CRACK GROWTH DATA FOR Ti 8Al-1Mo-1V, HEAT D4535

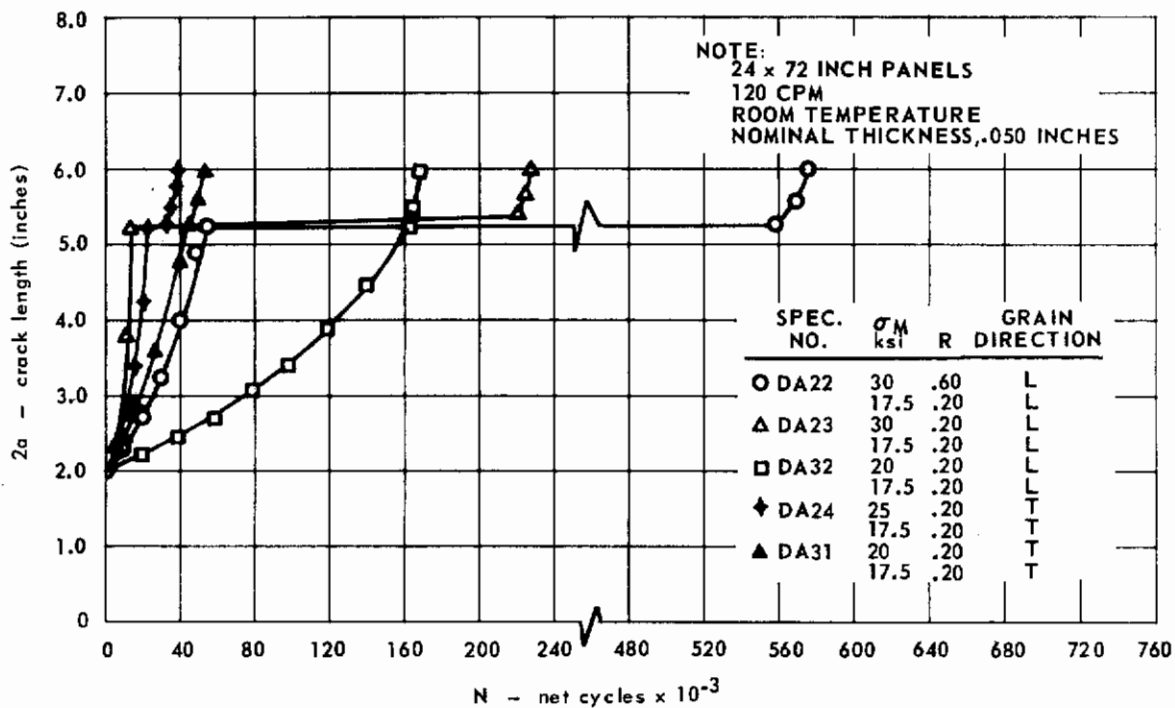


FIG. 22 CRACK GROWTH DATA FOR Ti 8Al-1Mo-1V, HEAT D3454

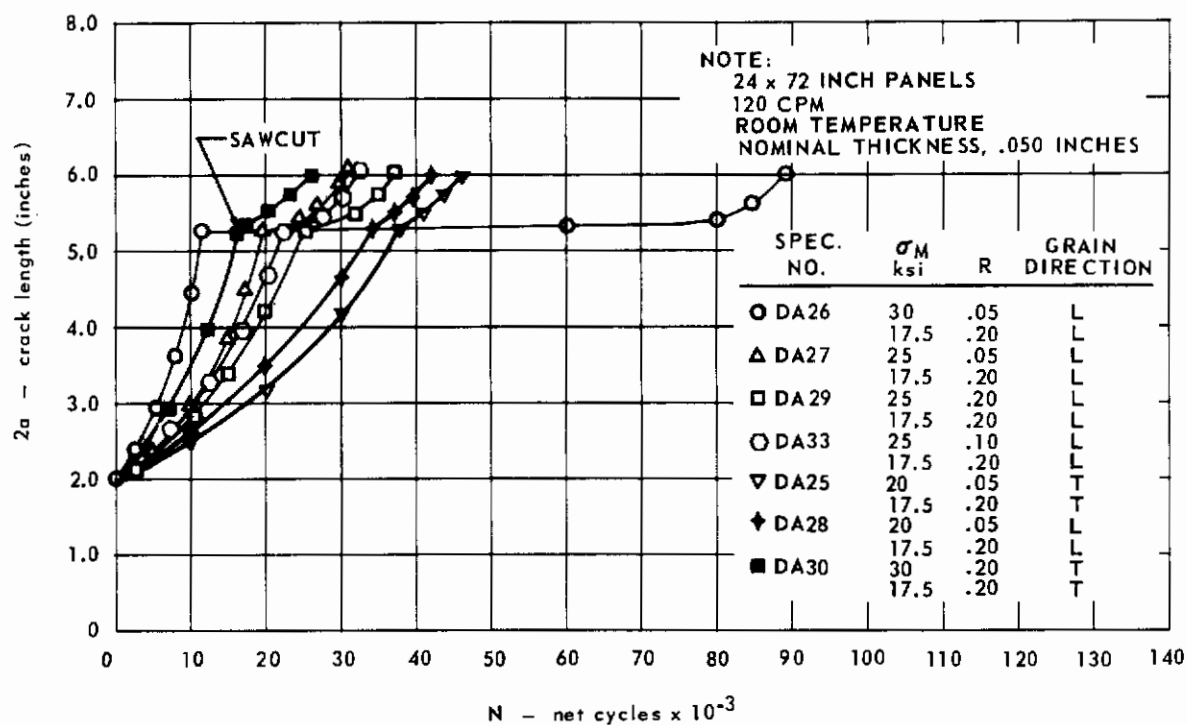


FIG. 23 CRACK GROWTH DATA FOR Ti 8Al-1Mo-1V, HEAT D3454

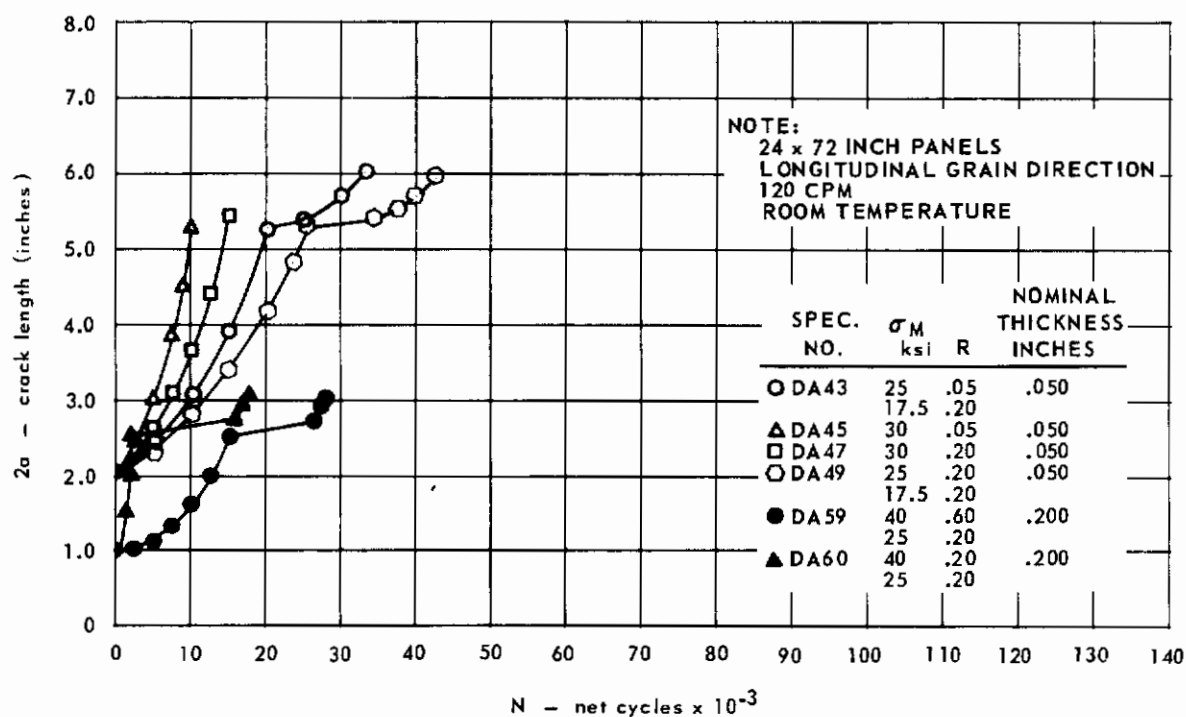


FIG. 24 CRACK GROWTH DATA FOR Ti 8Al-1Mo-1V HEAT D3457

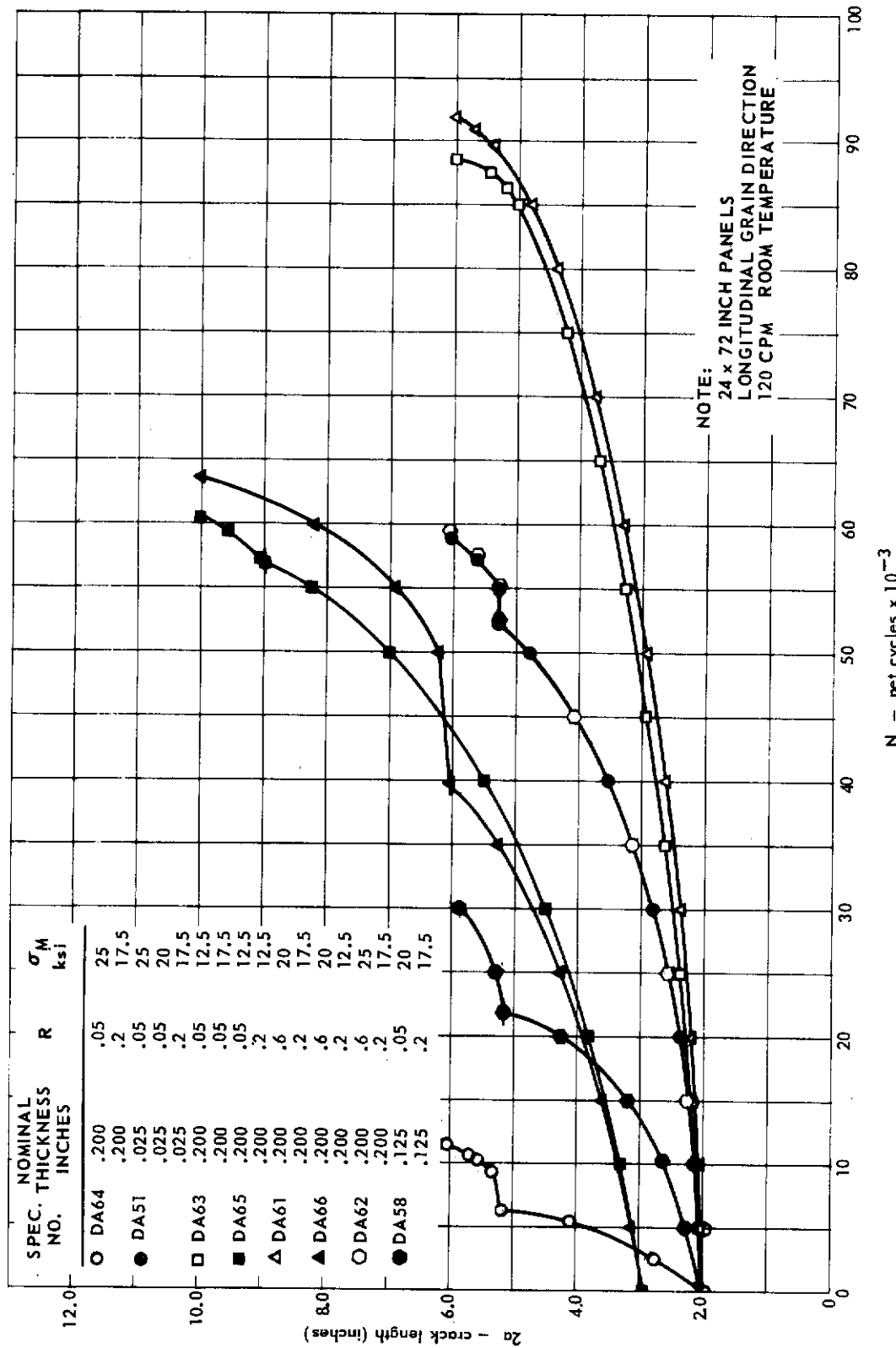


FIG. 25 CRACK GROWTH DATA FOR Ti 8Al-1Mo-1V, HEAT D3457

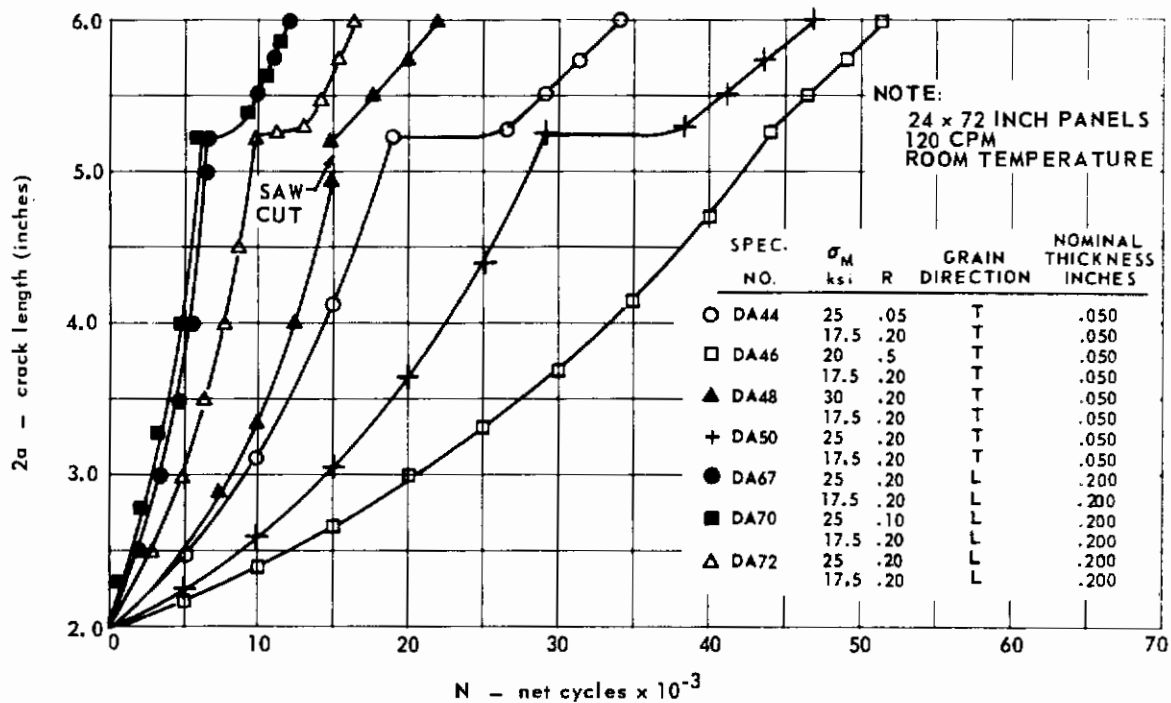


FIG. 26 CRACK GROWTH DATA FOR Ti 8Al-1Mo-1V, HEAT D3457

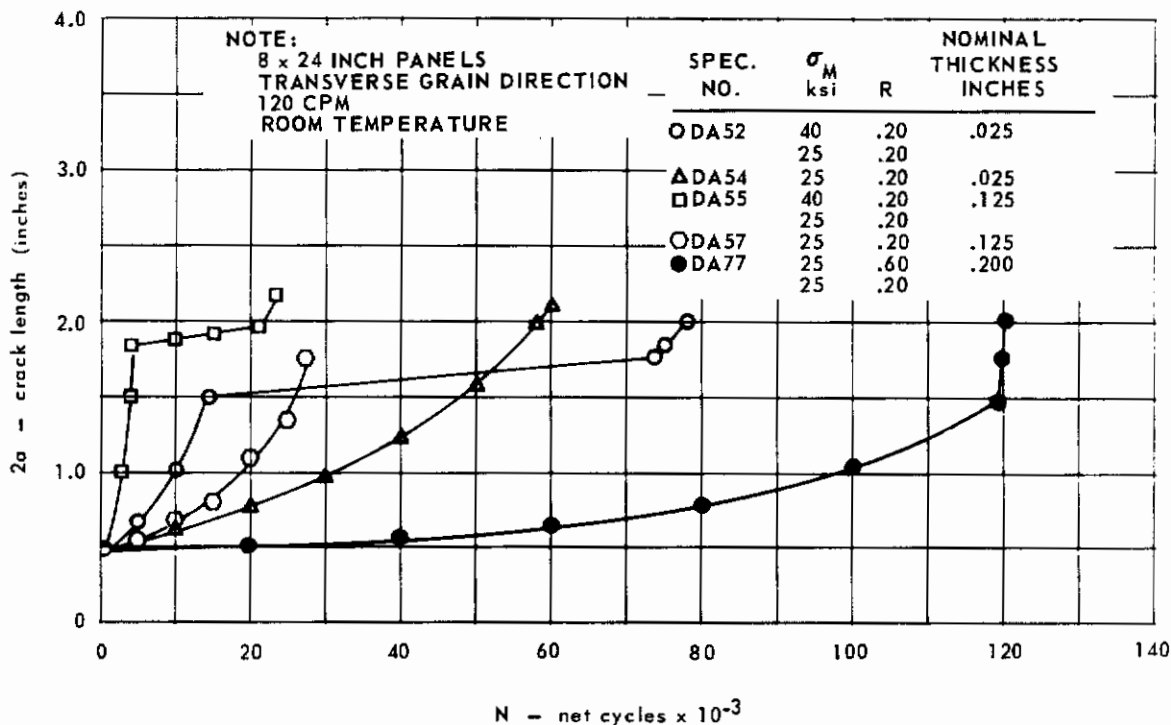


FIG. 27 CRACK GROWTH DATA FOR Ti 8Al-1Mo-1V HEAT D3457

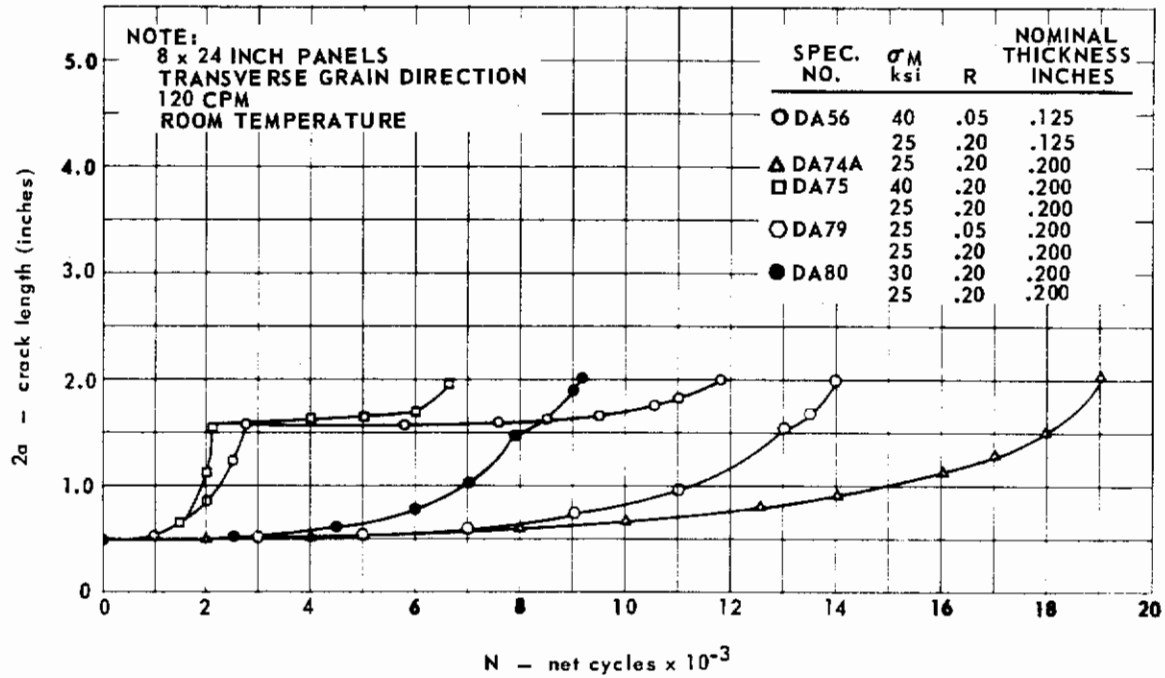


FIG. 28 CRACK GROWTH DATA FOR Ti 8Al-1Mo-1V, HEAT D3457

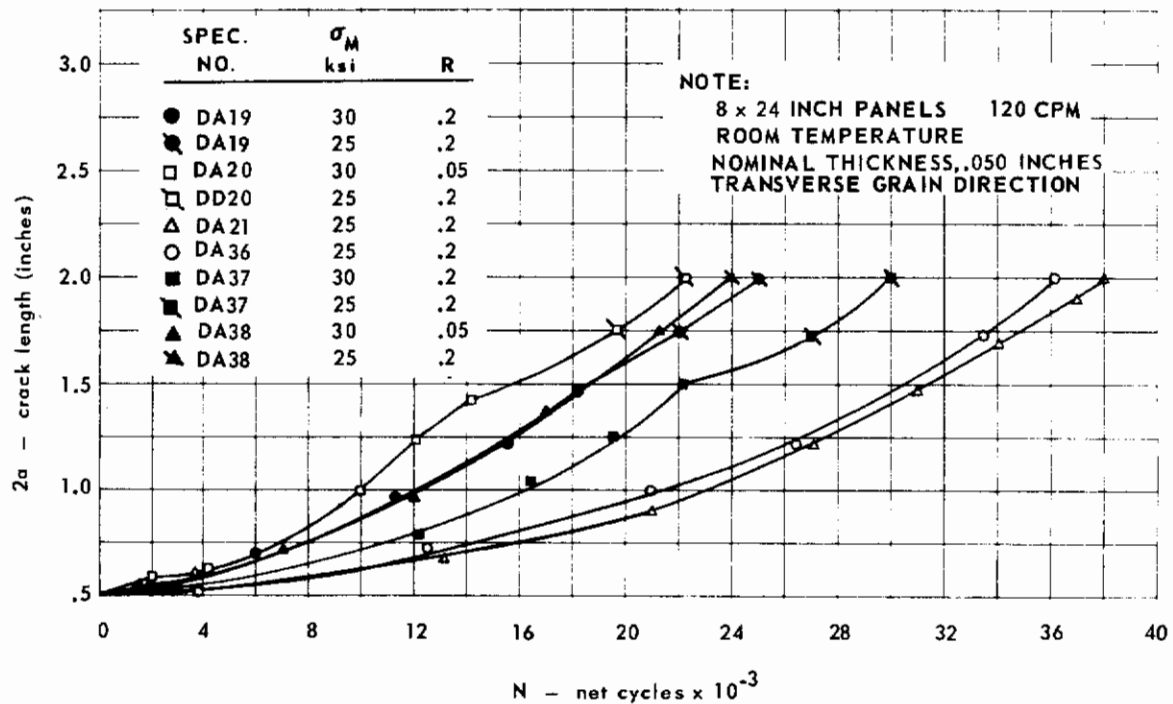


FIG. 29 CRACK GROWTH DATA FOR Ti 8Al-1Mo-1V, HEAT D3457

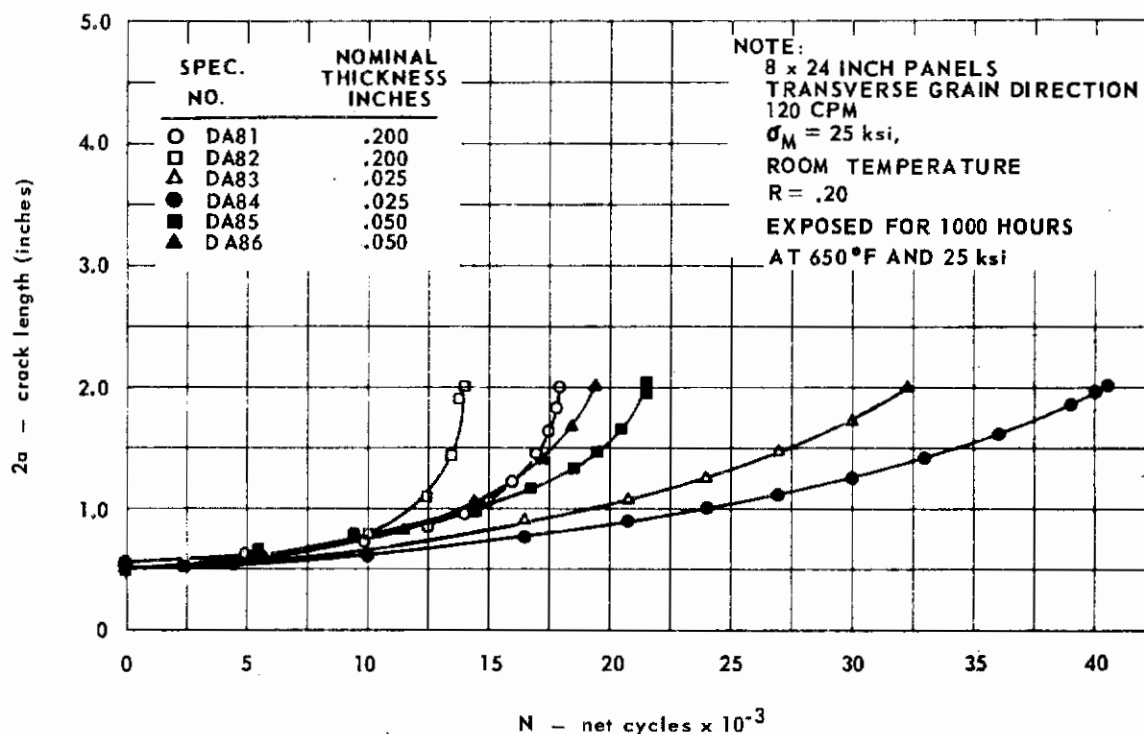


FIG. 30 CRACK GROWTH DATA FOR EXPOSED Ti 8Al-1Mo-1V PANELS, HEAT D3457

From these crack growth curves, several observations can be made. The cycles required to grow a given crack length decrease: with an increase in the gross stress level; with a decrease in the stress ratio; and with an increase in specimen thickness.

Crack Growth Rate Data

The crack growth rate data are plotted as K versus rate curves for all the unexposed panels in Figs. 31 through 39. Fig. 31 shows a comparison for 24 x 72-inch panels between longitudinal and transverse grain directions at $R = 0.06$. Specimen DA5 which is a transverse grain direction panel shows a much slower growth rate than the grouping which includes the remaining longitudinal and transverse panels. A similar situation is shown in Fig. 32 with specimen DA6 at R values of 0.20 and 0.05. Fig. 32 also shows that the 24 x 72-inch and 8 x 24-inch transverse grain direction panels have growth rates which lie in the same R -value band.

Fig. 33 shows the effect of stress ratio on crack growth rate. The growth rate is much faster for $R = 0.20$ than for $R = 0.60$. Fig. 34 shows that there is very little difference among the R values of 0.05, 0.10 and 0.20. Fig. 35 shows the difference between the $R = 0.60$ group and the $R = 0.05, 0.10$, and 0.20 group. There is also a marked difference between the growth rates of specimens DA22 and DA32 at $R = 0.60$. Since specimen DA22 was cycled at a higher stress, it is possible that this may indicate a stress level effect.

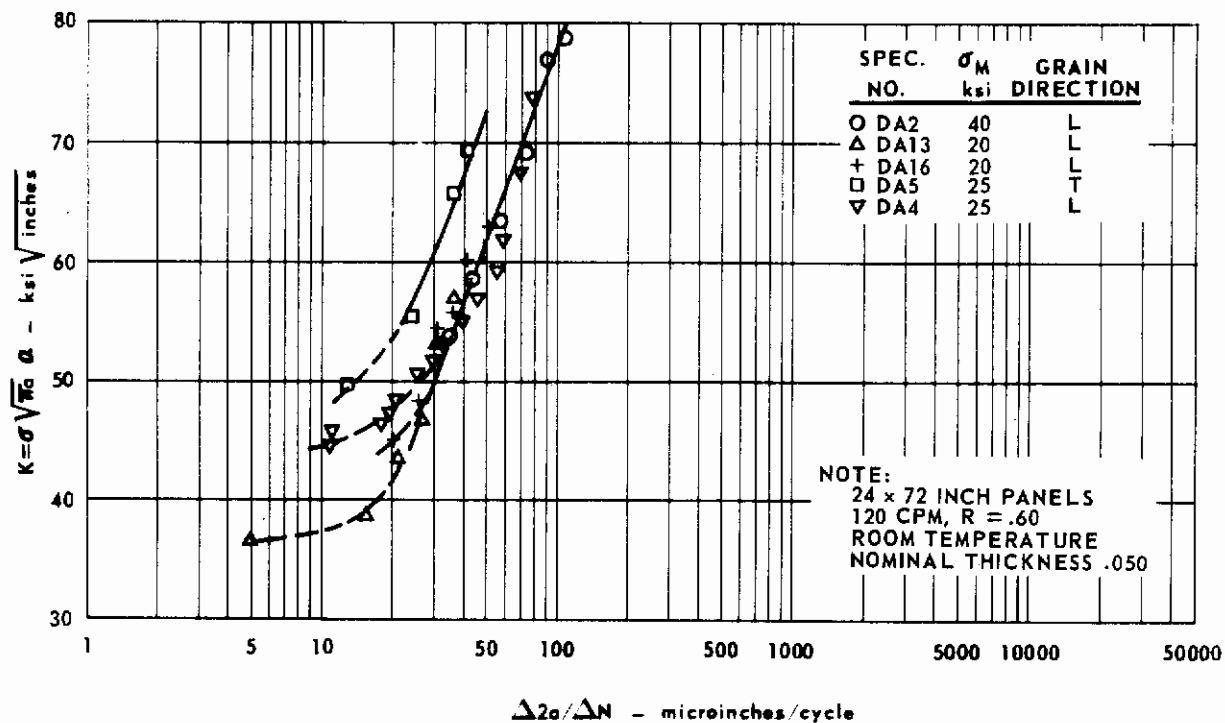


FIG. 31 CRACK GROWTH RATE DATA FOR Ti 8Al-1Mo-1V, HEAT 4535

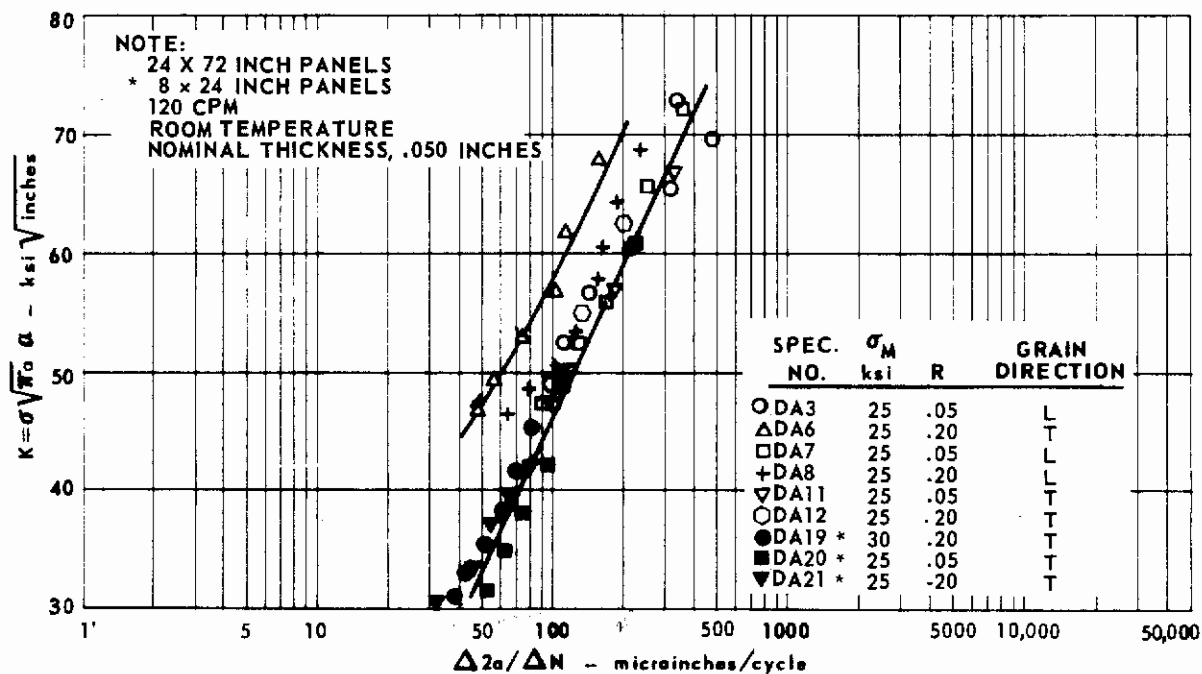


FIG. 32 CRACK GROWTH RATE DATA FOR Ti 8Al-1Mo-1V, HEAT 4535

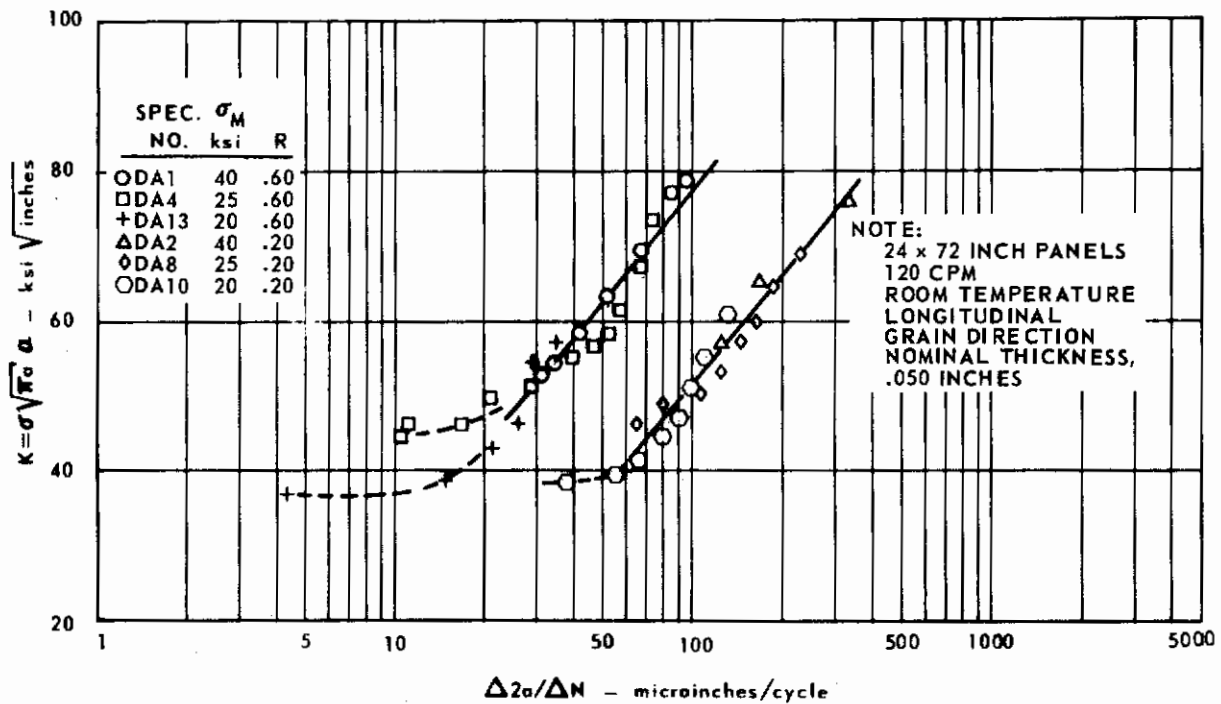


FIG. 33 CRACK GROWTH RATE DATA FOR Ti 8Al-1Mo-1V, HEAT 4535

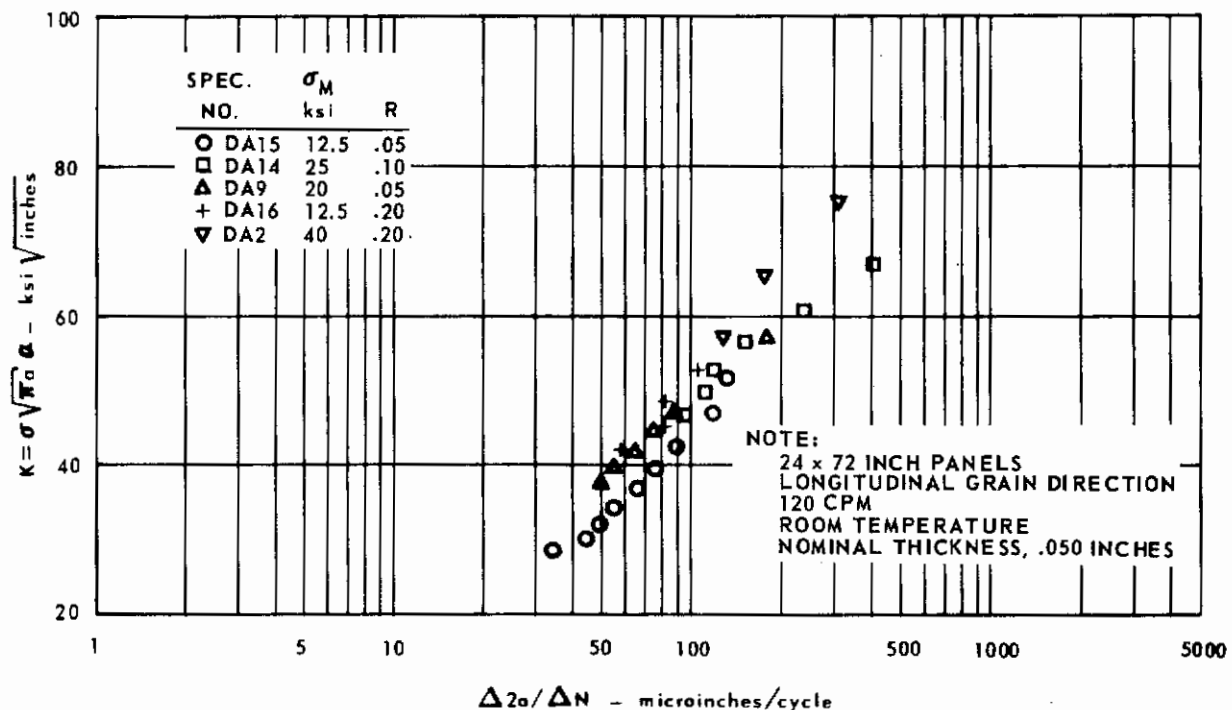


FIG. 34 CRACK GROWTH RATE DATA FOR Ti 8Al-1Mo-1V, HEAT 4535

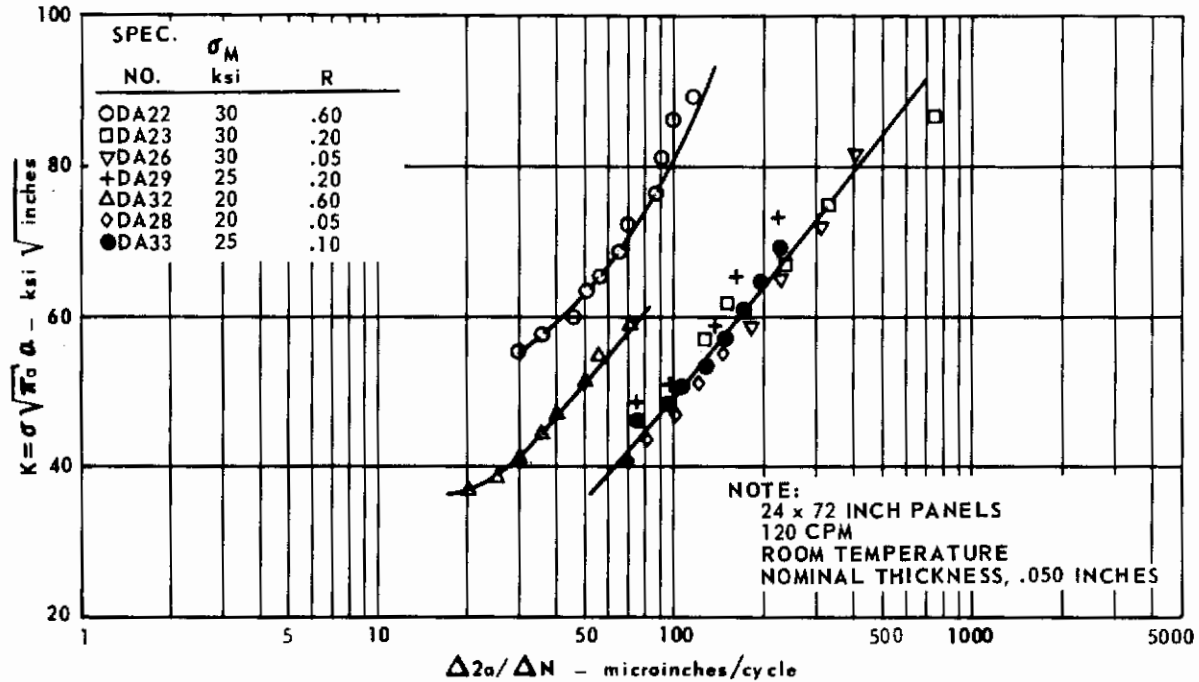


FIG. 35 CRACK GROWTH RATE DATA FOR Ti 8Al-1Mo-1V, HEAT 3454

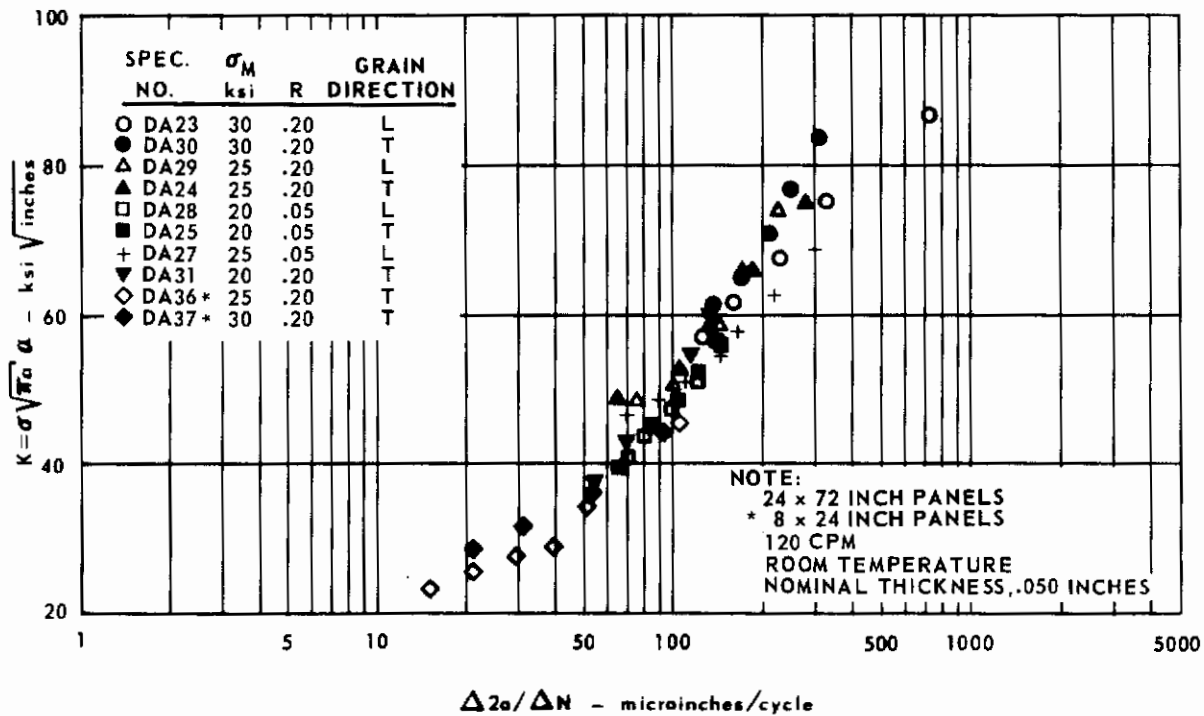


FIG. 36 CRACK GROWTH RATE DATA FOR Ti 8Al-1Mo-1V, HEAT 3454

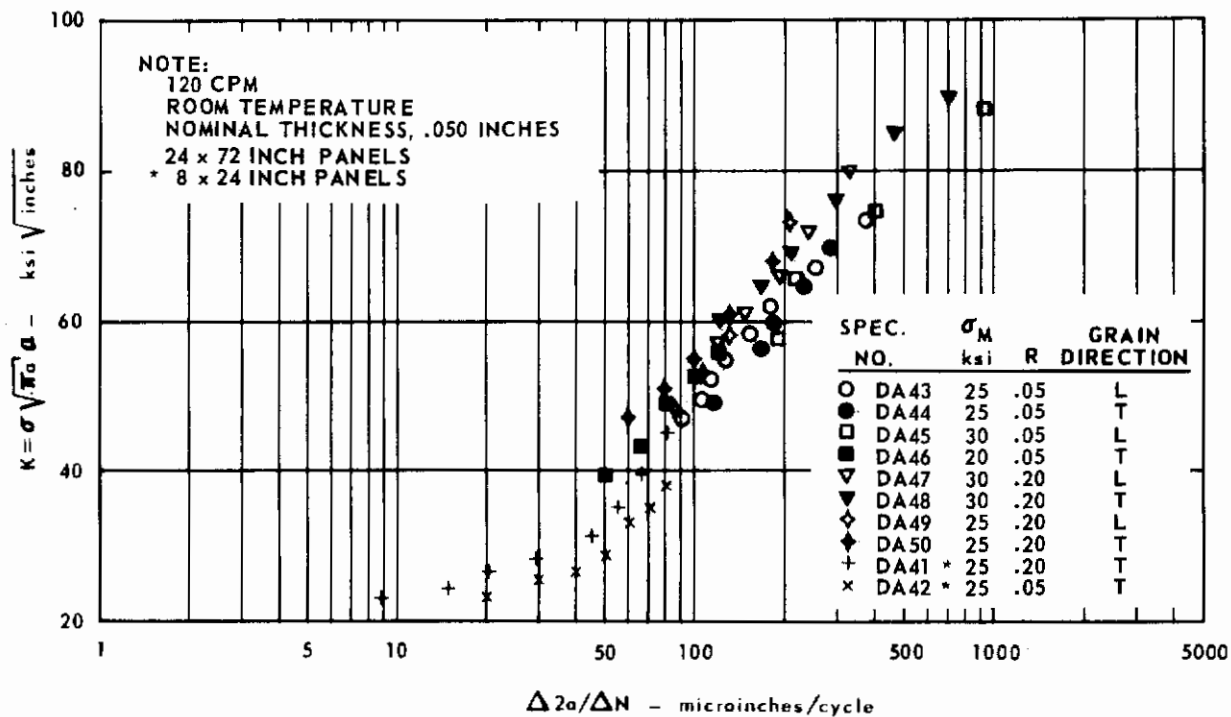


FIG. 37 CRACK GROWTH RATE DATA FOR Ti 8Al-1Mo-1V, HEAT 3457

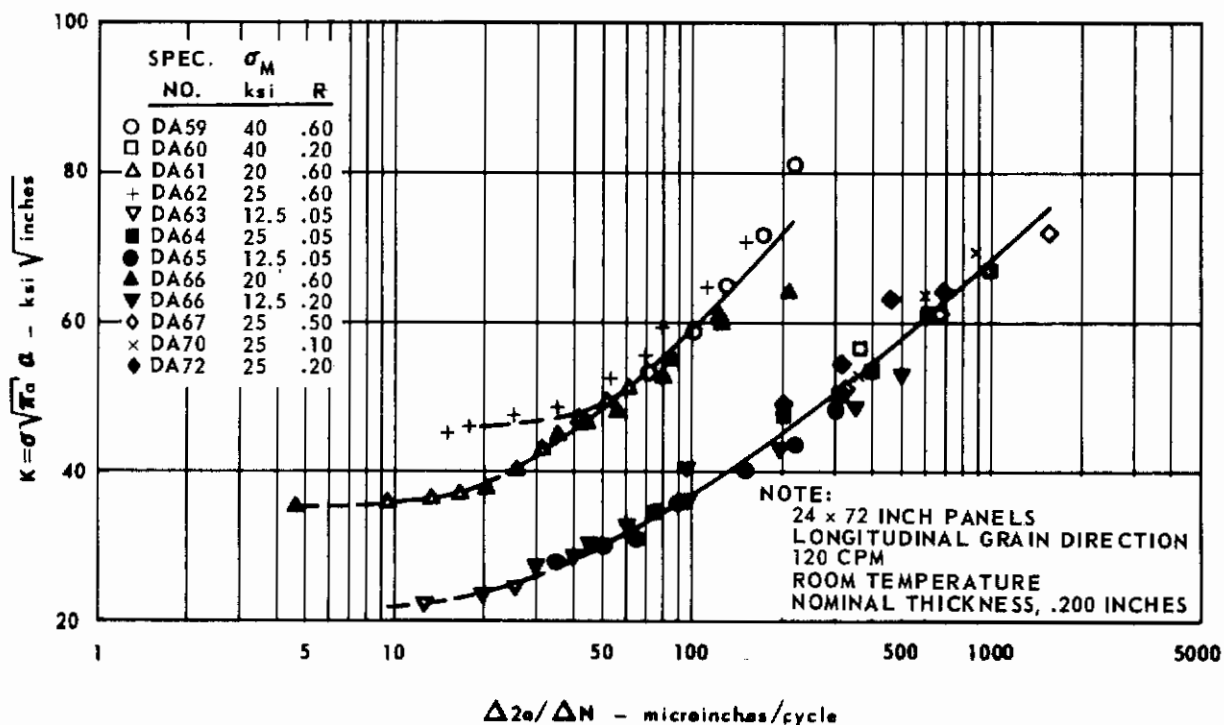


FIG. 38 CRACK GROWTH RATE DATA FOR Ti 8Al-1Mo-1V, HEAT 3457

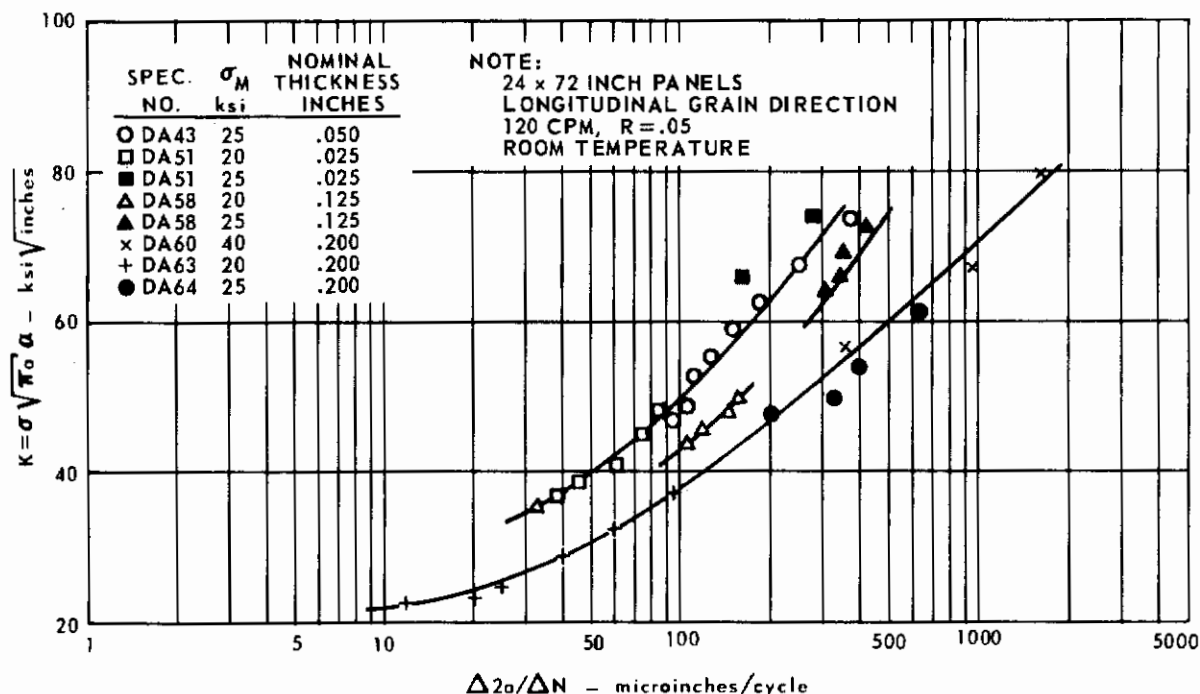


FIG. 39 CRACK GROWTH RATE DATA FOR Ti 8Al-1Mo-1V, HEAT 3457

Figs. 36 and 37 illustrate the consistency of crack growth rates between transverse and longitudinal panels and also between 24 x 72-inch and 8 x 24-inch panel tests. The difference between cracking rates at $R = 0.20$ and $R = 0.60$ are shown for the 0.200-inch thick panels in Fig. 38. For this thickness there does not appear to be a stress level effect (compare specimen DA59, DA61, and DA66). The effect of panel thickness is illustrated by the three curves in Fig. 39 for $R = 0.05$. There is no difference between thicknesses of 0.025 and 0.050 inches (compare specimens DA43 and DA51). The cracking rate increases for the 0.125-inch thickness (specimen DA58) and again for the 0.200-inch thickness (specimens DA60, 63, and 64).

A crack-growth-rate scatter band for all the 0.025- and 0.050-inch thick unexposed data is shown in Fig. 40. This band includes the three heats of material, both panel sizes and both grain directions, for $R = 0.20$ and $R = 0.05$.

Figs. 41, 42, and 43 show the effect of the 650° F-exposure on crack growth rate for the transverse, 8 x 24-inch panels. For the 0.025 and 0.050-inch thickness there is a marked increase in growth rate for the exposed panels (see Figs. 41 and 42). For the 0.200-inch thick panels both exposed and unexposed growth rates fall in the same data band (see Fig. 43). It is possible that any differences between exposed and unexposed rates for this thick material are masked because of the high crack growth rates with the thick material.

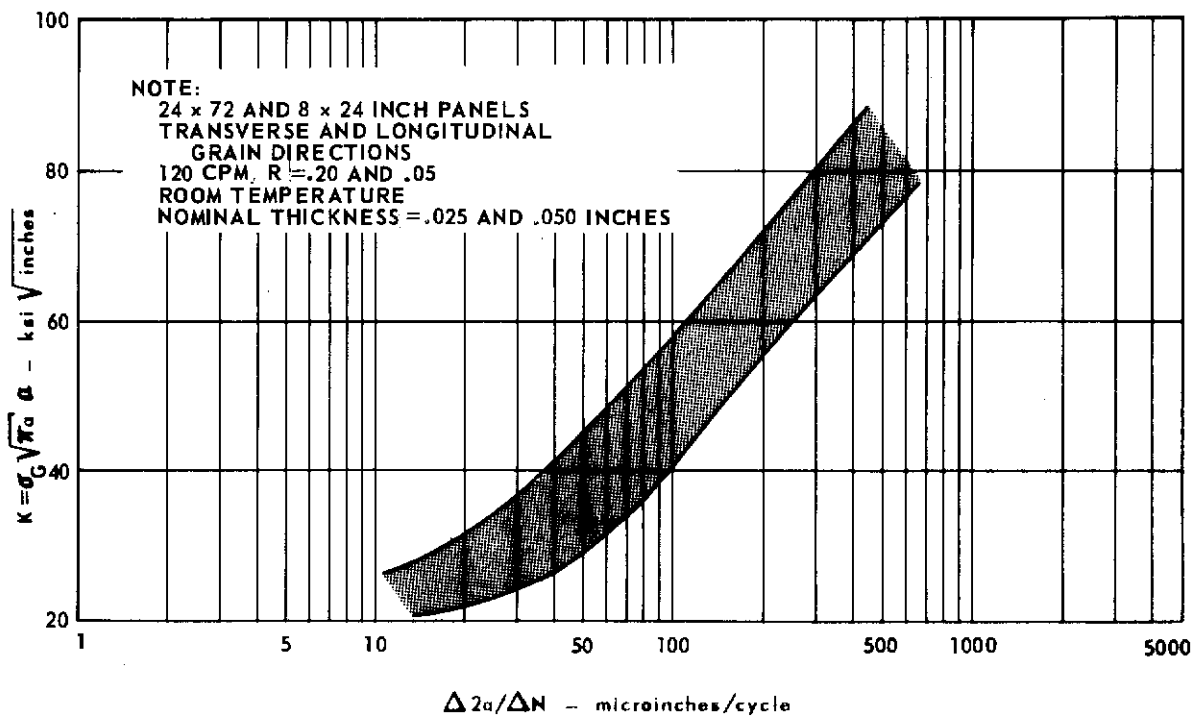


FIG. 40 CRACK GROWTH RATE DATA FOR Ti 8Al-1Mo-1V, HEATS 3454, 3457 AND 4535

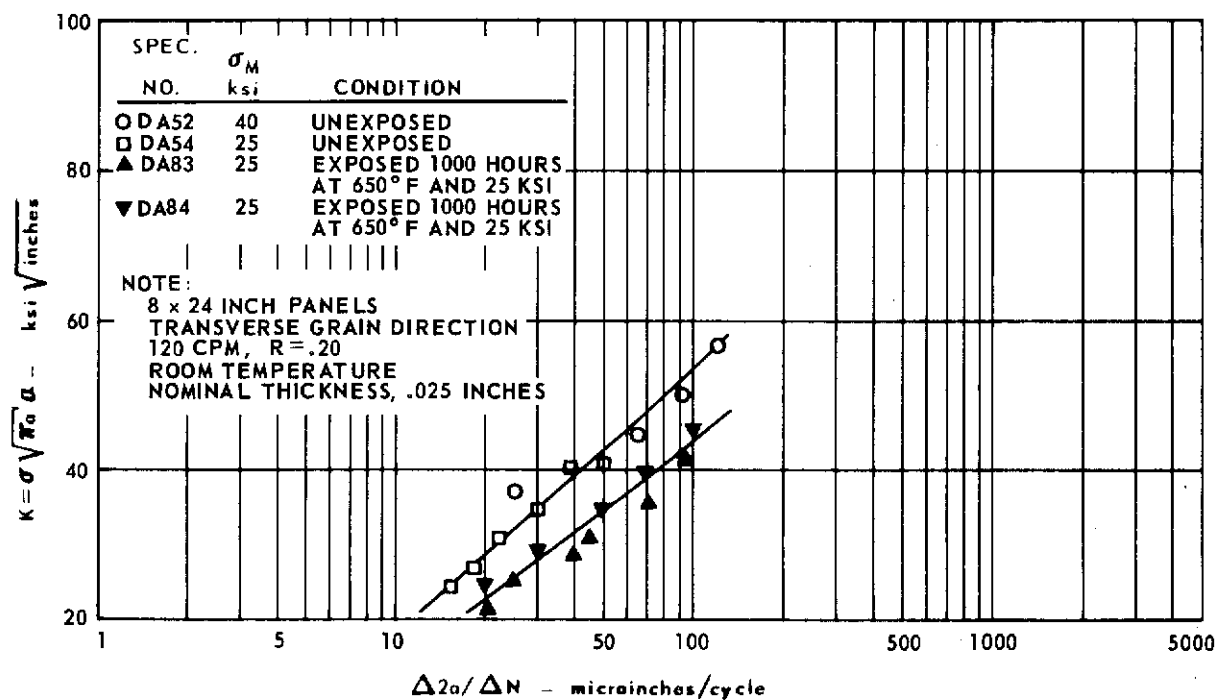


FIG. 41 COMPARISON OF EXPOSED AND UNEXPOSED CRACK GROWTH RATES FOR Ti 8Al-1Mo-1V, HEAT 3457

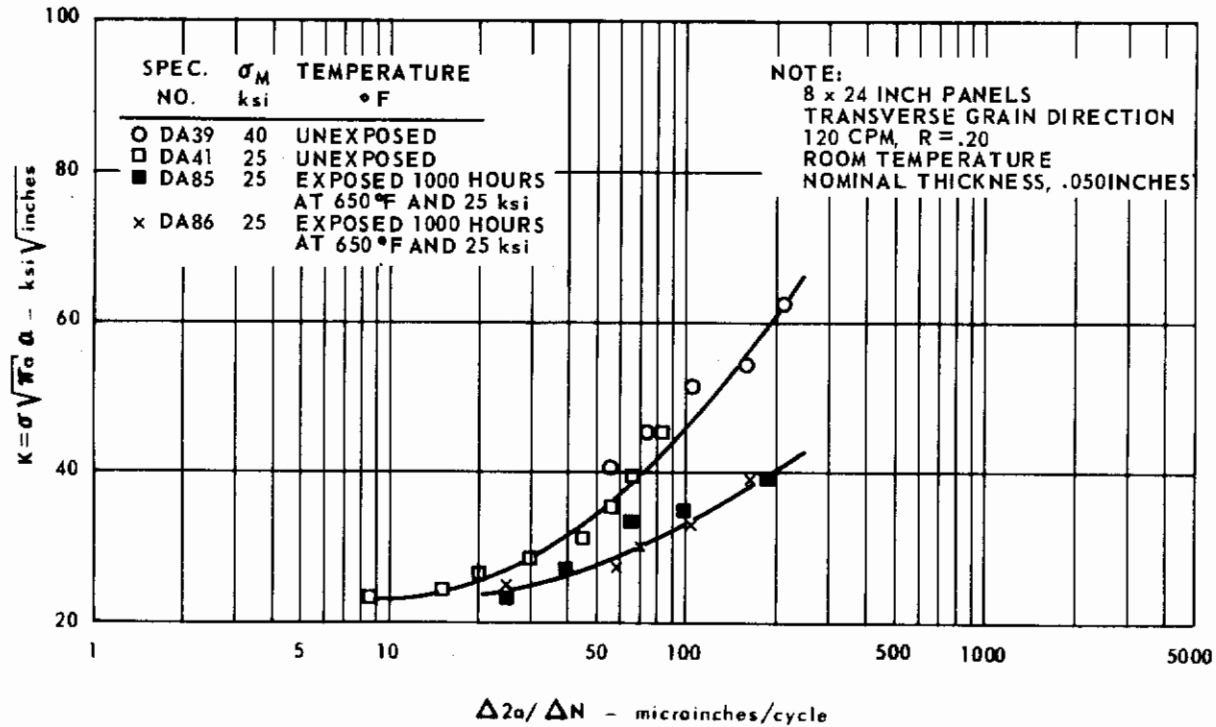


FIG. 42 COMPARISON OF EXPOSED AND UNEXPOSED CRACK GROWTH RATES FOR Ti 8Al-1Mo-1V, HEAT 3457

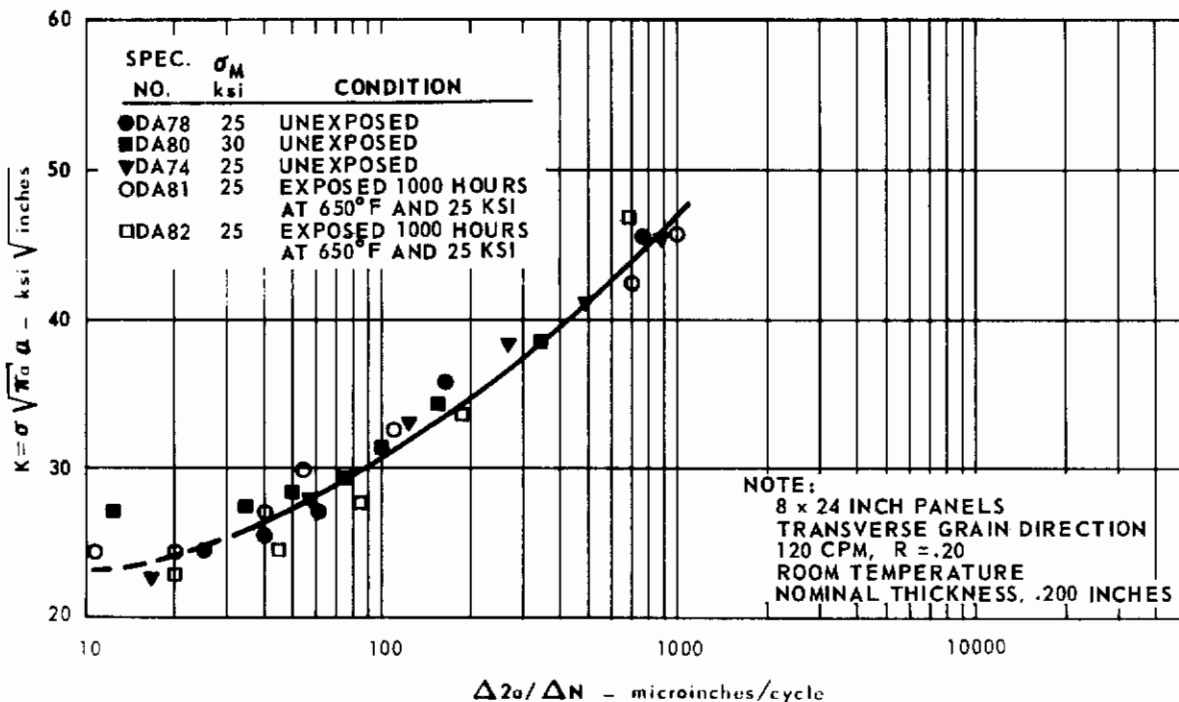


FIG. 43 COMPARISON OF EXPOSED AND UNEXPOSED CRACK GROWTH RATES FOR Ti 8Al-1Mo-1V, HEAT 3457

Residual Strength and Fracture Toughness

All pertinent test data for the static fracture testing are included in Table 8 for the 24 x 72-inch panels and in Table 9 for the 8 x 24-inch panels. The calculations based on σ_{yp} derived from high strain rate tensile data are accentuated by a darker background to simplify comparisons between the various data columns.

The Effect of Temperature

The effect of temperature is shown in Figs. 44 and 45 for both K_C and residual strength data. This comparison is made only for 24 x 72 x 0.050-inch longitudinal panels with $2a_0 = 6$ inches and at a stress rate of 10^6 psi/sec. Both curves show there is a drop in toughness at -110°F and an increase in toughness at 400 and 650°F . All the 400 and 650°F points on Fig. 44 exceed the ASTM criterion for valid K_C values and represent minimum (conservative) values. The drop in K_C and residual strength at -110°F is expected in part because of the significant increase in tensile ultimate and yield strengths at the low temperature.

A different comparison is shown in Fig. 46 on a panel damage-residual strength curve. Here transverse 8 x 24-inch panels are compared at a loading rate of 5×10^3 psi/sec. Again the -110°F residual strength is below that at room temperature and the 400 and 650°F residual strengths are above.

The Effect of Grain Direction

As noted previously, there appears to be no significant directionality effects detectable in the microstructure or shown by the tensile test data (section 6) for this alloy. This observation is substantiated by the K_C and residual strength data shown in Figs. 47 and 48. There is little difference between the longitudinal and transverse panel tests for any of the three heats when compared at a constant thickness of 0.050 inches, a crack length of 6 inches, and at a stress rate of 10^6 psi/sec. For the 5 longitudinal tests the average K_C value is $223.0 \text{ ksi } \sqrt{\text{in}}$; for the 5 transverse tests, the average K_C value is $230.3 \text{ ksi } \sqrt{\text{in}}$.

Similar results are shown by the residual strength panel damage graph in Fig. 49. This comparison is made at loading rates of 5×10^3 psi/sec for the longitudinal and transverse panels. For heat 4535, there is essentially no difference between longitudinal and transverse panels. For heat 3454, the longitudinal grain direction tests show higher values than the transverse tests.

The Effect of Thickness

For heat 3457, four specimen thicknesses were evaluated with both 8-inch and 24-inch wide panels. Figs. 50 and 51 illustrate the variation of K_C and residual strength, respectively, with specimen thickness. Curves are drawn only for the room temperature data to maintain graphic clarity.

There are variations in K_C and residual strength among the various thicknesses for each of the test temperatures. With the 24-inch wide panels, the 0.025 and 0.125-inch thicknesses have the highest toughness at room temperature. For the 8-inch wide panels, valid tests were attained with only the -110°F tests and the room temperature tests for the 0.200-inch thick material. A comparison made at -110°F for the 8-inch panels (transverse grain direction) shows that the 0.050 inch thickness is the toughest.

TABLE 8 FRACTURE TOUGHNESS DATA FOR 24 X 72-INCH PANELS OF Ti 8Al-1Mo-1V

SPECIMEN NO.	HEAT NO.	THICKNESS inches	WIDTH inches	GRAIN DIRECTION	TEMP. °F	$\dot{\sigma}$ psi/sec	$2\sigma_0$ inches	σ_G ksi	σ_N ksi	F_{tu} ksi	σ_{yp}^* ksi	σ_{yp}^* ksi	σ_{yp}^* ksi	σ_N^* ksi	σ_N^{**} ksi	$K_{CN} = \sigma_G \sqrt{\pi a}$ ksi \sqrt{in}	$\frac{\sigma_G^*}{F_{tu}}$	$K_{C^*} = \frac{\sigma_G^* \sqrt{a}}{\sqrt{W}}$ ksi \sqrt{in}	SHEAR %
DA 1	D4535	.053	24.08	L	RT	1.09×10^6	3.00	97.178	111.06	139.5	128.6	146.6	146.6	.86	.76	212.7	.676	248.0	100
DA 2	D4535	.051	23.98	L	650	1.14×10^6	3.00	85.568	97.79	105.0	79.9	103.1	103.1	1.22	.95	187.0	.815	236.7	100
DA 3	D4535	.052	24.00	L	70	5.4×10^3	6.00	58.230	77.64	139.5	128.6	132.1	132.1	.60	.59	185.2	.417	197.5	100
DA 4	D4535	.051	23.98	L	72	4.8×10^3	6.00	59.130	78.86	139.5	128.6	132.1	132.1	.61	.60	188.1	.424	198.3	100
DA 5	D4535	.050	23.99	T	75	4.25×10^3	6.00	53.667	71.58	140.0	130.7	134.0	134.0	.55	.53	170.6	.383	177.2	100
DA 6	D4535	.050	24.00	T	75	5.11×10^3	6.01	61.333	81.76	140.0	130.7	134.0	134.0	.63	.61	194.7	.438	207.1	100
DA 7	D4535	.050	24.04	L	65	1.02×10^5	6.00	64.642	86.19	139.5	128.6	140.2	140.2	.67	.61	205.6	.464	218.2	100
DA 8	D4535	.052	24.00	L	65	$.99 \times 10^5$	6.00	60.897	81.19	139.5	128.6	140.2	140.2	.63	.58	193.7	.434	202.8	100
DA 9	D4535	.049	24.04	L	RT	1.09×10^6	6.00	62.564	83.42	139.5	128.6	146.6	146.6	.65	.57	198.9	.449	208.2	100
DA 10	D4535	.052	23.98	L	RT	1.08×10^6	6.00	59.823	79.76	139.5	128.6	146.6	146.6	.62	.54	190.3	.428	197.5	100
DA 11	D4535	.051	24.01	T	67	$.98 \times 10^6$	6.00	59.184	78.92	140.0	130.7	146.6	146.6	.60	.53	188.0	.423	195.3	100
DA 12	D4535	.051	23.98	T	67	$.99 \times 10^6$	6.00	72.389	96.51	140.0	130.7	146.6	146.6	.74	.65	230.0	.512	244.8	100
DA 13	D4535	.051	24.07	L	650	1.02×10^6	6.00	71.528	95.37	105.0	79.9	103.1	103.1	1.19	.92	227.4	.681	267.0	100
DA 14	D4535	.050	23.96	L	650	1.03×10^6	6.00	72.228	96.30	105.0	79.9	103.1	103.1	1.20	.93	229.6	.688	272.0	100
DA 15	D4535	.052	24.00	L	650	1.08×10^6	10.00	54.870	94.06	105.0	79.9	103.1	103.1	1.18	.91	245.2	.531	272.9	100
DA 16	D4535	.050	24.03	L	RT	1.12×10^6	10.00	47.504	81.44	139.5	128.6	146.6	146.6	.63	.55	212.2	.341	213.5	100
DA 17	D4535	.052	24.01	L	-110	$\sim 10^6$	3.00	82.626	94.50	162.1	151.3	171.8	171.8	.63	.55	180.8	.510	191.5	100
DA 18	D4535	.048	24.00	L	400	1.07×10^6	6.00	75.694	100.93	115.4	94.5	110.3	110.3	1.07	.91	240.9	.656	282.3	100
DA 68	D4535	.050	24.00	L	-110	1.00×10^6	6.00	58.583	78.11	162.1	151.3	171.8	171.8	.52	.45	186.3	.362	192.7	100
DA 22	D3454	.048	24.00	L	66	4.7×10^3	6.00	69.444	92.59	141.6	129.2	132.5	132.5	.72	.70	220.8	.490	238.5	100
DA 23	D3454	.048	23.98	L	66	4.9×10^3	6.00	63.944	85.26	141.6	129.2	132.5	132.5	.66	.64	203.8	.451	216.2	100
DA 24	D3454	.046	23.99	T	75	4.85×10^3	6.00	57.790	77.09	141.1	131.0	134.0	134.0	.59	.58	183.9	.410	190.9	100
DA 25	D3454	.046	24.00	T	75	4.95×10^3	6.00	57.796	77.05	141.1	131.0	134.0	134.0	.59	.58	183.9	.410	191.0	100
DA 26	D3454	.047	24.01	L	68	1.06×10^5	6.00	76.064	101.42	141.6	129.2	141.0	141.0	.78	.72	242.0	.537	263.7	100
DA 27	D3454	.048	24.00	L	68	1.00×10^5	6.00	72.222	96.27	141.6	129.2	141.0	141.0	.74	.68	229.0	.510	248.9	100
DA 28	D3454	.049	23.99	L	68	1.06×10^6	6.00	63.149	75.76	141.6	129.2	147.0	147.0	.59	.52	200.8	.446	208.4	100

* TENSILE PROPERTIES OBTAINED FROM STANDARD STRAIN RATE TESTS OF .005 in./in./min
 ** σ_{yp} EXTRAPOLATED FROM HIGH STRAIN RATE TENSILE DATA FOR 5Al-2.5Sn TITANIUM (REFERENCE 26)

TABLE 8 FRACTURE TOUGHNESS DATA FOR 24 X 72-INCH PANELS OF Ti 8Al-1Mo-1V (Continued)

SPECIMEN NO.	HEAT NO.	THICKNESS inches	WIDTH inches	GRAIN DIRECTION	TEMP. °F	$\dot{\sigma}$ psi/sec	2 σ_0 inches	σ_G ksi	σ_N ksi	F_{10} ksi	σ_{yp}^* ksi	σ_{yp}^* ksi	σ_N^* ksi	σ_N^* ksi	σ_N^* ksi	$K_{CN} = \sigma_G \sqrt{\pi a}$ ksi \sqrt{in}	$\frac{\sigma_G}{F_{10}}$	$K_C = \frac{\sigma_G \sqrt{a_0 W}}{\sigma_{G0} \sqrt{a_0 W}}$ ksi \sqrt{in}	SHEAR %
DA 29	D3454	.052	24.00	L	RT	1.06×10^6	6.00	72.276	96.42	141.6	129.2	147.0	.74	.65	.65	229.1	.510	245.5	100
DA 30	D3454	.046	24.00	T	70	$\sim 10^6$	6.00	69.565	92.76	141.1	131.0	148.8	.71	.62	.62	221.2	.493	234.9	100
DA 31	D3454	.046	23.99	T	70	1.01×10^6	6.00	70.072	93.45	141.1	131.0	148.8	.71	.63	.63	224.8	.497	236.3	100
DA 32	D3454	.052	24.01	L	650	1.12×10^6	6.00	70.351	93.80	106.0	83.4	107.7	1.12	.87	.87	223.7	.664	238.5	100
DA 33	D3454	.053	24.03	L	650	1.03×10^6	6.00	68.737	91.65	106.0	83.4	107.7	1.10	.85	.85	218.6	.649	249.8	100
DA 43	D3457	.049	24.03	L	-110	1.07×10^6	6.00	56.949	76.00	180.9	162.3	184.5	.47	.41	.41	181.2	.315	193.5	100
DA 44	D3457	.047	24.00	T	-110	10.3×10^6	6.00	57.624	76.83	177.0	164.5	186.7	.47	.41	.41	183.0	.326	198.1	100
DA 45	D3457	.048	24.04	L	RT	1.07×10^6	6.00	74.437	98.25	142.6	129.4	147.2	.76	.67	.67	236.5	.522	235.5	100
DA 46	D3457	.046	24.00	T	70	1.01×10^6	6.00	70.788	94.38	142.0	129.0	146.7	.73	.64	.64	225.0	.500	240.1	100
DA 47	D3457	.048	24.04	L	400	1.12×10^6	5.40	82.810	101.36	117.9	95.3	121.0	1.06	.84	.84	249.8	.702	209.8	100
DA 48	D3457	.046	24.00	T	400	1.11×10^6	6.00	74.826	99.78	113.8	93.0	118.1	1.07	.85	.85	237.4	.659	271.9	100
DA 49	D3457	.046	24.04	L	650	1.03×10^6	6.00	68.314	91.03	104.7	82.7	106.7	1.10	.85	.85	217.3	.655	248.3	100
DA 50	D3457	.046	24.02	T	650	1.07×10^6	6.00	75.294	100.37	104.8	82.4	106.4	1.22	.94	.94	239.0	.720	205.5	100
DA 51	D3457	.026	24.03	L	70	$.77 \times 10^6$	6.00	81.920	109.23	140.8	128.6	146.2	.85	.75	.75	260.5	.582	286.2	100
DA 58	D3457	.127	24.02	L	66	$.90 \times 10^6$	6.00	83.262	111.02	138.2	128.2	145.8	.87	.76	.76	264.7	.603	292.3	100
DA 59	D3457	.204	24.19	L	69	1.06×10^6	3.00	101.763	116.17	136.9	126.3	143.6	.92	.81	.81	222.6	.743	240.0	100
+ DA 60	D3457	.204	24.24	L	650	1.13×10^6	3.00	82.735	94.50	105.8	83.4	88.9	1.13	1.06	1.06	181.0	.782	246.7	100
DA 61	D3457	.206	24.25	L	66	$.69 \times 10^6$	6.03	77.497	103.14	136.9	126.3	143.6	.82	.72	.72	246.8	.566	266.0	93
DA 62	D3457	.198	24.22	L	67	$.78 \times 10^6$	6.02	82.048	109.19	136.9	126.3	143.6	.86	.76	.76	261.3	.599	288.5	95
+ DA 63	D3457	.204	24.25	L	650	1.07×10^6	6.00	74.801	99.37	105.8	83.4	88.9	1.19	1.12	1.12	237.9	.707	313.2	100
+ DA 64	D3457	.200	24.25	L	650	1.04×10^6	6.00	73.034	97.05	105.8	83.4	88.9	1.16	1.09	1.09	232.3	.690	310.0	100
DA 65	D3457	.200	24.24	L	65	$.89 \times 10^6$	10.05	53.073	90.66	136.9	126.3	143.6	.72	.63	.63	237.2	.388	238.5	93
+ DA 66	D3457	.208	24.25	L	650	$.99 \times 10^6$	10.00	54.490	92.73	105.8	83.4	88.9	1.11	1.04	1.04	243.2	.515	294.5	100
DA 67	D3457	.206	24.25	L	-110	$.69 \times 10^6$	6.00	47.547	63.17	162.6	151.4	172.1	.42	.37	.37	151.2	.292	156.2	71
DA 70	D3457	.201	24.23	L	73	4.88×10^6	6.00	52.423	69.67	136.9	126.3	143.6	.55	.49	.49	166.8	.383	174.8	100
DA 72	D3457	.203	24.15	L	75	$.91 \times 10^5$	6.00	69.762	92.82	136.9	126.3	143.6	.73	.64	.64	221.9	.509	244.5	100

* TENSILE PROPERTIES OBTAINED FROM STANDARD STRAIN RATE TESTS OF .005 in./in./min
 ** σ_{yp} EXTRAPOLATED FROM HIGH STRAIN RATE TENSILE DATA FOR SA1-2.5 Sn TITANIUM (REFERENCE 26)

+ NO BUCKLING RESTRAINT

TABLE 9 FRACTURE TOUGHNESS DATA FOR 8 x 24 INCH PANELS OF Ti 8Al - 1Mo - 1V (continued)

SPECIMEN NO.	HEAT NO.	THICKNESS inches	WIDTH inches	GRAIN DIRECTION	TEMP. °F	$\dot{\sigma}$ psi/sec	$2a_0$ inches	σ_G ksi	σ_N ksi	F_{tu} ksi	σ_{yp} ksi	σ_{yp} ksi	σ_{yp} ksi	σ_{yp} ksi	$K_{CN} = \sigma_G \sqrt{\pi a_0}$ ksi \sqrt{in}	$\sigma_G^* F_{tu}$	$K_{CN} = \sigma_G \sqrt{\pi a_0}$ ksi \sqrt{in}	SHEAR %
DA 80	D3457	.214	8.00	T	650	1.30×10^6	2.04	71.813	96.3	105.8	83.4	94.8	1.15	1.01	132.9	.686	146.3	100
▲ DA 81	D3457	.215	8.00	T	73	1.31×10^6	2.00	70.349	93.8	143.6	130.0	147.8	.72	.64	128.9	.490	137.7	40
▲ DA 82	D3457	.215	8.00	T	73	1.56×10^6	2.00	67.384	89.9	143.6	130.0	147.8	.69	.61	123.4	.470	131.1	38
▲ DA 83A	D3457	.027	7.98	T	70	1.05×10^6	2.01	77.898	106.5	144.6	126.4	143.6	.84	.74	143.1	.540	157.3	100
▲ DA 84A	D3457	.027	7.99	T	70	1.06×10^6	1.99	79.860	104.1	144.6	126.4	143.6	.82	.73	146.5	.553	162.1	100
▲ DA 85	D3457	.049	8.02	T	70	1.02×10^6	2.03	65.869	88.9	150.0	132.7	150.6	.67	.59	121.6	.439	127.9	100
▲ DA 86	D3457	.049	8.02	T	70	1.03×10^6	2.02	66.499	88.2	150.0	132.7	150.6	.66	.59	122.2	.443	129.1	100

* TENSILE PROPERTIES OBTAINED FROM STANDARD STRAIN RATE TESTS OF .005 in./in./min
 ** σ_{yp} EXTRAPOLATED FROM HIGH STRAIN RATE TENSILE DATA FOR 5Al-2.5 Sn TITANIUM (REFERENCE 26)
 ▲ EXPOSED @ 650°F FOR 1000 HRS @ $\sigma_G = 25$ ksi

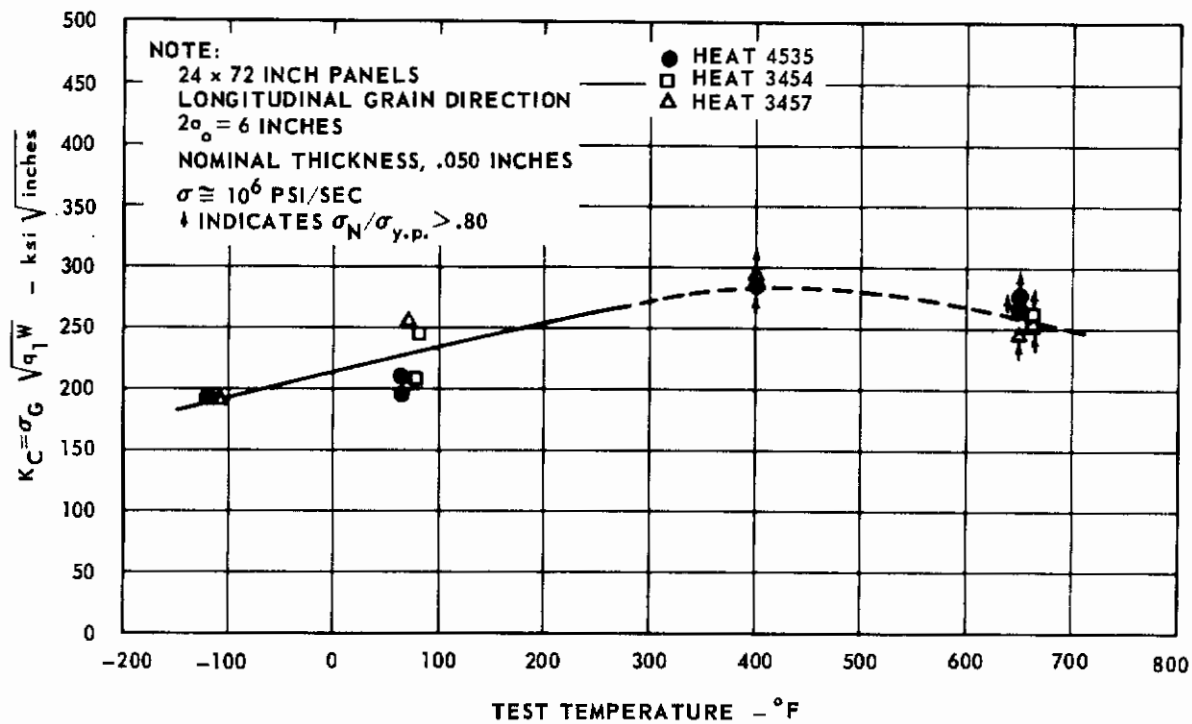


FIG. 44 EFFECT OF TEST TEMPERATURE ON K_C FOR Ti 8Al-1Mo-1V

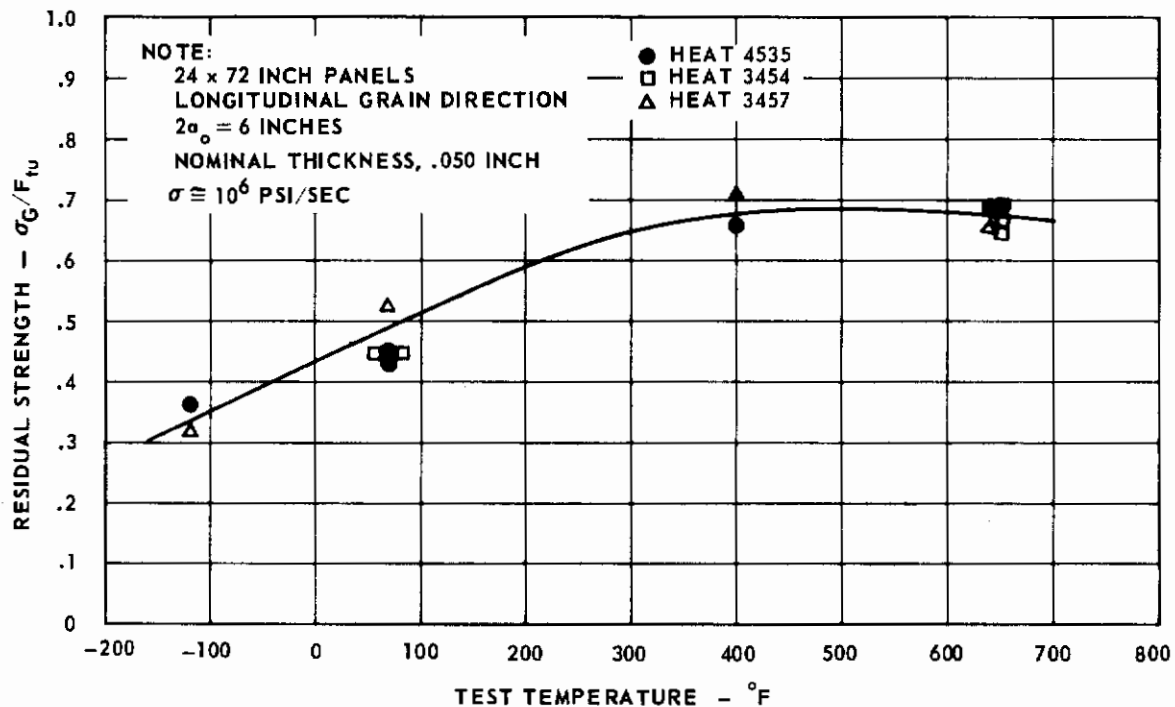


FIG. 45 EFFECT OF TEST TEMPERATURE ON RESIDUAL STRENGTH FOR Ti 8Al-1Mo-1V

NOTE:

$\dot{\sigma} \cong 5 \times 10^3$ PSI/SEC
TRANSVERSE GRAIN DIRECTION

NOMINAL THICKNESS INCHES	TEMPERATURE ° F
HEAT D4535 ○ .050	-110
HEAT D3454 □ .050	-110
HEAT D3457 △ .050	R. T.
◇ .200	R. T.
◊ .200	400
▽ .200	650
◇ .200	-110

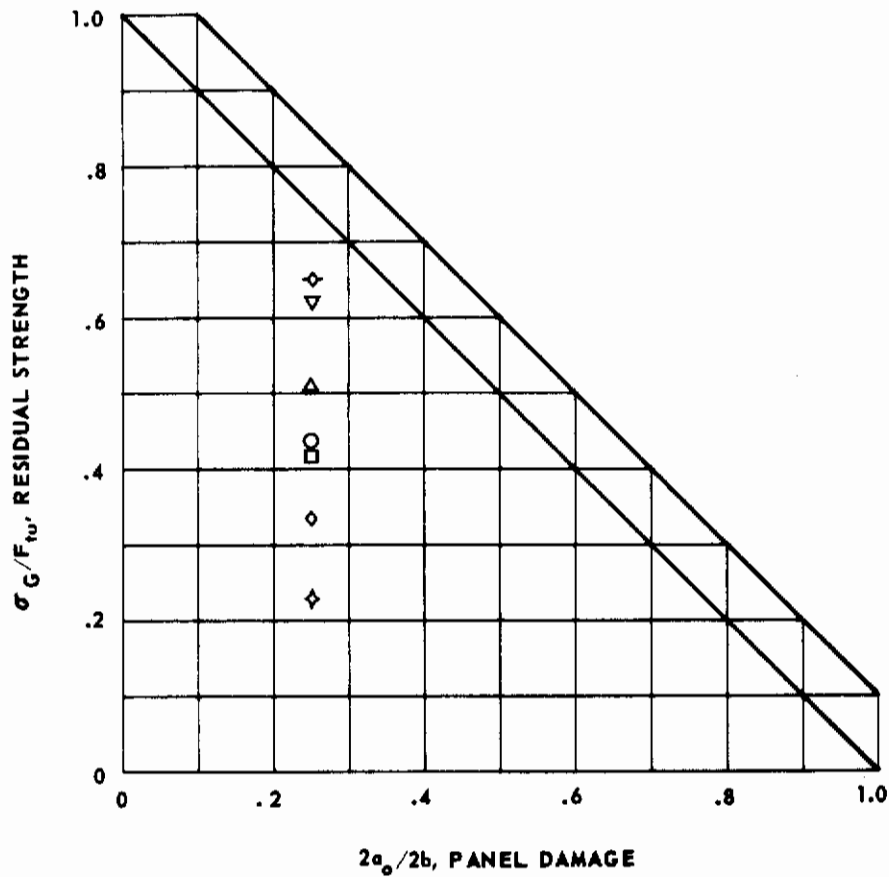


FIG. 46 RESIDUAL STRENGTH vs DAMAGE FOR 8 x 24 INCH Ti 8Al-1Mo-1V PANELS, HEATS D4535, D3454 AND D3457

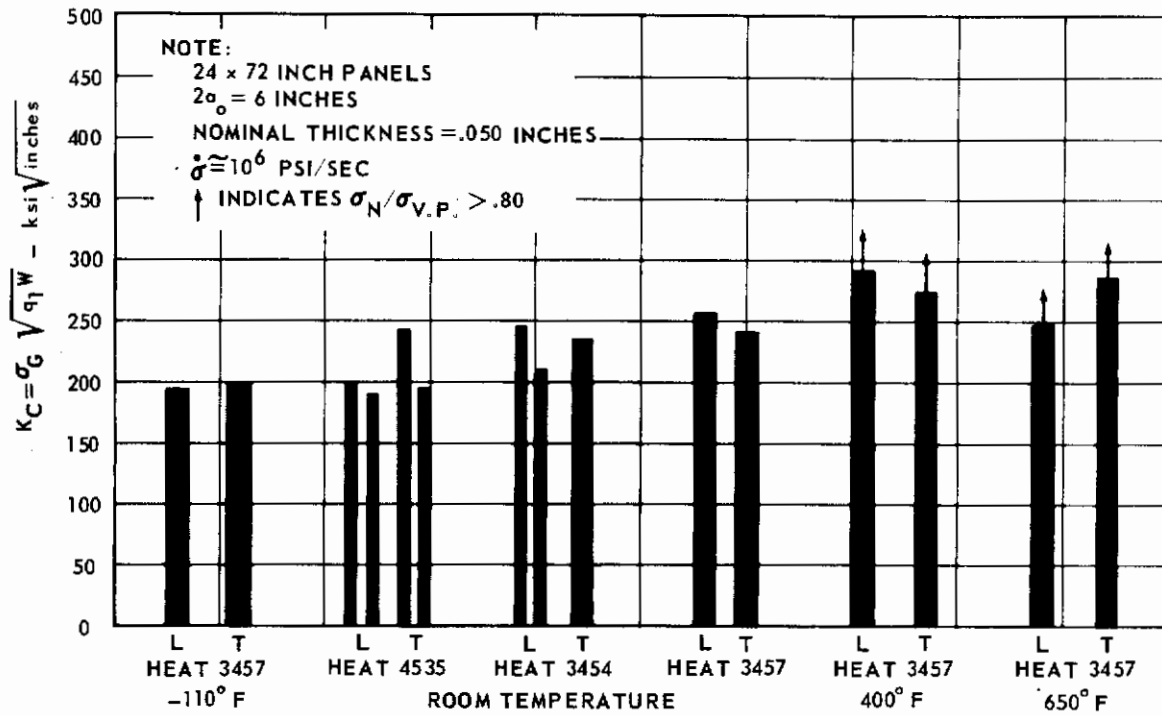


FIG. 47 VARIATION OF K_C WITH GRAIN DIRECTION FOR Ti 8Al-1Mo-1V

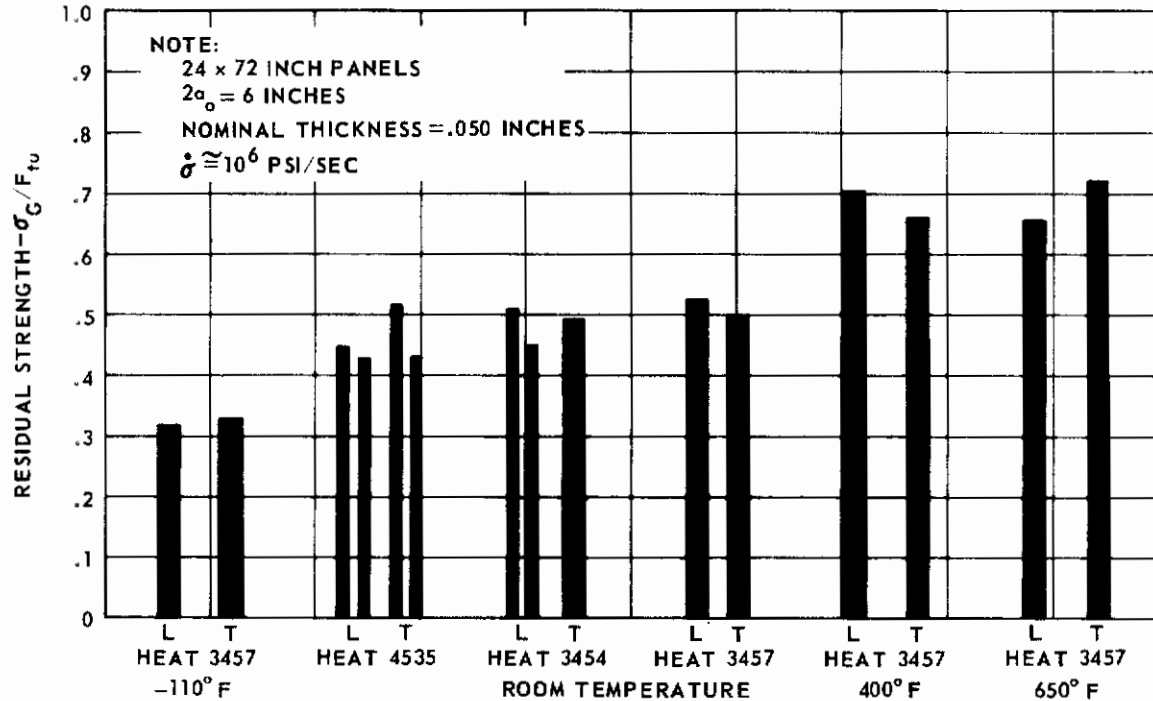


FIG. 48 VARIATION OF RESIDUAL STRENGTH WITH GRAIN DIRECTION FOR Ti 8Al-1Mo-1V

NOTE:
ROOM TEMPERATURE
NOMINAL THICKNESS, .050
Points at $2a_0/2b = .25$ were Displaced
Laterally to Avoid Overplotting.

	GRAIN DIRECTION	$\dot{\sigma}$ psi/sec
HEAT D4535		
○	L	5×10^3
□	T	5×10^3
△	L	1×10^5
HEAT D3454		
◇	L	5×10^3
▽	T	5×10^3
◊	L	1×10^5

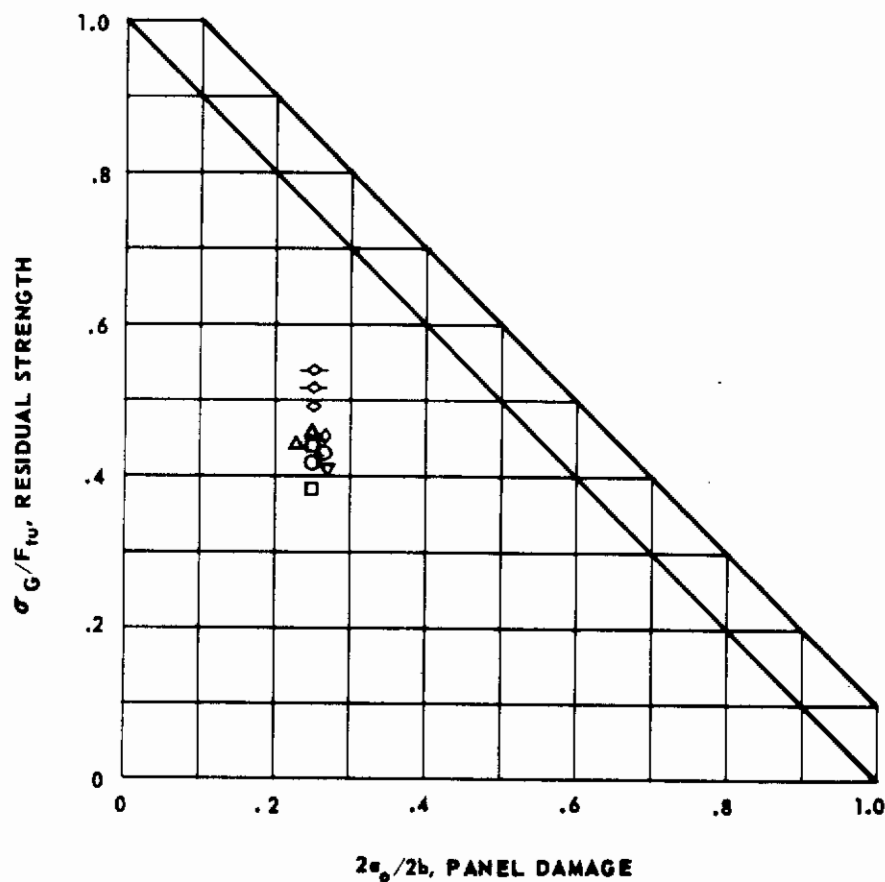


FIG. 49 RESIDUAL STRENGTH vs DAMAGE FOR 24 x 72 INCH Ti 8Al-1Mo-1V PANELS,
HEATS D4535 AND D3454

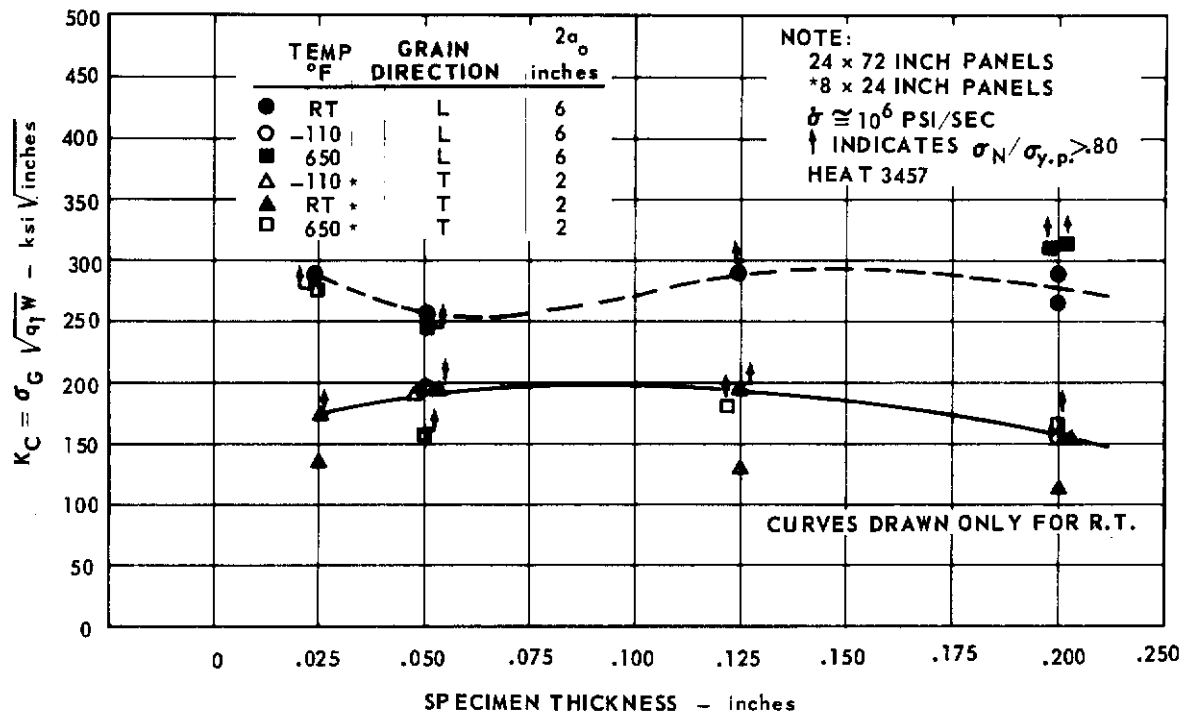


FIG. 50 VARIATION OF K_C WITH THICKNESS FOR Ti 8Al-1Mo-1V

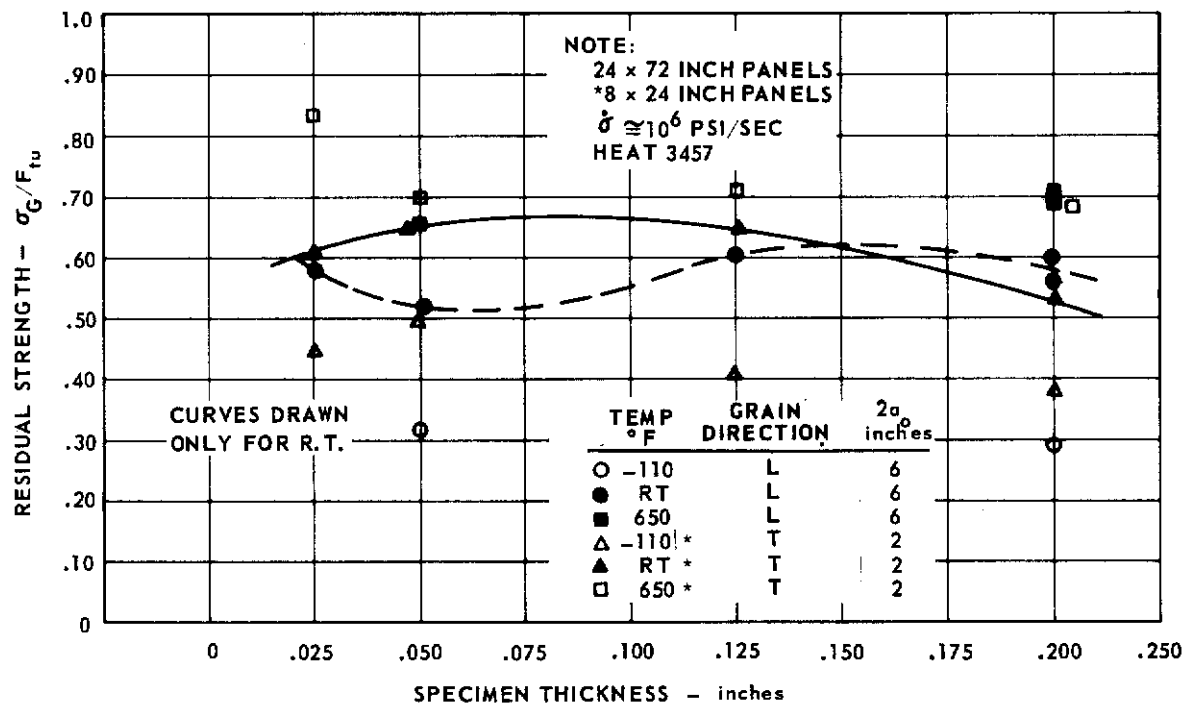


FIG. 51 VARIATION OF RESIDUAL STRENGTH WITH THICKNESS FOR Ti 8Al-1Mo-1V

The Effect of Crack Length

The effect of crack length expressed as the ratio of crack-length to panel-width is shown in Figs. 52 and 53 for K_C and in Figs. 54 and 55 for residual strength for the 24-inch wide panels. Parametrically superimposed on these graphs are grain direction, temperature and thickness variables. All comparisons are made at a stress rate of 10^6 psi/sec.

Fig. 52 shows that K_C is virtually unaffected by crack length for a given test temperature when tests are valid. All 650°F-tests have undergone net section yielding and exceed the ASTM criterion for validity of test data. The K_C value for the 10-inch crack length for the 0.200 inch thick panels at room temperature has a slightly lower K_C value than the 6-inch crack-length panels (see Fig. 53). Both Figs. 52 and 53 show that K_C is a function of σ_N / σ_{yp} even when this ratio is below 0.80. This may indicate that a more strict criterion for valid tests should be at σ_N / σ_{yp} ratios below the present 0.80 value. For plane stress fracture tests of tough materials with such a criterion, it might be impossible to obtain valid tests with any practically-sized test panel.

Figs. 54 and 55 show that the 400 and 650°F tests approach the theoretical upper limit of residual strength for all thicknesses and all crack lengths tested. For the room temperature and -110°F tests, residual strength decreases linearly with increasing panel damage.

The Effect of Stress Rate

The effect of stress rate is shown in Fig. 56 for both 8-inch-wide and 24-inch-wide panels. In general, the variation of K_C with stress rate is within the scatter of K_C values (all other variables being held constant). Specifically, there is a consistent increase in K_C with increasing stress rate for the 8-inch-wide panels tested at -110°F and room temperature and the thick 24-inch wide panels tested at room temperature. In order to maintain graphic clarity, no lines have been drawn through the test points on Fig. 56.

The Effect of Exposure

The effect of the 650°F exposure for 1000 hours at 25 ksi on K_C is shown in Fig. 57 for the 8 x 24-inch panels. Data are included for unexposed panels from the same heat of material for comparison. There is a consistent drop in exposed K_C values which varies from 8 percent for the 0.025-inch thickness, to 11 percent for the 0.200-inch thickness, to 33 percent for the 0.050-inch thickness.

In the Douglas program (Ref. 1), no exposure effect was found for 4-inch-wide and 8-inch-wide transverse panels exposed in a similar manner for triplex annealed 8Al-1Mo-1V. Although the Douglas panels were notched and fatigue-cracked before exposure, as compared to notching and cracking after exposure with the present panels, it is not known what effect this might have had on the K_C data. As Freeman (Ref. 25) has pointed out, a pre-cracked exposure panel would tend to undergo stress relaxation around the crack tip during exposure. The gross panel stress should still have a similar effect, however, in promoting any metallurgical changes associated with instability. On the other hand, it is possible that the triplex annealed condition provides a more stable metallurgical structure.

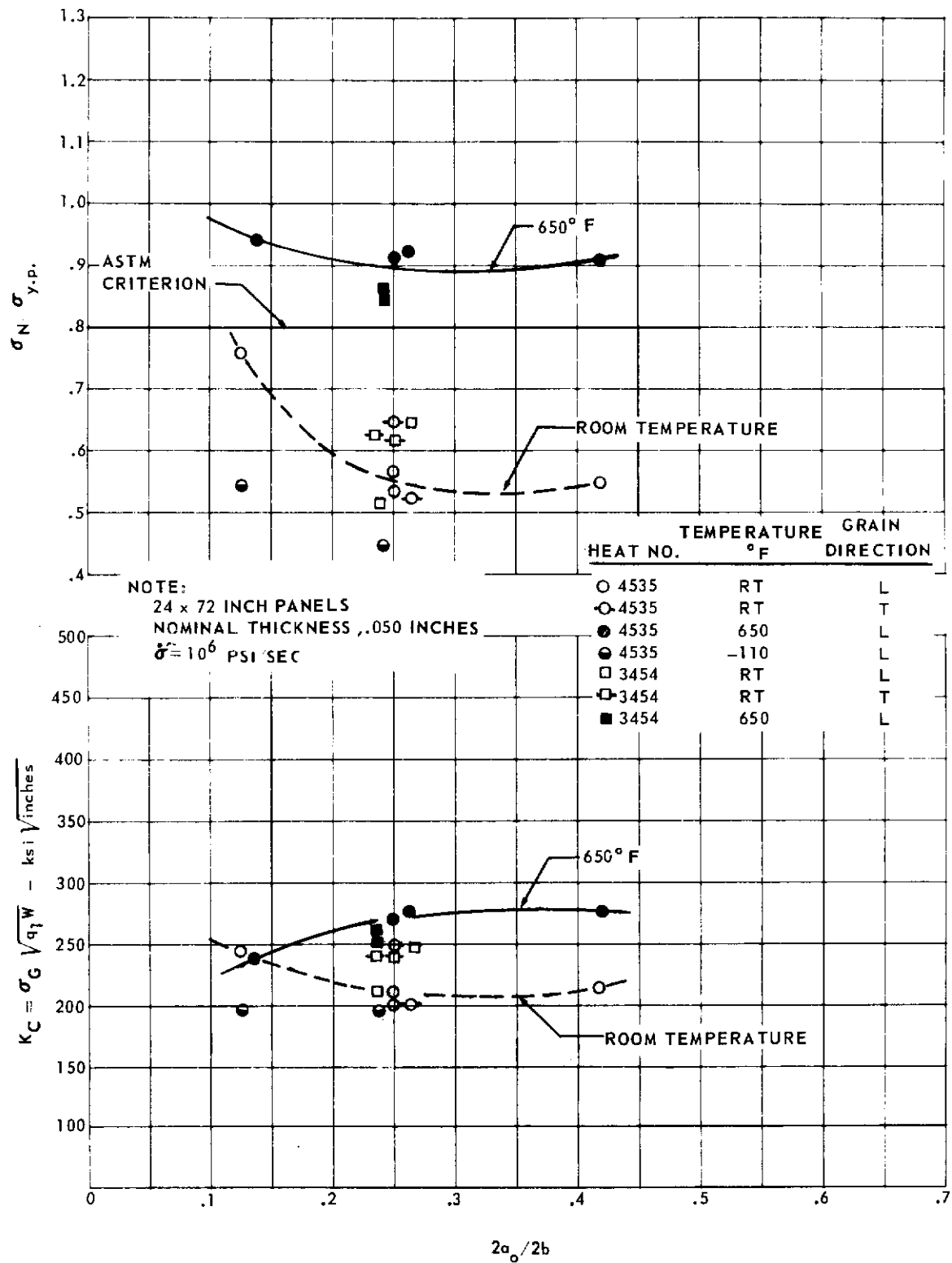


FIG. 52 VARIATION OF K_C WITH TEMPERATURE, CRACK LENGTH AND GRAIN DIRECTION FOR Ti 8Al-1Mo-1V

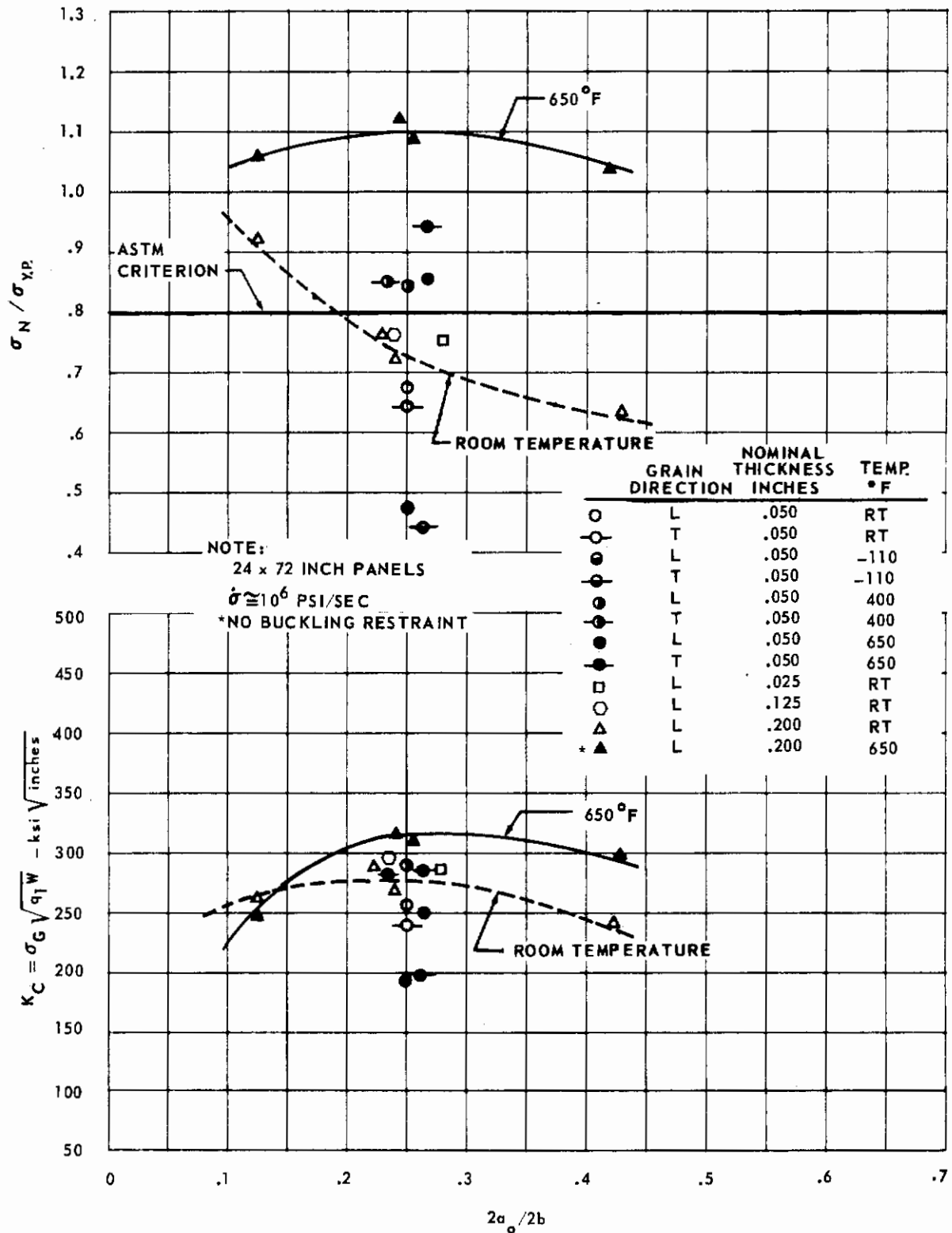


FIG. 53 VARIATION OF K_C WITH TEMPERATURE, CRACK LENGTH, THICKNESS AND GRAIN DIRECTION FOR Ti 8Al-1Mo-1V HEAT 3457

NOTE:
 $\dot{\sigma} \approx 10^6$ PSI/SEC
 LONGITUDINAL GRAIN DIRECTION
 Points at $2a_0/2b = .25$ were Displaced
 Laterally to Avoid Overplotting.

NOMINAL THICKNESS INCHES	TEMP °F
○ .025	R.T.
□ .125	R.T.
△ .200	R.T.
◇ .200	650
▽ .200	-110

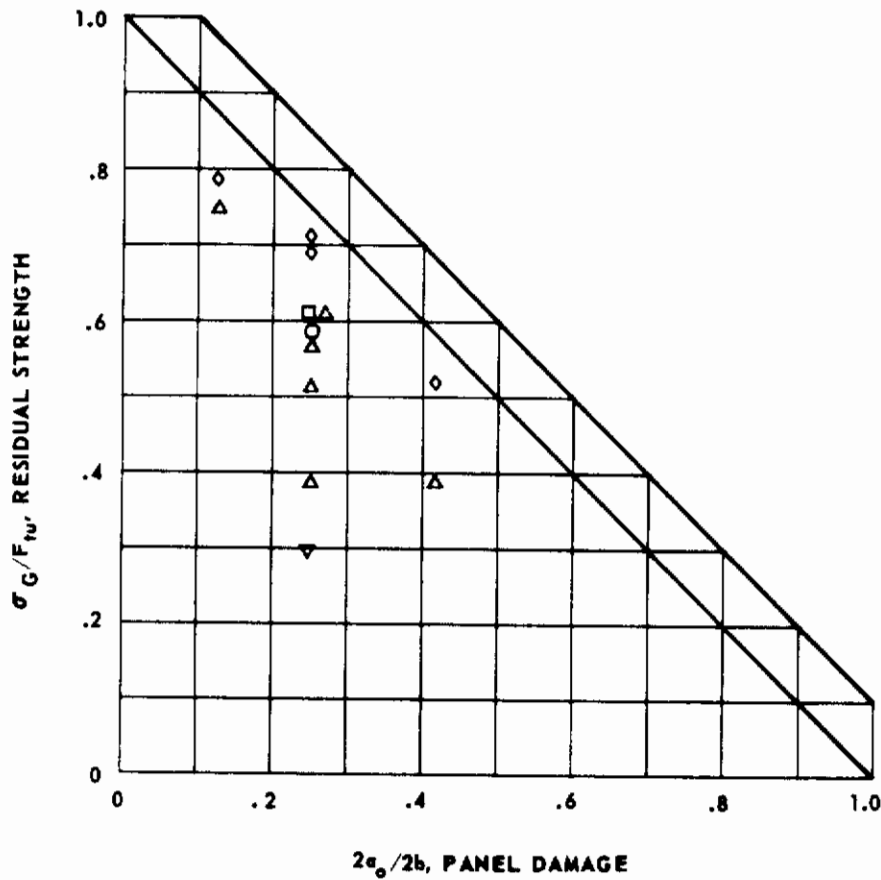


FIG. 54 RESIDUAL STRENGTH vs DAMAGE FOR 24 x 72 INCH Ti 8Al-1Mo-1V PANELS, HEAT D3457

NOTE:
 $\dot{\epsilon} \approx 10^6$ PSI/SEC
 NOMINAL THICKNESS, .050 INCHES
 Points at $2a_0/2b = .25$ were Displaced
 Laterally to Avoid Overplotting.

	GRAIN DIRECTION	TEMPERATURE ° F
HEAT D4535		
○	L'	R.T.
□	L	650
■	L	-110
●	T	R.T.
○	L	400
HEAT D3454		
△	L	R.T.
▲	L	650
★	T	R.T.
HEAT D3457		
◇	L	R.T.
◆	L	400
◇	L	650
▽	L	-110
▽	T	R.T.
▽	T	400
◇	T	650
◆	T	-110

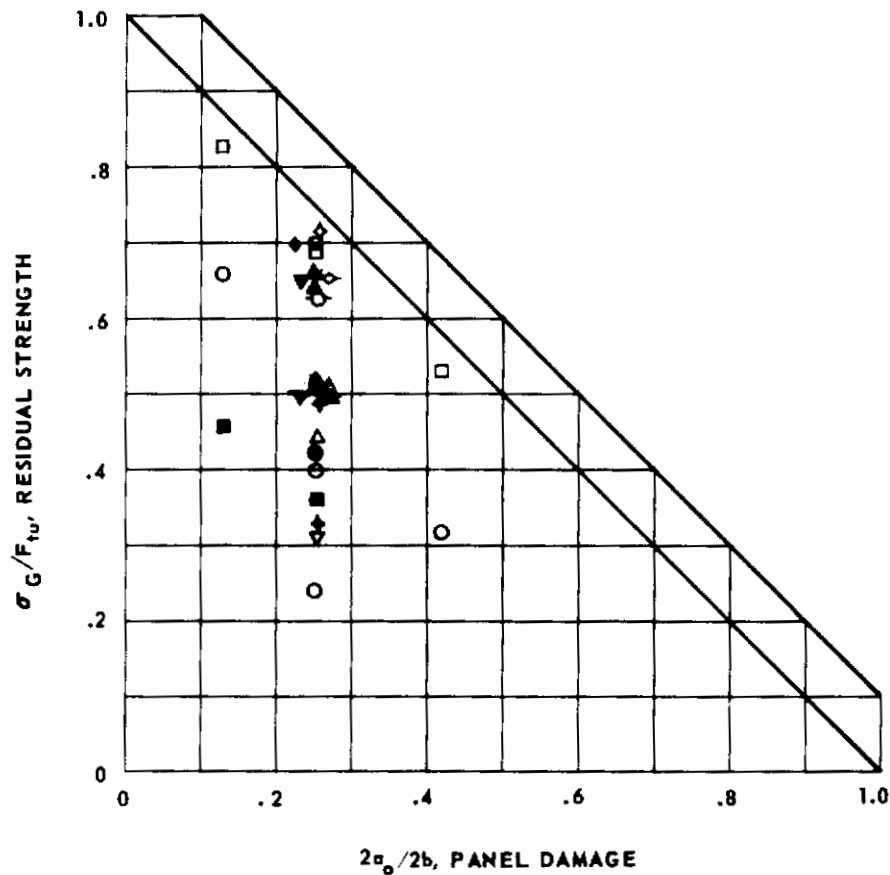


FIG. 55 RESIDUAL STRENGTH vs DAMAGE FOR 24 x 72 INCH Ti 8Al-1Mo-1V PANELS, HEATS D4535, D3454 AND D3457

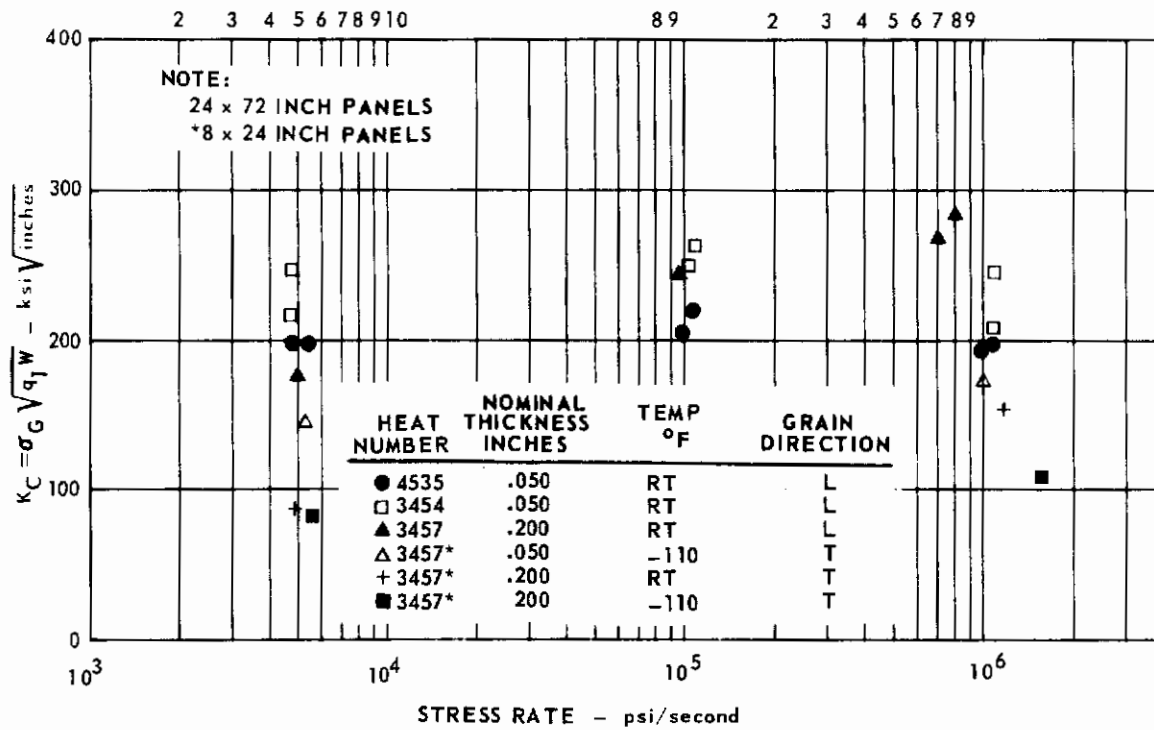


FIG. 56 THE EFFECT OF STRESS RATE ON K_C FOR Ti 8Al-1Mo-1V

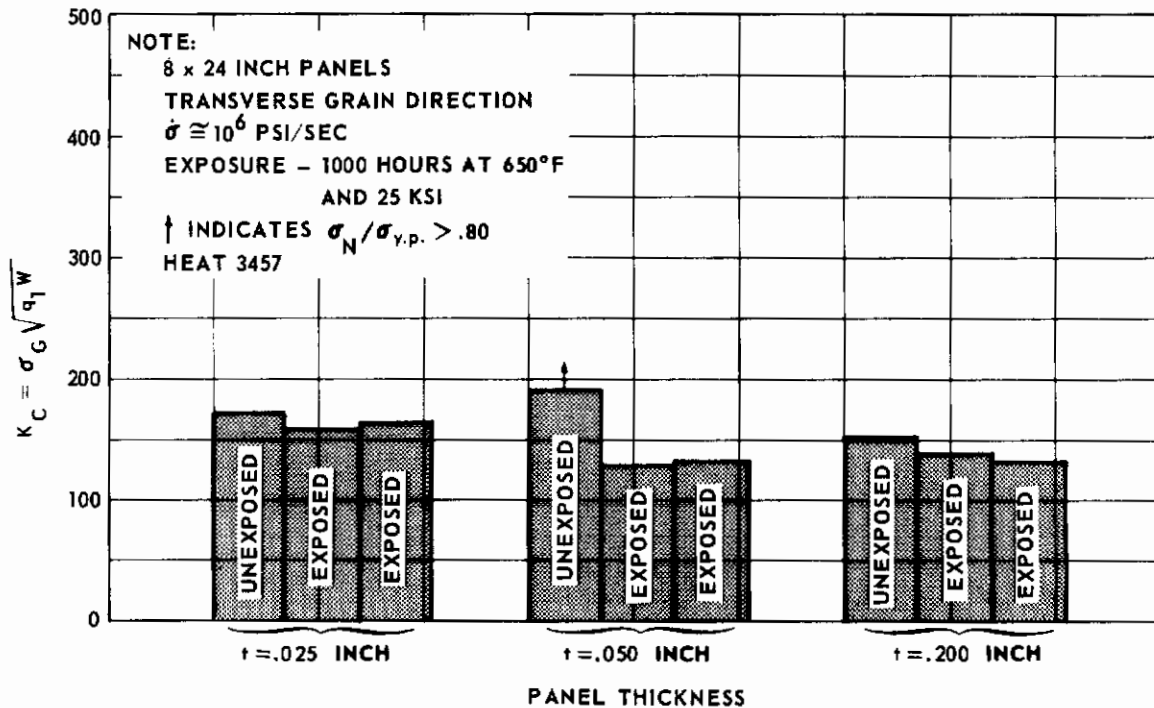


FIG. 57 COMPARISON OF EXPOSED AND UNEXPOSED K_C VALUES FOR Ti 8Al-1Mo-1V

The Effect of Heat Variation

The effect of heat variation is shown partly by Fig. 47 in the previous subsection on grain direction. There, it was pointed out that for three heats of the 0.050-inch-thick material the average K_C for the longitudinal grain direction was 223.0 ksi $\sqrt{\text{in.}}$ and for the transverse grain direction, 230.3 ksi $\sqrt{\text{in.}}$ The average K_C value for both grain directions is 226.7 ksi $\sqrt{\text{in.}}$ The range in values considering both grain directions is from 195.3 to 255.5 ksi $\sqrt{\text{in.}}$ All these K_C values are from valid tests with σ_N / σ_{yp} less than 0.70 in each case.

A similar comparison can be made from the -110°F tests of the 8 x 24 x 0.050-inch transverse panels from the three heats. Only the -110°F tests are compared since at higher temperatures most 8-inch-wide panels underwent net section yielding. For the three panels tested at a stress rate of 5×10^3 psi per second (one panel from each heat), the K_C values are 142.7, 141.6, and 144.7 ksi $\sqrt{\text{in.}}$ For similar panels tested at a stress rate of 10^6 psi per second, the K_C values are 185.2, 179.2, and 172.5 ksi $\sqrt{\text{in.}}$

One method of comparing the variation among the three heats is to use the range in K_C values expressed as a percent of the average value. For the large panels tested at room temperature, both the longitudinal and transverse grain directions are considered since there is no consistent difference between them. The following comparison can be made when these computations are carried out:

For the longitudinal and transverse 24 x 72-inch panels tested at room temperature at a stress rate of 10^6 psi per second, the range is 26.6 percent; for the 8 x 24-inch transverse panels tested at -110°F at a stress rate of 10^6 psi per second, the range is 7 percent; and, for the 8 x 24-inch panels tested at -110°F at a stress rate of 5×10^3 psi per second, the range is 2.2 percent. It is possible that preferred orientation studies could explain in part the large range variation with the 24 x 72-inch panels.

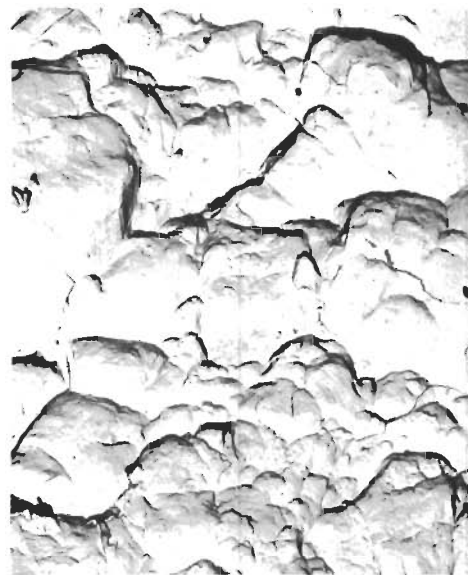
Fractographic Studies

Macrophotographs from four panels of Ti 8Al-1Mo-1V are included in Figs. 58, 59, 60, and 61. Only one-half of the panel width is shown to maintain detail in the photographs. Fig. 58 shows electron micrographs from representative fracture areas from an 8 x 24 x 0.050-inch panel fractured at room temperature. Striations were found over most of the completely flat fatigue crack area, as shown in the lower-right-hand picture. The transition from the fatigue-cracked surface to the rapid fracture area is shown in the lower-left-hand micrograph. This small, triangular, plane strain fracture area consists of dimples which are different in appearance from those of the rapid shear lip fracture area. This difference is shown by the upper-left-hand and upper-right-hand micrographs in Fig. 58.

Fig. 59 shows the results of the electron microscope study from a 24 x 72 x 0.200-inch panel also fractured at room temperature. An interesting observation was made in the fatigue cracked area where the stress level has been changed from 25 ksi to 17.5 ksi. The lower-right-hand micrograph shows the very fine striations at the mid-thickness point where crack growth has been delayed by the reduction in stress level. It is possible that careful exhaustive



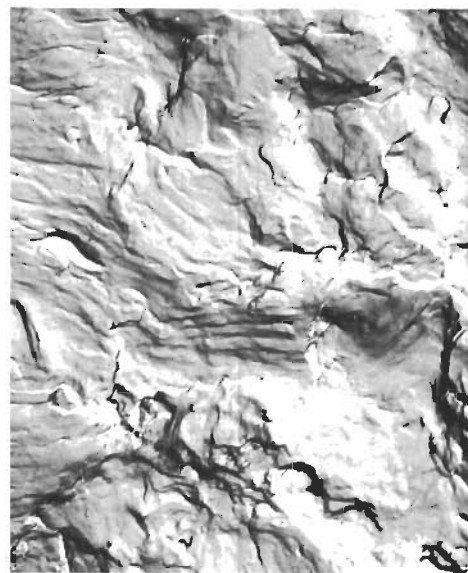
(A) TYPICAL AREA FROM PLANE STRAIN ZONE (1700x)



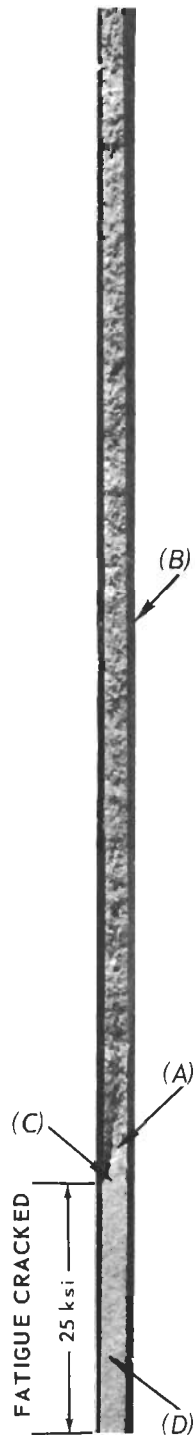
(B) DIMPLES FROM SHEAR LIP AREA (1700x)



(C) TRANSITION ZONE FROM FATIGUE TO RAPID FRACTURE (1700x)

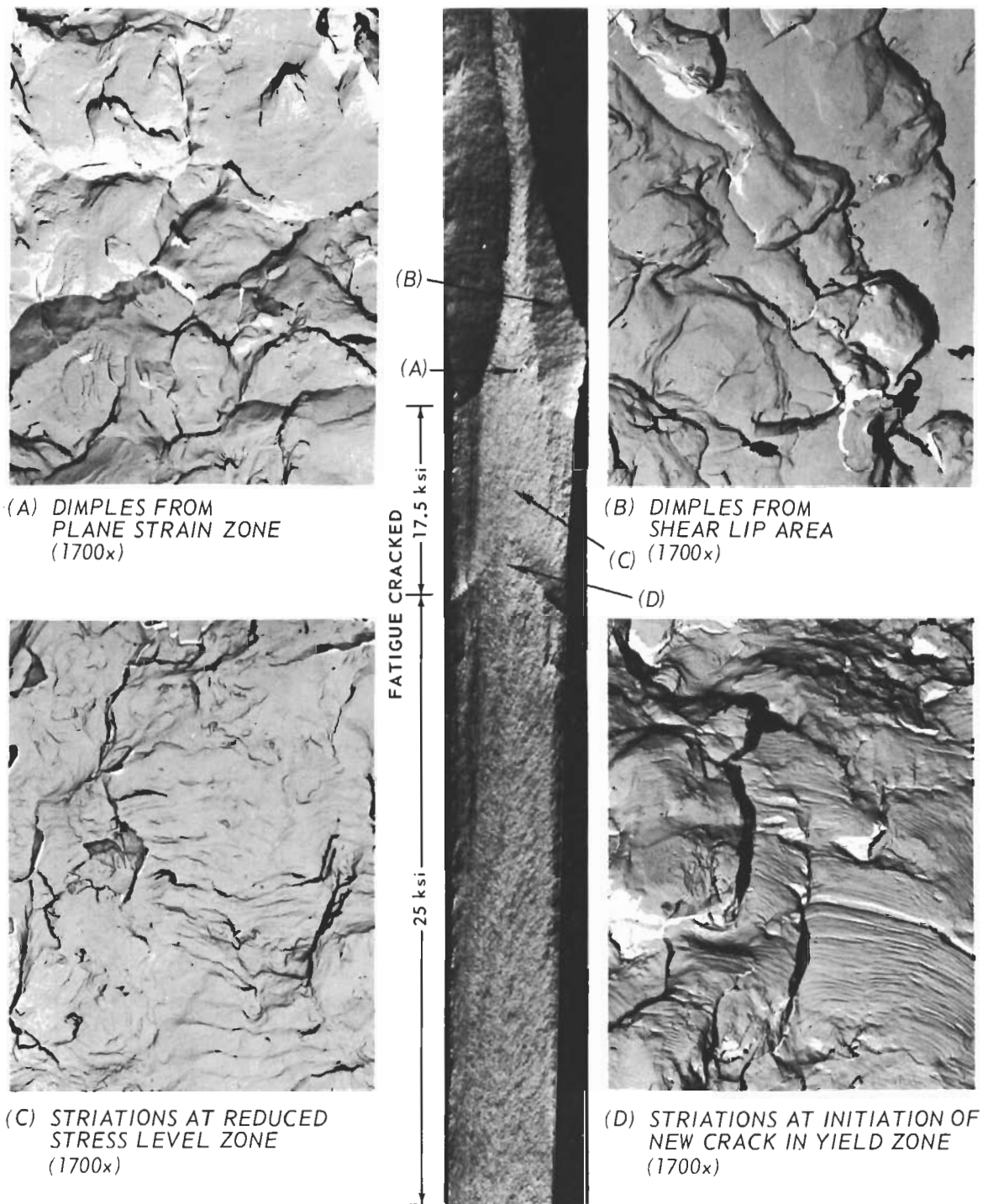


(D) TYPICAL STRIATIONS FROM FATIGUE AREA (1700x)



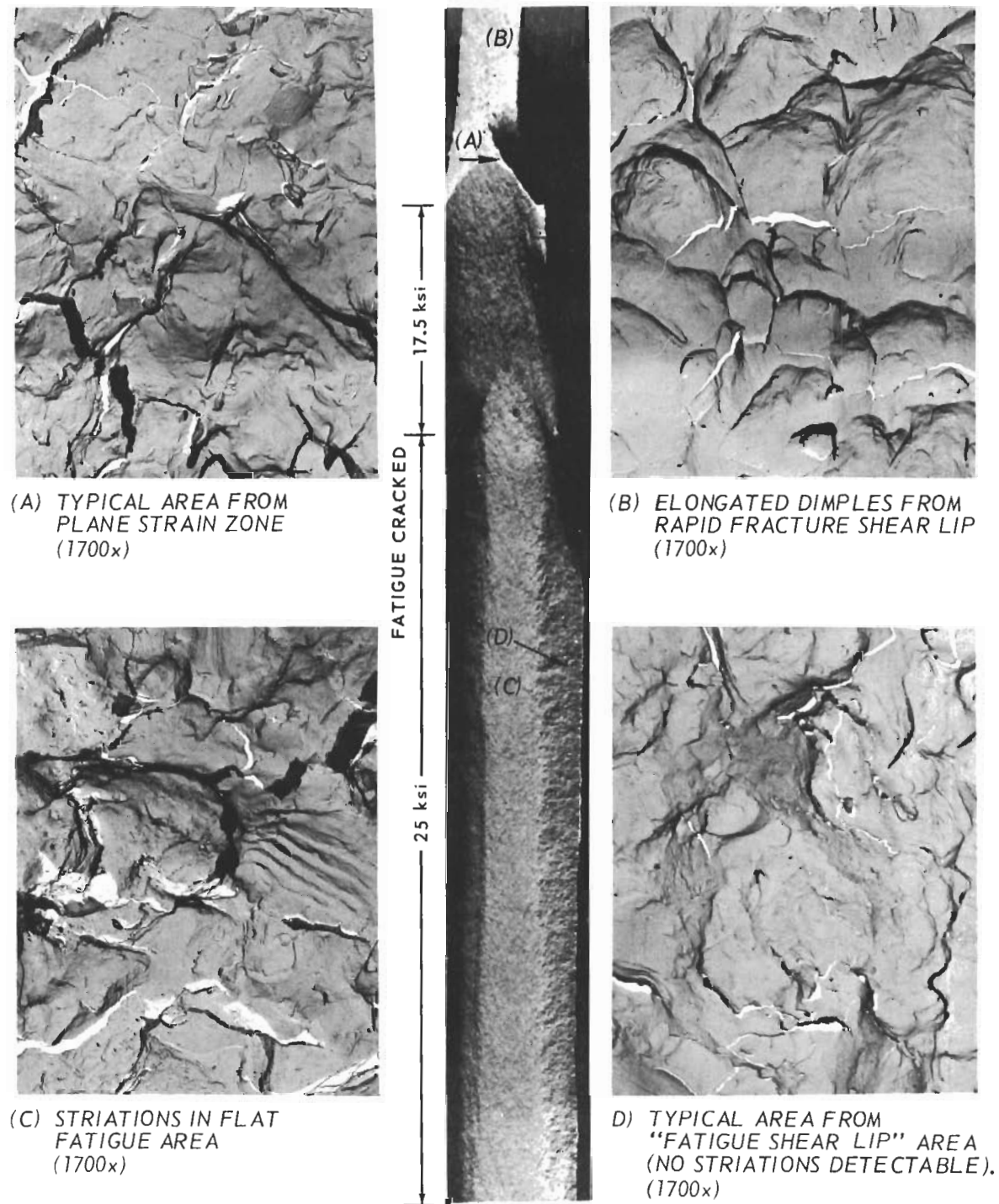
NOTE: Fatigue Cracked and Fractured at Room Temperature

FIG. 58 FRACTOGRAPHIC STUDY OF Ti 8Al-1Mo-1V SPECIMEN DA21



NOTE: Fatigue Cracked and Fractured at Room Temperature

FIG. 59 FRACTOGRAPHIC STUDY OF Ti 8Al-1Mo-1V SPECIMEN DA62



NOTE: Fatigue Cracked at Room Temperature and Fractured at 650°F

FIG. 60 FRACTOGRAPHIC STUDY OF Ti 8Al-1Mo-IV SPECIMEN DA64

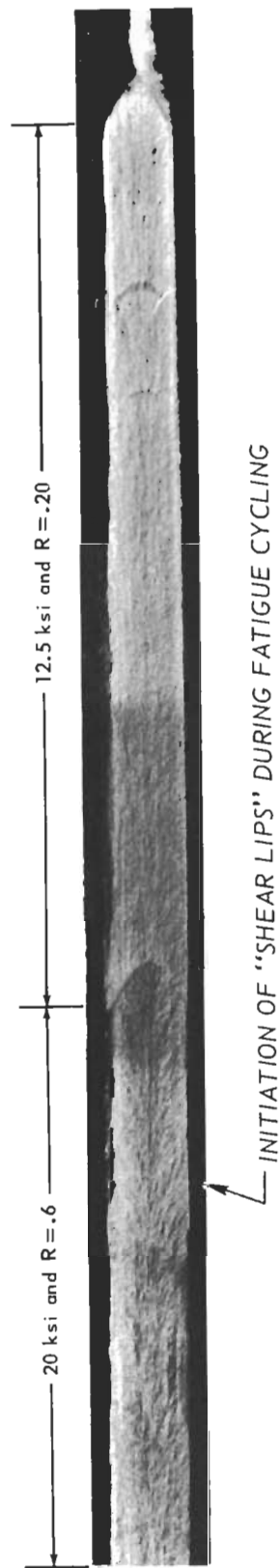


FIG. 61 MACROPHOTOGRAPH OF SPECIMEN DA 66 SHOWING FRACTURE MODE TRANSITION

replica mapping of this area to delineate the boundary area of fine striations would permit an estimate of the yield zone size for the 25 ksi stress level. The lower-left-hand micrograph shows the striation spacing in the reduced stress level zone.

Fig. 59 also shows that the dimples from the plane strain area have a slightly different appearance from those of the shear lip area. This difference is not as marked as it is for specimen DA21 shown in Fig. 58.

The macrophotograph in Fig. 59 also shows the transition from a completely plane strain fracture mode to a mixed plane stress-plane strain mode in the fatigue area. An estimate of the nominal plane strain fracture toughness parameter, K_{1CN} , can be made from the crack length where shear lips first appear on the fatigue portion of the fracture. With panel DA62, for example, $2a_0 = 3.50$ inches and K_{1CN} from the formula $K_{1CN} = \sigma_G \sqrt{\pi a_0}$ is 59.9 ksi $\sqrt{\text{inches}}$.

Fig. 60 shows fractographic results for a 24 x 72 x 0.200-inch panel fatigued cracked at room temperature and fractured at 650°F. Electron microscope surveys were made with replicas taken from both the flat and shear lip-type fatigue areas. The lower-left-hand micrograph shows the striations typical of the flat plane strain fatigue area. No striations were found on any of the shear lip-type fatigue area. The two upper micrographs again show a difference between the small triangular plane-strain rapid-fracture area and the shear-lip rapid-fracture area.

Fig. 61 contains a macrophotograph of the fatigue fracture surface from a 24 x 72 x 0.200-inch panel. Here, the fracture mode transition is shown for a 10 inch final crack length. Measurements of the surface fatigue crack length at the point of initiation of shear lips were made for several similar specimens. These measurements along with calculations of K_{1CN} are included in Table 10. The average value of K_{1CN} for the 12 panels is 45.6 ksi $\sqrt{\text{inches}}$. This value should be recognized as an estimate only. The stress ratio appears to have an effect on K_{1CN} . Higher values of R correspond to higher K_{1CN} values.

AM 350 STAINLESS STEEL

Chemistry and Mill Processing History

The chemical composition of the three heats of material are shown in Table 11 along with specification ranges. All elements meet the specification requirement when check analysis ranges are considered. Heat 55538 has a slightly higher phosphorous content than the other two heats. Both heats 19020 and 19207 have lower carbon contents than heat 55538. All the heats purchased were certified by Allegheny Ludlum to pass a salt spray stress corrosion test. This test utilizes longitudinal grain direction specimens stressed to 70 percent of the ultimate tensile strength. The material is guaranteed to pass one week of this exposure without cracking.

The following list describes the processing history for heats 19020 and 19207. Heat 55538 was purchased from warehouse stock and no history was available.

TABLE 10 ROOM TEMPERATURE PLANE STRAIN FRACTURE TOUGHNESS ESTIMATES FOR Ti 8Al-1Mo-1V

SPECIMEN NO.	THICKNESS inches	GRAIN DIRECTION	σ_M ksi	R	$2a_p$ FOR SHEAR LIP INITIATION inches	$K_{ICN} = \sigma_G \sqrt{\pi a_0} a$ ksi $\sqrt{\text{inches}}$
DA 55	.125	T	40	.20	.60	38.9
DA 56	.125	T	40	.05	.55	37.2
DA 57	.125	T	25	.20	1.60	40.5
DA 59	.200	L	40	.60	1.00	50.2
DA 60	.200	L	25	.20	2.80	52.8
DA 61	.200	L	20	.60	5.10	57.9
DA 62	.200	L	25	.60	3.50	59.9
DA 63	.200	L	12.5	.05	5.22	36.6
DA 64	.200	L	25	.05	2.05	44.9
DA 65	.200	L	12.5	.05	5.80	39.0
DA 66	.200	L	20	.60	5.00	57.1
DA 66	.200	L	12.5	.10	6.80	42.8
DA 72	.200	L	25	.20	2.10	45.5

AVERAGE $K_{ICN} = 45.6 \text{ ksi} \sqrt{\text{inches}}$

TABLE 11 VENDOR CERTIFIED CHEMICAL ANALYSES FOR 3 HEATS AT AM 350 (WEIGHT PERCENT)

HEAT NO.	C	Mn	P	S	Si	Cr	Ni	Mo	Fe	N
19020	.074	.76	.018	.010	.26	16.58	4.32	2.84	BAL.	.092
55538	.090	.71	.028	.010	.30	16.80	4.34	2.78	BAL.	.089
19207	.076	.70	.015	.009	.24	16.40	4.30	2.95	BAL.	.088
SPEC.	MIN.	.08	.50			16.00	4.00	2.50	BAL.	.07
	MAX.	.12	.04	.03	.50	17.00	5.00	3.25	BAL.	.13

- 1) Both heats were air melted in a 25-ton basic electric arc furnace using a two slag practice. A lime-alumina slag was used during the refining period.
- 2) The ingot size for heat 19020 was 19 x 35 inches; for heat 19207, 20 x 38 inches.
- 3) The ingots were charged hot into a pit at 2150 to 2180°F and held until uniform in temperature.
- 4) The 19 x 35-inch ingot from heat 19020 was rolled on a blooming mill to a section size of 8 to 12 inches thick and 29 inches wide and was reheated and rolled to a 5 x 29-inch slab. The 20 x 38-inch ingot from heat 19207 was similarly rolled to a section 8 to 12 inches thick and 36 inches wide, reheated, and rolled to a 5 x 34-inch slab.
- 5) The 5-inch slabs were over-all conditioned and cropped.
- 6) The conditioned slabs were heated to 2150 and 2180°F, rolled to a thickness of 0.8 to 1.0 inch on a Universal Mill, then continuously rolled to a 0.200-inch thick coil on a six stand hot tandem mill.
- 7) Cold rolling was carried out on a four-high United Reversing Mill with a final reduction of approximately 50 percent made in six passes.
- 8) Final annealing was done continuously at 1950°F for a time based on 100 minutes per inch of thickness.

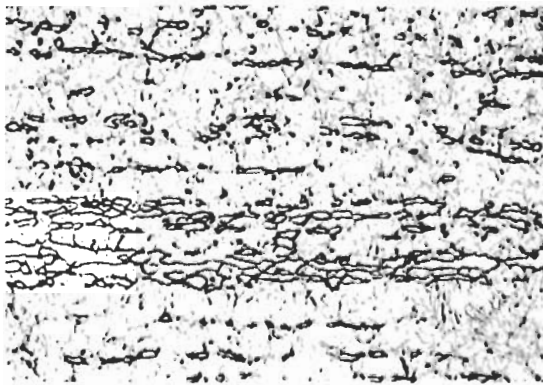
The foregoing process steps present a detailed account of the major steps involved in producing two of the three heats. It is probable that heat 55538 was processed in a similar manner. One point to be noted here is that this alloy has been rolled continuously in one direction from the 5-inch slab stage. For both the titanium alloys, hand-rolling methods were used so that reductions were probably made in both directions. Because of this mill-processing difference, the AM 350 alloy was expected to show a greater variation of structure sensitive properties with grain direction than the titanium alloys.

Microstructure

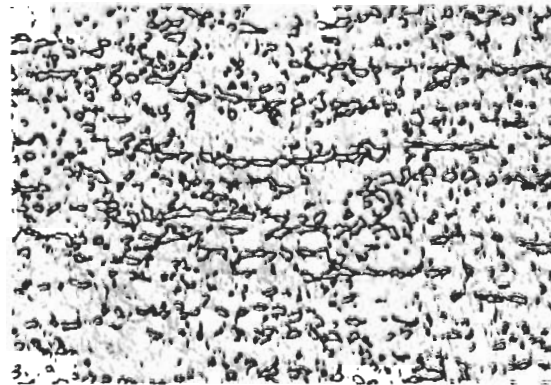
Typical microstructures for the three heats of AM 350 in the SCT 850 condition are shown in Figs. 62 and 63. Fig. 62 shows the variation between longitudinal and transverse grain directions for three thicknesses of heat 19020. A directionality effect is easily seen between the longitudinal and transverse grain directions for each thickness of material. The longitudinal sections show long stringers of delta ferrite. The transverse sections show that these stringers are flattened slightly in the plane of the sheet. These stringers increase in coarseness and spacing with increasing material thickness.

Fig. 63 shows the variation among the three heats of material at a thickness of 0.025 inch. There are no significant differences revealed in these microstructures among any of the heats. The variation between longitudinal and transverse sections resulting from the delta ferrite stringers is evident with

$t = .050$ INCHES

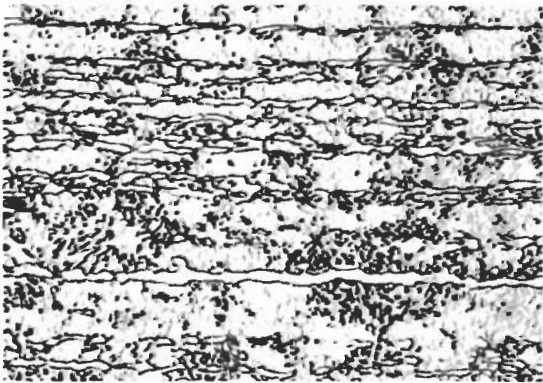


(A) LONGITUDINAL GRAIN (500x)

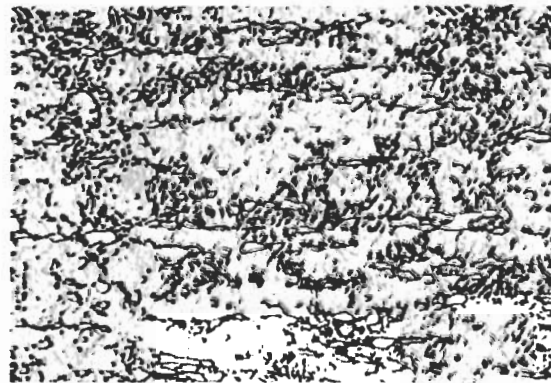


(B) TRANSVERSE GRAIN (500x)

$t = .093$ INCHES

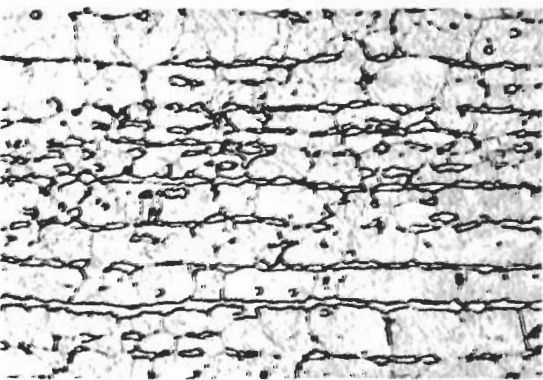


(C) LONGITUDINAL GRAIN (500x)

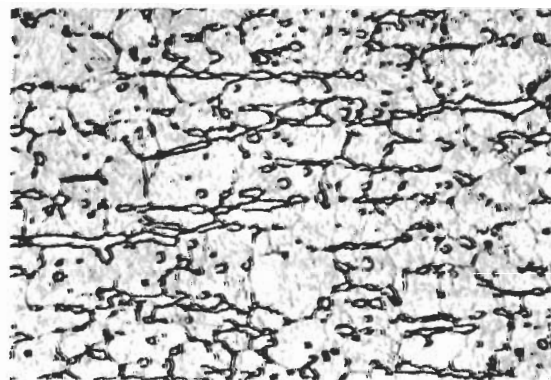


(D) TRANSVERSE GRAIN (500x)

$t = .125$ INCHES



(E) LONGITUDINAL GRAIN (500x)



(F) TRANSVERSE GRAIN (500x)

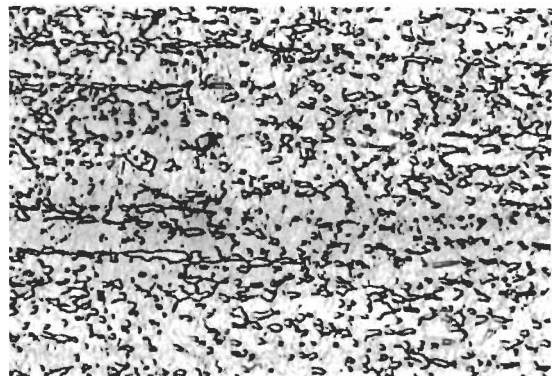
NOTE: Kallings Etchant

FIG. 62 PHOTOMICROGRAPHS OF AM 350 SHOWING THICKNESS VARIATION, HEAT 19020

HEAT 19207, $t = .025$ INCHES

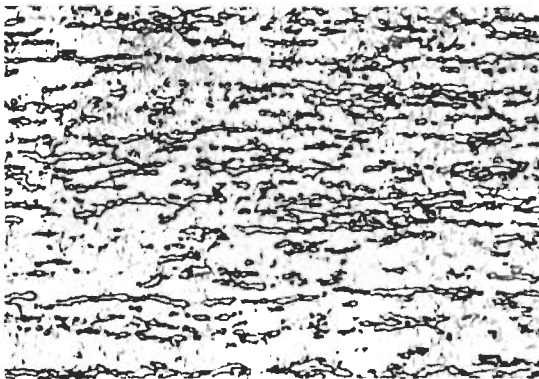


(A) LONGITUDINAL GRAIN (500x)

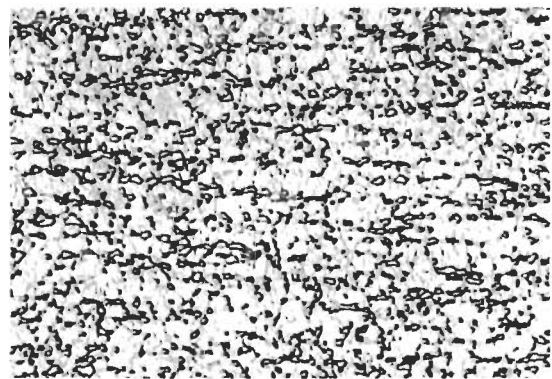


(B) TRANSVERSE GRAIN (500x)

HEAT 55538, $t = .025$ INCHES

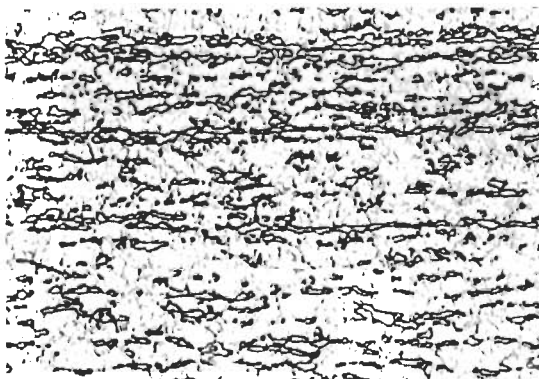


(C) LONGITUDINAL GRAIN (500x)



(D) TRANSVERSE GRAIN (500x)

HEAT 19020, $t = .025$ INCHES



(E) LONGITUDINAL GRAIN (500x)



(F) TRANSVERSE GRAIN (500x)

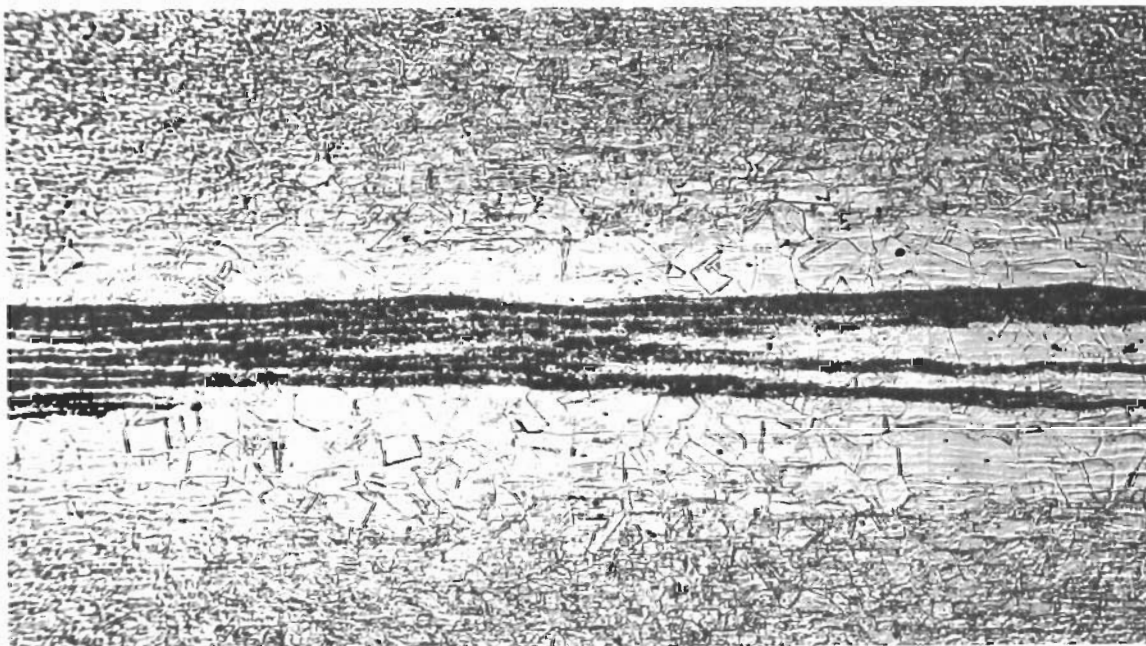
NOTE: Kallings Etchant

FIG. 63 PHOTOMICROGRAPHS OF AM 350, HEATS 19207, 55538 AND 19020

each of the heats. These stringers appear to be somewhat more discontinuous and closely spaced with this thickness of material, probably as a result of the greater reduction during rolling.

At the initiation of the project, segregation was found in some of the 0.125-inch thick sheets of AM 350. At the time, it was felt that this segregation which occurred near the center of the thickness dimension of the sheets would act only in a "mechanical" way within the structure; and hence, it would have a negligible effect on fracture toughness properties since the sheet would behave as a laminated sheet at these local segregation areas. Also, it was recognized from past experience with precipitation hardening stainless steels that this type of laminar segregation was often present in this family of alloys and could be considered typical of the alloy. In addition, the required tensile properties were achieved after the SCT 850 treatment with all of the thick material whether or not the segregation was present.

In the course of testing however, it was found that several panels of the 0.125-inch thick material behaved in an erratic manner. Several panels fractured during fatigue cracking at K levels of less than 100 ksi $\sqrt{\text{inches}}$. A brief metallurgical study was made on several of the fractured panels. In each case of premature fracture at relatively low K levels at room temperature, some segregated areas were found in the panel. A typical example is shown in Fig. 64.



NOTE: Kalling's Etchant (200x) $t = .125$ INCH

FIG. 64 PHOTOMICROGRAPH SHOWING SEGREGATION IN AM 350, HEAT 19020

Two brief studies were carried out to determine what elements were present in this segregation band and to qualitatively determine their effect on fracture properties. An electron microprobe analysis was made across this segregated area with an ARL model microprobe. Traverses were made for the following elements: Cu, Cr, Cb, Fe, Mg, Mo, Mn, P, S, Si, Ti. The only significant variation was found with Cr, Fe and Cb. The band was found to be higher in Cr and Cb and lower in Fe.

Several bend specimens were cut from a fractured panel containing segregated areas. Some were re-heat-treated using a one-half hour, 1950°F, H-annealing treatment followed by the standard SCT treatment. The bend test results showed that the re-heat-treated material had twice the toughness (as measured by the area under the load-deflection curves) of the material with the original heat treat. From these qualitative tests, it appeared that the segregation was caused in part by an insufficient solution treatment.

Two of the panels which broke during fatigue cycling were re-solution-heat-treated at 1950°F and welded to small pieces of excess AM 350 material to make 24 x 72 inch panels (DB59X and DB73X in the tabular data). These were then given the standard SCT 850 treatment.

None of the other thick fracture panels were re-heat-treated with a 1950°F annealing treatment since this would have introduced a variable which would have complicated the planned comparisons. Also, the original SCT 850 treatment was considered "standard" for this alloy and the test results obtained would be typical of this standard treatment. Many of the large panel tests showed that high K_{IC} values could be attained with most of the tests.

Tensile Properties

Tensile properties representing the three heats of AM 350 (SCT 850) over the temperature range -110 to 650°F are included in Table 12. The tensile ultimate and yield strength values are relatively constant for the three heats and for the four thicknesses of one heat. The elongation values are slightly below the specification guarantee of 10 percent for the longitudinal grain direction for heat 55538. Otherwise, the elongation met or exceeded the 10 percent value in each case. Transverse and longitudinal tests show no significant differences. One interesting result shown in Table 12 which has been previously observed is that the tensile ultimate strength increases slightly as the test temperature is raised from 400 to 650°F. This change is probably the result of a metallurgical precipitation process which may cause some degree of instability at elevated temperature.

Tensile test results from specimens cut from the failed halves of the exposed fracture panels are also included in Table 12. There appears to be no significant difference between exposed and unexposed tensile properties.

Crack Propagation Results

Crack Growth Data

Crack propagation data are plotted as crack length versus cycles curves for

TABLE 12 TENSILE TEST DATA FOR AM 350

HEAT NO.	NOMINAL THICKNESS inches	GRAIN DIRECTION	TEST TEMPERATURE											
			-110° F			R. T. (68° F)			400° F			650° F		
			F _{TU} (ksi)	F _{TY} (ksi)	ELONG.*	F _{TU} (ksi)	F _{TY} (ksi)	ELONG.*	F _{TU} (ksi)	F _{TY} (ksi)	ELONG.*	F _{TU} (ksi)	F _{TY} (ksi)	ELONG.*
19207	.025	T	223.2	—	10.0	201.1	176.7	10.5				175.9	137.9	5.5
	.025	T				202.3	177.7	9.5				176.1	136.7	4.5
	.025	L	226.2	205.6	12.5	203.6	178.8	10.0				180.4	141.2	5.5
	.025	L				204.8	179.8	11.0				180.4	140.8	6.0
55538	.025	T	230.8	208.8	—	212.0	183.8	9.5				191.9	145.9	5.5
	.025	T				211.2	182.2	9.0				191.9	143.1	5.5
	.025	L	228.0	205.3	—	211.4	182.3	9.5				186.6	140.7	
	.025	L				210.9	182.1	9.5				193.5	141.1	
19020	.025	T	226.9	203.1	14.0	206.9	177.6	9.5	184.4	148.0	5.5	185.8	141.5	4.5
	.025	T				206.0	177.4	11.0	176.1	143.8	6.5			
	.025	L	222.3	200.0	13.0	207.0	179.1	10.0	181.7	146.4	7.5	188.2	135.3	6.0
	.025	L				204.9	189.6	10.5	182.0	146.8	6.5			
	.050	T	227.2	202.7	10.0	209.3	177.4	9.5	187.6	148.2	6.5	189.1	135.2	4.5
	.050	T				209.8	180.3	10.0						
	.050	L	227.3	206.8	16.0	208.7	177.3	11.0	190.2	150.0	7.5	193.7	137.8	6.5
	.050	L	230.5	203.5	16.5	209.0	177.5	11.0	188.2	149.2	9.0	193.7	141.5	7.5
	.093	T	225.1	199.5	15.0	199.7	170.9	10.5				182.3	145.4*	7.0
	.093	T				200.0	169.6	11.0						
	.093	L	228.4	197.4	17.5	199.5	169.5	11.5				183.8	131.6	6.0
	.093	L				201.2	171.0	12.0						
	.125	T	218.3	190.3	13.0	200.6	167.0	12.0	180.7	141.7	9.0	184.3	132.0	8.5
	.125	T				200.9	168.0	12.0				182.9		9.5
	.125	L	220.0	195.2	15.5	200.6	167.5	13.5	180.7	138.6	10.0	182.9	134.7	10.0
	.125	L	218.1	188.1	15.0	200.4	167.7	13.0	180.5	143.2	10.0	183.1	134.0	10.5

* ELONGATION MEASURED AS % IN 2 INCHES.

TABLE 12 TENSILE TEST DATA FOR AM 350 (continued)

HEAT NO.	NOMINAL THICKNESS inches	GRAIN DIRECTION	TEST TEMPERATURE												
			-110° F			R. T. (68° F)			400° F			650° F			
			F _{TU} (ksi)	F _{TY} (ksi)	ELONG.*	F _{TU} (ksi)	F _{TY} (ksi)	ELONG.*	F _{TU} (ksi)	F _{TY} (ksi)	ELONG.*	F _{TU} (ksi)	F _{TY} (ksi)	ELONG.*	
19020**	.025	T				208.0	180.0	9.0							
		T				208.0	178.4	8.0							
	.050	T				214.2	—	9.5							
		T				214.4	183.2	9.5							
	.125	T				208.6	175.3	11.0							
		T				207.5	171.9	11.5							

* ELONGATION MEASURED AS % IN 2 INCHES.

** AFTER EXPOSURE AT 650° F FOR 1000 HOURS AT A GROSS STRESS LEVEL OF 40 ksi

the 24 x 72-inch panels in Figs. 65 through 71; and for the 8 x 24-inch panels in Figs. 72 through 74. Fig. 75 includes the crack growth curves for the exposed panels. All data were gathered at room temperature at a cycling frequency of 120 cpm.

As pointed out in Section 6, the final increment of crack growth for each specimen was carried out at $R = 0.20$ and at a stress level to produce a final K of approximately 75 ksi $\sqrt{\text{inches}}$. For the 24 x 72-inch panels, the 3-inch final crack lengths were grown from 2.5 inches at stress levels of 32 to 40 ksi; the 6-inch final crack lengths were grown from 5.25 inches at stress levels of 24 or 28 ksi; and the 10-inch final crack lengths were grown from 9 inches at stress levels of 15 or 20 ksi. The final crack tip preparation for the 8 x 24-inch panels was carried out at stress levels of 36 or 40 ksi.

A discontinuity was nearly always noted on the crack length cycles curves at the point of stress level change. Crack growth was retarded by dropping to a lower stress level (see specimen DB22, Fig. 67), and accelerated in raising to a higher stress level. (See Fig. 69).

Some of the large transverse grain direction specimens showed erratic behavior during cyclic cracking (See Fig. 66 and 71) with unexpected fracturing occurring in some cases.

From these crack growth curves, several observations can be made. The cycles required to grow a given crack length decrease with an increase in the gross stress level. The cycles required to grow a given crack length decrease with a decrease in the stress ratio. The cycles required to grow a given crack length are reduced for the transverse grain direction.

Crack Growth Rate Data

The AM 350 crack growth rate data are plotted as K versus rate curves for all the unexposed panels in Figs. 76 through 83. Fig. 76 shows a comparison for 24 x 72-inch panels between longitudinal and transverse grain directions at $R = 0.20$. These curves show that cracks in the transverse grain direction panels propagate at a much faster rate than in the longitudinal grain panels. Fig. 76 also shows that the rate data for both the 8-inch wide and 24-inch wide panels falls on the same curve. Similar effects of grain direction on crack growth rate are shown in Figs. 79, 80, 81 and 82. In general the transverse grain direction has the higher propagation rate, but several specimens (DB30 in Fig. 79 and DB44 in Fig. 81) do not fall directly on the curves. One of the reasons for this is that cracks grew somewhat erratically in some cases and caused some difficulty in deriving growth rate data from the crack length-cycles curves.

Higher R values result in slower cracking rates when comparisons are made at constant K levels. This result is illustrated in Figs. 77 and 79. The greatest difference is evident by a comparison of the R values of 0.60 and 0.05, 0.10, and 0.20. Cracking rates for R values of 0.05, 0.10, and 0.20 all fall in a relatively narrow scatter band for longitudinal grain direction specimens (see Figs. 78 and 83). Fig. 83 shows that there is essentially no difference in crack growth rates for the range of thicknesses studied (0.025 inches to 0.125 inches).

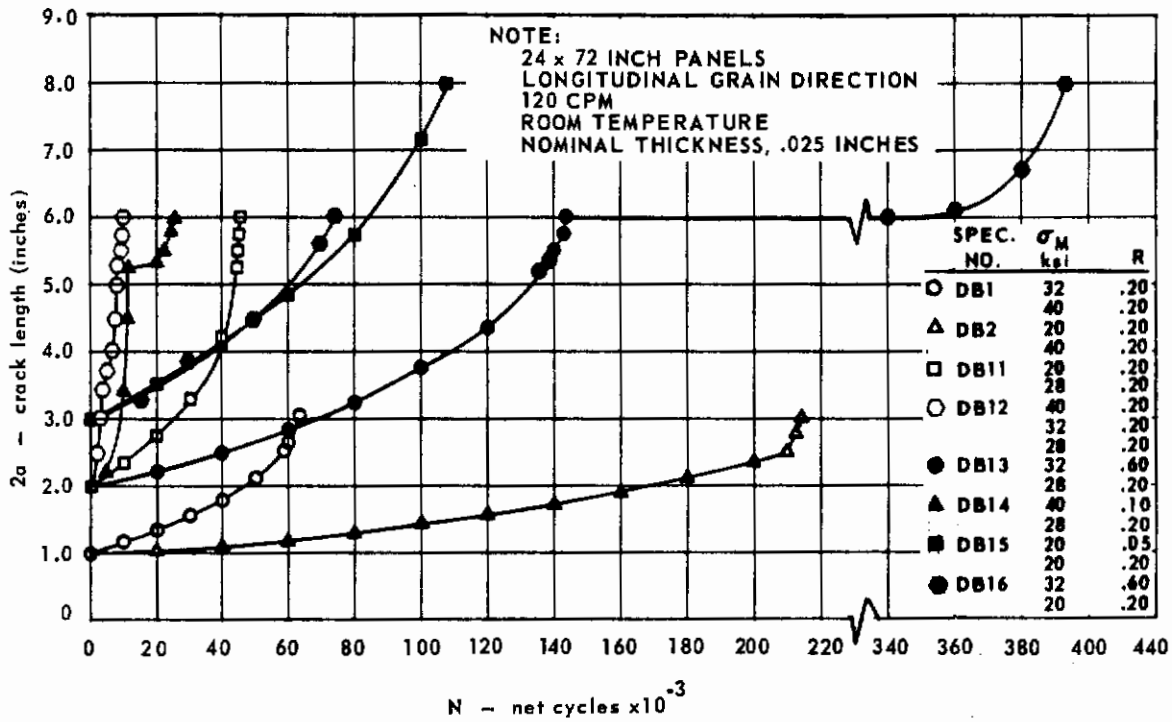


FIG. 65 CRACK GROWTH DATA FOR AM 350, HEAT 19207

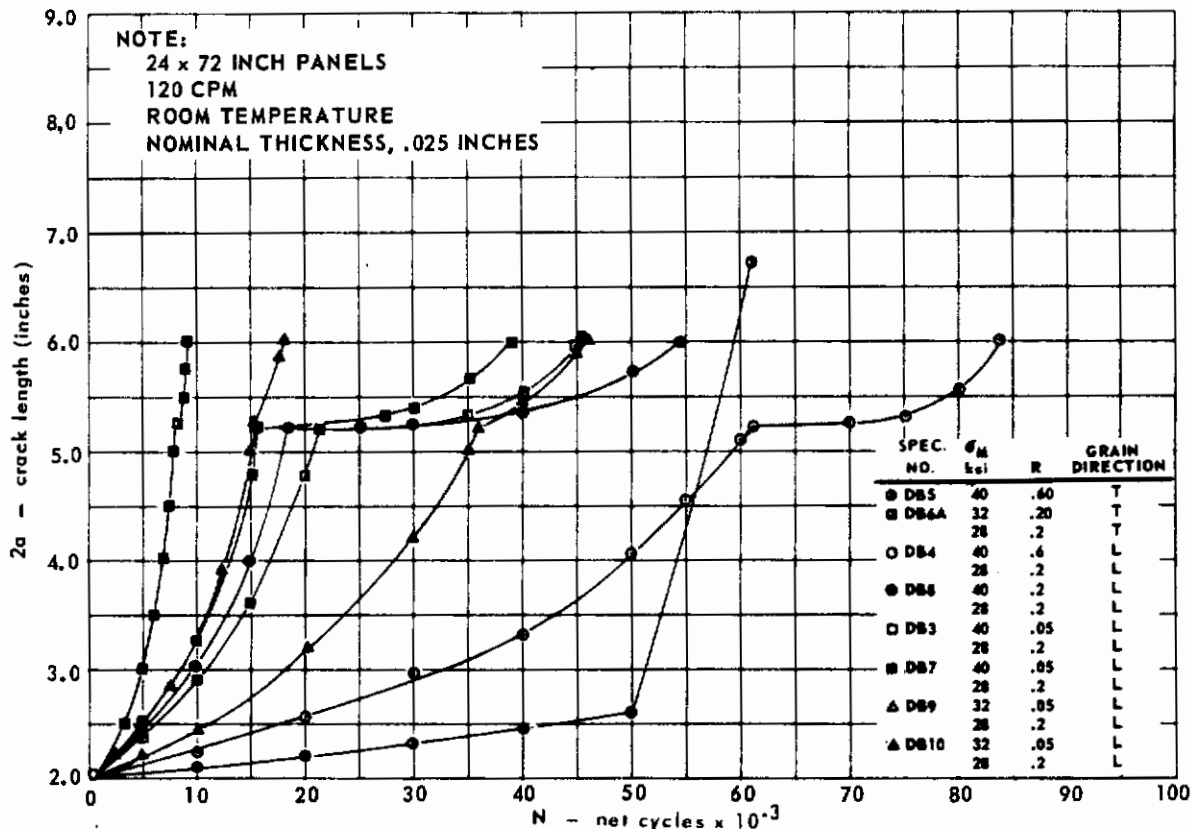


FIG. 66 CRACK GROWTH DATA AM 350, HEAT 19207

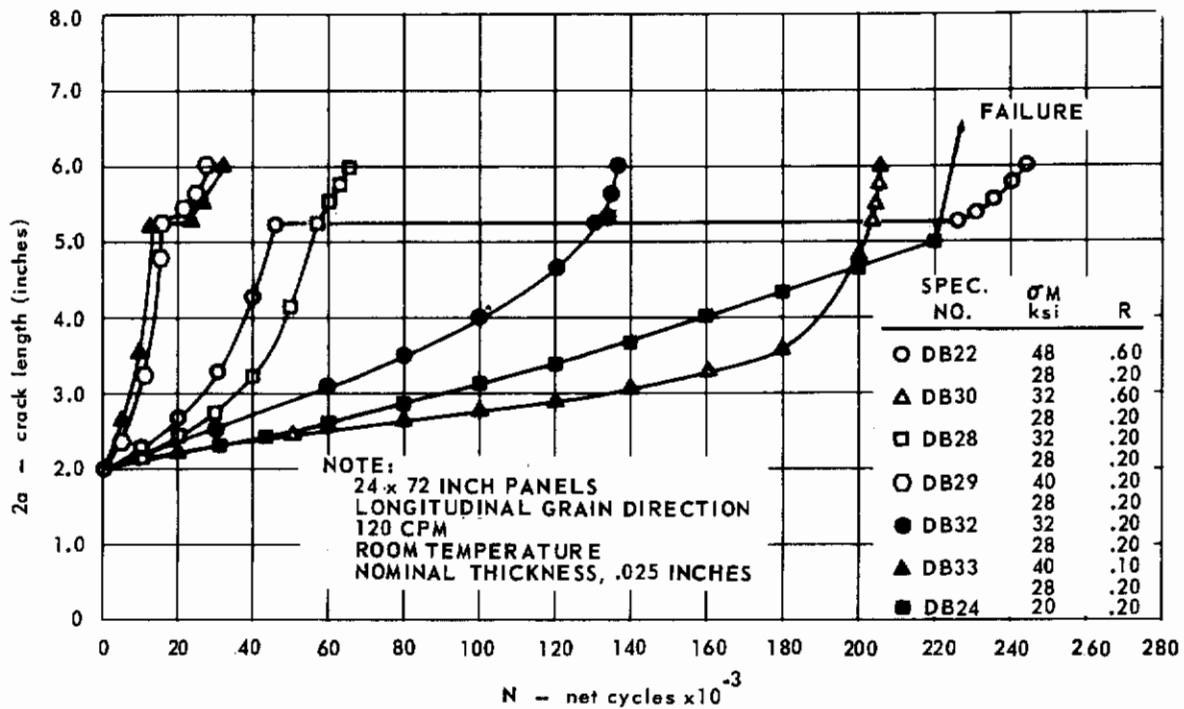


FIG. 67 CRACK GROWTH DATA FOR AM 350, HEAT 55538

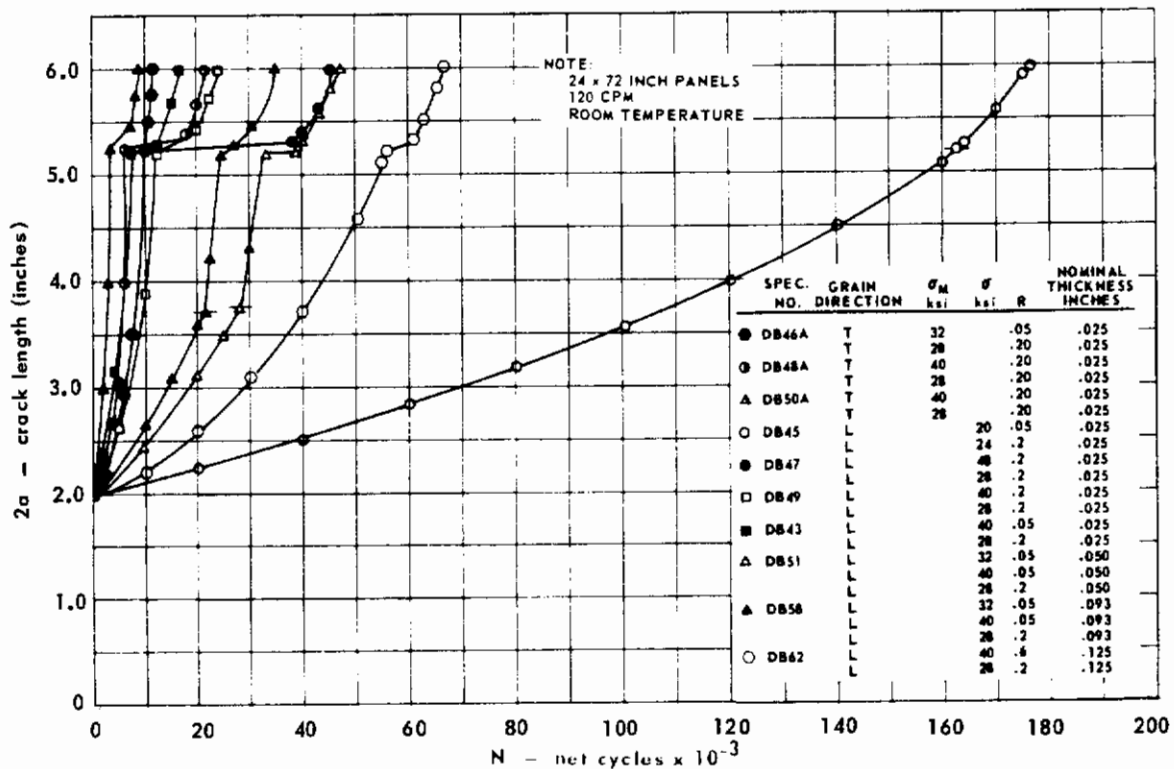


FIG. 68 CRACK GROWTH DATA AM 350, HEAT 19020

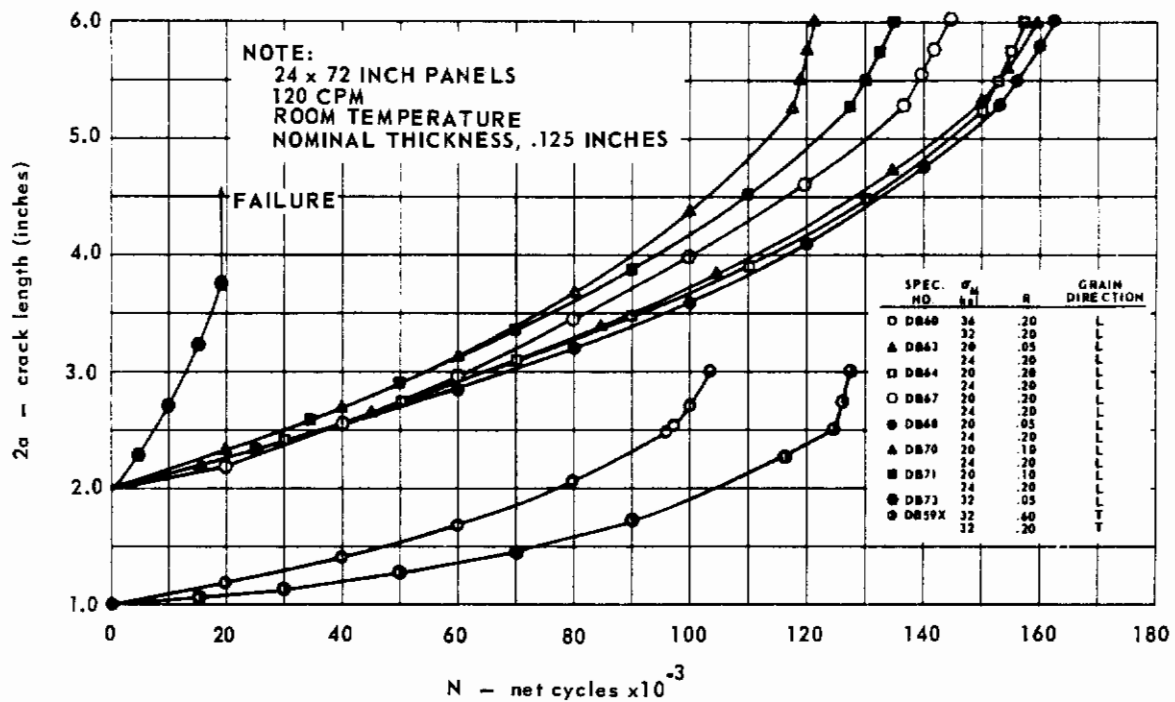


FIG. 69 CRACK GROWTH DATA FOR AM 350, HEAT 19020

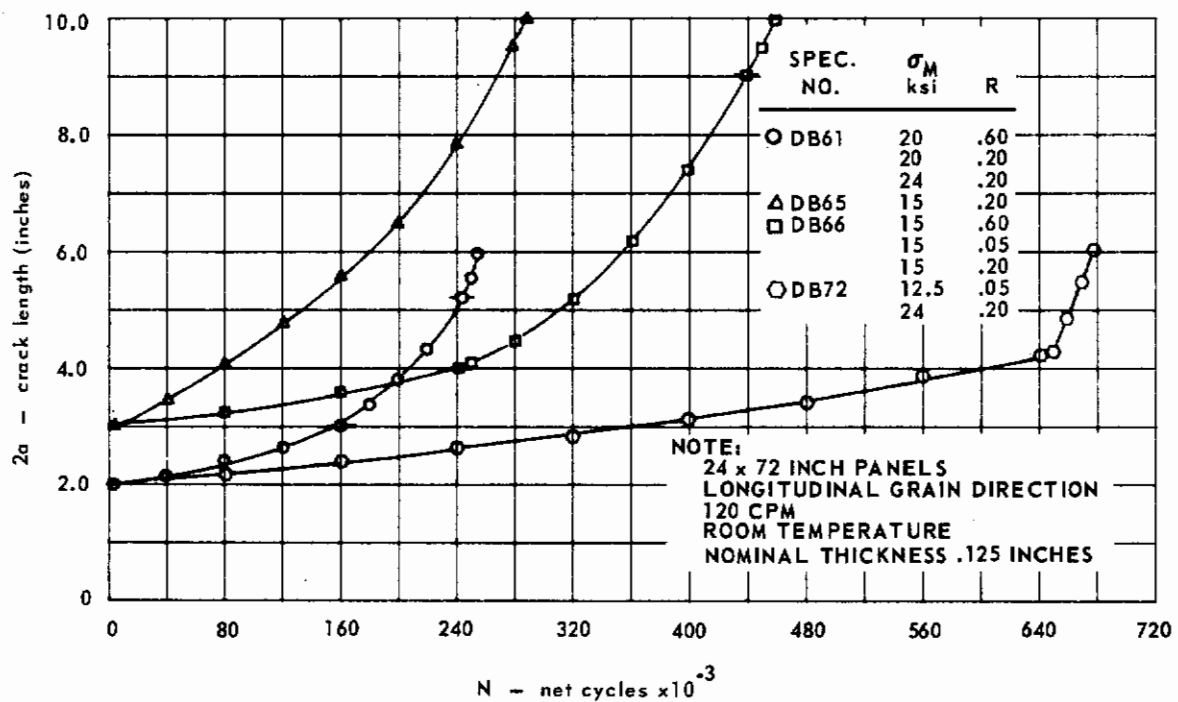


FIG. 70 CRACK GROWTH DATA FOR AM 350, HEAT 19020

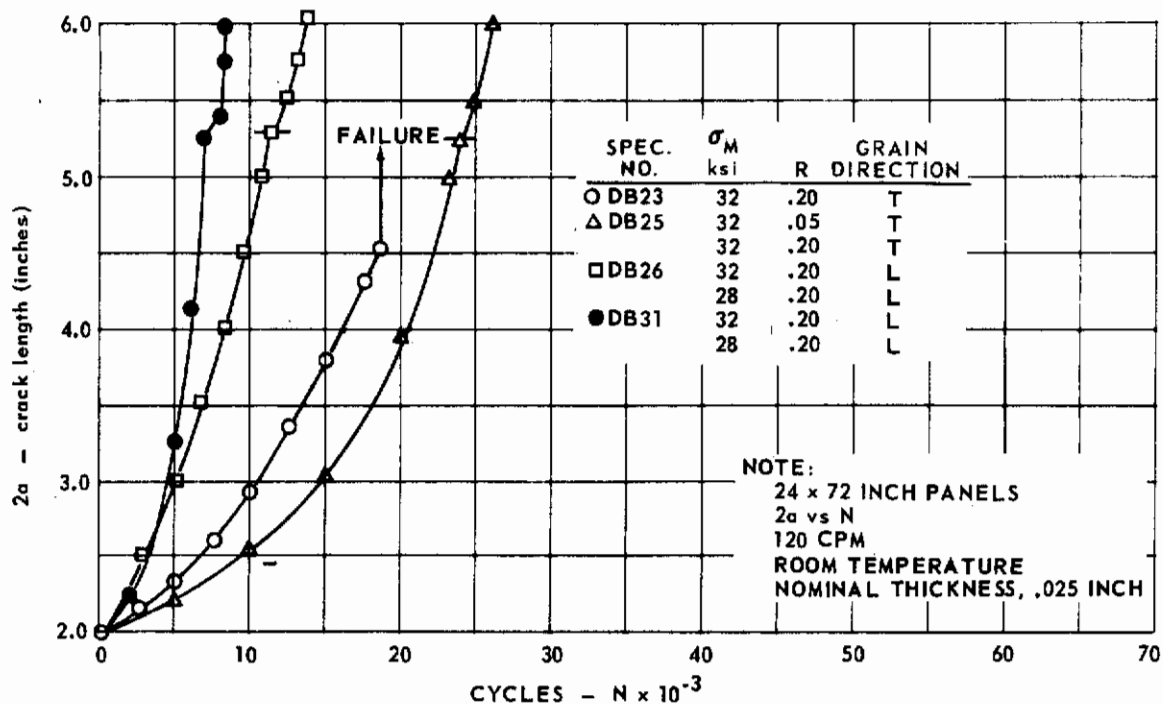


FIG. 71 CRACK GROWTH DATA FOR AM 350, HEAT 55538

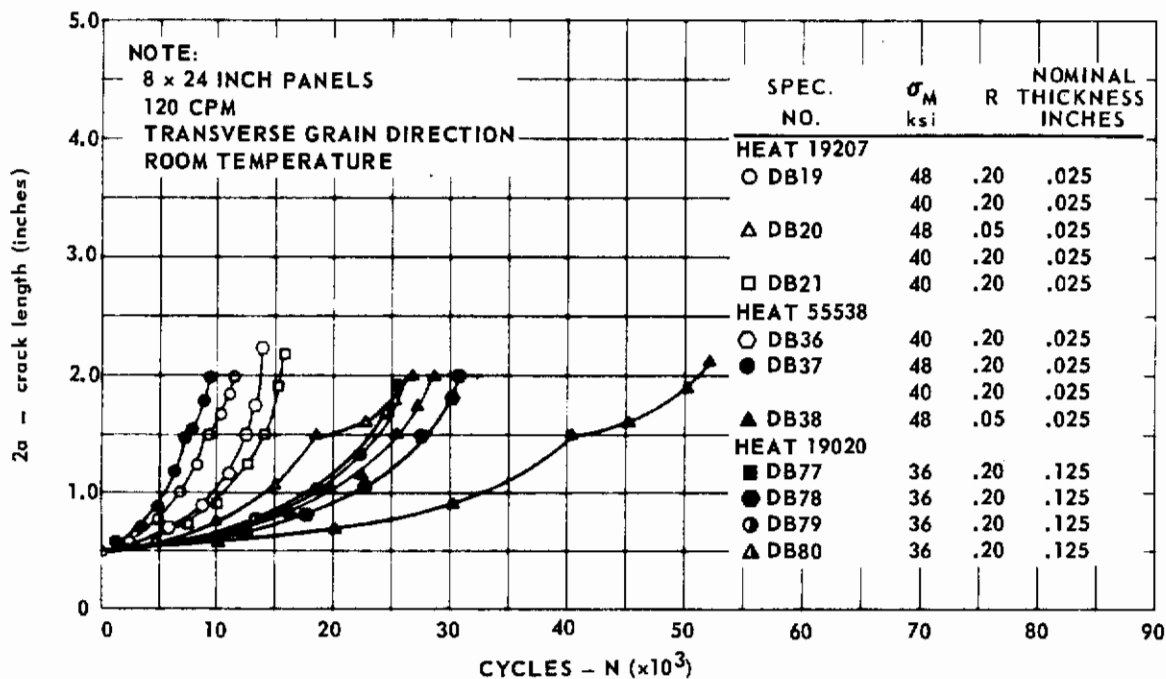


FIG. 72 CRACK GROWTH DATA FOR AM 350, HEATS 19020, 19207 AND 55538

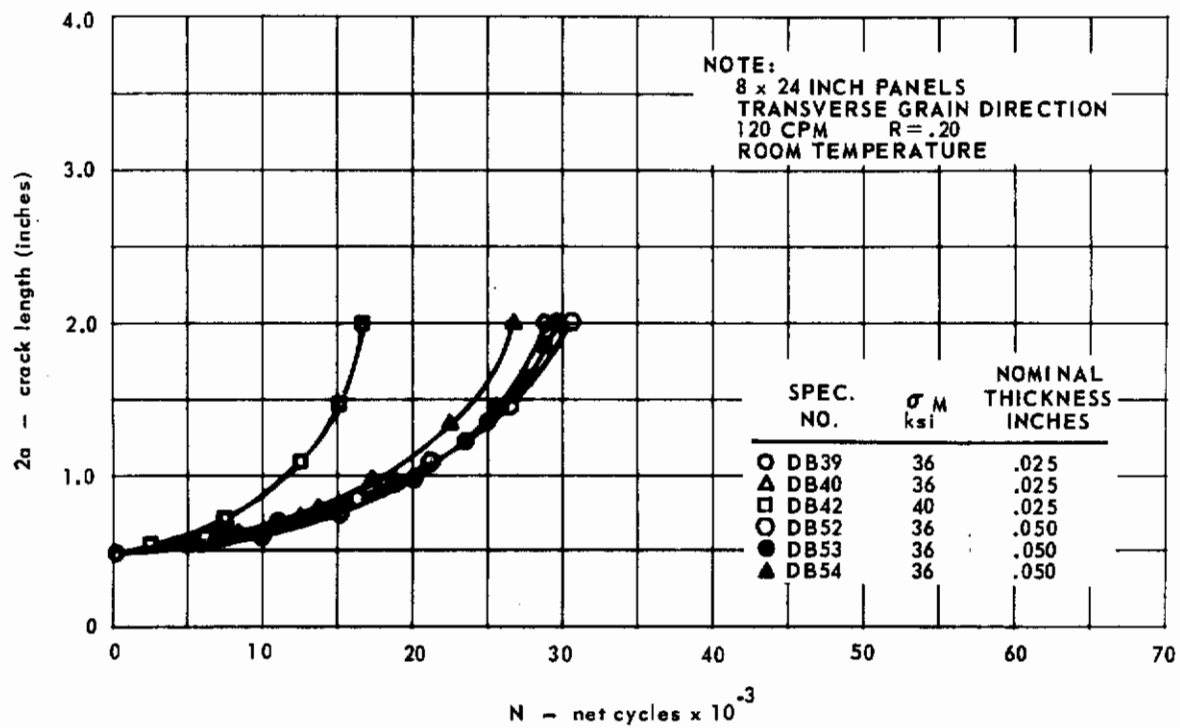


FIG. 73 CRACK GROWTH DATA FOR AM 350, HEAT 19020

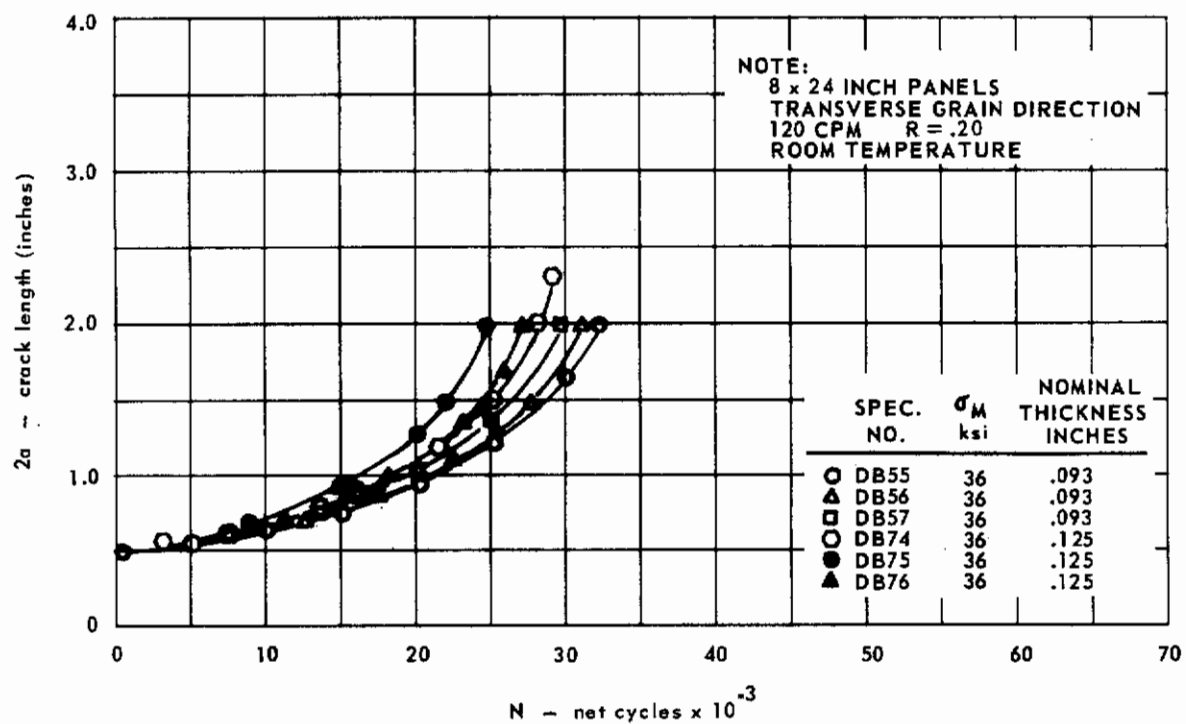


FIG. 74 CRACK GROWTH DATA FOR AM 350, HEAT 19020

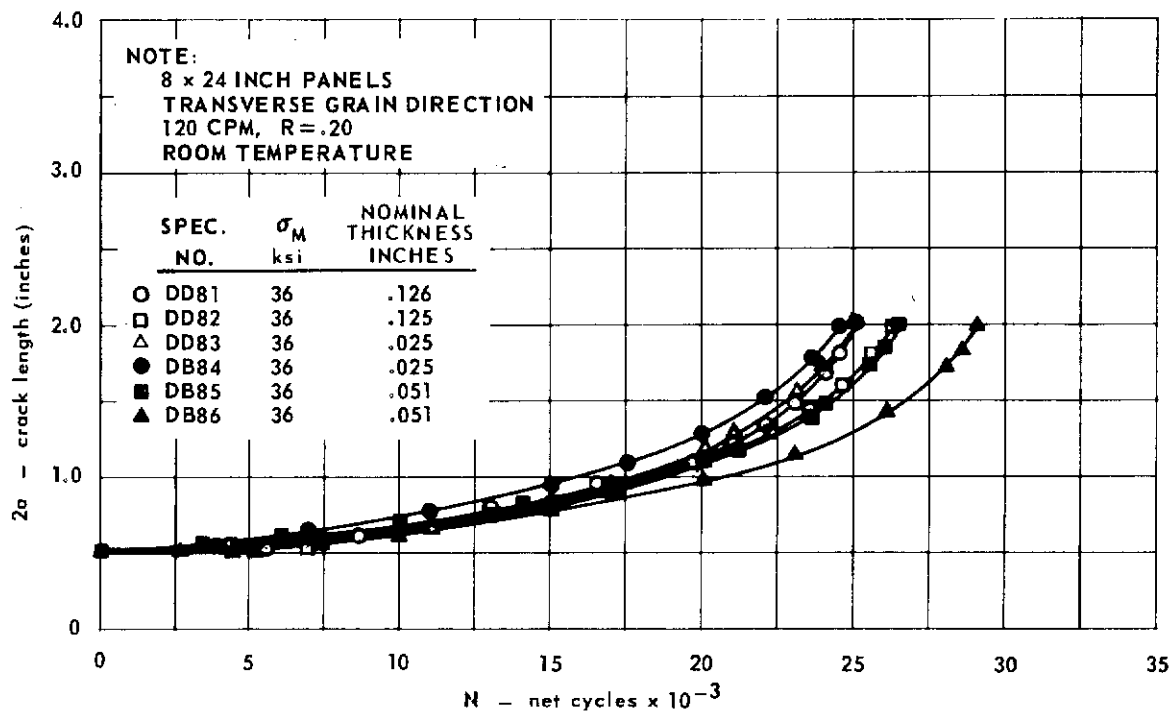


FIG. 75 CRACK GROWTH DATA FOR EXPOSED AM 350 PANELS, HEAT 19020

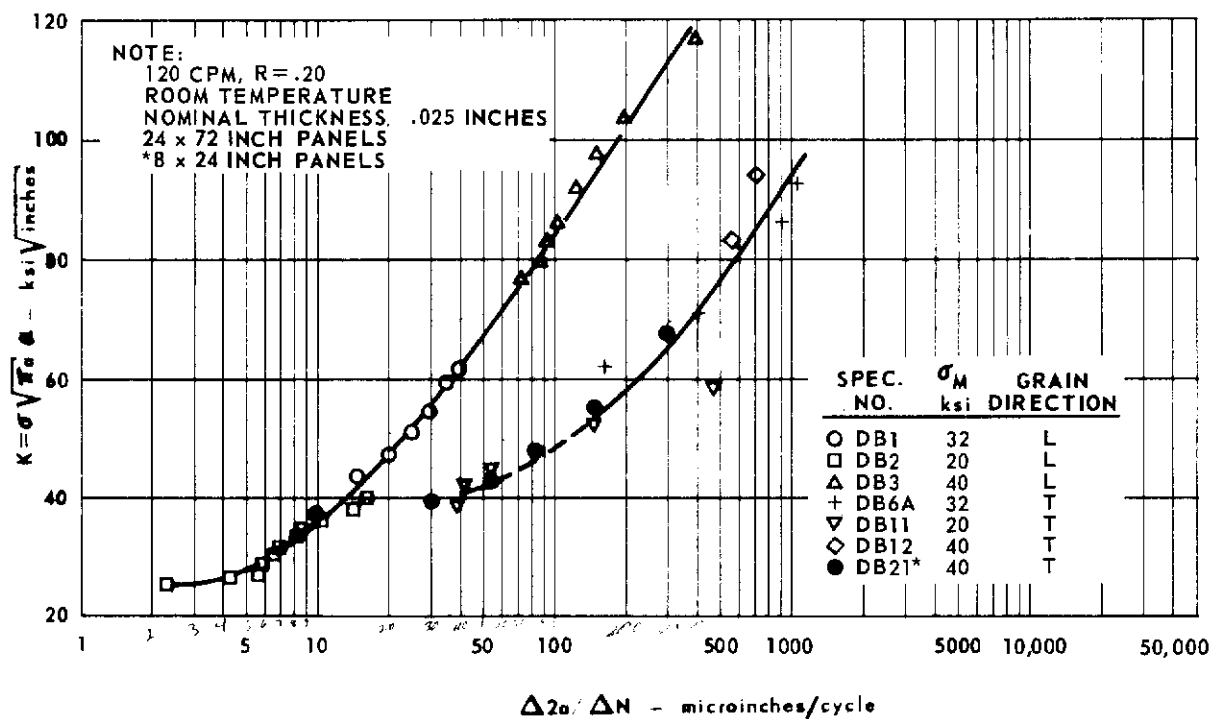


FIG. 76 CRACK GROWTH RATE DATA FOR AM 350 (SCT 850) HEAT 19207

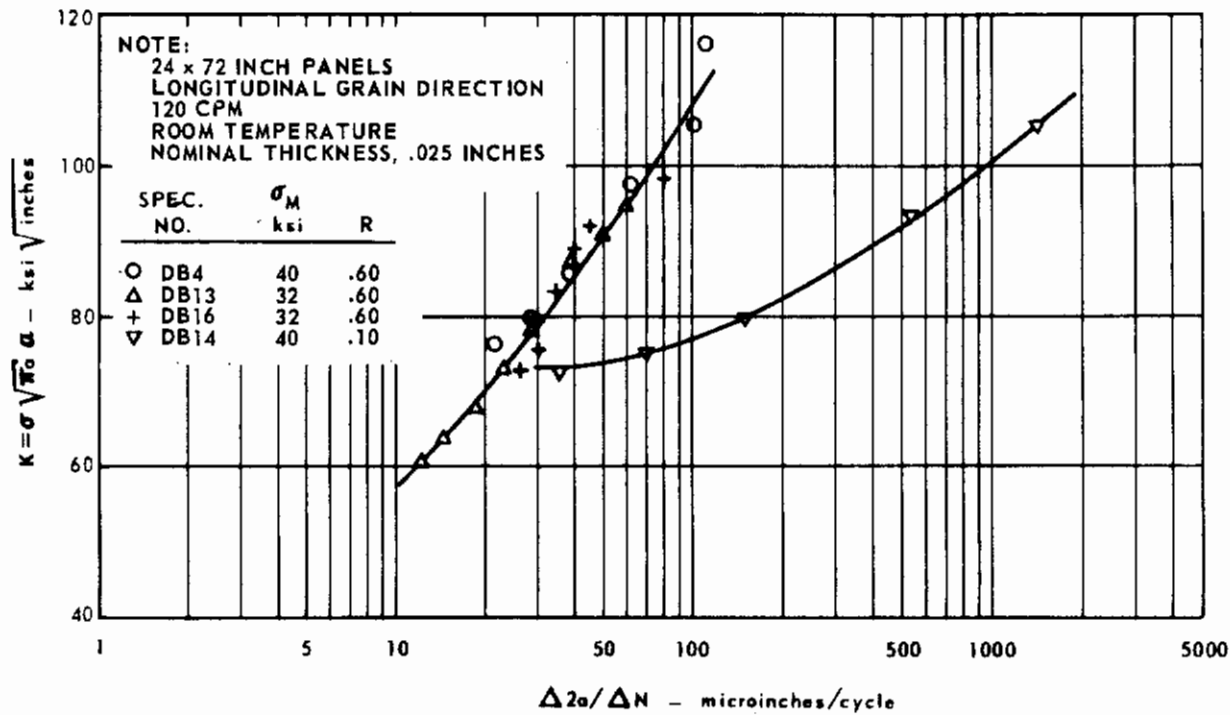


FIG. 77 CRACK GROWTH RATE DATA FOR AM 350 (SCT 850) HEAT 19207

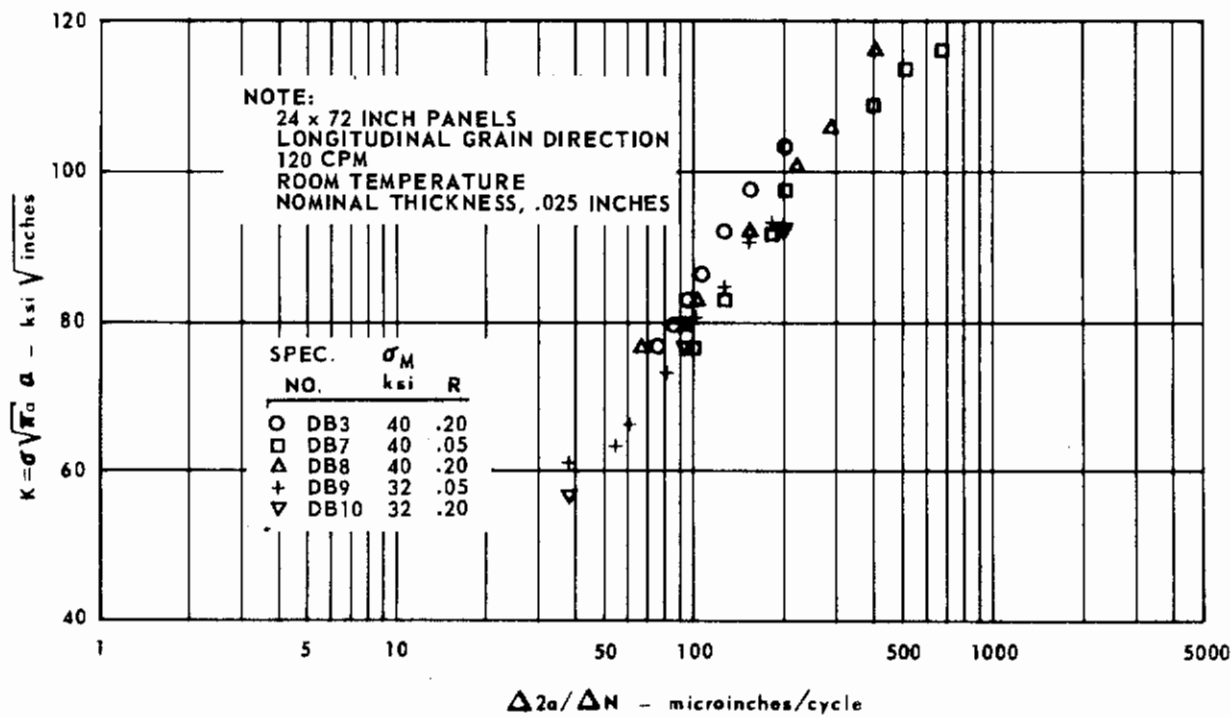


FIG. 78 CRACK GROWTH RATE DATA FOR AM 350, HEAT 19207

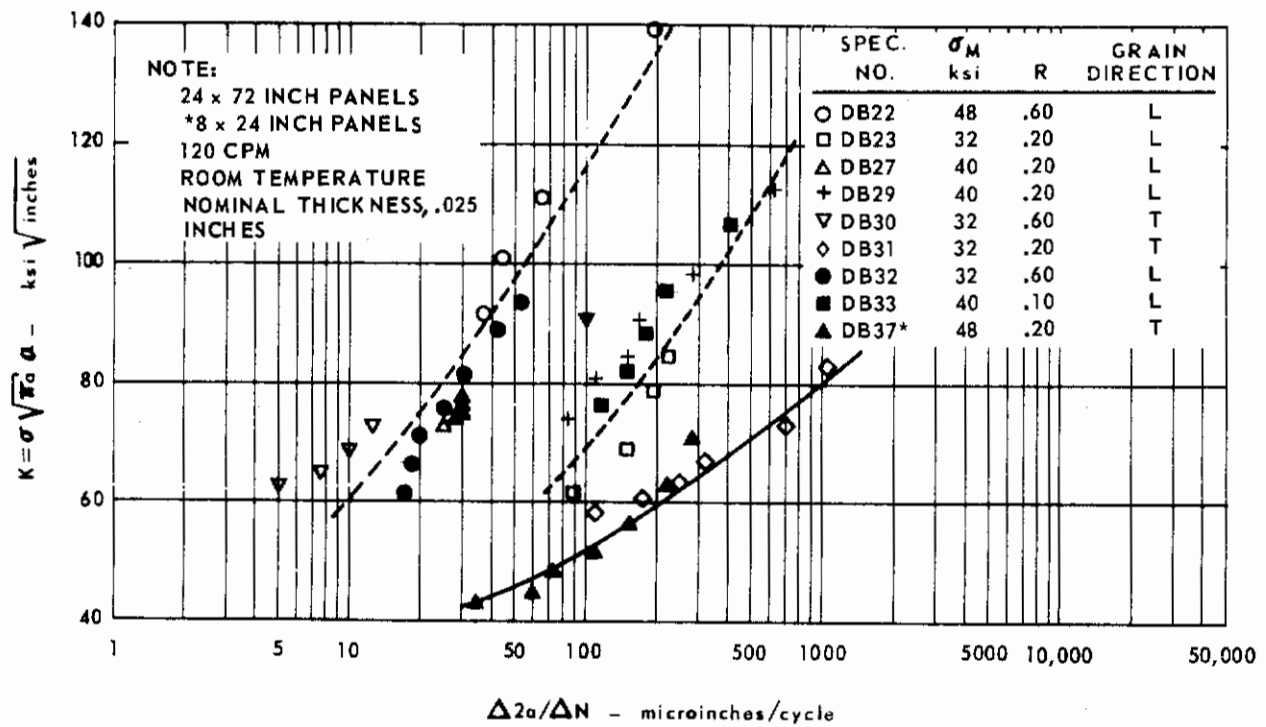


FIG. 79 CRACK GROWTH RATE DATA FOR AM 350, HEAT 55538

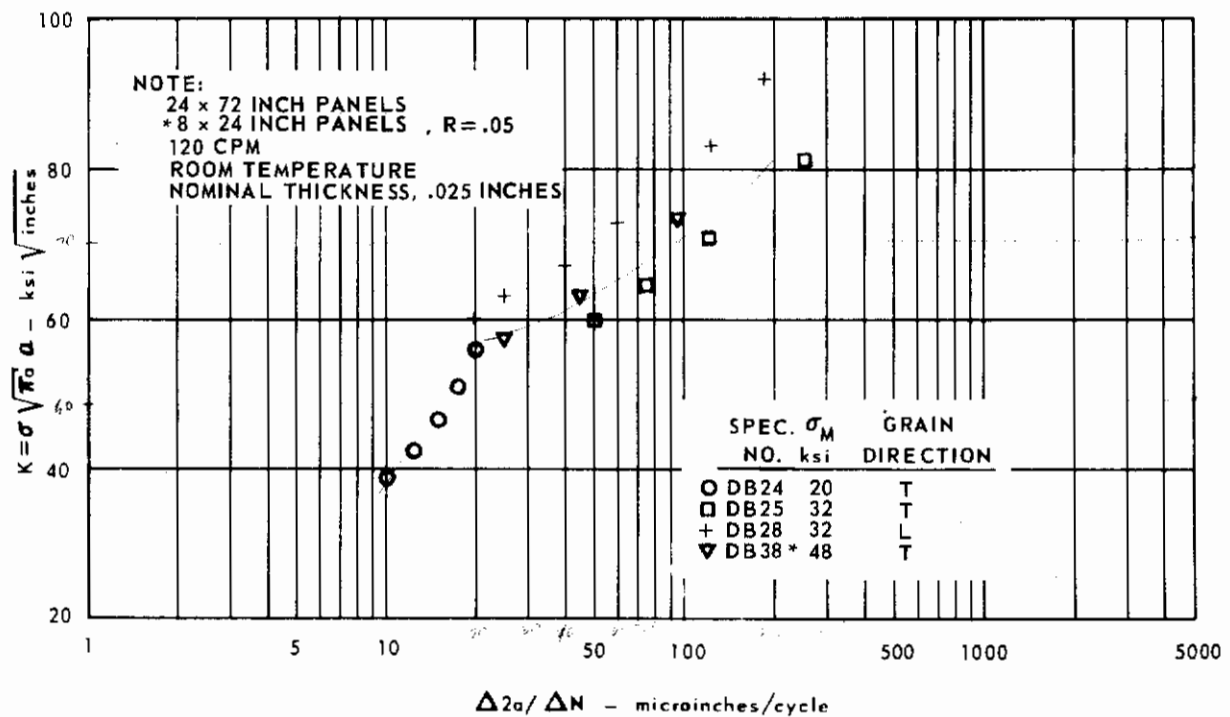


FIG. 80 CRACK GROWTH RATE DATA FOR AM 350, HEAT 55538

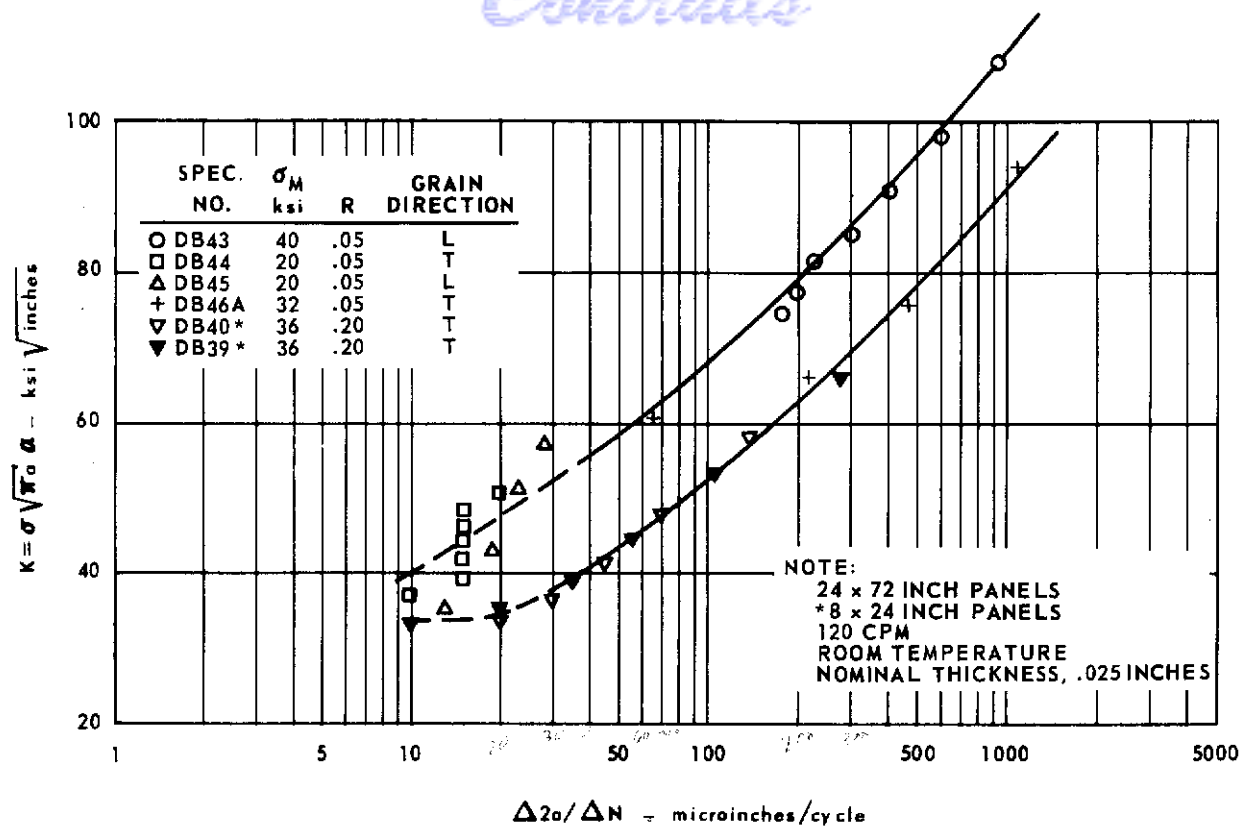


FIG. 81 CRACK GROWTH RATE DATA FOR AM 350, HEAT 19020

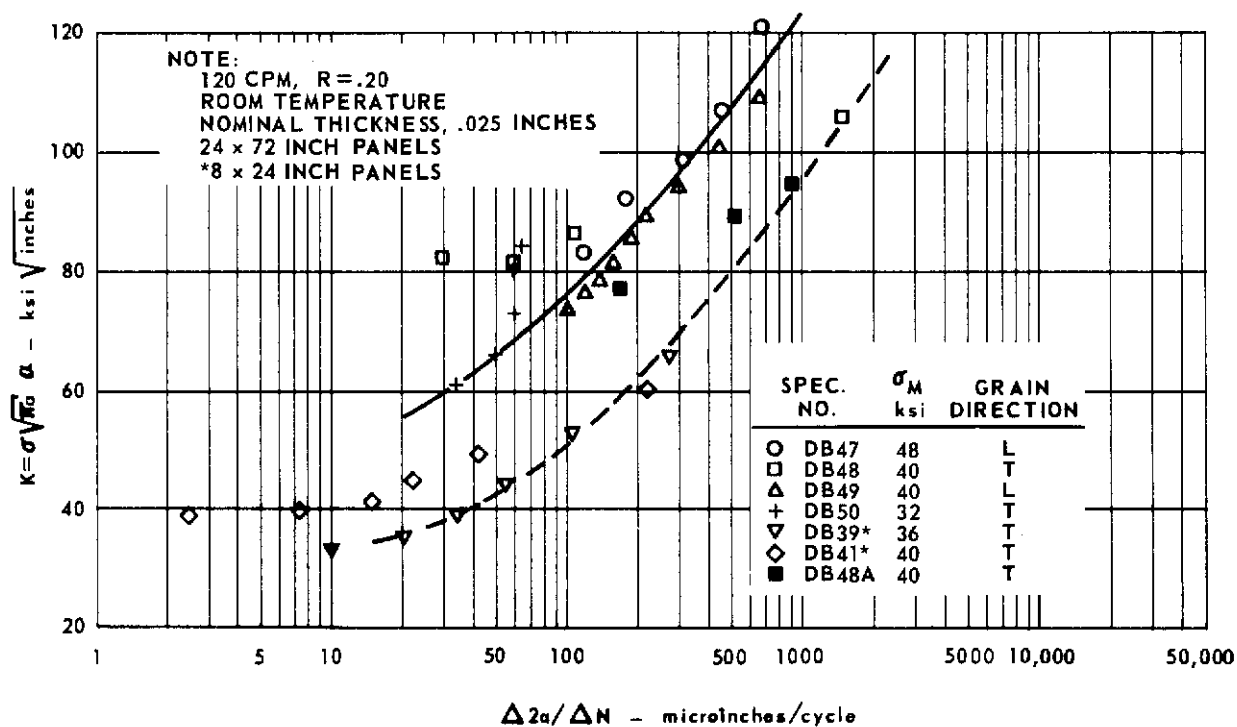


FIG. 82 CRACK GROWTH RATE DATA FOR AM 350, HEAT 19020

Contrails

GRAPH IS BACKWARDS?

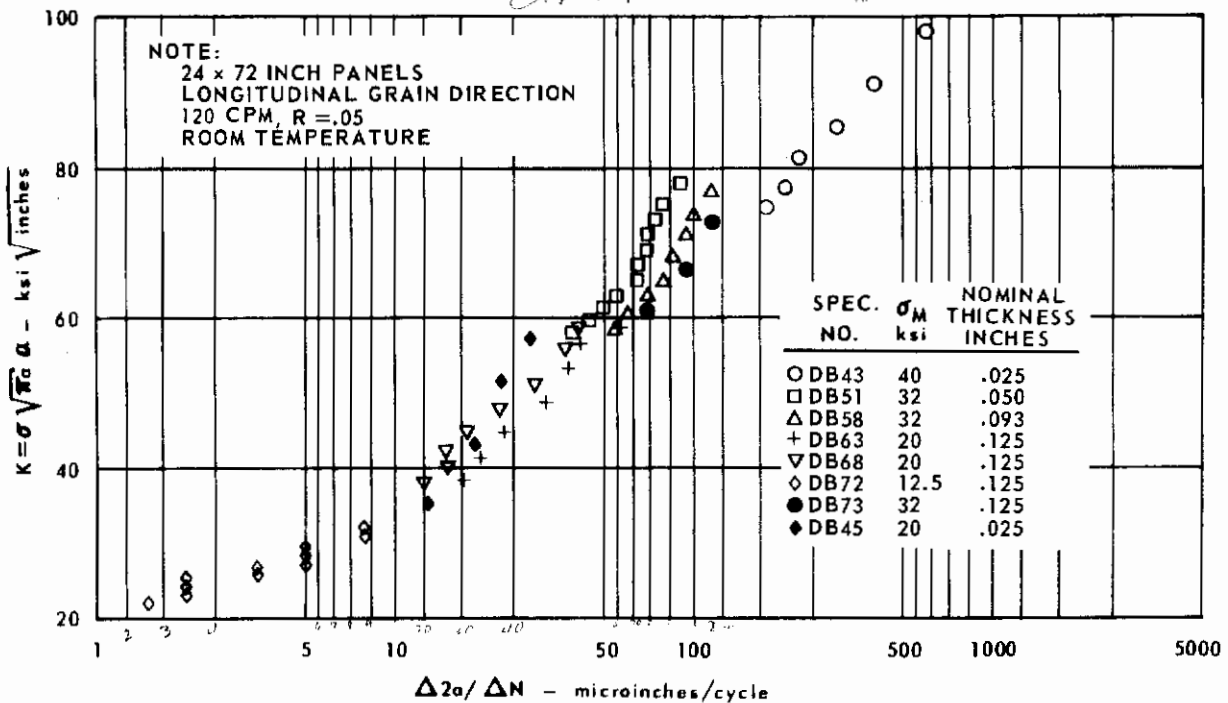


FIG. 83 CRACK GROWTH RATE DATA FOR AM 350, HEAT 19020

A crack-growth-rate scatter band for all the unexposed panel data is shown in Fig. 87. This graph includes the three heats of material, both panel sizes and both grain directions for $R = 0.20$ and $R = 0.05$.

Figs. 84, 85 and 86 include comparisons for exposed and unexposed 8 x 24-inch transverse panels. There is no difference between exposed and unexposed panel data. All points again fall within a relatively narrow scatter band. These figures also show that there is no variation of crack growth rate for the three thicknesses tested.

Fracture Toughness Test Data

Tabular Data

All pertinent test data for the fracture tests on the 24 x 72-inch panels are included in Table 13. Table 14 gives the data for the 8 x 24-inch panels. The calculations based on σ_{yp} derived from the high strain rate tensile data are accentuated by a darker background to simplify comparisons among the various columns.

The Effect of Temperature

The effect of temperature on K_C and residual strength for the three heats of AM 350 is shown in Figs. 88 and 89. This comparison is made for only the 24 x 72 x 0.025-inch longitudinal panels with $2a_0 = 6$ inches and at a stress rate of 10^6 psi/sec. Both curves show that there is a very sharp drop in fracture toughness at -110°F . There is essentially no increase in residual strength at temperatures above the room temperature test values. Almost all of the K_C computations from the 400 and 650°F tests are conservative values since the σ_N/σ_{yp} ratio exceeds 0.80.

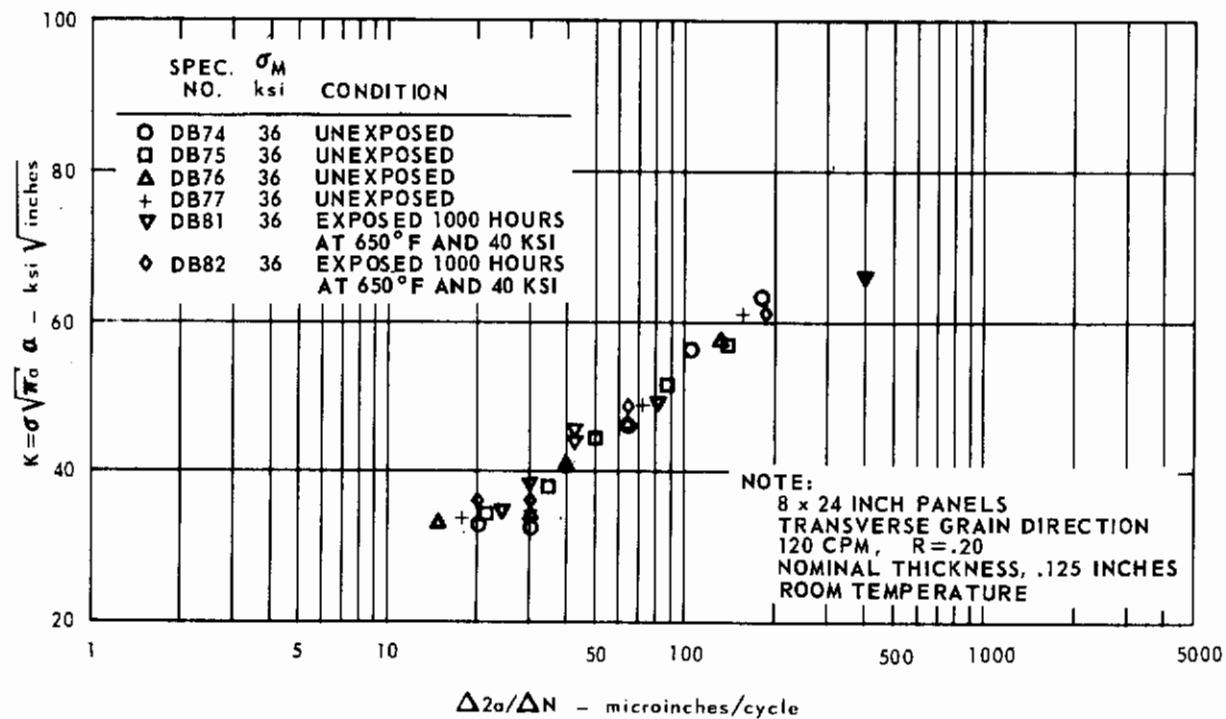


FIG. 84 COMPARISON OF EXPOSED AND UNEXPOSED CRACK GROWTH RATES FOR AM 350, HEAT 19020

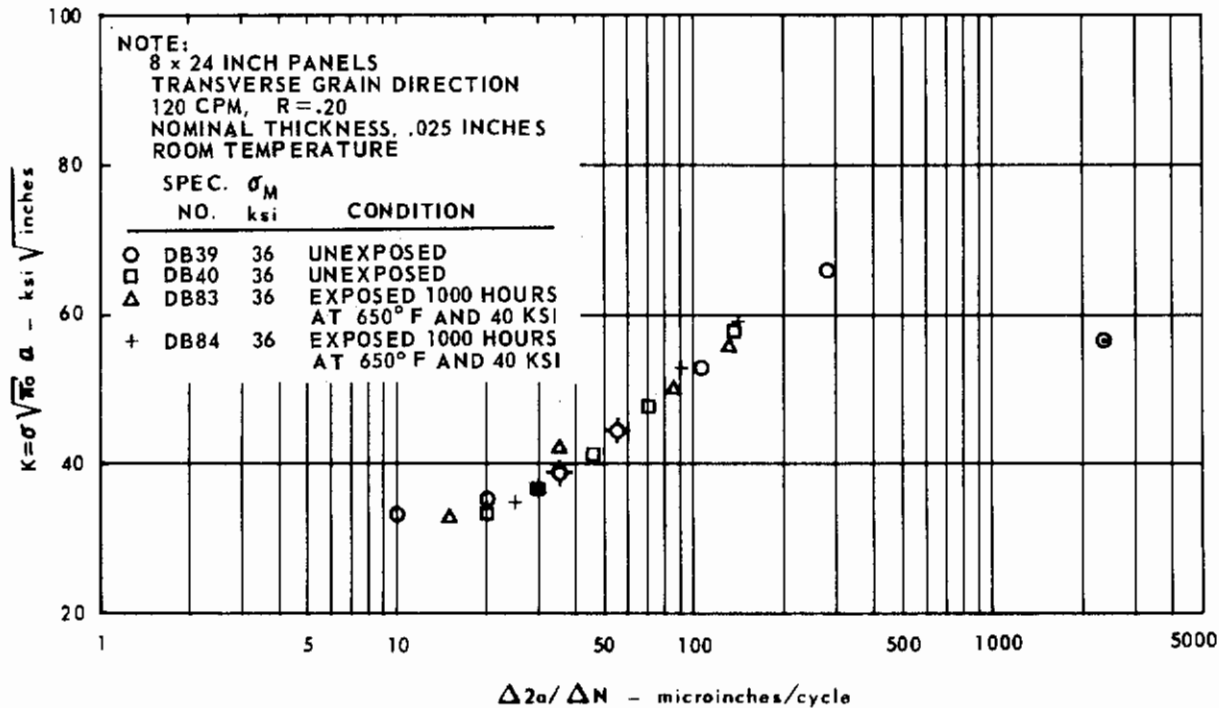


FIG. 85 COMPARISON OF EXPOSED AND UNEXPOSED CRACK GROWTH RATES FOR AM 350, HEAT 19020

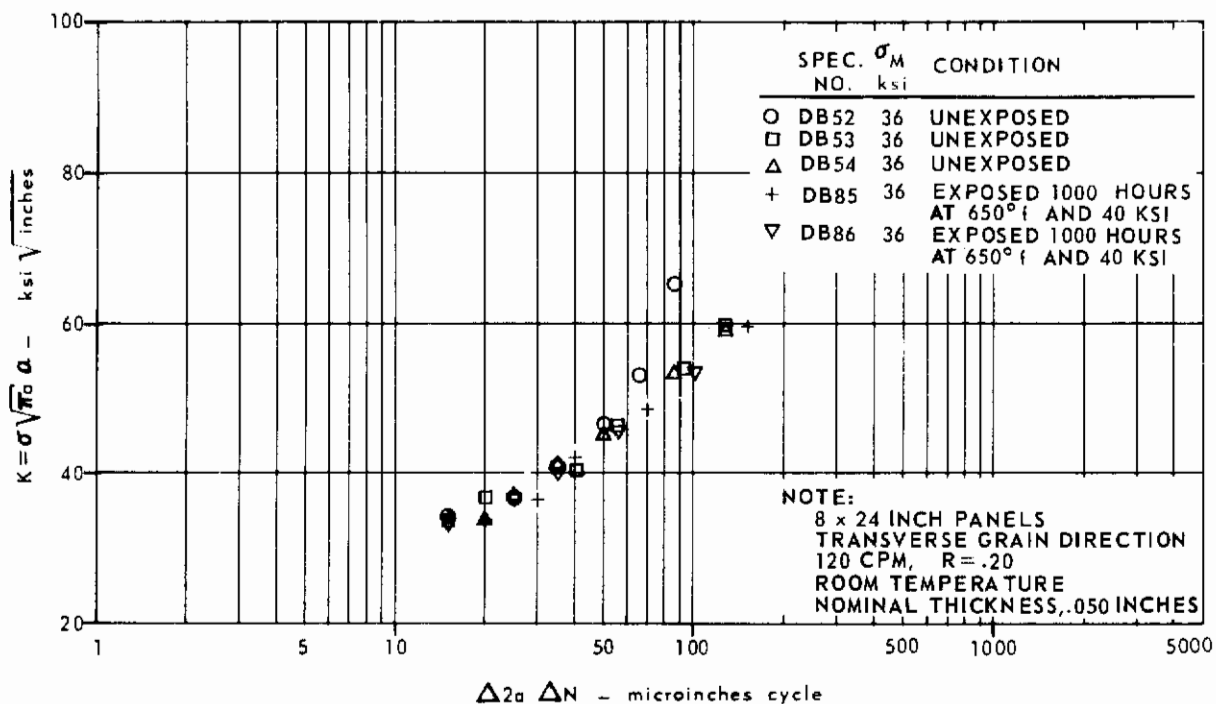


FIG. 86 COMPARISON OF EXPOSED AND UNEXPOSED CRACK GROWTH RATES FOR AM 350, HEAT 19020

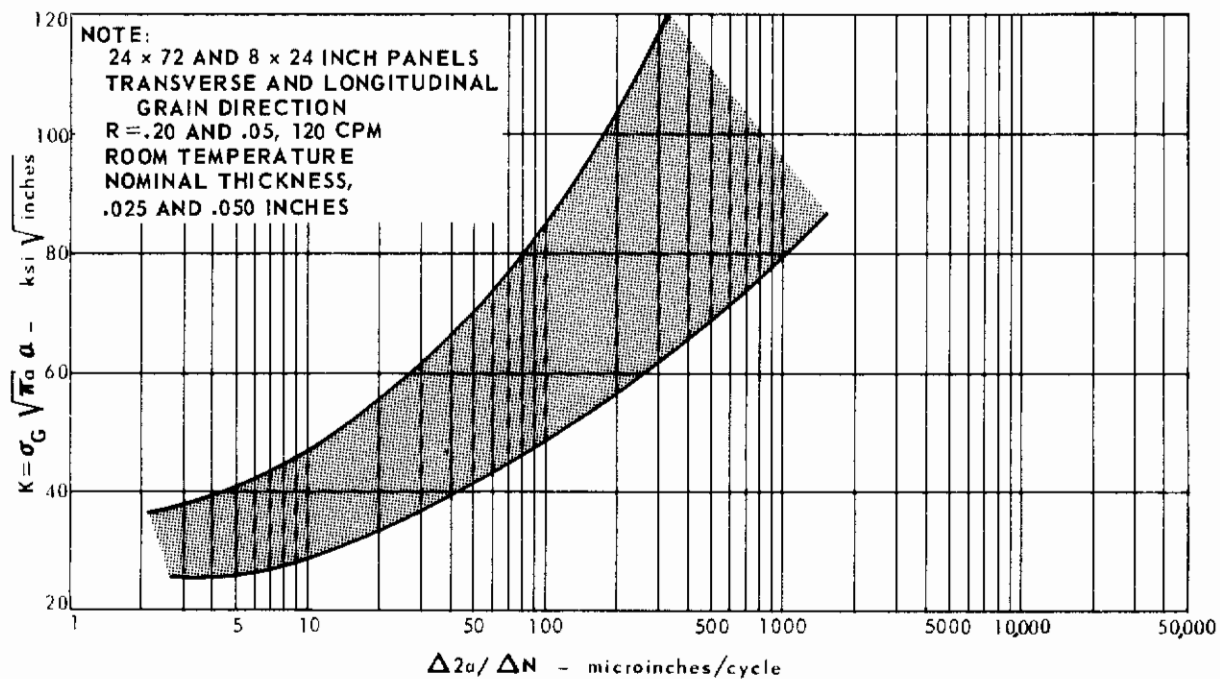


FIG. 87 CRACK GROWTH RATE DATA FOR AM 350, HEATS 19020, 19207 and 55538

TABLE 13 FRACTURE TOUGHNESS DATA FOR 24 X 72-INCH PANELS OF AM350

SPECIMEN NO.	HEAT NO.	THICKNESS inches	WIDTH inches	GRAIN DIRECTION	TEMP. ° F	$\dot{\sigma}$ psi/sec	$2a_0$ inches	σ_G ksi	σ_N ksi	F_{tu} ksi	σ_{yp} @TEMP. ksi	σ_{yp} @TEMP. AND $\dot{\sigma}$ ksi	σ_N^* @TEMP. AND $\dot{\sigma}$ ksi	σ_N^{**} @TEMP. AND $\dot{\sigma}$ ksi	$K_{CN} = \sigma_G \sqrt{\pi a}$ ksi \sqrt{in}	$\frac{\sigma_G^*}{F_{tu}}$	$K_{IC} = \sigma_G \sqrt{a}$ ksi \sqrt{in}	SHEAR %
DB 1	19207	.025	24.11	L	62	$.84 \times 10^6$	3.00	130.719	149.2	204.2	179.3	190.2	.83	.78	285.2	.640	332.8	100
DB 2	19207	.025	24.10	L	650	$.94 \times 10^6$	3.00	102.925	117.6	180.4	141.0	138.0	.83	.85	225.2	.570	267.2	100
DB 2X	19207	.027	24.12	L	-110	$.81 \times 10^6$	3.00	31.413	41.82	226.2	205.6	225.0	.20	.19	68.7	.139	69.5	8
DB 3	19207	.025	24.11	L	68	5.05×10^3	6.00	99.692	132.8	204.2	179.3	180.5	.74	.74	317.1	.488	347.4	100
DB 4	19207	.025	24.11	L	68	4.20×10^3	6.00	102.967	137.0	204.2	179.3	180.5	.76	.76	327.5	.504	360.5	100
DB 5	19207	.026	24.12	T	67	4.32×10^3	6.68	56.190	77.7	201.7	177.2	178.0	.44	.44	190.6	.298	193.8	80
DB 6A	19207	.026	24.12	T	75	4.83×10^3	6.00	54.382	72.4	201.7	177.2	178.0	.41	.41	172.9	.268	176.1	85
DB 7	19207	.025	24.14	L	67	1.03×10^5	6.00	97.340	129.5	204.2	179.3	186.0	.72	.78	309.5	.477	334.2	100
DB 8	19207	.025	24.11	L	68	1.04×10^5	6.00	104.261	138.8	204.2	179.3	186.0	.77	.75	332.0	.511	365.5	100
DB 9	19207	.025	24.10	L	RT	1.01×10^6	6.00	94.070	125.2	204.2	179.3	190.2	.70	.66	299.0	.461	318.5	100
DB 9X	19207	.026	24.12	L	RT	1.00×10^6	6.03	80.223	106.9	204.2	179.3	190.2	.60	.55	255.0	.392	267.0	100
DB 10A	19207	.026	24.12	L	69	$.91 \times 10^6$	6.00	66.980	89.2	204.2	179.3	190.2	.50	.47	212.8	.328	218.2	100
DB 10X	19207	.026	24.12	L	-110	$.45 \times 10^6$	6.00	23.318	31.0	226.2	205.6	225.0	.15	.14	74.0	.103	75.8	4
DB 11	19207	.027	24.11	T	70	$.94 \times 10^6$	6.00	55.155	73.4	201.7	177.2	188.0	.41	.39	175.3	.273	191.3	90
DB 12	19207	.026	24.13	T	68	$.96 \times 10^6$	6.00	51.014	70.2	201.7	177.2	188.0	.40	.37	162.1	.253	164.0	86
DB 13	19207	.025	24.12	L	650	$.90 \times 10^6$	6.00	85.742	114.2	180.4	141.0	138.0	.81	.83	272.7	.475	309.0	100
DB 14A	19207	.026	24.12	L	650	$.46 \times 10^6$	6.00	80.861	107.6	180.4	141.0	138.0	.76	.78	256.9	.448	291.3	100
DB 15	19207	.025	24.12	L	650	$.94 \times 10^6$	10.00	60.324	103.0	180.4	141.0	138.0	.73	.75	282.0	.334	283.5	100
DB 16	19207	.025	24.11	L	63	$.88 \times 10^6$	10.00	62.540	106.9	204.2	179.3	190.2	.60	.54	282.5	.347	282.0	100
DB 16X	19207	.026	24.14	L	-110	$.50 \times 10^6$	10.00	16.172	21.5	226.2	205.6	225.0	.10	.10	75.4	.071	76.8	0
DB 22	55538	.025	24.13	L	68	5.06×10^3	6.00	104.040	138.6	211.1	182.2	182.2	.76	.76	330.7	.473	364.5	100
DB 25	55538	.026	24.08	T	69	5.45×10^3	6.00	63.929	85.1	211.6	183.0	184.0	.46	.46	203.0	.302	208.0	100
DB 26	55538	.024	23.99	L	78	1.07×10^5	6.00	80.505	107.5	211.2	182.2	188.5	.59	.57	256.0	.382	269.0	100
DB 28	55538	.024	24.09	L	68	1.06×10^6	6.00	100.000	133.2	211.1	182.2	193.1	.73	.69	318.0	.474	343.0	100
DB 29	55538	.025	24.16	L	68	1.06×10^6	6.00	90.741	120.7	211.1	182.2	193.1	.66	.62	288.6	.430	306.5	100
DB 30	55538	.025	24.11	T	70	1.02×10^6	6.04	51.980	69.4	211.6	183.0	194.0	.38	.38	165.9	.246	167.2	76
DB 31	55538	.025	24.13	T	70	$.94 \times 10^6$	6.00	51.709	68.8	211.6	183.0	194.0	.38	.35	164.7	.239	166.3	84

* TENSILE PROPERTIES OBTAINED FROM STANDARD STRAIN RATE TESTS OF .005 in/in/min
 ** σ_{yp} BASED ON HIGH STRAIN RATE TENSILE DATA FOR AM 350 (SCT 850) (REFERENCE 26)

TABLE 13 FRACTURE TOUGHNESS DATA FOR 24 X 72-INCH PANELS OF AM350 (continued)

SPECIMEN NO.	HEAT NO.	THICKNESS inches	WIDTH inches	GRAIN DIRECTION	TEMP. ° F	$\dot{\sigma}$ psi/sec	2a ₀ inches	σ_G ksi	σ_N ksi	F _{tu} ksi	σ_{yp} @ TEMP. ksi	σ_{yp} @ TEMP. AND $\dot{\sigma}$ ksi	σ_N^* @ TEMP. AND $\dot{\sigma}$ ksi	KCN = $\sigma_G \sqrt{\pi a_0}$ ksi \sqrt{in}	$\frac{\sigma_G^*}{F_{tu}}$	K _C = $\frac{\sigma_G \sqrt{a_0 W}}{ksi \sqrt{in}}$	SHEAR %
DB 32	55538	.025	24.15	L	650	1.07x10 ⁶	6.00	86.377	115.0	190.5	140.9	137.8	.82	274.7	.453	311.5	100
DB 33	55538	.025	24.15	L	650	1.00x10 ⁶	6.00	84.219	112.2	190.5	140.9	137.8	.80	267.9	.442	300.5	100
DB 43	19020	.025	24.17	L	-110	.89x10 ⁶	6.00	26.821	35.7	222.3	200.0	219.0	.18	85.3	.12	88.5	38
DB 44A	19020	.026	24.17	T	-110	.74x10 ⁶	6.00	18.790	25.0	226.9	203.1	222.0	.12	59.6	.083	59.0	25
DB 45	19020	.026	24.16	L	70	.99x10 ⁶	6.00	94.382	125.5	205.9	184.3	195.3	.61	300.18	.458	321.0	100
DB 46A	19020	.026	24.17	T	68	.80x10 ⁶	6.00	66.980	89.2	206.4	177.5	188.2	.50	212.8	.325	219.3	100
DB 47	19020	.026	24.14	L	400	1.03x10 ⁶	6.00	97.416	129.7	181.8	146.6	146.6	.88	309.8	.536	358.0	100
DB 48A	19020	.025	24.12	T	400	1.01x10 ⁶	6.00	66.179	88.1	180.2	146.4	146.4	.60	210.0	.367	222.3	100
DB 49	19020	.025	24.18	L	650	1.07x10 ⁶	6.00	83.667	111.3	188.2	135.3	132.4	.82	266.1	.445	304.7	100
DB 50A	19020	.026	24.06	T	650	1.02x10 ⁶	6.00	67.504	89.9	185.8	141.5	138.5	.64	214.5	.364	229.1	100
DB 51	19020	.049	24.16	L	70	1.00x10 ⁶	6.00	107.073	142.5	208.8	177.4	188.1	.80	340.6	.513	375.5	100
DB 58	19020	.094	24.14	L	68	1.00x10 ⁶	6.04	121.340	161.9	200.4	170.2	188.5	.95	387.3	.605	443.3	100
DB 59X	19020	.128	24.01	T	73	.81x10 ⁶	3.02	38.155	43.6	200.8	167.6	177.5	.26	121.1	.190	97.3	19
DB 60	19020	.124	24.14	L	650	.97x10 ⁶	3.00	119.243	136.1	183.0	134.3	131.3	1.01	260.9	.652	352	100
DB 61	19020	.121	24.14	L	65	.93x10 ⁶	6.00	115.516	153.7	200.5	167.6	177.6	.92	367.4	.576	432.0	88
DB 62	19020	.128	24.12	L	68	1.01x10 ⁶	6.00	118.096	157.2	200.5	167.6	177.6	.94	375.6	.589	446.8	92
DB 63	19020	.124	24.16	L	650	1.06x10 ⁶	6.00	89.773	119.4	183.0	134.3	131.3	.89	285.5	.491	333.2	100
DB 64	19020	.125	24.15	L	650	.98x10 ⁶	6.00	91.126	121.3	183.0	134.3	131.3	.90	289.8	.498	343.0	—
DB 65	19020	.125	24.15	L	RT	.93x10 ⁶	10.02	17.573	29.0	200.5	167.6	177.6	.17	77.9	.088	75.8	12
DB 66	19020	.126	24.15	L	650	.94x10 ⁶	10.00	65.573	111.8	183.0	134.3	131.3	.83	290.4	.358	321.0	100
DB 67	19020	.125	24.16	L	-110	.38x10 ⁶	6.00	8.851	11.8	219.0	191.6	218.0	.06	28.1	.040	27.8	3
DB 68	19020	.119	24.14	L	-110	.95x10 ⁶	6.01	19.112	25.4	219.0	191.6	210.0	.13	60.7	.087	68.5	3
DB 70	19020	.125	24.15	L	71	3.15x10 ³	6.00	53.268	70.9	200.5	167.6	168.5	.42	169.4	.266	173.2	32
DB 71	19020	.122	24.15	L	72	5.15x10 ³	6.00	37.120	49.4	200.5	167.6	168.5	.29	118.1	.185	118.0	25
DB 72	19020	.120	24.16	L	68	.90x10 ⁵	6.00	28.850	38.4	200.5	167.6	174.5	.23	91.8	.144	91.5	26
DB 73X	19020	.128	24.15	T	73	~ 10 ⁵	6.00	28.150	37.5	200.8	167.5	174.5	.22	89.4	.140	89.0	16

* TENSILE PROPERTIES OBTAINED FROM STANDARD STRAIN RATE TESTS OF .005 in./in./min

** σ_{yp} BASED ON HIGH STRAIN RATE TENSILE DATA FOR AM 350 (SCT 850) (REFERENCE 26)

TABLE 14 FRACTURE TOUGHNESS DATA FOR 8 x 24 INCH PANELS OF AM 350

SPECIMEN NO.	HEAT NO.	THICKNESS inches	WIDTH inches	GRAIN DIRECTION	TEMP. °F	$\dot{\sigma}$ psi/sec	$2a_0$ inches	σ_G ksi	F_{tu} * @TEMP. ksi	σ_{yp} * @TEMP. ksi	σ_{yp} * @TEMP. AND $\dot{\sigma}$ ksi	σ_N * @TEMP. AND $\dot{\sigma}$	σ_N^{**} * @TEMP. AND $\dot{\sigma}$	$K_{CN} = \sigma_G \sqrt{\pi a_0}$ ksi \sqrt{in}	$\frac{\sigma_G}{F_{tu}}$	$K_{IC} = \sigma_G \sqrt{a_0}$ ksi \sqrt{in}	SHEAR %
DB 19	19207	.025	8.00	T	-110	4.60×10^3	2.00	37.393	223.2	205.6	205.6	.26	.25	72.3	.167	71.5	25
DB 20	19207	.025	8.00	T	-110	$.86 \times 10^6$	2.00	35.000	223.2	205.6	205.6	.23	.21	64.3	.157	63.5	20
DB 21	19207	.025	8.07	T	RT	1.02×10^6	2.00	92.136	201.7	177.2	177.2	.69	.65	169.2	.457	169.5	100
DB 36A	55538	.025	8.02	T	-110	—	2.00	~2.25	230.8	208.8	208.8	.01	—	~4.0	.097	4.1	20
DB 37	55538	.025	8.02	T	-110	1.08×10^6	2.00	37.055	230.8	208.8	208.8	.24	.22	68.0	.161	67.2	28
DB 38	55538	.025	8.06	T	RT	$.90 \times 10^6$	2.00	86.834	211.6	183.0	183.0	.63	.59	159.4	.410	159.0	98
DB 39	19020	.025	8.00	T	-110	4.68×10^3	2.00	39.832	226.9	203.1	203.1	.26	.26	73.1	.176	72.4	40
DB 40	19020	.025	8.02	T	-110	1.02×10^6	2.01	30.585	226.9	203.1	203.1	.20	.18	56.2	.135	55.4	48
DB 41	19020	.025	8.00	T	RT	1.05×10^6	2.00	90.500	206.4	177.5	177.5	.68	.64	166.2	.438	174.0	100
DB 42	19020	.025	8.01	T	650	$.70 \times 10^6$	2.00	87.030	185.8	141.5	141.5	.82	.84	160.0	.468	181.5	100
DB 52	19020	.051	8.00	T	650	1.06×10^6	2.00	99.264	189.1	135.2	135.2	.98	1.00	182.1	.525	226.5	100
DB 53	19020	.051	8.00	T	-110	1.89×10^6	2.02	37.759	227.2	202.7	202.7	.25	.23	69.2	.166	75.5	26
DB 54	19020	.051	8.00	T	68	$.96 \times 10^6$	2.00	102.604	209.6	178.8	178.8	.76	.72	188.4	.489	205.2	81
DB 55	19020	.096	8.00	T	-110	$.88 \times 10^6$	2.00	33.487	225.1	199.5	199.5	.22	.20	61.6	.149	65.5	11
DB 56	19020	.095	8.00	T	RT	1.06×10^6	2.00	95.362	199.8	170.2	170.2	.75	.70	175.3	.478	189.9	52
DB 57	19020	.096	8.00	T	650	$.85 \times 10^6$	2.00	94.197	182.3	145.4	145.4	.86	.98	173.0	.516	210.8	100
DB 74	19020	.128	8.01	T	68	1.07×10^6	2.29	93.246	200.7	167.5	167.5	1.00	.94	183.3	.455	185.0	.48
DB 75	19020	.128	8.01	T	68	3.5×10^3	2.01	94.891	200.7	167.5	167.5	.77	.75	174.5	.473	191.7	68
DB 76	19020	.129	8.00	T	400	3.85×10^3	2.00	96.255	180.7	141.7	141.7	.90	.90	176.6	.532	206.5	100
DB 77	19020	.129	8.00	T	650	5.9×10^3	2.00	87.691	183.6	132.0	132.0	.89	.89	161.1	.478	187.1	100
DB 78	19020	.128	8.00	T	-110	4.6×10^3	2.00	34.008	218.3	190.3	190.3	.24	.24	62.5	.156	62.2	5
DB 79	19020	.127	8.01	T	-110	$.78 \times 10^6$	2.00	31.881	218.3	190.3	190.3	.22	.20	58.6	.146	58.3	8

* TENSILE PROPERTIES OBTAINED FROM STANDARD STRAIN RATE TESTS OF .005 in./in./min
 ** σ_{yp} BASED ON HIGH STRAIN RATE TENSILE DATA FOR AM 350 (SCT 850) (REFERENCE 26)

TABLE 14 FRACTURE TOUGHNESS DATA FOR 8 x 24 INCH PANELS OF AM 350 (continued)

SPECIMEN NO.	HEAT NO.	THICKNESS inches	WIDTH inches	GRAIN DIRECTION	TEMP. °F	$\dot{\sigma}$ psi/sec	$2a_0$ inches	σ_G ksi	σ_N ksi	F_{tu} #TEMP. ksi	σ_{yp} #TEMP. ksi	σ_{yp} #TEMP. AND σ ksi	σ_N #TEMP. AND σ ksi	σ_N #TEMP. AND σ ksi	$K_{CN} = \sigma_G \sqrt{\pi a_0}$ ksi \sqrt{in}	$\frac{\sigma_G}{F_{tu}}$	$K_{IC} = \frac{\sigma_G \sqrt{a_0 W}}{\sqrt{in}}$	SHEAR %
DB 80	19020	.126	8.02	T	650	1.08×10^6	2.00	92.702	123.5	183.6	132.0	129.1	.94	.96	170.2	.505	204.8	100
▲ DB 81	19020	.126	8.01	T	70	$.89 \times 10^6$	2.00	51.585	68.8	208.0	173.6	184.0	.40	.37	94.5	.248	96.0	16
▲ DB 82	19020	.125	8.00	T	70	1.07×10^6	2.00	65.526	87.4	208.0	173.6	184.0	.50	.47	120.3	.315	123.4	26
▲ DB 83	19020	.025	8.00	T	68	$.92 \times 10^6$	2.00	91.615	122.2	208.0	179.2	190.0	.68	.64	168.2	.440	178.9	100
▲ DB 84	19020	.025	8.00	T	68	$.91 \times 10^6$	2.00	92.745	123.7	208.0	179.2	190.0	.69	.65	170.1	.446	181.0	100
▲ DB 85	19020	.051	8.00	T	70	1.09×10^6	2.00	93.610	125.0	214.3	183.2	194.3	.68	.64	171.8	.437	183.0	78
▲ DB 86	19020	.051	8.01	T	70	$.90 \times 10^6$	2.00	97.799	130.7	214.3	183.2	194.3	.71	.67	179.5	.456	192.6	73

* TENSILE PROPERTIES OBTAINED FROM STANDARD STRAIN RATE TESTS OF .005 in./min

** σ_{yp} BASED ON HIGH STRAIN RATE TENSILE DATA FOR AM 350 (SCT 850) (REFERENCE 26)

▲ EXPOSED @ 650°F FOR 1000 HRS @ $\sigma_G = 40$ ksi

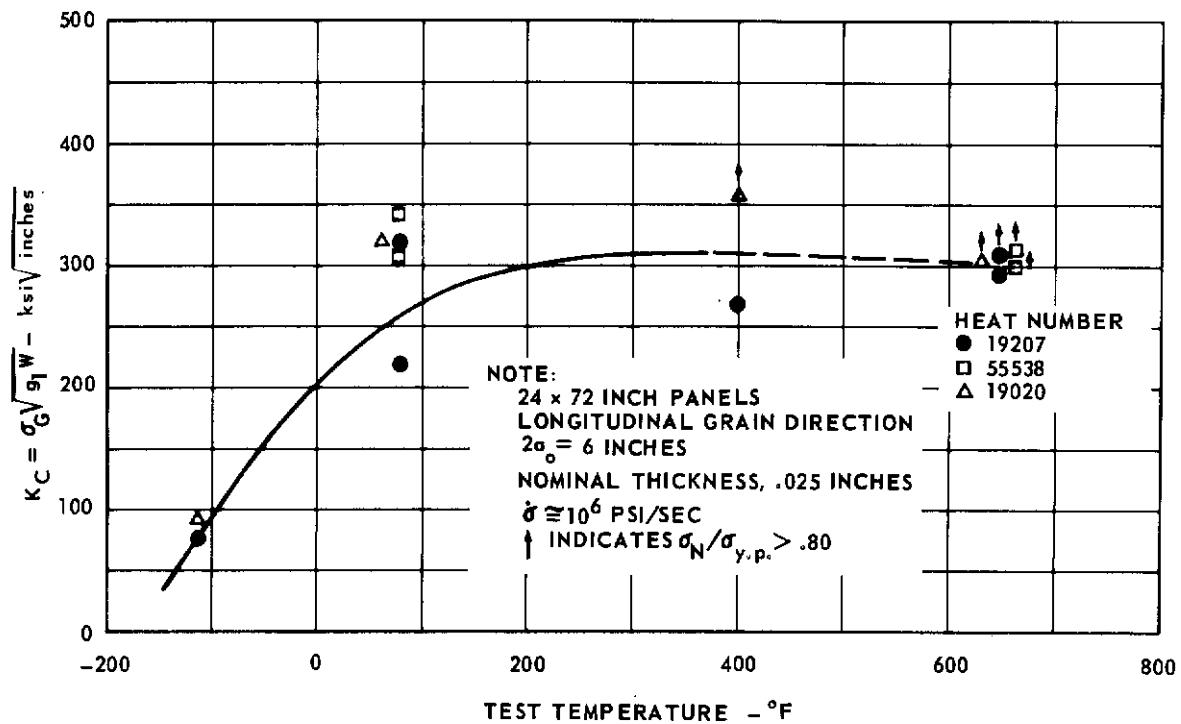


FIG. 88 EFFECT OF TEST TEMPERATURE ON K_C FOR AM 350

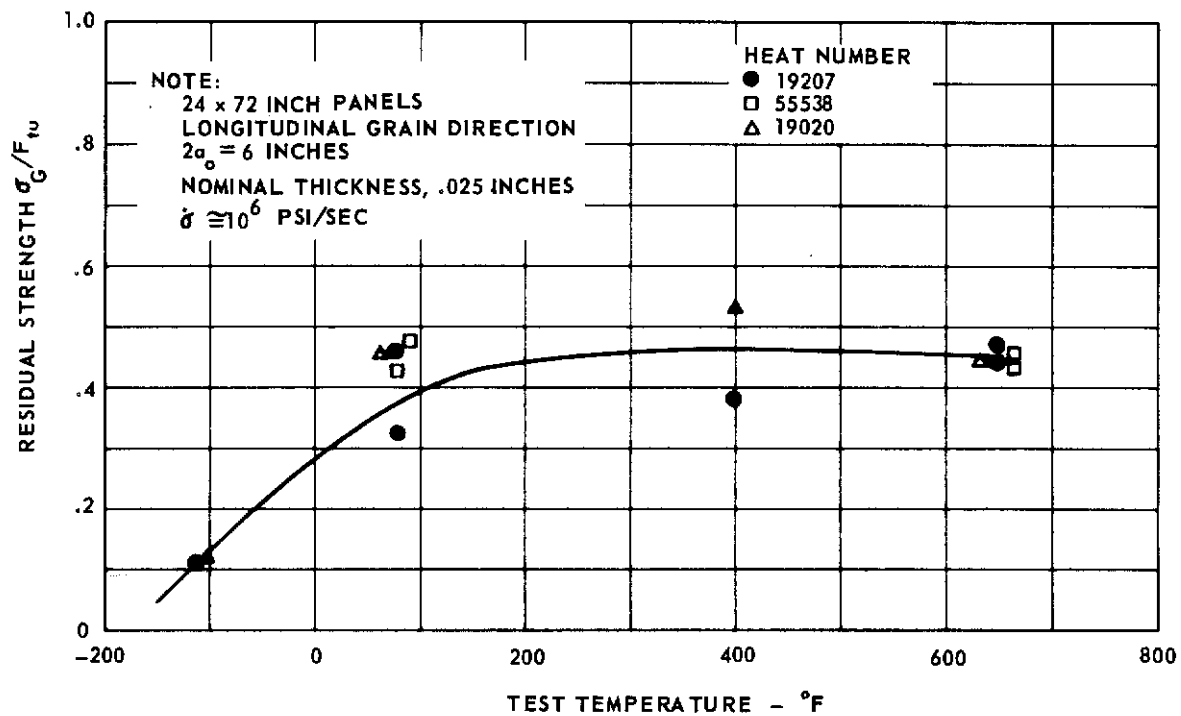


FIG. 89 EFFECT OF TEST TEMPERATURE ON RESIDUAL STRENGTH FOR AM 350

The Effect of Grain Direction

The effect of grain direction on both K_C and residual strength is shown in Figs. 90 and 91 for each of the four test temperatures. The transverse grain direction has nearly a 40 percent lower K_C and residual strength than the longitudinal grain direction at room temperature. This difference is less marked but still very apparent at the test temperatures of -110, 400 and 650°F. For the five longitudinal room temperature tests, the average K_C value is 301.7 ksi $\sqrt{\text{inches}}$; and 181.6 ksi $\sqrt{\text{inches}}$ for the 5 transverse tests.

The Effect of Thickness

For heat 19020, four specimen thicknesses were evaluated with both 8-inch and 24-inch wide panels. Figs. 92 and 93 illustrate the variation of K_C and residual strength with specimen thickness. Curves are drawn only for the room temperature data to maintain clarity.

K_C increases with thickness for the 24-inch wide longitudinal panels. At thicknesses of 0.093 and 0.125 inches, valid tests were not obtained since σ_N/σ_{yp} exceeded 0.80. For the transverse 8-inch wide panels, K_C increases at the 0.050 inch thickness point and drops somewhat for the 0.093 and 0.125-inch thickness points. At -110°F, both longitudinal and transverse test points are close together. The longitudinal tests show a greater drop for the 0.125 inch thickness than the transverse tests. The segregation problem discussed in the Microstructure Subsection could be responsible for this test result.

The residual strength curves in Fig. 93 parallel the K_C data for the most part. The highest residual strength value occurs at the 0.093 inch thickness point for the 24-inch wide longitudinal panel tests and at the 0.050 inch thickness point for the 8-inch wide transverse panel tests.

The Effect of Crack Length

The effect of crack length expressed as the ratio of crack-length to panel-width for the 24-inch wide panels is shown in Figs. 94 and 95 for K_C and in Figs. 96 and 97 for residual strength. Grain direction, temperature, and thickness are included as variables on these graphs. All comparisons are made at a stress rate of 10^6 psi/sec.

Fig. 94 shows that K_C at room temperature is relatively constant for the three crack lengths studied. The two test points at $2a/2b = 0.25$ for the longitudinal tests show considerable variation and obscure the best direct comparison among the three crack lengths. At -110°F, K_C is constant for the three crack lengths and this is also reflected by the very low consistent ratios of σ_N/σ_{yp} . The very minor variation of K_C with crack length for AM 350 at -110°F illustrates the strict applicability of the fracture mechanics theory to brittle material behavior. For the 650°F tests, (Figs. 94 and 95) most of the tests exceeded the ASTM criterion for valid tests.

Figs. 96 and 97 show that residual strength decreases with increasing panel damage for the room and elevated temperature tests. At -110°F the decrease in residual strength with increasing panel damage is less marked.

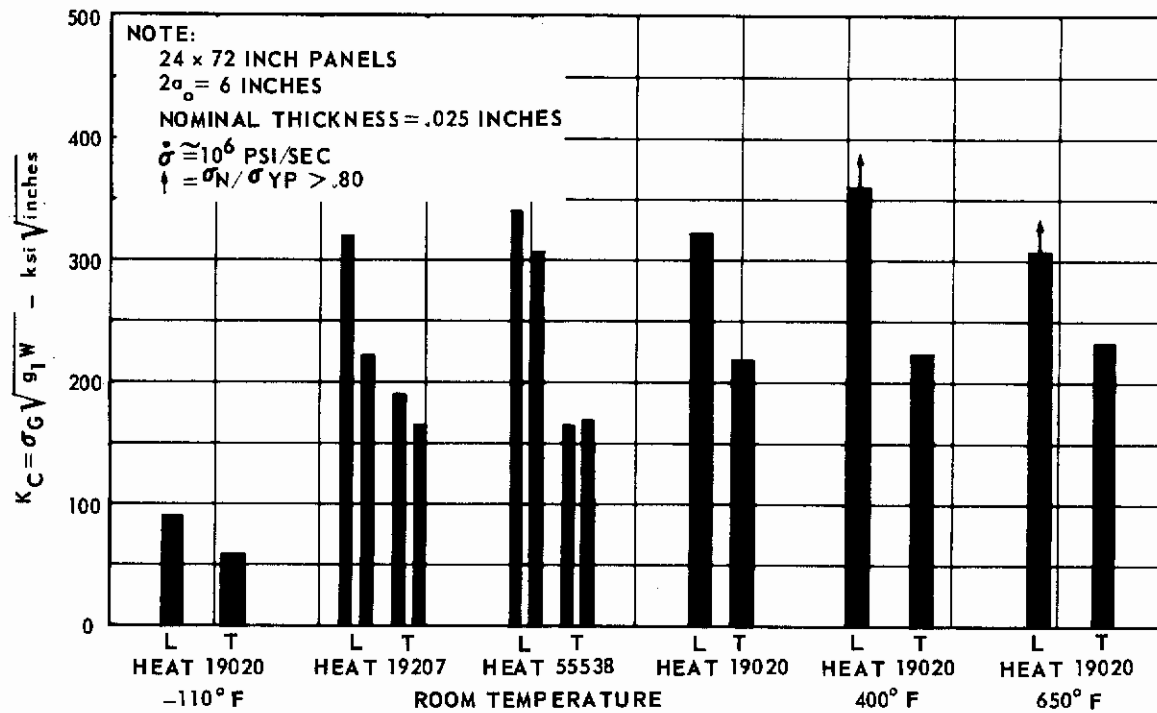


FIG. 90 VARIATION OF K_C WITH GRAIN DIRECTION FOR AM 350

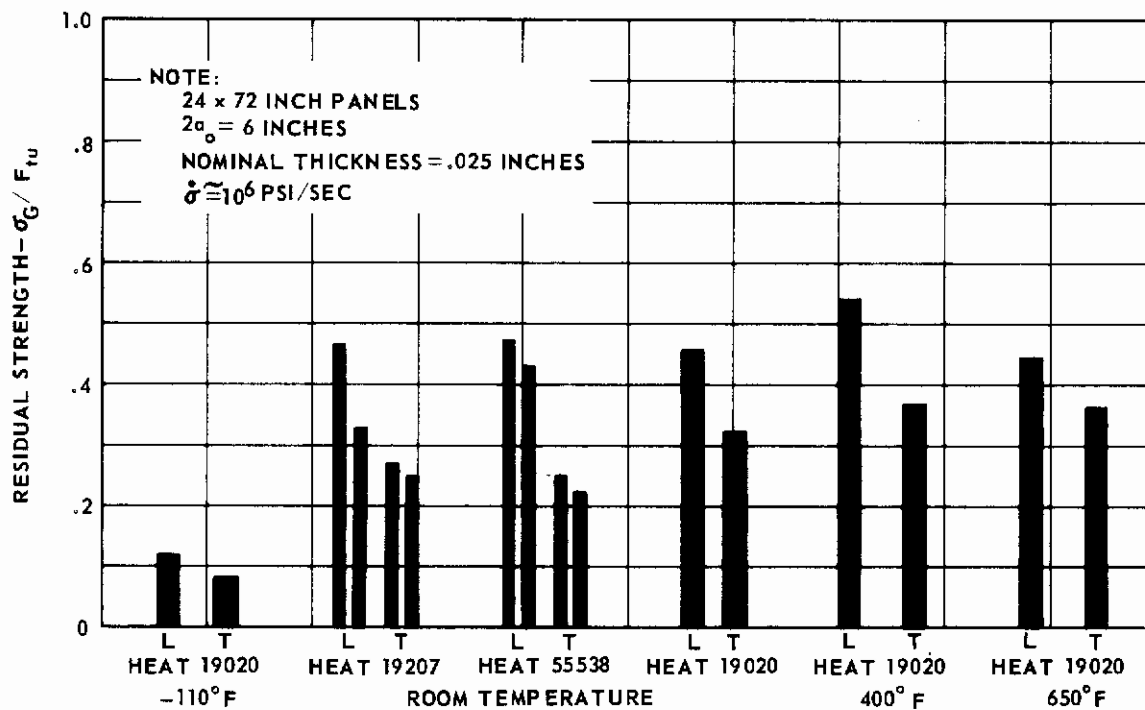


FIG. 91 VARIATION OF RESIDUAL STRENGTH WITH GRAIN DIRECTION FOR AM 350

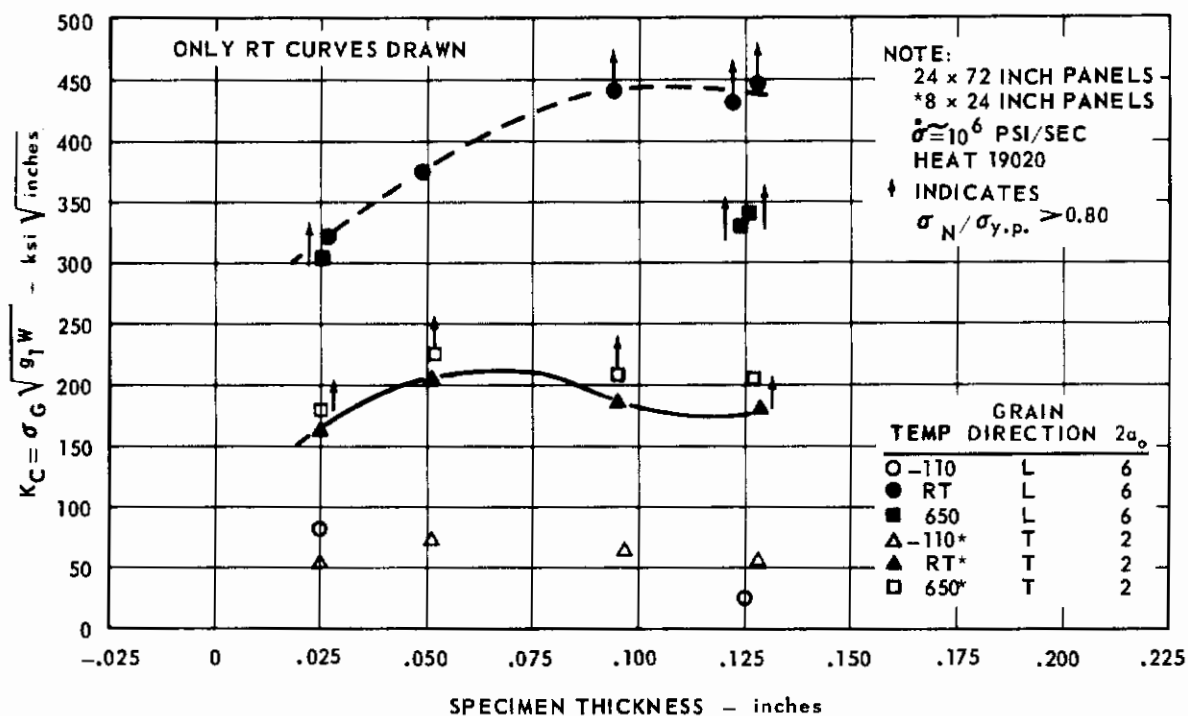


FIG. 92 VARIATION OF K_C WITH THICKNESS FOR AM 350

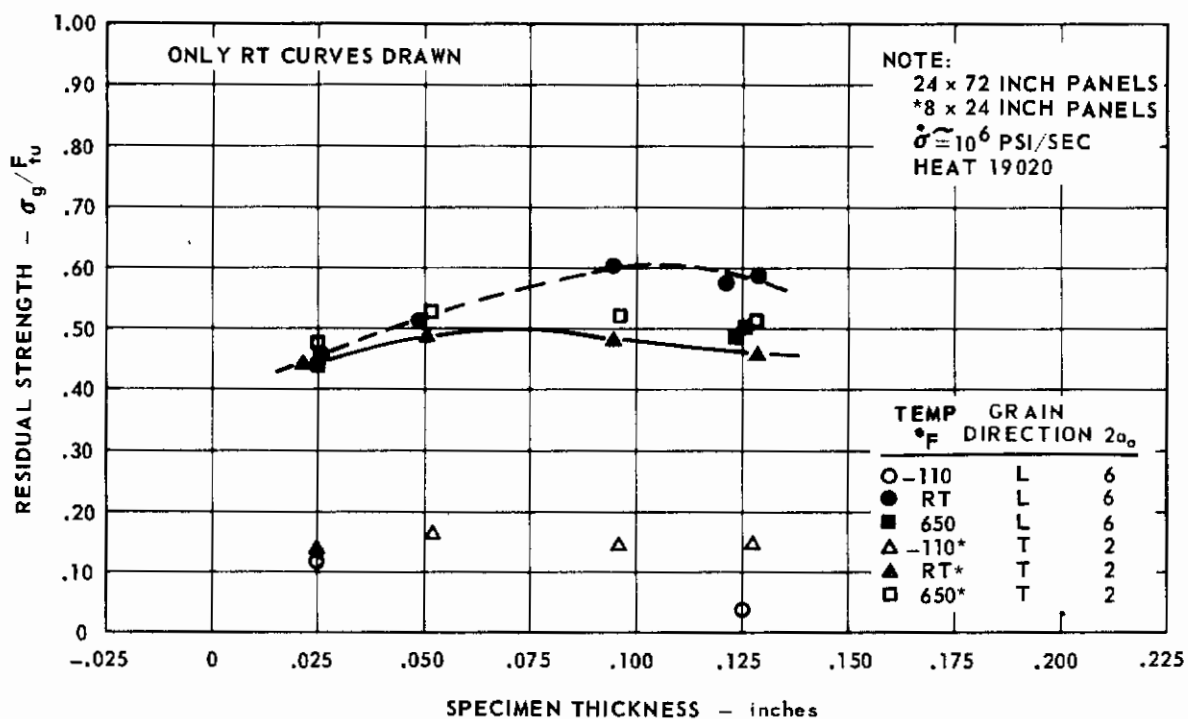


FIG. 93 VARIATION OF RESIDUAL STRENGTH WITH THICKNESS FOR AM 350

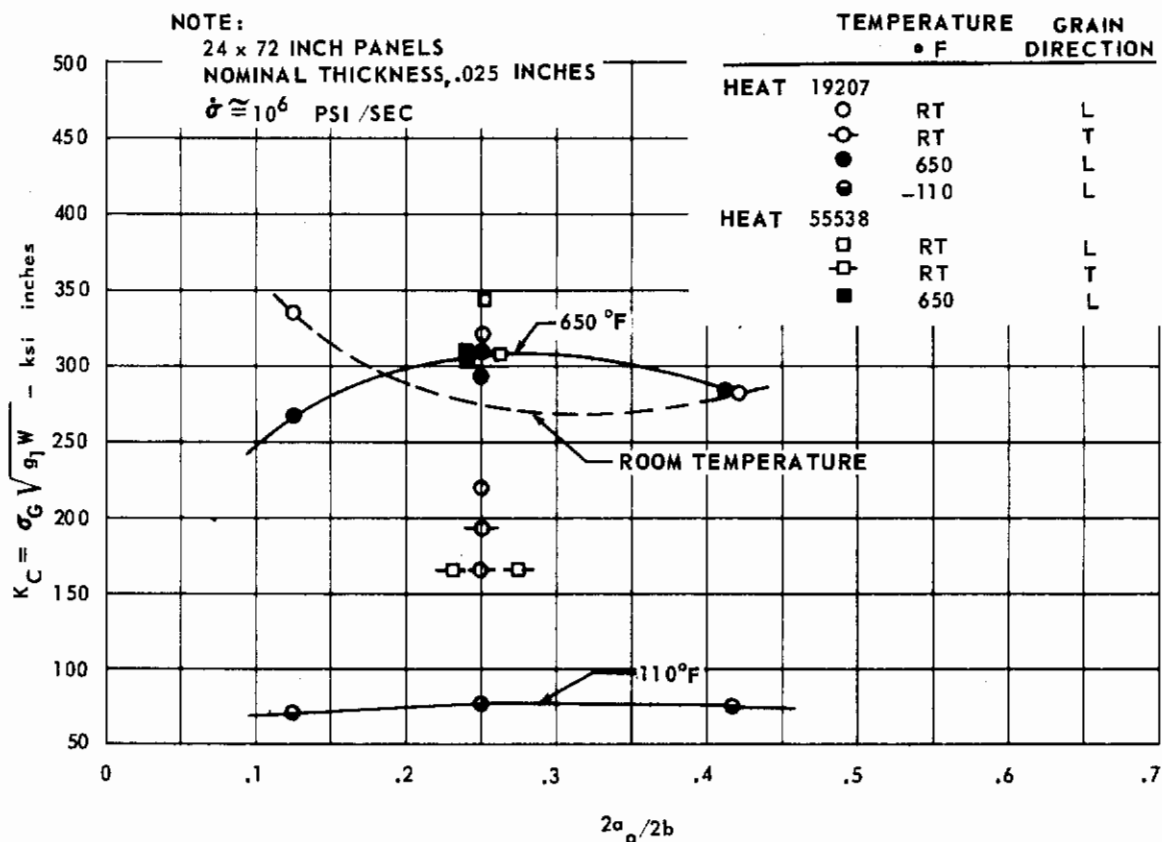
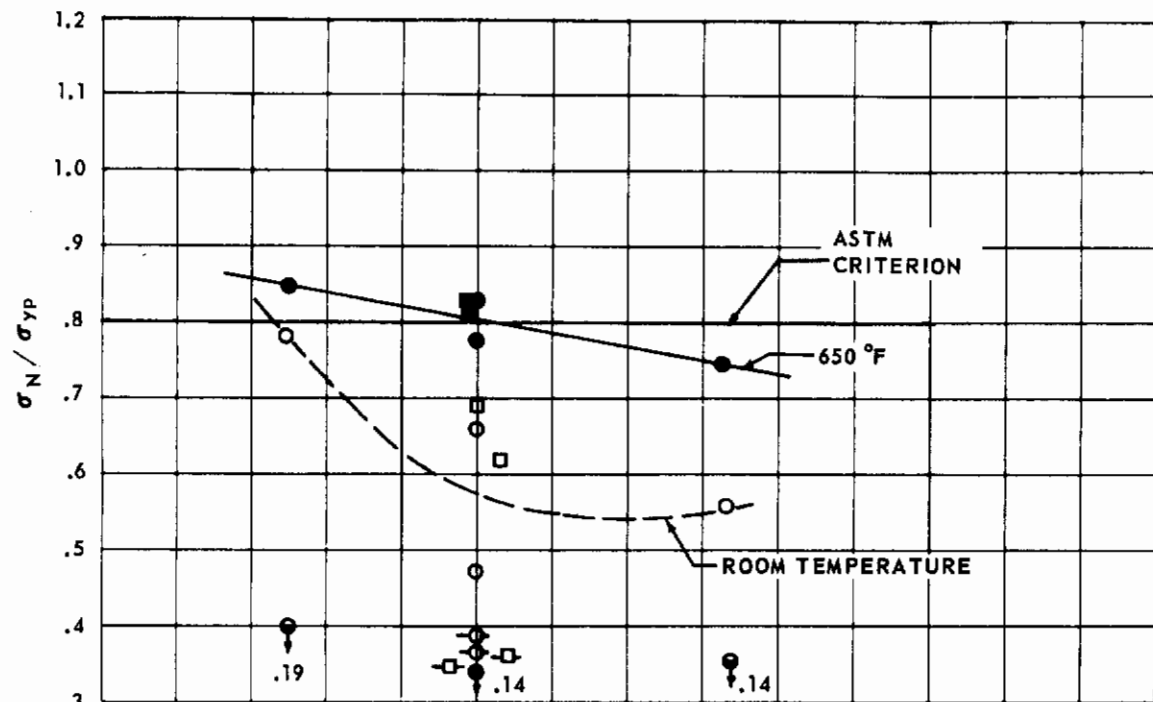


FIG. 94 VARIATION OF K_C WITH TEMPERATURE, CRACK LENGTH AND GRAIN DIRECTION FOR AM 350

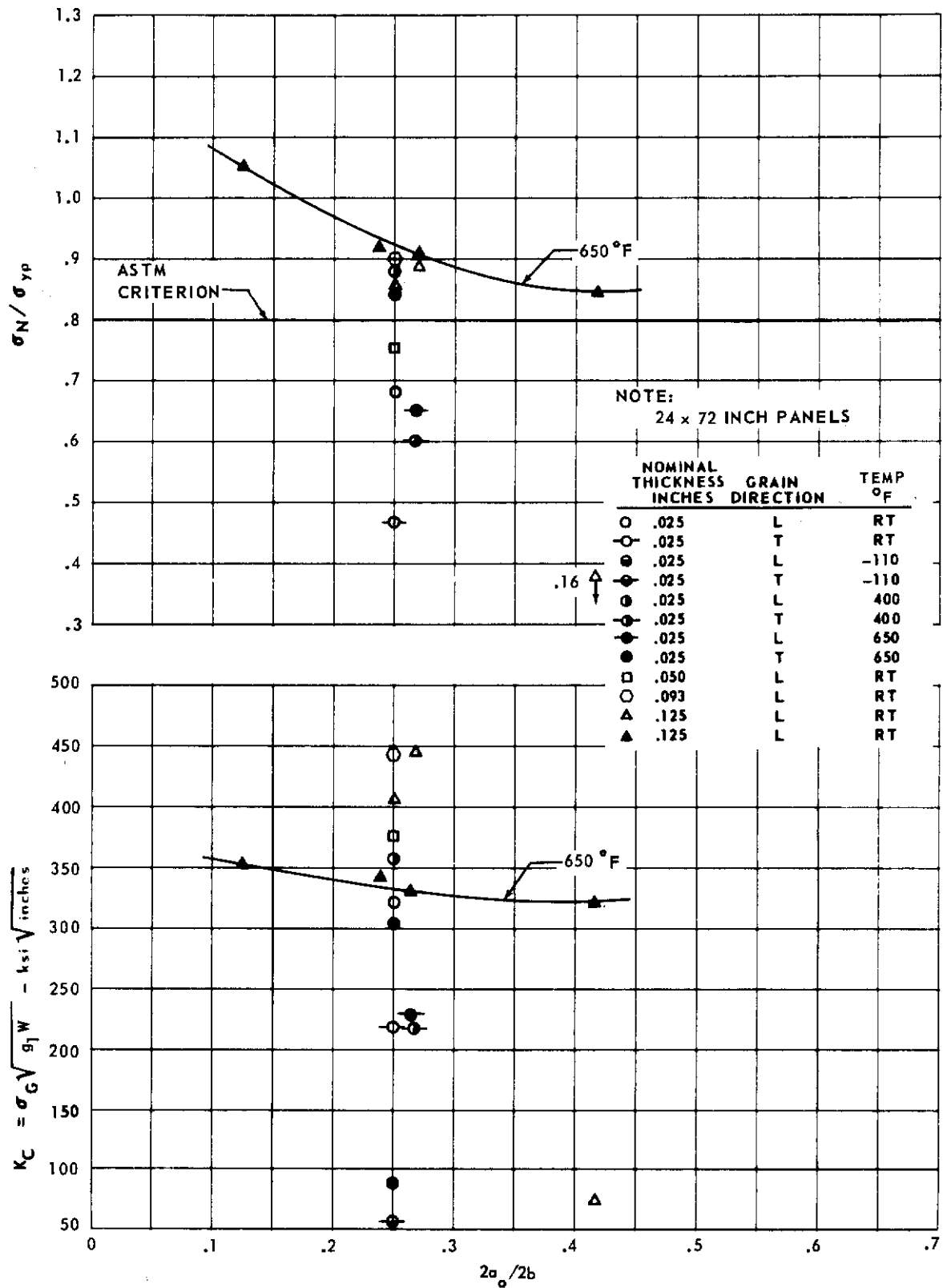


FIG. 95 VARIATION OF K_C , CRACK LENGTH, THICKNESS AND GRAIN DIRECTION FOR AM 350, HEAT 19020

NOTE:

$\dot{\sigma} \approx 10^6$ PSI/SEC
 NOMINAL THICKNESS, .025 INCHES
 Points at $2a_0/2b = .25$ were Displaced
 Laterally to Avoid Overplotting.

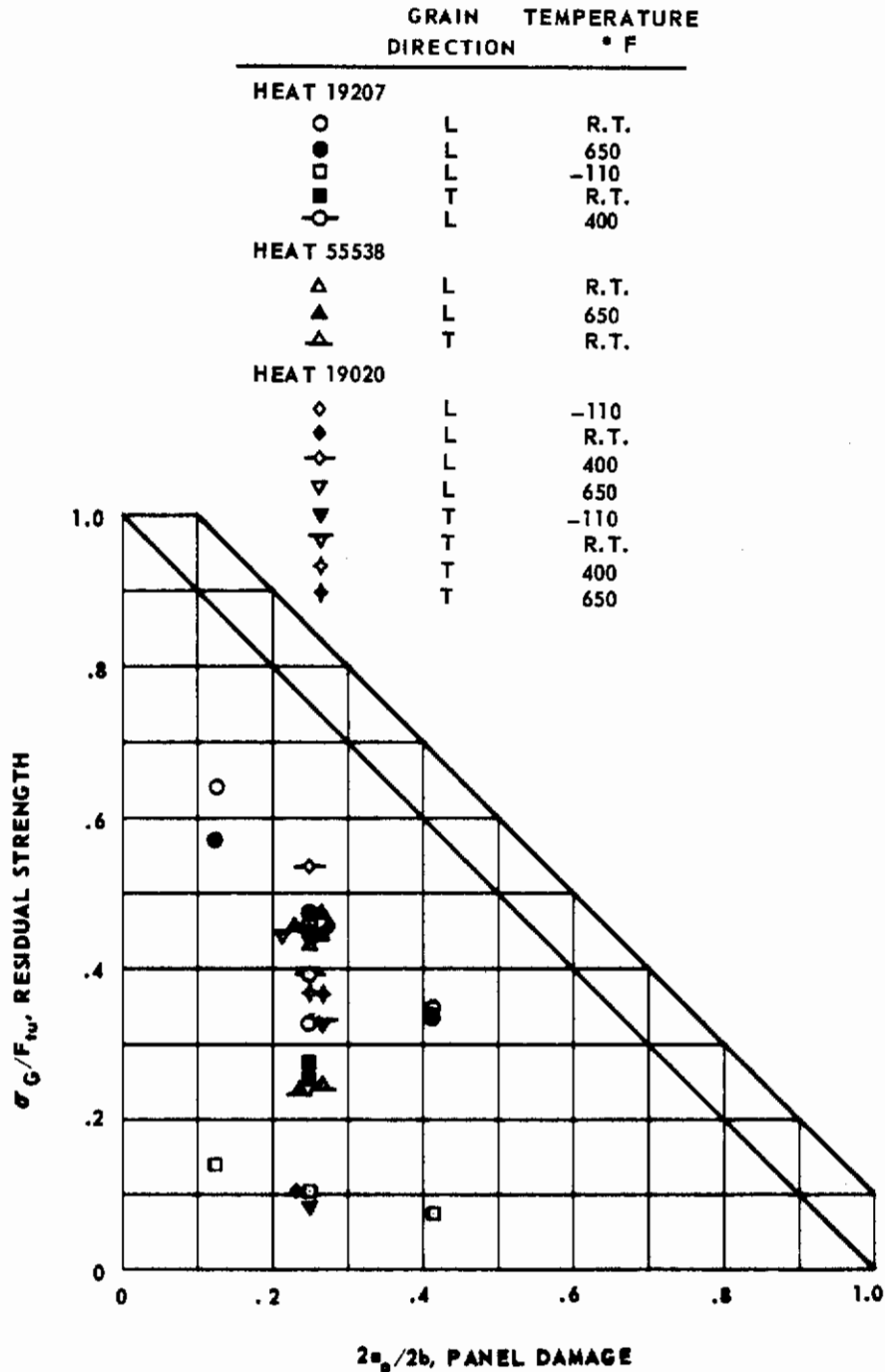


FIG. 96 RESIDUAL STRENGTH vs DAMAGE FOR 24 x 72 INCH AM 350 PANELS, HEATS 19207, 55538 AND 19020

NOTE:

$\dot{\sigma} \cong 10^6$ PSI/SEC

Points at $2a_0/2b = .25$ were Displaced

Laterally to Avoid Overplotting

	NOMINAL THICKNESS INCHES	GRAIN DIRECTION	TEMPERATURE ° F
O	.050	L	R.T.
□	.093	L	R.T.
△	.125	L	-110
◇	.125	L	R.T.
▽	.125	L	650
◊	.125	T	R.T.

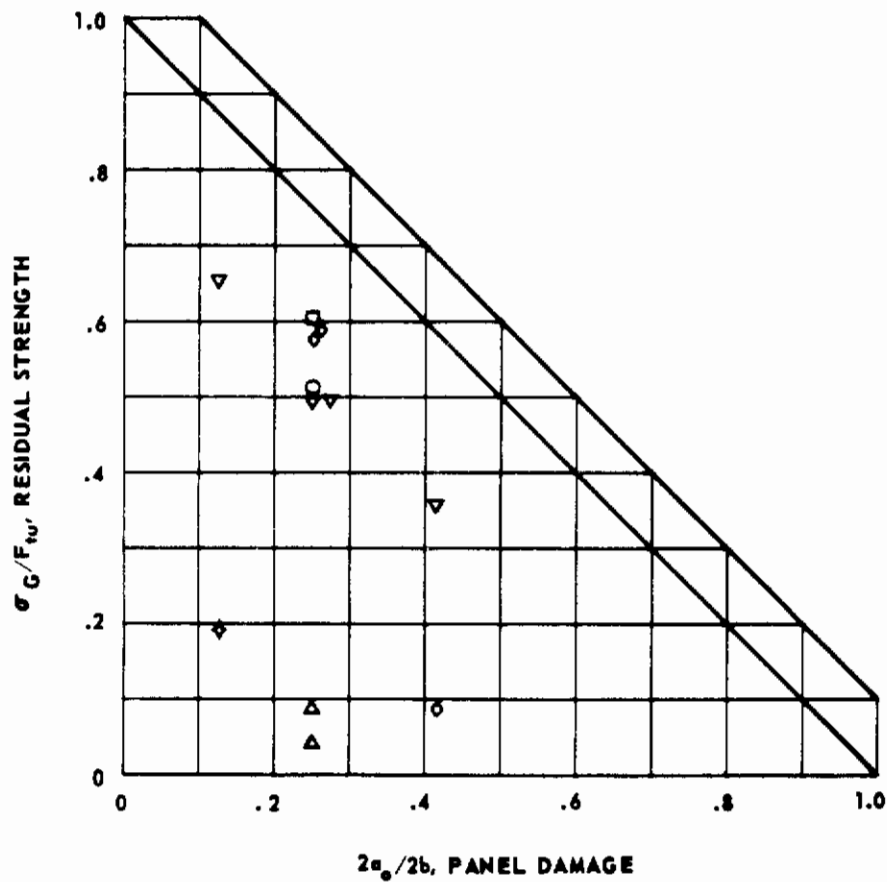


FIG. 97 RESIDUAL STRENGTH vs DAMAGE FOR 24 x 72 INCH AM 350 PANELS, HEAT 19020

The Effect of Stress Rate

The effect of stress rate on K_C is shown in Fig. 98 for both 8-inch and 24-inch wide panels. It is very difficult to generalize on the stress rate effect because of the large scatter in test points. For example, the 24-inch wide panels from heat 19207 show an almost negligible stress rate effect except for one very low K_C value at the 10^6 psi/sec stress rate. With the 24-inch wide panels from heat 55538, there is marked consistent increase in K_C with increasing stress rate. Tests from both these heats were made from 0.025 inch thick sheets from the longitudinal grain direction. The 0.125-inch longitudinal tests from heat 19020 show tremendous scatter which is probably the result of the metal-lurgical segregation effects previously discussed.

For the 8-inch wide transverse grain direction panels tested at stress rates of 5×10^3 and 10^6 psi/sec, there is no stress rate effect for either the 0.025 or the 0.125-inch thicknesses.

The Effect of Exposure

The effect of the 650° F exposure for 1000 hours at 40 ksi on K_C is shown in Fig. 99 for the 8 x 24-inch panels. Unexposed panel data are included for comparison. The exposure effect appears to be thickness dependent. For the 0.025-inch thick panel tests, exposure has resulted in a slight increase in K_C values. For the 0.050-inch panel tests, exposure has resulted in a very slight decrease in K_C values. For the 0.125-inch thick panel tests however, exposure has resulted in a 40 percent decrease in K_C values. Douglas exposure test results (Ref. 1) from 0.025-inch thick AM 350 SCT material paralleled those included herein for the 0.025-inch thickness.

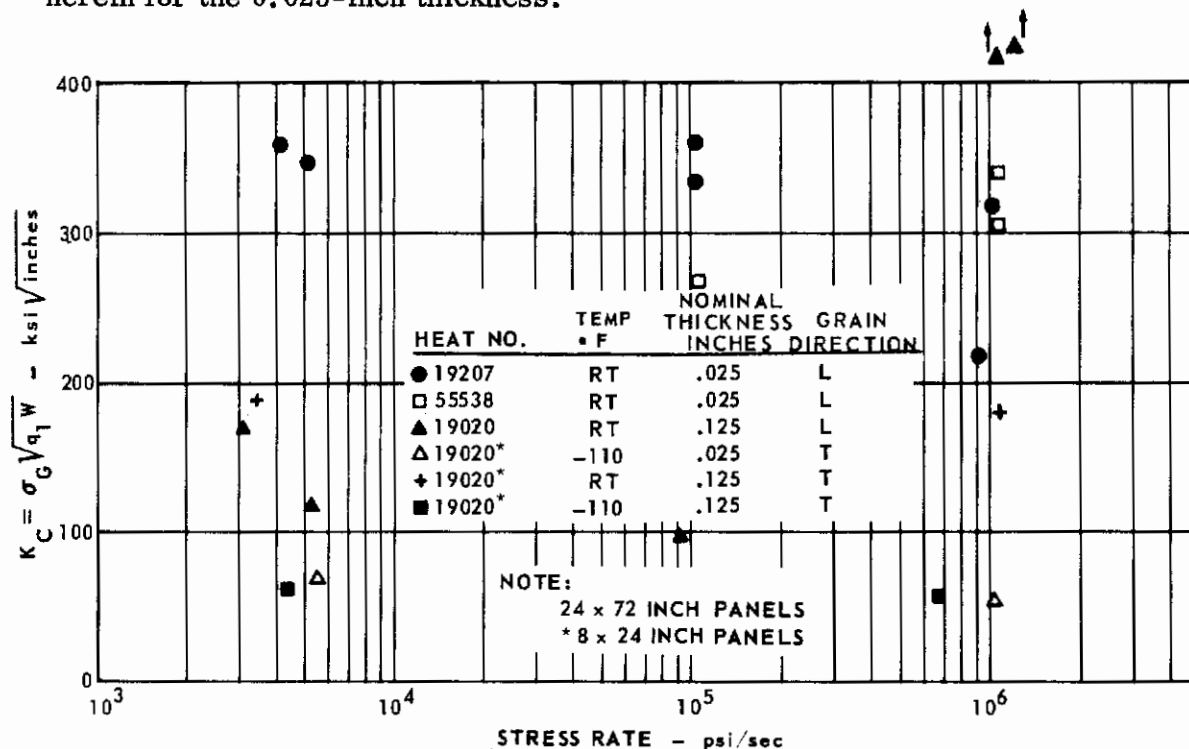


FIG. 98 THE EFFECT OF STRESS RATE ON K_C FOR AM 350

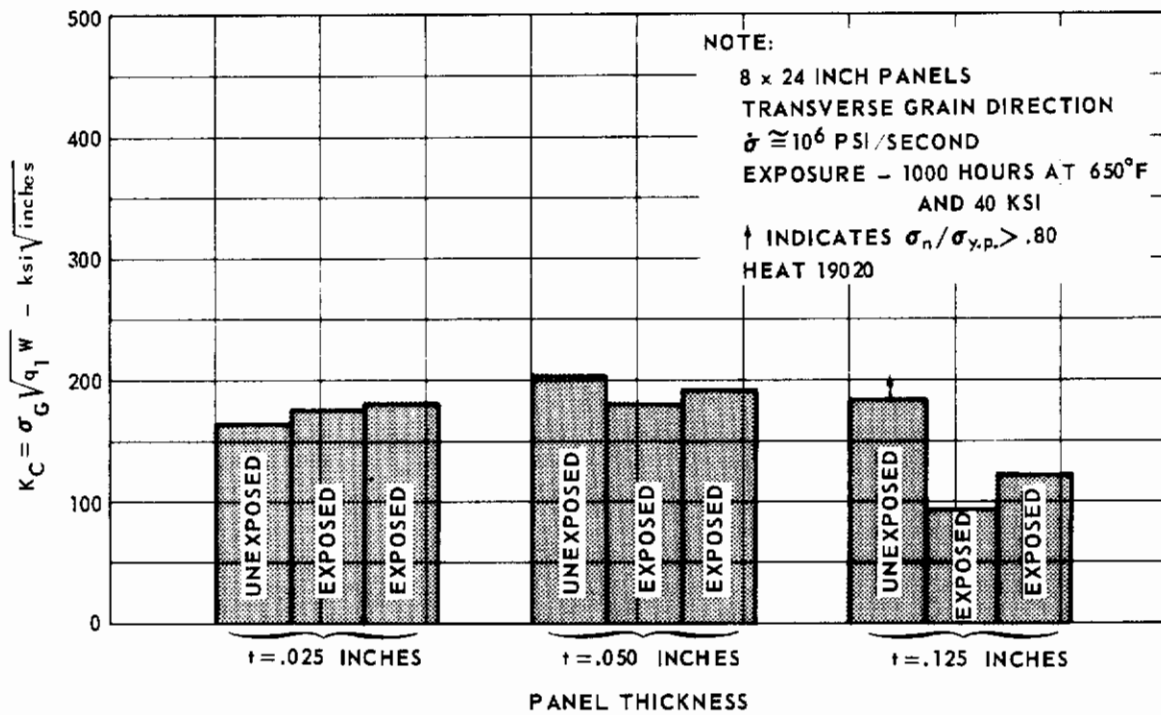


FIG. 99 COMPARISON OF EXPOSED AND UNEXPOSED K_C VALUES FOR AM 350

As discussed previously, the main microstructural differences existing among the various sheet thicknesses were the size and spacing of the delta ferrite stringers. It is possible that detailed metallurgical studies could explain how the morphology and distribution of the delta ferrite phase affects the alloy behavior under exposure conditions.

The Effect of Heat Variation

The effect of heat variation is shown partly by Fig. 90 in the previous subsection of grain direction. For the 24 x 72-inch room temperature tests of the three heats of material, K_{IC} varies as follows:

For the longitudinal grain direction, the average K_{IC} value is 301.7 ksi $\sqrt{\text{inches}}$ and values range from 218.5 to 343.0 ksi $\sqrt{\text{inches}}$. This range expressed as a percentage of the average value is 41 percent.

For the transverse grain direction, the average K_{IC} value is 181.6 ksi $\sqrt{\text{inches}}$ and values range from 164.0 to 219.3 ksi $\sqrt{\text{inches}}$. This range expressed as a percentage of the average value is 30 percent.

A similar comparison can be made from the room temperature and -110°F tests of the 8 x 24 x 0.025-inch transverse panels from the three heats for the 10^6 psi/sec stress rate. For the -110°F tests the average K_{IC} value is 62.3 ksi $\sqrt{\text{inches}}$ and the range in values as a percent of the average is 19 percent. For the room temperature tests, the average K_{IC} is 164.8 ksi $\sqrt{\text{inches}}$ and the range is 6.4 percent.

It is recognized that K_{IC} is a very sensitive material property and using the range in K_{IC} values as a measure of heat variation is probably a very severe evaluation method. However, many material comparisons are made based on K_{IC} values, and it is necessary to consider the most conservative value. A range in K_{IC} values of 40 percent among various heats would indicate that there is still a lack of complete understanding of how to control the basic metallurgical structure to produce consistent fracture toughness properties.

Fractographic Studies

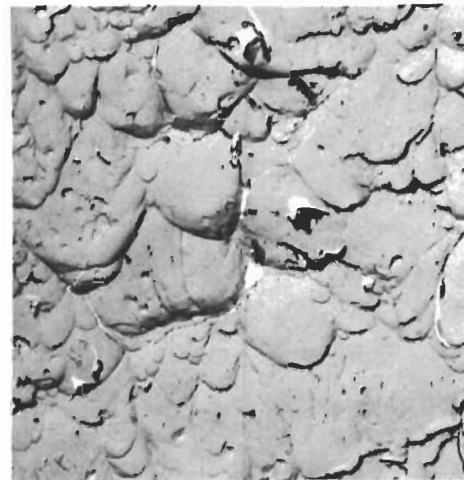
Several fracture specimens were examined with the wide-field microscope and the electron microscope. Fig. 100 includes the results of an analysis of specimen DB74 which best represents the typical results of all the panels studied.

The lower right-hand electron micrograph shows the fine striations typical of fatigue cracked areas in AM 350. In the thick specimens (0.125 inch) many of the electron micrographs showed a gross lamellar texture in addition to the fine striations. It is believed that this fracture morphology is the result of the banded AM 350 microstructure.

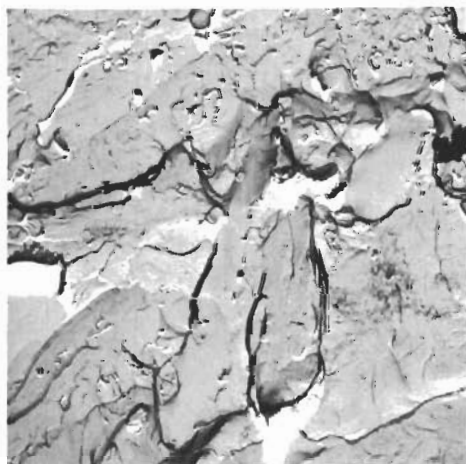
The lower left-hand electron micrograph shows an isolated cleavage area found in the rapid fracture portion of the surface. This mode of cracking is the characteristic brittle cracking mode for alloys with the body-centered cubic crystal



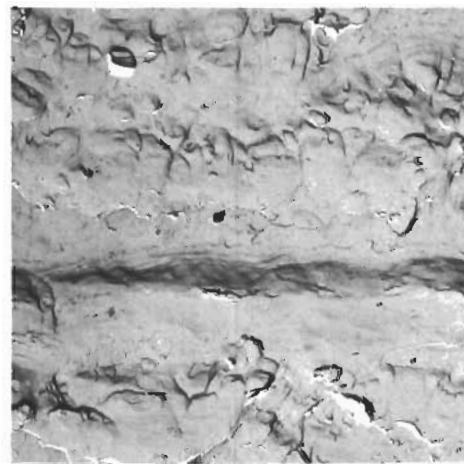
(A) PLANE STRAIN AREA OF RAPID FRACTURE (1700x)



(B) ELONGATED DIMPLES AT SHEAR LIP (1700x)



(C) ISOLATED CLEAVAGE ISLAND (1700x)



(D) FINE FATIGUE STRIATIONS IN A BANDED STRUCTURE (1700x)

NOTE: Fatigue Cracked and Fractured at Room Temperature

FIG. 100 FRACTOGRAPHIC STUDY OF AM 350 SPECIMEN DB74

structure. Generally the tendency toward this brittle fracture mode increases with decreasing temperature. The AM 350 panels tested at -110°F showed that a large portion of the rapid fracture surface was of the cleavage fracture mode.

The two upper micrographs illustrate the difference in typical fracture characteristics between the flat and shear-lip areas. Dimples from the plane strain flat area tend to be blocky and somewhat featureless, while dimples from the shear lip area have dominant features and are elongated to some extent. In future fracture studies, particularly with thicker sections, this method of study may be useful in determining plane strain material characteristics from plane stress fracture tests.

Inco 718 NICKEL ALLOY

Chemistry and Mill Processing History

The chemical composition of the three heats of material are shown in Table 15 along with the specification ranges. Variation in composition among the heats is small and all elements meet the specification requirements.

The mill processing history received from the Huntington Alloy Products Division of Inco is described in the following list.

- 1) Vacuum arc melt
- 2) Condition and convert ingot to sheet bar

TABLE 15 VENDOR CERTIFIED CHEMICAL ANALYSIS FOR INCO 718 (WEIGHT, PERCENT)

		C	Mn	S	Si	Cr	Ni	Al	Mo	Fe	Cu	Ti	Cb+Ta	B
INCO 718	6713 EV	.03	.22	.007	.42	18.45	52.85	.35	3.11	18.45	.04	.94	4.88	
	6905 EV	.04	.18	.007	.27	18.68	52.00	.33	3.07	19.16	.04	1.01	5.19	
	6902 EV	.05	.17	.007	.35	18.70	52.46	.22	2.99	19.29	.03	.80	4.91	
	SPEC. MIN.					17.0	50.0	.1	2.80			.70	4.75	.002
	SPEC. MAX.	.10	.35	.015	.45	21.0	55.0	.6	3.30	BAL.	.30	1.40	5.25	.010

- 3) Hot roll sheet bars to sheet
- 4) Anneal sheet
- 5) Pickle sheet
- 6) Cold roll sheets approximately 20 to 30 percent. The actual reduction was 27 percent for the 0.025-inch thick material from heats 6713, 6902, and 6905; 21 percent for the 0.050-inch thick material from heat 6902; 18 percent for the 0.093-inch thick material from heat 6902; and 23 and 26 percent for the 0.125-inch thick material from heat 6902
- 7) Level
- 8) Cut to length

This processing history lacks many of the specific details such as ingot size, the amount of reduction, rolling temperatures, and annealing temperatures. It should be noted that there is some variation in the amount of cold reduction among the various sheet thicknesses.

Microstructure

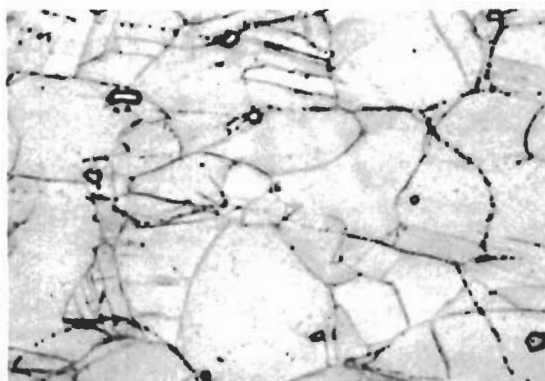
Micrographs representing both longitudinal and transverse sections from the three heats of Inco 718 are shown in Fig. 101. It is very difficult to etch this material to show general microstructural details. Because of this limitation and because the microstructural makeup of this alloy is rather complex, the detection of variations among the three heats is virtually impossible. There is evidence shown in Fig. 101 that some recrystallization has occurred. Twinning in the structure also appears to be rather general. Fig. 102 shows typical micrographs of both longitudinal and transverse sections from three material thicknesses of heat 6902. Differences in grain size, the amount of twinning and the degree of recrystallization do not seem to form a consistent pattern. It was not possible to correlate any of the microstructural features with the different amounts of cold reduction.

Tensile Properties

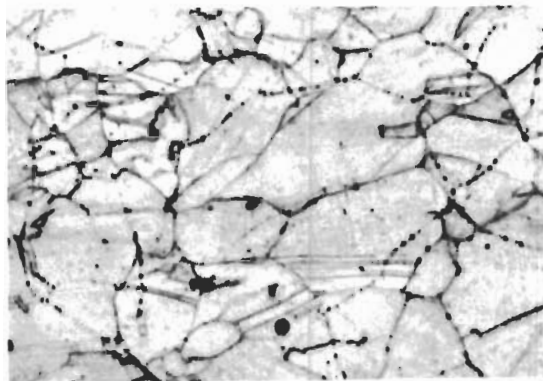
Tensile test results for the temperature range -110 to 650°F for the three Inco 718 heats are included in Table 16. The tensile properties show little variation among the three heats of material or among the three thicknesses of heat 6902. The thick (0.125-inch) material does have the highest strength properties, however. Generally the longitudinal test results are higher than the transverse.

Initially, 10 percent elongation was required in the proposed specification. However, purchase of the material on a "best effort" basis resulted in a guarantee of only 6 percent elongation. Table 16 shows that the original 10 percent elongation value was met or exceeded by the tests for all but the 0.125-inch thick material.

HEAT 6713, $t = .025$ INCHES

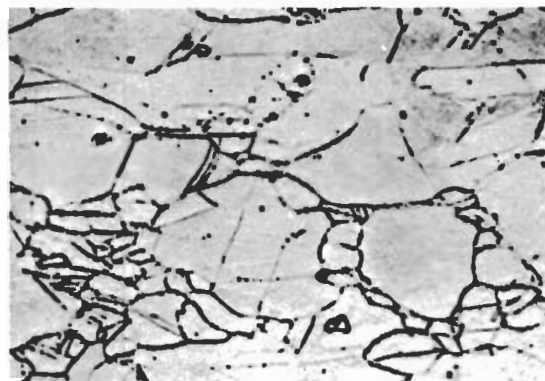


(A) LONGITUDINAL GRAIN (500x)

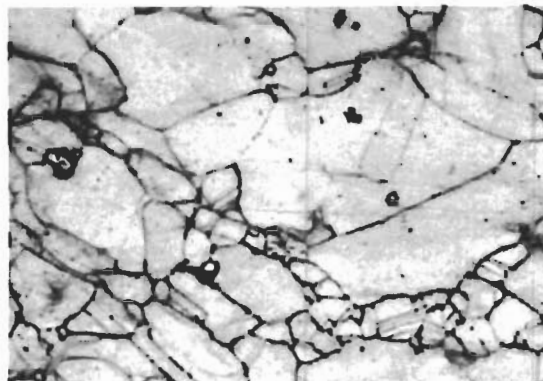


(B) TRANSVERSE GRAIN (500x)

HEAT 6905, $t = .025$ INCHES



(C) LONGITUDINAL GRAIN (500x)

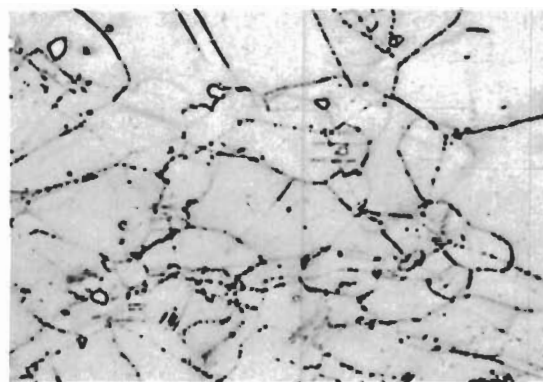


(D) TRANSVERSE GRAIN (500x)

HEAT 6902, $t = .025$ INCHES



(E) LONGITUDINAL GRAIN (500x)



(F) TRANSVERSE GRAIN (500x)

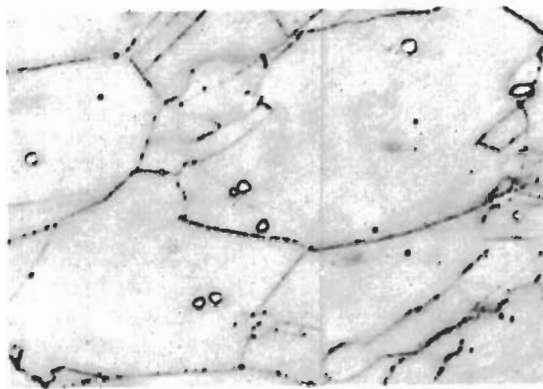
NOTE: Tartaric Acid Etchant

FIG. 101 PHOTOMICROGRAPHS OF INCO 718, HEATS 6713, 6905 AND 6902

$t = .050$ INCHES

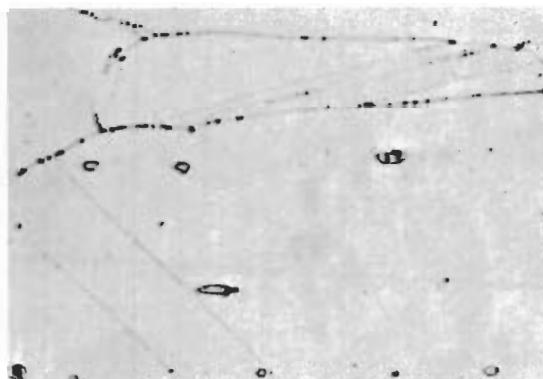


(A) LONGITUDINAL GRAIN (500x)

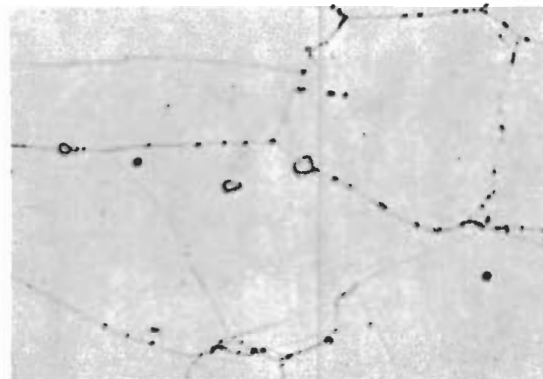


(B) TRANSVERSE GRAIN (500x)

$t = .093$ INCHES



(C) LONGITUDINAL GRAIN (500x)

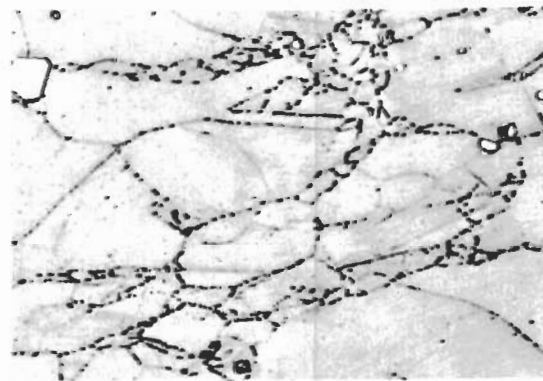


(D) TRANSVERSE GRAIN (500x)

$t = .125$ INCHES



(E) LONGITUDINAL GRAIN (500x)



(F) TRANSVERSE GRAIN (500x)

NOTE: Tartaric Acid Etchant

FIG. 102 PHOTOMICROGRAPHS OF INCO 718 SHOWING THICKNESS VARIATION, HEAT 6902

TABLE 16 TENSILE TEST DATA FOR INCO 718

HEAT NO.	NOMINAL THICKNESS inches	GRAIN DIRECTION	TEST TEMPERATURE											
			-110° F				R. T. (68° F)				400° F			
			F TU (ksi)	F TY (ksi)	ELONG.*	F TU (ksi)	F TY (ksi)	ELONG.*	F TU (ksi)	F TY (ksi)	ELONG.*	F TU (ksi)	F TY (ksi)	ELONG.*
6713	.025	T	229.3	199.2	13.0	213.2	193.1	11.5	194.6	178.2	7.5	188.2	173.8	9.5
		T				213.8	193.0	11.0	196.2	178.1	7.5	187.1	173.8	9.0
		L	232.8	210.8	11.5	218.4	201.5	11.5	200.7	185.9	8.5	188.7	177.8	9.0
		L				219.3	202.6	12.0				190.9	179.9	10.5
6905	.025	T	225.5	201.8	11.5	212.8	191.6	11.0				190.2	169.9	11.5
		T				211.2	-	10.5						
		L	237.4	222.1	10.5	222.1	-	11.0				192.5	178.7	7.0
		L				220.3	201.1	10.0				192.2	179.2	6.0
6902	.025	T	233.5	205.3	11.5	213.9	194.3	10.5	198.4	-	7.5	187.5	172.3	10.0
		T				213.5	194.1	10.5	198.8	183.3	7.5	190.8	177.0	8.0
		L	232.9	215.8	10.5	217.1	201.9	10.0	201.5	187.8	8.5	192.0	180.3	9.0
		L				217.7	202.4	10.5	201.8	187.8	9.0			
	.050	T	226.5	198.8	13.0	200.0	180.2	11.0	192.0	172.6	9.0	182.5	170.7	9.5
		T				200.0	180.6	11.0						
		L	229.8	201.9	14.5	211.4	193.5	14.0	194.2	178.3	13.0	183.9	175.4	11.0
		L	230.1	204.5	14.0	213.6	193.1	13.5	194.6	179.3	12.5	184.6	175.0	11.0
	.093	T	228.2	197.9	15.0	208.3	187.2	11.0				182.8	170.2	5.0
		T				207.7	186.8	11.5						
		L	232.9	207.9	14.0	214.6	196.0	13.5				185.7	177.2	10.0
		L				214.1	196.2	13.5						
	.125	T	233.0	212.2	8.5	218.5	199.3	8.5	200.4	183.4	6.5	193.9	177.9	9.0
		T				218.5	199.4	8.5				193.8	177.2	7.5
		L	241.0	225.7	7.5	224.6	212.1	8.0	205.4	197.6	6.0	197.6	187.1	6.0
		L	240.8	217.8	9.5	224.6	212.0	8.5	205.2	197.4	6.0	197.4	187.4	6.0

* ELONGATION MEASURED AS % IN 2 INCHES

TABLE 16 TENSILE TEST DATA FOR INCO 718 (continued)

HEAT NO.	NOMINAL THICKNESS inches	GRAIN DIRECTION	TEST TEMPERATURE												
			-110° F			R. T. (68° F)			400° F			650° F			
			F _{TU} (ksi)	F _{TY} (ksi)	ELONG.*	F _{TU} (ksi)	F _{TY} (ksi)	ELONG.*	F _{TU} (ksi)	F _{TY} (ksi)	ELONG.*	F _{TU} (ksi)	F _{TY} (ksi)	ELONG.*	
6902 **	.025	T				215.3	195.9	10.0							
		T				214.9	195.9	10.0							
	.050	T				209.4	188.2	11.0							
		T				208.2	187.1	11.0							
	.125	T				218.2	198.4	10.0							
		T				217.9	197.9	9.0							

* ELONGATION MEASURED AS % IN 2 INCHES

**AFTER EXPOSURE AT 650° F FOR 1000 HOURS AT A GROSS STRESS LEVEL OF 40 ksi

Tensile test data from specimens cut from failed halves of the exposed fracture panels are also included in Table 16. For the 0.025 and the 0.125-inch thick material, there was no change in tensile properties as a result of the exposure treatment. For the 0.050-inch thick material, the tensile ultimate and yield strengths are approximately 4 percent higher for the exposed material.

Fatigue Crack Propagation Results

Crack Growth Data

Crack growth test results for the 24 x 72-inch Inco 718 panels are shown in Figs. 103 through 110. The final increment of crack growth was carried out in each case at a stress level that put the final stress intensity factor at approximately 75 ksi $\sqrt{\text{inches}}$. With the 24-inch wide panels, this meant the final cycling stress for 3-inch cracks was 40 ksi; for 6-inch cracks, 28 ksi; and for 10-inch cracks, 20 ksi. All final crack tip preparation was carried out at a stress ratio of 0.20.

For many of the specimens, it was virtually impossible to reinitiate cracking when the stress level was reduced for the final crack tip preparation. In order to circumvent this problem, a small cut was made with a jewellers' saw at each end of the crack tip as noted on the appropriate figures.

Crack growth data for the unexposed 8 x 24-inch panels are included in Figs. 111 through 114. Data for exposed panels are included in Fig. 115. Final crack tip preparation was also carried out with these small panels to produce a final K level of approximately 75 ksi $\sqrt{\text{inches}}$. For the one inch final crack length, a stress level of 60 ksi was used. For the 2-inch final crack length, which was the principal length tested, a stress level of either 36 or 40 ksi was used. For the 3-inch final crack length, a stress level of 32 ksi was used. All final cracking was made at a stress ratio of 0.20. Two specimens DC94 and DC95 (Fig. 114) were cycled to failure to parallel Douglas testing (Ref. 1).

From these crack growth curves, two general observations can be made about the cycles required to grow a given crack length: (1) they decrease with an increase in the gross stress level and (2) they decrease with a decrease in the stress ratio.

Crack Growth Rate Data

Crack growth rate data are shown in Figs. 116 through 122 for the unexposed panels. Fig. 116 shows two somewhat indistinct data groupings for heat 6713. In general, the data gathered at a stress ratio of 0.60 show the slowest cracking rate. However, for two panels (DC8 and DC16) that were fatigue cracked at a stress ratio of 0.20 the test data also lie in this grouping. Testing records and computations were rechecked but these data appear to be correct. The second grouping contains both longitudinal and transverse test results and there does not appear to be any significant difference.

Fig. 117 again shows two general data groupings. The majority of data was derived at a stress ratio of 0.05 and the two boundaries indicate a rather broad scatter band. The transverse panel test points for both 8-inch and 24-inch wide panels lie near the boundary exhibiting the fastest rate of crack growth.

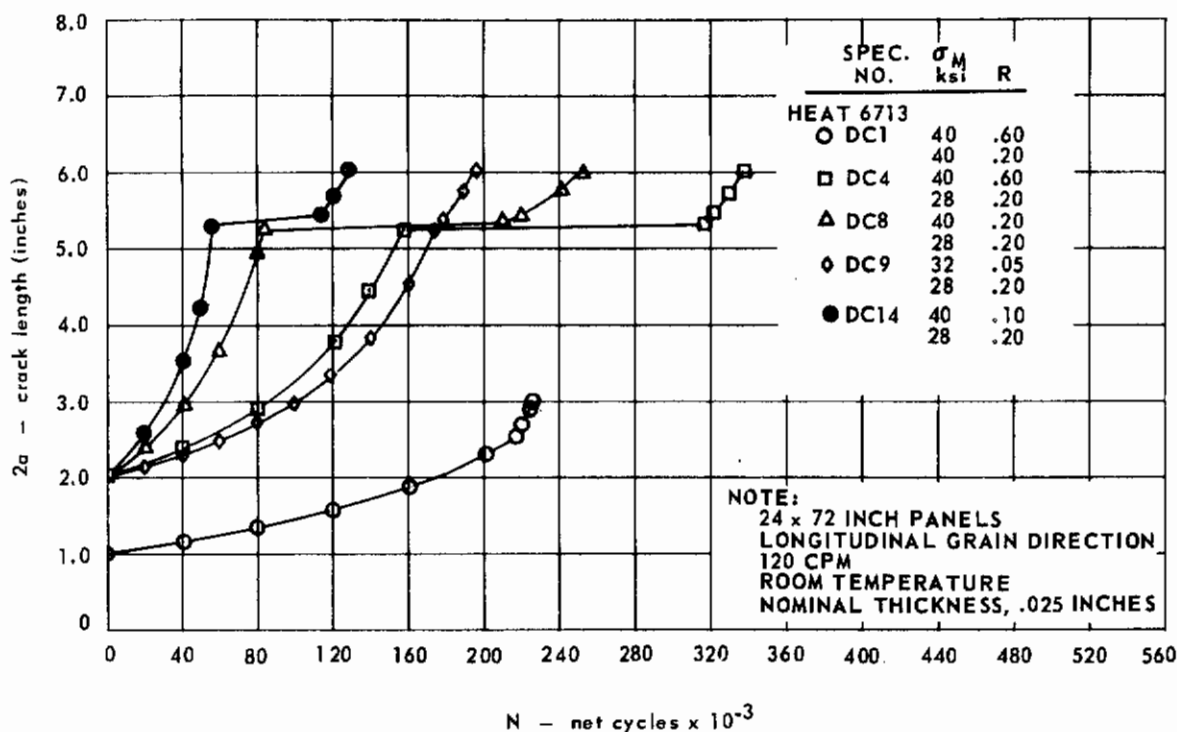


FIG. 103 CRACK GROWTH DATA FOR INCO 718, HEAT 6713

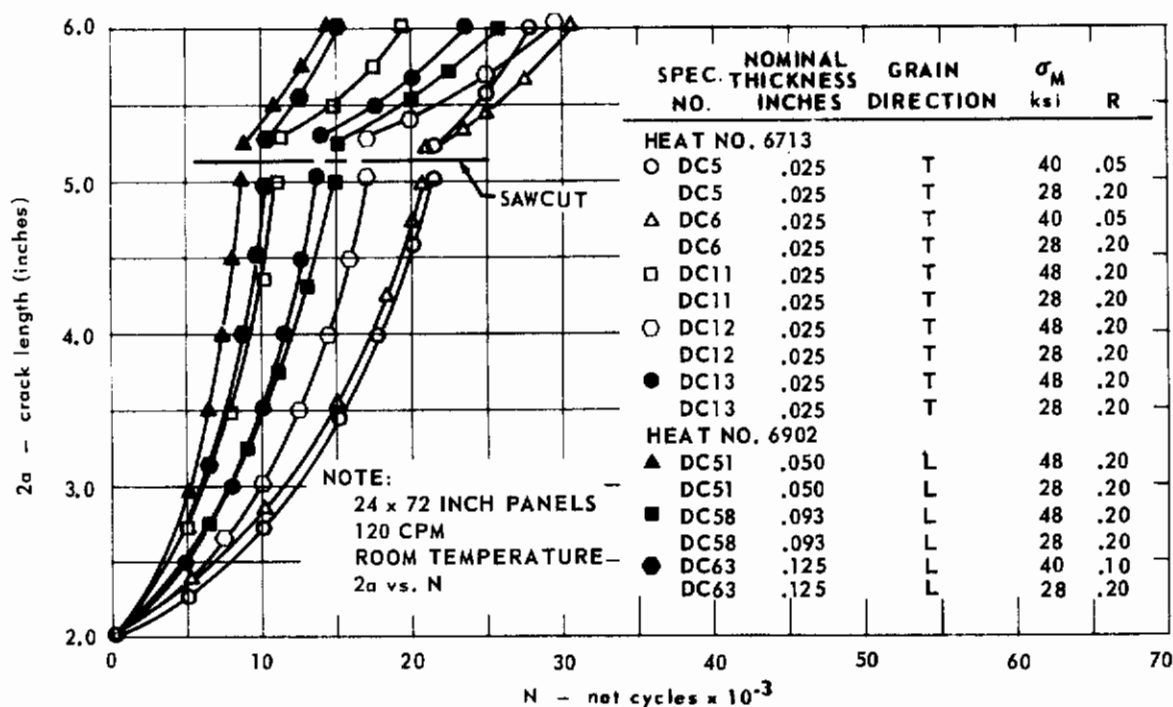


FIG. 104 CRACK GROWTH DATA FOR INCO 718, HEAT 6713 AND 6902

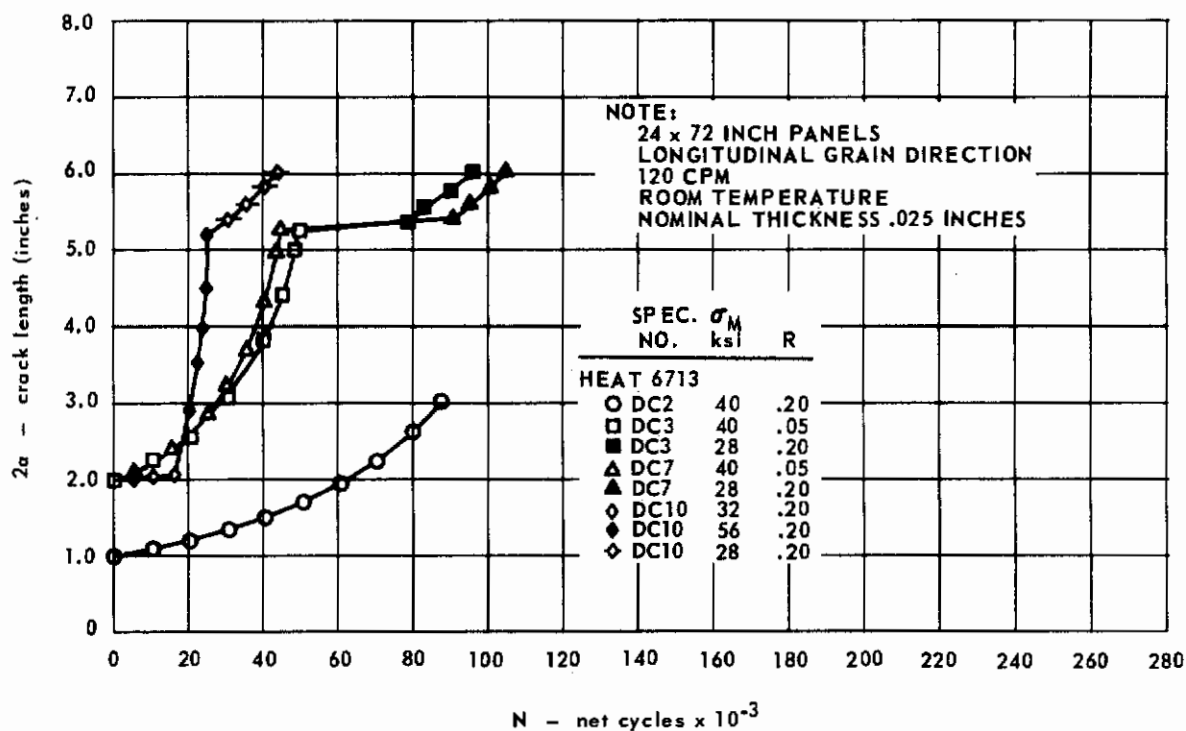


FIG. 105 CRACK GROWTH DATA FOR INCO 718, HEAT 6713

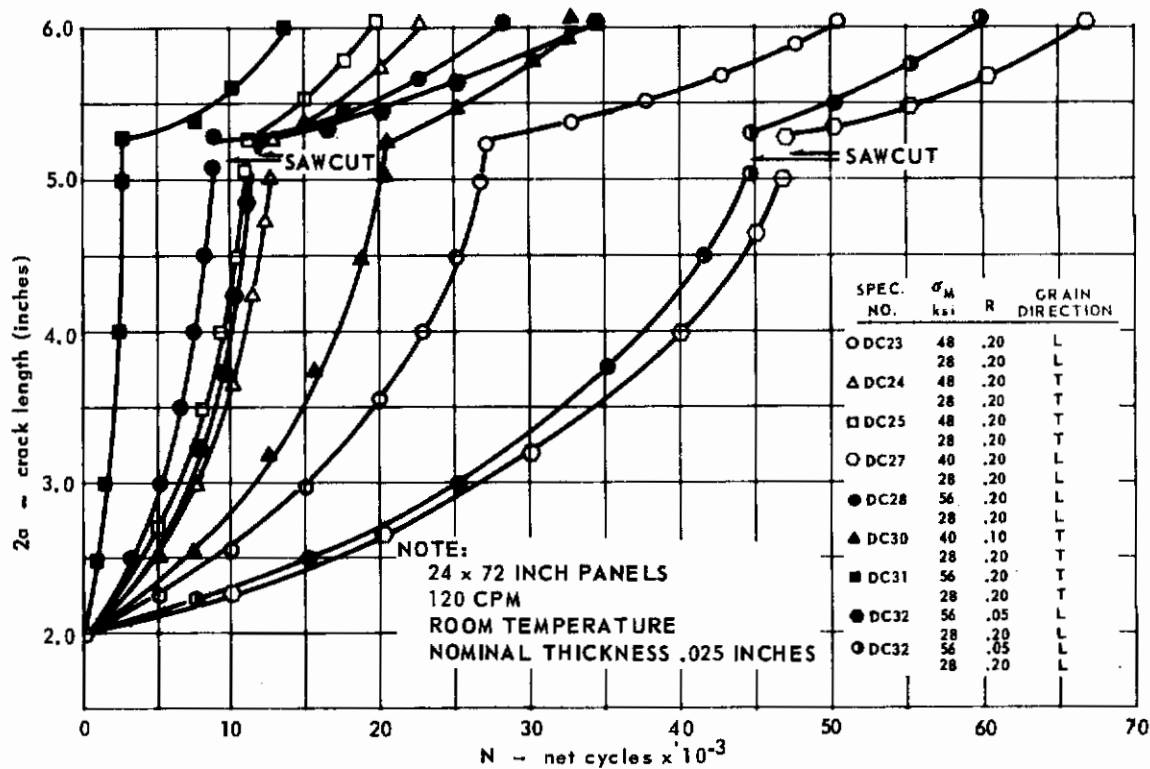


FIG. 106 CRACK GROWTH DATA FOR INCO 718, HEAT 6905

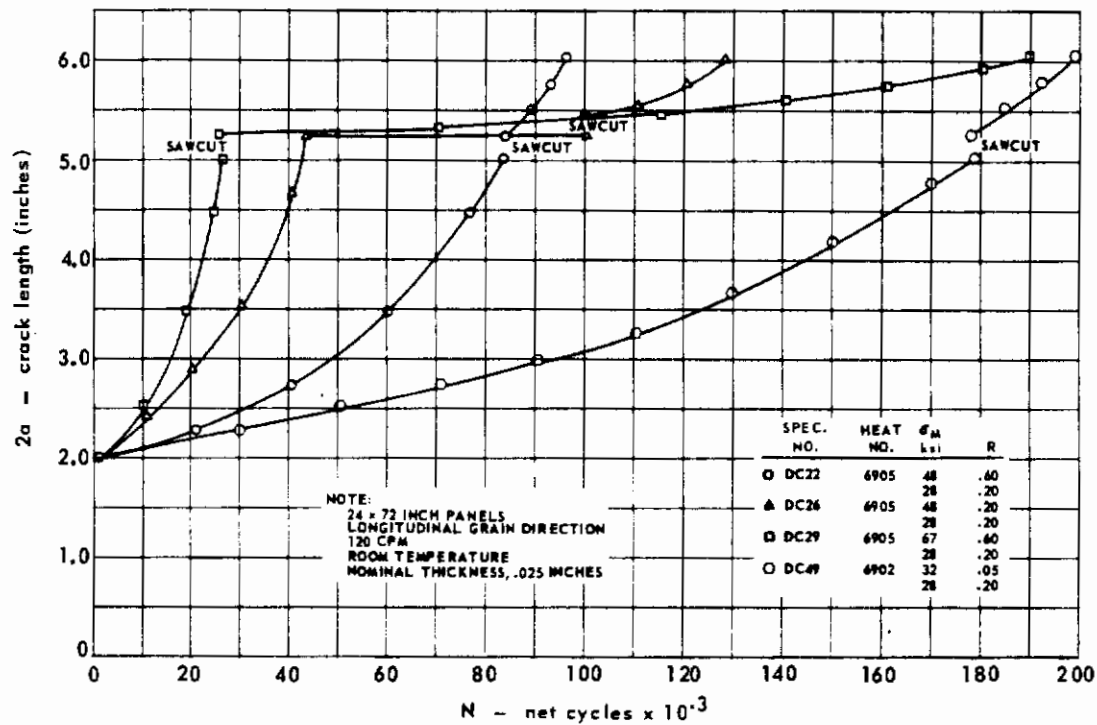


FIG. 107 CRACK GROWTH DATA FOR INCO 718, HEATS 6905 AND 6902

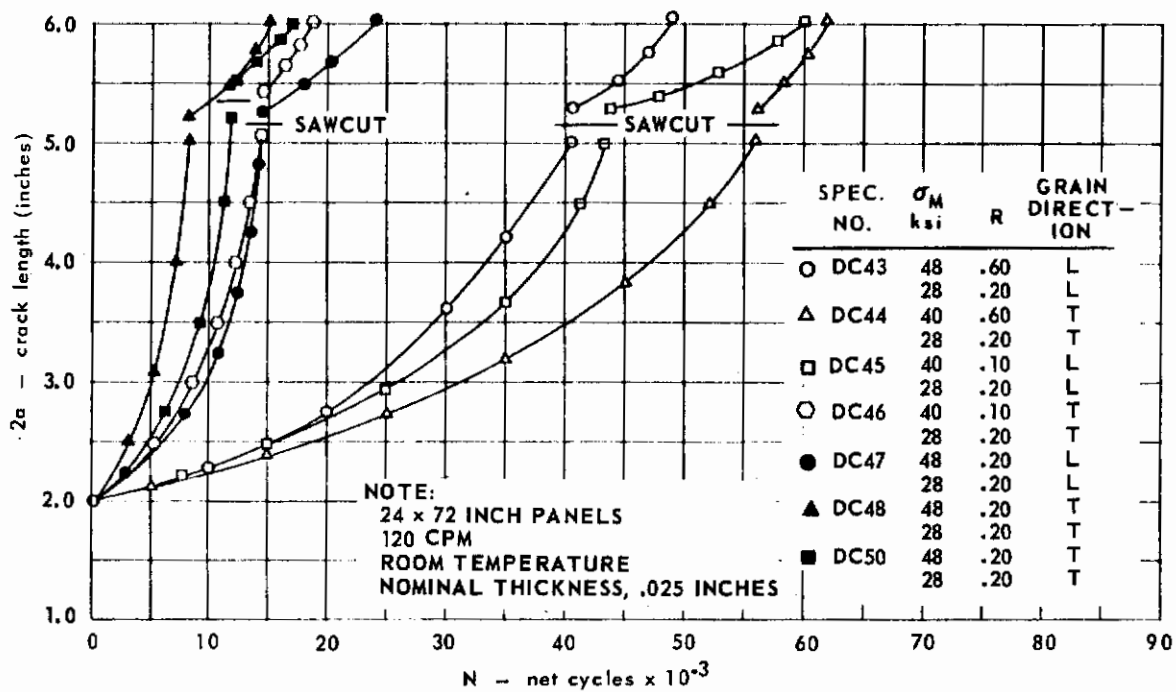


FIG. 108 CRACK GROWTH DATA FOR INCO 718, HEAT 6902

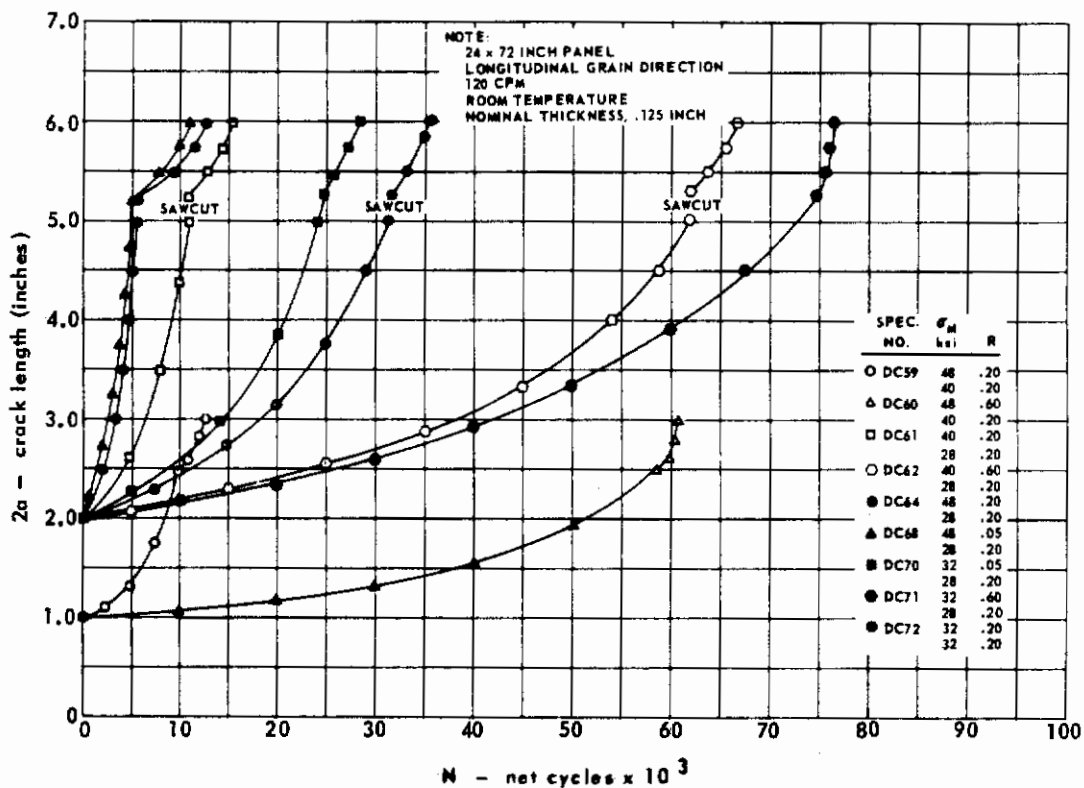


FIG. 109 CRACK GROWTH DATA FOR INCO 718, HEAT 6902

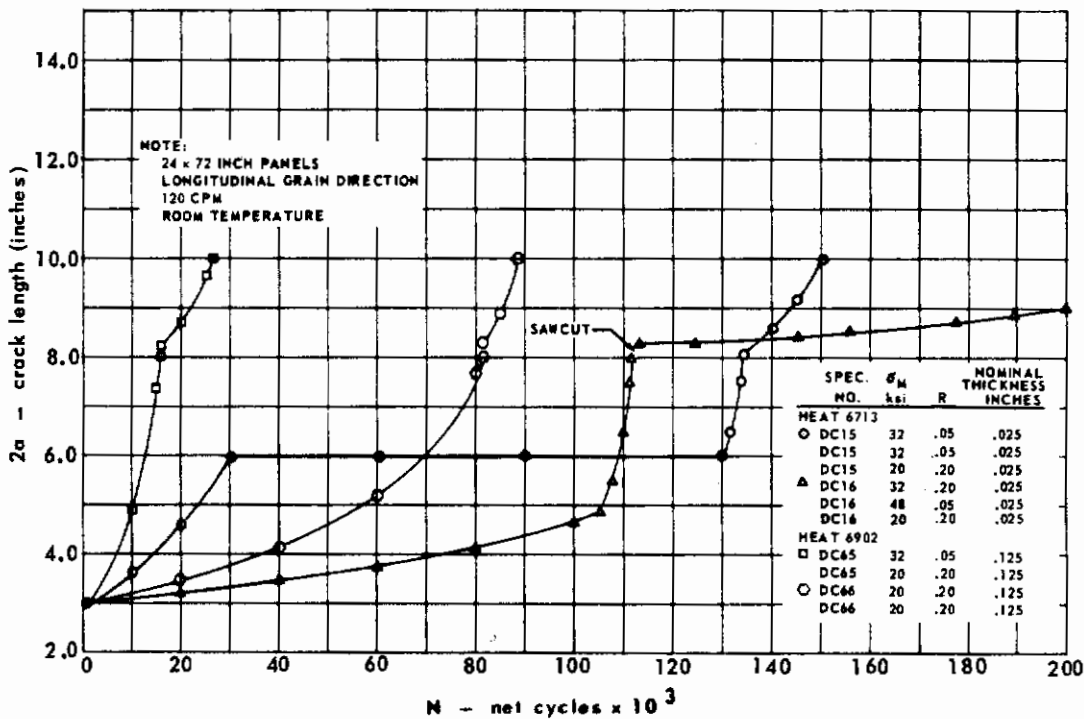


FIG. 110 CRACK GROWTH DATA FOR INCO 718, HEATS 6713 AND 6902

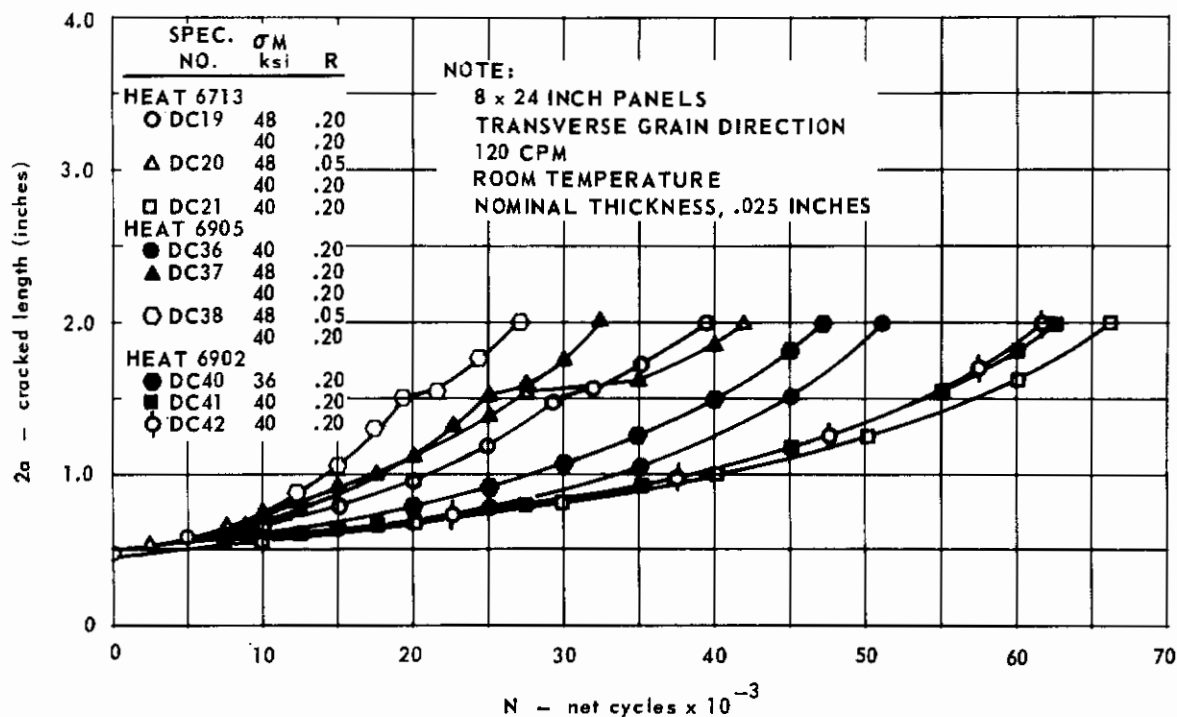


FIG. 111 CRACK GROWTH DATA FOR INCO 718, HEATS 6713, 6905 AND 6902

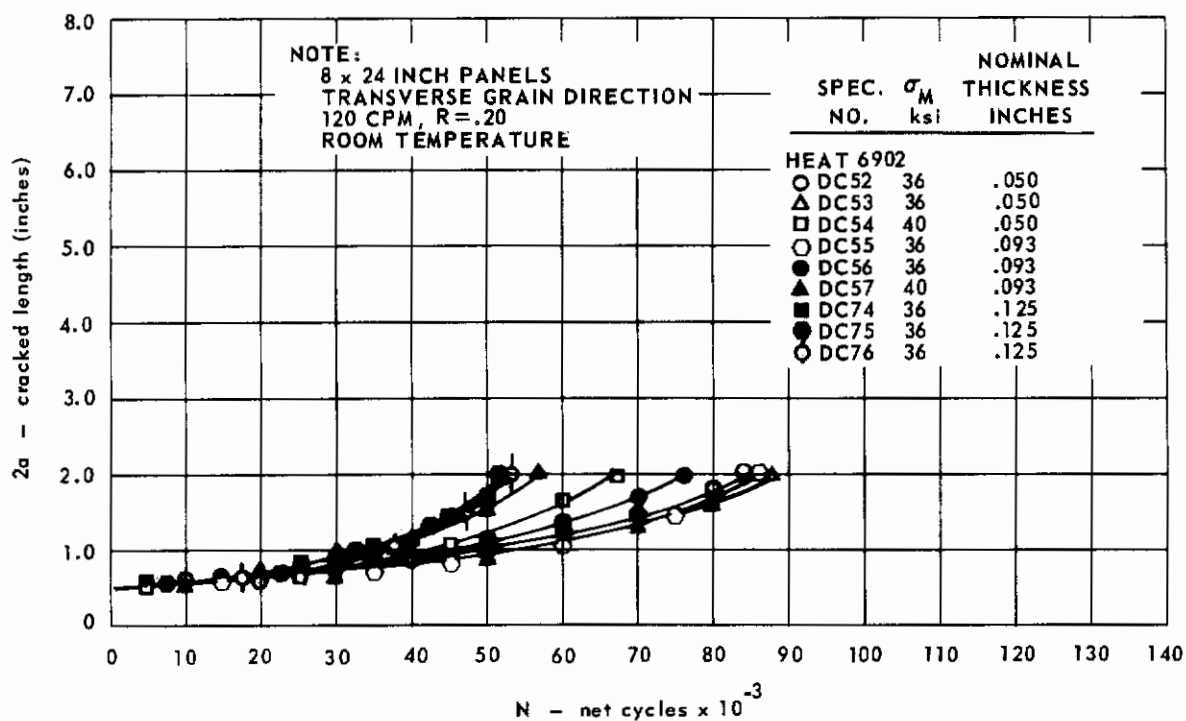


FIG. 112 CRACK GROWTH DATA FOR INCO 718, HEAT 6902

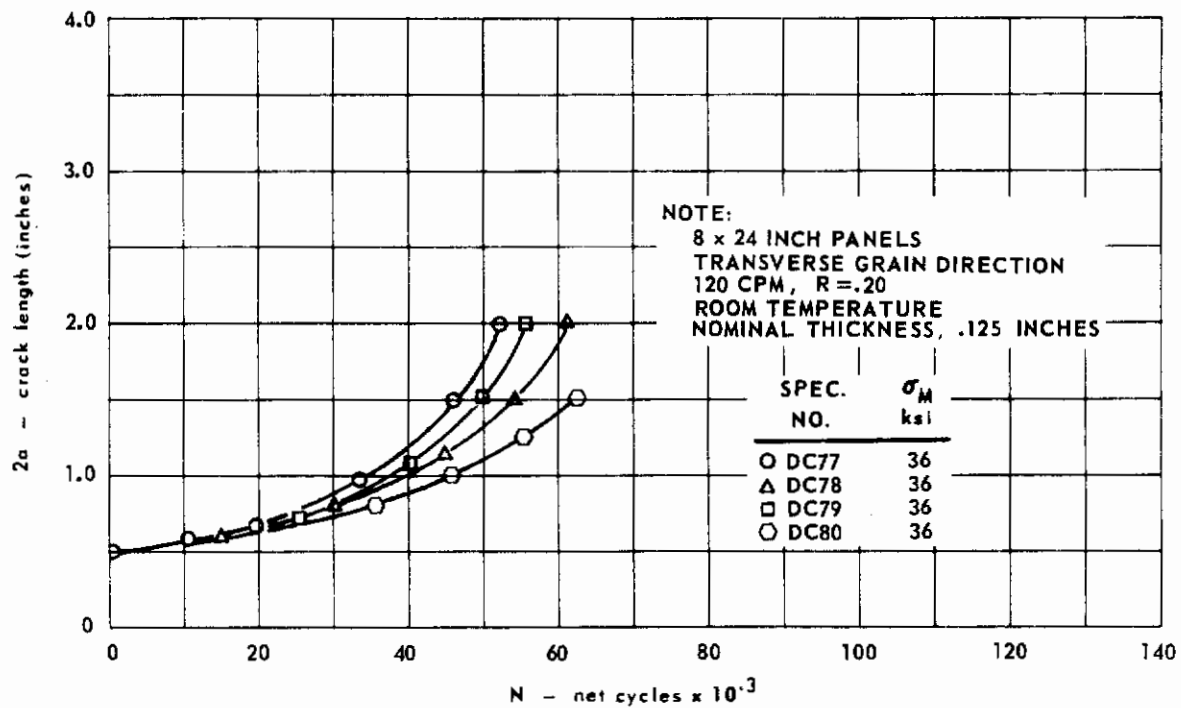


FIG. 113 CRACK GROWTH DATA FOR INCO 718, HEAT 6902

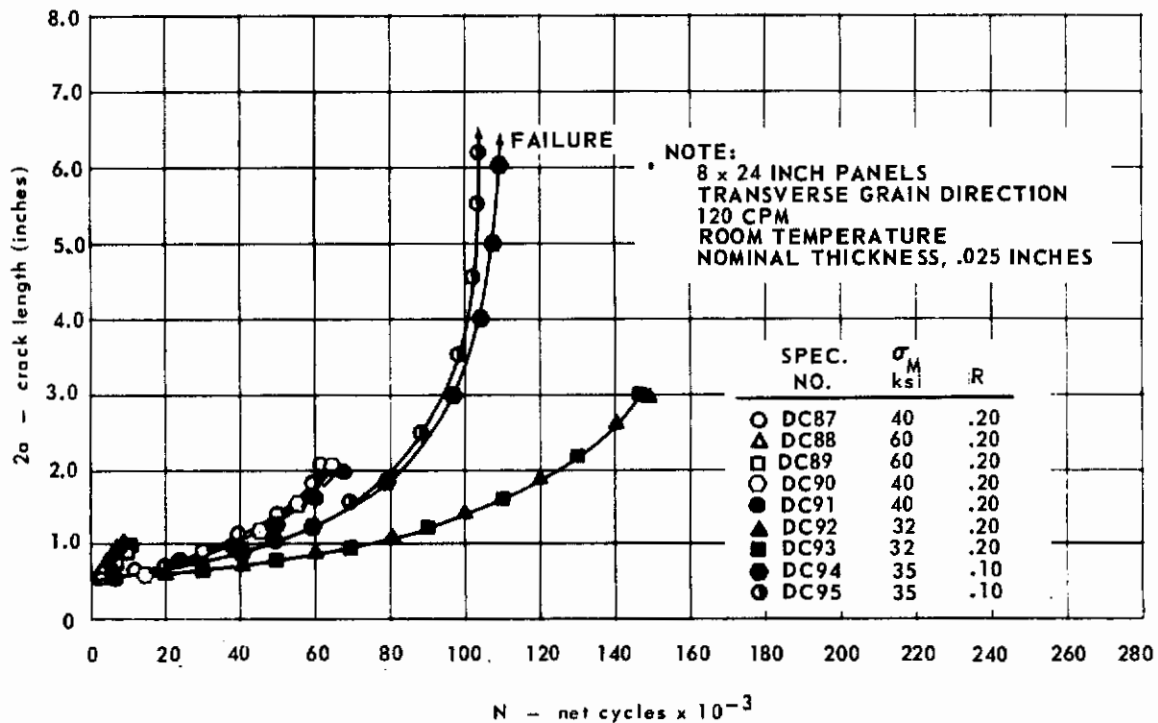


FIG. 114 CRACK GROWTH DATA FOR INCO 718, HEAT 6902

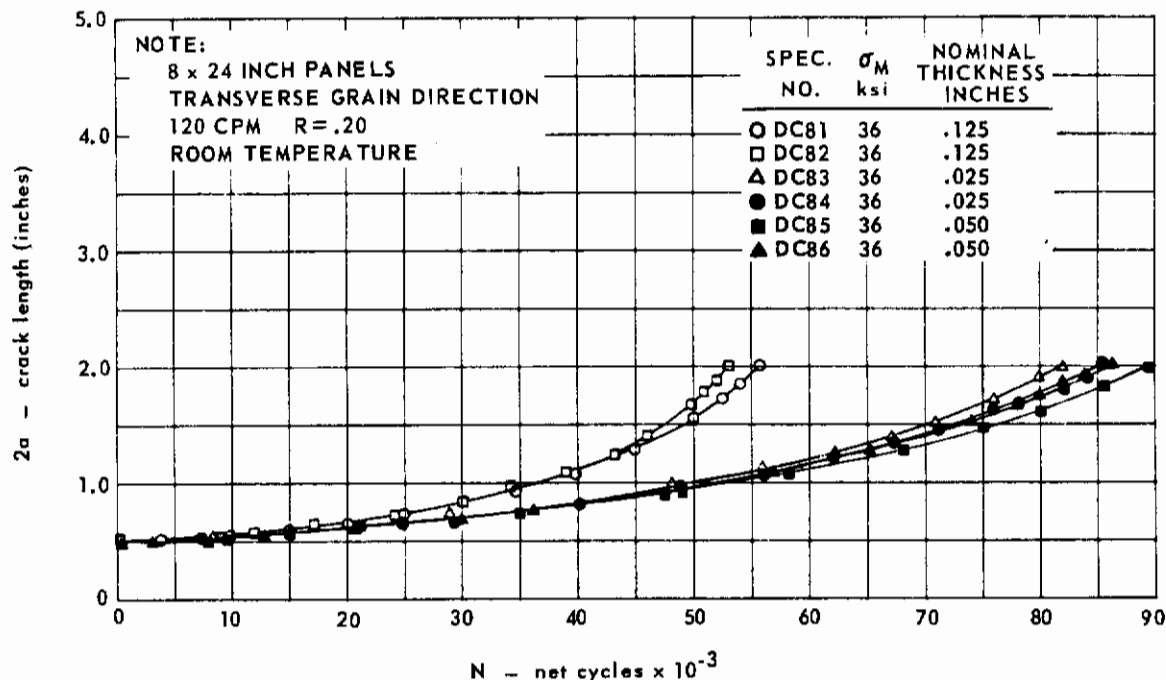


FIG. 115 CRACK GROWTH DATA FOR EXPOSED INCO 718 PANELS, HEAT 6902

Fig. 118 shows the expected distinct difference in cracking rates between the stress ratios of 0.20 and 0.60 for heat 6905. For this heat, both the 8-inch and 24-inch wide transverse panel tests show a higher crack propagation rate than the longitudinal tests. Fig. 119 shows that this heat of Inco 718 has a relatively wide scatter band.

Fig. 120 shows the expected distinct difference in cracking rates for the stress ratios of 0.20 and 0.60 for heat 6902. The results of these test data parallel those of heat 6905 (Fig. 118). Again, tests in the transverse grain direction show the most rapid crack propagation rate. Both the 8-inch and 24-inch wide transverse panel test data fall on the same curve under similar test conditions.

Fig. 121 shows that there is very little difference in cracking rates among the thicknesses of 0.025, 0.050 and 0.093-inch. For the 0.125-inch thickness there appears to be an increased cracking rate compared to the thinner materials. Fig. 121 also shows that with the 0.125-inch thick material, the crack growth rates of the 8-inch wide transverse panels are similar to those of the 24-inch wide longitudinal panels. Fig. 122 shows similar test results for the 8-inch wide transverse and 24-inch wide longitudinal panels.

Figs. 123, 124 and 125 show crack growth rate comparisons for both exposed and unexposed panels from heat 6902. The exposure treatment appears to have had no effect on the crack growth rate for any of the three thicknesses studied. The 0.125-inch thick panel data show the greatest amount of scatter for both conditions.

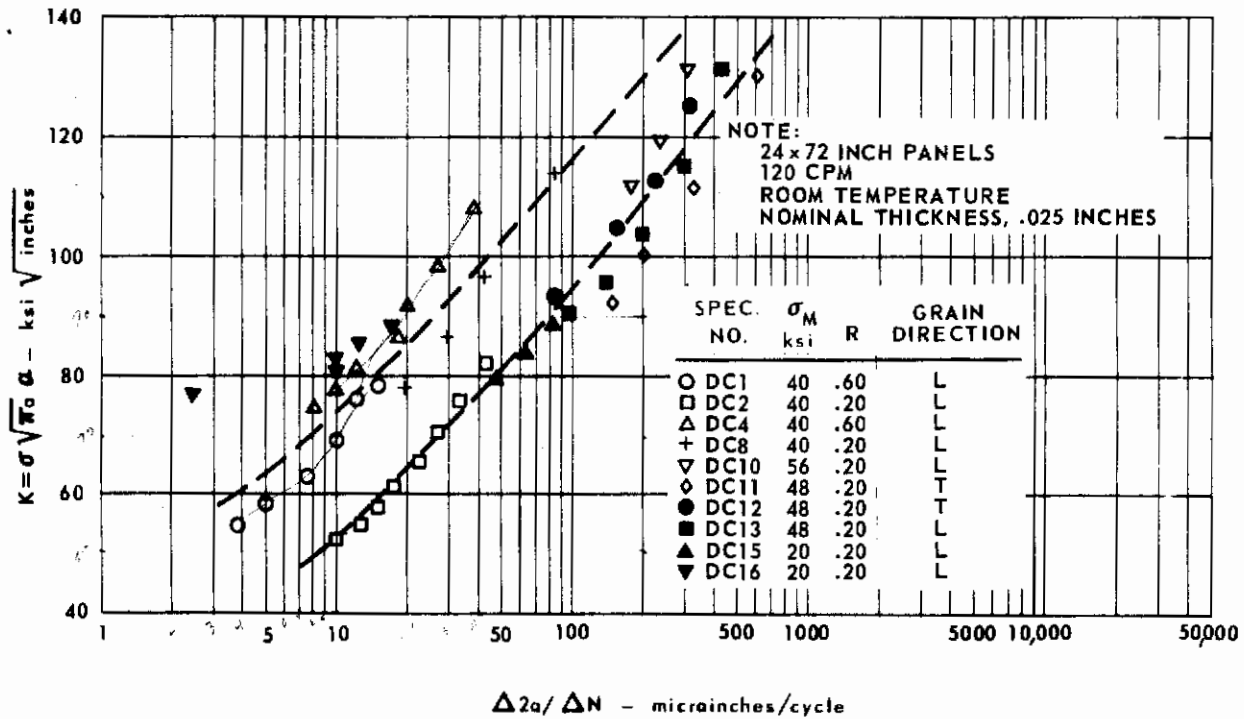


FIG. 116 CRACK GROWTH RATE DATA FOR INCO 718, HEAT 6713

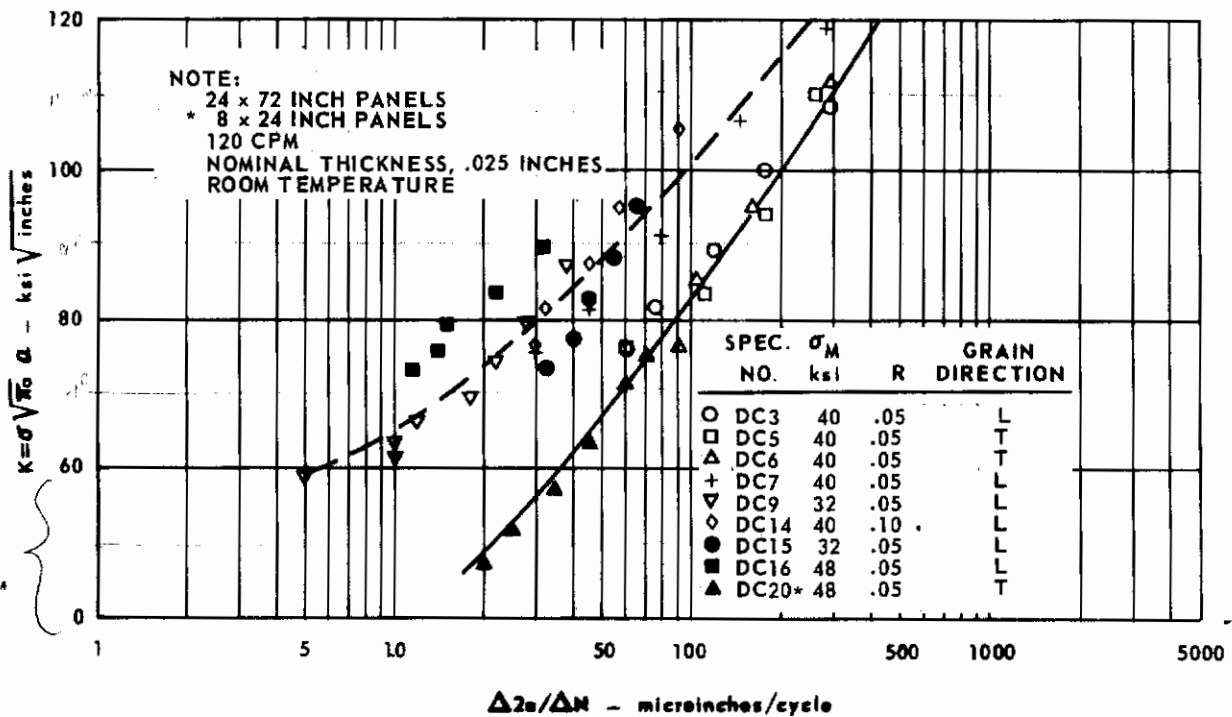


FIG. 117 CRACK GROWTH RATE DATA FOR INCO 718, HEAT 6713

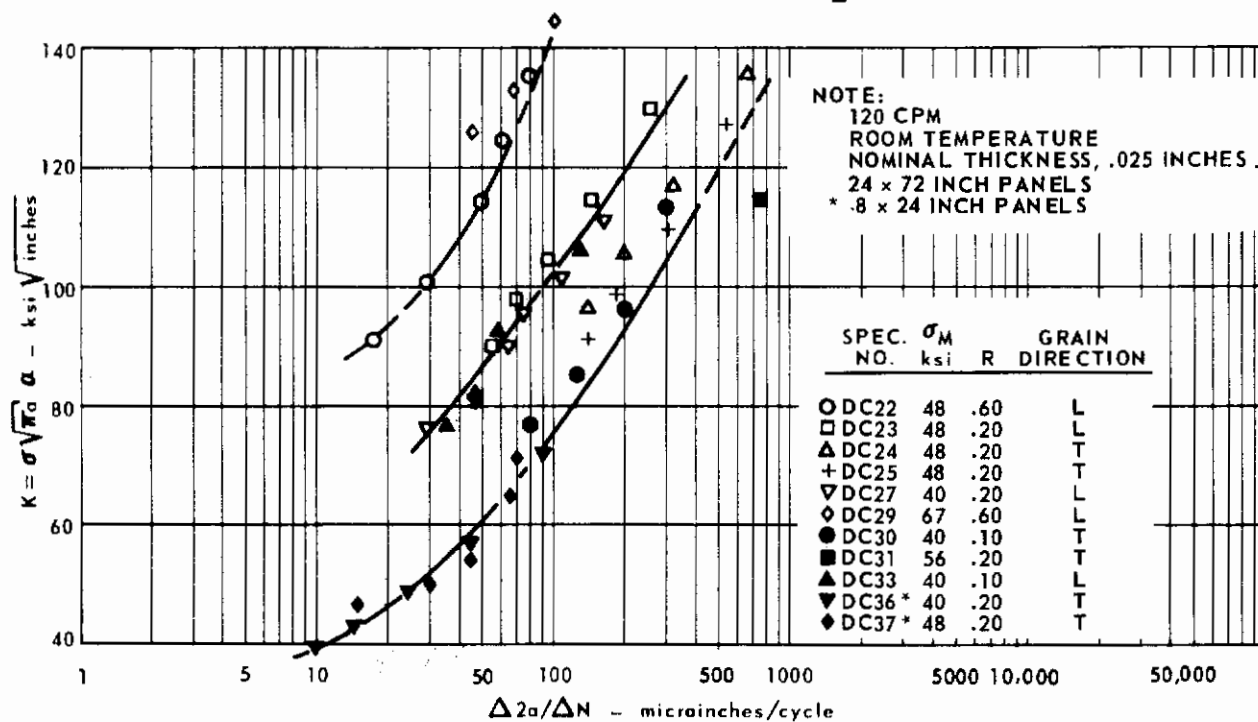


FIG. 118 CRACK GROWTH RATE DATA FOR INCO 718, HEAT 6905

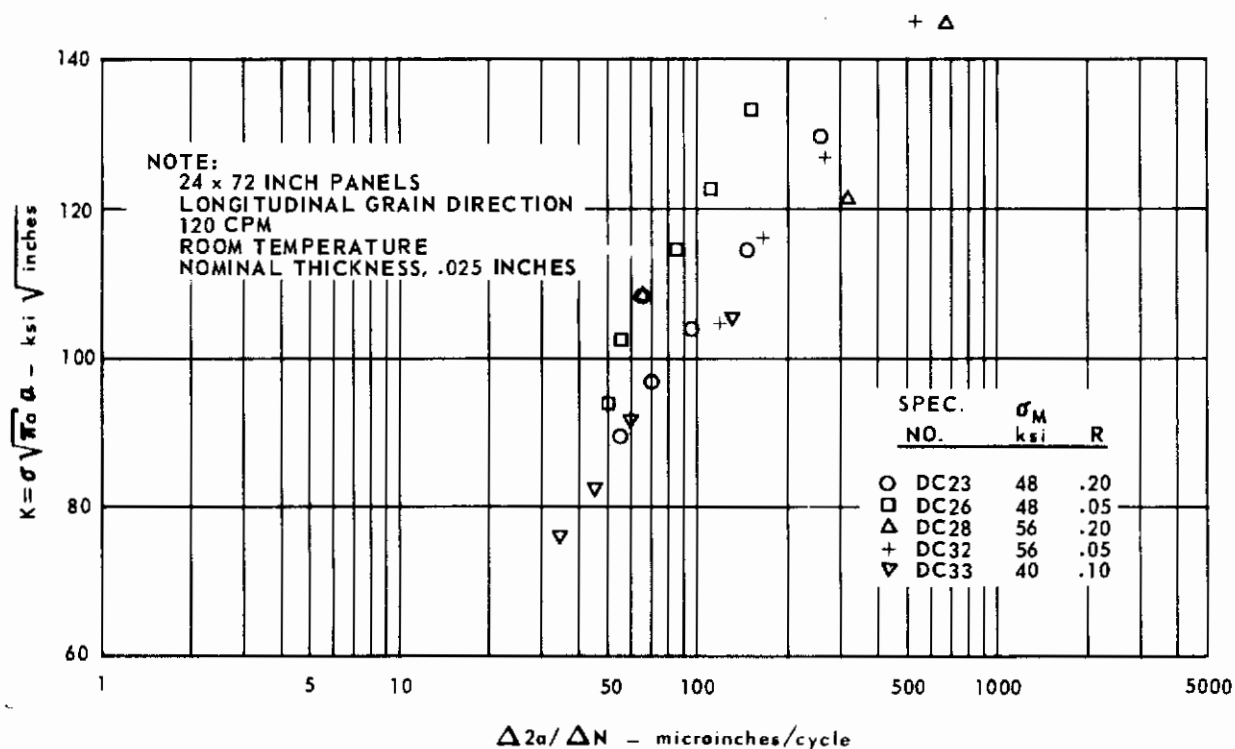


FIG. 119 CRACK GROWTH RATE DATA FOR INCO 718, HEAT 6905

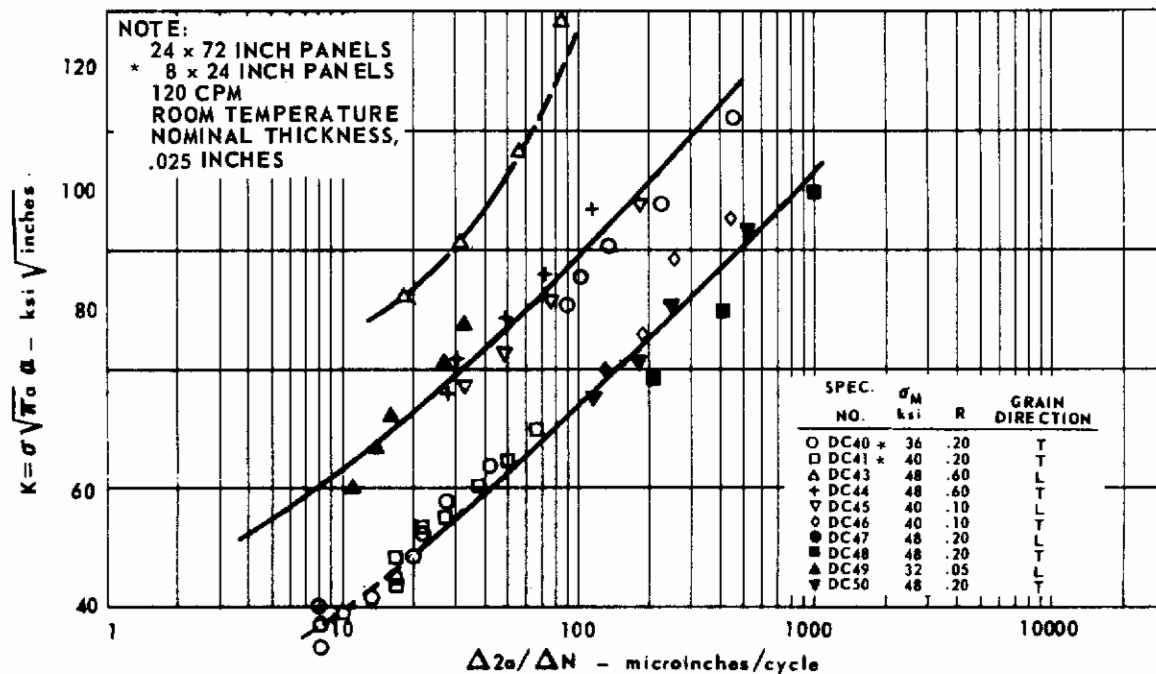


FIG. 120 CRACK GROWTH RATE DATA FOR INCO 718, HEAT 6902

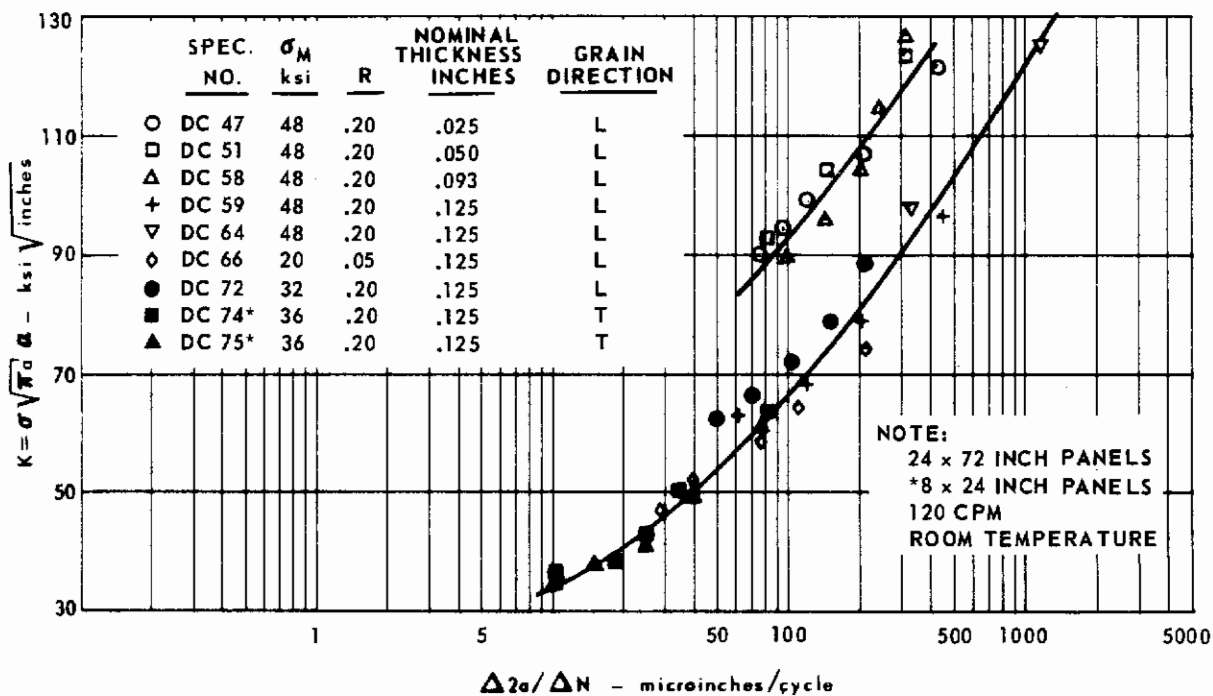


FIG. 121 CRACK GROWTH RATE DATA FOR INCO 718, HEAT 6902

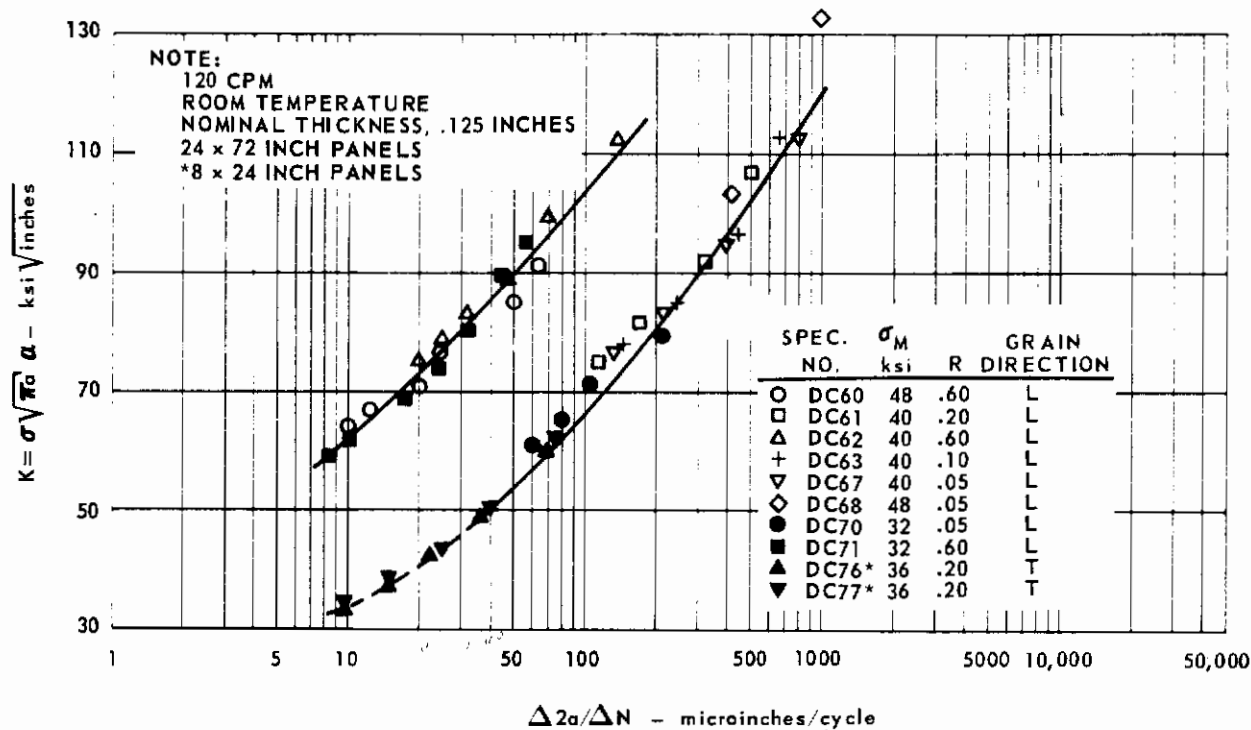


FIG. 122 CRACK GROWTH RATE DATA FOR INCO 718, HEAT 6902

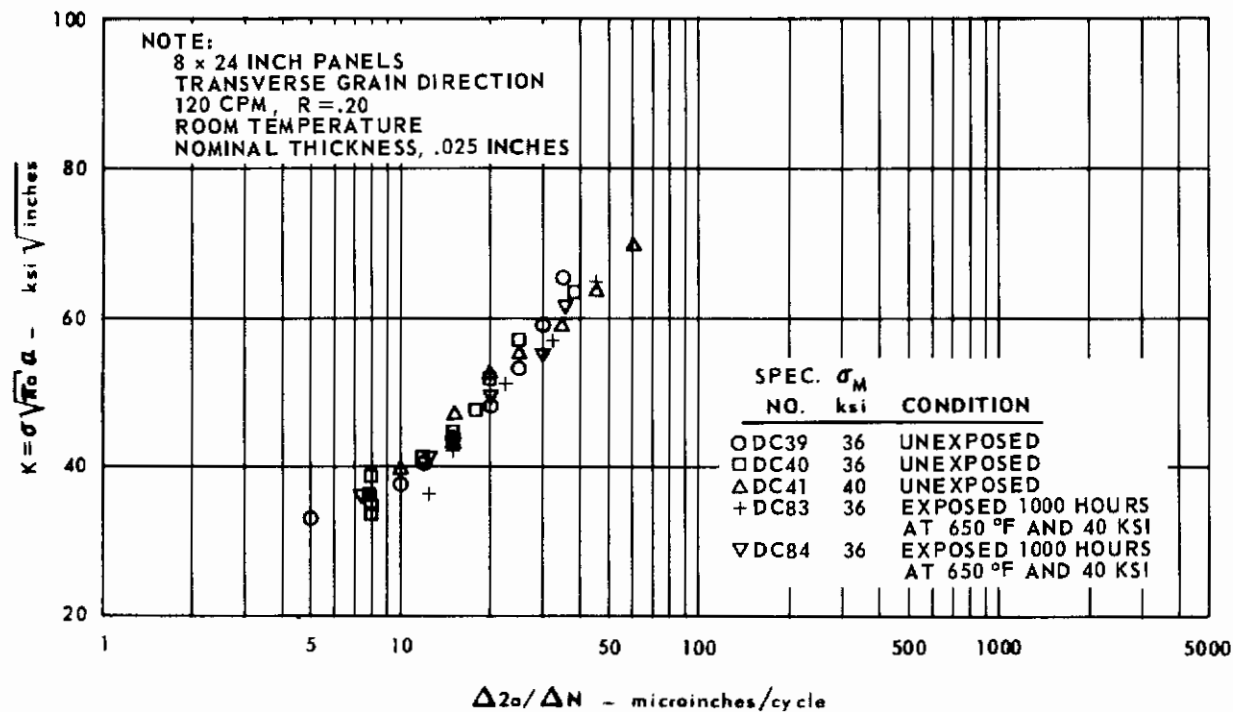


FIG. 123 COMPARISON OF EXPOSED AND UNEXPOSED CRACK GROWTH RATES FOR INCO 718, HEAT 6902

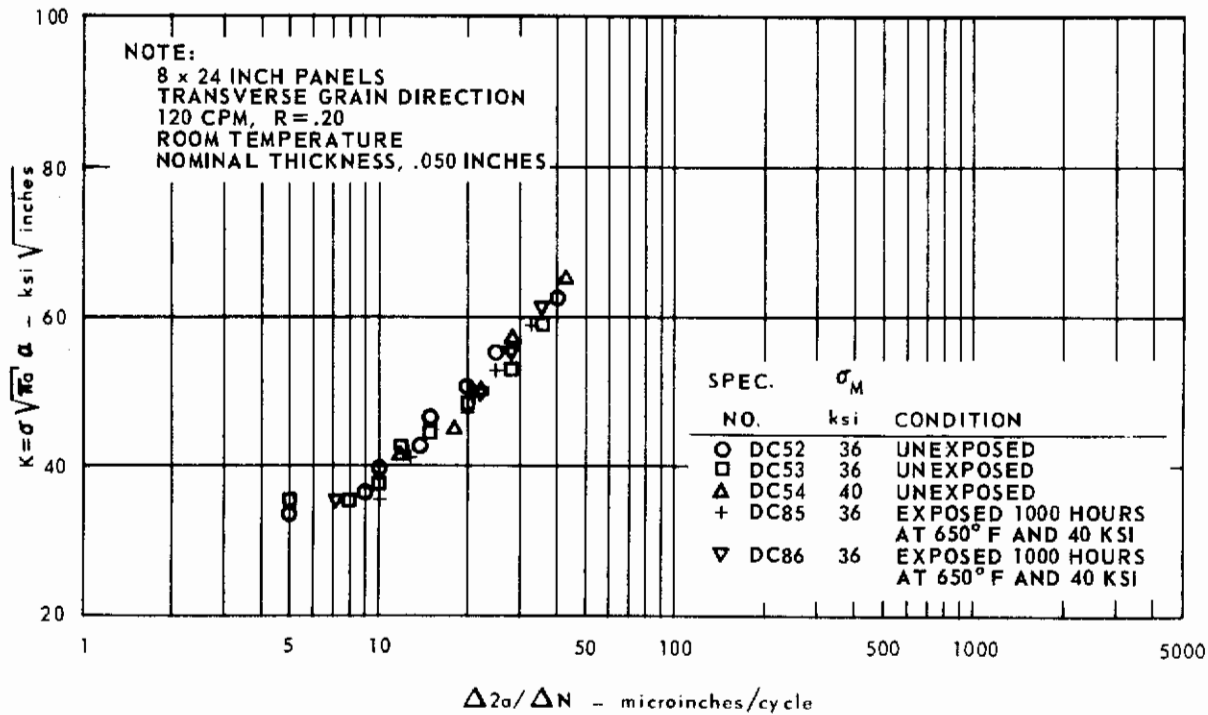


FIG. 124 COMPARISON OF EXPOSED AND UNEXPOSED CRACK GROWTH RATES FOR INCO 718, HEAT 6902

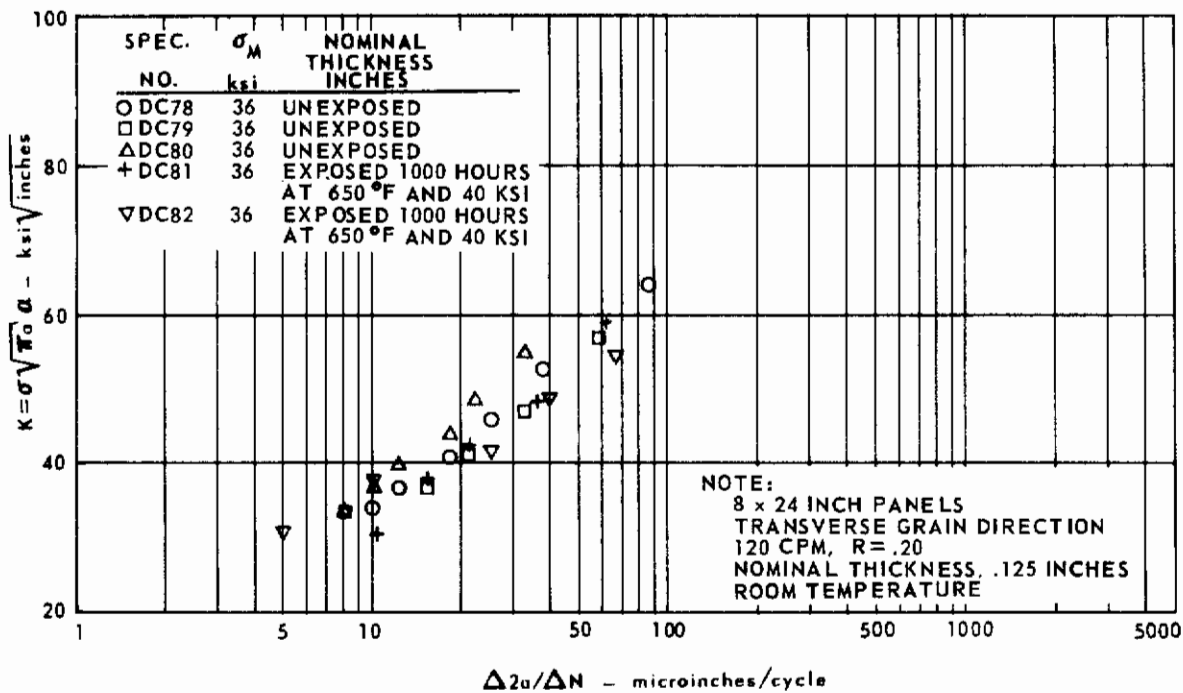


FIG. 125 COMPARISON OF EXPOSED AND UNEXPOSED CRACK GROWTH RATES FOR INCO 718, HEAT 6902

A crack growth rate scatter band for all the 0.025 and 0.050-inch thick unexposed panel data is shown in Fig. 126. This band includes the three heats of material, both panel sizes, and both grain directions for stress ratios of 0.20 and 0.05. The relatively large spread of data is caused by the variation of heat 6713. It is possible that this spread in data reflects the developmental status of Inco 718.

Fracture Test Data

Tabular Data

Detailed data for the fracture tests are included in Table 17 for the 24 x 72-inch panels and in Table 18 for the 8 x 24-inch panels. On the basis of high strain rate tensile data (Ref. 25) for Inconel X, it was assumed that increasing strain rate has the same negligible effect on the tensile yield point for Inco 718 as for Inconel X. The columns for high strain rate tensile data have therefore been left blank in Tables 17 and 18.

Effect of Temperature

The effect of temperature on both K_{IC} and residual strength is shown in Figs. 127 and 128. This effect is only shown for the longitudinal 24 x 72-inch panels which are 0.025 inches thick and which were tested at a stress rate of 10^6 psi/sec. Both curves indicate that the fracture properties (both K_{IC} and residual strength) are at a minimum at 400° F, otherwise, temperature does not have a significant effect on fracture properties. They remain relatively constant over the range of -110 to 650° F. Three of the five test points at 650° F exceed the ASTM criterion for valid tests.

Effect of Grain Direction

Figs. 129 and 130 show the effect of grain direction on both K_{IC} and residual strength for 0.025-inch thick 24 x 72-inch panels tested at a stress rate of 10^6 psi/sec. A significantly lower value exists for the transverse tests at each of the four temperatures. For the five longitudinal room temperature tests, the average K_{IC} value is 388.3 ksi $\sqrt{\text{inches}}$ and for the five transverse room temperature tests, the average value is 264.7 ksi $\sqrt{\text{inches}}$. This difference represents a drop of 32 percent in K_{IC} compared with the longitudinal average.

Effect of Thickness

Figs. 131 and 132 contain K_{IC} and residual strength test results plotted as a function of thickness for the four thicknesses studied with Inco 718. Only the room temperature curves are drawn to maintain graphic clarity. It appears that both fracture parameters have maximum values near the 0.050-inch thickness point. This trend is consistent both for grain directions and panel sizes. The data for the 650° F tests with the 8 x 24-inch panels show very little effect of thickness. The K_{IC} computations from the small panel tests should be considered conservative since the σ_N / σ_{yp} ratio exceeds 0.80 in each case.

Effect of Crack Length

The effect of crack length expressed as the ratio of crack-length to panel-width is shown in Figs. 133, 134 and 135 for K_{IC} and in Figs. 136, 137 and 138 for residual strength. Grain direction temperature and thickness are also included

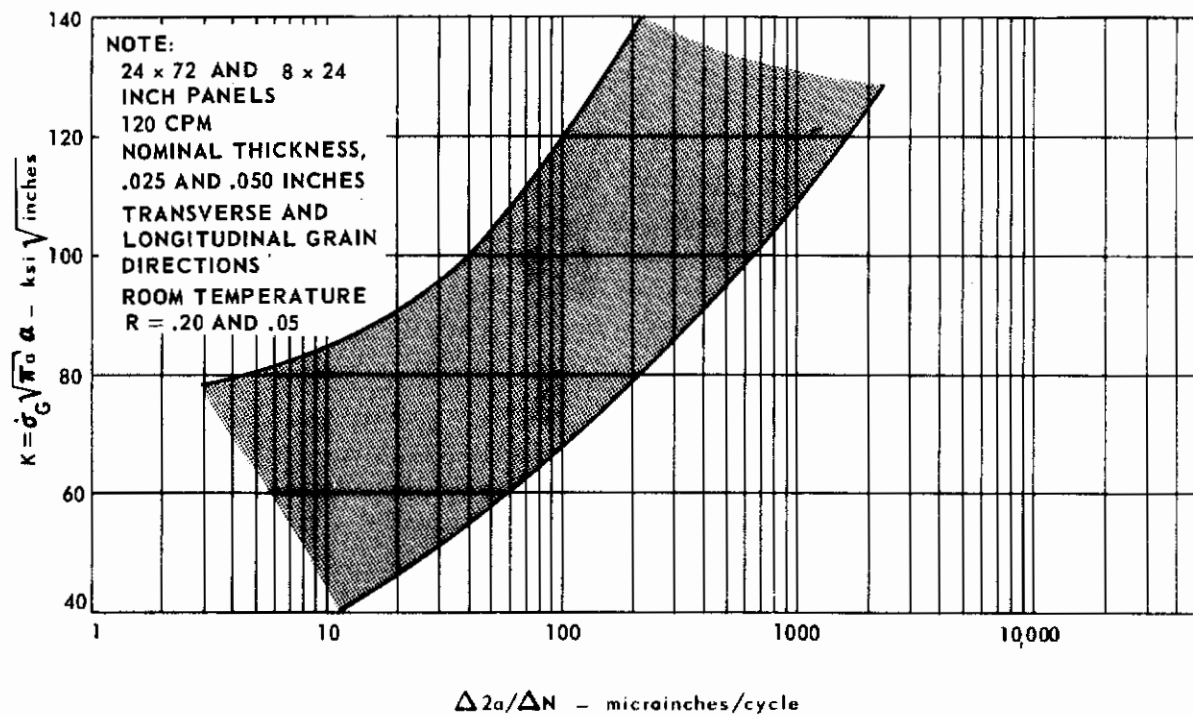


FIG. 126 CRACK GROWTH RATE DATA FOR INCO 718, HEATS 6713, 6902 AND 6905

TABLE 17 FRACTURE TOUGHNESS DATA FOR 24 x 72 INCH PANELS OF INCO 718

SPECIMEN NO.	HEAT NO.	THICKNESS inches	WIDTH inches	GRAIN DIRECTION	TEMP. °F	$\dot{\sigma}$ psi/sec	$2a_0$ inches	σ_G ksi	σ_N ksi	F_{tu} ksi	σ_{yp} ksi	σ_{yp} TEMP. AND $\dot{\sigma}$ ksi	σ_N^* TEMP. AND $\dot{\sigma}$ ksi	σ_N^{**} TEMP. AND $\dot{\sigma}$ ksi	$K_{CN} = \sigma_G \sqrt{a}$ ksi \sqrt{in}	$\frac{\sigma_G}{F_{tu}}$	$K_C = \frac{\sigma_G \sqrt{a}}{\sigma_{yp} \sqrt{a}}$ ksi \sqrt{in}	SHEAR %
DC 1	6713	.025	24.02	L	68	1.13×10^6	3.00	145.677	166.4	218.0	202.0		.82		316.0	.668	374.5	100
DC 2	6713	.025	24.02	L	650	1.09×10^6	3.01	139.097	159.0	189.8	178.3		.88		303.7	.733	371.2	100
DC 3	6713	.026	24.02	L	70	4.83×10^3	6.00	103.837	138.2	218.0	202.0		.68		329.5	.476	355.5	100
DC 4	6713	.026	24.02	L	71	4.55×10^3	6.00	107.300	143.0	218.0	202.0		.71		341.4	.493	370.8	100
DC 5	6713	.026	24.06	T	75	5.13×10^3	6.00	82.704	110.2	213.5	193.0		.57		262.9	.387	275.2	100
DC 6	6713	.026	24.02	T	75	5.08×10^3	6.00	86.656	115.6	213.5	193.0		.60		275.1	.406	291.0	100
DC 7	6713	.026	24.03	L	72	1.03×10^5	6.00	102.897	137.1	218.0	202.0		.68		327.0	.472	352.0	100
DC 8	6713	.026	24.02	L	73	1.0×10^5	6.00	112.853	151.4	218.0	202.0		.74		358.5	.517	394.8	100
DC 9	6713	.026	24.02	L	72	$.99 \times 10^6$	6.00	118.514	158.1	218.0	202.0		.78		376.5	.544	419.2	100
DC 10	6713	.026	24.02	L	72	1.07×10^6	6.00	106.873	142.6	218.0	202.0		.70		339.2	.490	368.0	100
DC 11	6713	.026	23.97	T	70	1.16×10^6	6.00	81.701	108.9	213.5	193.0		.56		259.6	.383	271.6	100
DC 12	6713	.026	23.90	T	70	1.16×10^6	6.00	78.989	105.4	213.5	193.0		.55		251.0	.370	260.8	100
DC 13	6713	.025	24.02	L	650	1.04×10^6	6.00	104.151	138.9	189.8	178.3		.78		331.5	.548	368.0	100
DC 14	6713	.026	24.02	L	650	1.05×10^6	6.00	109.226	145.6	189.8	178.3		.82		352.0	.576	392.9	100
DC 15	6713	.025	24.01	L	650	$.96 \times 10^6$	10.00	74.232	127.3	189.8	178.3		.71		331.6	.391	345.0	100
DC 16	6713	.025	24.02	L	70	$.94 \times 10^6$	10.00	84.485	144.6	218.0	202.0		.72		395.0	.388	394.5	100
DC 22	6905	.025	24.02	L	72	4.20×10^3	6.00	109.641	146.0	221.2	201.1		.73		348.1	.496	380.0	100
DC 23	6905	.026	24.02	L	72	5.20×10^3	6.00	110.625	147.1	221.2	201.1		.73		351.2	.500	383.1	100
DC 24	6905	.026	24.04	T	75	4.97×10^3	6.00	89.920	119.8	212.0	191.6		.63		285.4	.424	303.1	100
DC 25	6905	.025	24.02	T	75	5.09×10^3	6.04	85.785	114.5	212.0	191.6		.60		273.4	.405	288.7	100
DC 26	6905	.026	24.02	L	71	1.00×10^5	6.00	114.339	152.4	221.2	201.1		.76		363.2	.517	400.0	100
DC 27	6905	.025	24.02	L	71	1.02×10^5	6.00	109.098	145.5	221.2	201.1		.72		346.3	.494	377.8	100
DC 28	6905	.025	24.02	L	71	1.02×10^6	6.00	110.822	147.7	221.2	201.1		.73		352.0	.501	384.5	100
DC 29	6905	.026	24.03	L	72	$.98 \times 10^6$	6.00	112.262	149.6	221.2	201.1		.74		356.1	.507	392.9	100
DC 30	6905	.025	23.96	T	70	$.94 \times 10^6$	6.00	87.398	116.6	212.0	191.6		.61		277.5	.412	293.9	100
DC 31	6905	.026	24.03	T	70	$.72 \times 10^6$	6.00	76.609	102.1	212.0	191.6		.53		243.2	.361	253.1	100

* TENSILE PROPERTIES OBTAINED FROM STANDARD STRAIN RATE TESTS OF .005 in/in/min
 ** THE EFFECT OF STRAIN RATE ON σ_{yp} ASSUMED NEGLIGIBLE BASED ON INCONEL X DATA (REFERENCE 26)

TABLE 17 FRACTURE TOUGHNESS DATA FOR 24 x 72 INCH PANELS OF INCO 718 (continued)

SPECIMEN NO.	HEAT NO.	THICKNESS inches	WIDTH inches	GRAIN DIRECTION	TEMP. °F	$\dot{\sigma}$ psi/sec	$2a_0$ inches	σ_G ksi	σ_N ksi	F_{tu} ksi	σ_{yp} ksi	σ_{yp} ksi	σ_{yp} ksi	σ_N ksi	σ_N ksi	$K_{CN} = \sigma_G \sqrt{\pi a_0}$ ksi \sqrt{in}	$\frac{\sigma_G}{F_{tu}}$	$K_C = \frac{\sigma_G \sqrt{a_0}}{\sqrt{W}}$ ksi \sqrt{in}	SHEAR %
DC 32	6905	.026	24.02	L	650	.76x10 ⁶	6.00	111.103	148.2	192.4	179.0			.83		353.2	.577	399.8	100
DC 33	6905	.026	24.06	L	650	.91x10 ⁶	6.00	111.284	184.3	192.4	171.1			.87		353.6	.579	400.9	100
DC 43	6902	.026	24.04	L	-110	.92x10 ⁶	6.00	101.769	135.4	232.9	215.8			.63		323.1	.437	342.8	100
DC 44	6902	.026	23.98	T	-110	.97x10 ⁶	6.00	88.679	118.4	233.5	205.3			.58		282.1	.380	296.0	100
DC 45	6902	.025	24.04	L	71	1.03x10 ⁶	6.00	108.825	145.2	217.4	202.2			.72		345.5	.501	376.9	100
DC 46	6902	.026	24.02	T	66	1.05x10 ⁶	6.00	74.240	99.0	213.7	194.2			.51		236.1	.348	243.9	100
DC 47	6902	.026	24.01	L	400	1.11x10 ⁶	6.00	90.931	121.2	201.6	187.8			.64		289.3	.451	307.5	100
DC 48	6902	.026	24.01	T	400	.92x10 ⁶	6.02	78.302	104.4	198.6	183.3			.57		249.1	.394	261.2	100
DC 49	6902	.026	24.03	L	650	.83x10 ⁶	6.00	98.454	131.2	192.0	180.3			.73		316.2	.512	341.3	100
DC 50	6902	.027	21.95	T	650	.95x10 ⁶	6.00	81.956	112.9	189.2	174.6			.65		262.9	.434	264.0	100
DC 51	6902	.050	24.04	L	68	1.08x10 ⁶	6.00	121.428	161.9	212.5	193.3			.84		386.5	.572	440	100
DC 58	6902	.093	24.02	L	66	.90x10 ⁶	6.00	115.073	153.5	214.4	196.1			.78		365.3	.537	407	100
DC 59	6902	.128	24.02	L	67	1.20x10 ⁶	3.02	120.593	137.9	224.6	212.0			.65		264.2	.537	289.0	100
DC 60	6902	.124	24.07	L	650	.94x10 ⁶	3.00	148.157	168.9	197.4	187.4			.90		323.5	.750	397.3	100
DC 61	6902	.127	24.01	L	66	1.03x10 ⁶	6.00	97.634	117.9	224.6	212.0			.56		310.6	.435	328.8	100
DC 62	6902	.129	24.01	L	72	.90x10 ⁶	6.00	99.178	132.5	224.6	212.0			.62		315.5	.432	335.3	100
DC 63	6902	.128	24.01	L	650	.92x10 ⁶	6.00	107.400	143.4	197.4	187.4			.76		341.4	.545	377.0	100
DC 64	6902	.124	24.03	L	650	.99x10 ⁶	6.00	113.332	151.0	197.4	187.4			.81		360.0	.573	404.1	100
DC 65	6902	.122	24.02	L	66	1.01x10 ⁶	10.00	64.862	111.1	224.6	212.0			.52		290.1	.289	289.7	100
DC 66	6902	.124	24.03	L	650	.98x10 ⁶	10.00	78.759	135.0	197.4	187.4			.72		352.5	.399	367.2	100
DC 67	6902	.124	24.02	L	-110	.91x10 ⁶	6.00	95.346	127.0	241.0	217.8			.58		303.1	.396	318.6	100
DC 68	6902	.122	24.02	L	-110	.98x10 ⁶	6.00	91.863	122.5	241.0	217.8			.56		291.8	.382	305.5	100
DC 70	6902	.124	24.01	L	74	7.0 x10 ³	6.00	81.584	108.8	224.6	212.0			.51		259.6	.359	264.7	100
DC 71	6902	.127	24.01	L	69	3.86x10 ³	6.00	79.054	105.4	224.6	212.0			.50		251.3	.352	259.7	100
DC 72	6902	.129	24.00	L	70	.96x10 ⁵	6.01	87.186	121.0	224.6	212.0			.57		277.3	.388	289.0	100
DC 73	6902	.126	24.01	L	72	.94x10 ⁵	6.00	90.726	121.1	224.6	212.0			.57		288.5	.404	301.9	100

* TENSILE PROPERTIES OBTAINED FROM STANDARD STRAIN RATE TESTS OF .005 in./in./min
 ** THE EFFECT OF STRAIN RATE ON σ_{yp} ASSUMED NEGLECTABLE BASED ON INCONEL X DATA (REFERENCE 26)

TABLE 18 FRACTURE TOUGHNESS DATA FOR 8 x 24 INCH PANELS OF INCO 718

SPECIMEN NO.	HEAT NO.	THICKNESS inches	WIDTH inches	GRAIN DIRECTION	TEMP. °F	$\dot{\sigma}$ psi/sec	$2a_0$ inches	σ_G ksi	σ_N ksi	F_{tu} ksi	σ_{yp}^* ksi	σ_{yp}^* ksi	σ_N^* ksi	σ_N^* ksi	σ_N^* ksi	σ_N^* ksi	$K_{CN} = \sigma_G \sqrt{\pi a}$ ksi \sqrt{in}	$\frac{\sigma_G}{F_{tu}}$	$K_C = \frac{\sigma_G \sqrt{a_1}}{\sigma_{yp} \sqrt{a_1}}$ ksi \sqrt{in}	SHEAR %
DC 19	6713	.026	8.05	T	-110	4.95×10^3	2.00	140.881	187.5	229.3	199.2		.94				258.0	.614	309.5	100
DC 20	6713	.026	8.02	T	-110	$.90 \times 10^6$	2.00	140.070	187.0	229.3	199.2		.94				257.0	.612	306.0	100
DC 21	6713	.026	8.02	T	RT	1.05×10^6	2.00	134.104	178.9	213.5	193.0		.93				245.8	.629	292.0	100
DC 36	6905	.026	8.00	T	-110	5.45×10^3	2.00	128.660	171.3	225.5	201.8		.85				236.0	.571	269.6	100
DC 37	6905	.026	8.01	T	-110	4.35×10^3	2.00	131.322	175.1	225.5	201.8		.87				240.9	.584	278.0	100
DC 38	6905	.026	8.01	T	71	1.03×10^6	2.00	123.657	165.1	212.0	191.6		.86				226.8	.583	260.2	100
DC 39	6902	.027	8.02	T	-110	3.80×10^3	2.00	137.000	182.4	233.5	205.3		.89				251.5	.586	292.9	100
DC 40	6902	.026	8.02	T	-110	1.00×10^6	2.00	140.845	188.7	233.5	205.3		.92				258.4	.603	305.0	100
DC 41	6902	.026	8.02	T	73	$.92 \times 10^6$	2.00	134.594	179.5	213.7	194.2		.92				247.0	.630	292.0	100
DC 42	6902	.026	8.02	T	650	1.01×10^6	2.00	124.967	167.4	189.1	174.6		.96				229.3	.662	276.1	100
DC 52	6902	.051	8.01	T	650	$.99 \times 10^6$	2.00	120.656	160.9	182.5	170.7		.94				221.3	.661	264.3	100
DC 53	6902	.051	8.01	T	-110	$.99 \times 10^6$	2.00	135.289	180.5	226.5	198.8		.91				248.3	.598	290.8	100
DC 54	6902	.051	8.01	T	68	1.00×10^6	2.00	135.125	180.7	200.0	180.4		1.00				247.9	.676	308.2	100
DC 55	6902	.095	8.00	T	-110	94×10^6	2.00	141.690	187.0	228.2	197.9		.96				259.9	.620	312.0	100
DC 56	6902	.094	8.01	T	69	$.79 \times 10^6$	2.00	138.850	185.1	208.0	187.0		.99				254.7	.667	314.0	100
DC 57	6902	.094	8.01	T	650	1.29×10^6	2.00	125.722	167.6	182.8	170.2		.98				230.6	.689	282.0	100
DC 74	6902	.124	8.00	T	72	$.74 \times 10^6$	2.00	115.468	154.0	218.5	199.4		.77				211.8	.529	235.4	100
DC 75	6902	.124	8.01	T	72	5.95×10^3	2.00	111.567	148.7	218.5	199.4		.74				204.6	.512	224.9	92
DC 76	6902	.124	8.02	T	400	4.85×10^3	2.00	118.404	157.8	200.4	183.4		.86				217.2	.592	252.0	100
DC 77	6902	.124	8.01	T	650	4.55×10^3	2.00	119.492	152.5	193.8	177.6		.86				219.2	.617	256.0	100
DC 78	6902	.124	8.01	T	-110	5.05×10^3	2.00	103.777	138.3	228.2	212.2		.65				190.4	.454	203.6	86
DC 79	6902	.124	8.01	T	-110	1.11×10^6	2.00	101.455	135.2	228.2	212.2		.64				184.9	.444	198.2	80
DC 80	6902	.124	8.01	T	650	1.14×10^6	2.00	119.008	158.6	182.8	170.2		.93				218.3	.652	258.9	100
▲ DC 81	6902	.124	8.02	T	72	1.11×10^6	2.00	98.366	130.7	218.4	198.6		.66				180.4	.451	194.0	68
▲ DC 82	6902	.125	7.93	T	72	1.07×10^6	2.00	98.649	132.0	218.4	198.6		.66				181.0	.452	193.6	70
▲ DC 83	6902	.027	8.03	T	75	1.19×10^6	2.00	133.640	178.2	215.1	195.9		.91				245.1	.622	287.3	100

* TENSILE PROPERTIES OBTAINED FROM STANDARD STRAIN RATE TESTS OF .005 in./in./min
 ** THE EFFECT OF STRAIN RATE ON σ_{yp} ASSUMED NEGLIGIBLE BASED ON INCONEL X DATA (REFERENCE 26)
 ▲ EXPOSED @ 650°F FOR 1000 HRS @ $\sigma_G = 40$ ksi

TABLE 18 FRACTURE TOUGHNESS DATA FOR 8 x 24 INCH PANELS OF INCO 718 (continued)

SPECIMEN NO.	HEAT NO.	THICKNESS inches	WIDTH inches	GRAIN DIRECTION	TEMP. °F	$\dot{\sigma}$ psi/sec	$2a_0$ inches	σ_G ksi	σ_N ksi	F_{tu} ksi	σ_{yp}^* ksi	σ_{yp}^* ksi	σ_N^* ksi	σ_N^* ksi	σ_N^* ksi	$KCN = \sigma_G \sqrt{\pi a_0}$ ksi \sqrt{in}	$\frac{\sigma_G}{F_{tu}}$	$K_C = \frac{\sigma_G \sqrt{a_0}}{\sqrt{W}}$ ksi \sqrt{in}	SHEAR %
▲ DC 84	6902	.027	8.04	T	75	1.04×10^6	1.98	131,336	174.1	215.1	195.9		.89			240.9	.612	281.0	100
▲ DC 85	6902	.052	8.01	T	72	1.21×10^6	2.00	135,252	180.3	208.8	187.6		.96			248.1	.648	299.3	100
▲ DC 86	6902	.052	8.02	T	72	1.02×10^6	2.00	134,053	178.5	208.8	187.6		.95			245.9	.642	296.5	100
DC 87	6902	.026	8.01	L	70	1.00×10^6	2.00	143,115	190.6	217.4	202.4		.94			262.6	.708	311.3	100
DC 88	6902	.026	8.01	T	71	1.03×10^6	1.00	162,570	186.2	213.7	194.2		.96			204.9	.762	260.0	100
DC 89	6902	.026	8.02	T	650	.97x10	1.00	150,617	172.3	189.1	174.6		.99			189.7	.797	252.0	100
DC 90	6902	.026	8.01	T	400	.91x10 ⁶	2.00	127,819	170.4	198.6	183.3		.93			234.5	.644	277.4	100
DC 91	6902	.026	8.01	T	650	1.01×10^6	2.00	121,385	161.8	189.1	174.6		.93			222.7	.642	263.5	100
DC 92	6902	.026	8.02	T	72	1.03×10^6	3.01	103,071	164.8	213.7	202.4		.81			244.0	.483	268.0	100
DC 93	6902	.026	8.02	T	650	1.03×10^6	3.00	101,531	162.2	189.1	174.6		.93			240.3	.583	277.0	100
CYCLED TO FAILURE																			
DC 94	6902	.026	8.01	T	72	-	6.02	35,000	-	213.7	202.4						.173		
DC 95	6902	.026	8.01	T	72	-	6.17	35,000	-	213.7	202.4						.173		

* TENSILE PROPERTIES OBTAINED FROM STANDARD STRAIN RATE TESTS OF .005 in./in./min
 ** THE EFFECT OF STRAIN RATE ON σ_{yp} ASSUMED NEGLIGIBLE BASED ON INCONEL X DATA (REFERENCE 26)
 ▲ EXPOSED @ 650°F FOR 1000 HRS @ $\sigma_G = 40$ ksi

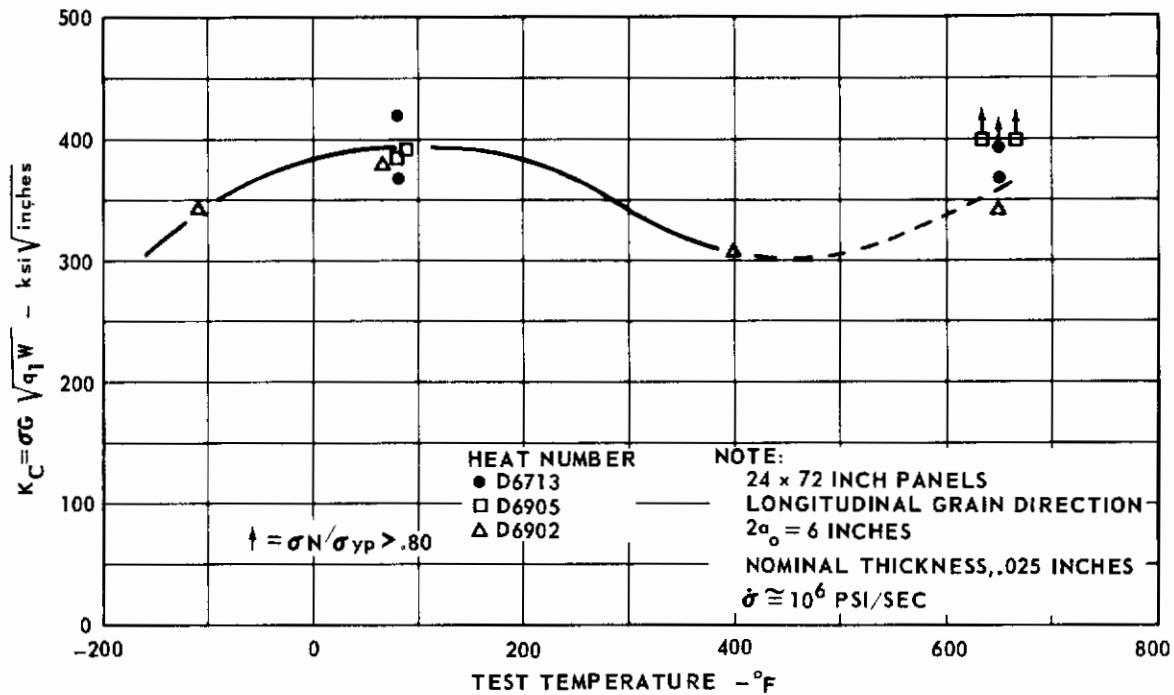


FIG. 127 EFFECT OF TEST TEMPERATURE ON K_C FOR INCO 718

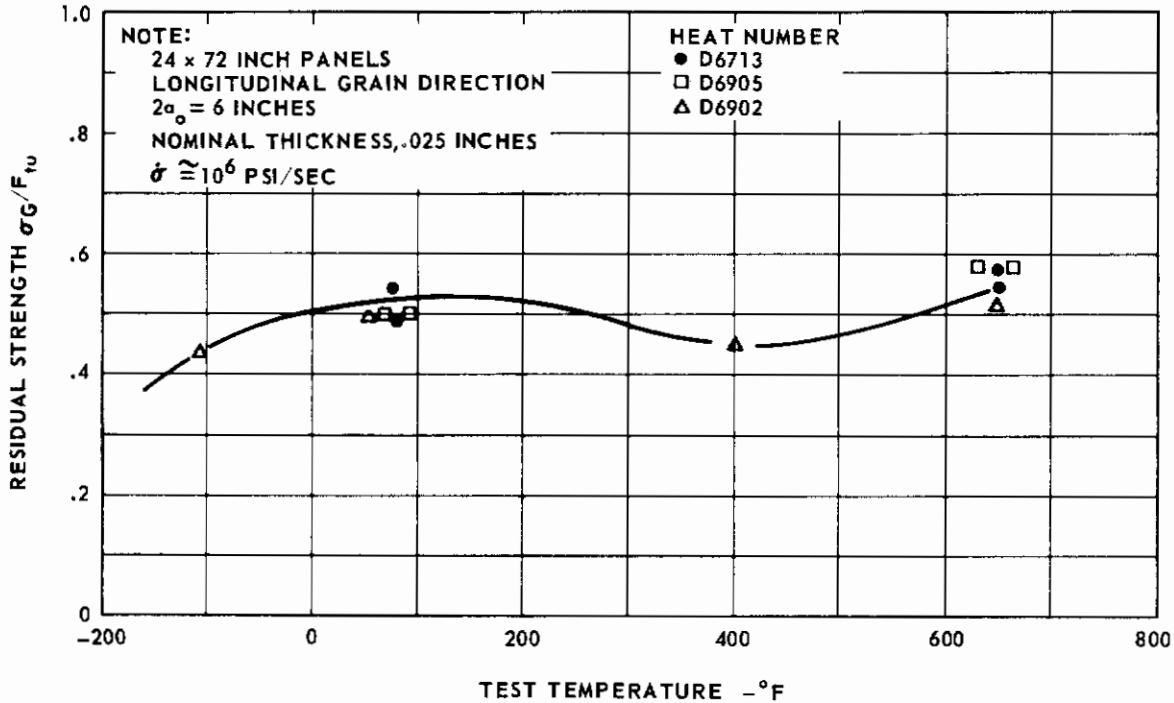


FIG. 128 EFFECT OF TEST TEMPERATURE ON RESIDUAL STRENGTH FOR INCO 718

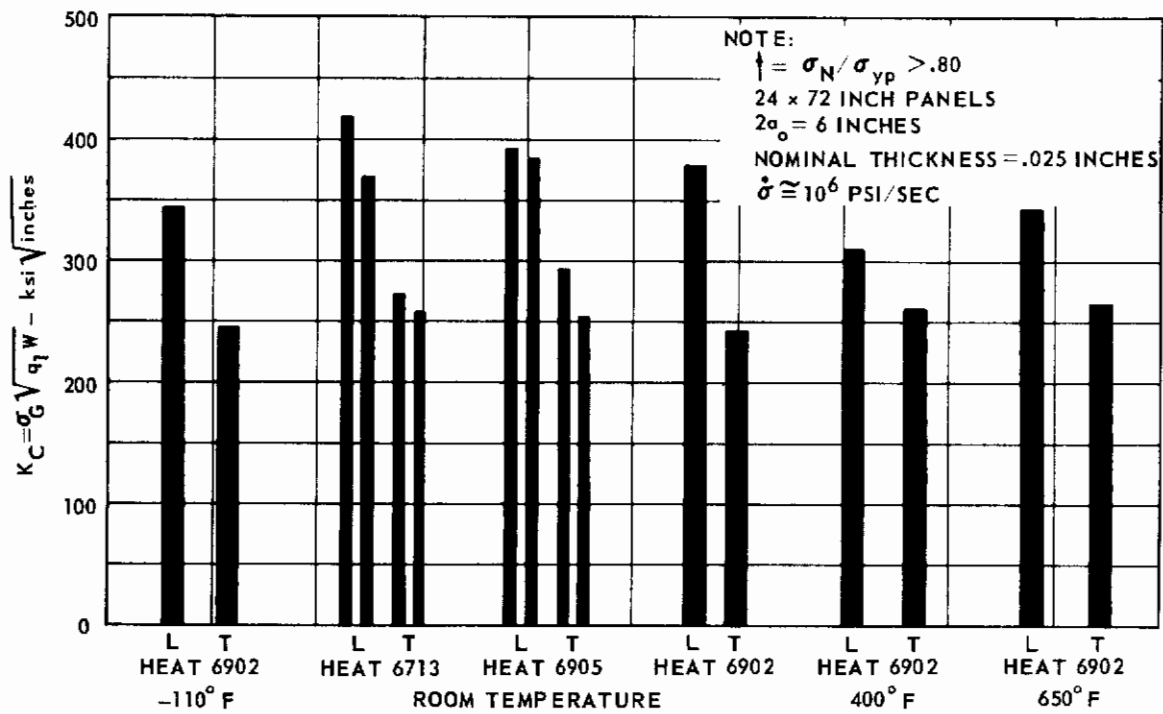


FIG. 129 VARIATION OF K_C WITH GRAIN DIRECTION FOR INCO 718

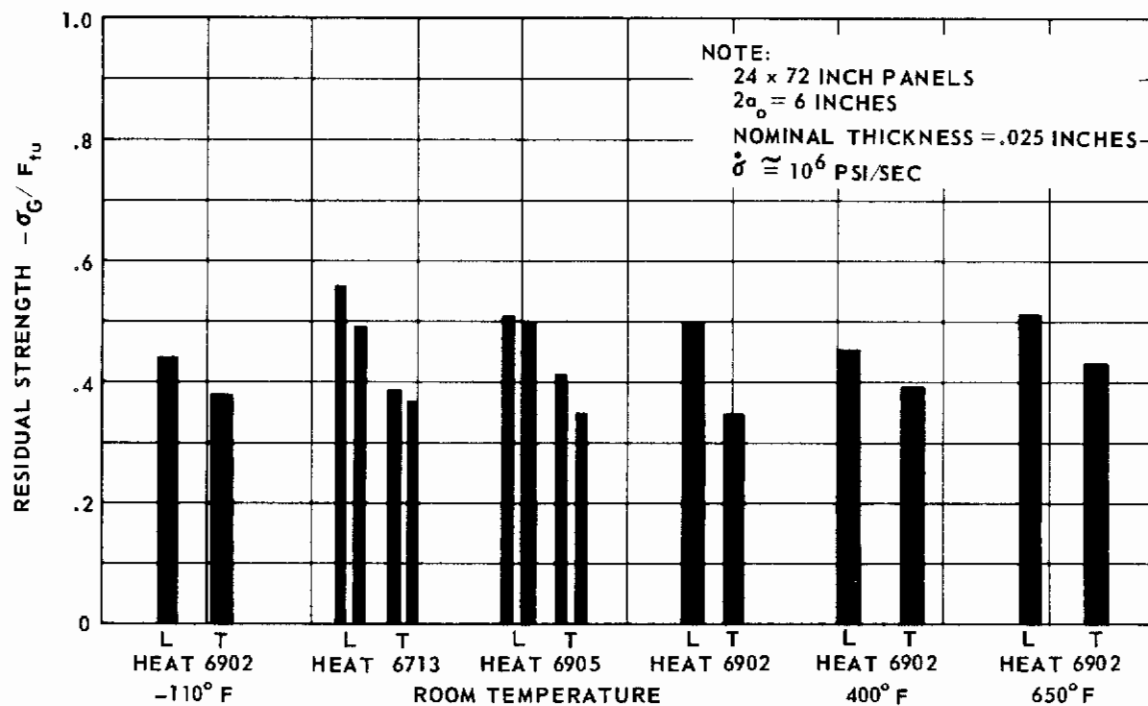


FIG. 130 VARIATION OF RESIDUAL STRENGTH WITH GRAIN DIRECTION FOR INCO 718

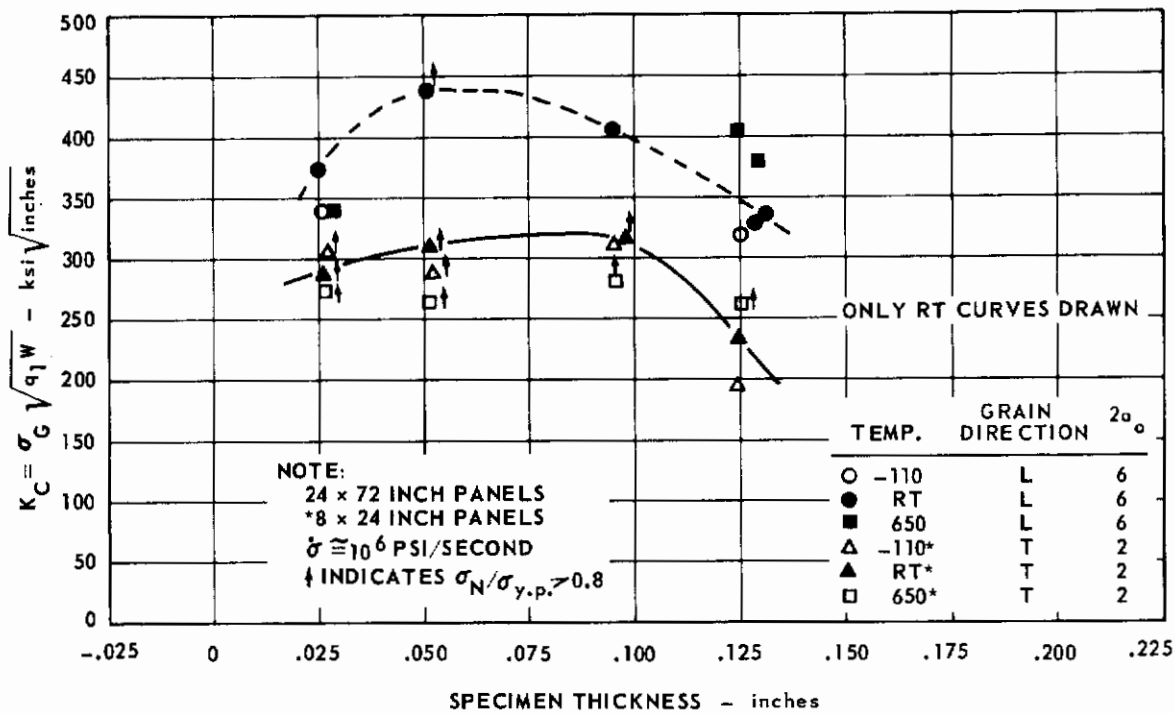


FIG. 131 VARIATION OF K_C WITH THICKNESS FOR INCO 718

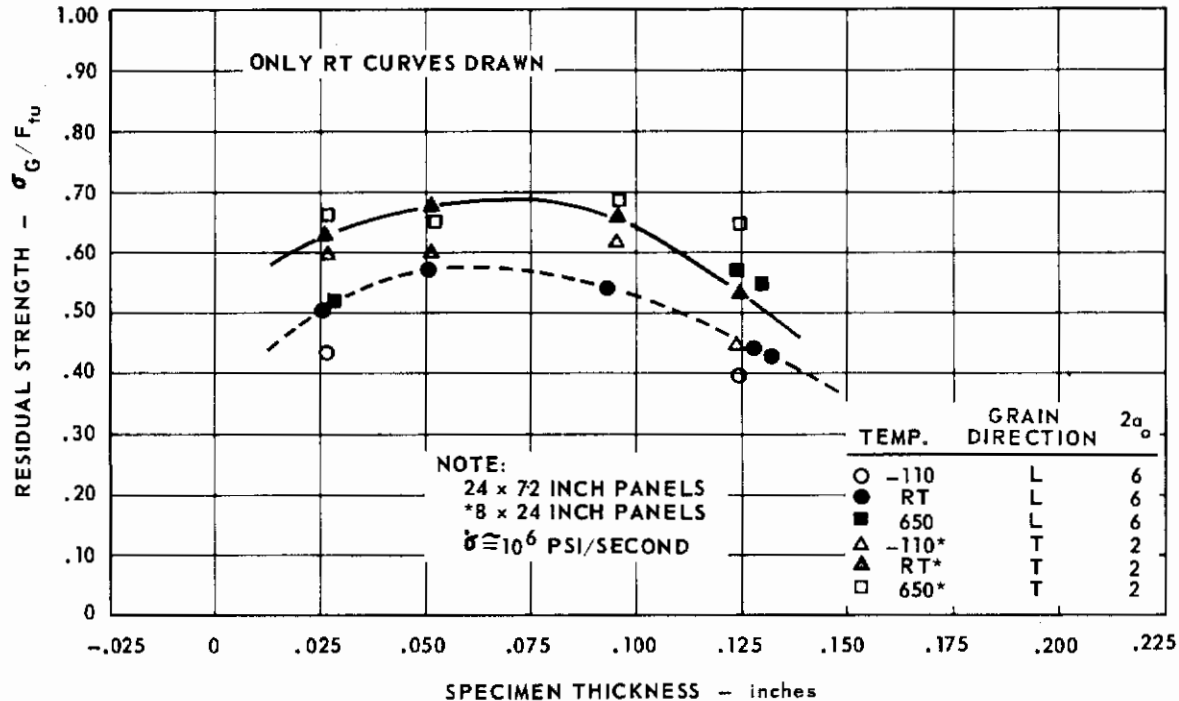


FIG. 132 VARIATION OF RESIDUAL STRENGTH WITH THICKNESS FOR INCO 718

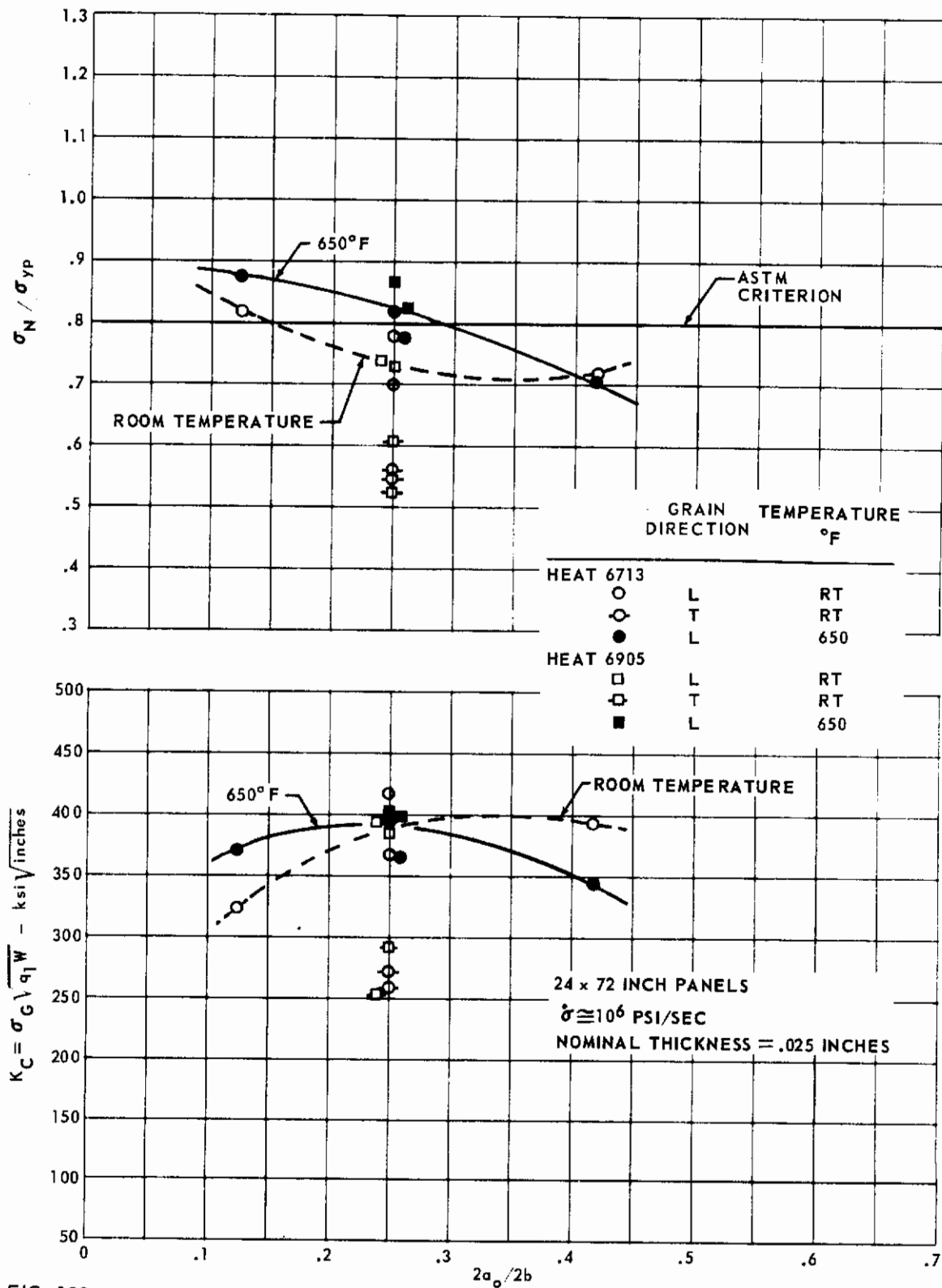


FIG. 133 VARIATION OF K_C WITH TEMPERATURE, CRACK LENGTH AND GRAIN DIRECTION FOR INCO 718

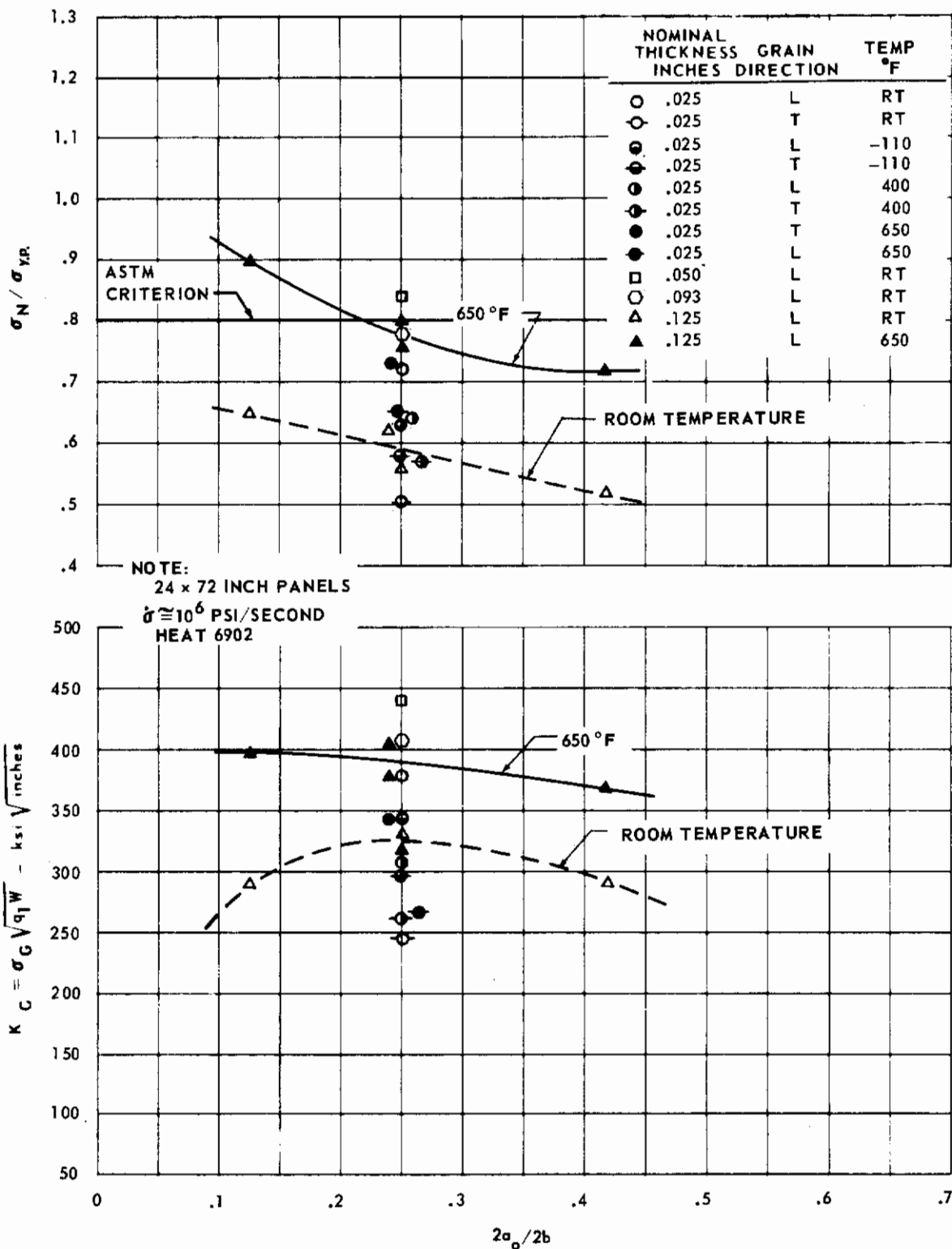


FIG. 134 VARIATION OF K_C WITH TEMPERATURE, CRACK LENGTH, THICKNESS AND GRAIN DIRECTION FOR INCO 718

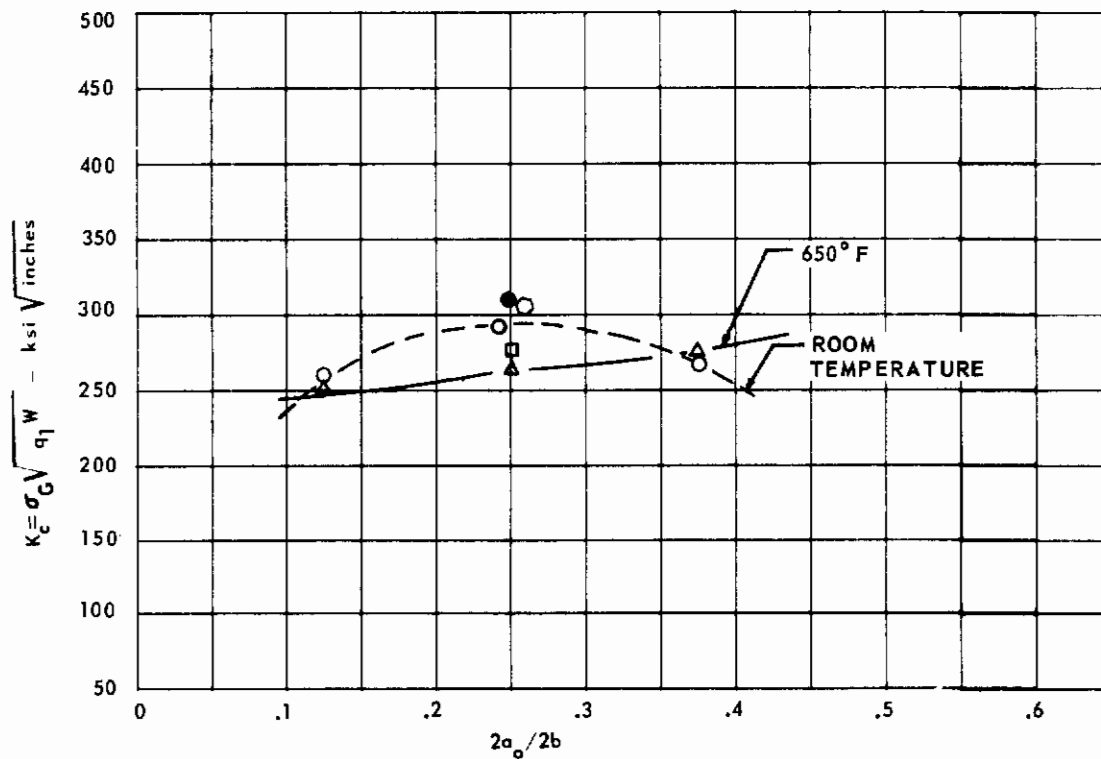
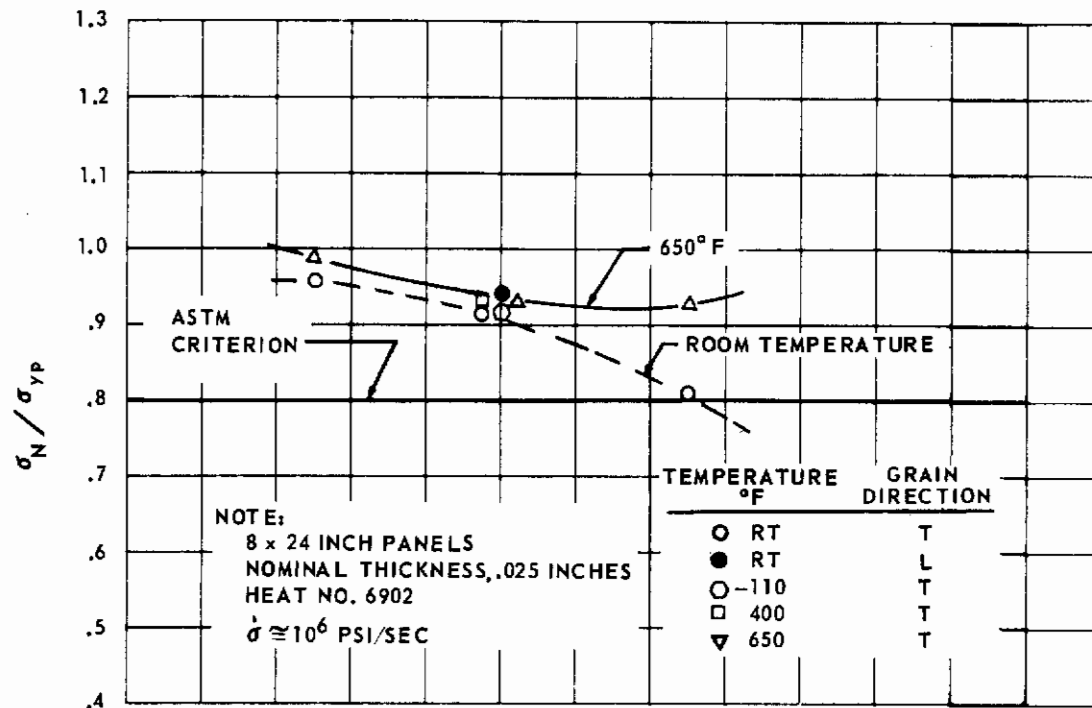


FIG. 135 VARIATION OF K_C WITH TEMPERATURE, CRACK LENGTH AND GRAIN DIRECTION FOR INCO 718

NOTE:
LONGITUDINAL GRAIN
Points at $2a_0/2b = .25$ were Displaced
Laterally to Avoid Overplotting.

	NOMINAL THICKNESS INCHES	$\dot{\sigma}$ psi/sec	TEMPERATURE ° F
○	.050	1×10^6	R.T.
□	.093	1×10^6	R.T.
△	.125	1×10^6	-110
◇	.125	1×10^6	R.T.
▽	.125	1×10^6	650
◇	.125	1×10^5	R.T.
◆	.125	5×10^3	R.T.

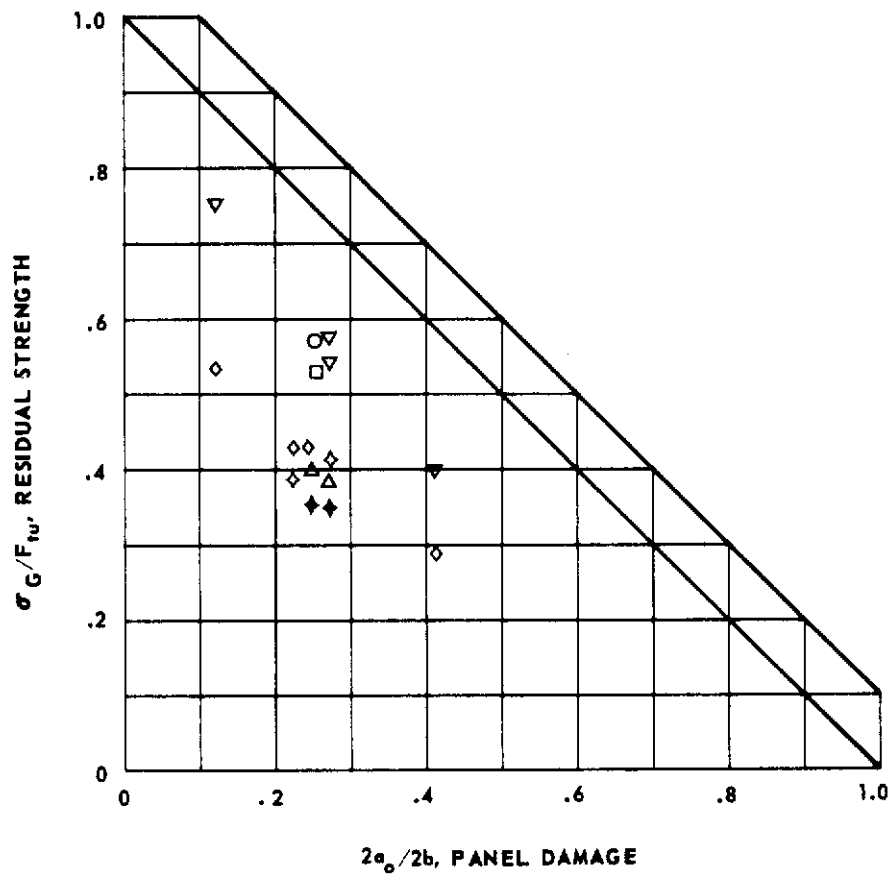


FIG. 136 RESIDUAL STRENGTH vs DAMAGE FOR 24 x 72 INCH INCO 718 PANELS , HEAT 6902

NOTE:
 TRANSVERSE GRAIN DIRECTION
 NOMINAL THICKNESS, .025 INCHES
 Points at $2a_0/2b = .25$ were Displaced
 Laterally to Avoid Overplotting.

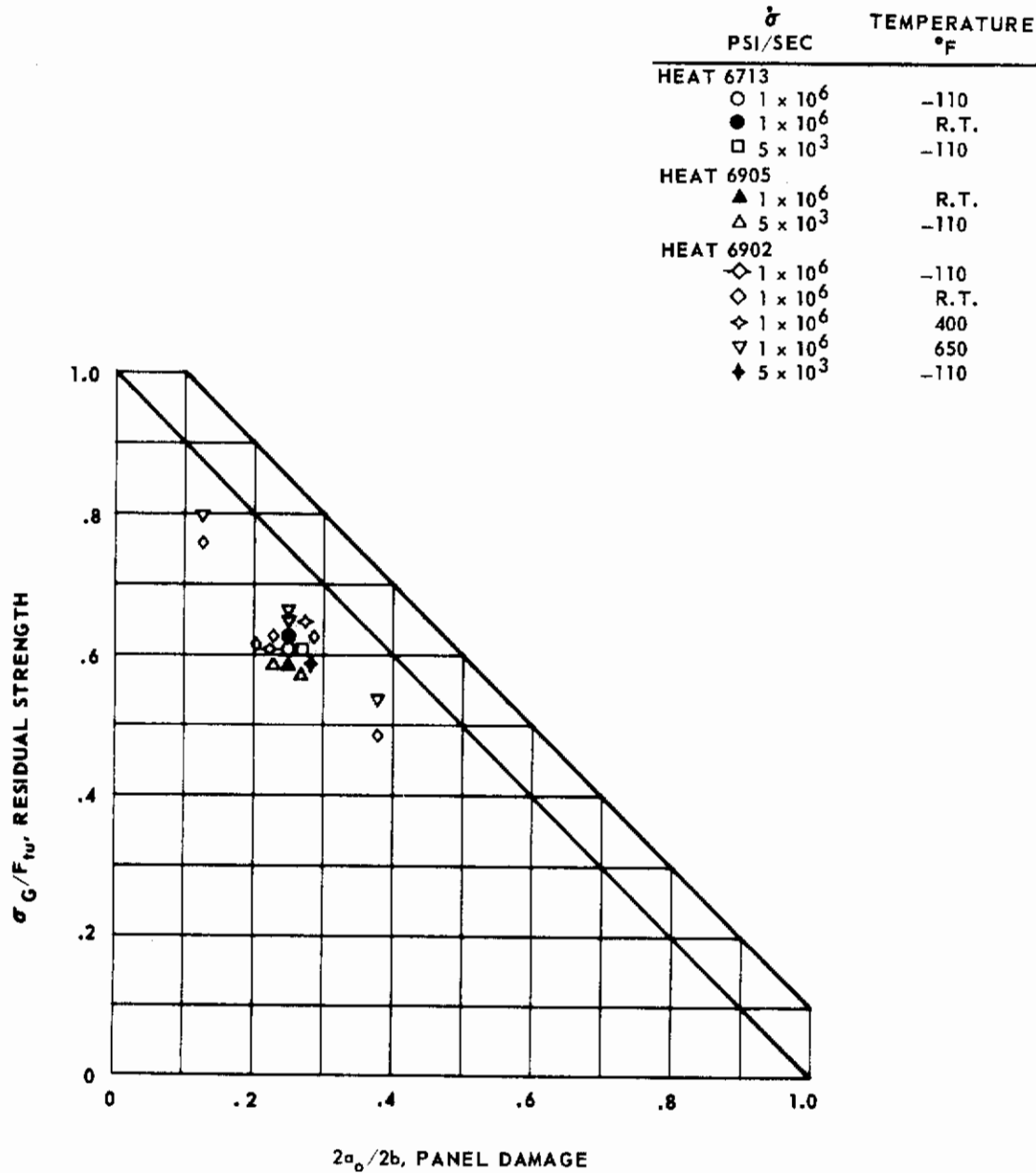


FIG. 137 RESIDUAL STRENGTH VS DAMAGE FOR 8 X 24 INCH INCO 718 PANELS, HEATS 6713, 6905 AND 6902

NOTE:

$\dot{\epsilon} \cong 10^6$ PSI/SEC

NOMINAL THICKNESS = .025

Points at $2a_o/2b = .25$ were Displaced
Laterally to Avoid Overplotting.

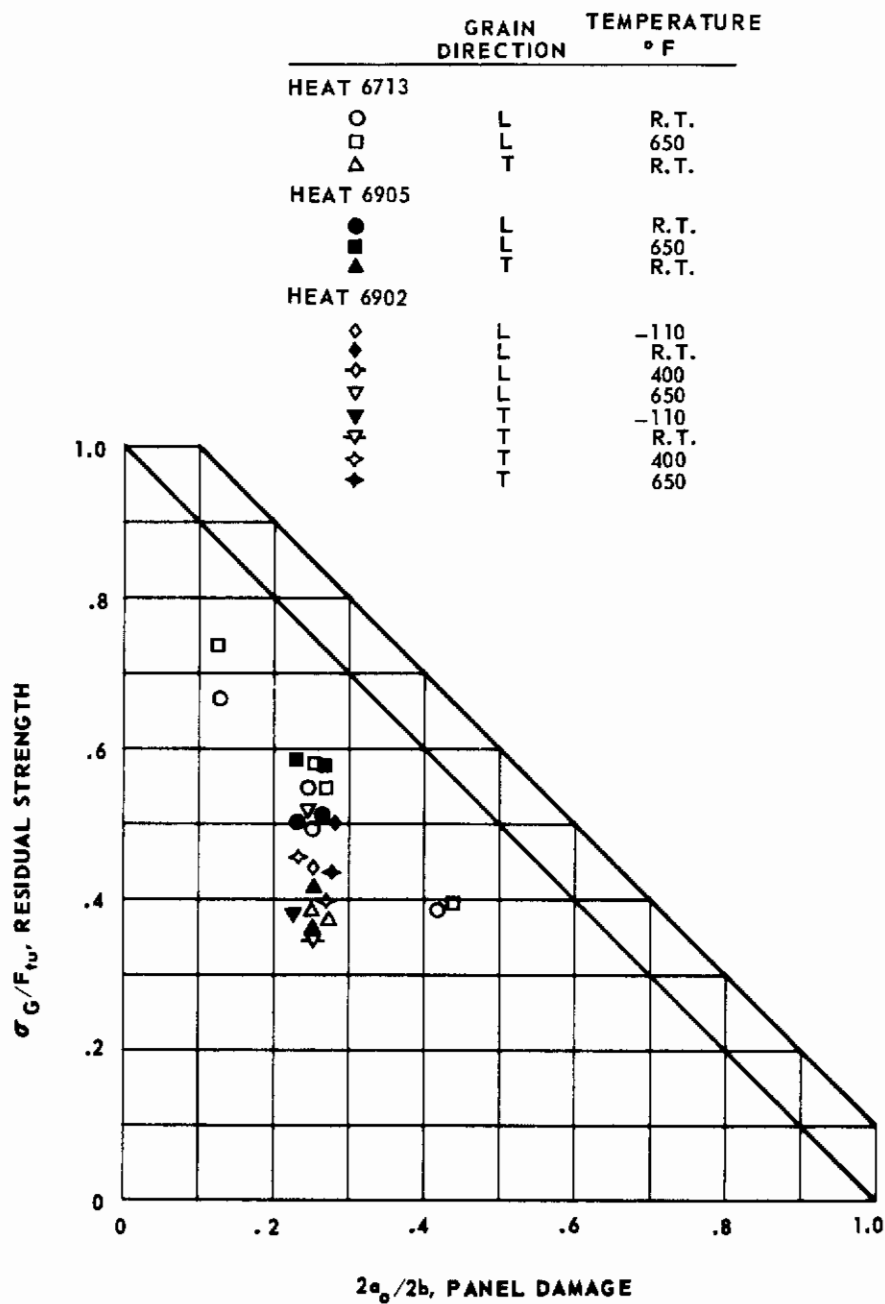


FIG. 138 RESIDUAL STRENGTH vs DAMAGE FOR 24 x 72 INCH INCO 718, HEATS 6713, 6905 AND 6902

as parameters on these graphs. Most of the data are from tests made at the high stress rate of 10^6 psi/sec.

Figs. 133 and 134 include only 24 x 72-inch panel data. Many of the elevated temperature tests result in the σ_N/σ_{yp} ratio exceeding the ASTM criterion. For the room temperature tests, K_C shows some variation with the σ_N/σ_{yp} ratio even at ratios below 0.80. For the 10-inch crack lengths ($2a_0/2b = 0.417$), the K_C variation may be due to the inapplicability of the geometry correction factor. For the 3-inch crack lengths, the net section yielding condition is being approached. Fig. 135 indicates test results for only the 8 x 24-inch panels and the ASTM criterion for valid tests has been exceeded in each case.

The residual strength data shown in Figs. 136, 137 and 138 generally show the expected variation of residual strength with crack length.

Effect of Stress Rate

The effect of stress rate on K_C is shown in Fig. 139. In general, stress rate has a negligible effect on K_C . For the 0.125-inch thick 24 x 72-inch panels from heat 6902 tested at room temperature, there appears to be a consistent increase in K_C with increasing stress rate.

Effect of Exposure

The effect of the 650° F exposure for 1000 hours at 40 ksi on K_C is shown in Fig. 140 for the 8 x 24-inch transverse panels. Data are included for unexposed panels from the same heat of material for comparison. Although all the 0.025 and 0.050-inch thick panels, both exposed and unexposed, exceed the ASTM validity criterion, there is a consistent trend to lower K_C values for the exposed panels. Because of this net section yielding condition, it is not strictly correct to compare K_C values, since the linear elasticity theory underlying the fracture mechanics approach is strictly applicable for elastic behavior.

For these thinner panels, a comparison based on residual strength can be made. For the unexposed 0.025-inch thick panel, the residual strength ($\sigma_{G/F_{tu}}$) is 0.630; for the exposed panels, 0.622 and 0.612. For the unexposed 0.050-inch thick panel, the residual strength is 0.676; for the exposed panels, 0.648 and 0.642. This comparison also shows a consistent reduction in residual strength values with the exposed panels. The argument for the 0.125-inch thick panels is clear-cut, since all K_C tests met the ASTM criterion. A drop of approximately 18 percent in K_C was found with exposed panels.

Effect of Heat Variation

The effect of heat variation is shown partly by Fig. 129 in a previous subsection on grain direction. The room temperature test data for the three heats of material can also be used to assess the heat-to-heat variation at a constant thickness of 0.025-inch. All these tests were made with 24 x 72-inch panels with a crack length of 6 inches and at a stress rate of 10^6 psi/sec.

For the five longitudinal tests, the average K_C value was 388.3 ksi $\sqrt{\text{inches}}$ and the range in values was 51.2 ksi $\sqrt{\text{inches}}$. This range expressed as a percentage of the average value is approximately 13 percent. A similar com-

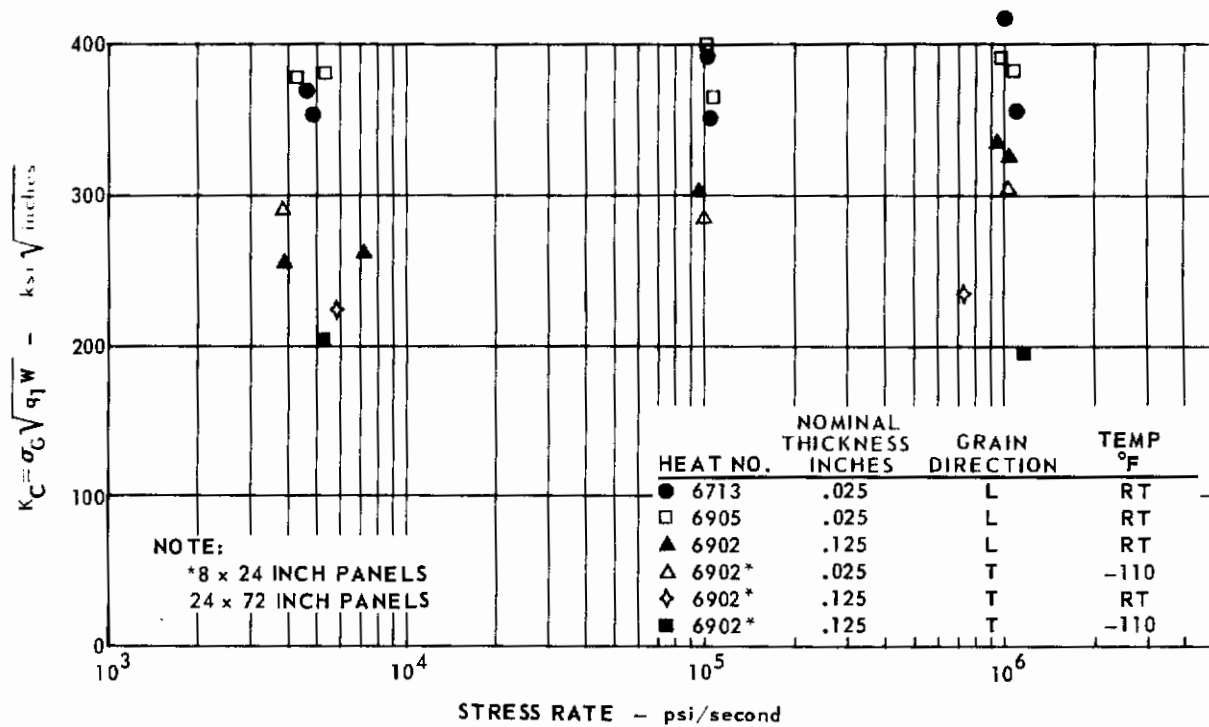


FIG. 139 THE EFFECT OF STRESS RATE ON K_C FOR INCO 718

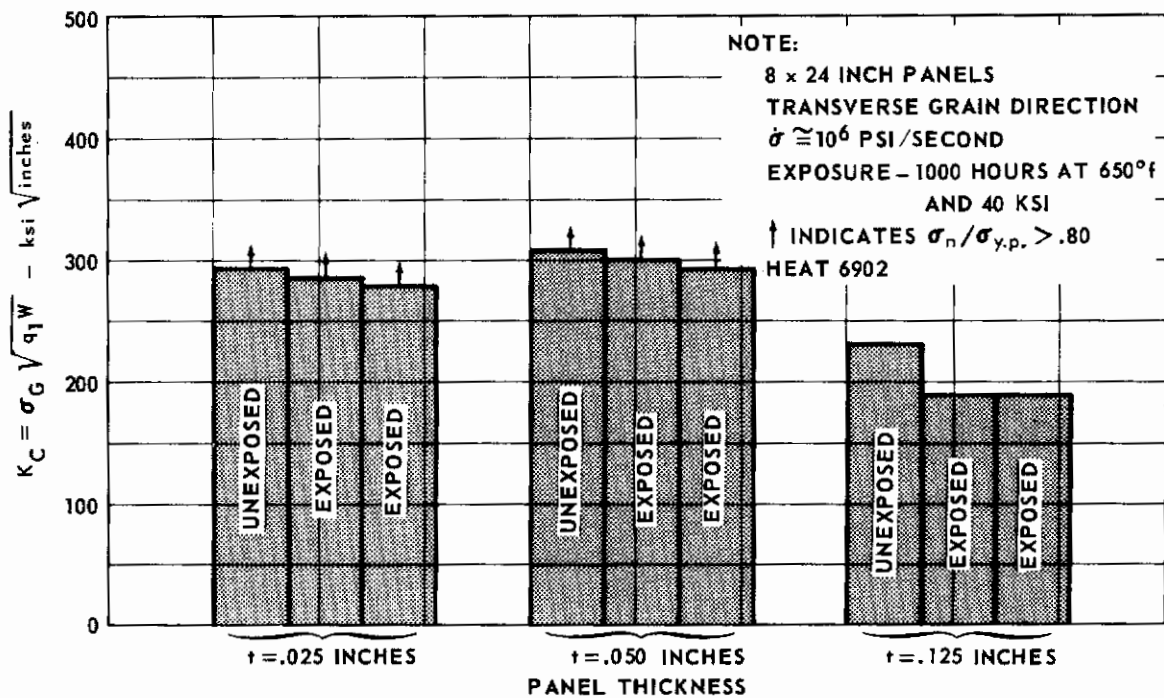
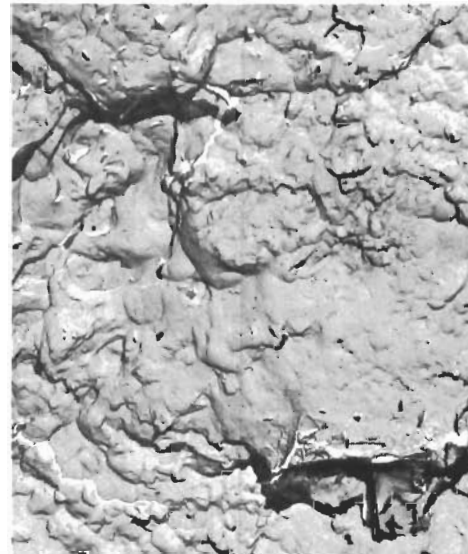


FIG. 140 COMPARISON OF EXPOSED AND UNEXPOSED K_C VALUES FOR INCO 718



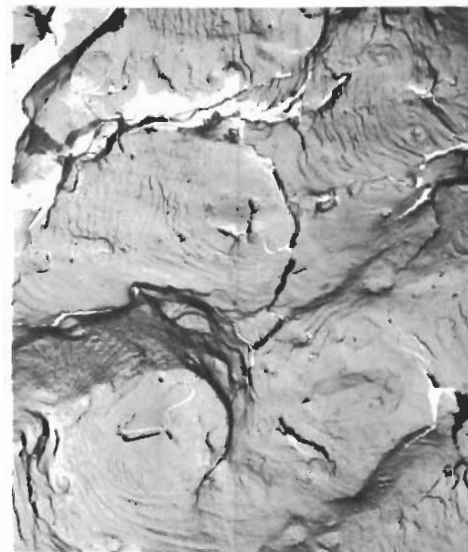
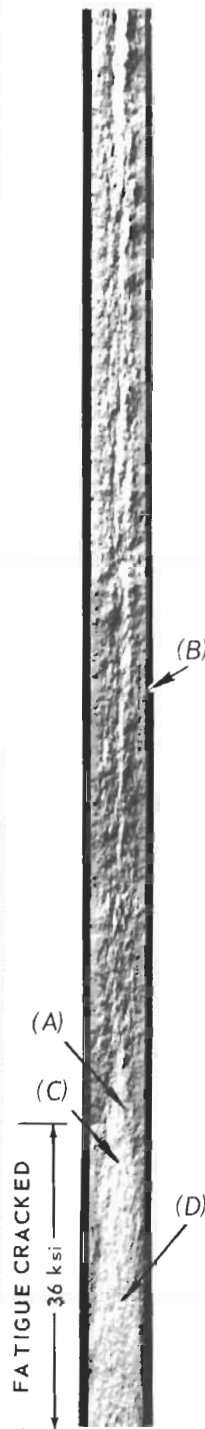
(A) INITIATION OF RAPID FRACTURE (1700x)



(B) DIMPLES FROM SHEAR LIP AREA (1700x)



(C) STRIATIONS TYPICAL OF TWINNED MICROSTRUCTURE (1700x)



(D) STRIATIONS FROM FATIGUE AREA (1700x)

NOTE: Fatigue Cracked and Fractured at Room Temperature

FIG. 141 FRACTOGRAPHIC STUDY OF INCO 718 SPECIMEN DC74

parison based on the transverse K_{IC} average of 264.7 ksi $\sqrt{\text{inches}}$ shows a range variation of approximately 19 percent.

Fractographic Studies

A macrophotograph of specimen DC74, along with results of the electron micrographic survey, is shown in Fig. 140. Note that the macrophotograph shows the fracture face representing only one-half the panel width in order to show as much detail as possible.

The electron micrographs typical of the fatigue crack area show two characteristic types of fatigue striations. The lower right hand micrograph shows the most general type found over this fracture area. It appears that the second phase particles may have retarded cracking to some extent in the immediate vicinity. The lower left hand micrograph shows the geometrically shaped striations which are often found and which are believed to be caused by twins in the microstructure.

The upper right-hand micrograph shows dimples characteristic of the room temperature shear fracture area. Isolated areas as shown in the upper left-hand micrograph were often found in the rapid fracture portion of the fracture surface. The small blocky shapes are believed to be second-phase particles in the microstructure.

TITANIUM 6Al-4V

Chemistry and Mill Processing History

Chemical analyses of each of the heats are listed in Table 19; also included are the ranges allowed for the principal elements by the material specification. All of the elements are within the specified ranges.

The material used in this program was melted by the double vacuum consumable electrode method from sponge having a Brinnell hardness greater than 120. Breakdown reduction was accomplished in steps from full-sized ingots at temperatures which permitted finishing of the sheet bar below the beta transus of the material.

Reheating and hot rolling were performed below the beta transus; hot rolling was initiated when the material was in the 1650° to 1750°F range. Finish rolling was also initiated in the 1650° to 1750°F range.

Flattening was accomplished in a car bottom annealing furnace that permitted the material to creep during annealing.

Sheets were sized and decontaminated by belt grinding. After grinding, the sheets were pickled to provide a matte finish and minimize the effects of grind lines.

TABLE 19 VENDOR CERTIFIED CHEMICAL ANALYSIS FOR Ti 6Al-4V (WEIGHT, PERCENT)

		C	Al	Fe	V	N ₂	H ₂	O ₂
Ti 6Al-4V	D 4949	.025	5.9	.14	4.1	.012	.008	.090
	D 5256	.026	6.0	.12	4.1		.006	.110
	D 5257	.023	6.0	.13	4.1		.006	.120
	SPEC. $\left\{ \begin{array}{l} \text{MIN.} \\ \text{MAX.} \end{array} \right.$.10	5.50 6.75	.30	3.50 4.50	.070	.0125	.20

Microstructure

Typical microstructures are shown in Figs. 142 and 143. The structure consists of grains of primary alpha phase in a matrix of retained beta phase. Comparing microstructures from heat to heat, they are relatively uniform and are for the most part equi-axed structures which give good mechanical properties. Comparing microstructures for the 0.025, 0.050, and 0.200-inch nominal thicknesses within heat D4949, the 0.050-inch thickness reveals a grain structure which is coarser than the grain structure of the other two gages. Practically, the microstructures appear normal for this alloy.

Tensile Properties

Tensile properties for -110°F, room temperature, 400°F, and 650°F are listed in Table 20. For the 0.050-inch thickness, the variation between the heats is small. Within heat D4949, the properties increase in magnitude with an increase in thickness. Tensile ultimate and tensile yield strengths decrease with an increase in temperature, and elongation decreases as the temperatures progress away from room temperature.

After the exposed fracture toughness specimens were failed, a tensile specimen was fabricated from each failed specimen. The measured tensile properties, which are included in Table 20, have consistently higher tensile ultimate and tensile yield strengths than the unexposed material, but the elongation of the exposed material decreases. Considering that none of the exposed fracture toughness specimens had net failing stresses exceeding the yield strength of

the material, the exposed tensile properties should be reliable.

Fatigue Crack Propagation

Fatigue crack growth curves are plotted in Figs. 144 through 153 for the 24 x 72-inch panels and in Figs. 154 through 157 for the 8 x 24-inch panels. All data were generated at room temperature at a cycling frequency of 120 cpm for the 24 x 72-inch specimens, and 1200 cpm and 120 cpm for the 8 x 24-inch specimens.

The final increment of crack growth for each specimen was performed at a stress ratio of 0.20 and a gross level to approximate a final stress intensity of 50 ksi $\sqrt{\text{inches}}$. For the 8 x 24-inch panels, the final stress was 25 ksi; for the 24 x 72-inch panels, the final stress was 25 ksi for the last 0.50 inch of the 3-inch final crack length, 17.5 ksi for the last 0.75 inches of the 6-inch final crack length, and 12.5 ksi for the last 1.0 inch of the 10-inch final crack length.

In general, it is shown by the crack growth curves that fatigue crack growth is a function of:

- 1) Gross stress level; cycles required to grow a given crack length decrease with an increase in the gross stress level.
- 2) Stress ratio; cycles required to grow a given crack length decrease with a decrease in the stress ratio. The effect of the stress ratio increases with an increase in the gross stress level.
- 3) Thickness; cycles required to grow a given crack length decrease with an increase in the thickness.
- 4) Grain direction; cycles required to grow a given crack length are smaller for the transverse grain direction.
- 5) Cycling frequency; for the 8 x 24-inch specimens examined, cycles required to grow a given crack length are larger for the slower cycling rate.
- 6) Exposure; for the 8 x 24-inch specimens examined, cycles required to grow a given crack length are smaller for the exposed specimens.

Changes in the gross stress level and/or the stress ratio during cycling may retard or prohibit crack growth for a number of cycles. Lowering the gross stress level and/or raising the stress ratio tend to retard or prohibit crack growth; elevating the gross stress level and/or lowering the stress ratio does not.

The fatigue crack of DD13 (Fig. 145) was grown beyond the intended length of 6 inches to a 14-inch length to determine if the net failing stress level (during static failure) could be considerably lowered.

TABLE 20 TENSILE TEST DATA FOR Ti 6Al-4V

HEAT NO.	NOMINAL THICKNESS inches	GRAIN DIRECTION	TEST TEMPERATURE											
			-110° F			R. T. (80° F)			400° F			650° F		
			F _{TU} (ksi)	F _{TY} (ksi)	ELONG.*	F _{TU} (ksi)	F _{TY} (ksi)	ELONG.*	F _{TU} (ksi)	F _{TY} (ksi)	ELONG.*	F _{TU} (ksi)	F _{TY} (ksi)	ELONG.*
D5257	.050	L	170.8	165.4	13.0	143.6	135.9	13.5				96.9	81.2	11.5
		L				143.0	137.1	14.0				98.3	82.7	10.5
		T	167.2	161.4	16.5	141.2	134.7	16.5				97.4	81.1	12.0
		T	167.8	165.2	15.5	139.9	132.9	14.5				97.4	81.0	12.0
D5256	.050	L	172.1	167.2	7.5	143.3	136.9	15.5				102.9	85.1	9.5
		L				143.5	136.5	15.0				103.3	86.1	9.1
		T	170.1	165.2	12.5	142.2	136.8	12.0				100.0	83.3	11.0
		T	178.5	163.4	12.0	142.5	135.1	13.5				100.6	84.3	11.5
D4949	.025	L	167.0	161.5	12.0	142.1	136.5	10.5	112.5	100.7	9.5	103.6	89.1	7.5
		L	167.5	166.2	12.0	139.4	136.8	12.5	114.9	102.8	10.5	99.5	85.4	8.5
		L	166.0	163.1	10.0									
		T	165.6	156.4	13.0	139.5	125.0	12.0	112.1	97.8	12.5	98.2	80.6	10.0
		T	167.2	158.0	13.0	139.3	128.9	12.5	113.2	98.0	11.5	97.4	79.9	9.6
		T										99.3	79.8	10.0
		T										100.0	80.3	11.0
		L	164.7	160.6	11.5	140.1	134.1	13.5	108.7	96.2	13.5	98.0	82.3	11.0
		L	164.5	161.4	10.0	140.0	134.3	15.0	109.6	97.8	13.0	97.8	82.4	11.0
		L										97.7	81.9	11.0
		T	163.5	158.3	11.0	139.6	132.4	14.5	109.3	96.3	13.0	97.5	81.5	11.5
		T	164.6	160.0	12.0	138.8	131.9	14.5	109.5	95.7	14.0			
	.125	L	166.3	161.8	11.0	138.8	135.2	16.0				98.2	82.6	17.0
		L				138.9	134.0	14.5						
		T	169.5	165.8	9.5	140.3	139.0	16.5				100.8	86.9	14.5
		T	172.0	166.6	12.0	141.3	140.4	16.0				100.0	86.0	13.5

* ELONGATION MEASURED AS % IN 2 INCHES

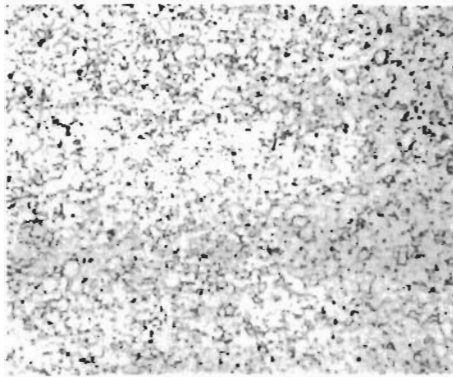
TABLE 20 TENSILE TEST DATA FOR Ti 6Al-4V (continued)

HEAT NO.	NOMINAL THICKNESS inches	GRAIN DIRECTION	TEST TEMPERATURE											
			-110° F			R. T. (80° F)			400° F			650° F		
			F _{TU} (ksi)	F _{TY} (ksi)	ELONG.*	F _{TU} (ksi)	F _{TY} (ksi)	ELONG.*	F _{TU} (ksi)	F _{TY} (ksi)	ELONG.*	F _{TU} (ksi)	F _{TY} (ksi)	ELONG.*
D4949	.200	L	164.6	157.7	9.0	138.5	129.0	14.5	112.1	97.0	15.5	99.4	84.0	13.5
		L	169.4	162.7	6.0	138.5	129.6	13.0				99.0	84.4	13.0
		T	171.5	166.6	10.5	145.7	140.0	15.0	117.4	103.3	15.5	106.3	92.6	13.5
		T	171.1	169.0	8.0	144.1	139.3	15.5	119.0	105.8	15.5	104.9	91.4	13.5
**D4949	.025	T				139.1	129.8	11.5						
		T				140.6	133.1	12.0						
	.050	T				140.0	132.7	14.0						
		T				140.2	133.9	12.5						
	.200	T				146.5	141.8	13.0						
		T				143.2	143.0	13.0						

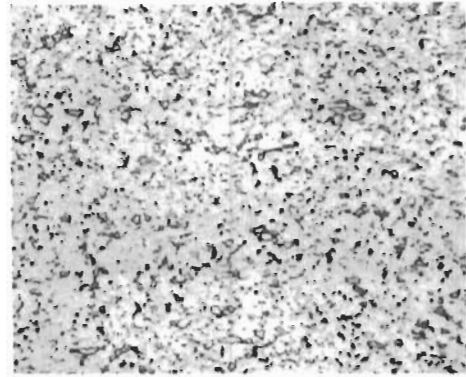
* ELONGATION MEASURED AS % IN 2 INCHES

** AFTER EXPOSURE AT 650° F FOR 1000 HOURS AT A GROSS STRESS LEVEL OF 25ksi

$t = .025$ INCHES

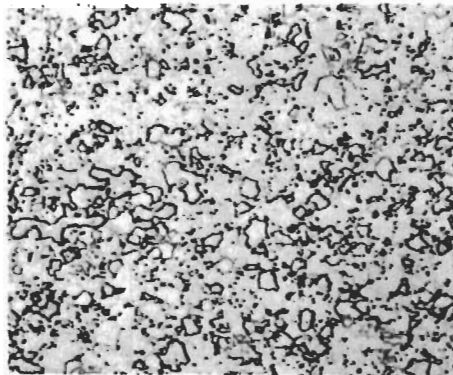


(A) LONGITUDINAL GRAIN
(250x)

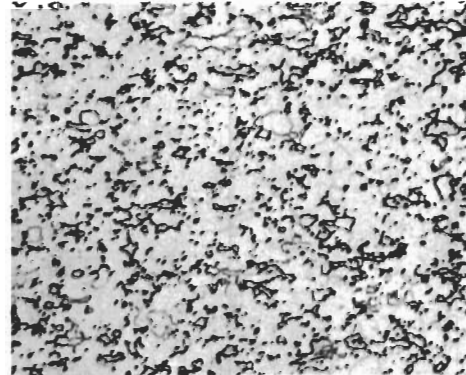


(B) TRANSVERSE GRAIN
(250x)

$t = .050$ INCHES

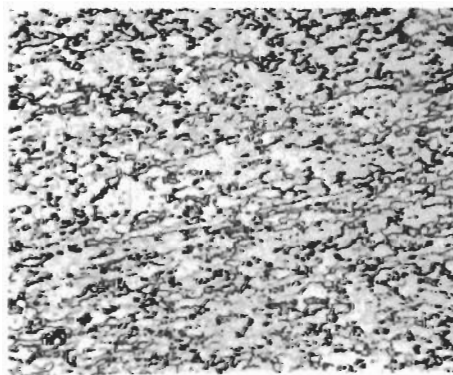


(C) LONGITUDINAL GRAIN
(250x)

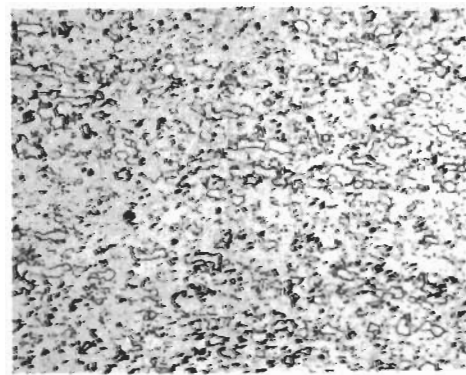


(D) TRANSVERSE GRAIN
(250x)

$t = .200$ INCHES



(E) LONGITUDINAL GRAIN
(250x)

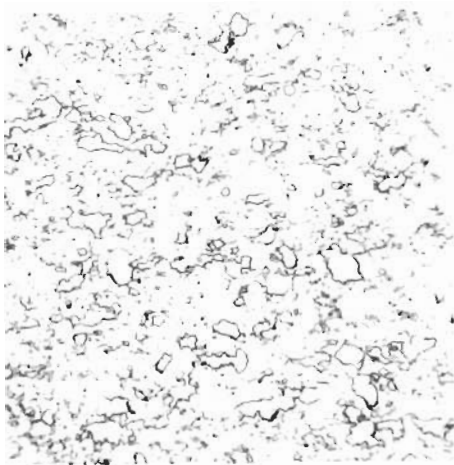


(F) TRANSVERSE GRAIN
(250x)

NOTE: Nitric-Hydrofluoric Acid Etchant

FIG. 142 PHOTOMICROGRAPHS OF Ti 6Al - 4V SHOWING THICKNESS VARIATION, HEAT 4949

HEAT 5257, $t = .050$ INCHES



(A) LONGITUDINAL GRAIN (250x)



(B) TRANSVERSE GRAIN (250x)

NOTE: Nitric-Hydrofluoric Acid Etchant.

FIG. 143 PHOTOMICROGRAPHS OF Ti 6Al-4V, HEAT 5257

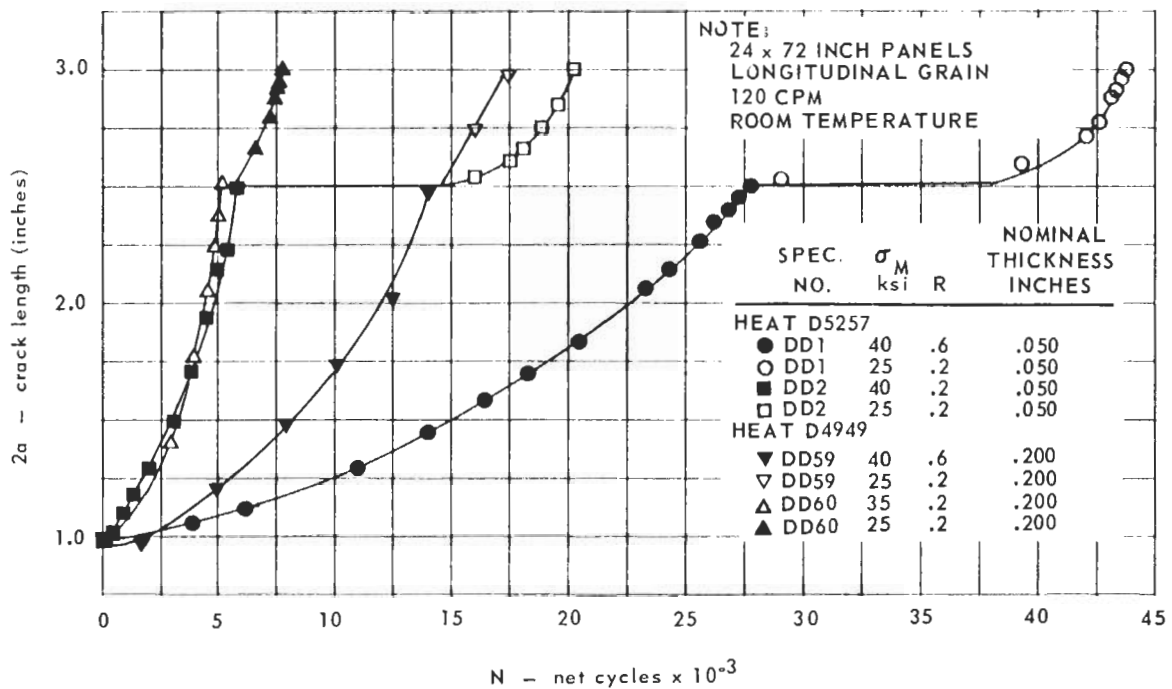


FIG. 144 CRACK GROWTH DATA FOR Ti 6Al-4V, HEATS D5257 AND D4949

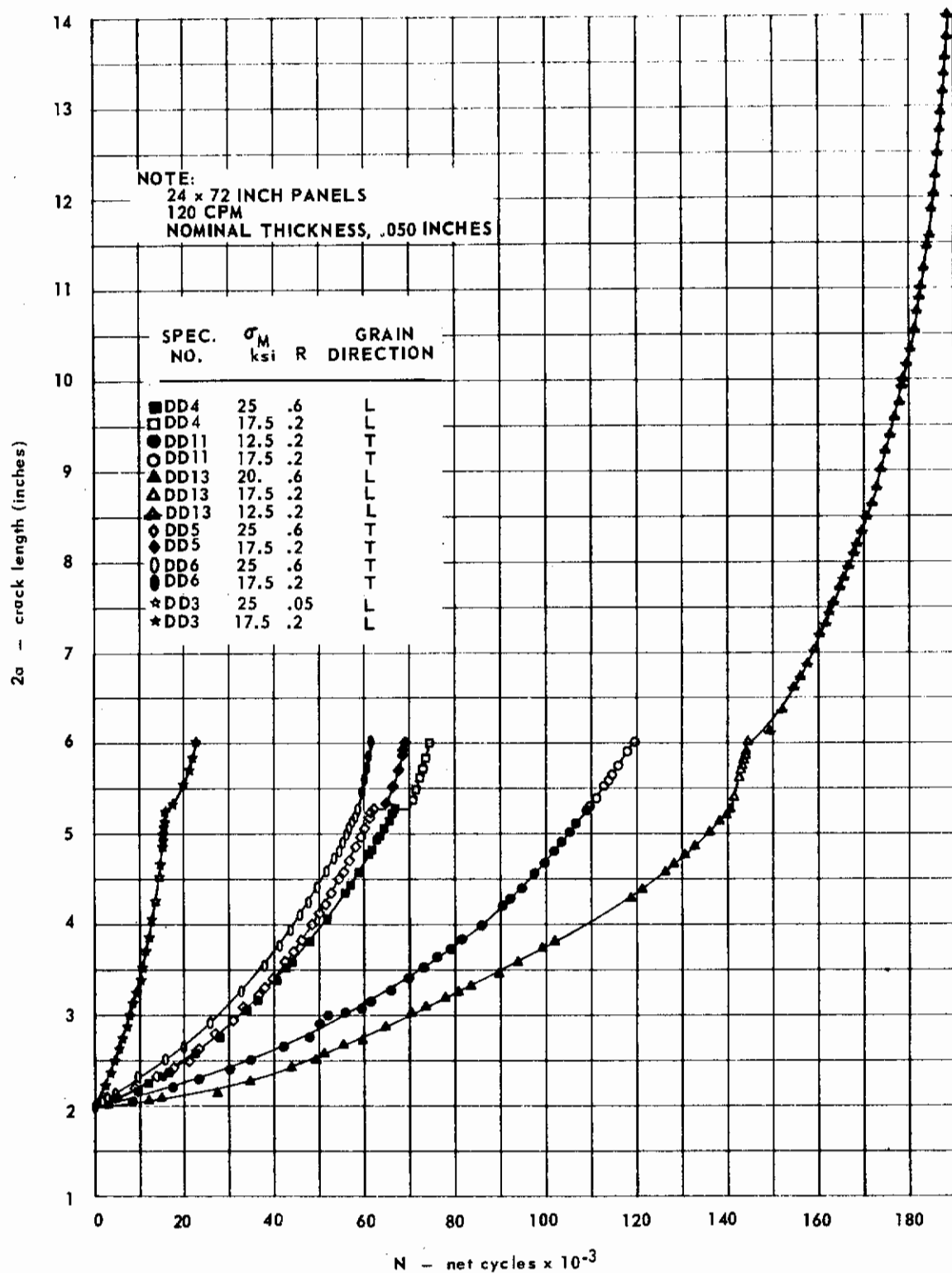


FIG. 145 CRACK GROWTH DATA FOR Ti 6Al-4V, HEAT DS257

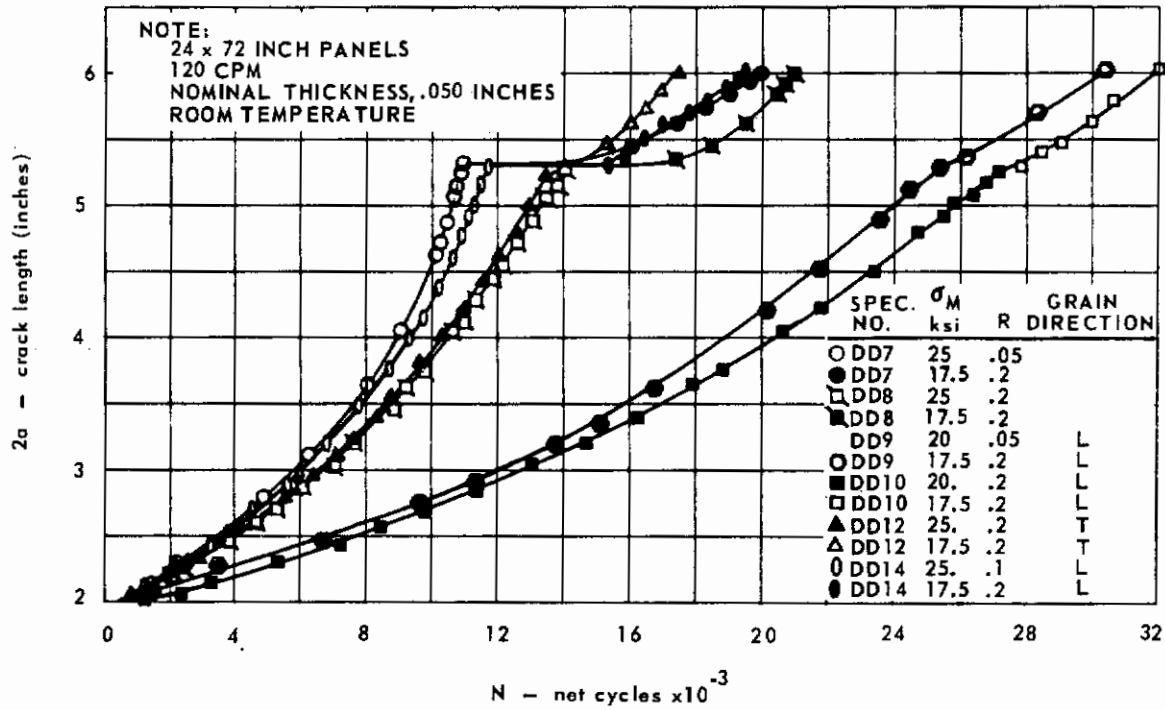


FIG. 146 CRACK GROWTH DATA FOR Ti 6Al-4V, HEAT D5257

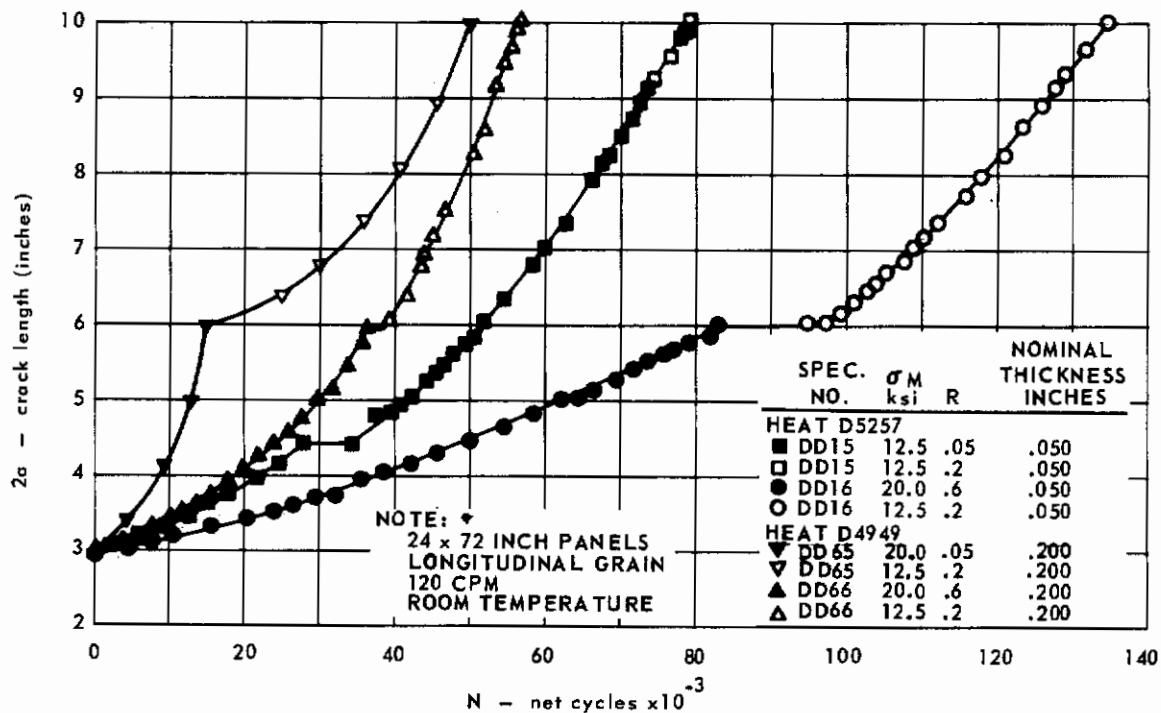


FIG. 147 CRACK GROWTH DATA FOR Ti 6Al-4V, HEATS D5257 AND D4949

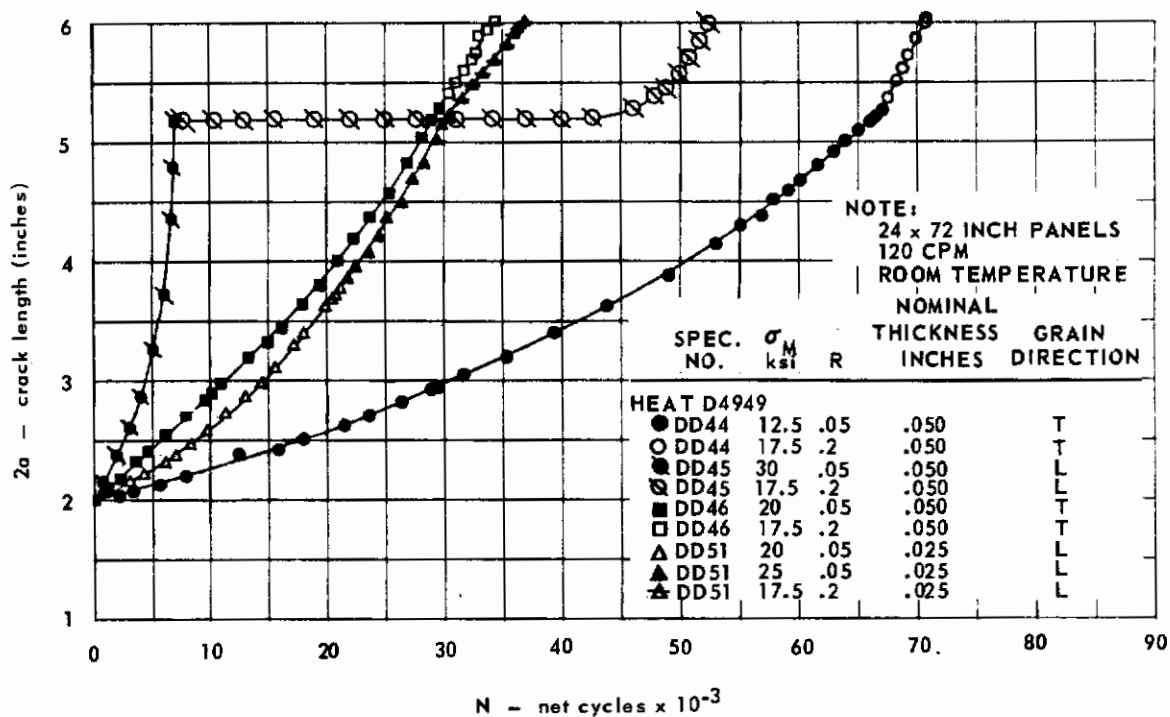


FIG. 148 CRACK GROWTH DATA FOR Ti 6Al-4V, HEAT D4949

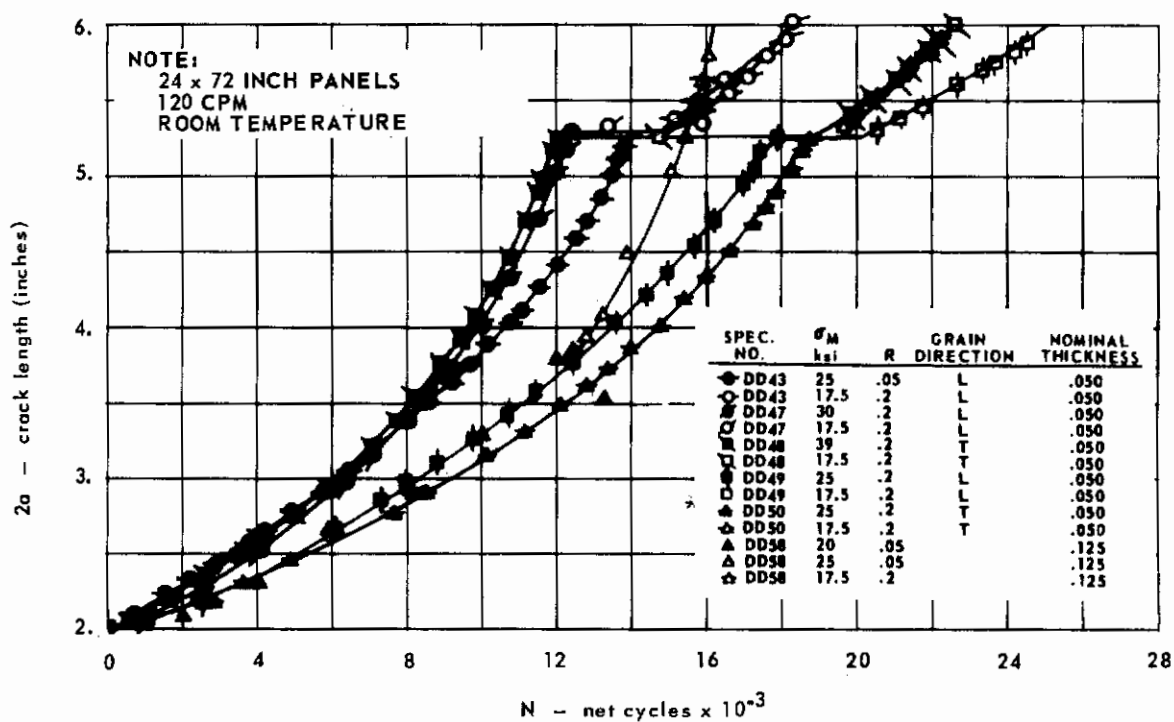


FIG. 149 CRACK GROWTH DATA FOR Ti 6Al-4V, HEAT D4949

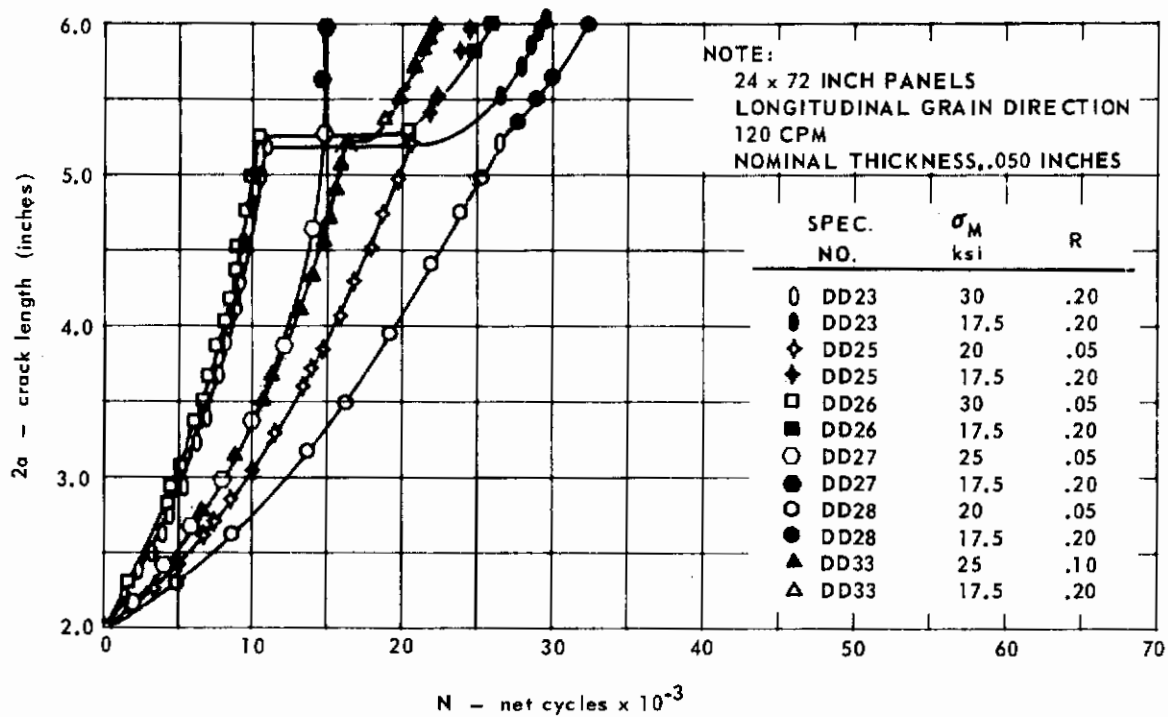


FIG. 150 CRACK GROWTH DATA FOR Ti 6Al-4V, HEAT D5256

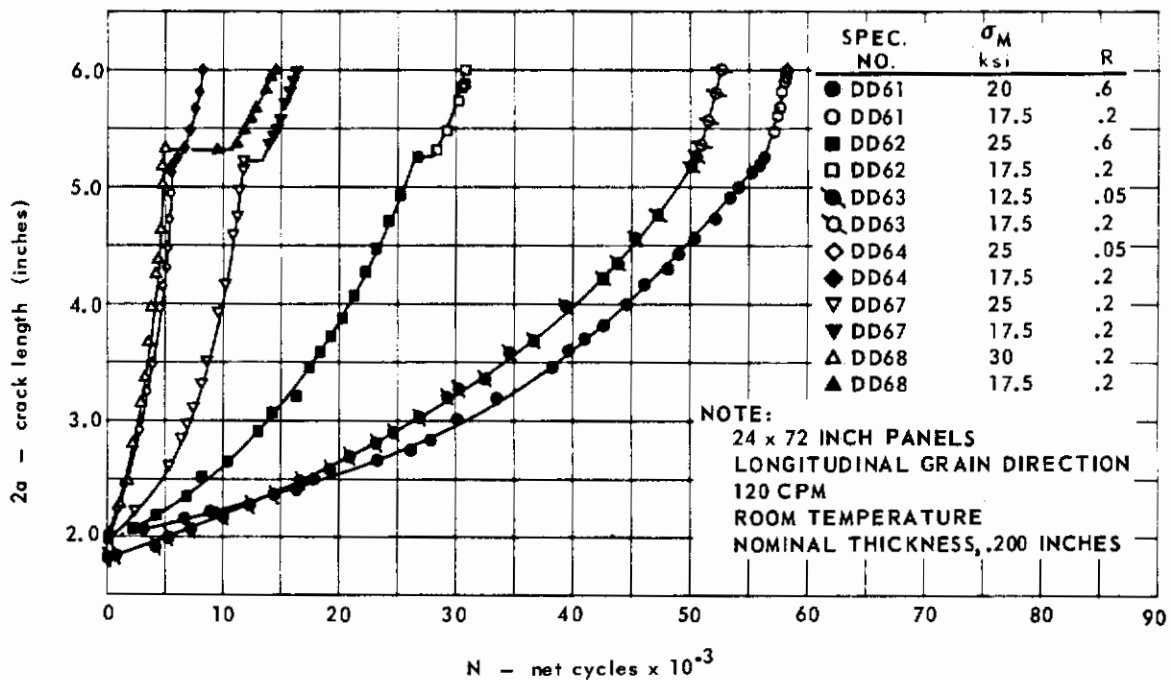


FIG. 151 CRACK GROWTH DATA FOR Ti 6Al-4V, HEAT D4949

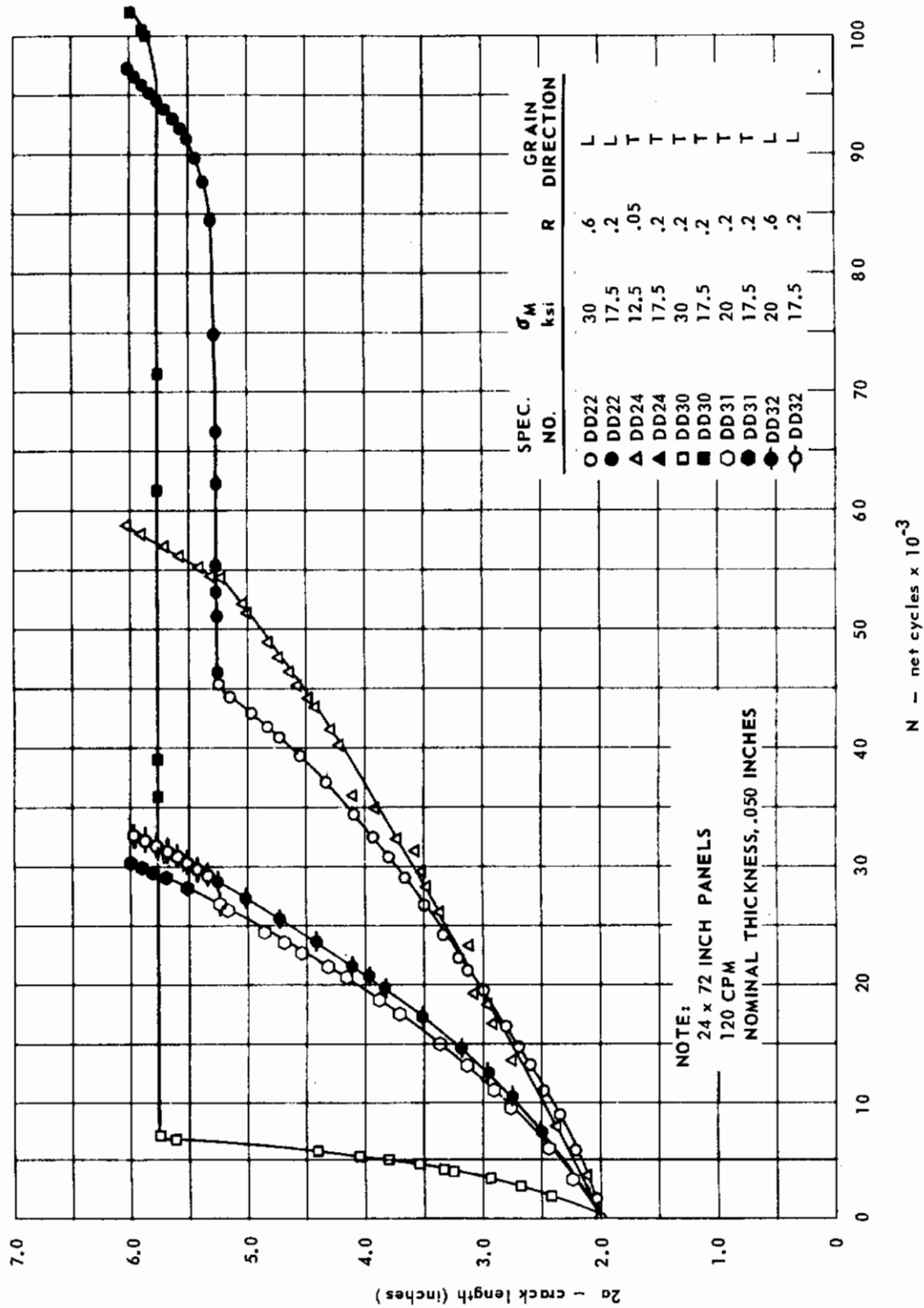


FIG. 152 CRACK GROWTH DATA FOR Ti 6Al-4V, HEAT D5256

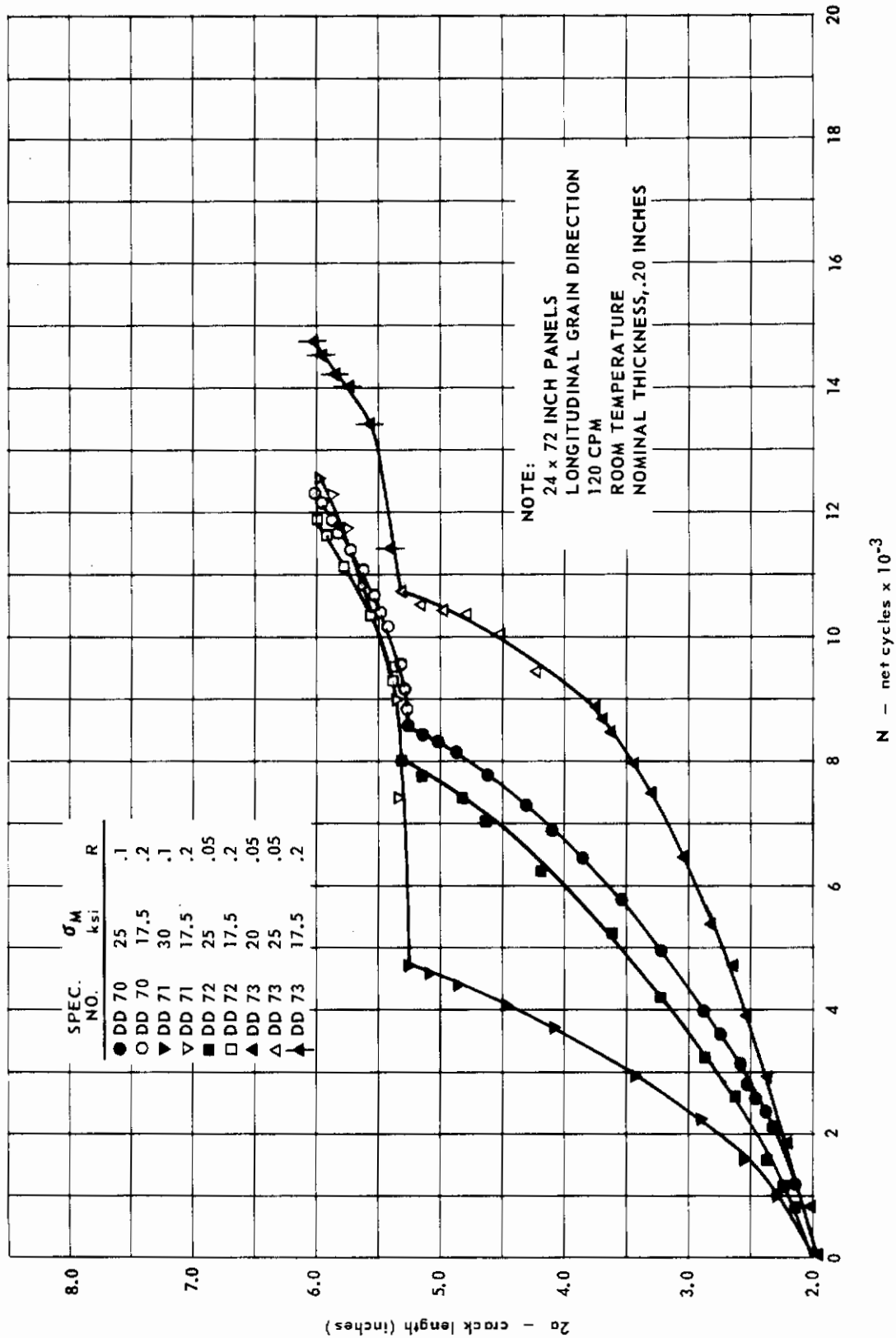


FIG. 153 CRACK GROWTH DATA FOR Ti 6Al-4V, HEAT D4949

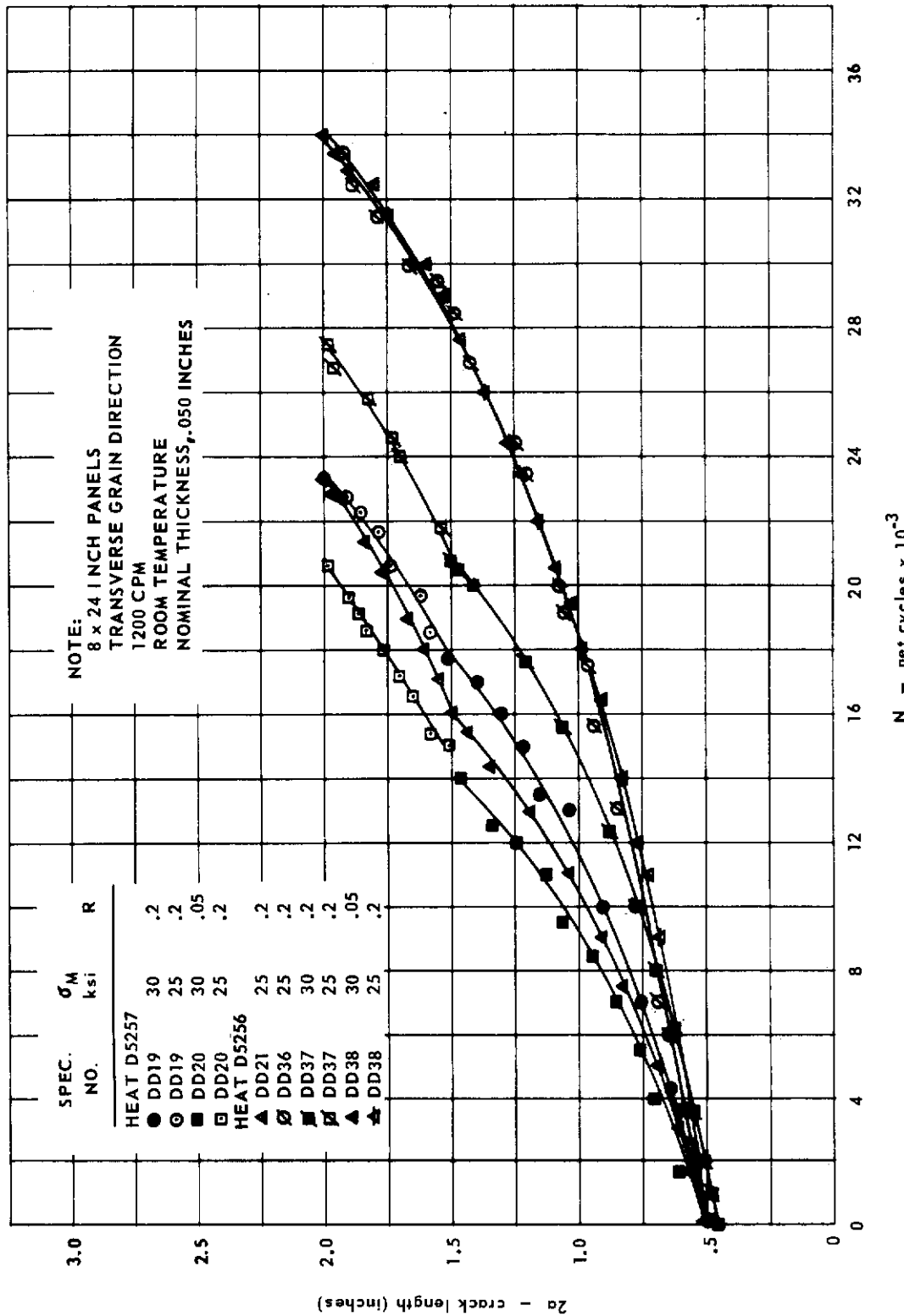


FIG. 154 CRACK GROWTH DATA FOR Ti 6Al-4V, HEATS D5257 AND D5256

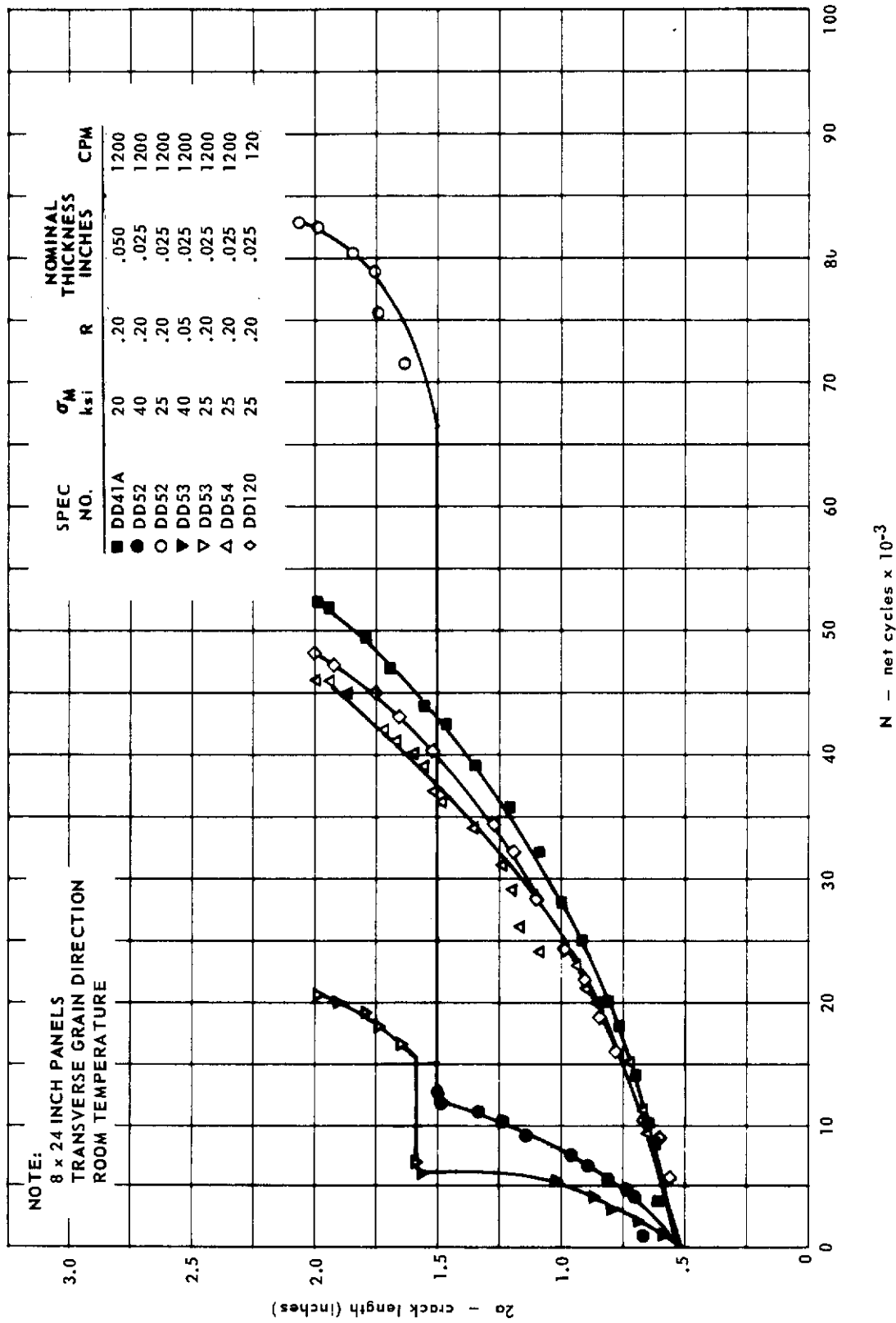


FIG. 155 CRACK GROWTH DATA FOR Ti 6Al-4V, HEAT D4949

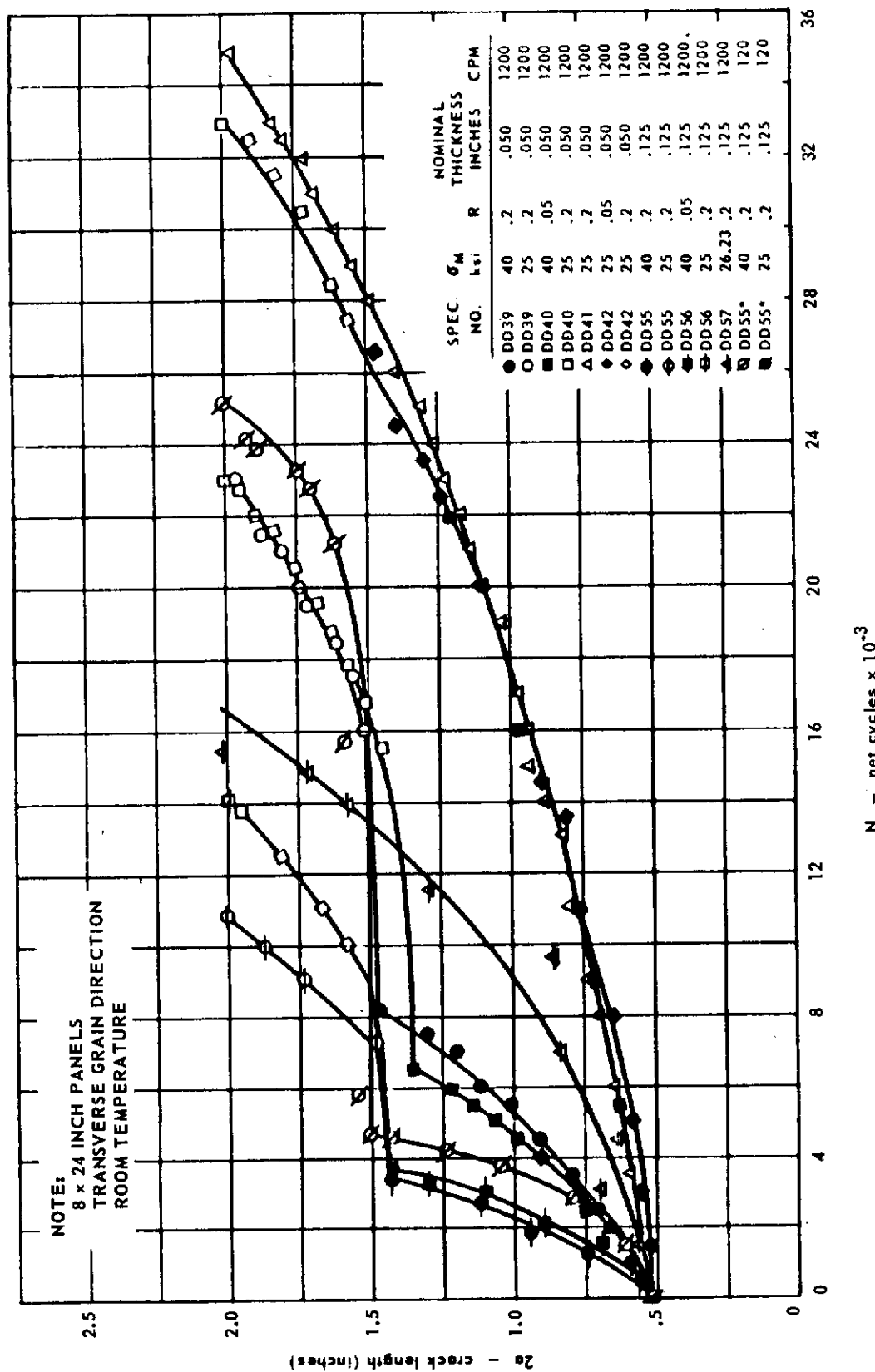


FIG. 156 CRACK GROWTH DATA FOR Ti 6Al-4V, HEAT D4949

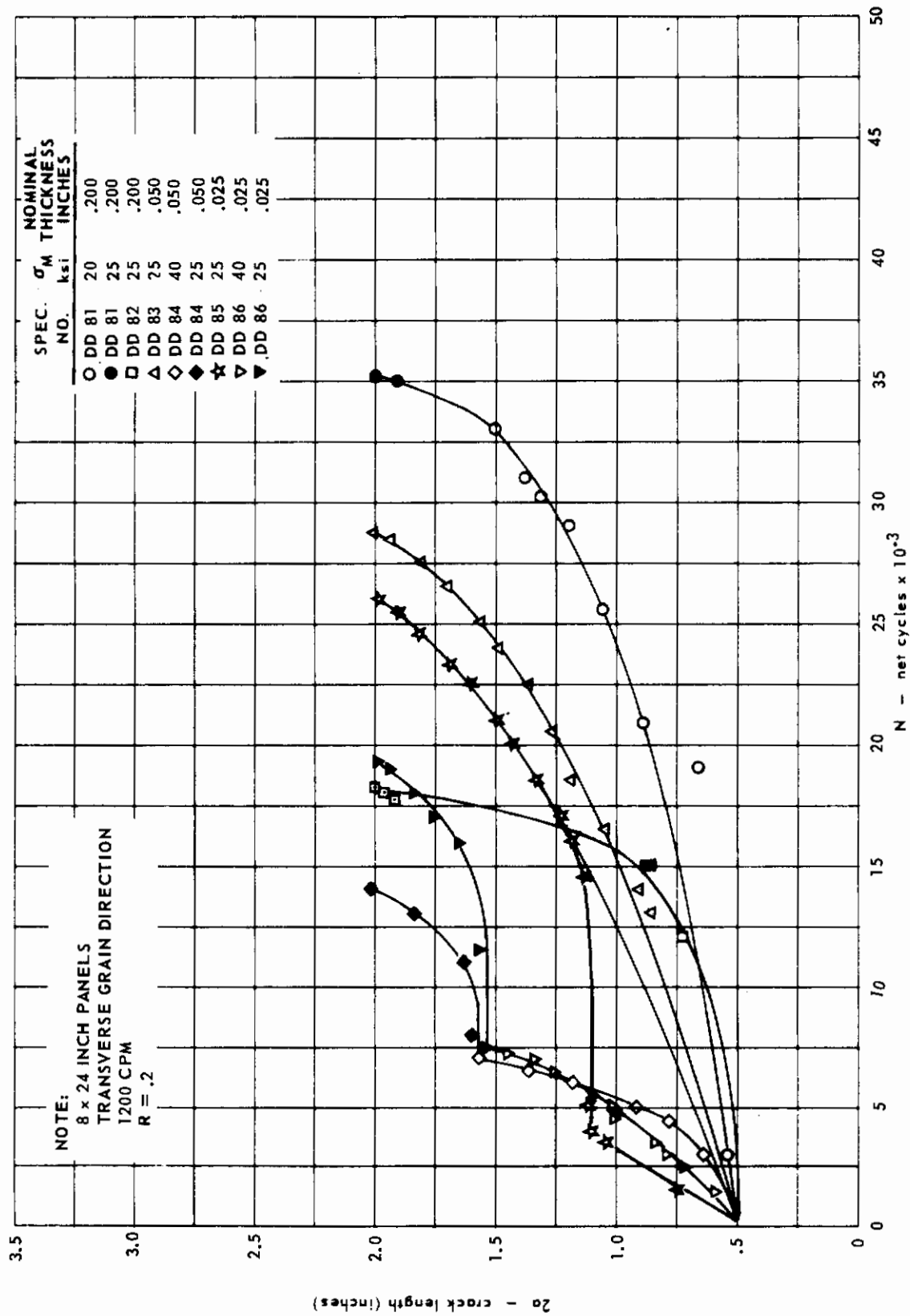


FIG. 157 CRACK GROWTH DATA FOR EXPOSED Ti 6Al-4V, HEAT D4949

A dwell period is shown at approximately 4.4 inches for DD15 (Fig. 147). This period occurred after the cycling was stopped for a reading of the crack length. The only plausible explanation is that the specimen was somehow accidentally overloaded.

Crack growth rate graphs are plotted in Figs. 158 through 171.

It is generally shown, in the graphs, that the fatigue crack growth rate is influenced by the test variables in the following manner:

- 1) Specimen Size. An influence on growth rate due to the specimen size was not found. Figs. 159, 160 and 162 illustrate how the data from the two specimen sizes blend together.
- 2) Thickness. The rate of crack growth increases with thickness. For the 24 x 72-inch specimen size, this is shown in Figs. 163 and 164; and for the 8 x 24-inch specimen size in Figs. 166 and 167.
- 3) Grain Direction. Crack growth rate is slightly larger for the transverse grain direction. For examples, note Figs. 161 and 162.
- 4) Stress Ratio. As expected, the growth rate increases with a decrease in the stress ratio. For the 24-inch wide specimens of 0.050-inch nominal thickness, a factor of approximately five exists between the rates for $R = .05$ and $R = .6$, while the rates for $R = .05$ and $R = .2$ differ by a factor less than two; this also is applicable to the 0.200-inch nominal thickness. The difference between the rates for $R = .05$ and $R = .2$ in the 0.050-inch and 0.125-inch nominal gages in the 8 x 24-inch specimen size is practically nil; in contrast the difference between the rates for $R = .05$ and $R = .2$ in the 0.025-inch and 0.200-inch nominal gages in the 8 x 24-inch specimen size varied up to a factor of approximately two. See Figs. 162, 165, 166 and 167.
- 5) Cycling Frequency. The effect of frequency on crack growth rate varies. In comparing 120 cpm and 1200 cpm frequencies on the 8 x 24-inch specimen size, growth rates are slightly less for 120 cpm in the 0.025 and 0.050-inch thicknesses, approximately the same for the 0.125-inch thickness and slightly more for 120 cpm for the 0.200-inch thickness. Refer to Figs. 167, 168, 169 and 170.
- 6) Heat. Fig. 171 depicts the scatter band for the 0.050-inch thicknesses for the three heats. The scatter band for the 0.050-inch thickness of each heat almost completely covers the scatter band in Fig. 171. It is concluded that the heat variable did not have any appreciable effect on the 0.050-inch thickness.
- 7) Exposure. Figs. 168, 169 and 170 show the effect of exposure on crack growth. The growth rate is increased throughout the range of the stress intensity for the exposed 0.025-inch thickness, while the growth of the exposed 0.050 and 0.200-inch thicknesses is increased only as the stress intensity increases.

Residual Strength and Fracture Toughness

All pertinent test data for the static fracture testing are included in Table 21 for the 24 x 72-inch panels and in Table 22 for the 8 x 24-inch panels. The calculations based on σ_{yp} , derived from high strain rate tensile data, are accentuated by a darker background to simplify comparisons among the various columns.

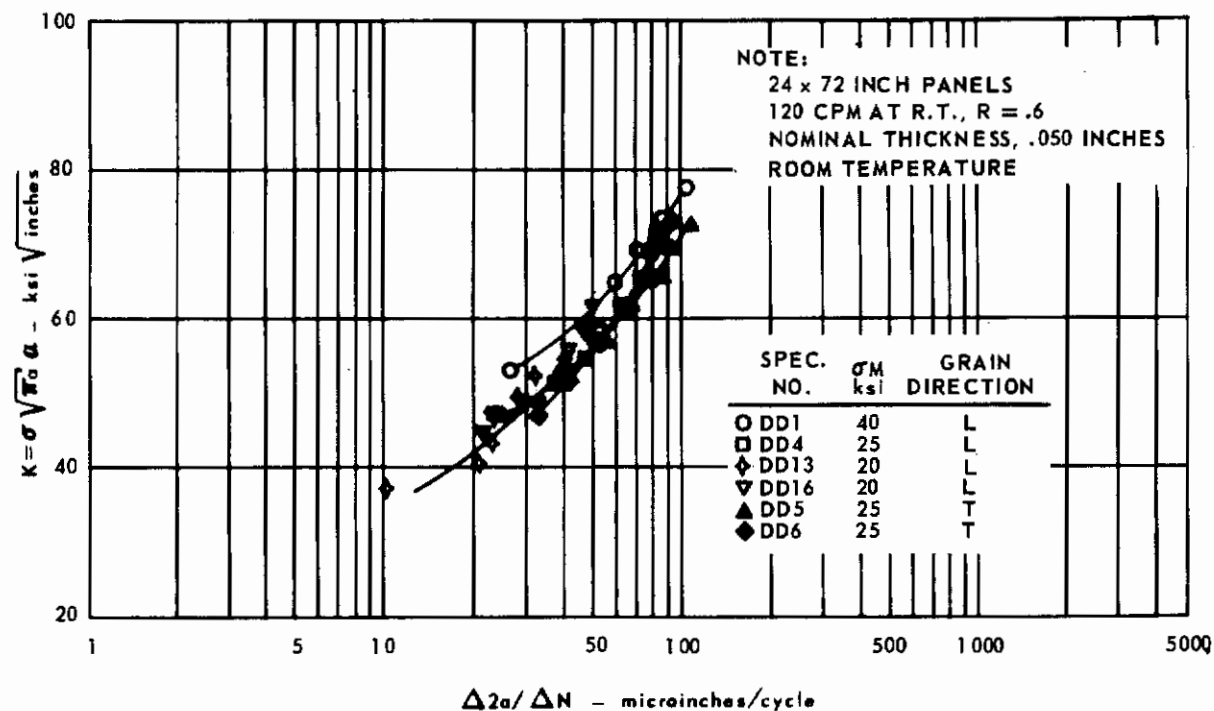


FIG. 158 CRACK GROWTH RATE DATA FOR Ti 6Al-4V, HEAT D5257

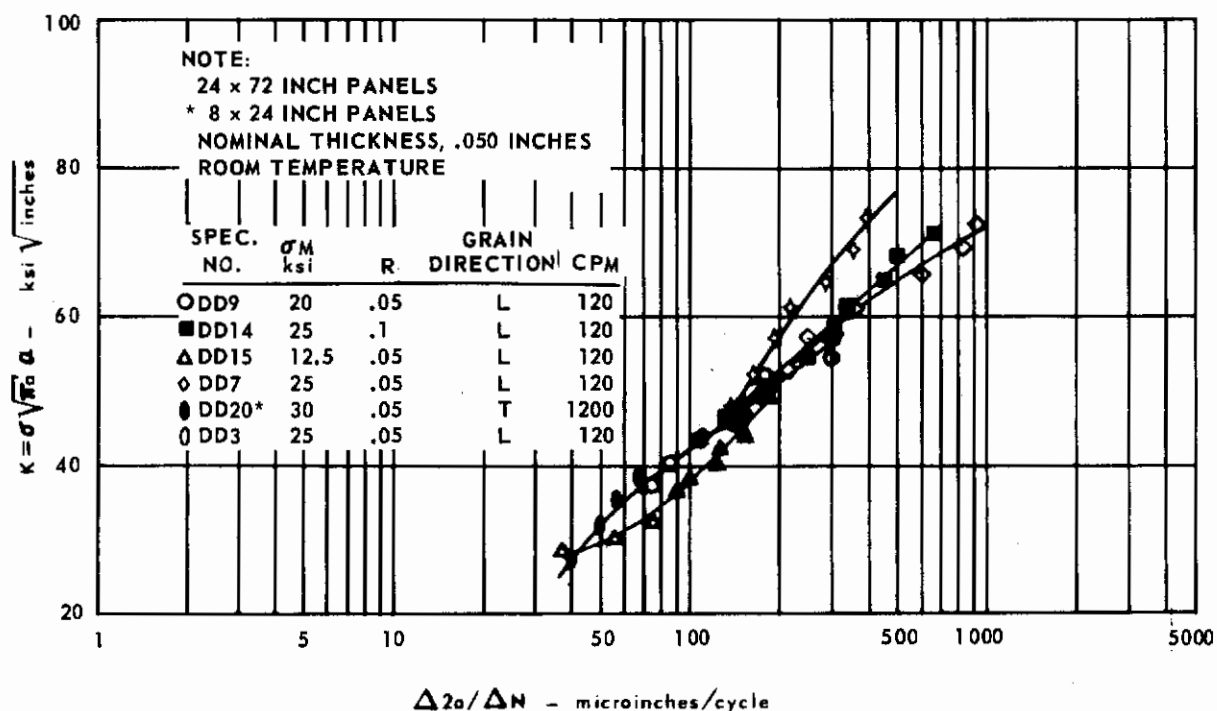


FIG. 159 CRACK GROWTH RATE DATA FOR Ti 6Al-4V, HEAT D5257

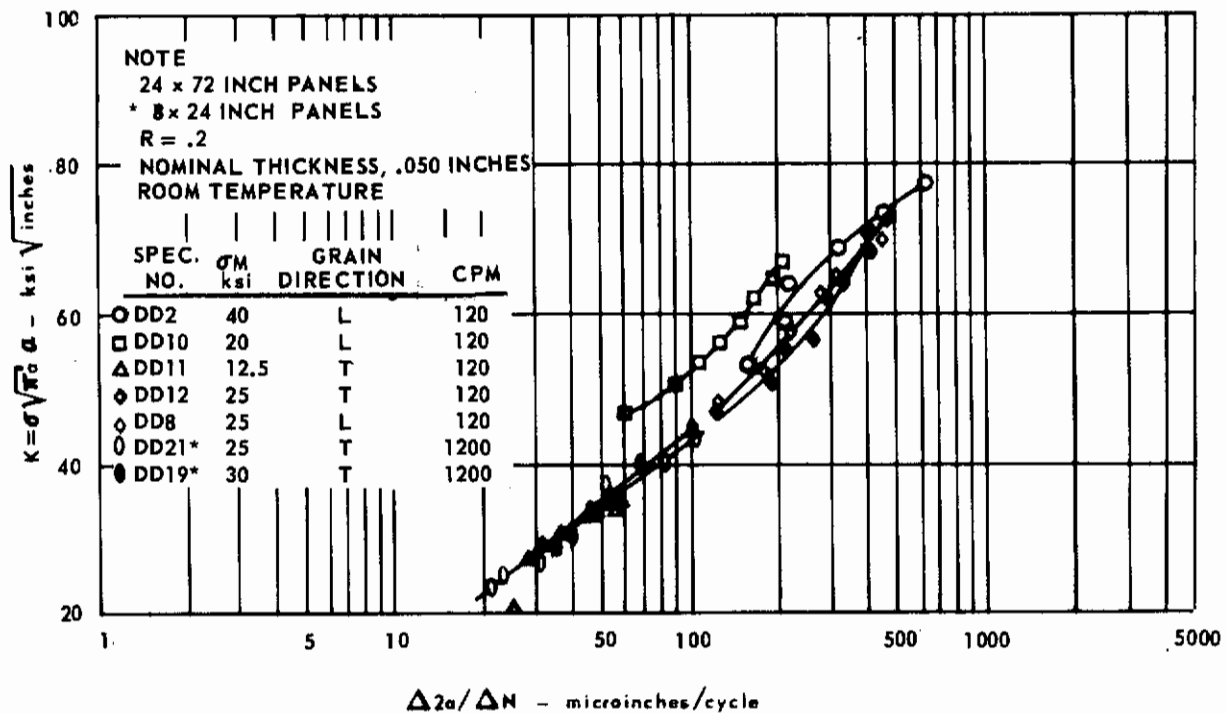


FIG. 160 CRACK GROWTH RATE DATA FOR Ti 6Al-4V HEAT D5257

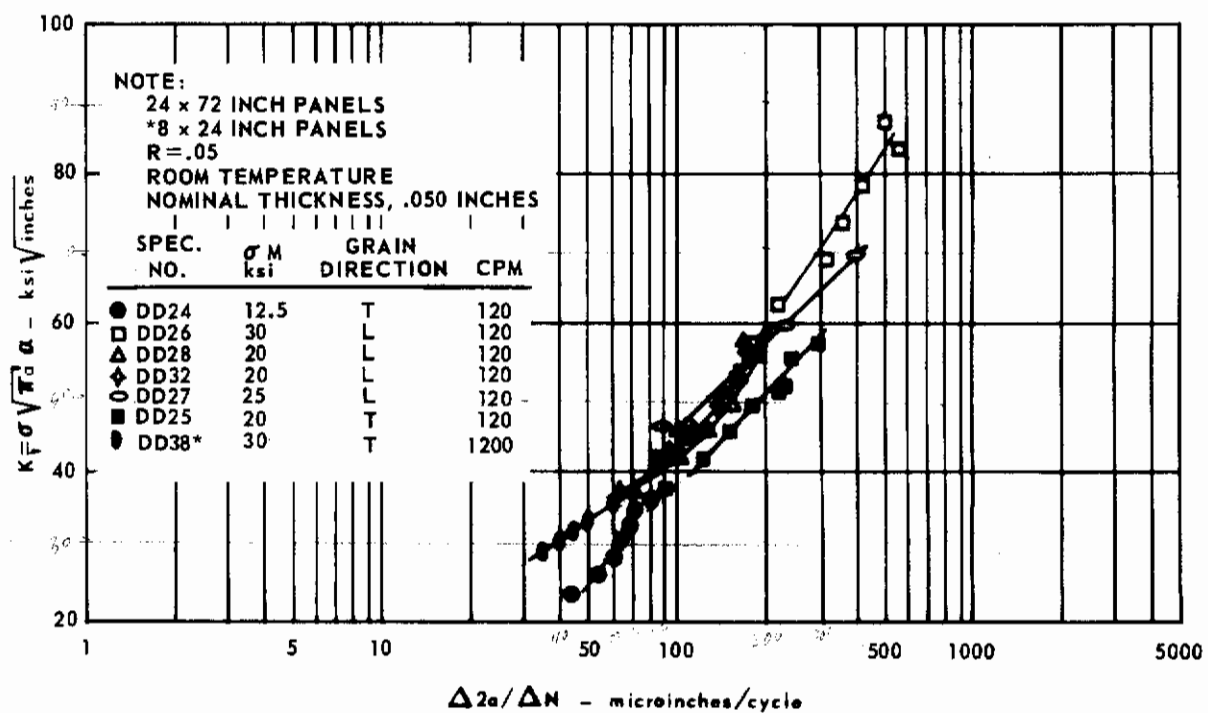


FIG. 161 CRACK GROWTH RATE DATA FOR Ti 6Al-4V, HEAT D5256

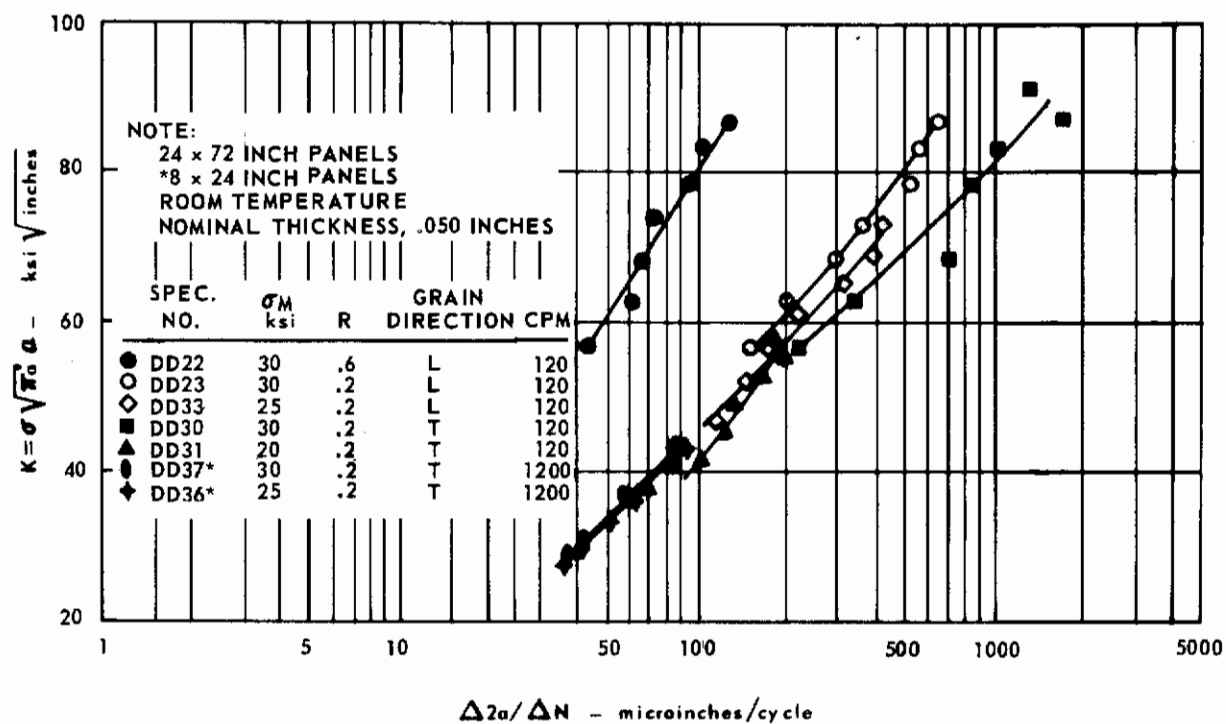


FIG. 162 CRACK GROWTH RATE DATA FOR Ti 6Al-4V, HEAT D5256

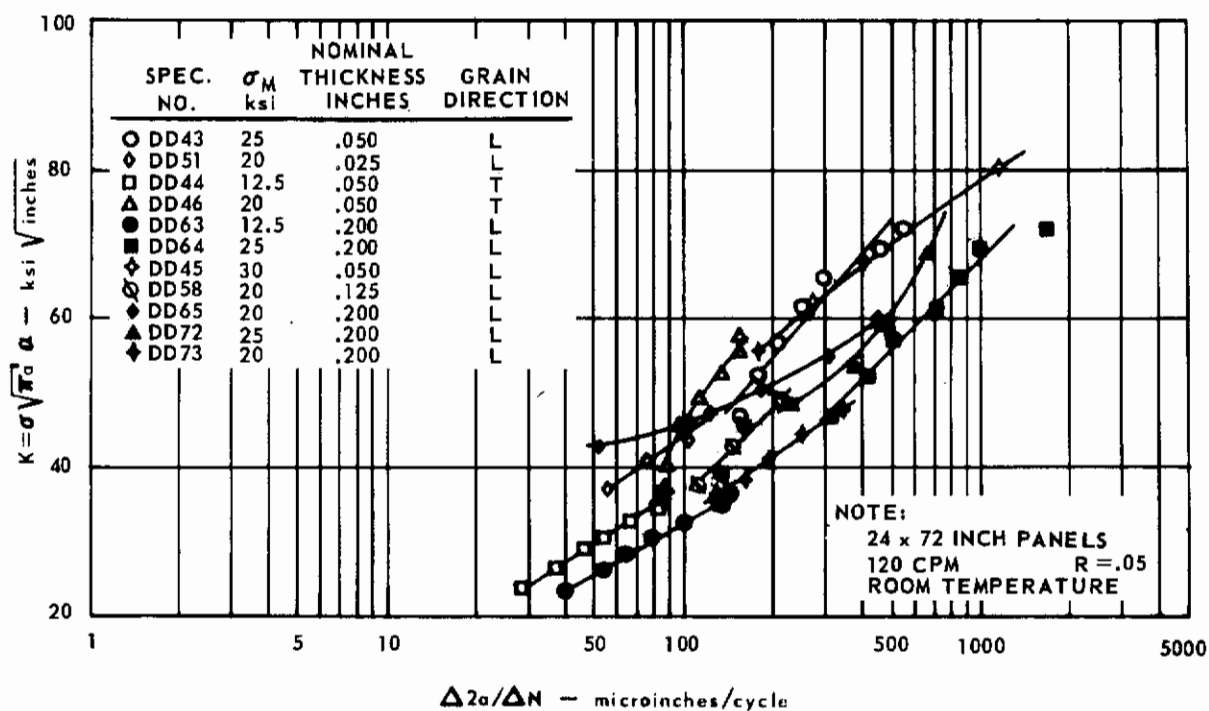


FIG. 163 CRACK GROWTH RATE DATA FOR Ti 6Al-4V, HEAT D4949

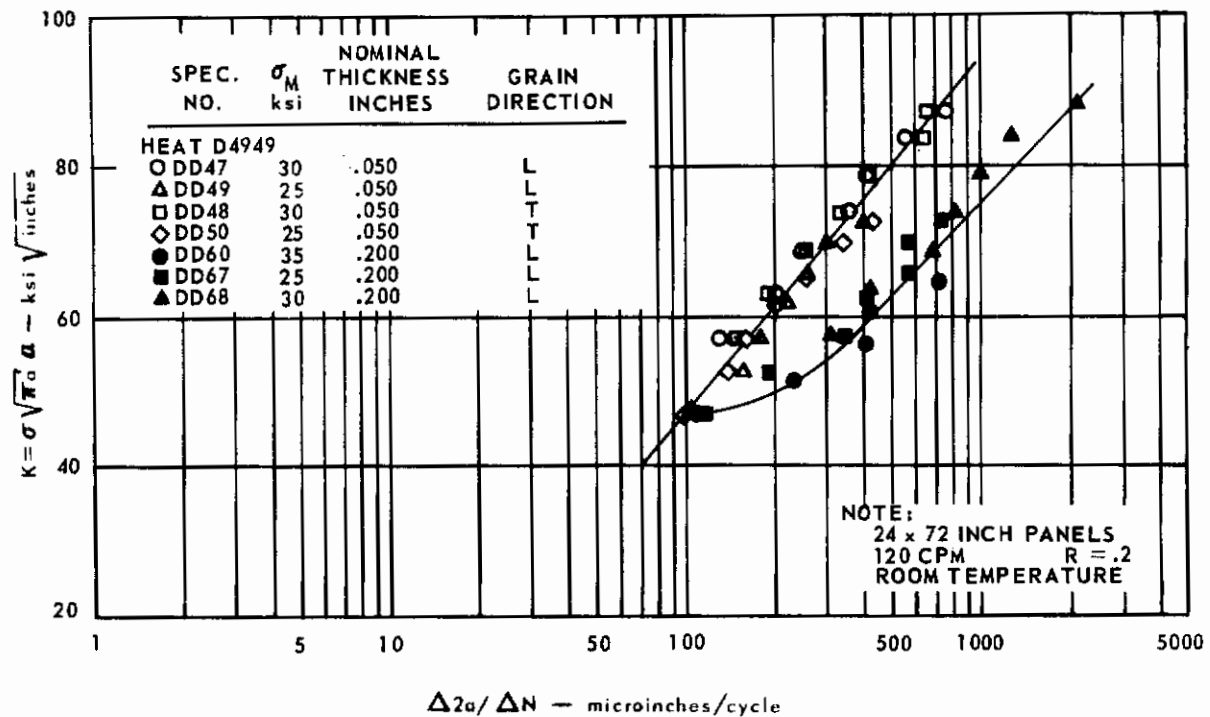


FIG. 164 CRACK GROWTH RATE DATA FOR Ti 6Al-4V, HEAT D4949

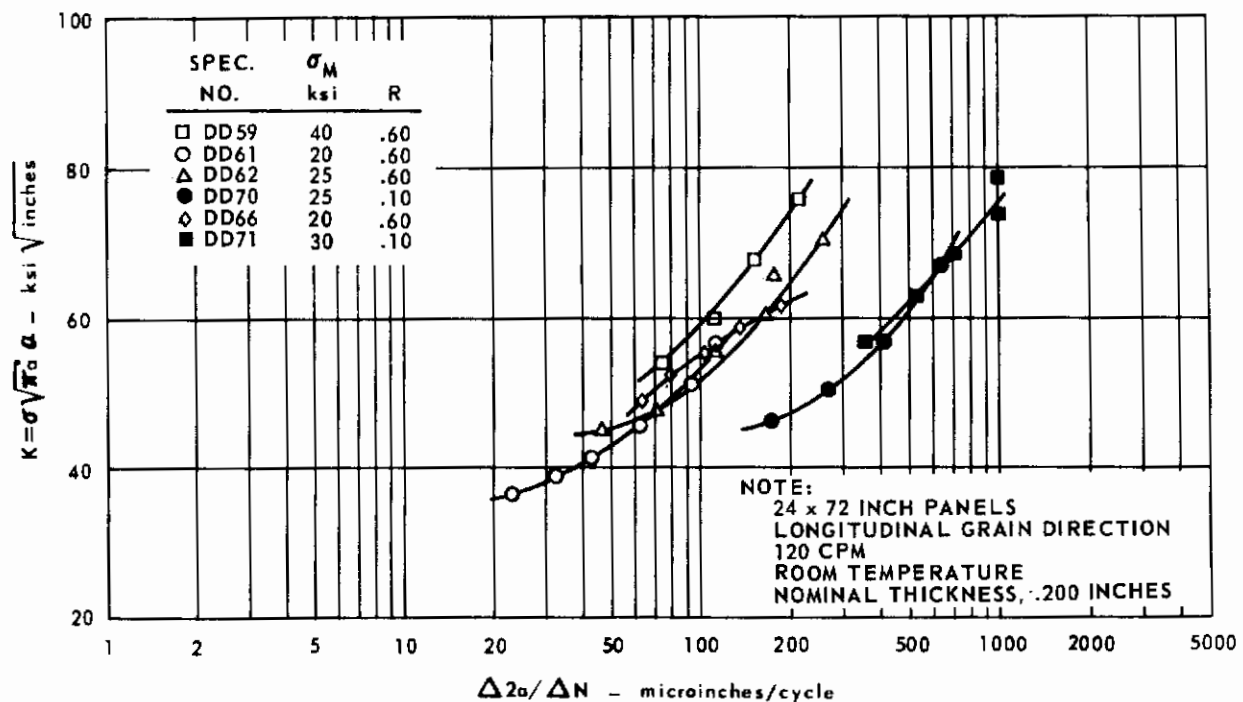


FIG. 165 CRACK GROWTH RATE DATA FOR Ti 6Al-4V, HEAT D4949

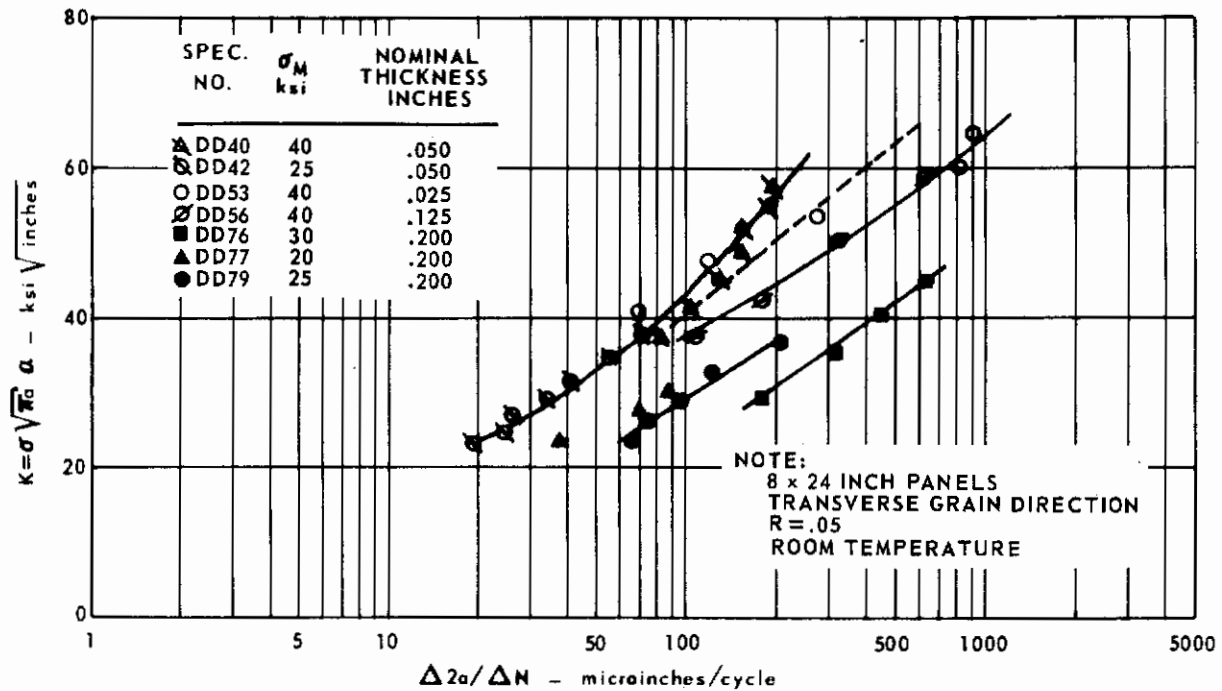


FIG. 166 CRACK GROWTH RATE DATA FOR Ti 6Al-4V, HEAT D4949

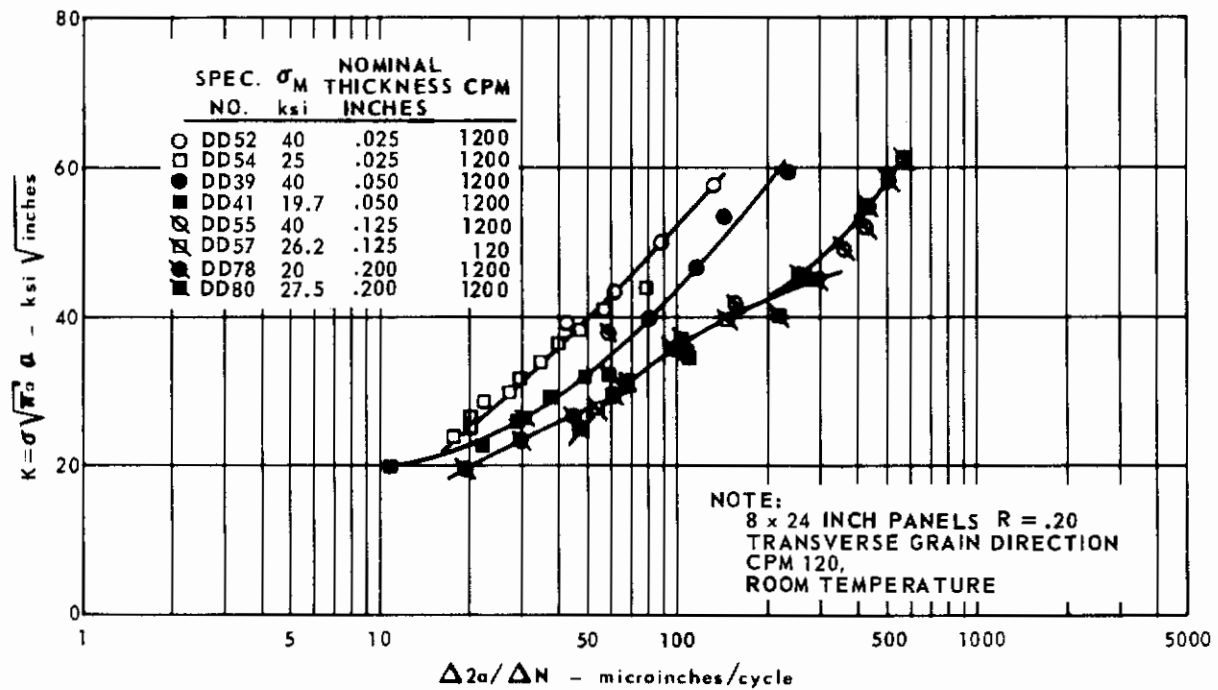


FIG. 167 CRACK GROWTH RATE DATA FOR Ti 6Al-4V, HEAT D4949

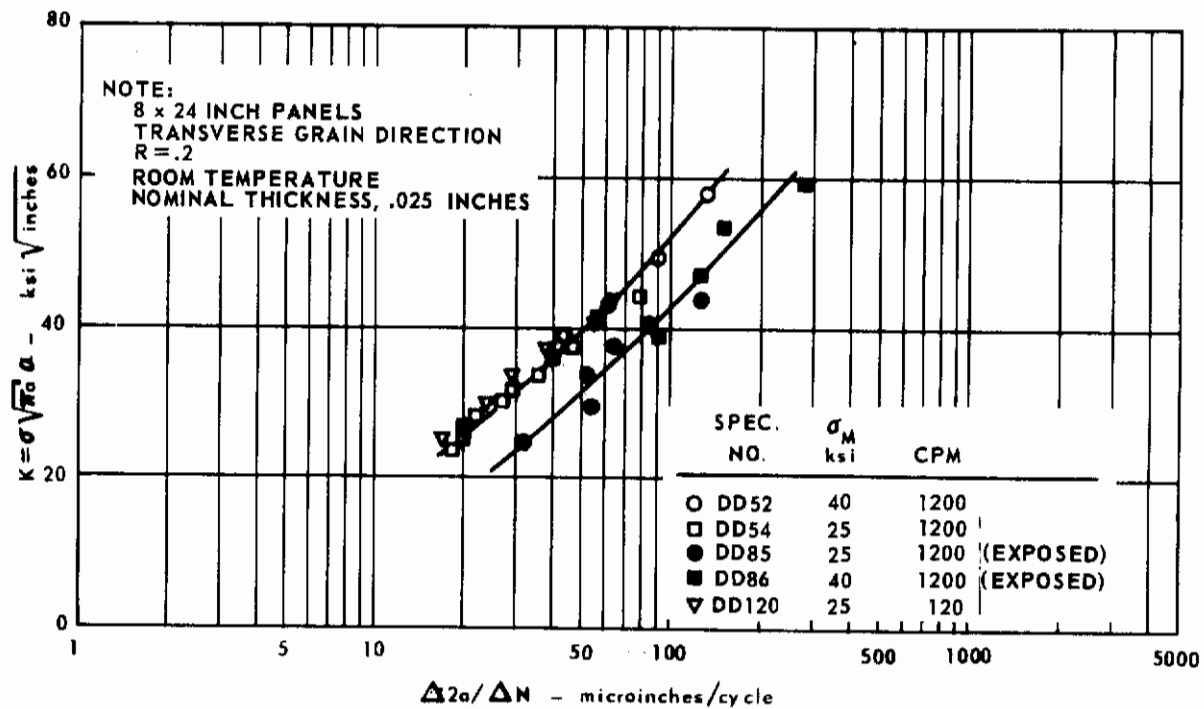


FIG. 168 CRACK GROWTH RATE DATA FOR Ti 6Al-4V, HEAT D4949

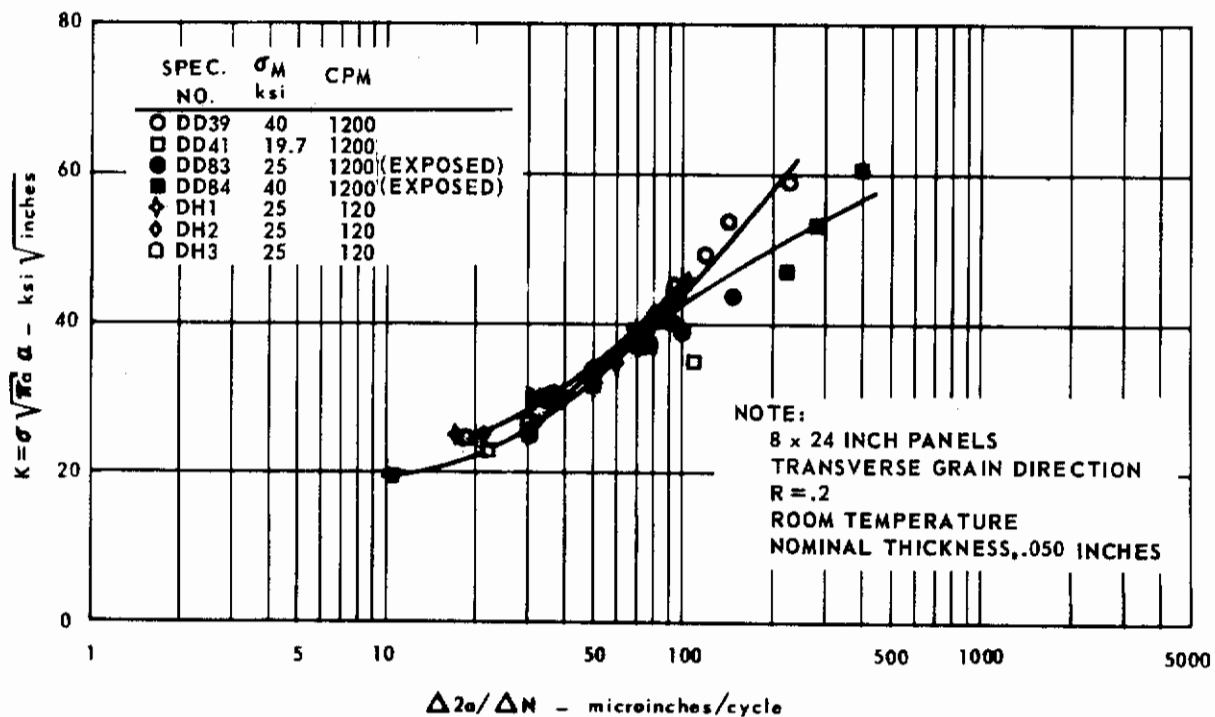


FIG. 169 CRACK GROWTH DATA FOR Ti 6Al-4V, HEAT D4949

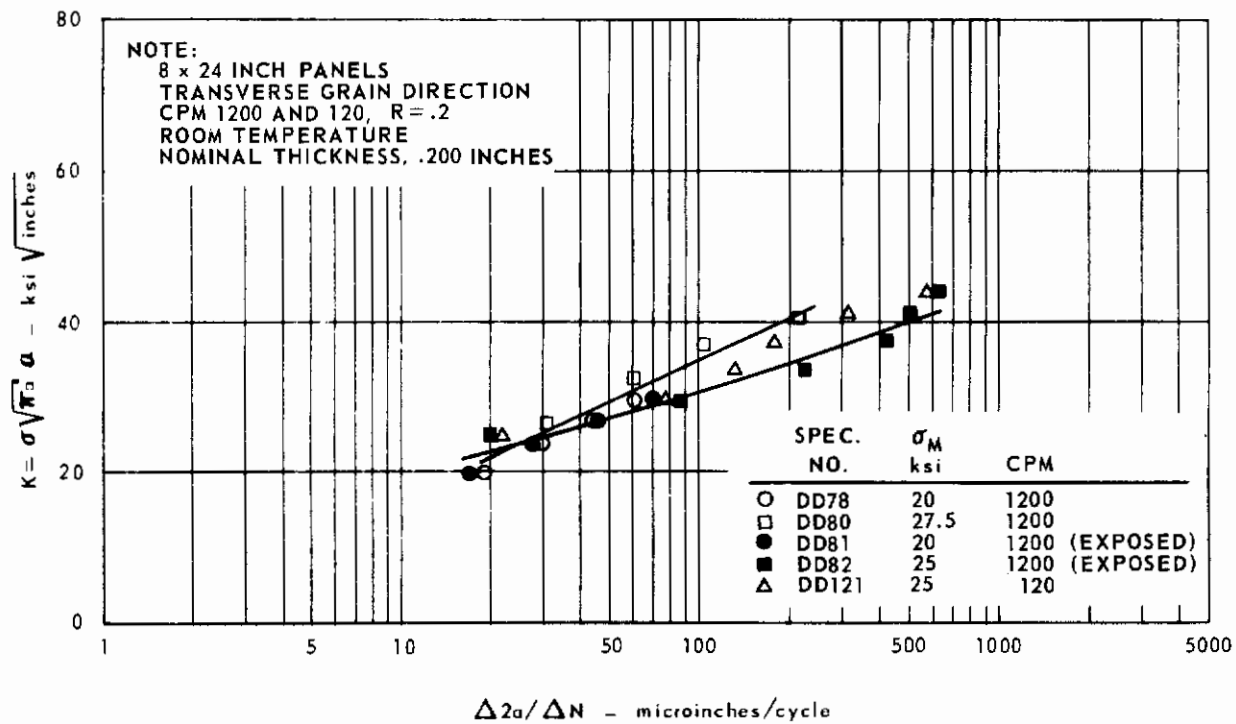


FIG. 170 CRACK GROWTH DATA FOR Ti 6Al-4V, HEAT D4949

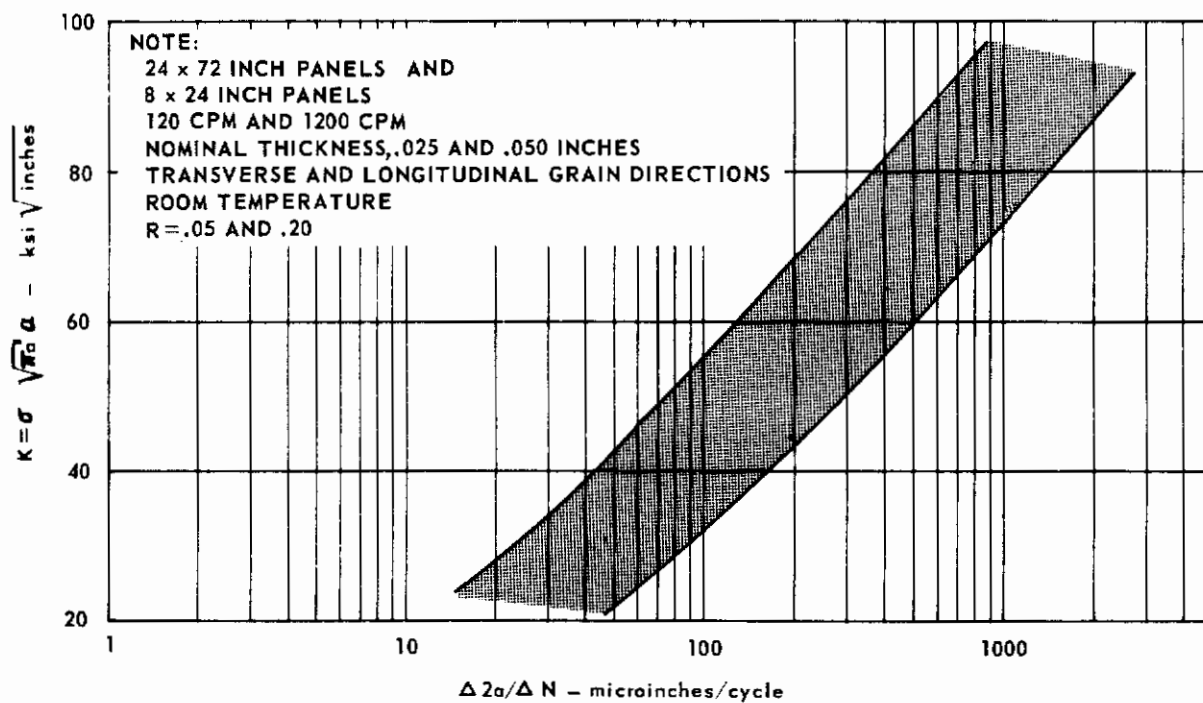


FIG. 171 CRACK GROWTH RATE DATA FOR Ti 6Al-4V, HEATS D5257, D5256 AND D4949

TABLE 21 FRACTURE TOUGHNESS DATA FOR 24 X 72- INCH PANELS OF TITANIUM 6Al-4V (MILL ANNEAL) (continued)

SPECIMEN NO.	HEAT NO.	THICKNESS inches	WIDTH inches	GRAIN DIRECTION	TEMP. °F	$\dot{\sigma}$ psi/sec	$2a_0$ inches	σ_G ksi	σ_N ksi	F_{tu} ksi	σ_{yp}^* ksi	σ_{yp}^* ksi	σ_N^* ksi	σ_N^* ksi	$K_{CN} = \sigma_G \sqrt{\pi a}$ ksi \sqrt{in}	$\frac{\sigma_G}{F_{tu}}$	$K_C = \frac{\sigma_G \sqrt{VqW}}{ksi \sqrt{in}}$	SHEAR %
DD 32	D5256	.052	24.07	L	650	1.10×10^6	6.00	74.840	99.68	103.1	85.6	111.3	1.16	.99	237.8	.726	277.3	100
DD 33	D5256	.055	24.07	L	650	$.93 \times 10^6$	6.00	73.112	97.38	103.1	85.6	110.2	1.14	.98	232.4	.709	278.9	100
DD 43	D4949	.0515	24.06	L	-110	$.95 \times 10^6$	6.00	53.834	71.72	164.6	161.0	183.1	.44	.39	171.1	.327	173.2	100
DD 44	D4949	.0515	24.09	T	-110	$.97 \times 10^6$	6.01	58.179	77.55	164.0	159.2	181.2	.49	.43	185.1	.355	189.1	100
DD 45	D4949	.051	24.06	L	73	$.36 \times 10^6$	7.16	57.865	82.37	140.0	134.2	149.8	.61	.55	204.3	.413	212.4	100
DD 46	D4949	.052	24.08	T	70	1.04×10^6	6.00	59.425	79.15	139.0	132.2	138.6	.60	.52	188.8	.428	196.7	100
DD 47	D4949	.052	24.06	L	400	1.10×10^6	6.01	81.535	108.63	109.2	97.0	123.6	1.12	.88	259.4	.747	300.9	100
DD 48	D4949	.0515	24.08	T	400	$.97 \times 10^6$	6.00	81.452	108.48	109.4	96.0	121.7	1.13	.89	258.8	.745	302.2	100
DD 49	D4949	.0515	24.06	L	650	1.40×10^6	6.00	71.751	95.59	97.8	82.2	108.4	1.16	.88	228.0	.734	264.4	100
DD 50	D4949	.050	24.08	T	650	$.84 \times 10^6$	6.01	69.020	91.92	97.5	81.5	104.3	1.13	.88	219.6	.708	254.8	100
DD 51	D4949	.022	24.03	L	66	1.42×10^6	6.00	60.337	80.35	140.8	136.6	146.5	.59	.51	135.6	.429	198.7	100
DD 58	D4949	.1235	24.02	L	71	1.04×10^6	6.04	80.580	107.66	138.8	134.6	153.3	.80	.70	257.1	.581	278.0	100
DD 59	D4949	.2115	24.07	L	69	$.80 \times 10^6$	3.01	93.105	106.52	138.5	129.3	146.5	.82	.73	204.1	.672	230.5	100
DD 60	D4949	.213	24.05	L	650	$.79 \times 10^6$	2.99	80.226	91.62	99.2	84.2	107.3	1.09	.85	175.3	.809	208.8	100
DD 61	D4949	.212	24.06	L	72	$.72 \times 10^6$	6.00	80.964	107.86	138.5	129.3	146.4	.83	.74	257.3	.585	282.2	100
DD 62	D4949	.2175	24.07	L	75	$.65 \times 10^6$	6.00	76.409	101.78	138.5	129.3	146.0	.79	.70	242.8	.552	263.6	100
DD 63	D4949	.2235	24.07	L	650	$.77 \times 10^6$	6.00	70.074	97.57	99.2	84.2	107.2	1.16	.91	222.7	.706	256.5	100
DD 64	D4949	.209	24.09	L	650	$.82 \times 10^6$	6.00	71.698	95.48	99.2	84.2	107.5	1.13	.89	227.8	.723	265.4	100
DD 65	D4949	.220	24.08	L	70	$.58 \times 10^6$	10.00	55.325	94.64	138.5	129.3	145.7	.73	.65	245.8	.399	253.2	100
DD 66	D4949	.213	24.08	L	650	$.70 \times 10^6$	10.00	56.346	96.36	99.2	84.2	106.3	1.14	.90	250.3	.568	278.9	100
DD 67	D4949	.216	24.04	L	-110	$.54 \times 10^6$	6.01	59.503	79.35	164.6	157.7	177.3	.50	.45	189.3	.362	194.0	100
DD 68	D4949	.215	24.05	L	-110	$.81 \times 10^6$	6.00	87.024	115.95	164.6	157.7	178.7	.73	.65	276.6	.529	295.9	100
DD 70	D4949	.212	24.07	L	75	4.10×10^3	6.01	70.547	94.02	138.5	129.3	132.0	.73	.71	224.4	.509	244.8	100
DD 71	D4949	.208	24.09	L	71	4.47×10^3	6.01	66.055	88.01	138.5	129.3	132.3	.68	.66	210.11	.477	226.0	100
DD 72	D4949	.2045	24.07	L	70	1.07×10^5	6.01	73.954	98.56	138.5	129.3	140.9	.76	.70	235.2	.534	255.7	100
DD 73	D4949	.204	24.08	L	74	$.90 \times 10^5$	6.01	69.625	92.78	138.5	129.3	140.8	.72	.66	221.5	.503	278.8	100

* TENSILE PROPERTIES OBTAINED FROM STANDARD STRAIN RATE TESTS OF .005 in./in./min
 ** σ_{yp} EXTRAPOLATED FROM HIGH STRAIN RATE TENSILE DATA FOR SA1-2.5 Sn (REFERENCE 26)

190

* TENSILE PROPERTIES OBTAINED FROM STANDARD STRAIN RATE TESTS OF .005 in./in./min
 **** σ_{yp} EXTRAPOLATED FROM HIGH STRAIN RATE TENSILE DATA FOR SA1-2.5 Sn (REFERENCE 26)
 ▲ EXPOSED @ 650°F FOR 1000 HRS @ $\sigma_G = 25$ ksi

* TENSILE PROPERTIES OBTAINED FROM STANDARD STRAIN RATE TESTS OF .005 in/in/min

TABLE 22 FRACTURE TOUGHNESS DATA FOR 8 x 24 INCH PANELS OF Ti 6Al-4V (continued)

SPECIMEN NO.	HEAT NO.	THICKNESS inches	WIDTH inches	GRAIN DIRECTION	TEMP. °F	$\dot{\sigma}$ psi/sec	2 σ_0 inches	σ_G ksi	σ_N ksi	F_{T0} ksi	$\sigma_{yp} \frac{\partial}{\partial TEMP.}$ ksi	$\sigma_{yp} \frac{\partial}{\partial TEMP.}$ ksi	$\sigma_N^{**} \frac{\sigma_{yp}}{\sigma_{yp} \frac{\partial}{\partial TEMP.}}$	$K_{CN} = \sigma_G \sqrt{\pi a_0}$ ksi \sqrt{in}	$\frac{\sigma_G}{F_{T0}}$	$K_C = \sigma_G \sqrt{a_1}$ ksi \sqrt{in}	SHEAR %
▲ DD 84	D4949	.026	8.01	T	76	.79x10 ⁶	2.01	67.691	90.38	140.6	133.1	130.8	.68	124.6	.481	131.7	100
▲ DD 85	D4949	.049	8.01	T	70	1.01x10 ⁶	1.98	89.936	119.46	140.0	132.7	131.9	.90	164.1	.642	123.9	100
▲ DD 86	D4949	.049	8.01	T	71	1.08x10 ⁶	2.00	91.465	121.90	140.2	133.9	132.6	.91	167.8	.652	188.6	100
DD 120	D4949	.026	8.01	T	75	.83x10 ⁶	2.00	76.332	101.73	139.4	127.0	143.9	.80	140.0	.548	152.7	100
DD 121	D4949	.211	8.01	T	70	.63x10 ⁶	2.01	87.450	116.75	144.9	139.6	137.5	.84	160.4	.404	176.8	100
DH 1	D4949	.049	7.99	T	72	.96x10 ⁶	2.00	86.335	115.16	139.2	132.2	130.3	.87	158.5	.628	178.0	100
DH 2	D4949	.049	7.99	T	75	.94x10 ⁶	2.00	86.845	115.84	139.2	132.2	130.2	.88	159.4	.624	179.5	100
DH 3	D4949	.049	7.99	T	75	.97x10 ⁶	2.00	88.123	117.55	139.2	132.2	130.3	.78	161.7	.633	184.5	100
DH 4	D4949	.049	8.003	T	73	1.12x10 ⁶	2.00	87.350	116.46	139.2	132.2	130.8	.88	160.2	.628	178.3	100
DH 5	D4949	.049	8.008	T	73	1.14x10 ⁶	2.00	87.920	117.19	139.2	132.2	130.8	.89	161.2	.632	179.6	100
DH 6	D4949	.0488	8.00	T	73	1.15x10 ⁶	2.00	91.957	122.61	139.2	132.2	130.8	.93	168.6	.661	190.4	100

* TENSILE PROPERTIES OBTAINED FROM STANDARD STRAIN RATE TESTS OF .005 in./in./min
 ** σ_{yp} EXTRAPOLATED FROM HIGH STRAIN RATE TENSILE DATA FOR SA1-2.5 Sn (REFERENCE 26)
 ▲ EXPOSED @ 650°F FOR 1000 HRS @ $\sigma_G = 25$ ksi

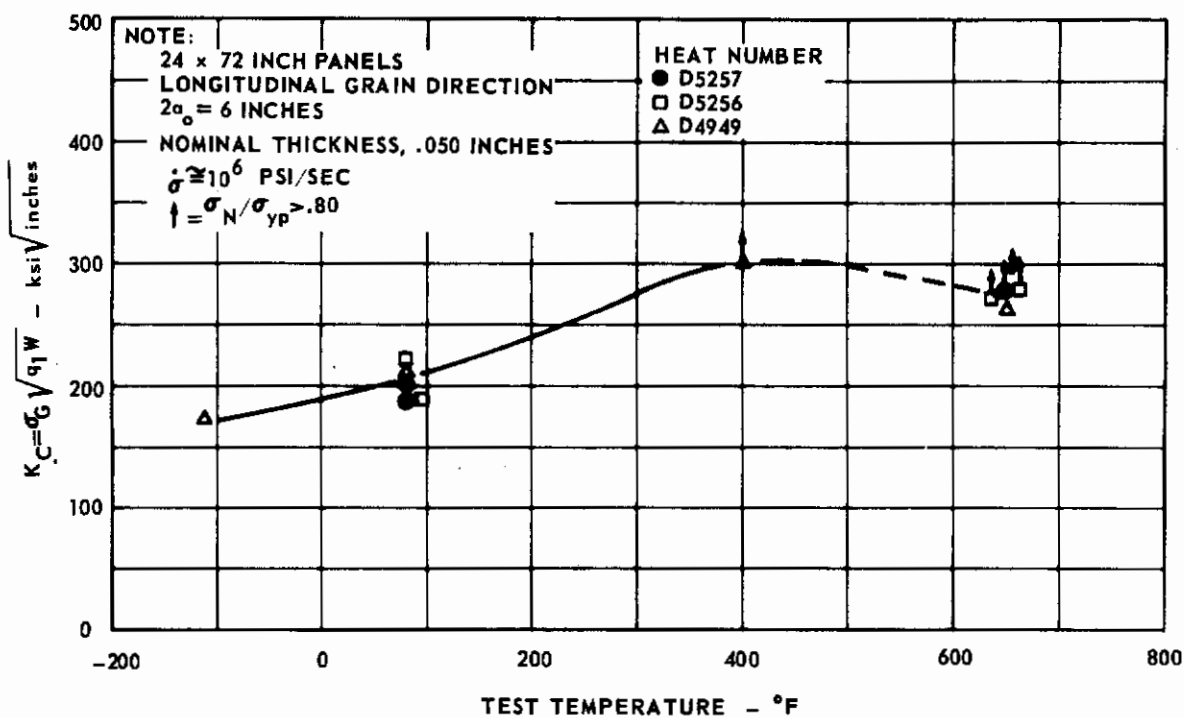


FIG. 172 EFFECT OF TEST TEMPERATURE ON K_C FOR Ti 6Al-4V

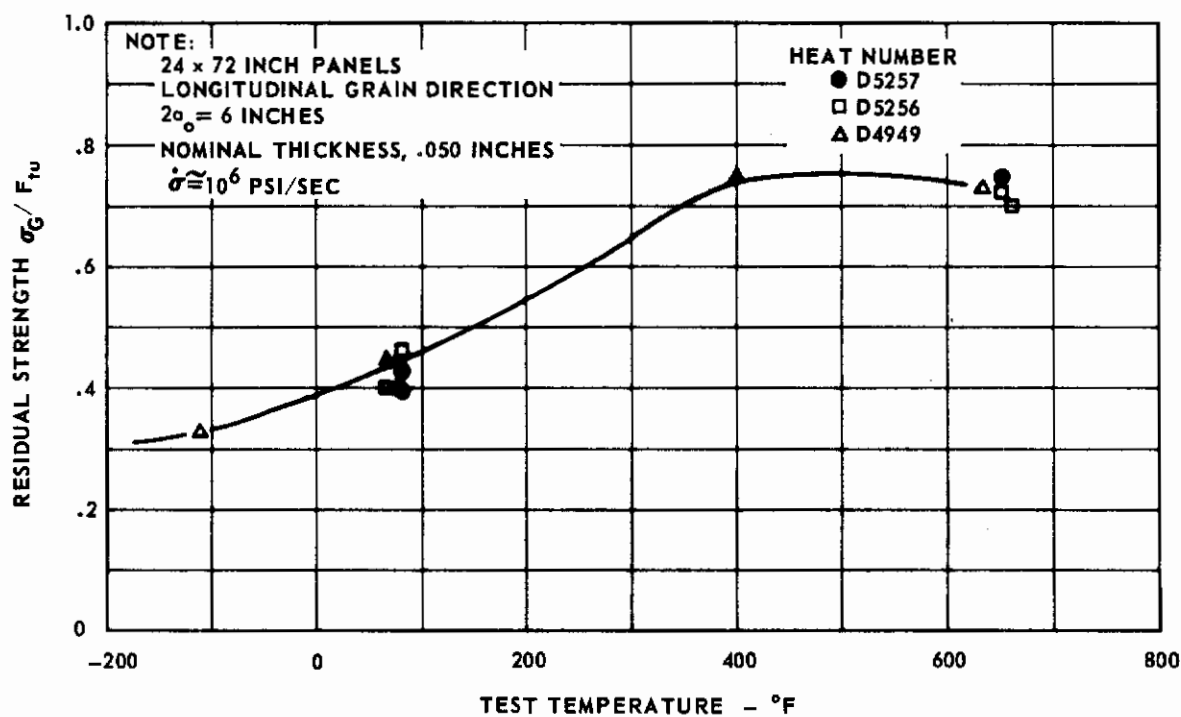


FIG. 173 EFFECT OF TEST TEMPERATURE ON RESIDUAL STRENGTH FOR Ti 6Al-4V

NOTE:

$\dot{\sigma} \cong 10^6$ PSI/SEC
 NOMINAL THICKNESS, .050 INCHES
 Points at $2a_0/2b = .25$ were Displaced
 Laterally to Avoid Overplotting.

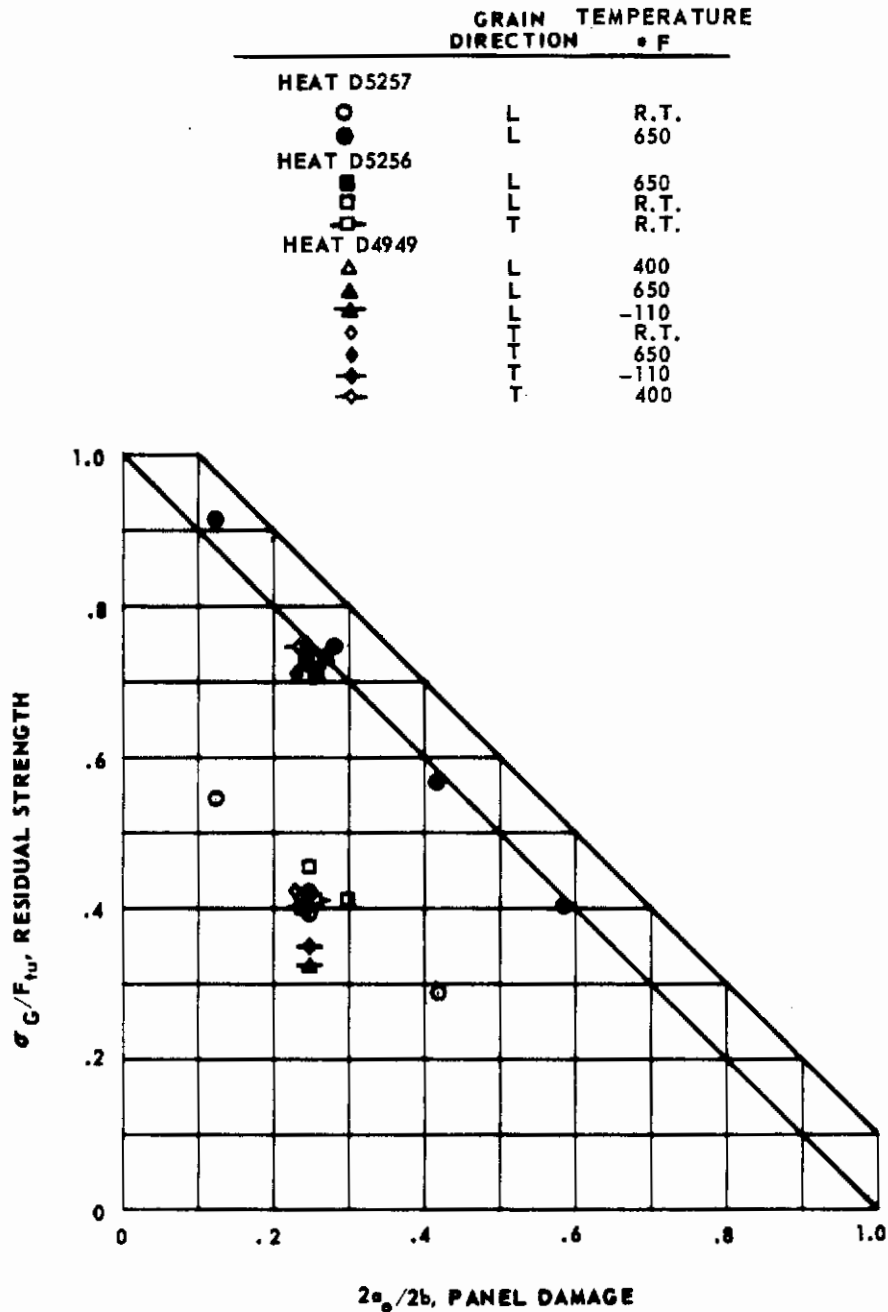


FIG.174 RESIDUAL STRENGTH vs DAMAGE FOR 24 x 72 INCH Ti 6Al-4V PANEL, HEATS D5257, D5256 AND D4949

NOTE:

$\dot{\sigma} \times \cong 10^6$ PSI/SEC
 LONGITUDINAL GRAIN
 Points were Displaced Laterally
 to Avoid Overplotting.
 at $2a_0/2b = .25$

	TEMPERATURE • F	NOMINAL THICKNESS INCHES
○	R.T.	.200
●	650	.200
○	-110	.200
□	R.T.	.125
△	R.T.	.025
◇	R.T.	.050
◆	650	.050
◊	-110	.050
◈	400	.050

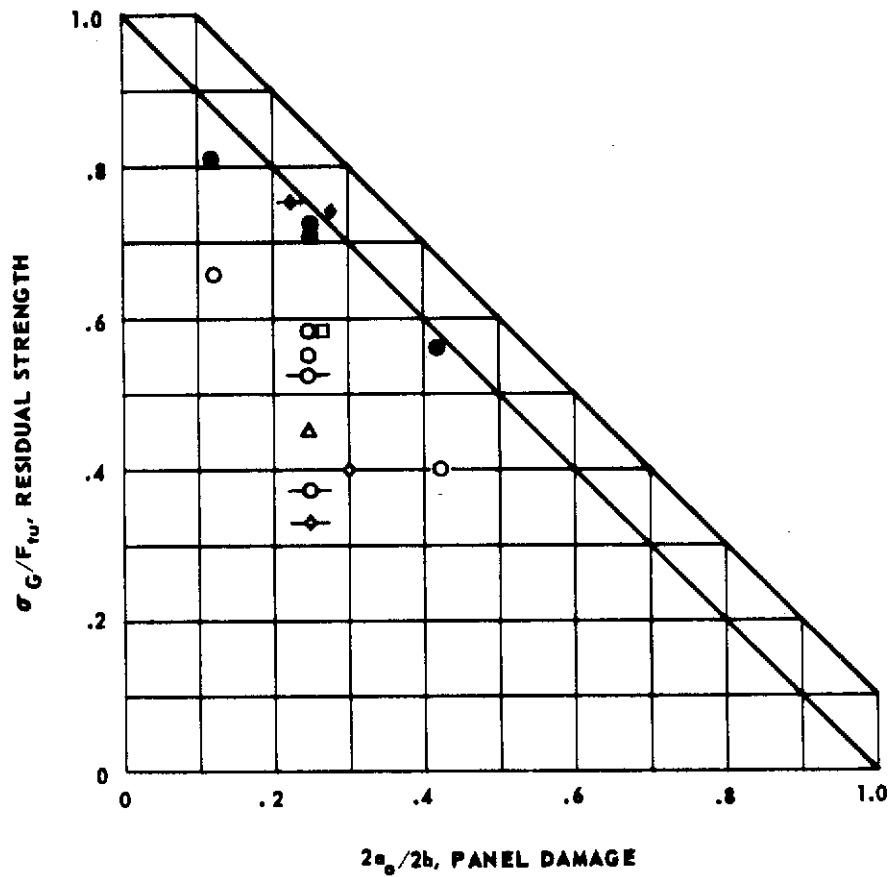


FIG. 175 RESIDUAL STRENGTH vs DAMAGE FOR 24 x 72 INCH Ti 6Al-4V, PANEL, HEAT 4949

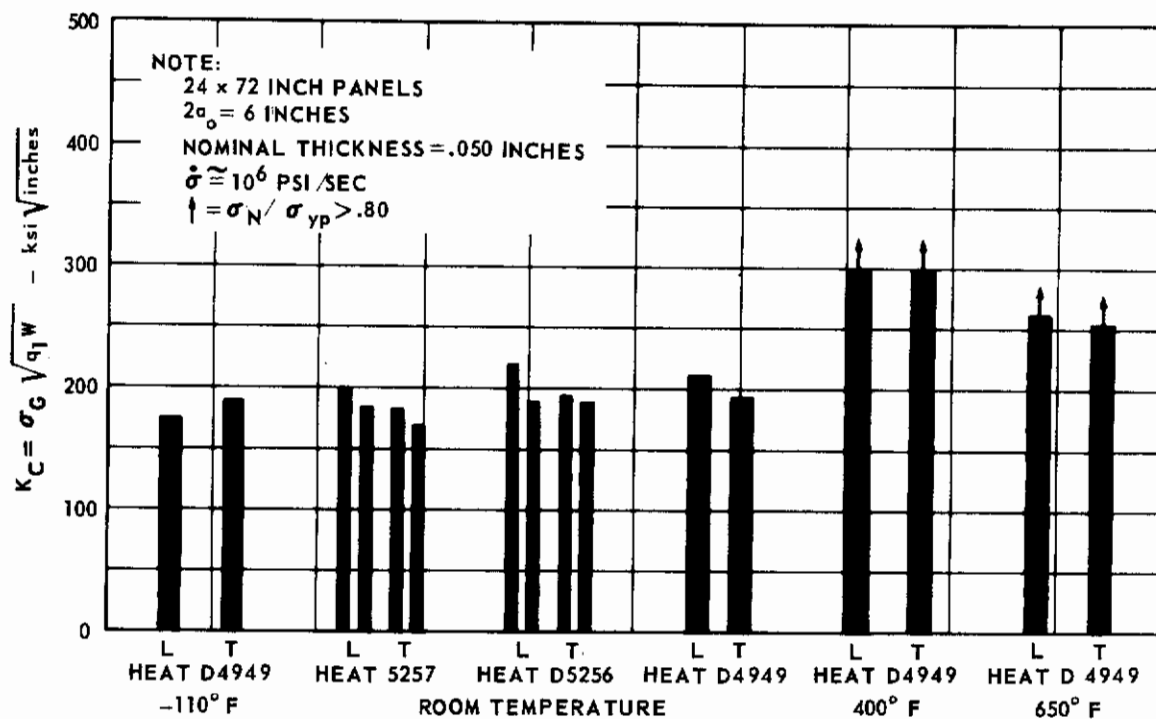


FIG.176 VARIATION OF K_C WITH GRAIN DIRECTION FOR Ti 6Al-4V

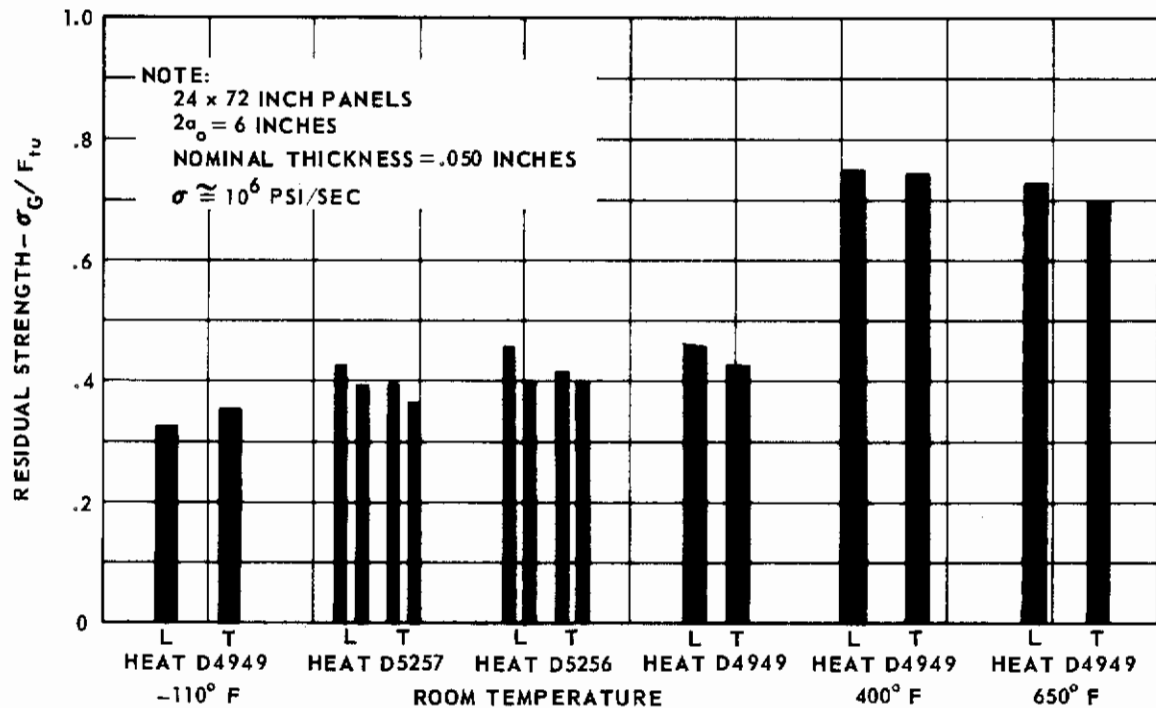


FIG.177 VARIATION OF RESIDUAL STRENGTH WITH GRAIN DIRECTION FOR Ti 6Al-4V

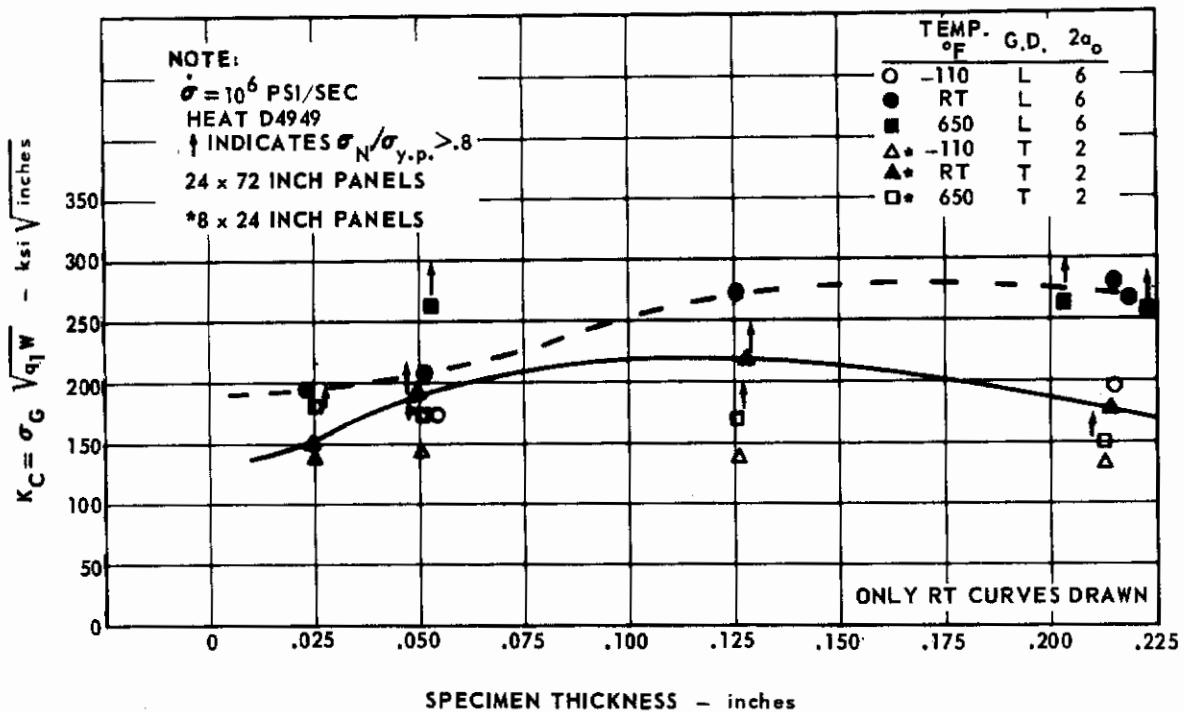


FIG.178 VARIATION OF K_C WITH THICKNESS FOR Ti 6Al-4V

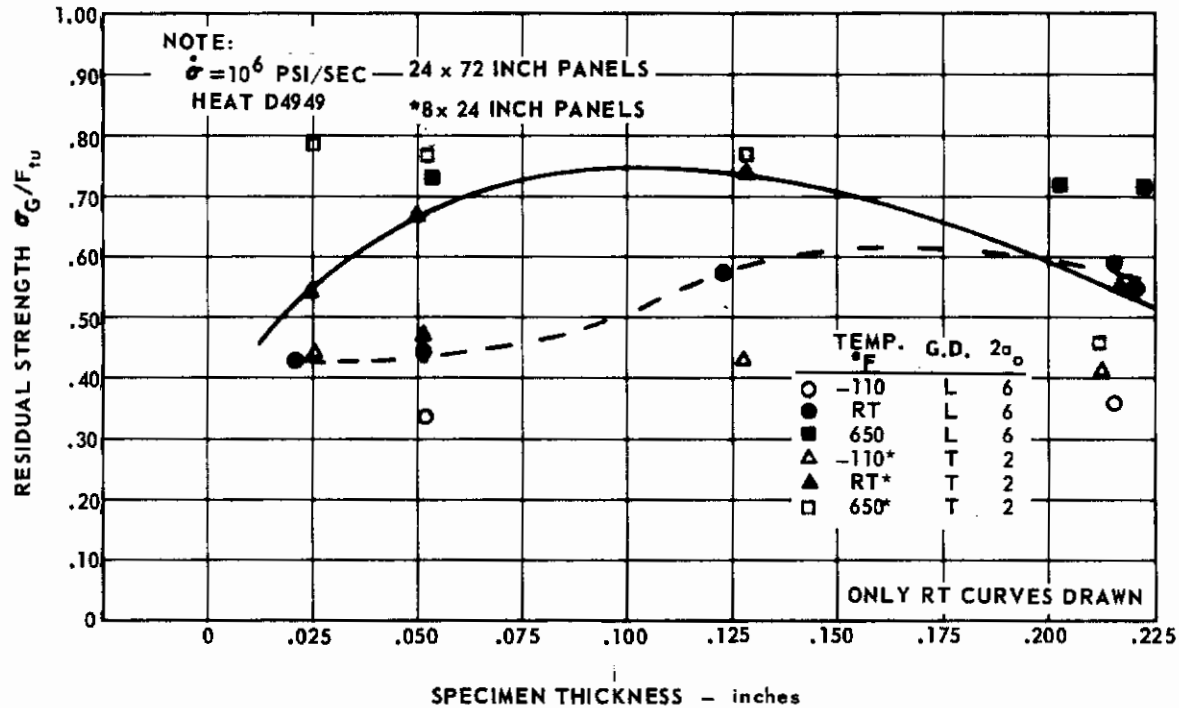


FIG.179 VARIATION OF RESIDUAL STRENGTH WITH THICKNESS FOR Ti 6Al-4V, HEAT D4949

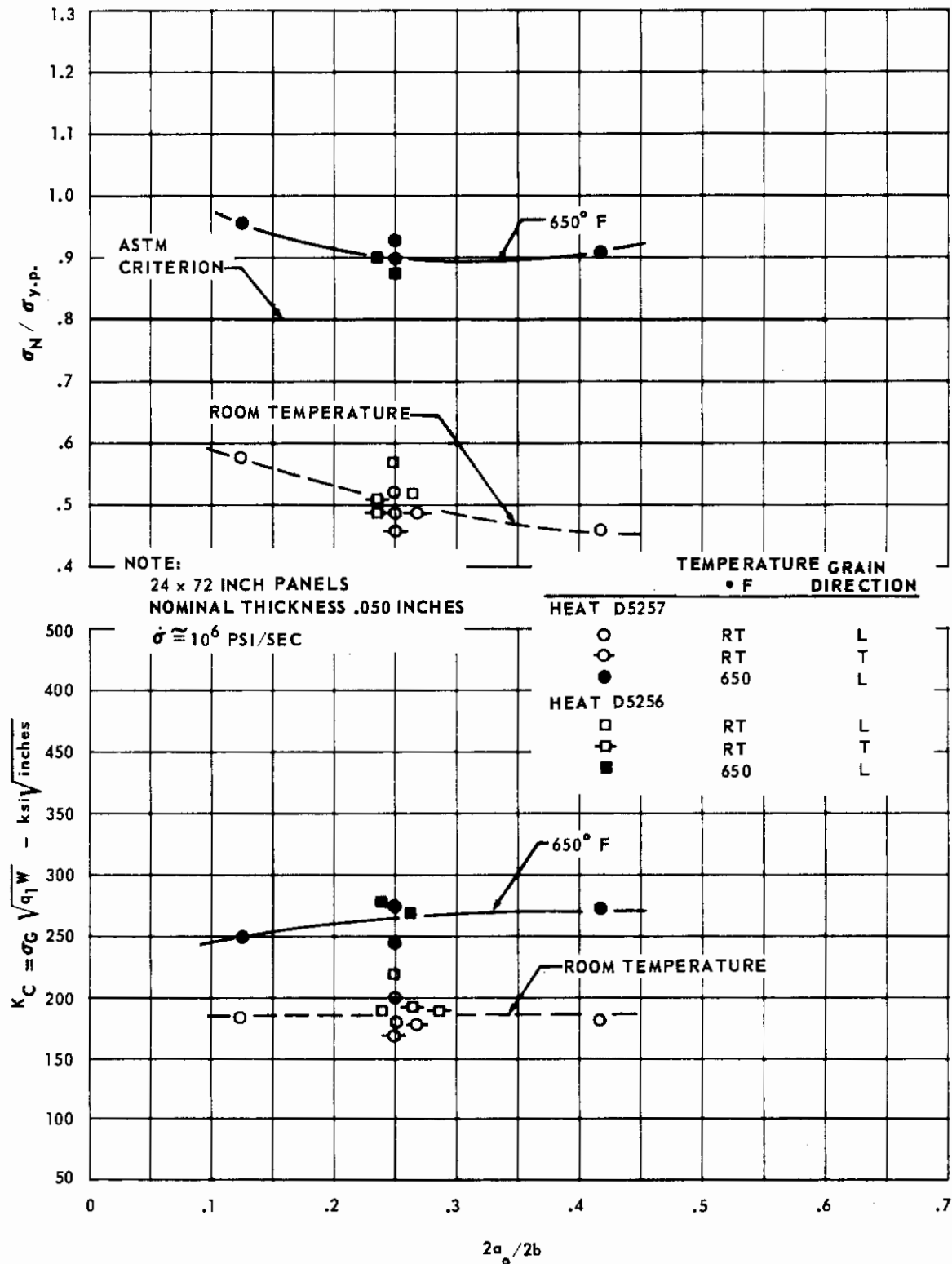


FIG.180 VARIATION OF K_C WITH TEMPERATURE, CRACK LENGTH AND GRAIN DIRECTION FOR Ti 6Al-4V

Effect of Temperature

Figs. 172 and 173 show the effect of test temperatures on fracture toughness and residual strength for 24 x 72 x 0.050-inch longitudinal panels with $2a_0 = 6$ inches tested at a stress rate of 10^6 psi/sec. These show that fracture toughness and residual strength decrease as the temperature decreases from 400°F, and increases from 400°F. At 400°F and 600°F the net failing stresses exceeded the ASTM criterion for valid fracture toughness values, and hence are conservative.

The plot of residual strength versus panel damage in Fig. 174 displays a practically linear relationship for 400 and 650°F for the 0.050-inch thickness, and Fig. 175 shows that the 0.200-inch thickness has an almost linear relationship for 650°F.

Effect of Grain Direction

Although not great, the longitudinal grain direction generally has the larger values of fracture toughness and residual strength; this is shown in Figs. 176 and 177 for the 24 x 72 x 0.050-inch panels with $2a_0 = 6$ inches and at a stress rate of 10^6 psi/sec for all temperatures except -110°F.

Effect of Thickness

Figs. 178 and 179 illustrate the variation of fracture toughness and residual strength with thickness for 8 x 24-inch and 24 x 72-inch panels of heat D4949.

For the 24 x 72-inch longitudinal panels, the fracture toughness increases with thickness at room temperatures and -110°F, and is practically constant at 650°F. The 8 x 24-inch transverse panels at room temperature have an increase in toughness with thickness up to 0.125 inches thickness and then toughness decreases with a further increase in thickness. For -110°F, the 8 x 24-inch panels show an increase in toughness with thickness, while for 650°F the fracture toughness decreases with increasing thickness.

Residual strengths are higher for the thicker 24 x 72-inch longitudinal panels at room temperatures and show a small decrease in strength with increasing thickness at -110°F and 650°F. The 8 x 24-inch transverse panels have an increase in residual strength with thickness up to 0.125 inches and then decrease in strength with a further increase in thickness at room temperature. At -110°F and 650°F, the 8 x 24-inch panels show a decrease in strength as the thickness increases.

Effect of Crack Length

The influence of crack length on fracture toughness is shown in Figs. 180 and 181. At 650°F, fracture toughness increases with panel damage for the 0.050 and 0.200-inch thicknesses, while the toughness is a maximum at a panel damage of approximately .25 for both thicknesses at room temperature. An influence of crack length on residual strength is depicted in Figs. 174 and 175 for the 24 x 72-inch panels. The decrease in strength at 400°F and 650°F is approximately linear with panel damage for the 0.050 and 0.200-inch thicknesses. For room temperature the loss in strength with panel damage is nonlinear.

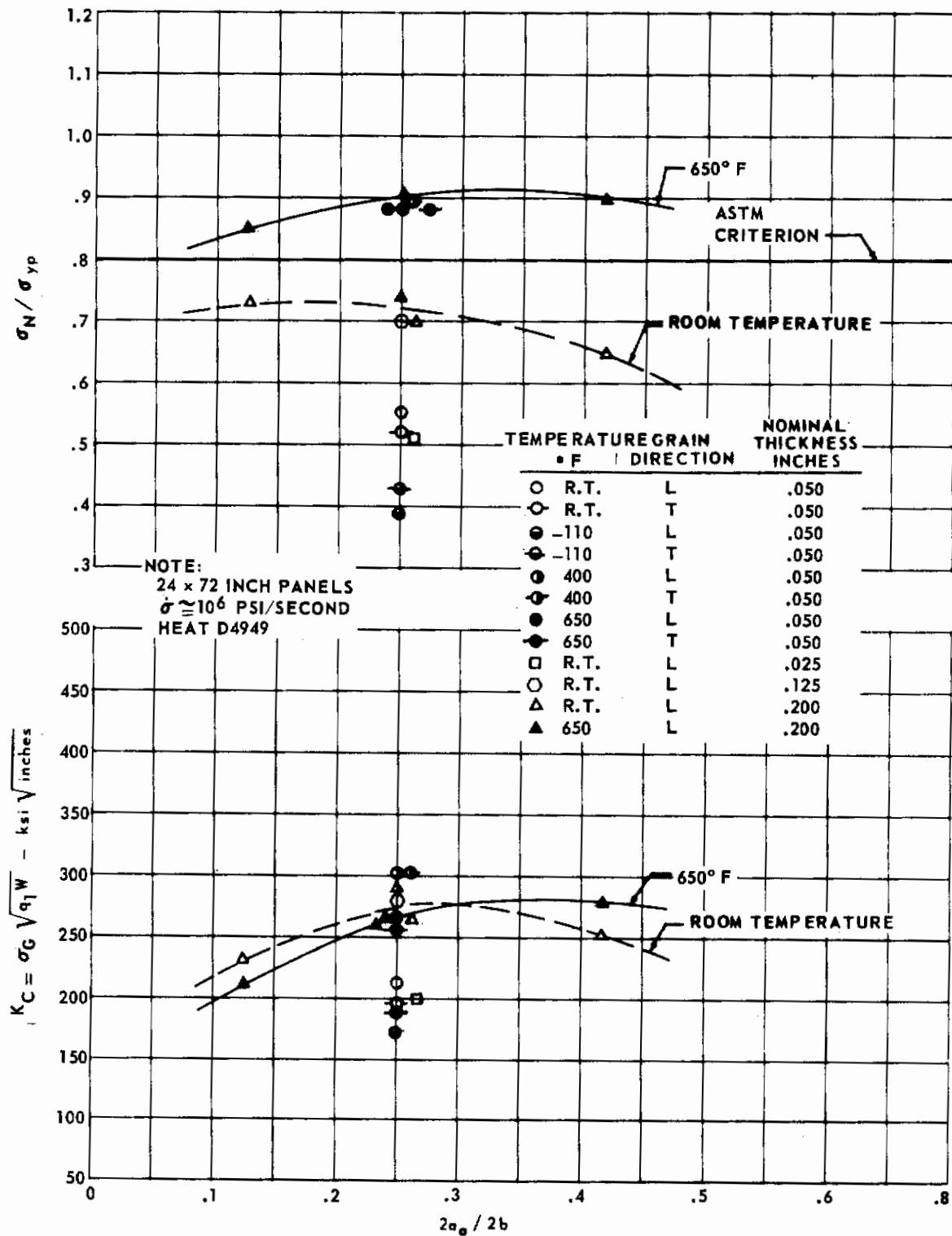


FIG.181 VARIATION OF K_C WITH TEMPERATURE, CRACK LENGTH, THICKNESS AND GRAIN DIRECTION FOR Ti 6Al-4V

Effect of Stress Rate

Fracture toughness and residual strength increase with an increase in the stress rate (See Fig. 182). The increases in toughness for the various heats and thicknesses for the 24 x 72-inch longitudinal panels are very similar. Conversely, the effects on the 8 x 24-inch transverse specimens are erratic. Similarly, the residual strengths for the two specimen sizes display the same type of behavior.

Effect of Exposure

Fig. 183 shows that the average fracture toughness values of the exposed specimens are higher than the unexposed specimens for the 0.050 and 0.200-inch thicknesses, but lower than the unexposed specimen of 0.025-inch thickness.

The residual strength of the exposed 0.200-inch thickness is higher than the strength of the unexposed material, while the exposed 0.025 and 0.050-inch thickness strengths are lower than the unexposed material.

Effect of Heat

Although not large, the heat variable does have an effect on fracture toughness and residual strength. This is shown in Figs. 176, 177 and well as 180 and 182.

Effect of Panel Size

Fracture toughness tends to be more conservative for the smaller size specimen, especially at 650°F.

Residual strength is a function of specimen size. Except at testing temperatures of 400°F and 650°F, where residual strengths for both sizes are approximately equal, more conservative data is obtained by testing of the larger specimen size. For the room temperature tests of the 0.050-inch thickness, residual strengths of the larger size specimen are only approximately .65 of those found for the smaller size specimen.

Fractographic Studies

Macrophotographs along with the corresponding electron micrographs for specimens DD21 and DD74 are shown in Figs. 184 and 185. These electron micrographs show striations characteristic of the fatigue area and also the ductile fracture mode characteristic of the rapid fracture area. In general, these fractographic studies for the 6Al-4V parallel those for the 8Al-1Mo-1V alloy.

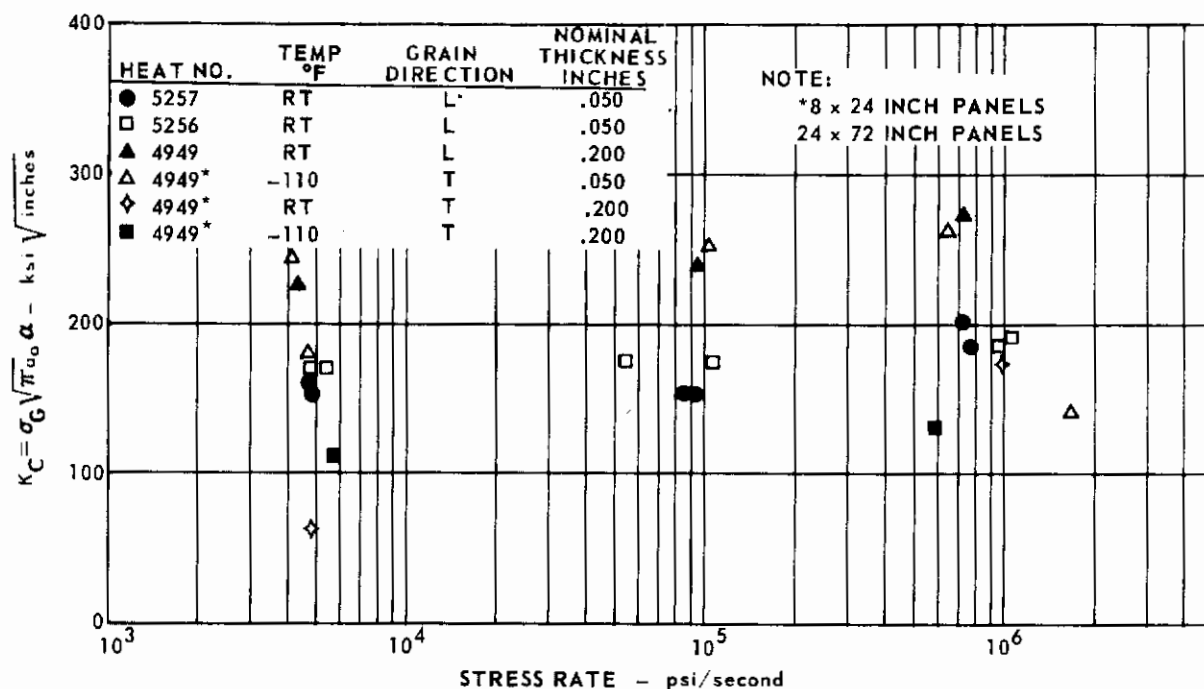


FIG.182 THE EFFECT OF STRESS RATE ON K_C FOR Ti 6Al-4V, HEATS 5257, 5256 AND 4949

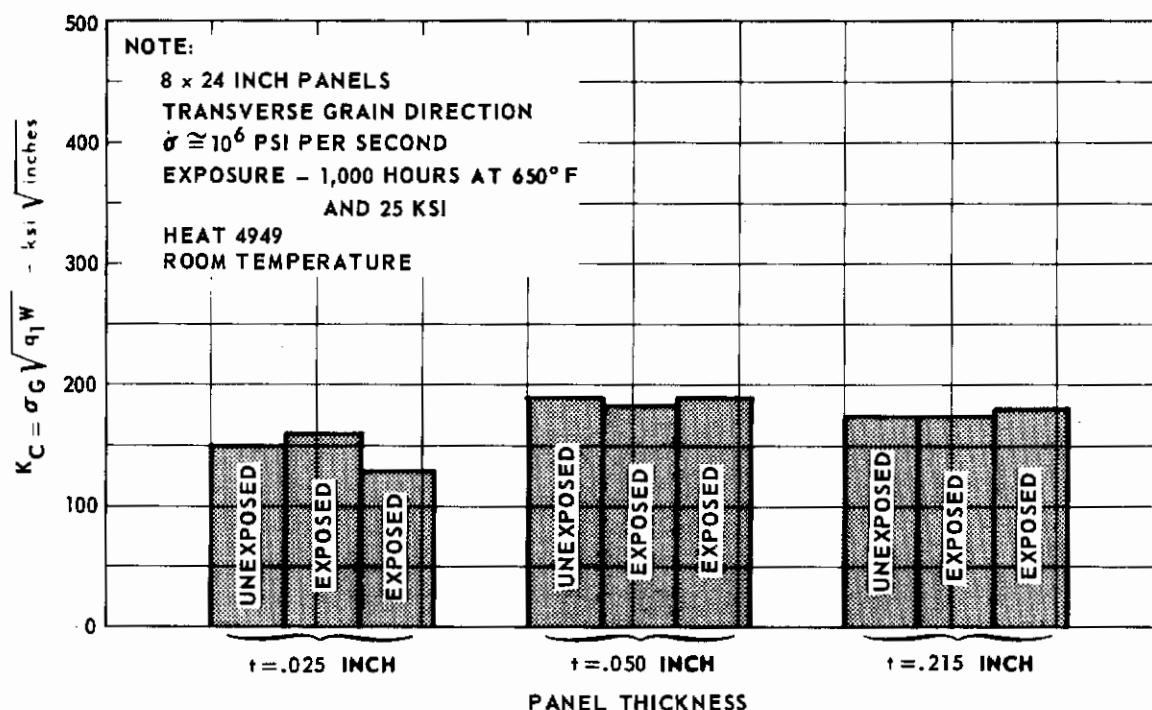
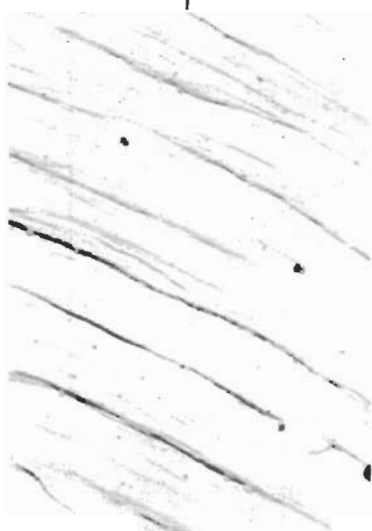
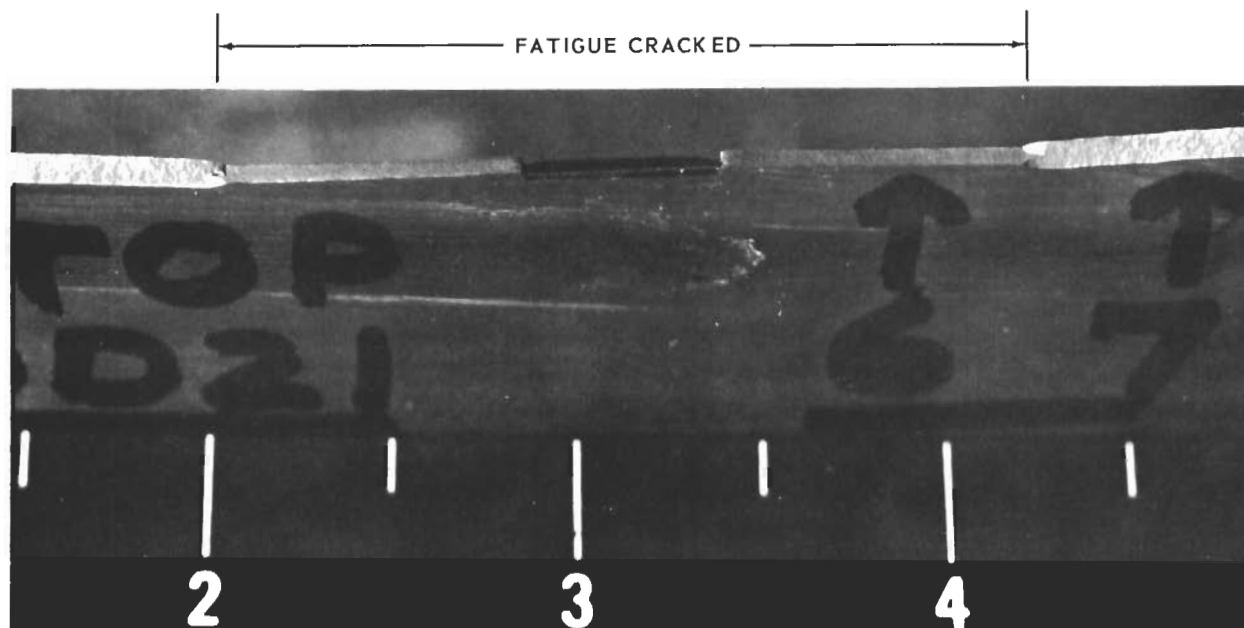
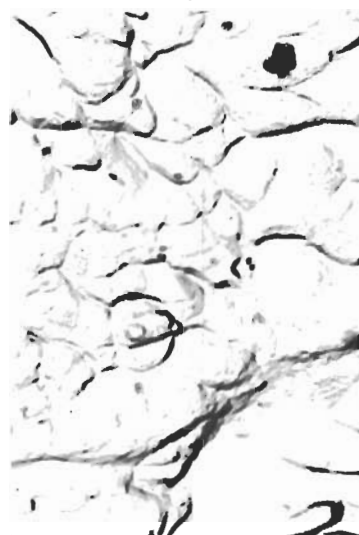


FIG.183 COMPARISON OF EXPOSED AND UNEXPOSED K_C VALUES FOR Ti 6Al-4V, HEAT 4949



(A) FATIGUE AREA SHOWING STRIATIONS (15,000x)



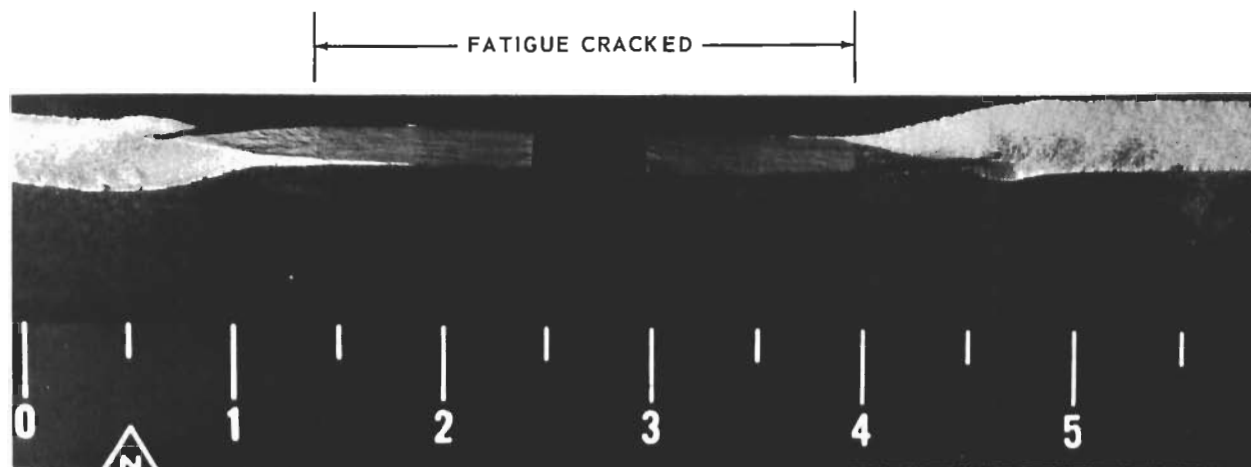
(B) DIMPLES FROM RAPID FRACTURE SHEAR LIP AREA (15,000x)

NOMINAL THICKNESS .050 INCHES

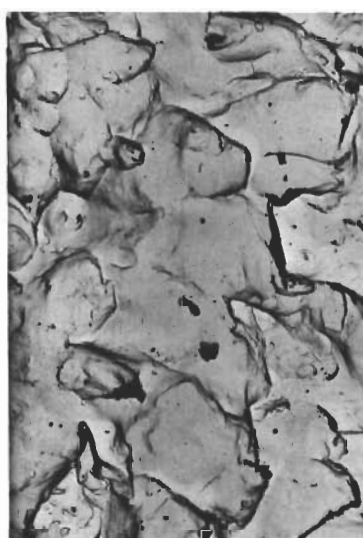
NOTE: Fatigue Cracked and Fractured at Room Temperature

FIG.184 FRACTOGRAPHIC STUDY OF Ti 6Al - 4V SPECIMEN DD21

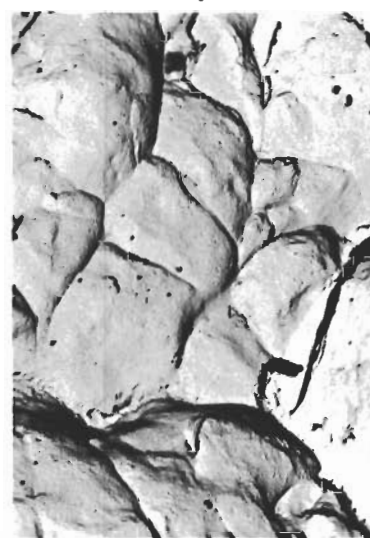
Contrails



(A) FATIGUE AREA SHOWING STRIATIONS (19,000x)



(B) TYPICAL AREA FROM PLANE STRAIN ZONE (3,000x)



(C) ELONGATED DIMPLES FROM RAPID FRACTURE SHEAR LIP (5,000x)

NOMINAL THICKNESS .200 INCHES

NOTE: Fatigue Cracked and Fractured at Room Temperature

FIG.185 FRACTOGRAPHIC STUDY OF Ti 6Al - 4V SPECIMEN DD74

PH 14-8Mo STAINLESS STEEL

The thickness tested in each heat was slightly different from that planned for this material. Material required for this program was properly ordered from the material producer, who agreed to fulfill the order; however, the producer was unable to completely satisfy the requirement for the 0.125-inch nominal thickness in the largest heat. Consequently, because of material coordination between the other programs, performed at Lockheed and the Joint-Venture, and also a shortage of lead time for a replacement heat, it was decided to accept some of the thickest material from one of the other heats used in this program.

Chemistry and Mill Processing History

Chemical analyses are listed in Table 23 for each of the heats. Also included are the ranges allowed for the principal elements by the material specification. All of the principal elements are within the specified ranges.

In answer to a letter requesting mill processing information, ARMCO answered: "we would suggest that the following description sufficiently categorizes the processing history of the sheets delivered for this program: 'Heats Number 33347, 33570 and 43208 were air melted by the electric arc process in 32,000 pound heat size. Ingots were full size as related to sizes normal for other stainless steels. Mill processing by continuous rolling, annealing and pickling practices was controlled to obtain the ordered sheet sizes with Condition A properties. Tests were made to assess capability of heat treating the sheets to high strength properties.'"

TABLE 23 VENDOR CERTIFIED CHEMICAL ANALYSIS FOR PH 14-8Mo (WEIGHT, PERCENT)

		C	Mn	P	S	Si	Cr	Ni	Al	Mo
PH 14-8Mo	43208	.033	.26	.033	.002	.38	14.71	8.16	1.09	2.21
	33570	.037	.36	.004	.002	.34	14.71	8.12	1.21	2.25
	33347	.031	.35	.002	.002	.37	14.44	8.27	1.23	2.33
	SPEC. {	MIN.					13.50	7.50	.75	2.00
		MAX.	.05	1.00	.015	.010	15.50	9.50	1.50	3.00

Microstructure

Photomicrographs of the thinnest and thickest gage of heat 33347 are shown in Fig. 186. In general, they appear typical of those examined for this alloy processed through the SRH 1050 heat treatment. Retained austenite in the form of bands is evident in these microstructures; 15 to 20 percent retained austenite is considered to be normal for this alloy in this heat treat condition.

Difficulty was experienced in obtaining satisfactory transformation in a portion of the PH 14-8Mo steel during heat treatment to the SRH 1050 condition.

Table 24 lists the mechanical properties of two heats of Ph 14-8Mo which were heat treated, in one batch, to the SRH 1050 condition per the recommended process of the material supplier.

For gages of .010 through .312 inch the material specification requires the following minimum values for the transverse grain direction:

- 1) $F_{tu} = 200$. ksi
- 2) $F_{ty} = 180$. ksi
- 3) 5.0 percent elongation in 2-inch gage length

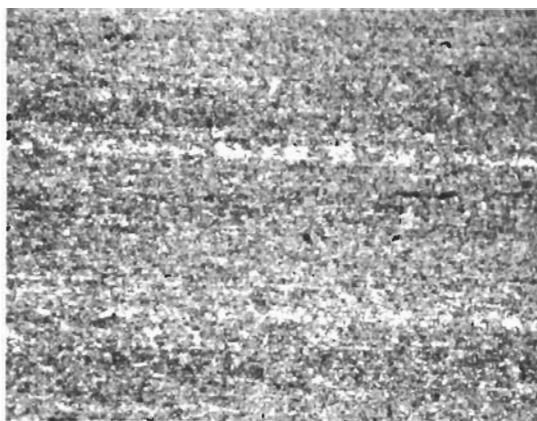
As may be seen, the 0.025-inch thickness from heat 33570 did not meet the specification. Photomicrographs of coupons tested for the listed heats are shown in Fig. 187; the numbers of the photomicrographs are listed in the Table 24 for their respective heats.

TABLE 24 TENSILE PROPERTIES OF PH 14-8 Mo, HEATS 43208 AND 33570

HEAT	GRAIN DIRECTION	NOMINAL GAGE (inches)	F_{tu} (ksi)	F_{ty} (ksi)	PERCENT OF ELONGATION *	PHOTO NUMBER
43208	L	.025	195. 193.	175. 174.	7.5 10.0	1
43208	T	.025	204. 204.	189. 188.	5.0 5.0	2
33570	L	.025	181. 173.	152. 119.	15.0 12.0	3
33570	T	.025	183. 186.	147. 161.	7.5 9.0	4
33570	L	.125	207. 204.	194. 193.	7.5 9.0	5

* 2 INCH GAGE LENGTH

$t = .025$ INCHES

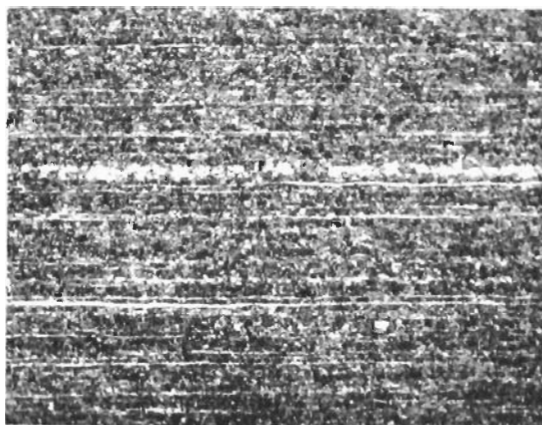


(A) LONGITUDINAL GRAIN
(100x)



(B) TRANSVERSE GRAIN
(100x)

$t = .125$ INCHES



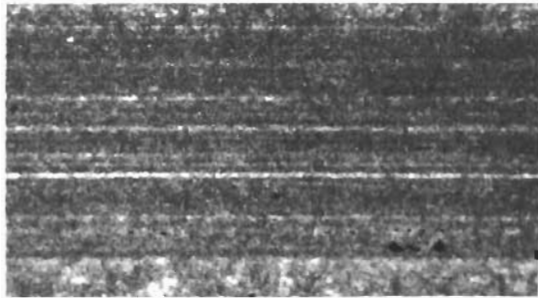
(C) LONGITUDINAL GRAIN
(100x)



(D) TRANSVERSE GRAIN
(100x)

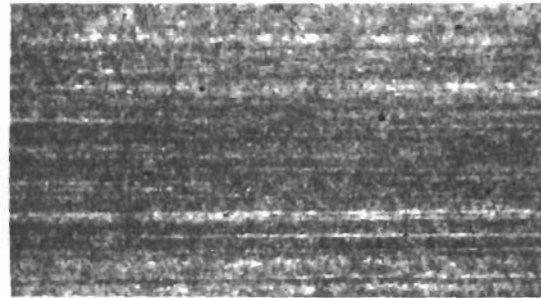
NOTE: Diluted Kalling's Etchant

FIG.186 PHOTOMICROGRAPHS OF PH 14-8Mo, HEAT 33347



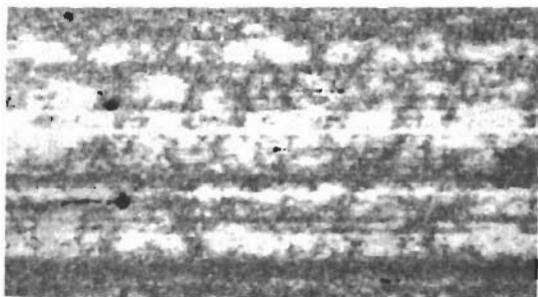
(100x)

NUMBER 1



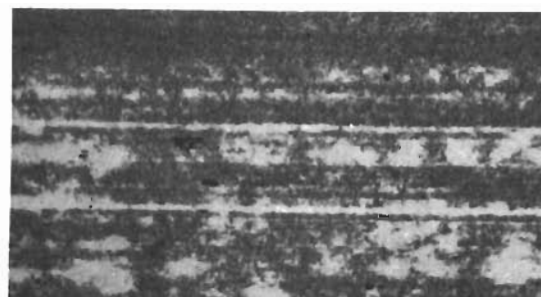
(100x)

NUMBER 2



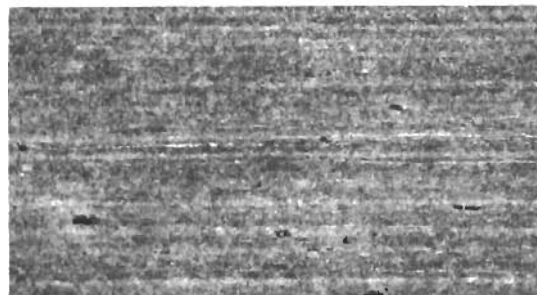
(100x)

NUMBER 3



(100x)

NUMBER 4



(100x)

NUMBER 5

NOTE: Diluted Kalling's Etchant

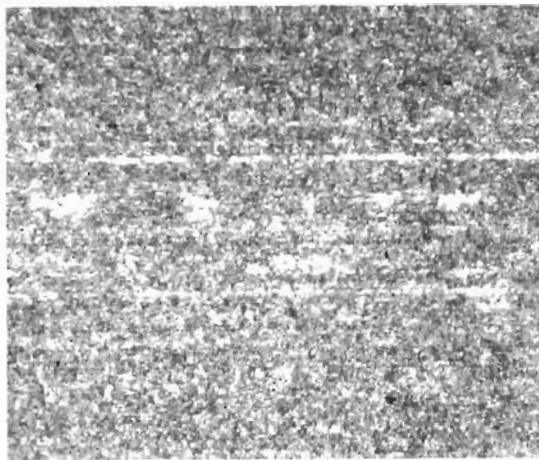
FIG.187 PHOTOMICROGRAPHS OF PH 14-8 Mo WITH UNACCEPTABLE
HEAT TREAT RESPONSE

An unacceptable amount of retained austenite is shown in the photomicrographs of the 0.025-inch thickness in heat 33570, whereas the photomicrographs for the other thickness and heat show adequate transformation of austenite to martensite.

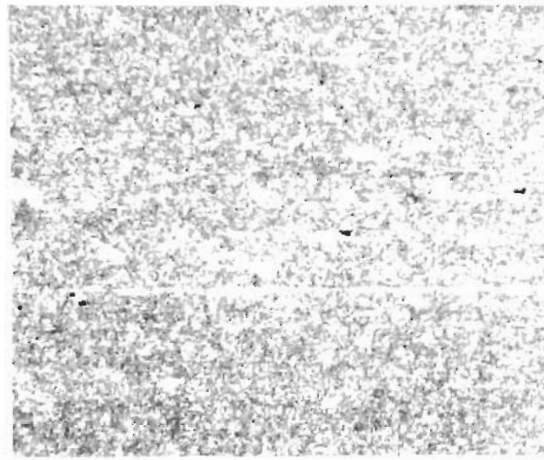
The 0.025-inch thickness of heat 33570 was re-heat-treated for the following reasons:

- A sufficient amount of material from a new heat was not immediately available, and time remaining in the program would not allow ordering a new heat.
- Fracture toughness properties that would be found for this material in the lower strength condition would not be conservative. Based on past experience with PH steels, the fracture toughness properties of the re-heat-treated material should be within the same scatter band as those for the single heat treatment material.
- Testing of re-heat-treated material and comparison with normally processed material is of value because re-heat-treatment would be performed should this situation be encountered in production use of this material.

After the re-heat-treat, the mechanical properties were found to be acceptable and are those listed in the Table of Mechanical Properties for the gage and heat. Photomicrographs of the re-heat-treated material are shown in Fig. 188.



(100x)



(100x)

NOTE: Diluted Kalling's Etchant

FIG. 188 PHOTOMICROGRAPHS OF PH 14-8 Mo THAT WAS RE-HEAT TREATED

Tensile Properties

Tensile properties are listed in Table 25 for temperatures of -110°F , room temperature, 400°F , and 650°F .

Because PH 14-8Mo was heat treated to the SRH 1050 condition and because the heat treatment will be a variable in the analysis of this material, the manner in which the material was heat treated is explained here. The delay in material delivery and the demands of the program schedule did not allow all of the PH 14-8Mo to be heat treated in one batch.

All the material in heat 33347 was heat treated in one batch. The total material for heats 33570 and 43208 were heat treated in one batch; but when the 0.025-inch nominal thickness of heat 33570 did not properly respond, the thickness was re-heat-treated. Thus, the 0.025-inch and 0.125-inch nominal thicknesses of each heat have a heat treat variable. The different thicknesses of heat 33347 do not have a heat treat variable.

In Table 25, the variation in properties between the 0.025-inch thickness of the heats is noteworthy but still within the limits of the specification. Although this may not be particularly desirable for a research program, it does allow the heat treat variable to be interjected for enhancing the value of the data for design application. The variations in properties between the different thicknesses of heat 33347 are smaller in magnitude than the differences between the heats in the 0.025-inch thickness.

After the exposed specimens had been fractured, a tensile coupon was cut from each specimen and tested at room temperature. These values are included in Table 25. The tensile ultimate and yield strengths of the 0.025-inch thickness was decreased by exposure while the 0.050-inch thickness was partially increased and the 0.125-inch thickness notably increased. Elongation increased for the 0.025-inch thickness but decreased for the 0.050 and 0.125-inch thicknesses. Considering that none of the exposed fracture toughness specimens had net failure stresses exceeding the yield strength of the material, the exposure tensile properties should be reliable.

Fatigue Crack Propagation

Crack Growth Data

Fatigue crack growth data are plotted for the 24 x 72-inch panels in Figs. 189 through 196, and in Figs. 197 through 201, for the 8 x 24-inch panels. All data were generated at room temperature at a cycling frequency of 120 cpm for the 24 x 72-inch specimens, and 1200 cpm and 120 cpm for the 8 x 24-inch specimens. The final increment of crack growth for each specimen was performed at a stress ratio of .20 and a gross stress level to approximate a final stress intensity of 75 ksi $\sqrt{\text{inches}}$. For the 8 x 24-inch panels, the final stress was 40 ksi; and for the 24 x 72-inch panels, the final stress was 40 ksi for the last 0.50 inch of the 3-inch final crack length, 28 ksi for the last 0.75 inch of the 6-inch final crack length, and 20 ksi for the last 1.0 inch of the 10-inch final crack length.

TABLE 25 TENSILE TEST DATA FOR PH 14-8Mo

HEAT NO.	NOMINAL THICKNESS inches	GRAIN DIRECTION	TEST TEMPERATURE											
			-110° F			R. T. (80° F)			400° F			650° F		
			F _{TU} (ksi)	F _{TY} (ksi)	* ELONG.	F _{TU} (ksi)	F _{TY} (ksi)	* ELONG.	F _{TU} (ksi)	F _{TY} (ksi)	* ELONG.	F _{TU} (ksi)	F _{TY} (ksi)	* ELONG.
43208	.025	L	226.4	189.6	13.0	194.7	174.8	7.5	177.7	159.4	4.0	164.5	146.6	5.0
		L				192.5	174.1	10.0				168.0	150.4	4.0
		T	229.1	200.8	11.0	204.4	188.8	5.0	180.9	158.3	3.0	176.7	163.1	3.0
		T	230.4	210.4	7.0	204.7	188.3	5.0	183.3	166.3	3.0	171.1	150.0	3.0
33570	.025	L	233.7	205.8	13.0	208.9	192.9	9.0				171.3	150.8	4.5
		L				209.8	191.8	6.0				172.1	154.9	4.5
		T	234.0	207.7	12.0	208.9	192.1	5.0				176.5	158.4	2.0
		T	238.8	205.2	12.0				188.9	172.2	7.5	177.6	162.8	7.0
33347	.125	L	235.0	210.8	14.5	207.0	194.2	7.5						
		L	229.2	194.9	14.5	204.0	193.0	9.0	188.3	170.8	6.5	178.0	160.4	7.0
		L	235.7	212.3	10.5	208.0	193.6	7.5	186.5	170.6	4.5	183.7	164.2	3.0
		L	237.9	211.7	10.5	209.1	196.4	7.0	181.3	163.5	4.0	173.8	148.4	4.0
	.050	T	240.5	216.3	9.5	211.0	191.9	5.5	193.6	177.8	3.0	179.5	157.5	3.0
		T	238.0	216.0	9.0	212.0	192.0	6.0	187.3	169.0	3.0	179.5	161.4	3.0
		L	241.3	217.9	12.0	208.2	193.9	10.0				178.2	160.2	4.5
		L				215.5	199.2	-						
	.093	T	234.0	200.8	15.5	204.9	188.5	10.0				174.3	151.8	4.5
		T	237.9	207.3	13.5	210.5	195.1	8.0				173.0	148.8	5.5
		L	238.6	213.5	15.5	214.7	197.8	10.0				181.8	159.7	6.5
		L				213.8	197.0	10.0						
		T	239.2	218.8	14.5	216.6	199.3	5.0				182.8	160.8	5.0
		T	240.6	219.7	14.0	215.2	192.2	5.5				183.9	162.5	5.5

*ELONGATION MEASURED AS % IN 2 INCHES

TABLE 25 TENSILE TEST DATA FOR PH 14-8Mo (Continued)

HEAT NO.	NOMINAL THICKNESS inches	GRAIN DIRECTION	TEST TEMPERATURE											
			-110° F			R. T. (80° F)			400° F			650° F		
			F _{TU} (ksi)	F _{TY} (ksi)	* ELONG.	F _{TU} (ksi)	F _{TY} (ksi)	* ELONG.	F _{TU} (ksi)	F _{TY} (ksi)	* ELONG.	F _{TU} (ksi)	F _{TY} (ksi)	* ELONG.
33347 **	.125	L	233.8	211.7	15.0	208.6	195.5	8.0	189.3	173.5	8.0	177.3	154.6	6.5
		L	235.2	213.5	15.5	210.4	195.3	10.0				178.1	156.9	6.0
		T	236.8	215.3	13.5	213.2	197.9	6.0	191.6	175.1	6.0	178.7	160.9	5.5
		T	235.4	214.2	14.0	211.4	196.4	8.0	190.9	176.7	6.5	178.0	158.3	5.5
	.025	T				208.0	186.7	6.0						
		T				210.4	186.4	8.5						
		T				209.7	187.0	4.5						
		T				212.3	194.5	4.5						
	.125	T				223.8	205.1	7.0						
		T				223.4	205.0	6.0						

**AFTER EXPOSURE AT 650° F FOR 1000 HOURS AT A GROSS STRESS LEVEL OF 40 ksi

*ELONGATION MEASURED AS % IN 2 INCHES

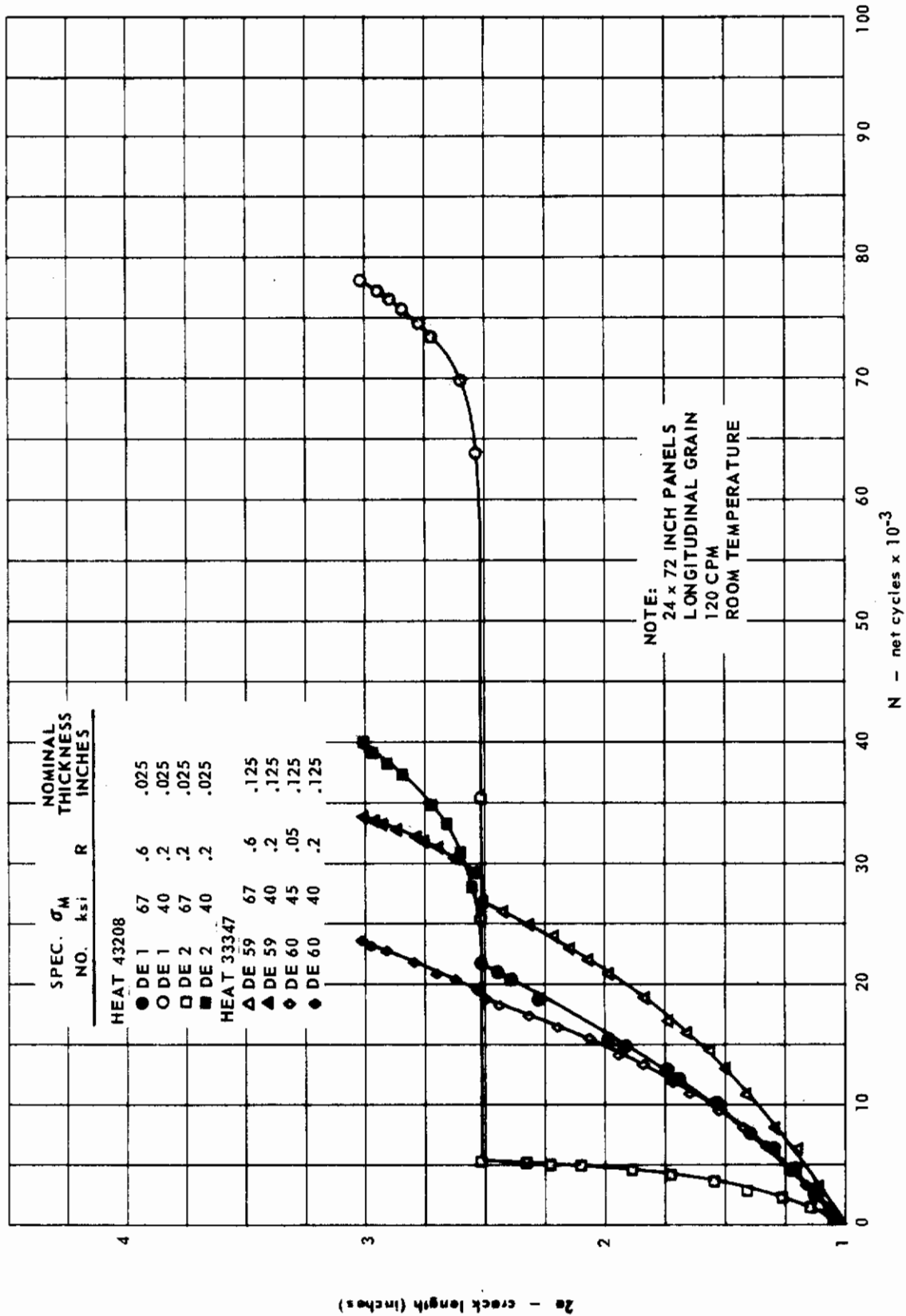


FIG.189 CRACK GROWTH DATA FOR PH 14-8Mo, HEATS 43208 AND 33347

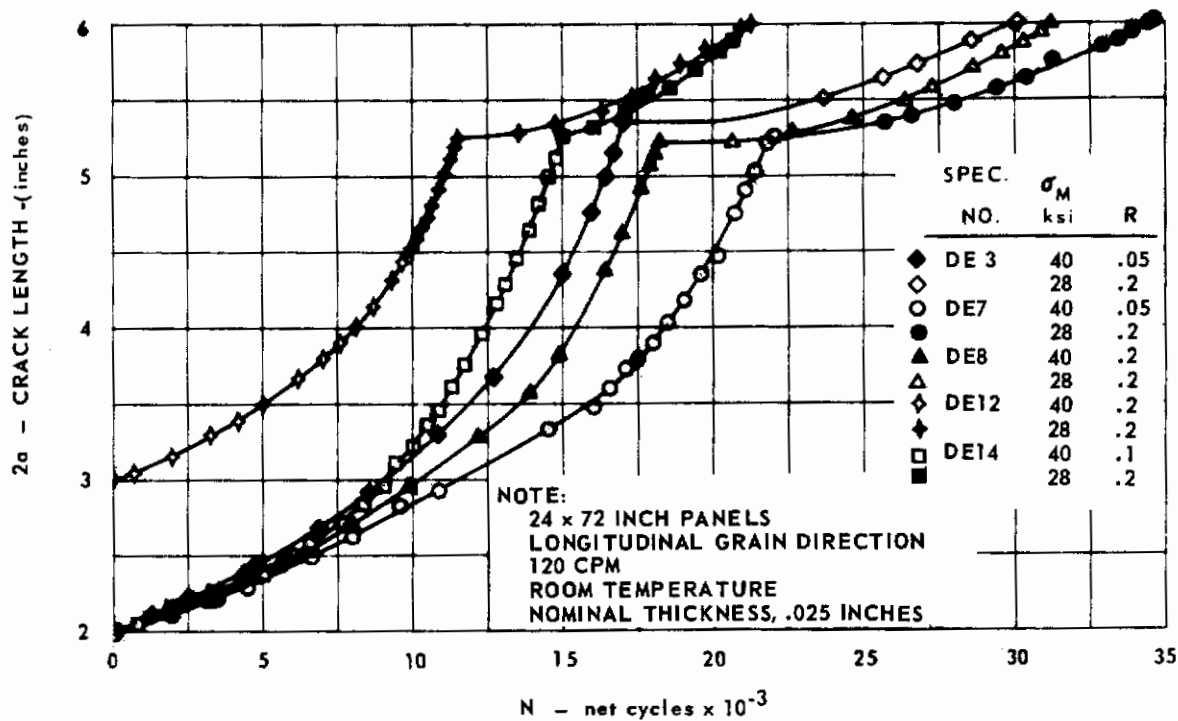


FIG.190 CRACK GROWTH DATA FOR PH 14-8Mo, HEAT 43208

In general, it is shown by the data that fatigue crack growth is a function of:

- Gross stress level; the cycles required to grow a given crack length decrease with an increase in the gross stress level.
- Stress ratio; the cycles required to grow a given crack length decrease with a decrease in the stress ratio.
- Grain direction; the number of cycles required to grow a given crack length is larger for the longitudinal grain direction.
- Cycling frequency; the number of the cycles required to grow a given crack length is larger for 120 cpm for thicknesses of 0.025, 0.050, and 0.093 inch and is also larger for 1200 cpm for a thickness of 0.125 inch. (See Figs. 200, 198 and 199.
- Exposure; for the 8 x 24-inch specimens which were examined, cycles required to grow a given crack length are fewer for the exposed specimens. Refer to Figs. 197, 198 and 199.

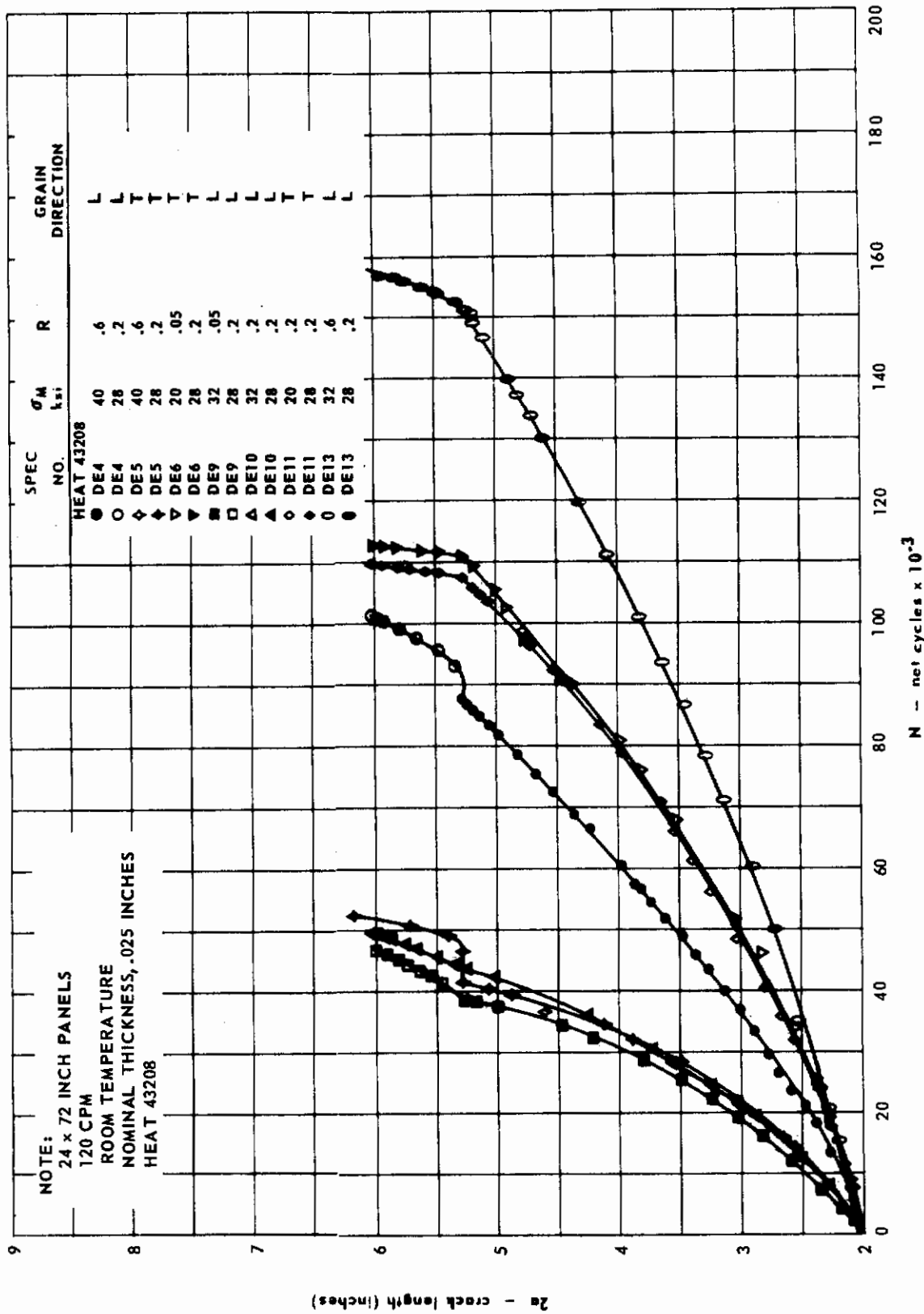


FIG.191 CRACK GROWTH DATA FOR PH 14-8Mo, HEATS 43208

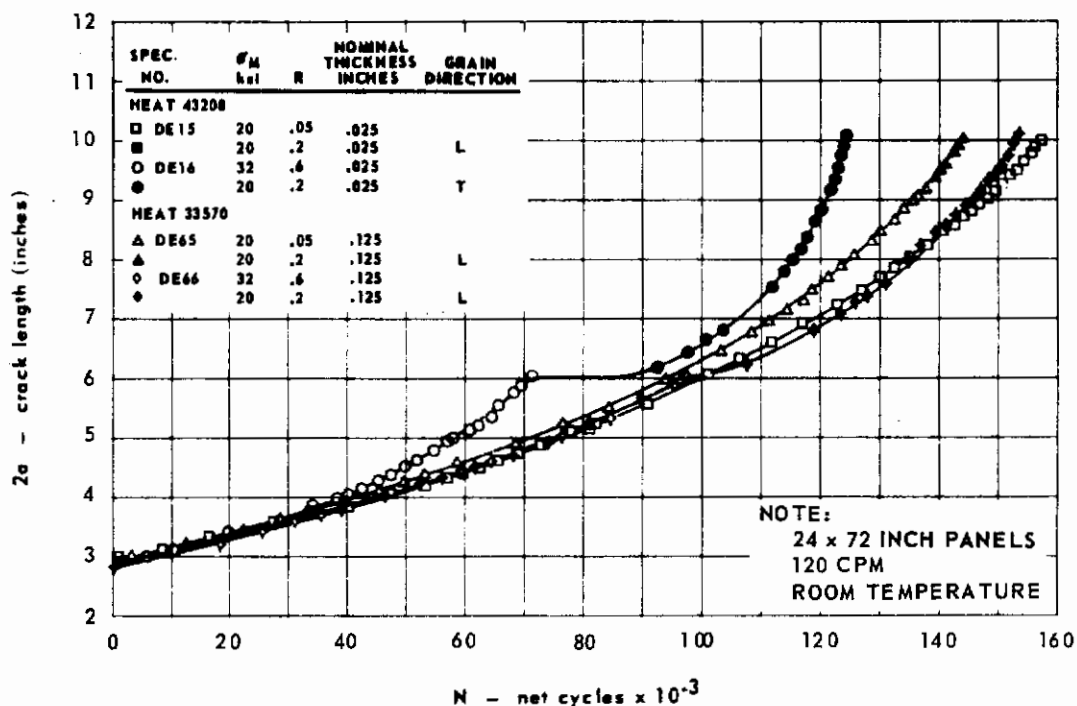


FIG. 192 CRACK GROWTH DATA FOR PH 14-8 Mo, HEATS 43208 AND 33570

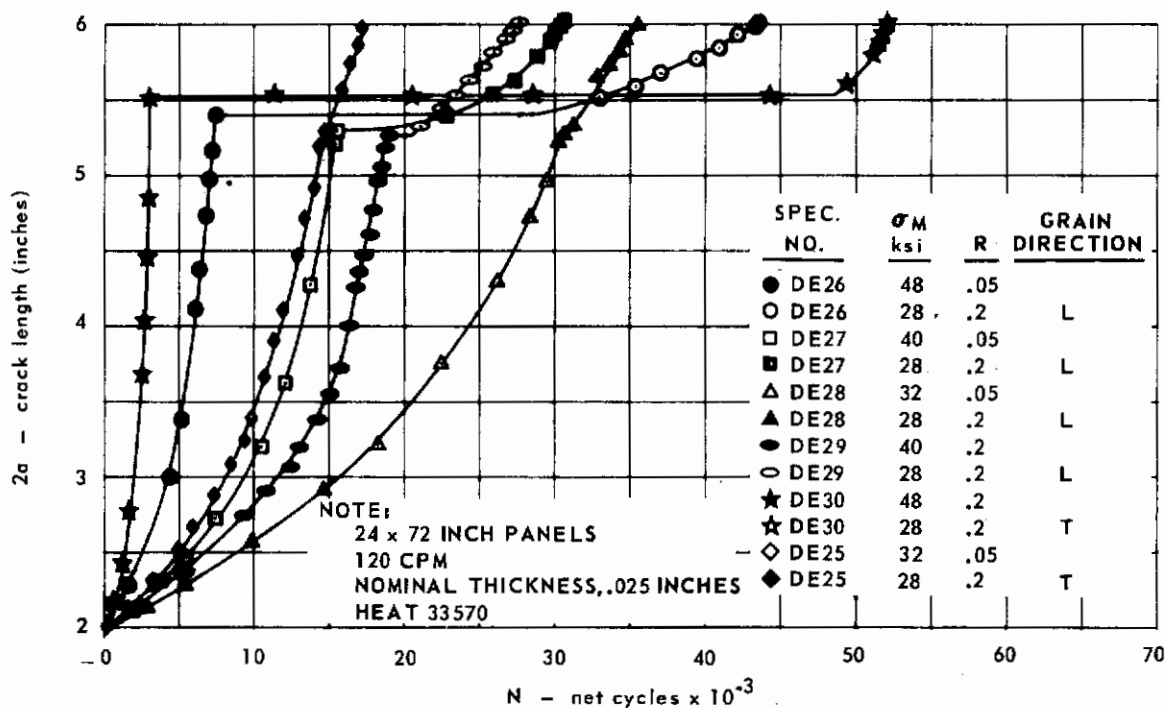


FIG. 193 CRACK GROWTH DATA FOR PH 14-8 Mo, HEAT 33570

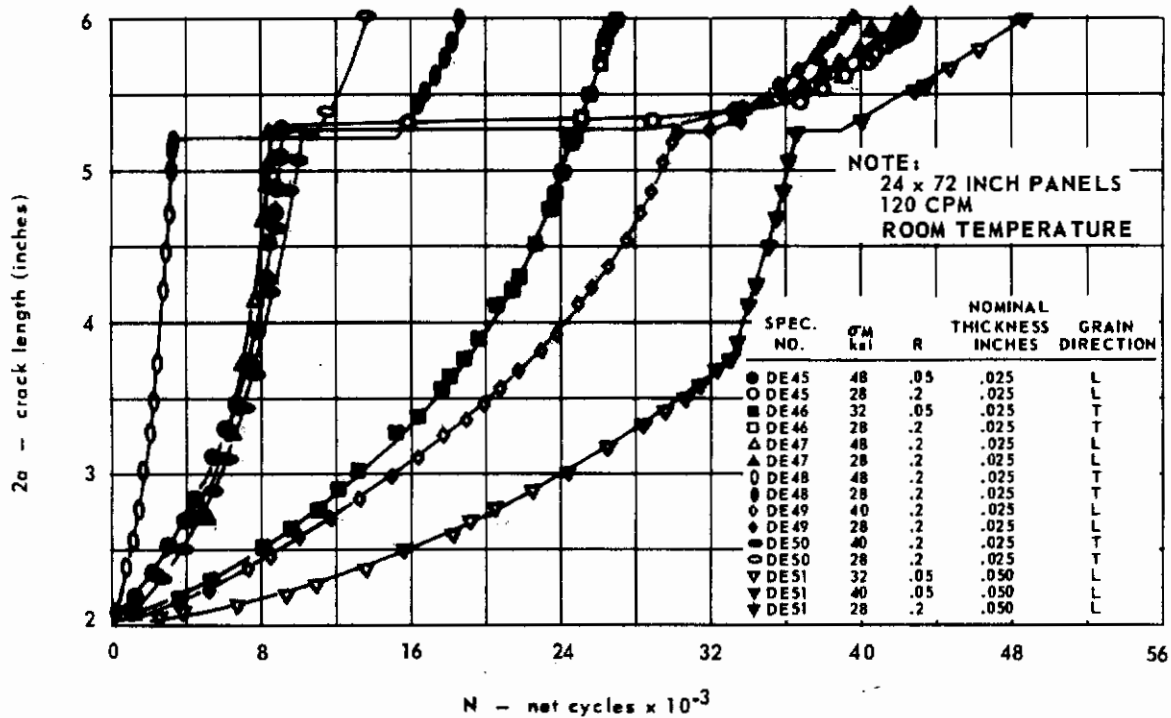


FIG. 194 CRACK GROWTH DATA FOR PH 14-8 Mo, HEAT 33347

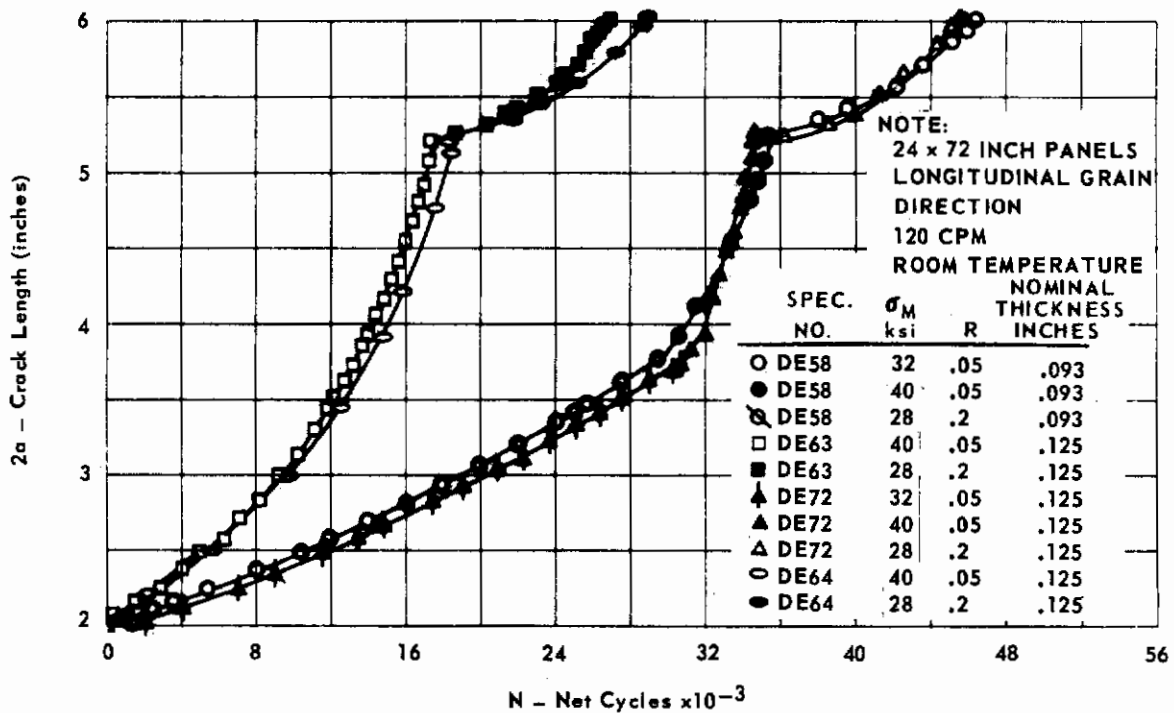


FIG. 195 CRACK GROWTH DATA FOR PH 14-8 Mo, HEAT 33347

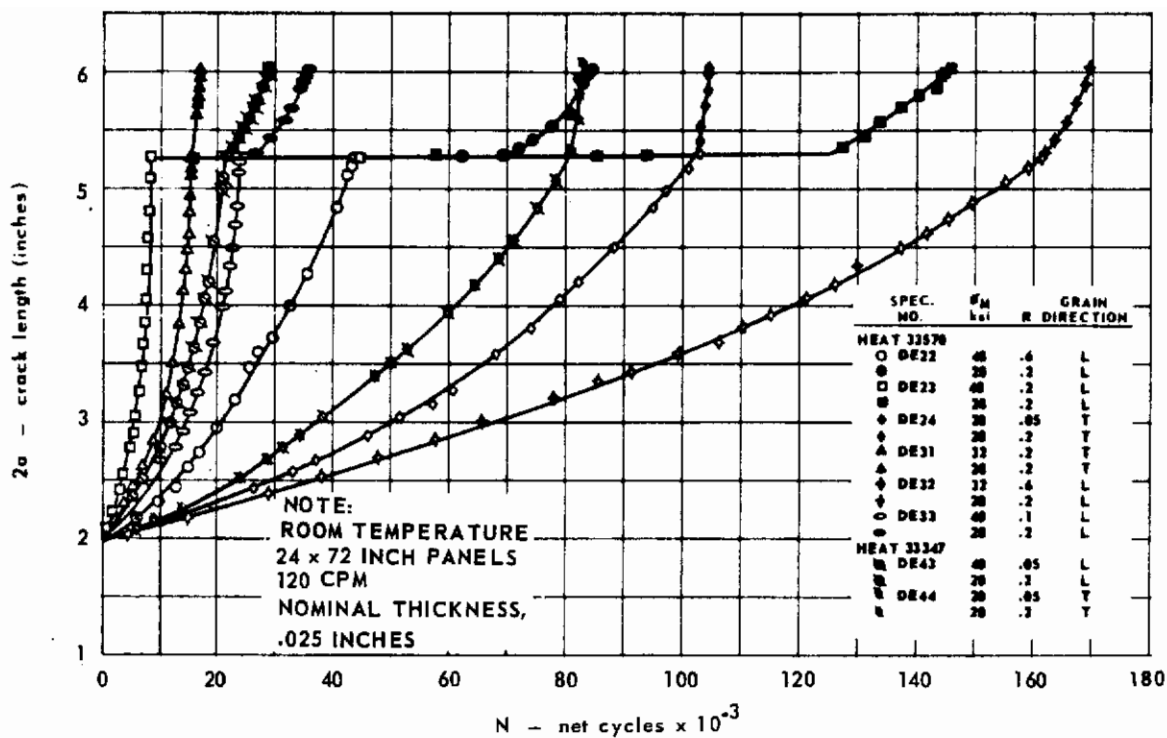


FIG. 196 CRACK GROWTH DATA FOR PH 14-8Mo, HEATS 33347 AND 33570

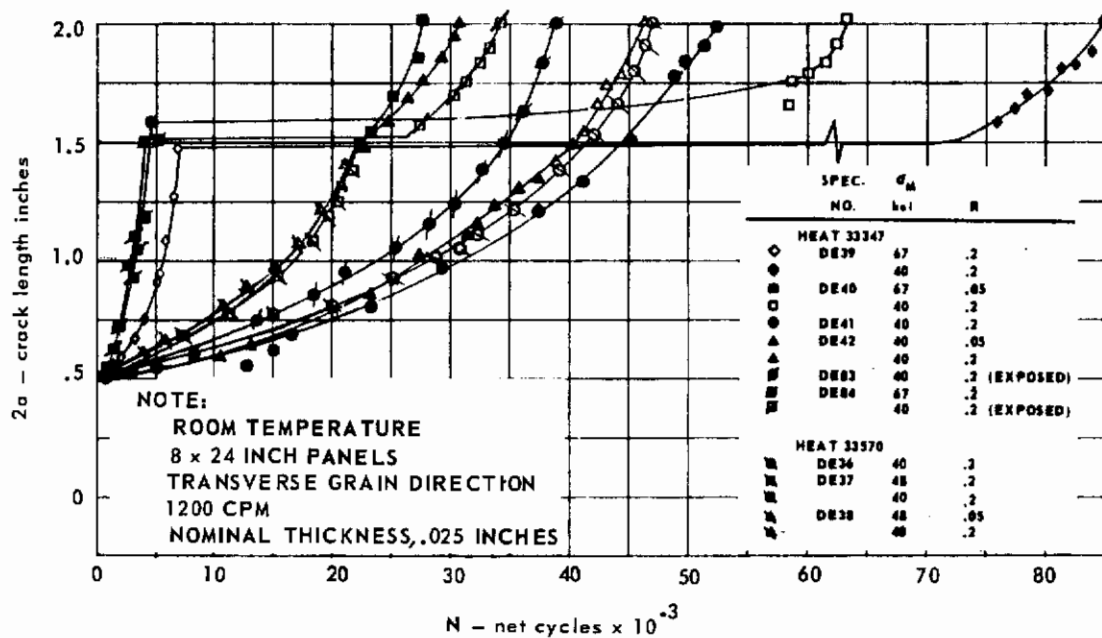


FIG. 197 CRACK GROWTH DATA FOR PH 14-8Mo, HEATS 33347 AND 33570

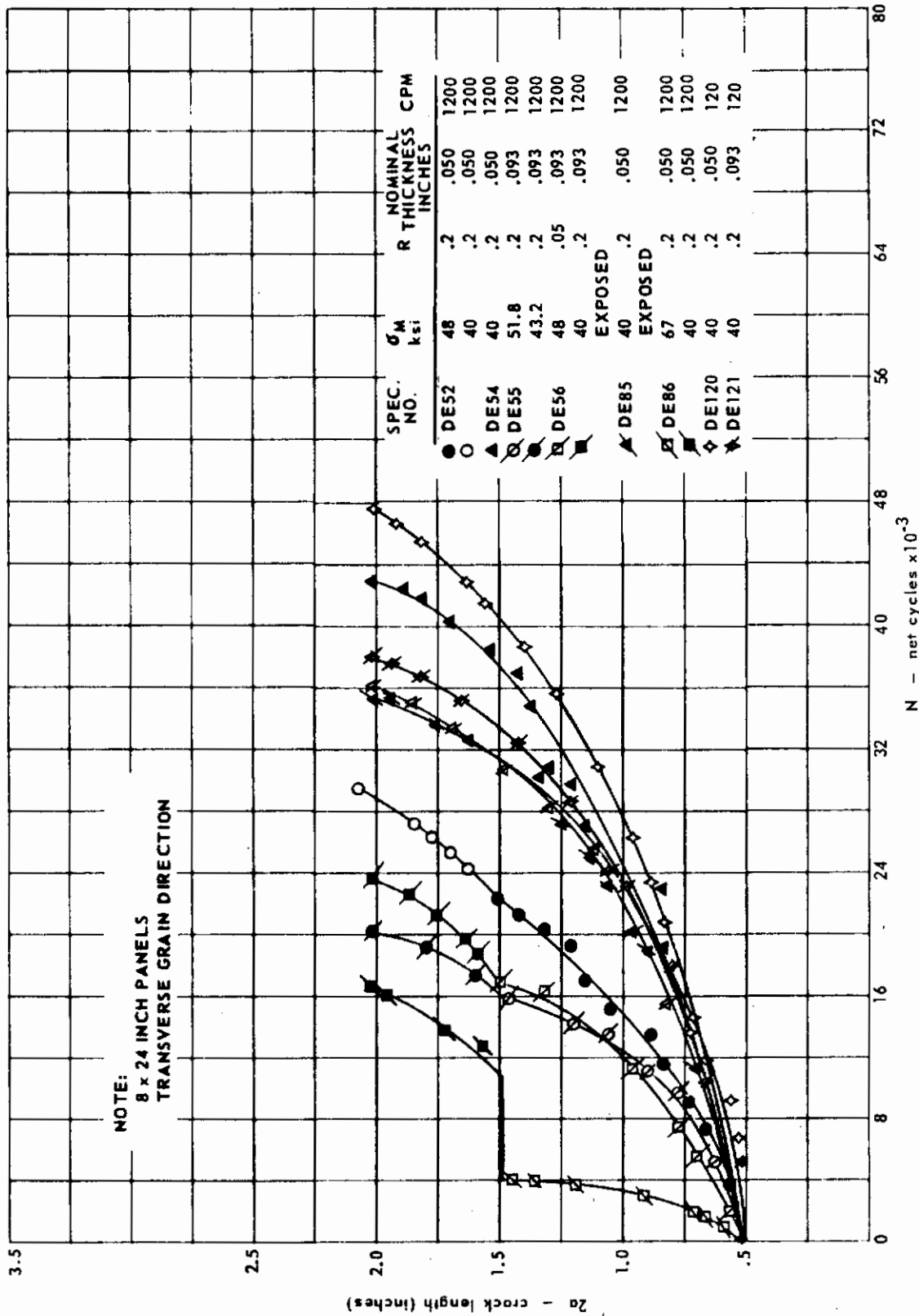


FIG. 198 CRACK GROWTH DATA FOR PH 14-8Mo, HEAT 33347

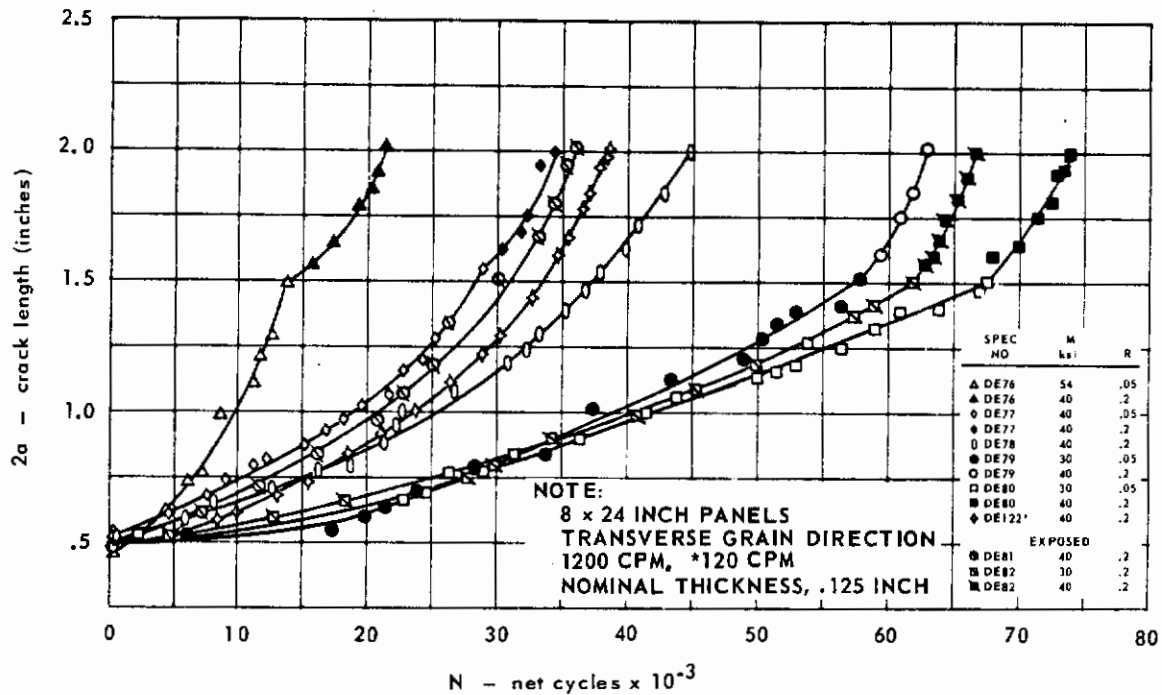


FIG. 199 CRACK GROWTH DATA FOR PH 14-8Mo, HEAT 33347

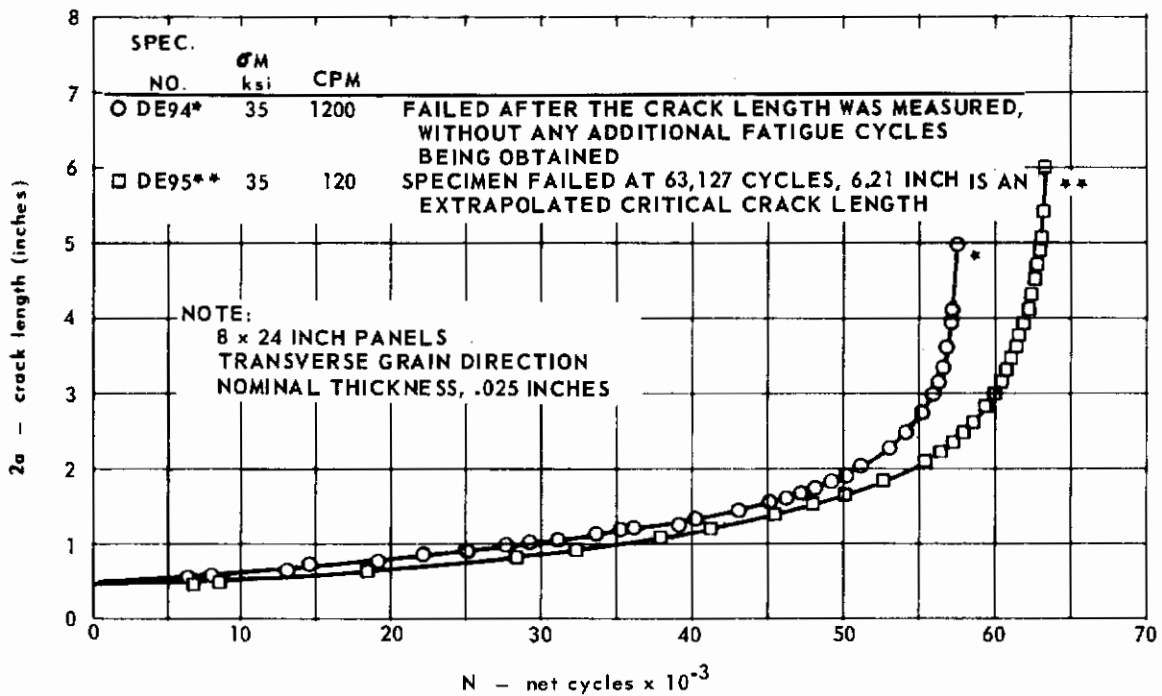


FIG. 200 CRACK GROWTH TO FRACTURE DATA FOR PH 14-8Mo, HEAT 43208

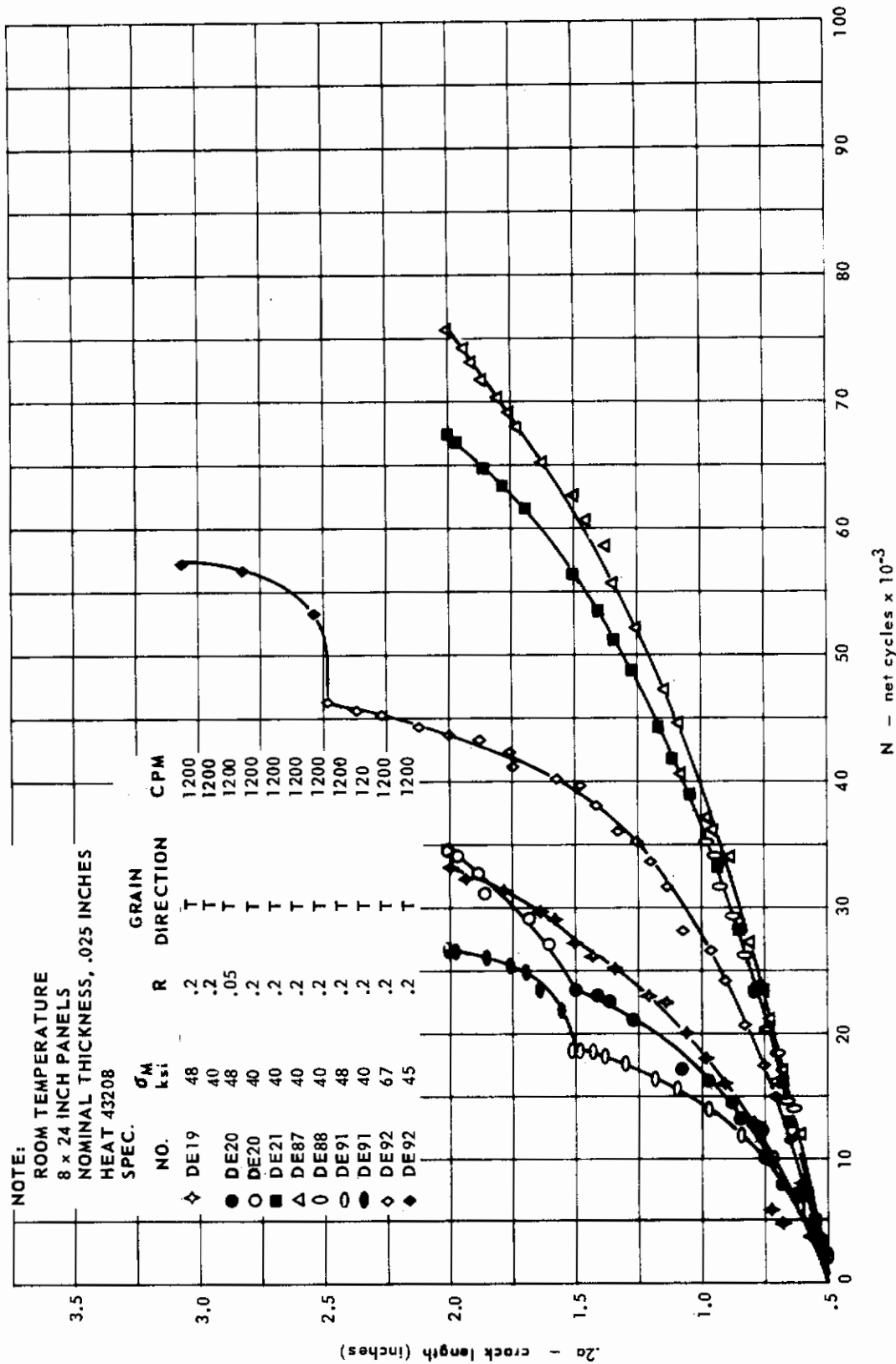


FIG. 201 CRACK GROWTH DATA FOR PH 14-8 Mo, HEAT 43208

It should be noted that changes in the gross stress level and/or the stress ratio during cycling may retard or prohibit crack growth for a number of cycles. Lowering the gross stress level and/or raising the stress ratio tend to retard or prohibit crack growth; whereas elevating the gross stress level and/or lowering the stress ratio do not.

Crack Growth Rate Data

The fatigue crack growth rate curves are plotted in Figs. 202 through 217.

It is shown that the test variables influence the rate of fatigue crack growth in the following manner:

- Specimen Size. The specimen size did not influence the growth rate. Figs. 202 through 206 show how the data for the two specimen sizes blend together.
- Thickness. Figs. 207, 211 and 212 illustrate that crack growth rate was not a function of specimen thickness.
- Grain Direction. Crack growth rate is a function of grain direction. Higher rates of crack growth were found for the transverse grain direction. Figs. 203 through 208 are typical examples.
- Stress Ratio. As expected, the crack growth rate is influenced by the stress ratio. For the 24 x 72-inch panels with 0.025-inch thickness, there is no apparent difference between the rates for stress ratios of 0.05 and 0.2, but the difference between the growth rate for stress ratios of 0.05 and 0.6 varies between factors of approximately 4 and 6. Similarly, for the large specimens of 0.125-inch thickness, a factor of approximately 4 exists between the crack growth rates for stress ratios of 0.05 and 0.6. The 8 x 24-inch panels also show there is no apparent difference in the crack growth rates of the stress ratios of 0.05 and 0.2.
- Cycling Frequency. The effect of cycling frequency varies with thickness and stress ratio. For the 0.025-inch thickness, the 120 cpm frequency has a higher rate of growth for $R = 0.2$ and $R = 0.6$, but a slower rate for $R = 0.1$. For $R = 0.2$, the frequency does not influence the 0.050-inch thickness, while the 0.125-inch thickness has a higher rate of crack growth for the 120 cpm frequency.
- Heat. Comparison of the crack growth rate envelopes for the 0.025 nominal thickness (longitudinal and transverse grain directions) of each of the heats shows that the heat variable has an effect. For $R = 0.05$ and $R = 0.1$, heat 33570 has the fastest rate of crack growth and heat 43208 has the slowest rate. For $R = 0.6$, where only two heats are compared, heat 43208 has a faster rate than does heat 33570.
In the 0.125-inch nominal thickness (with only a longitudinal grain direction and two heats compared) heat 33570 has a rate faster than heat 33347 for $R = 0.6$ while there is no difference for the two heats at $R = 0.05$.
- Exposure. Figs. 214, 215 and 216 contain plots of the exposed and unexposed specimens. The exposed specimens have a higher crack growth rate for each of the thicknesses tested. The difference in the rate increases as the thickness is decreased.

Residual Strength and Fracture Toughness

Tables 26 and 27 contain all the pertinent data for the fracture tests for the 24 x 72-inch and 8 x 24-inch panels. Calculations based on σ_{yp} , derived from high strain rate tensile data, are accentuated by a darker background to simplify comparisons among the various columns.

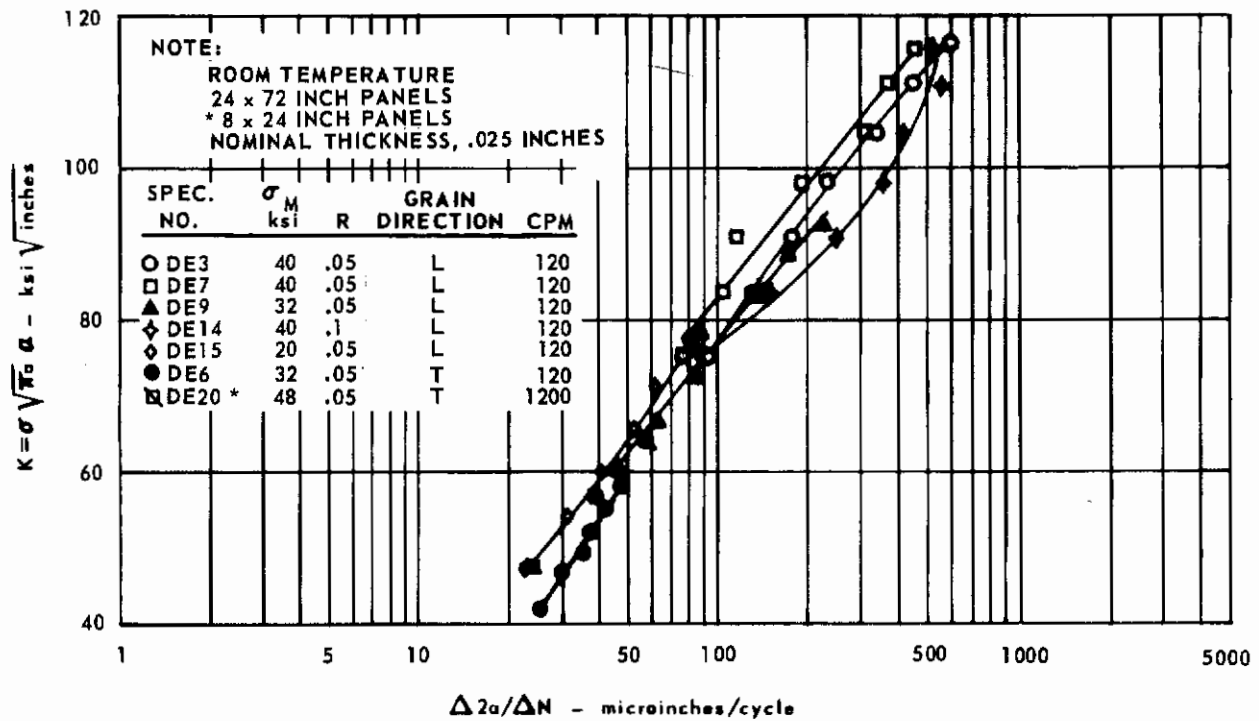


FIG. 202 CRACK GROWTH RATE DATA FOR PH 14-8Mo, HEAT 43208

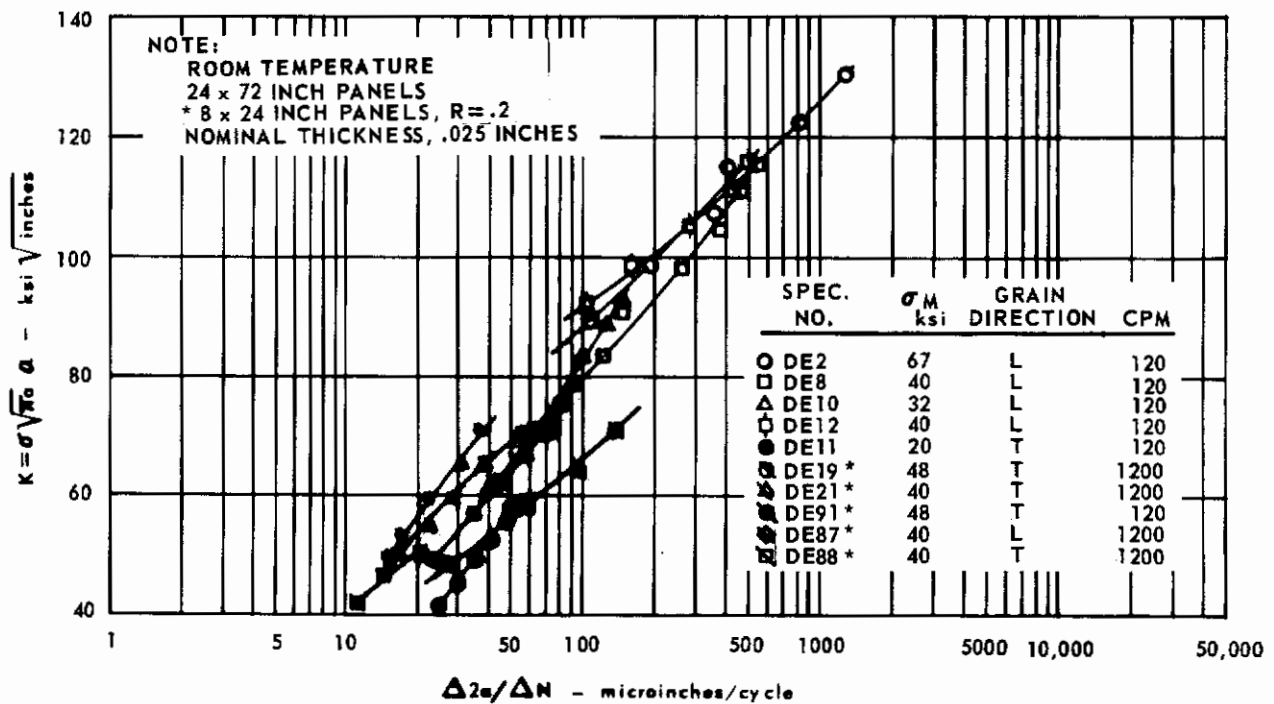


FIG. 203 CRACK GROWTH RATE DATA FOR PH 14-8Mo, HEAT 43208

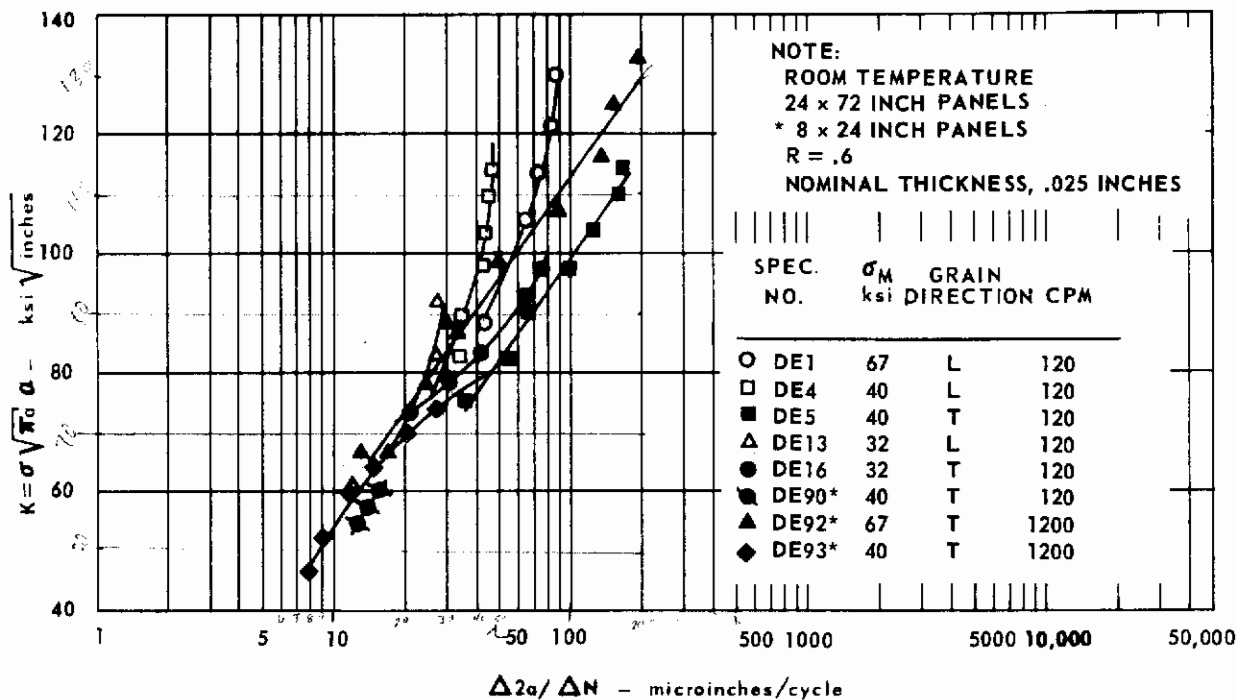


FIG. 204 CRACK GROWTH RATE DATA FOR PH 14-8Mo, HEAT 43208

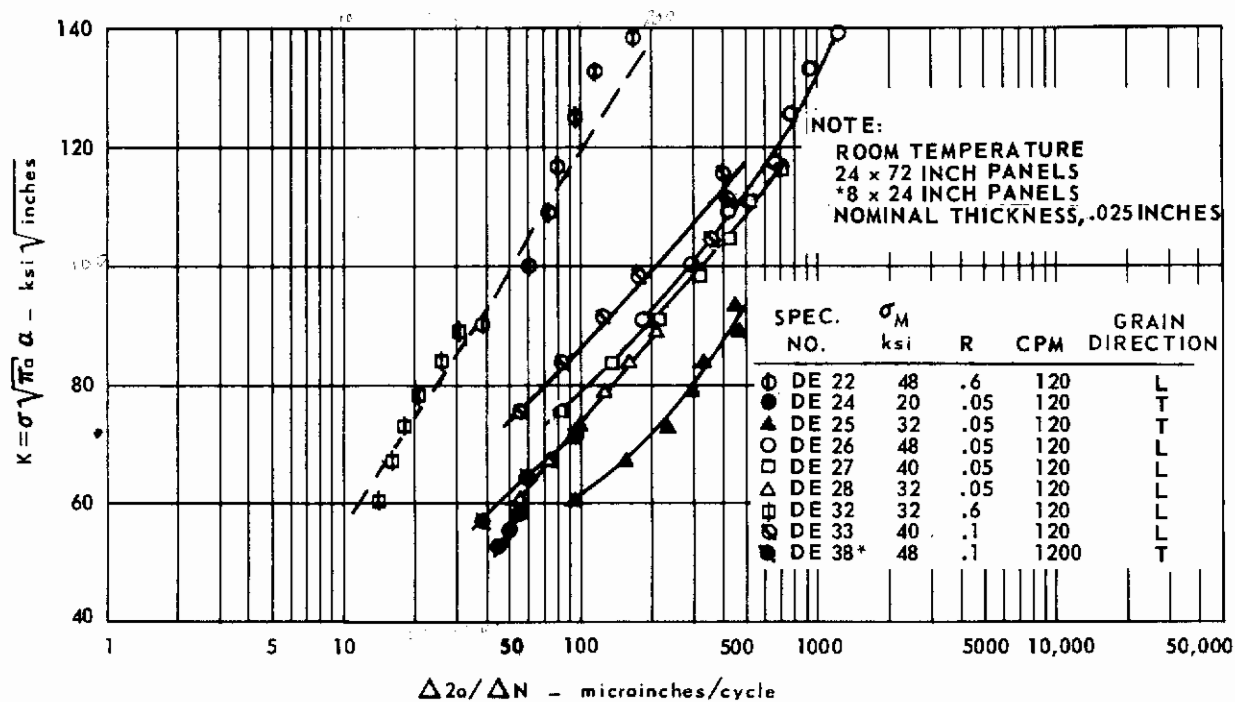


FIG. 205 CRACK GROWTH RATE DATA FOR PH 14-8 Mo, HEAT 33570

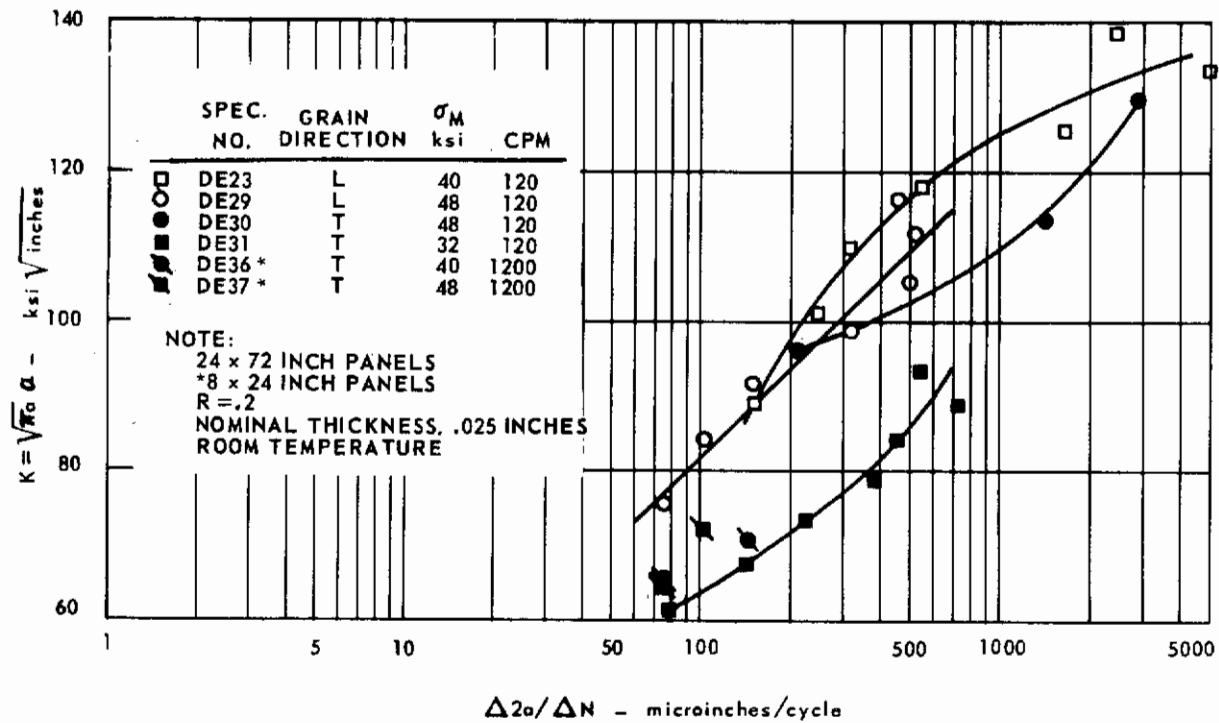


FIG. 206 CRACK GROWTH RATE DATA FOR PH 14-8 Mo, HEAT 33570

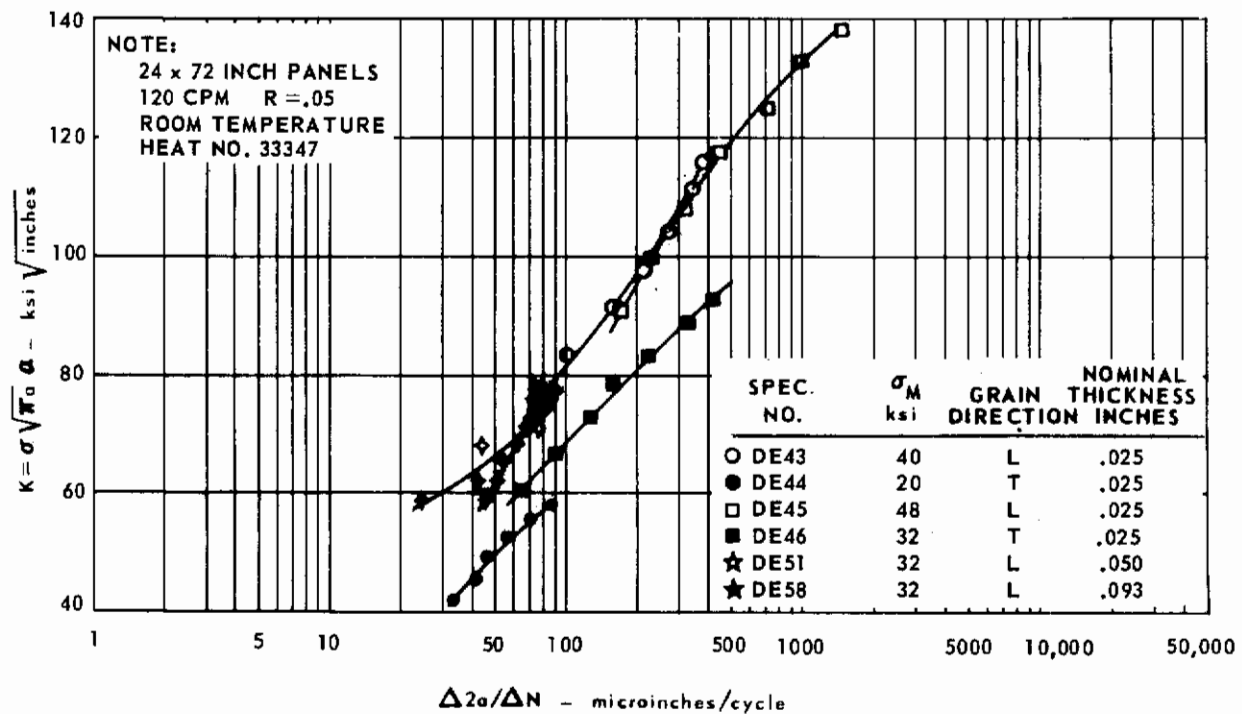


FIG. 207 CRACK GROWTH RATE DATA FOR PH 14-8 Mo, HEAT 33347

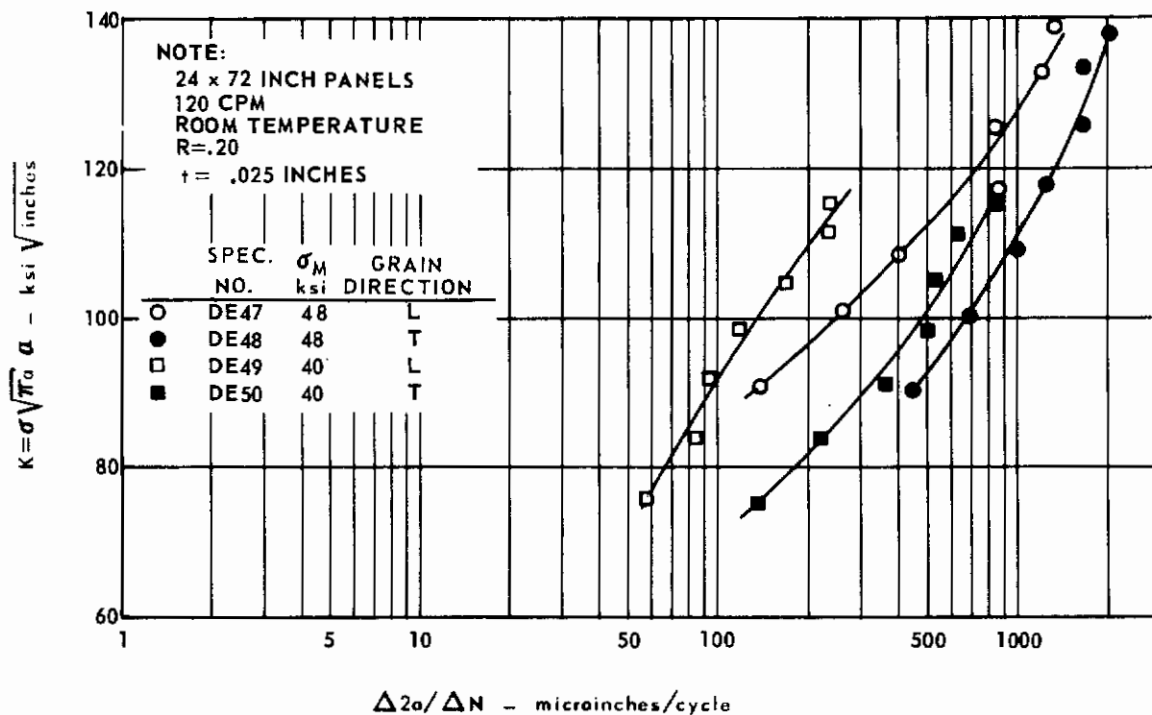


FIG. 208 CRACK GROWTH RATE DATA FOR PH 14-8 Mo, HEAT 33347

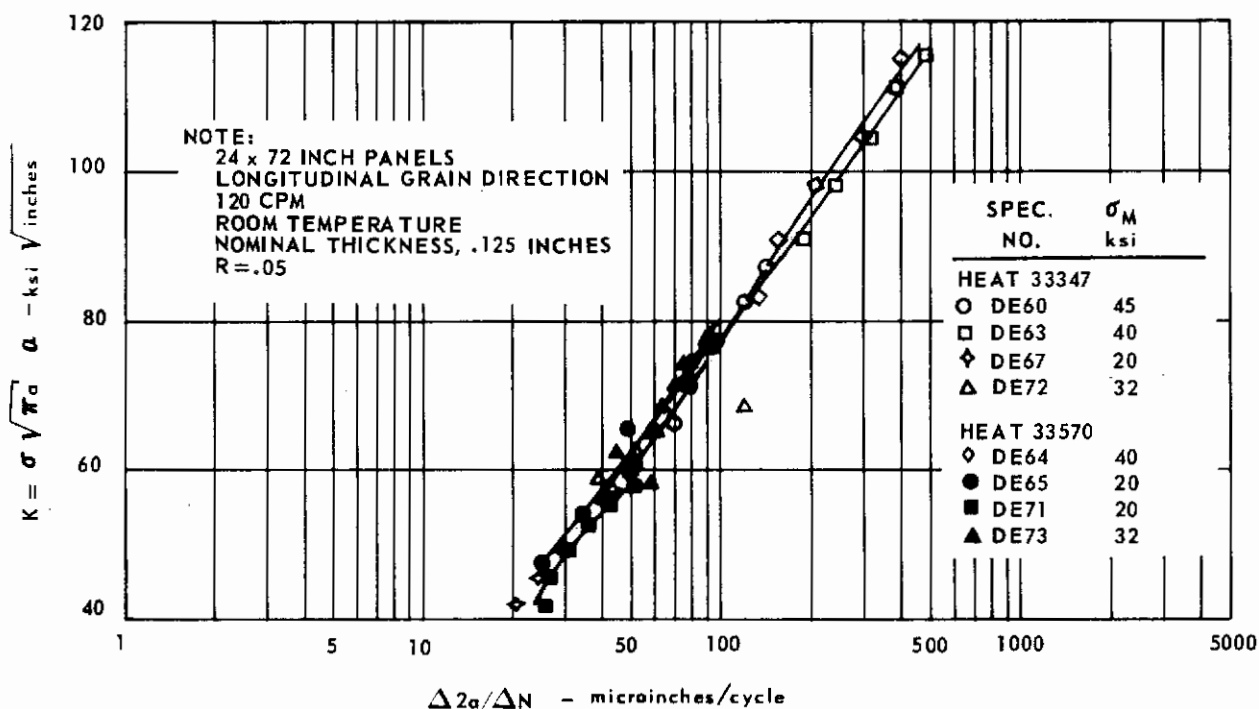


FIG. 209 CRACK GROWTH RATE DATA FOR PH 14-8 Mo, HEATS 33347 AND 33570

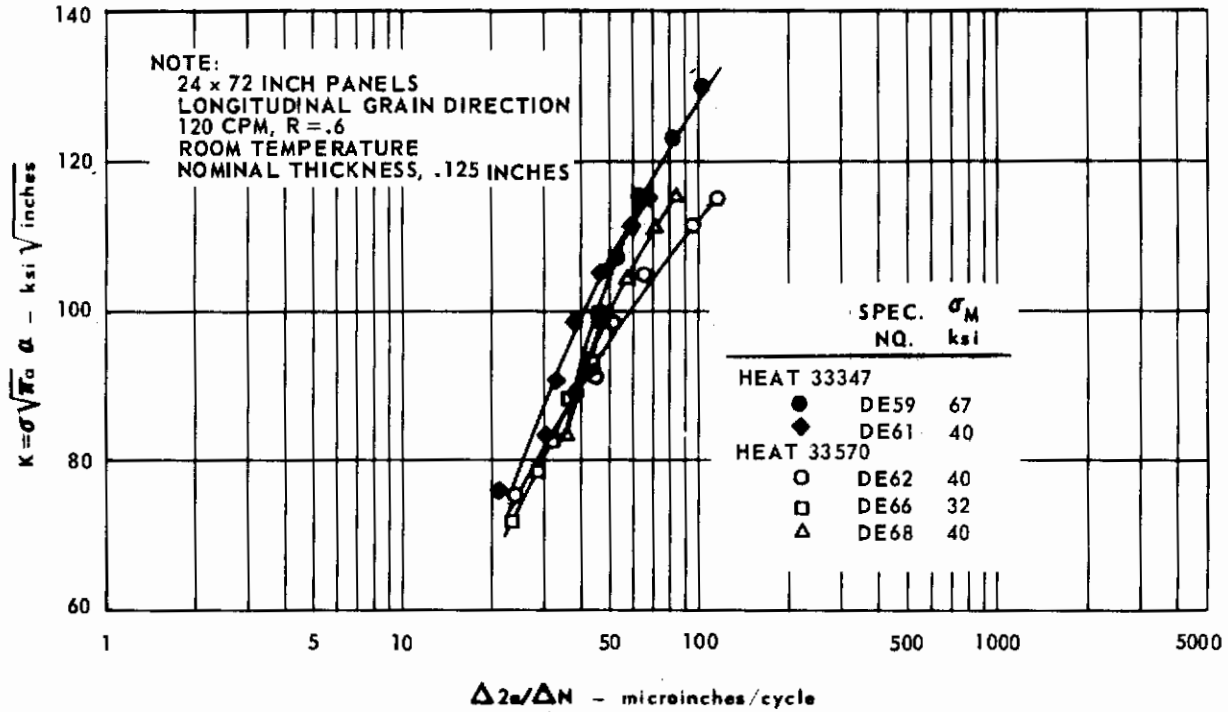


FIG. 210 CRACK GROWTH RATE DATA FOR PH 14-8 Mo, HEATS 33347 AND 33570

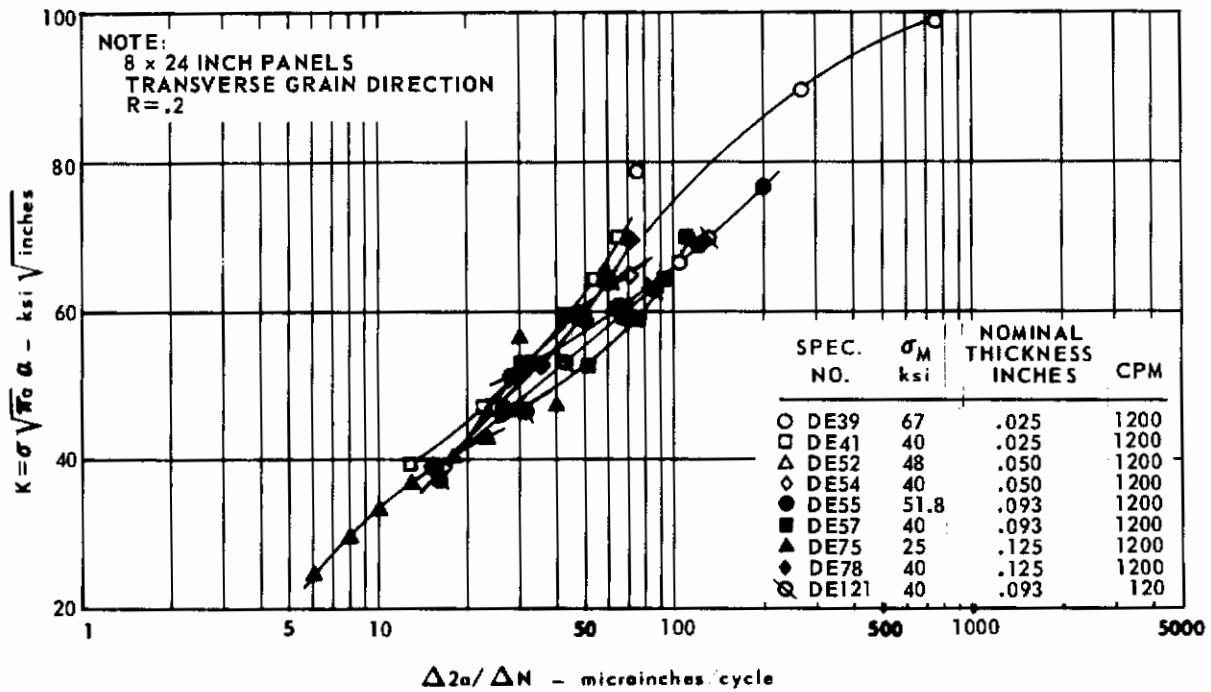


FIG. 211 CRACK GROWTH RATE DATA FOR PH 14-8 Mo, HEAT 33347

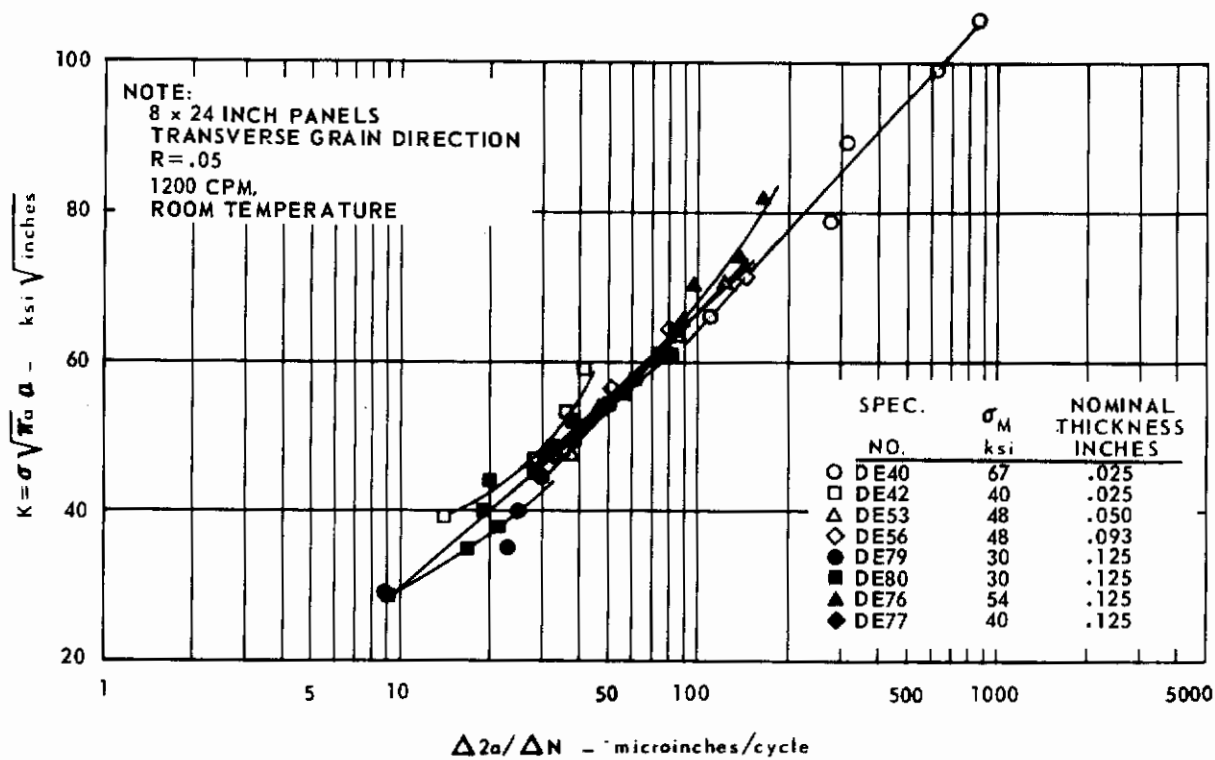


FIG. 212 CRACK GROWTH RATE DATA FOR PH 14-8 Mo, HEAT 33347

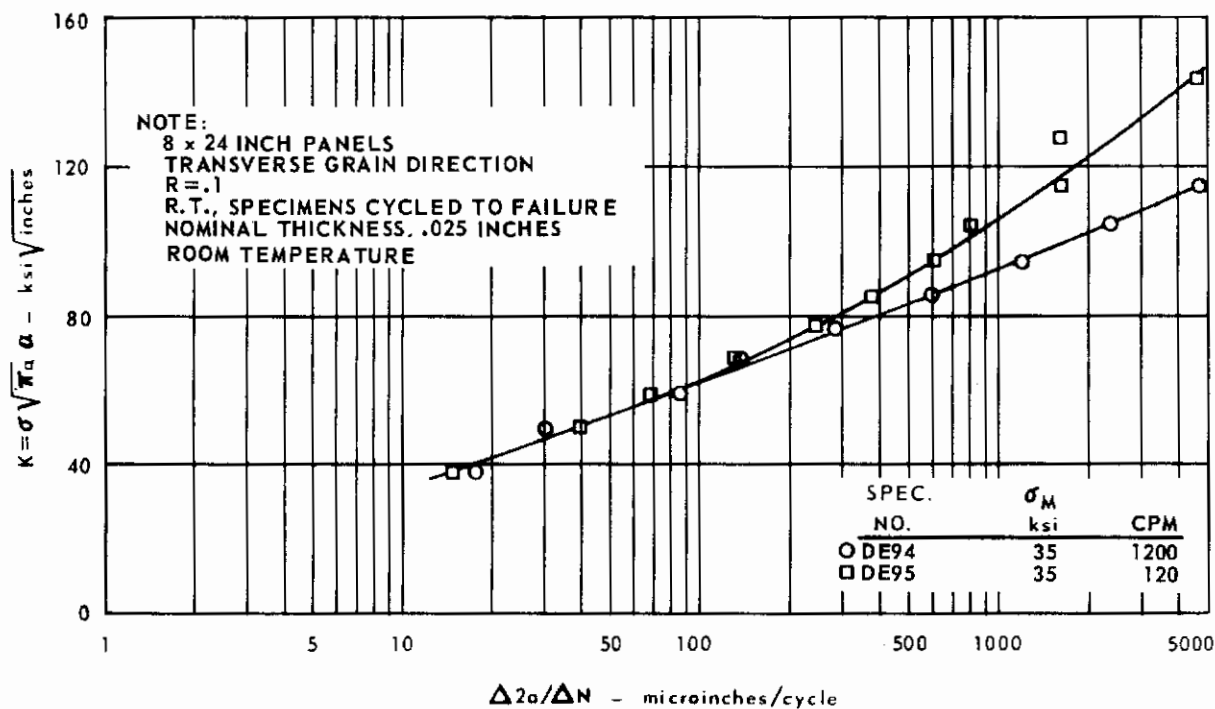


FIG. 213 CRACK GROWTH RATE DATA FOR PH 14-8 Mo, HEAT 43208

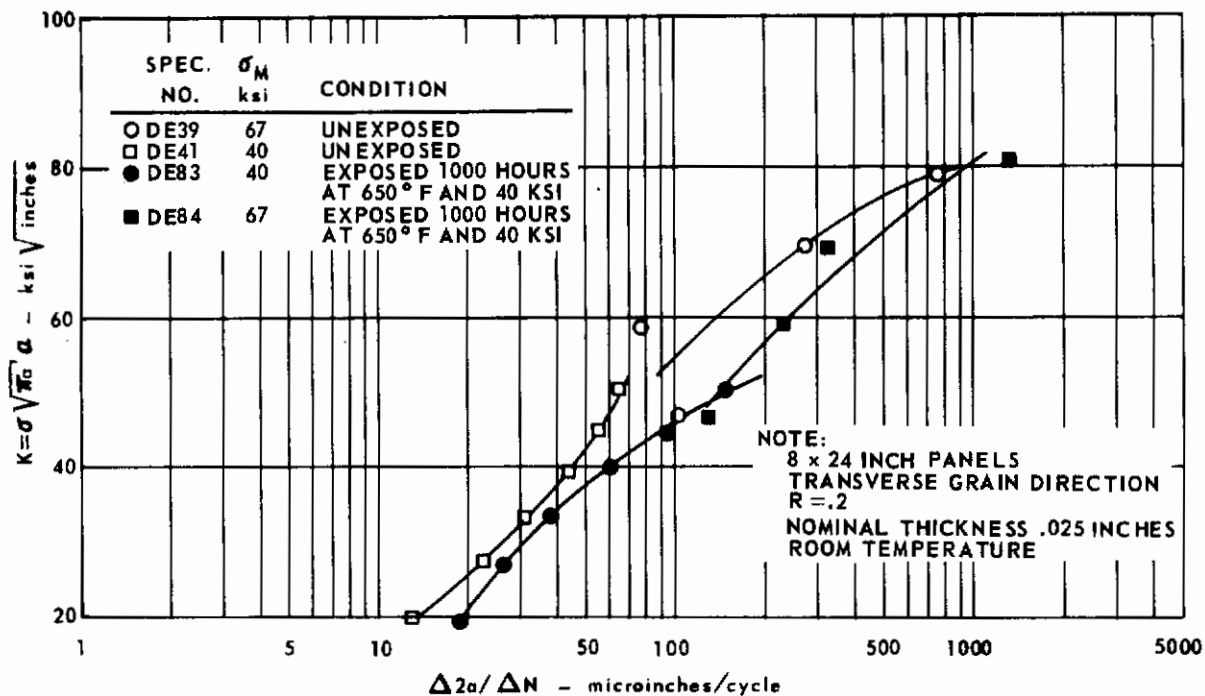


FIG. 214 COMPARISON OF EXPOSED AND UNEXPOSED CRACK GROWTH RATES FOR PH 14-8 Mo, HEAT 33347

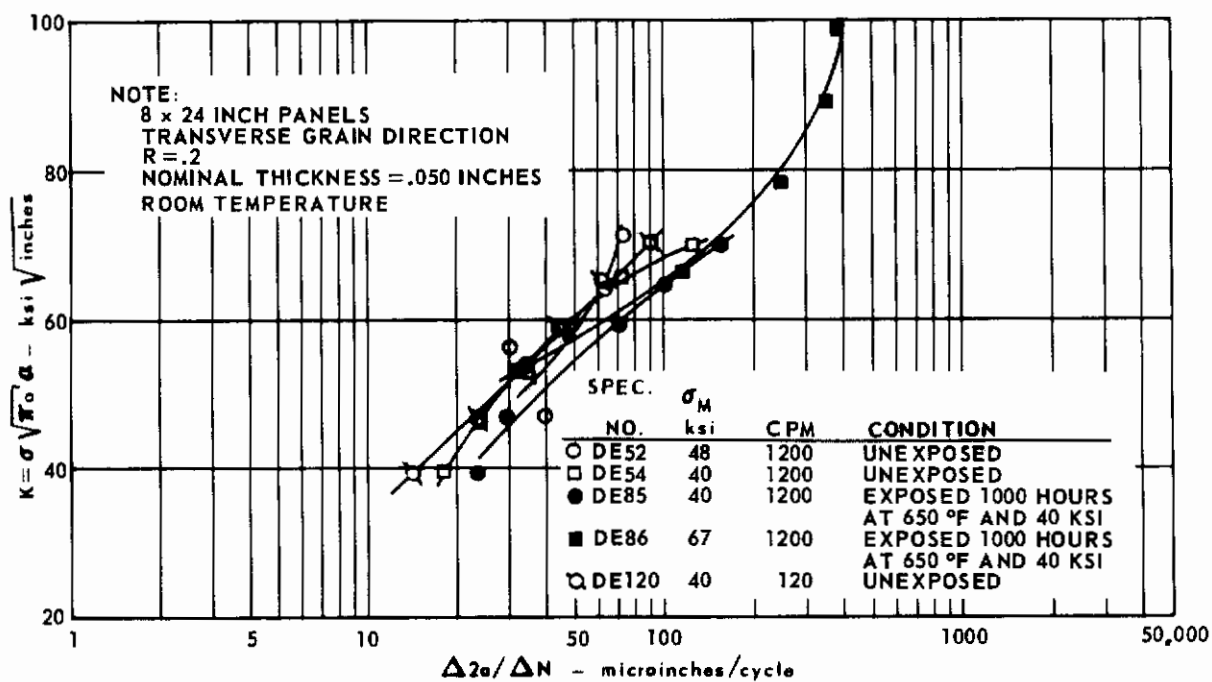


FIG. 215 COMPARISON OF EXPOSED AND UNEXPOSED CRACK GROWTH RATES FOR PH 14-8 Mo, HEAT 33347

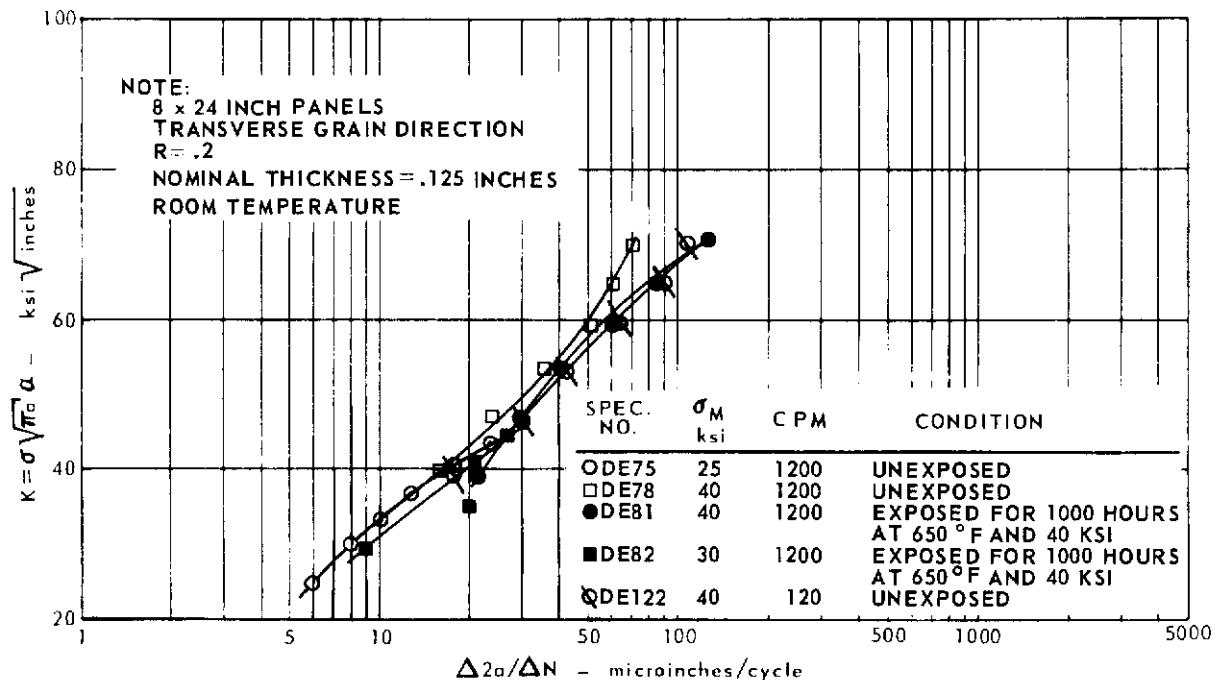


FIG. 216 COMPARISON OF EXPOSED AND UNEXPOSED CRACK GROWTH RATES FOR PH 14-8 Mo, HEAT 33347

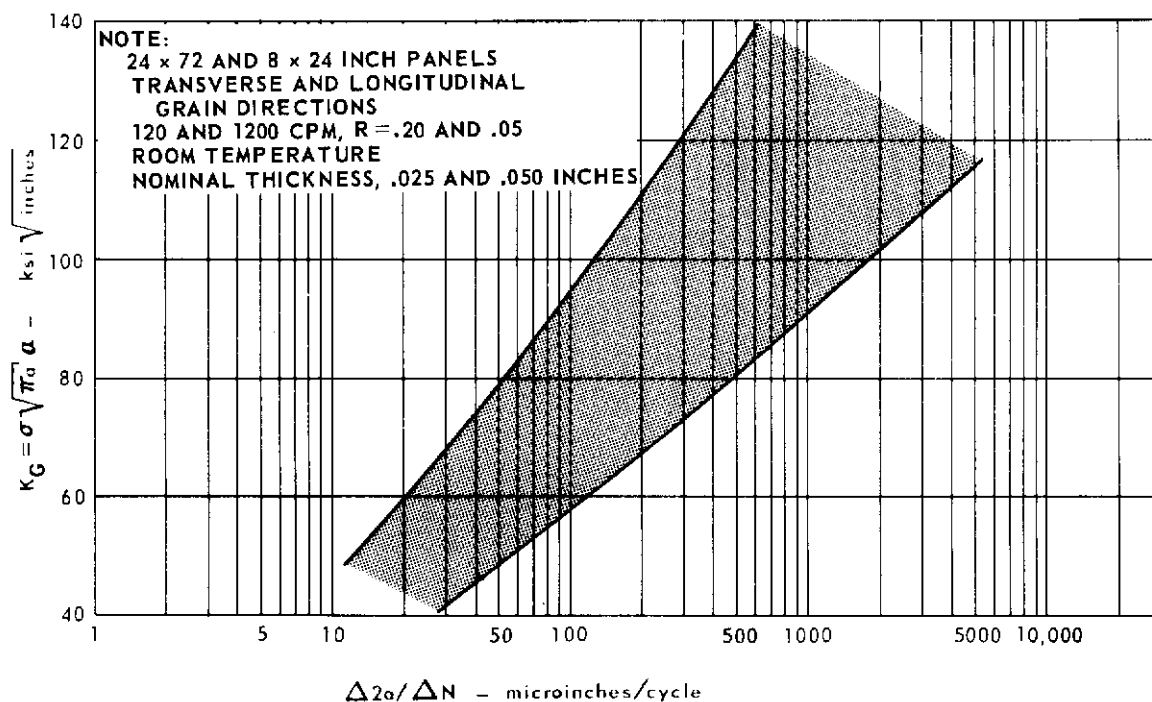


FIG. 217 CRACK GROWTH RATE DATA FOR PH 14-8 Mo, HEATS 33347, 33570 AND 43208

TABLE 26 FRACTURE TOUGHNESS DATA FOR 24 x 72 INCH PANELS OF PH 14-8 Mo (continued)

SPECIMEN NO.	HEAT NO.	THICKNESS inches	WIDTH inches	GRAIN DIRECTION	TEMP. °F	$\dot{\sigma}$ psi/sec	$2a_0$ inches	σ_G ksi	σ_N ksi	F_{tu} ksi	σ_{yp} ksi	σ_{yp} ksi	σ_{yp} ksi	σ_N^* ksi	σ_N^* ksi	σ_N^* ksi	$K_{CN} = \sigma_G \sqrt{\pi a_0}$ ksi \sqrt{in}	σ_G^* ksi	$K_{IC} = \sigma_G \sqrt{a_0}$ ksi \sqrt{in}	SHEAR %
DE 32	33570	.024	24.01	L	650	$.80 \times 10^6$	6.00	58,313	77.42	171.7	152.8	152.8	152.8	.51	.51	.51	185.4	.340	190.5	100
DE 33	33570	.024	24.02	L	650	$.88 \times 10^6$	6.00	57,155	76.18	171.7	152.8	152.8	152.8	.50	.50	.50	181.7	.332	186.6	100
DE 43	33347	.025	23.99	L	-110	1.30×10^6	6.00	82,361	109.83	235.8	212.0	212.0	212.0	.52	.52	.52	261.8	.349	270.7	100
DE 44	33347	.025	24.03	T	-110	$.99 \times 10^6$	6.02	70,240	93.74	239.2	216.2	216.2	216.2	.43	.43	.43	223.7	.294	227.6	100
DE 45	33347	.024	23.97	L	RT	1.56×10^6	6.00	81,251	107.81	208.6	195.0	195.0	195.0	.55	.55	.55	258.3	.390	268.3	100
DE 46	33347	.025	24.03	T	70	$.86 \times 10^6$	6.01	65,579	87.46	211.5	192.0	192.0	192.0	.46	.46	.46	208.6	.310	212.2	100
DE 47	33347	.025	23.97	L	400	1.64×10^6	6.02	68,091	90.93	183.9	174.2	174.2	174.2	.52	.52	.52	216.9	.370	224.1	100
DE 48	33347	.025	24.03	T	400	1.58×10^6	6.02	56,591	75.52	190.4	173.4	173.4	173.4	.44	.44	.44	180.2	.297	183.9	100
DE 49	33347	.026	23.98	L	650	$.73 \times 10^6$	6.00	62,550	83.42	178.8	156.3	156.3	156.3	.53	.53	.53	198.8	.350	205.3	100
DE 50	33347	.025	24.03	T	650	1.11×10^6	6.04	49,933	66.70	179.5	159.4	159.4	159.4	.42	.42	.42	159.3	.278	160.4	100
DE 51	33347	.050	24.01	L	72	1.07×10^6	6.00	92,083	122.71	211.8	196.6	196.6	196.6	.62	.62	.62	292.7	.435	305.5	100
DE 58	33347	.0925	24.10	L	74	1.27×10^6	6.00	115,747	154.12	214.2	197.4	197.4	197.4	.78	.78	.78	367.8	.540	402.7	100
DE 59	33347	.125	24.05	L	67	$.65 \times 10^6$	3.00	163,340	186.62	209.5	195.4	195.4	195.4	.95	.95	.95	357.4	.780	409.4	100
DE 60	33347	.1235	23.98	L	650	1.26×10^6	3.00	118,163	135.08	177.7	155.8	155.8	155.8	.87	.87	.87	258.6	.665	299.9	100
DE 61	33347	.122	23.99	L	RT	$.80 \times 10^5$	6.00	124,359	165.83	209.5	195.4	195.4	195.4	.85	.85	.85	395.3	.594	447.7	100
DE 62	33570	.124	24.08	L	70	$.98 \times 10^6$	6.00	112,860	150.31	205.5	193.6	193.6	193.6	.78	.78	.78	358.7	.549	383.4	100
DE 63	33347	.126	24.08	L	650	1.15×10^6	6.00	93,276	124.23	177.7	155.8	155.8	155.8	.80	.80	.80	296.4	.525	324.6	100
DE 64	33570	.119	24.07	L	650	$.74 \times 10^6$	6.01	89,735	119.59	177.7	155.8	155.8	155.8	.77	.77	.77	285.1	.505	306.4	100
DE 65	33570	.121	24.03	L	78	1.00×10^6	10.00	88,205	151.06	205.5	193.6	193.6	193.6	.78	.78	.78	392.0	.429	432.8	100
DE 66	33570	.119	24.03	L	650	$.96 \times 10^6$	10.01	73,427	125.90	177.8	161.2	161.2	161.2	.78	.78	.78	326.6	.413	343.4	100
DE 67	33347	.124	24.02	L	-110	$.92 \times 10^6$	6.01	119,543	159.43	234.5	212.6	212.6	212.6	.75	.75	.75	380.3	.510	414.3	100
DE 68	33570	.119	24.03	L	-110	1.01×10^6	6.00	114,685	152.84	232.1	202.8	202.8	202.8	.75	.75	.75	364.5	.494	397.6	100
DE 70	33347	.123	24.01	L	71	4.66×10^3	6.00	128,852	171.78	209.5	195.4	195.4	195.4	.88	.88	.88	409.6	.615	472.9	100
DE 71	33570	.119	24.06	L	74	4.51×10^3	6.00	129,235	172.17	205.5	193.6	193.6	193.6	.89	.89	.89	410.7	.629	475.6	100
DE 72	33347	.125	24.04	L	72	$.96 \times 10^6$	6.00	125,790	167.63	209.5	195.4	195.4	195.4	.86	.86	.86	399.8	.600	431.1	100
DE 73	33570	.119	24.07	L	74	1.14×10^6	6.00	117,318	156.28	205.5	193.6	193.6	193.6	.81	.81	.81	372.83	.571	412.5	100

* TENSILE PROPERTIES OBTAINED FROM STANDARD STRAIN RATE TESTS OF .005 in/in/min
 ** σ_{yp} EXTRAPOLATED FROM HIGH STRAIN RATE TENSILE DATA PH 27-7 STAINLESS STEEL (REFERENCE 26)

TABLE 27 FRACTURE TOUGHNESS DATA FOR 8 X 24-INCH PANELS OF PH 14-8Mo

SPECIMEN NO.	HEAT NO.	THICKNESS inches	WIDTH inches	GRAIN DIRECTION	TEMP. °F	$\dot{\sigma}$ psi/sec	$2a_0$ inches	σ_G ksi	σ_N ksi	F_{tu} ksi	σ_{yp}^* @ TEMP. ksi	σ_{yp}^* @ TEMP. AND $\dot{\sigma}$ ksi	σ_N^* @ TEMP. AND $\dot{\sigma}$ ksi	σ_N^* @ TEMP. AND $\dot{\sigma}$ ksi	KCN = $\sigma_G \sqrt{\pi a_0}$ ksi $\sqrt{\text{in}}$	$\frac{\sigma_G}{F_{tu}}$	$K_{IC} = \frac{\sigma_G \sqrt{a_0 W}}{\text{ksi} \sqrt{\text{in}}}$	SHEAR %
DE 19	43208	.0247	7.987	T	-110	5.48×10^3	2.00	108.718	145.03	229.8	205.6	208.3	.71	.70	199.5	.473	216.1	100
DE 20	43208	.0247	7.99	T	-110	1.00×10^6	2.00	107.396	143.24	229.8	205.6	217.3	.70	.66	197.1	.467	211.4	100
DE 21	43208	.025	7.99	T	78	$.97 \times 10^6$	2.00	108.458	144.66	204.6	188.6	199.2	.77	.73	199.1	.530	217.3	100
DE 36	33570	.024	8.00	T	-110	5.5×10^3	2.00	114.062	152.08	236.4	206.4	209.1	.74	.73	209.3	.482	229.3	100
DE 37	33570	.024	7.99	T	-110	1.07×10^6	2.01	110.532	147.74	236.4	206.4	218.2	.71	.69	203.4	.468	219.7	100
DE 38	33570	.024	7.99	T	78	1.02×10^6	2.00	99.583	132.82	208.9	192.1	203.0	.69	.65	182.8	.477	195.5	100
DE 39	33347	.0252	7.993	T	-110	4.75×10^3	2.01	120.159	160.48	239.2	216.2	218.6	.74	.73	221.2	.502	243.2	100
DE 40	33347	.0255	7.993	T	-110	1.04×10^6	2.02	108.685	145.44	239.2	216.2	228.5	.67	.64	200.6	.454	214.0	100
DE 41	33347	.0254	7.993	T	68	1.09×10^6	1.98	103.202	137.20	211.5	192.0	202.9	.72	.68	188.3	.488	203.0	100
DE 42	33347	.025	7.99	T	650	$.94 \times 10^6$	2.00	82.082	109.48	179.5	159.4	174.4	.69	.63	150.6	.458	160.2	100
DE 52	33347	.050	7.994	T	-110	$.98 \times 10^6$	2.05	136.102	183.04	236.0	207.6	219.2	.88	.84	253.4	.577	288.3	100
DE 53	33347	.051	8.00	T	76	1.04×10^6	2.01	119.853	160.06	207.7	191.8	202.7	.83	.79	220.6	.577	245.7	100
DE 54	33347	.049	7.99	T	650	1.00×10^6	2.00	101.405	135.26	173.6	150.3	164.6	.90	.82	186.1	.584	210.9	100
DE 55	33347	.092	8.00	T	-110	1.04×10^6	2.01	138.587	185.08	239.9	219.2	231.7	.85	.80	255.1	.578	279.3	100
DE 56	33347	.092	8.00	T	72	1.01×10^6	2.01	132.473	176.92	215.9	195.8	207.0	.90	.86	243.8	.614	279.0	100
DE 57	33347	.092	8.00	T	650	1.00×10^6	2.00	108.967	145.29	183.4	161.6	177.0	.90	.82	200.0	.594	276.7	100
DE 74	33347	.123	8.04	T	73	1.02×10^6	2.00	133.482	177.68	212.3	197.2	208.4	.90	.85	244.8	.629	280.6	100
DE 75	33347	.124	8.00	T	70	5.28×10^3	1.99	132.560	176.46	212.3	197.2	199.8	.90	.88	242.6	.624	282.0	100
DE 76	33347	.124	8.01	T	400	5.4×10^6	2.01	121.828	162.63	191.2	175.9	177.1	.92	.92	224.2	.637	283.8	100
DE 77	33347	.124	8.00	T	650	5.26×10^3	1.98	107.934	143.60	178.4	159.6	162.8	.90	.88	196.9	.605	228.5	100
DE 78	33347	.124	8.00	T	-110	5.31×10^3	2.00	128.071	107.97	236.1	214.8	217.4	.50	.79	235.04	.542	262.5	100
DE 79	33347	.124	8.00	T	-110	$.99 \times 10^6$	2.01	133.065	177.71	236.1	214.8	226.8	.83	.78	244.9	.564	272.8	100
DE 80	33347	.124	8.00	T	650	1.01×10^6	1.99	100.806	134.19	178.4	159.6	174.9	.84	.77	184.5	.565	264.6	100
DE 81	33347	.125	8.01	T	72	1.04×10^6	2.02	128.346	171.61	223.8	205.1	216.8	.84	.79	236.9	.573	263.4	100
DE 82	33347	.125	7.99	T	73	1.05×10^6	1.99	132.84	176.74	223.4	205.0	216.5	.86	.82	243.1	.595	275.00	100
DE 83	33347	.026	7.99	T	74	$.96 \times 10^6$	2.01	101.830	136.01	208.0	186.7	197.0	.73	.69	187.4	.490	262.8	100

* TENSILE PROPERTIES OBTAINED FROM STANDARD STRAIN RATE TESTS OF .005 in./in./min

** σ_{yp} BASED ON HIGH STRAIN RATE TENSILE DATA FOR PH 17-7 (REFERENCE 26)

▲ EXPOSED # 650°F FOR 1000 HRS @ $\sigma_G = 40$ ksi

TABLE 27 FRACTURE TOUGHNESS DATA FOR 8 X 24-INCH PANELS OF PH 14-8Mo (continued)

Effect of Temperature

Figs. 218 and 219 show the effect of test temperature on fracture toughness and residual strength for 24 x 72 x 0.050-inch longitudinal panels with $2a_0 = 6$ inches tested at a stress rate of 10^6 psi/sec. The toughness of each of the heats plotted in Fig. 217 decreased with an increase in temperature.

In Fig. 219, the residual strength value for the 0.025-inch thickness is the highest at room temperature, next at 400°F, and the lowest at 650°F and -110°F.

Plots of residual strength versus panel damage are shown in Figs. 220 and 221 for the 0.025-inch and 0.125-inch thicknesses, respectively. For the 0.025-inch thickness in Fig. 220, the residual strength is not a linear function of the panel damage. This is also shown in Fig. 221 for the 0.125-inch thickness, as well as the above mentioned residual strength-temperature relationship.

Effect of Grain Direction

There is a very consistent and significant superiority of the longitudinal grain direction for fracture toughness and residual strength. Values are depicted in Figs. 222 and 223 for the 24 x 72 x 0.025-inch specimens which have $2a_0 = 6$ inches and are tested at the fastest stress rate. This superiority for the longitudinal grain direction is also shown for two 8 x 24 x 0.025-inch specimens (DD21 and DD87).

Effect of Thickness

The variations of fracture toughness and residual strength with thickness for 8 x 24-inch and 24 x 72-inch panels of heat 33347, which were tested at the highest stress rate, are illustrated in Figs. 224 and 225.

For the 24 x 72-inch longitudinal panels the fracture toughness increases with thickness at room temperature and at 650°F. Values of fracture toughness for the 8 x 24-inch transverse panels are higher for the thicker specimens at room temperature; values increase with an increase in thickness up to 0.093 inches and then decrease with a further increase in thickness at -110°F; and at 650°F there is a maximum at 0.050 inches which decreases with any change in thickness.

Residual strength increases with thickness at room temperature, -110°F, and 650°F for the 24 x 72-inch longitudinal specimens. For the 8 x 24-inch transverse specimens, residual strength increases with thickness for -110°F, room temperature, and 650°F, but then decreases with a further increase in thickness after 0.093-inches for the temperatures of -110°F and 650°F.

Effect of Crack Length

Figs 226, 227, and 228 illustrate the effect of crack length on fracture toughness. For the 24 x 72 x 0.025-inch specimens in Fig. 226, fracture toughness values increase with crack length. This is also shown for the 0.125-inch thickness in Fig. 227. The 8 x 24 x 0.025-inch specimens in Fig. 228 display a drop in fracture toughness with an increase in crack length at room temperature.

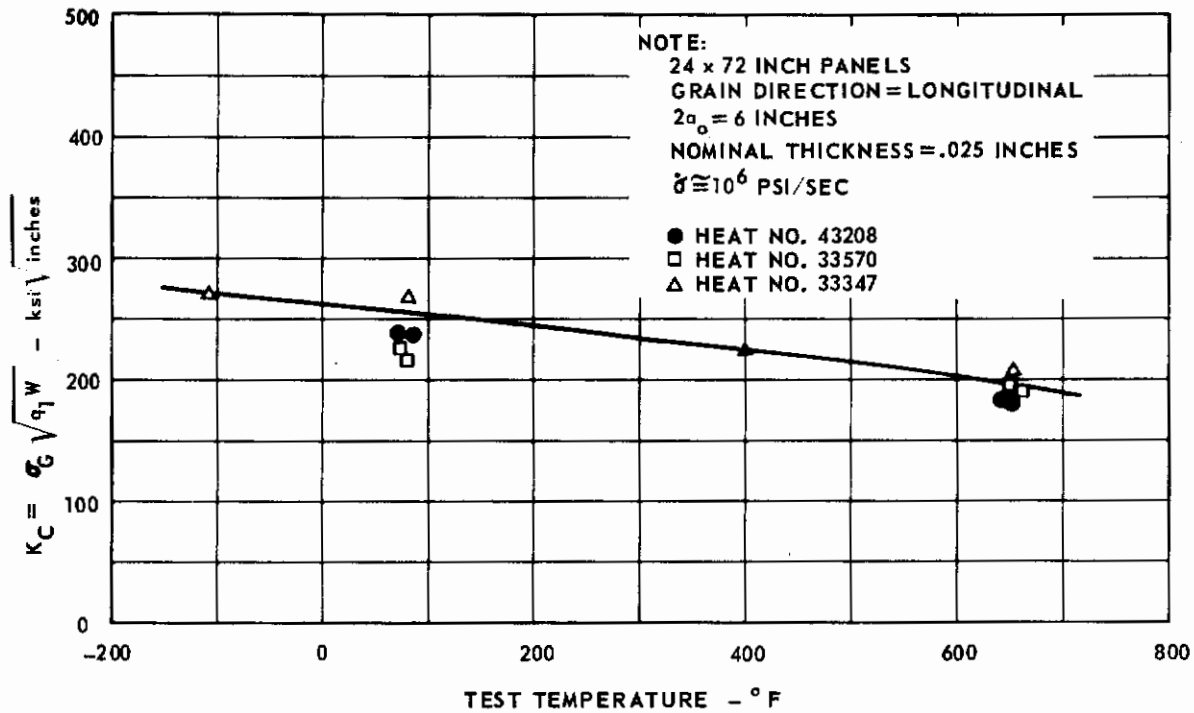


FIG. 218 EFFECT OF TEST TEMPERATURE ON K_C FOR PH 14-8 Mo

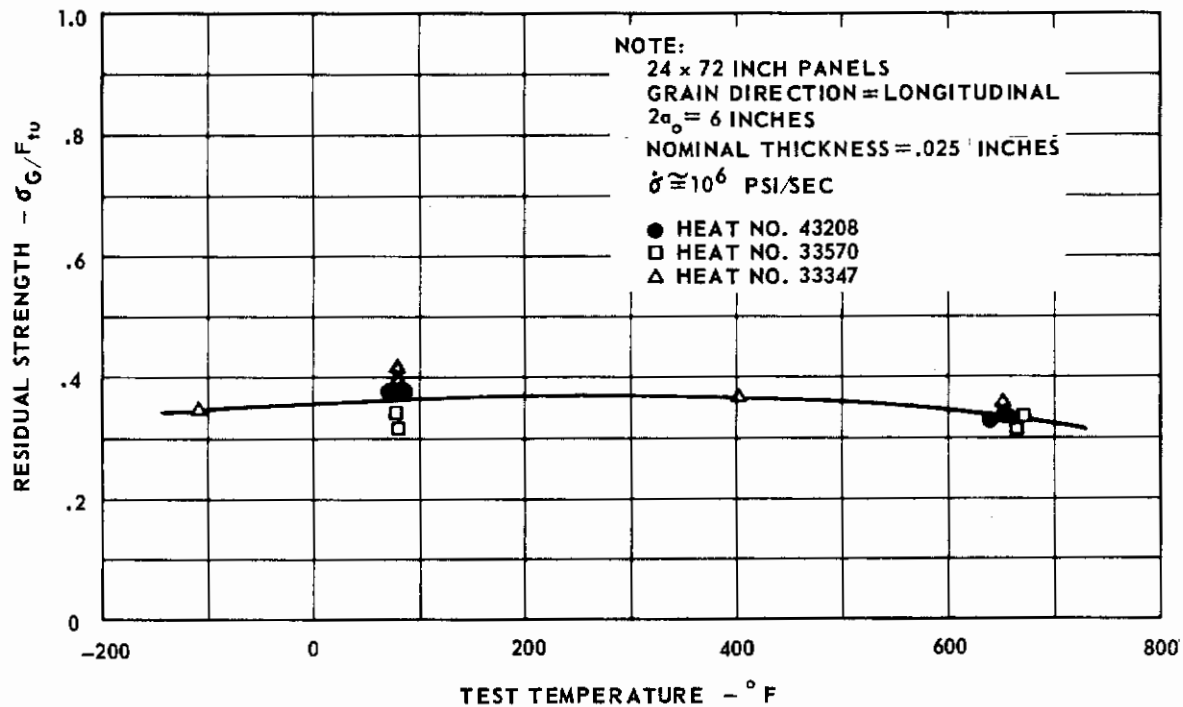


FIG. 219 EFFECT OF TEST TEMPERATURE ON RESIDUAL STRENGTH FOR PH 14-8 Mo

NOTE:

$\dot{\sigma} \approx 10^6$ PSI/SEC
LONGITUDINAL GRAIN DIRECTION

	NOMINAL THICKNESS INCHES	TEMPERATURE ° F
HEAT 33347		
○	.125	R.T.
●	.125	650
◐	.125	-110
HEAT 33570		
□	.125	R.T.
■	.125	650
◑	.125	-110

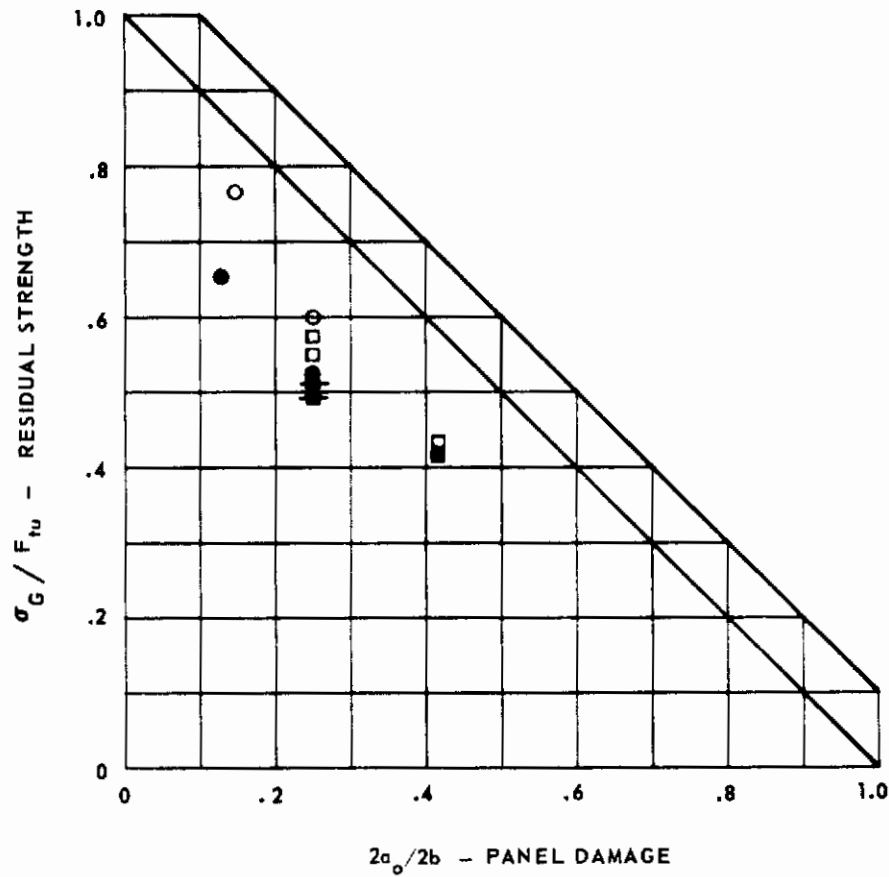


FIG. 220 RESIDUAL STRENGTH vs DAMAGE FOR 24 x 72 INCH PH 14-8 Mo PANELS, HEATS 33347 AND 33570

NOTE:

$\dot{\sigma} \approx 10^6$ PSI/SEC
 NOMINAL THICKNESS .025 INCH
 Points at $2a_0/2b = .25$ were Displaced
 Laterally to Avoid Overplotting.

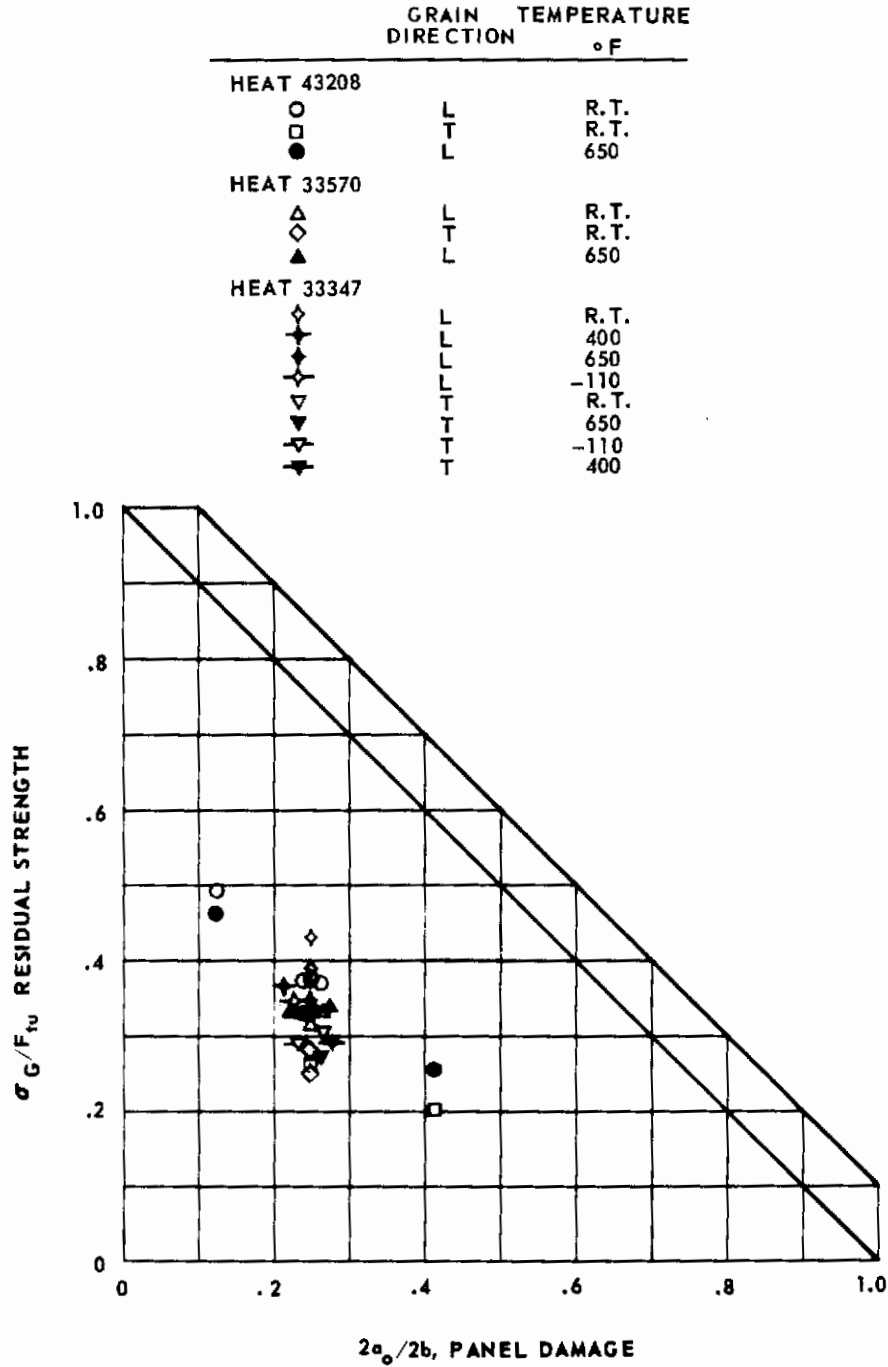


FIG. 221 RESIDUAL STRENGTH vs DAMAGE FOR 24 x 72 INCH PH 14-8 Mo PANELS, HEATS 43208, 33570 AND 33347

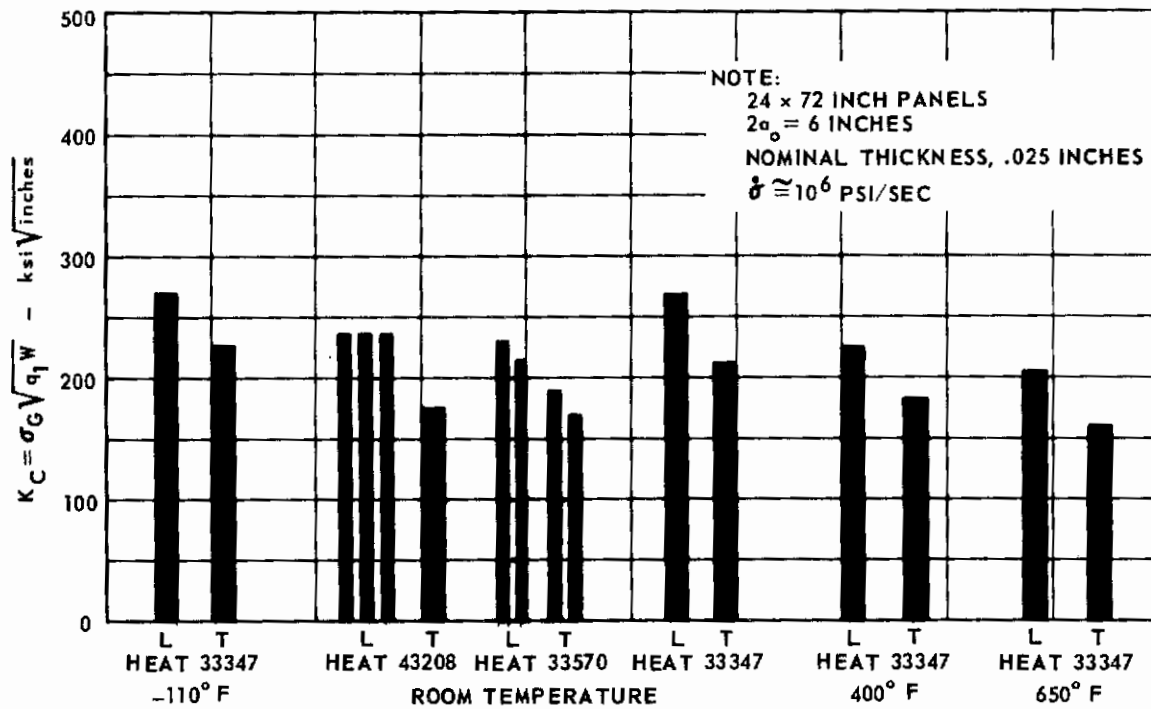


FIG. 222 VARIATION OF K_C WITH GRAIN DIRECTION WITH PH 14-8Mo

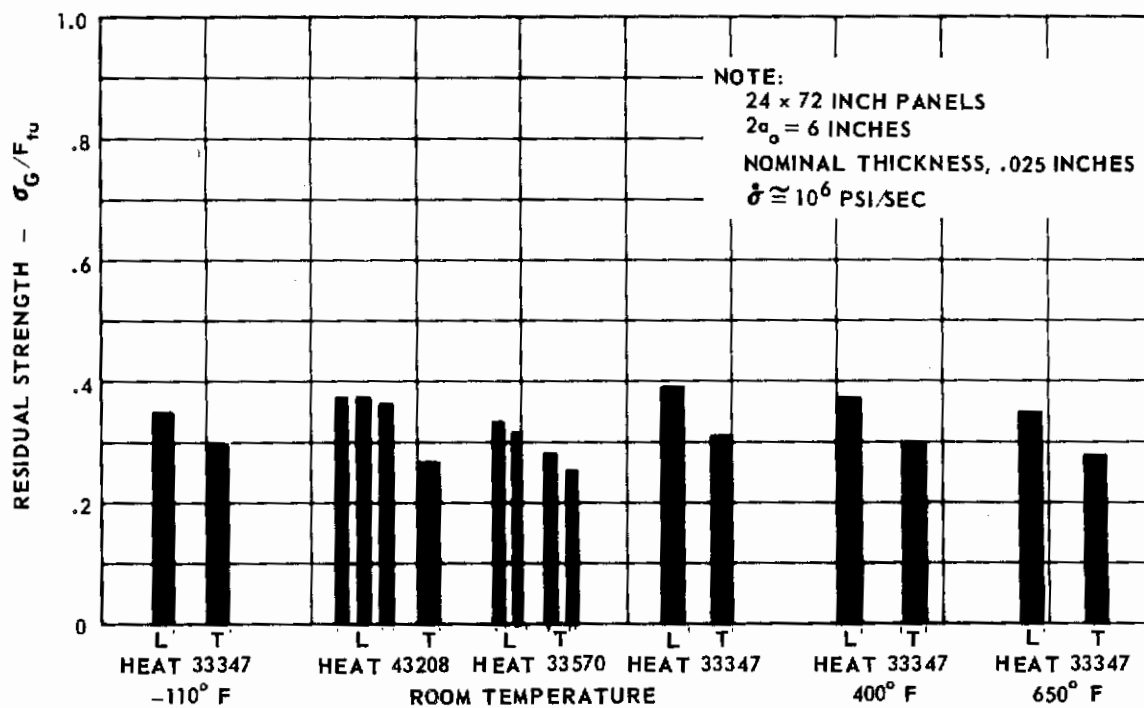


FIG. 223 VARIATION OF RESIDUAL STRENGTH WITH GRAIN DIRECTION FOR PH 14-8Mo

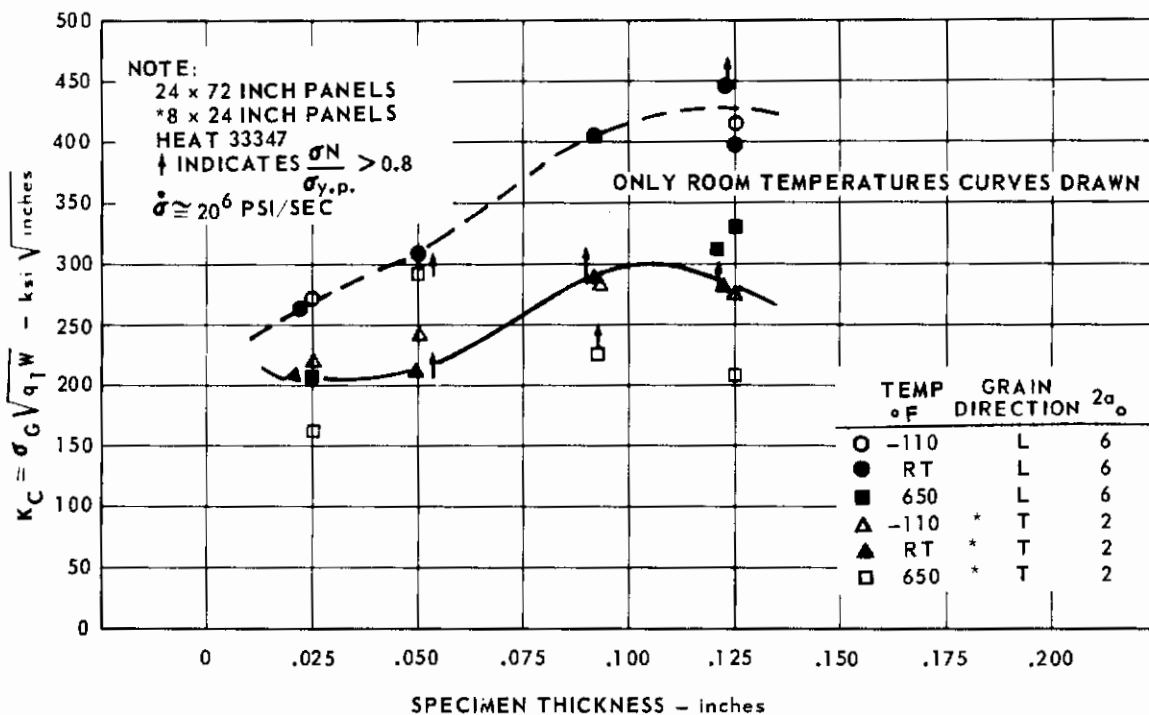


FIG. 224 VARIATION OF K_C WITH THICKNESS FOR PH 14-8 Mo

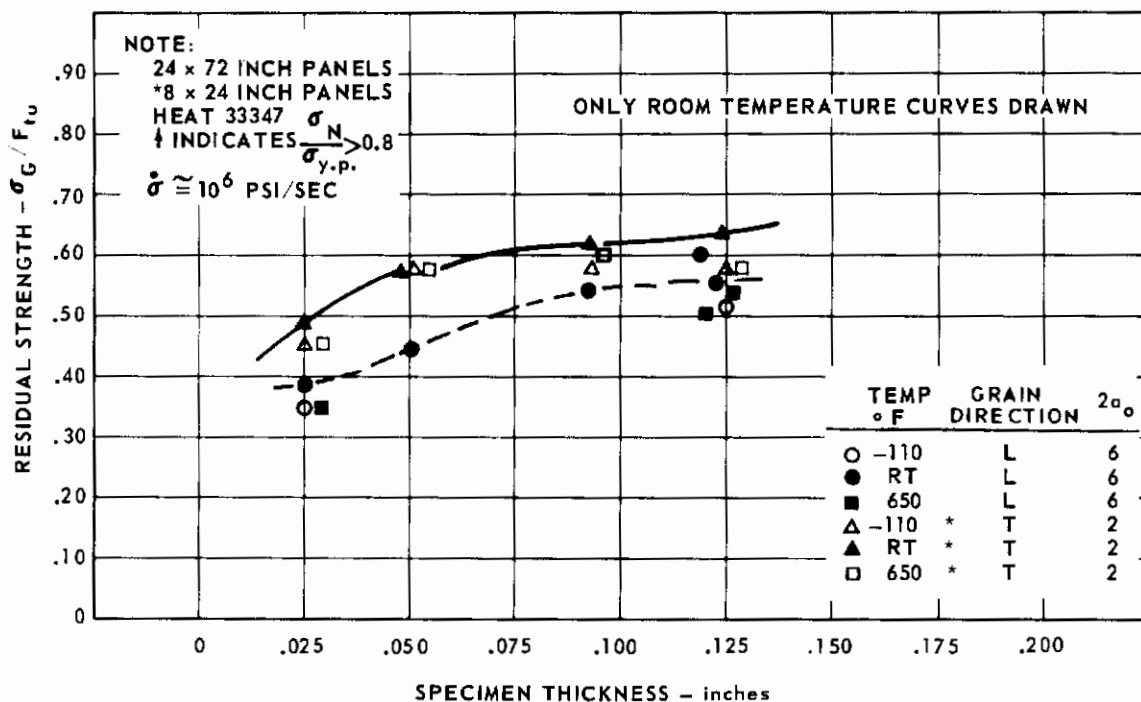


FIG. 225 VARIATION OF RESIDUAL STRENGTH WITH THICKNESS FOR PH 14-8 Mo

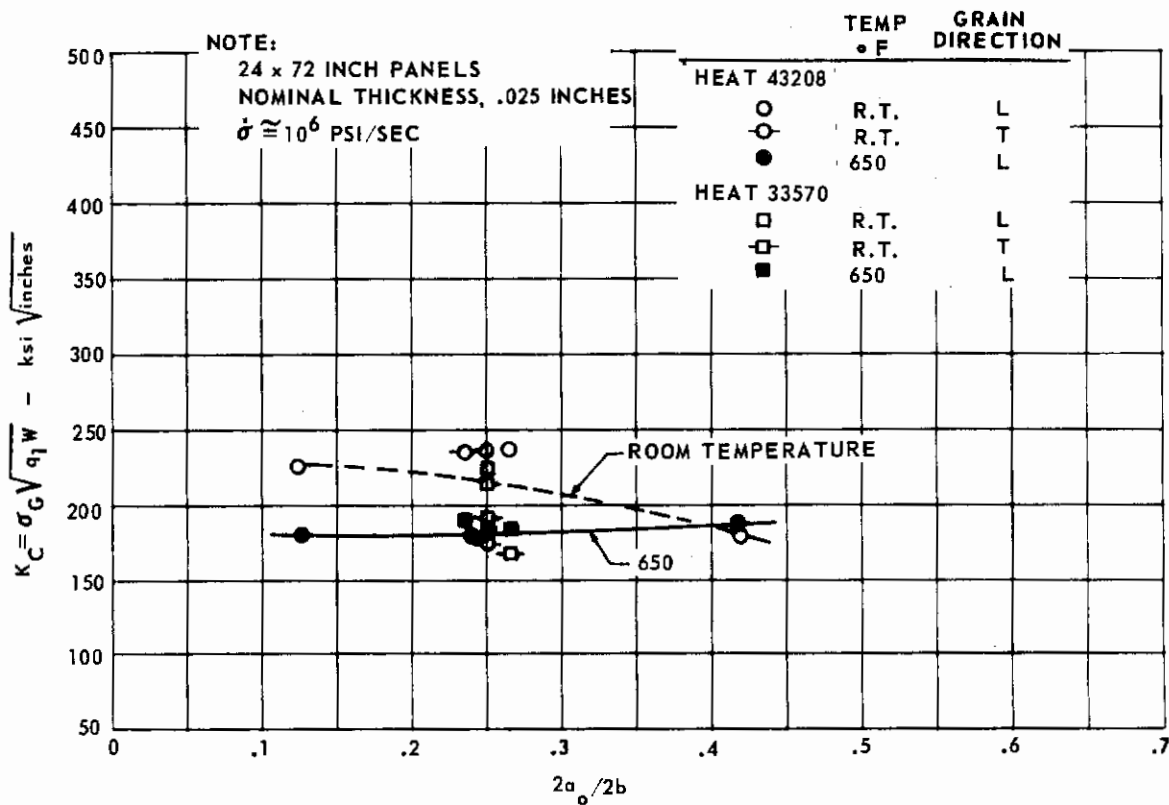
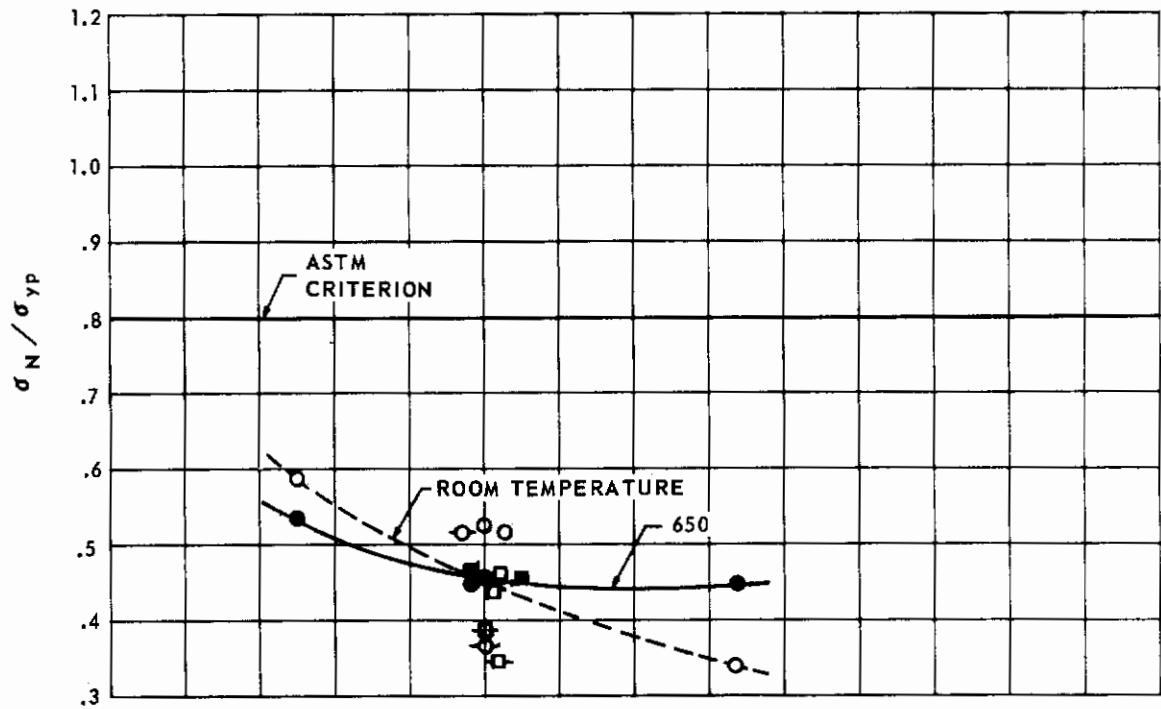


FIG. 226 VARIATION OF K_C WITH TEMPERATURE, CRACK LENGTH, AND GRAIN DIRECTION FOR PH 14-8Mo

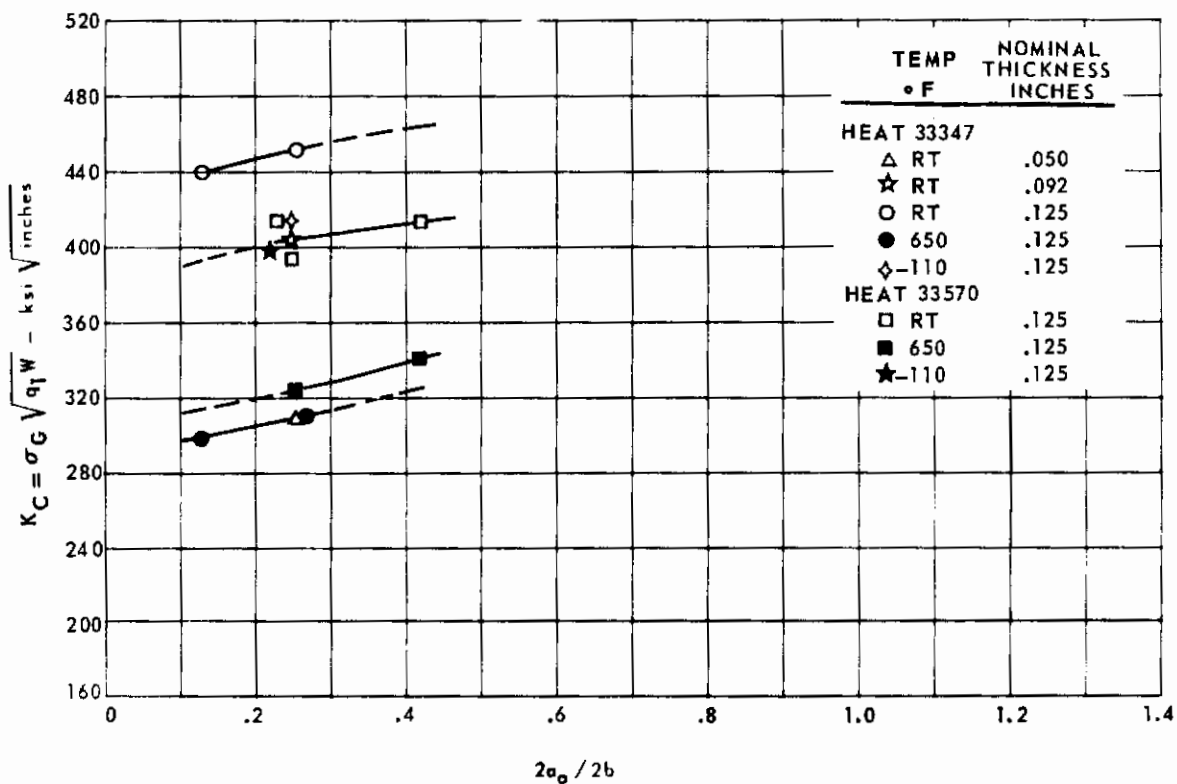
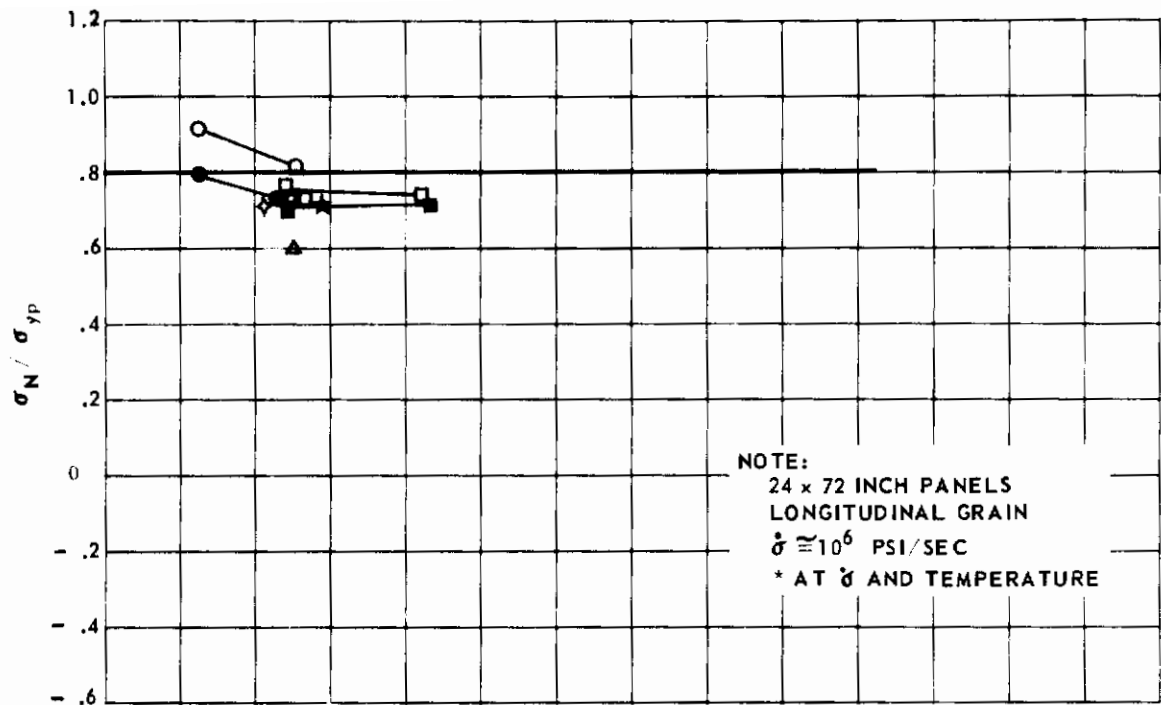


FIG. 227 VARIATION OF K_C WITH TEMPERATURE, CRACK LENGTH, THICKNESS AND GRAIN DIRECTION FOR PH 14-8Mo

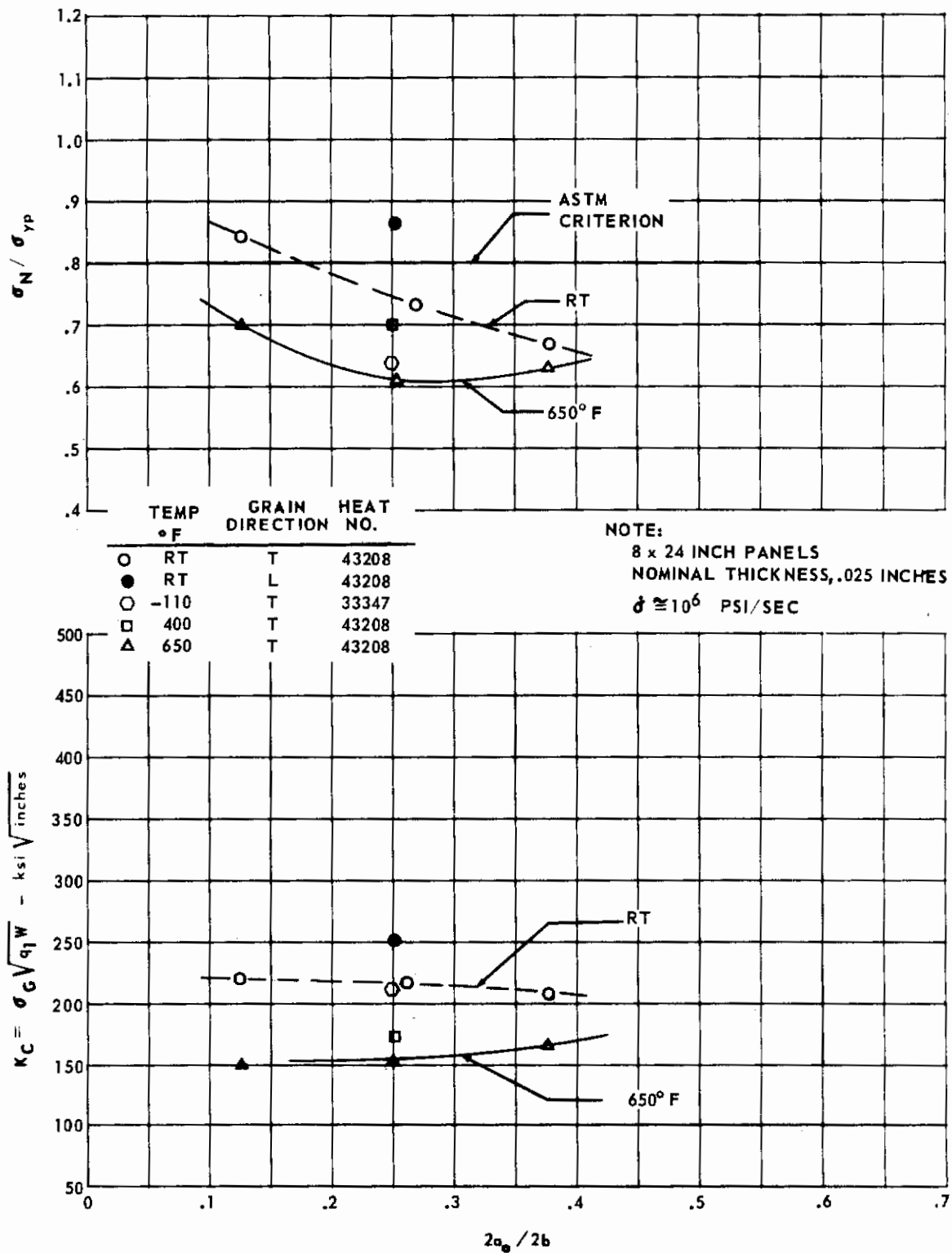


FIG. 228 VARIATION OF K_C WITH TEMPERATURE, CRACK LENGTH AND GRAIN DIRECTION FOR PH 14-8Mo

In Figs. 220 and 221, as expected, residual strength decreases nonlinearly with an increase in crack length.

Effect of Stress Rate

Fracture toughness and residual strength decrease with an increase in the stress rate. Fig. 229 shows typical data in a plot of fracture toughness versus stress rate. When the rate is increased to 10^6 psi/sec, this decrease in fracture toughness is shown to be on the order of 10 to 20 percent of the value for the rate of 5×10^3 psi/sec. Decreases in residual strength are on the order of 8 to 15 percent of the value for the rate of 5×10^3 psi/sec, when the rate is increased to 10^6 psi/sec.

Effect of Exposure

Fig. 230 shows that the exposed specimens have average fracture toughness values which are higher than the unexposed specimens for the 0.025 and 0.050-inch thickness but lower for the 0.125-inch thickness.

For residual strength, the value of the exposed 0.025-inch thickness is about 3 percent higher than the value of the unexposed material, exposed and unexposed strengths are approximately equal for the 0.050-inch thickness, and the strength of the exposed 0.125-inch thickness is about 8 percent lower than the unexposed residual strength.

Effect of Heat and/or Heat Treatment

Considering that the 0.025-inch thickness of each heat was heat treated separately, the significant differences in values of fracture toughness and residual strength between the heats must be attributed to the heat and/or the heat treatment variables.

Effect of Panel Size

More conservative values of fracture toughness are found for the 8 x 24-inch panel size. This may be explained in part by the consistently higher ratios of σ_N/σ_{yp} obtained with 8 x 24-inch panel tests. Conversely, more conservative values of residual strength are found by using the 24 x 72-inch panel size.

Fractographic Studies

Macrophotographs showing the fracture surfaces for the PH 14-8Mo specimens DE21 and DE74 are included in Figs. 230 and 231. Electron micrographs are included on each figure to show the detailed characteristics found from the electron microscope survey.

Striations were found within the fatigue regions of both specimens. The rapid fracture areas showed characteristic dimples in most areas. Some evidence of banding was believed to be indicated by the fractographic studies.

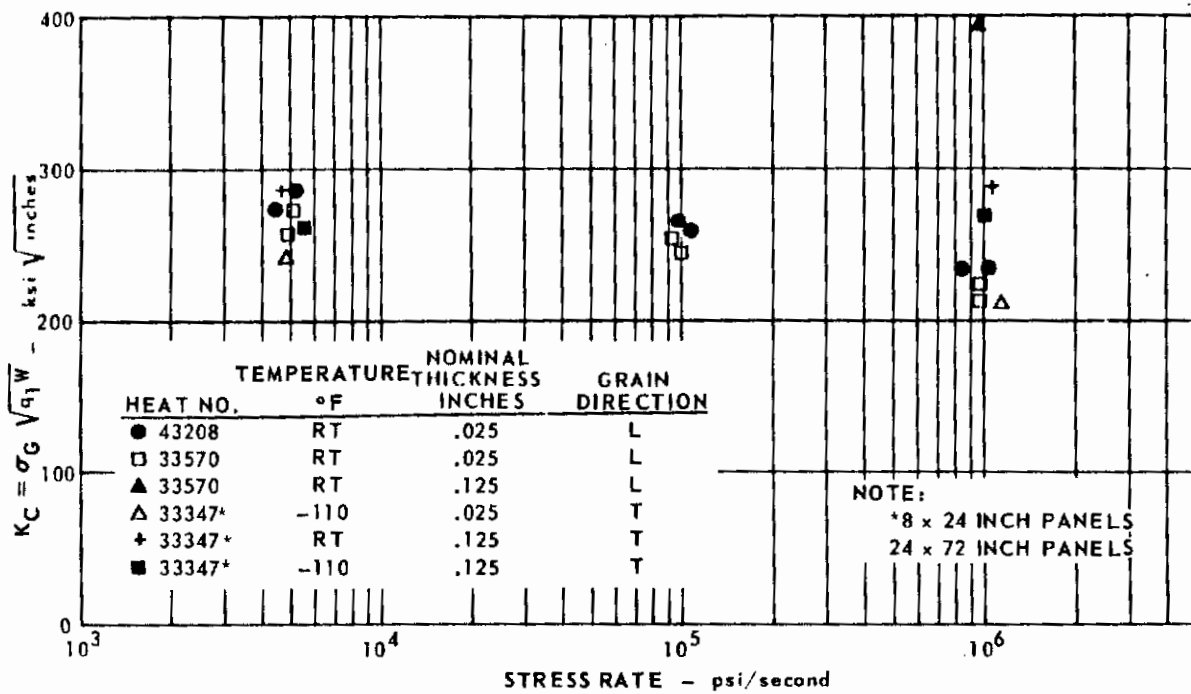


FIG. 229 THE EFFECT OF STRESS RATE ON K_C FOR PH 14-8Mo

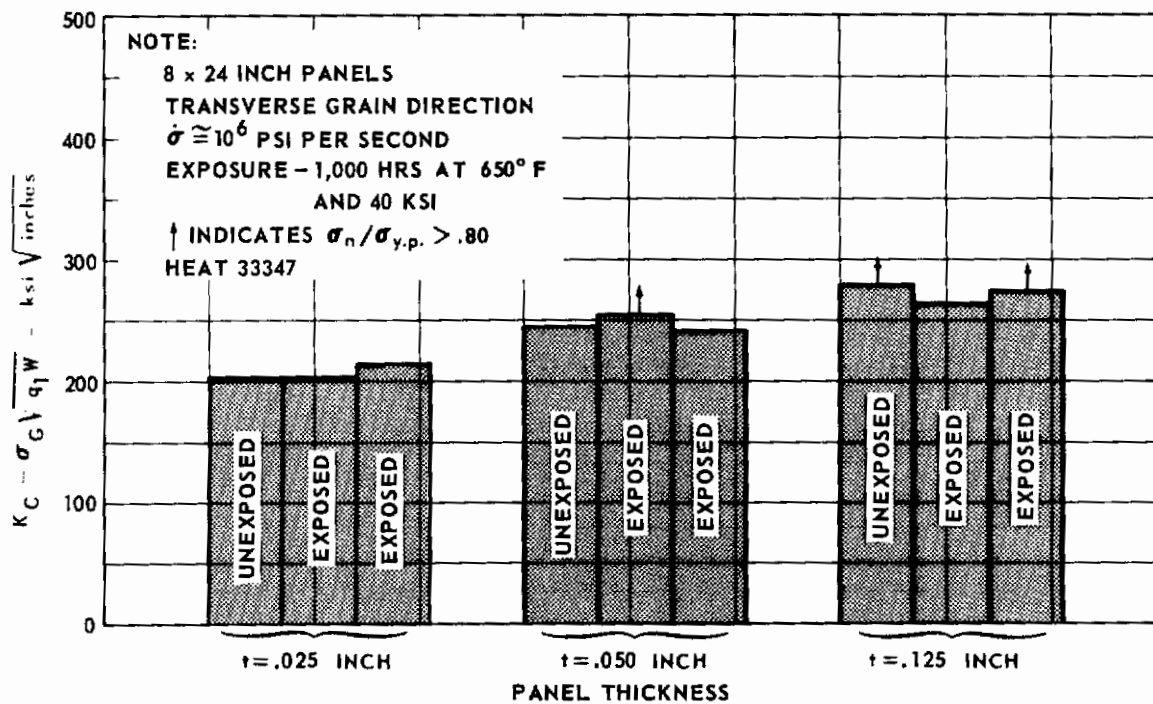
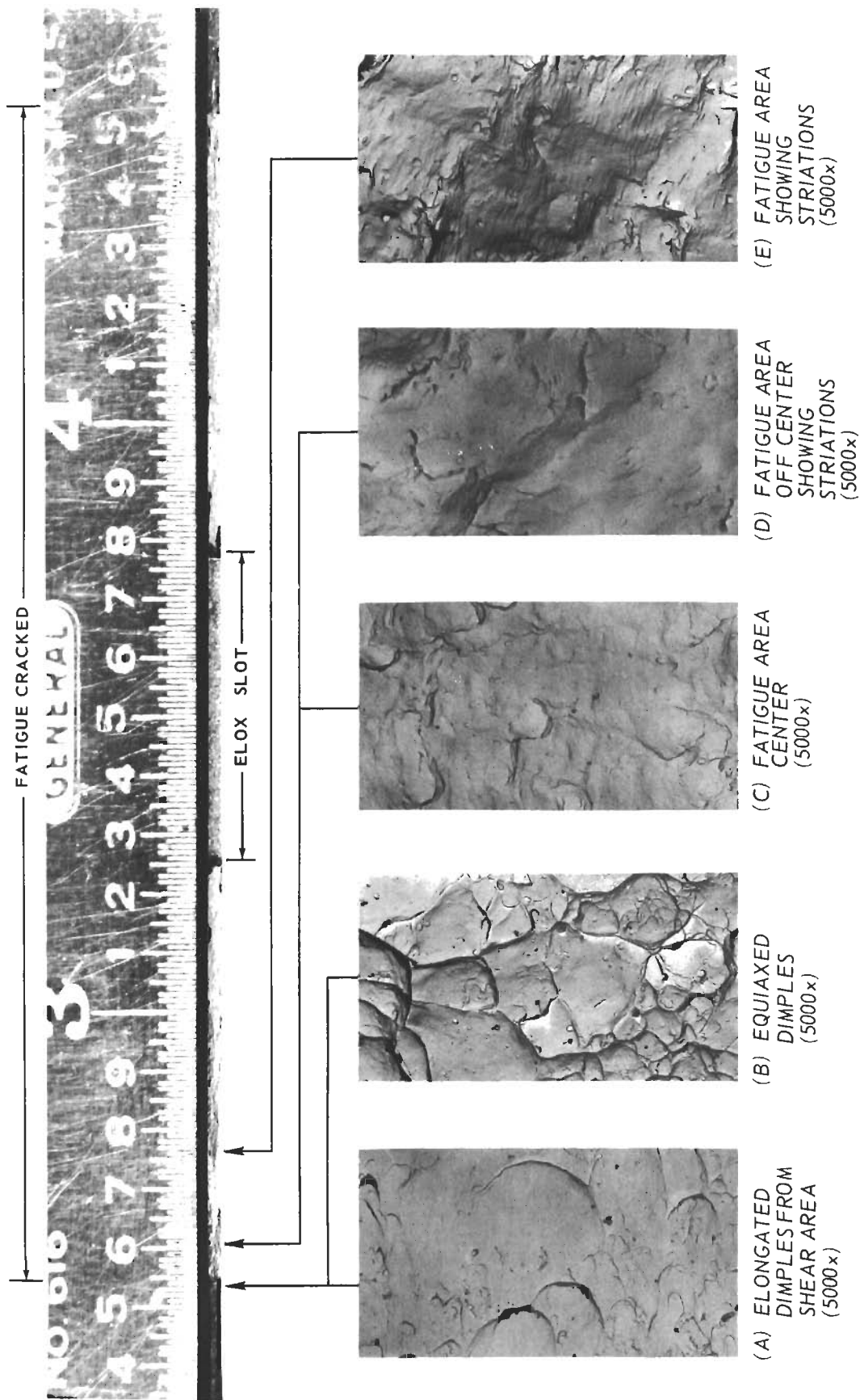
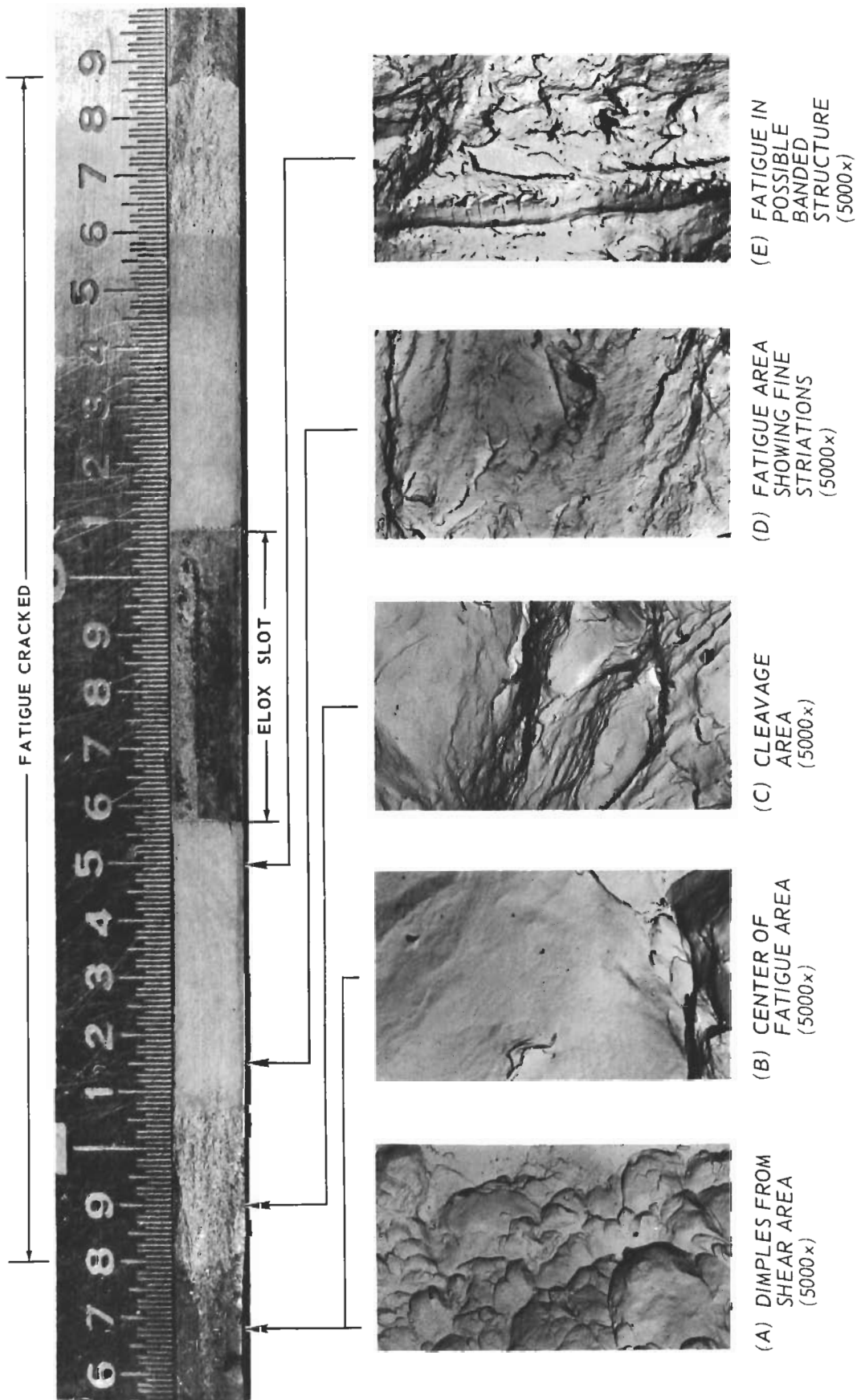


FIG. 230 COMPARISON OF EXPOSED AND UNEXPOSED K_C VALUES FOR PH 14-8Mo



NOTE: Fatigue Cracked and Fractured at Room Temperature

FIG. 231 FRACTOGRAPHIC STUDY OF PH 14 - 8Mo SPECIMEN DE21



NOTE: Fatigue Cracked and Fractured at Room Temperature

FIG. 232 FRACTOGRAPHIC STUDY OF PH 14 - 8 Mo SPECIMEN DE74

COORDINATION TESTING

The Boeing Company and North American Aviation, Inc.

A small program was initiated to check the agreement between the testing facilities at Boeing and North American Aviation. For this purpose Boeing and North American each tested three Ti 6Al-4V, 8 x 24-inch specimens made from one 0.050 inch thick sheet of heat D4949. Test conditions were identical for all specimens. Each specimen was cycled at 120 cpm, at a gross stress level of 25 ksi, to grow a 2.00 fatigue crack from a 0.50-inch starter notch. Specimens were then statically fractured at a stress rate of 10^6 psi/sec at room temperature.

Fig. 233 shows the crack growth data. Because the initial notches were slightly longer for the specimens tested at Boeing, and also because the determination of dwell cycles has a certain degree of inaccuracy, the average cycles required to grow the 2.0 inch crack for the Boeing specimens are approximately ten percent less than the average cycles required for the specimens tested at North American Aviation. However, the fatigue crack growth rate shown in Fig. 234 displays excellent agreement; this plot eliminated the influence of the initial notch length and determination of dwell cycles on the data.

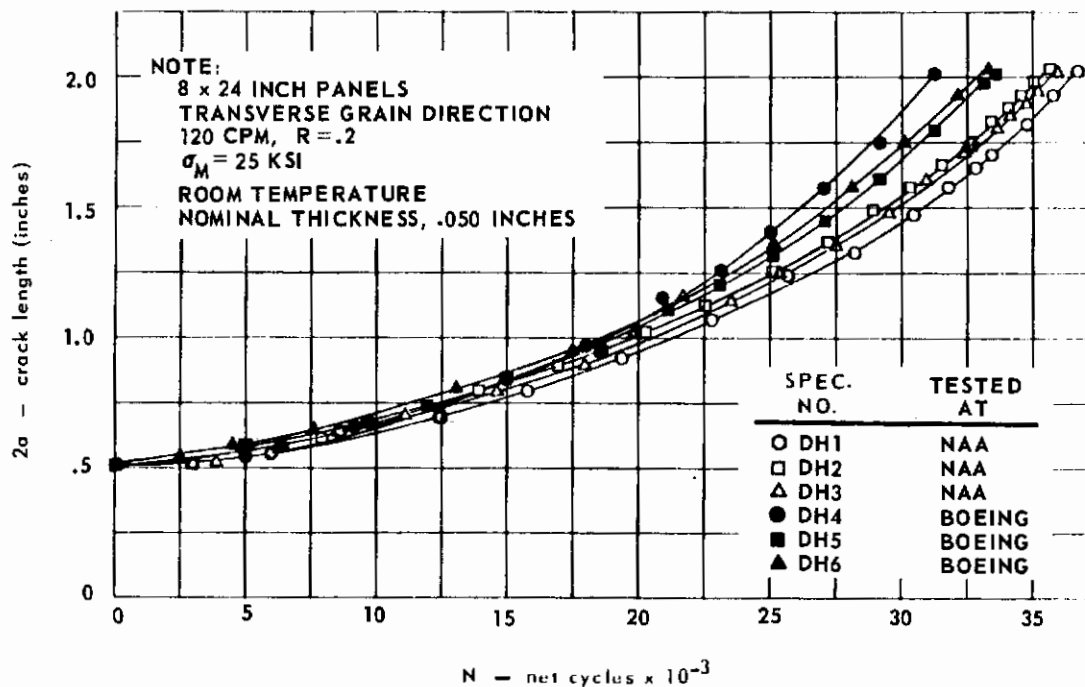


FIG. 233 COORDINATION TESTING CRACK GROWTH DATA FOR Ti 6Al-4V

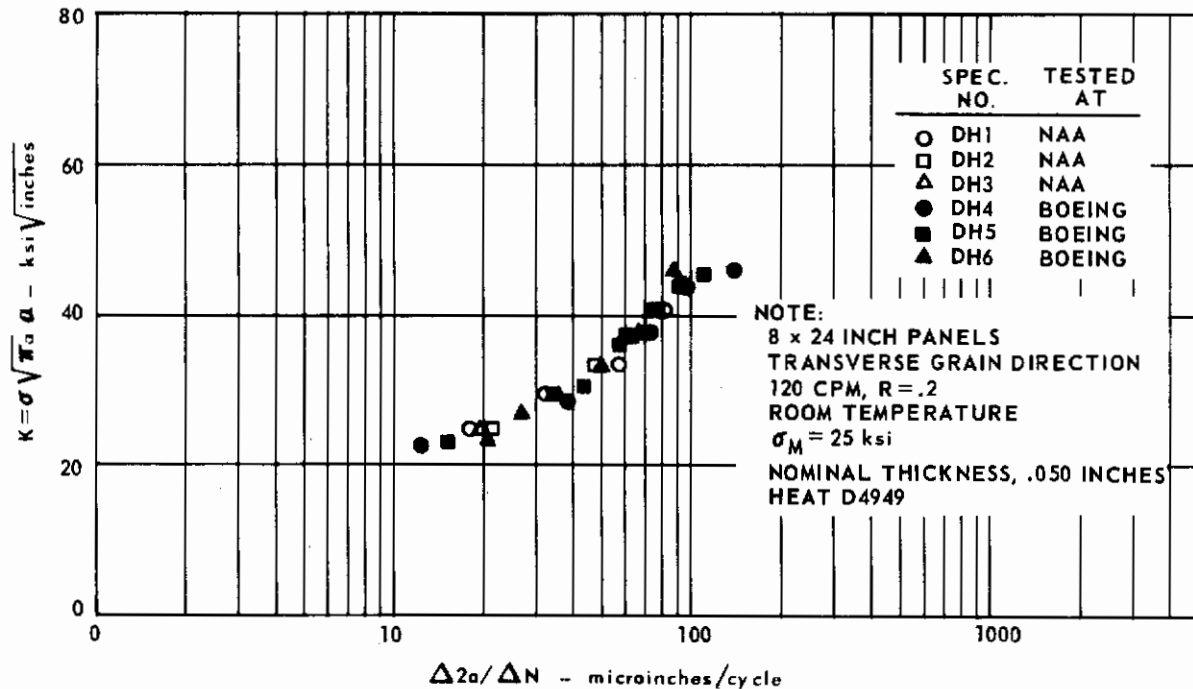


FIG. 234 COORDINATION TESTING CRACK GROWTH RATE DATA FOR Ti 6Al-4V

A summary of fracture toughness test data is shown in Table 28; more detailed data are given in Table 22.

The test data from the two testing facilities show excellent agreement. Boeing tests were made at a slightly higher loading rate than the North American Aviation tests and this difference is reflected by a small but consistent difference in fracture data. Both residual strength and K_{IC} are higher for the highest loading rate data.

The Joint Venture and The Douglas Aircraft Company

Six, Ti 8Al-1Mo-1V (triplex anneal), specimens were purchased from the Douglas Aircraft Company for coordination testing. The purpose of this testing was to determine if there was any difference between test data obtained from the various test facilities and to provide data on the effect of stress rate.

Specifically, the six 8 x 24-inch Ti 8Al-1Mo-1V specimens were from heat D3369, which was reported in Ref. 1. Specimen data are contained in Table 29. The specimens as received from Douglas had only to have the center notch machined prior to testing.

Each specimen was cycled at 120 cpm and at a gross stress level of 25 ksi, $R = 0.2$, for at least the last 0.5 inches of fatigue crack growth. After fatigue crack growth, the specimens were fractured at room temperature at a stress rate of approximately 1.67×10^3 and 10^6 psi/sec.

TABLE 28 COORDINATION TESTING FRACTURE TOUGHNESS DATA FOR 8 x 24 INCH
Ti 6Al-4V PANELS

SPECIMEN NO.	ACTUAL THICKNESS inches	σ_G ksi	$\dot{\sigma}$ psi/sec	$\frac{\sigma_G}{F_{tu}}$	$K_{CN} = \sigma_G \sqrt{\pi a_0} a$ ksi \sqrt{in}	$K_C = \sigma_G \sqrt{a_1 W}$ ksi \sqrt{in}
DH1	.049	86.335	.964x10 ⁶	.620	158.5	178.0
DH2	.049	86.845	.945x10 ⁶	.624	159.4	179.5
DH3	.049	88.123	.968x10 ⁶	.633	161.7	184.5
DH4	.049	87.350	1.12x10 ⁶	.628	160.2	178.3
DH5	.049	87.920	1.14x10 ⁶	.632	161.2	179.6
DH6	.0488	91.957	1.15x10 ⁶	.661	168.6	190.4

TABLE 29 COORDINATION TESTING SPECIMEN AND TEST DATA FOR Ti 8Al-1Mo-1V

TESTED BY	PANEL CODE	WIDTH inches	GROSS AREA sq in.	2a ₀ inches	TEST TEMP °F	P _{MAX} kips	2a ₀ /2b	$\dot{\sigma}$ psi/sec	σ ksi	σ/F_{tu}
DOUGLAS	15T9	7.997	.2039	2.032	80	13.8	.254	1.67x10 ³	67.68	.434
DOUGLAS	15T10	7.996	.1983	2.026	80	13.1	.253	1.67x10 ³	64.66	.419
NORTH AMERICAN	17T2	8.00	.216	2.00	74	16.2	.250	1.56x10 ³	75.00	.489
NORTH AMERICAN	17T3	8.00	.216	2.00	70	16.4	.250	1.67x10 ³	75.93	.495
NORTH AMERICAN	17T4	8.00	.216	2.00	72	16.5	.250	1.58x10 ³	76.39	.498
BOEING	----	8.00	.212	1.99	67	18.8	.250	.93x10 ⁶	88.68	.578
BOEING	----	8.00	.216	2.00	67	19.0	.250	.86x10 ⁶	88.15	.575
BOEING	----	8.00	.212	2.00	68	19.0	.250	.82x10 ⁶	83.68	.585

NOTE: TRIPLEX ANNEALED

t = .025 INCH NOMINAL THICKNESS

HEAT D3369

F_{TU} = 153.3 ksi

F_{TY} = 137.0 ksi

NOTE:
 WIDTH = 8.00 INCHES
 TRANSVERSE GRAIN
 ROOM TEMPERATURE
 NOMINAL THICKNESS, .025 INCHES
 HEAT D3369
 TRIPLEX ANNEALED
 COORDINATION TESTED BY NAA AND DAC

○ DAC
 - - - AVERAGE LINE BY DAC, REFERENCE 1
 △ NAA

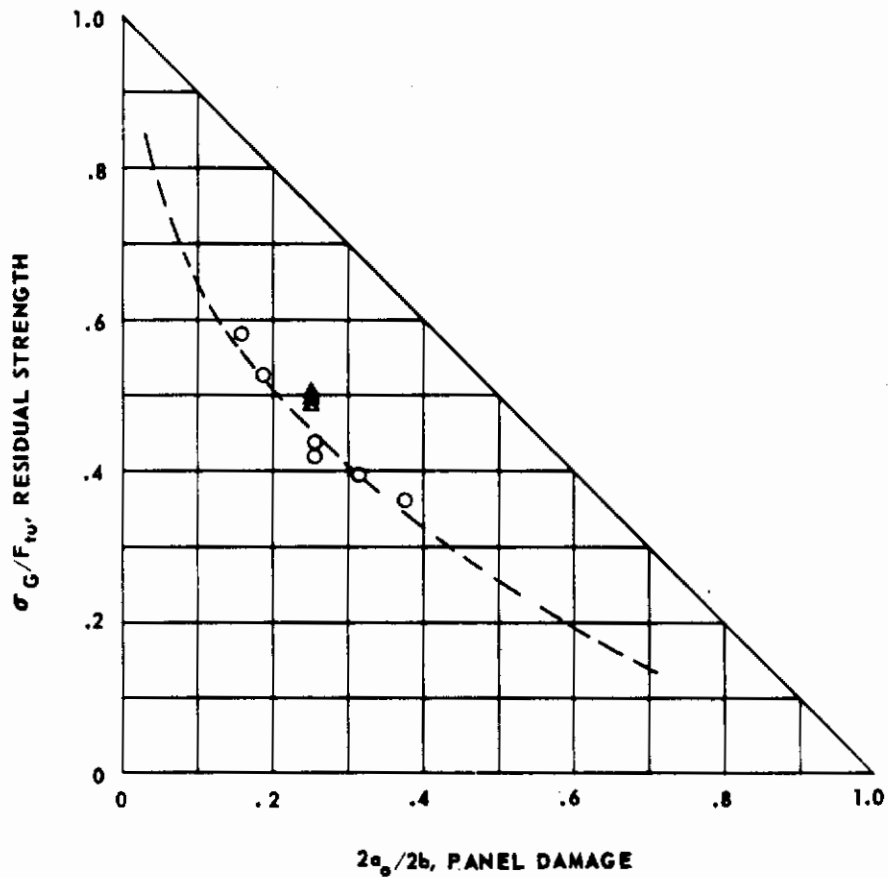


FIG. 235 COORDINATION TESTING RESIDUAL STRENGTH AND DAMAGE COMPARISON FOR Ti 8Al-1Mo-1V PANELS

The test data are listed in Table 29. Fig. 236 shows the residual strength for the specimens tested at North American is slightly above the average curve for the specimens tested at Douglas. In consideration of the scatter in the data for this alloy in both programs, the data agrees.

Fig. 235 shows residual strength versus stress rate for all the specimens. Data for duplex annealed material which were generated by the Joint Venture are included in Fig. 235 to display the influence of stress rate on residual strength. The dashed curve was drawn parallel to the curve through the duplex annealed material to establish a reference line for comparing the coordination testing.

The Douglas tests were made with standard tensile test equipment whereas the Joint Venture tests were made with testing equipment specially designed for fracture testing. The slightly lower Douglas test data may be due to differences in the test equipment. As shown in the previous subsection, testing between the Joint Venture companies shows excellent agreement.

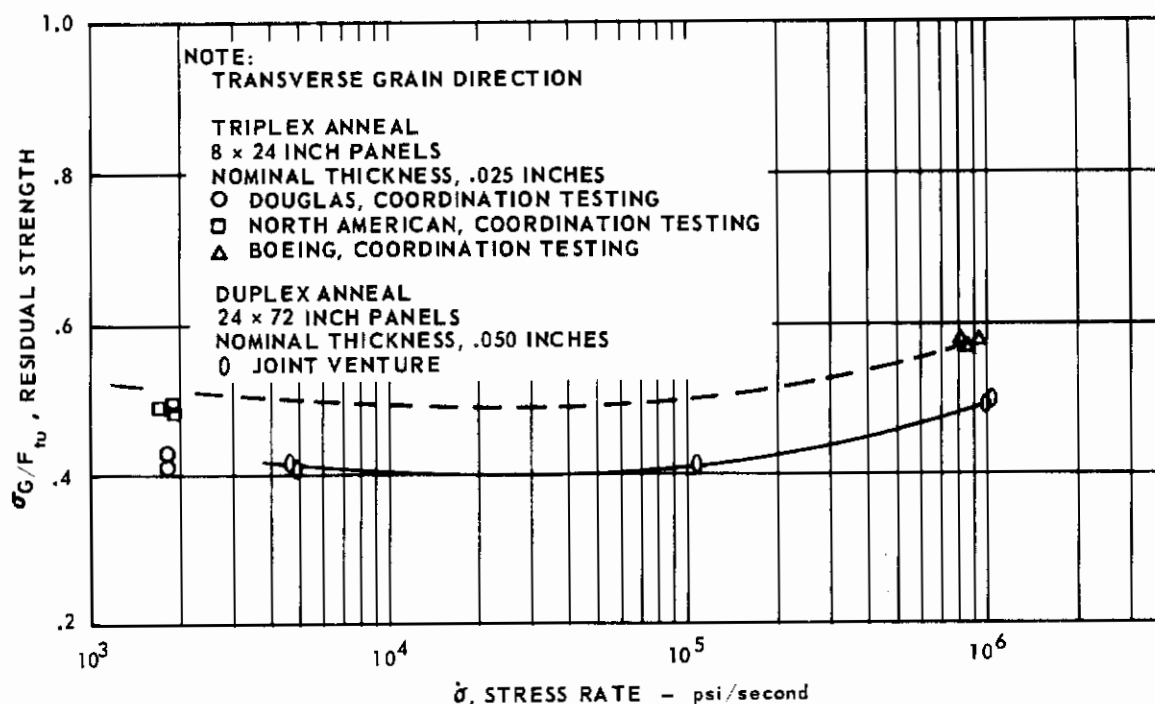


FIG. 236 COORDINATION TESTING RESIDUAL STRENGTH AND STRESS RATE RELATIONSHIP FOR Ti 8Al-1Mo-1V

Contrails

SECTION 7 COMPARISON OF ALLOYS

The alloys which were tested in this program are compared within this section only with regard to the specific properties examined.

FATIGUE CRACK GROWTH

Fig.237 shows the conservative boundary of the fatigue crack growth rate scatter band which was drawn for each alloy. Each scatter band included data for both grain directions of the 8-inch and 24-inch wide specimens which were cycled at stress ratios of 0.20 and 0.05. By using these stress intensity versus crack growth rate curves, it is shown that:

- 1) At K levels below $60 \text{ ksi}\sqrt{\text{inches}}$, both titanium alloys exhibit the most rapid crack growth rate. In this region, the Ti 6Al-4V alloy has the highest rate of crack propagation, followed by the Ti 8Al-1Mo-1V, AM 350, PH 14-8Mo, and Inco 718 alloys in that order.
- 2) At a K level of $80 \text{ ksi}\sqrt{\text{inches}}$, the alloys rank as follows in the order of decreasing crack growth rate: Ti 6Al-4V, AM 350, Ti 8Al-1Mo-1V, PH 14-8Mo, and Inco 718.

By taking the unit weight into consideration in Fig.238, which is of importance for design application, the order of the alloys changes significantly:

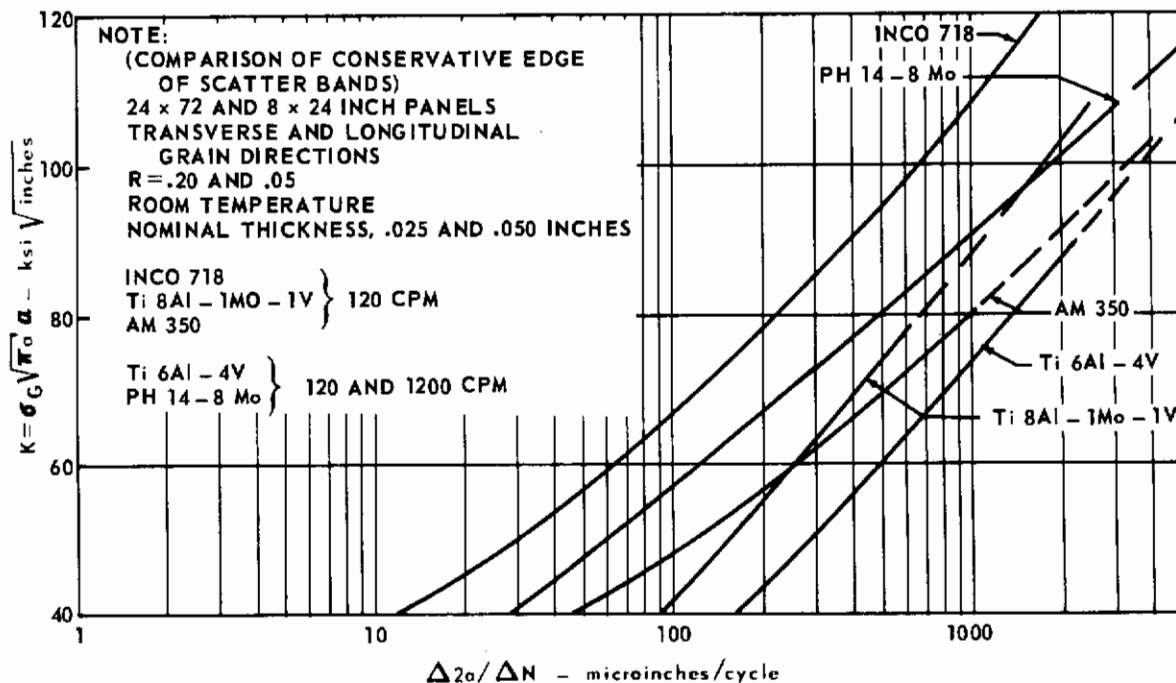


FIG. 237 COMPARISON OF CRACK GROWTH RATE FOR ALL ALLOYS, DENSITY NOT CONSIDERED

Below a stress intensity to density ratio of approximately 140, the order is practically the same as shown in Fig. 237 for values of the stress intensity less than 60.

Above a stress intensity to density ratio of approximately 260, the titanium alloys have crack growth rates which are less than those for the other alloys. A stress intensity to density ratio of 260 corresponds to a stress intensity value of 41 for the Ti 8Al-1Mo-1V and 42 for the Ti 6Al-4V. This corresponds further to an operating stress of approximately 33 ksi for a 1-inch crack length or an operating stress of approximately 46 ksi for a 1/2-inch crack length. Thus, this value for the stress intensity to density ratio is realistic for the titanium alloys. In a like manner this may also be shown for the steel and nickel base alloys.

On this basis, the alloys are rated for their fatigue crack growth properties in the following order:

- 1) Ti 8Al-1Mo-1V (Duplex Anneal) (Best)
- 2) Ti 6Al-4V (Mill Anneal)
- 3) Inco 718
- 4) PH 14-8Mo (SRH 1050)
- 5) AM 350 SCT 850 (Worst)

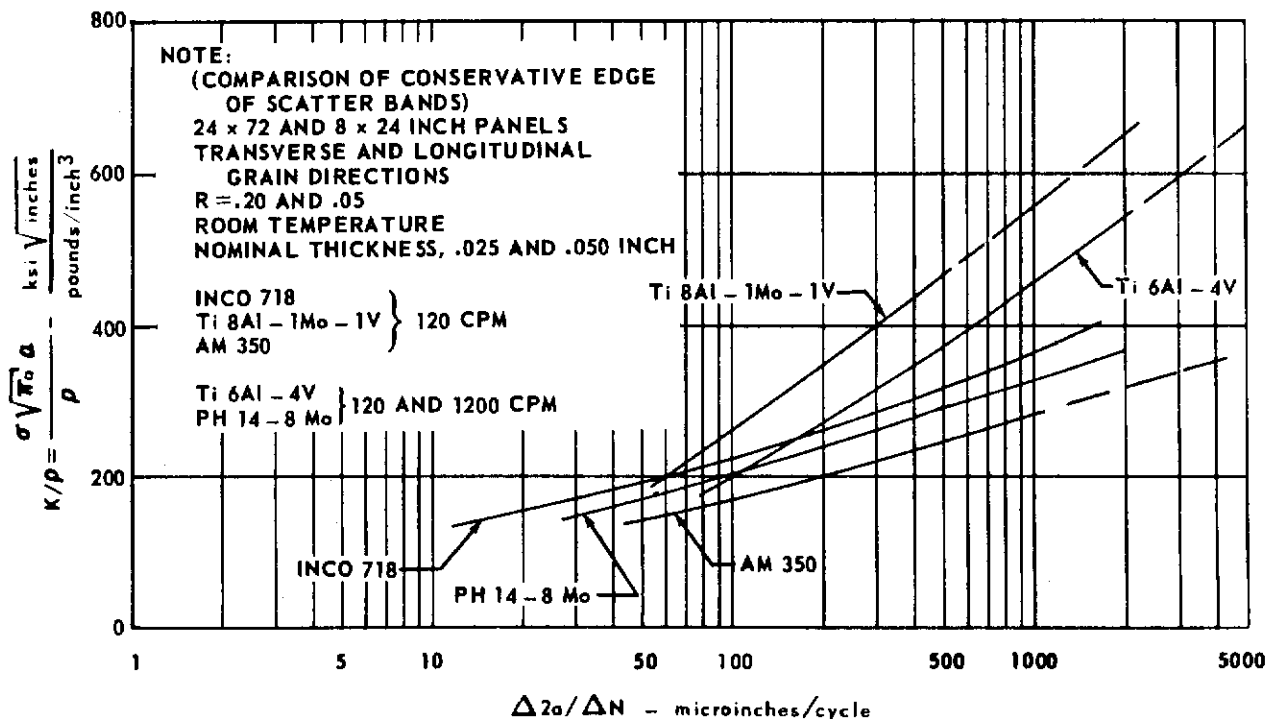


FIG. 238 COMPARISON OF CRACK GROWTH RATE FOR ALL ALLOYS, DENSITY CONSIDERED

FRACTURE PROPERTIES

Residual Strength

A comparison is made of the residual strength as a function of temperature for the principal thickness of each alloy in Fig. 239. This is based on the data for the 24 x 72-inch panel having a 6-inch crack and being tested at a stress rate of 10^6 psi/sec.

Using the value for the grain direction having the lower residual strength at each test temperature, the alloys are rated in Table 30, with the order of merit decreasing from 1 to 5.

With this approach, the general ranking of the alloys is:

- 1) Ti 6Al-4V (Mill Anneal) (Best)
- 2) Ti 8Al-1Mo-1V (Duplex Anneal)
- 3) Inco 718
- 4) AM 350 SCT 850
- 5) PH 14-8Mo (SRH 1050) (Worst)

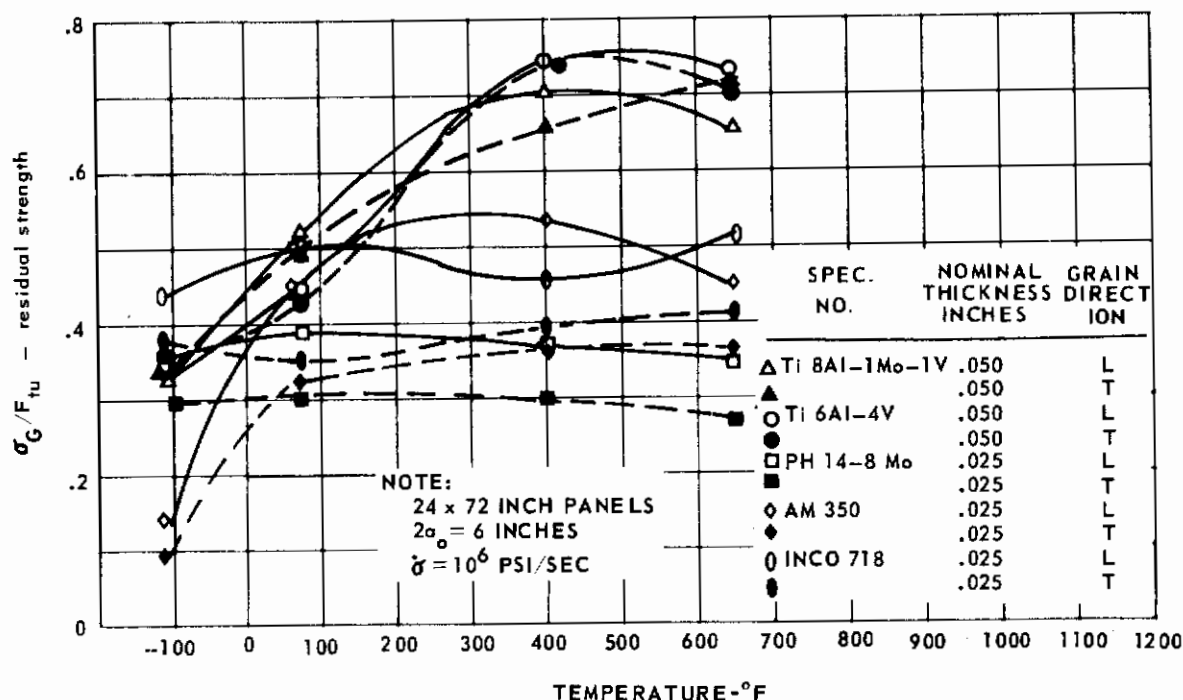


FIG. 239 VARIATION OF THE RESIDUAL STRENGTH WITH TEMPERATURE FOR ALL ALLOYS

TABLE 30 RATING OF RESIDUAL STRENGTH AT TEMPERATURE FOR ALL ALLOYS

	-110° F	ROOM TEMPERATURE	400° F	650° F
Ti 8Al-1Mo-1V (DUPLEX ANNEAL)	3	1	2	2
Ti 6Al-4V (MILL ANNEAL)	2	2	1	1
AM 350 (SCT 850)	5	4	4	4
PH 14-8 Mo (SRH 1050)	4	5	5	5
INCO 718	1	3	3	3

Fracture Toughness

The variation of fracture toughness with temperature is shown in Fig. 241. The fracture toughness to density ratio as a function of temperature is plotted for the principal thickness of each alloy in Fig. 240. These plots are made for 24 x 72-inch panels having a 6-inch crack length and tested at a stress rate of 10^6 psi/sec.

By using the more conservative grain direction for each alloy at the temperatures tested and considering density, the alloys are rated in Table 31 with the order of merit decreasing from 1 to 5.

This results in the following general ranking of alloys:

- 1) Ti 8Al-1Mo-1V (Duplex Anneal) (Best)
- 2) Ti 6Al-4V (Mill Anneal)
- 3) Inco 718
- 4) AM 350 SCT 850
- 5) PH 14-8Mo (SRH 1050) (Worst)

TABLE 31 RATING OF FRACTURE TOUGHNESS/DENSITY AT TEMPERATURE FOR ALL ALLOYS

	-110° F	ROOM TEMPERATURE	400° F	650° F
Ti 8Al-1Mo-1V (DUPLEX ANNEAL)	1	1	2	2
Ti 6 Al-4V (MILL ANNEAL)	2	2	1	1
AM 350 (SCT 850)	5	4	4	4
PH 14-8 Mo (SRH 1050)	4	5	5	5
INCO 718 (CRA)	3	3	3	3

NOTE:

24 x 72 INCH PANELS

2a = 6 INCHES

$\dot{\sigma} = 10^6$ PSI/SEC

$K_C = \sigma \sqrt{q_1 W}$

↑ INDICATES $\sigma_N / \sigma_{y.p.} = .80$

	NOMINAL THICKNESS INCHES	GRAIN DIRECTION	ALLOY	DENSITY pounds/inches ³	CONDITION	HEAT NO.
○	.050	L	Ti 6Al-4V	.161	MILL ANNEAL	4949
●	.050	T	Ti 6Al-4V	.161	MILL ANNEAL	4949
△	.025	L	PH 14-8 Mo	.278	SRH 1050	33347
▲	.025	T	PH 14-8 Mo	.278	SRH 1050	33347
□	.050	L	Ti 8Al-1Mo-1V	.158	D. ANN	3457
■	.050	T	Ti 8Al-1Mo-1V	.158	D. ANN	3457
○	.025	L	AM 350	.283	SCT 850	19020
●	.025	T	AM 350	.283	SCT 850	19020
○	.025	L	INCO 718	.296	CRA	6902
●	.025	T	INCO 718	.296	CRA	6902

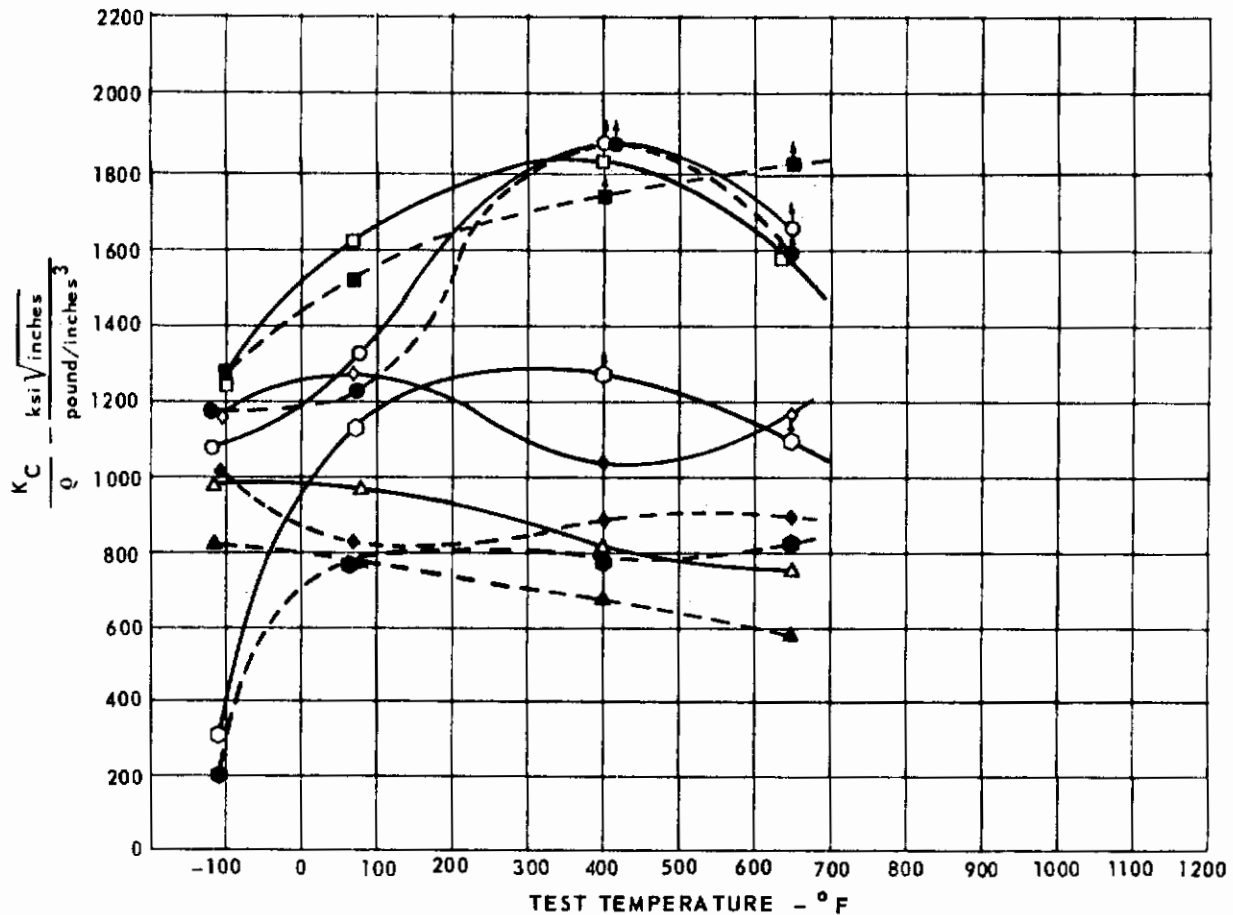


FIG. 240 VARIATION OF FRACTURE TOUGHNESS/DENSITY RATIO WITH TEMPERATURE FOR ALL ALLOYS

THICKNESS INCHES	GRAIN DIRECTION	ALLOY	CONDITION	HEAT NO.
○ .050	L	6Al-4V	MILL ANNEAL	4949
● .050	T	6Al-4V	MILL ANNEAL	4949
△ .025	L	PH 14-8Mo	SRH 1050	33347
▲ .025	T	PH 14-8Mo	SRH 1050	33347
□ .050	L	8Al-1Mo-1V	DUPLEX ANNEAL	3457
■ .050	T	8Al-1Mo-1V	DUPLEX ANNEAL	3457
○ .025	L	AM 350	SCT 850	19020
● .025	T	AM 350	SCT 850	19020
◇ .025	L	INCO 718	CRA	6902
◆ .025	T	INCO 718	CRA	6902

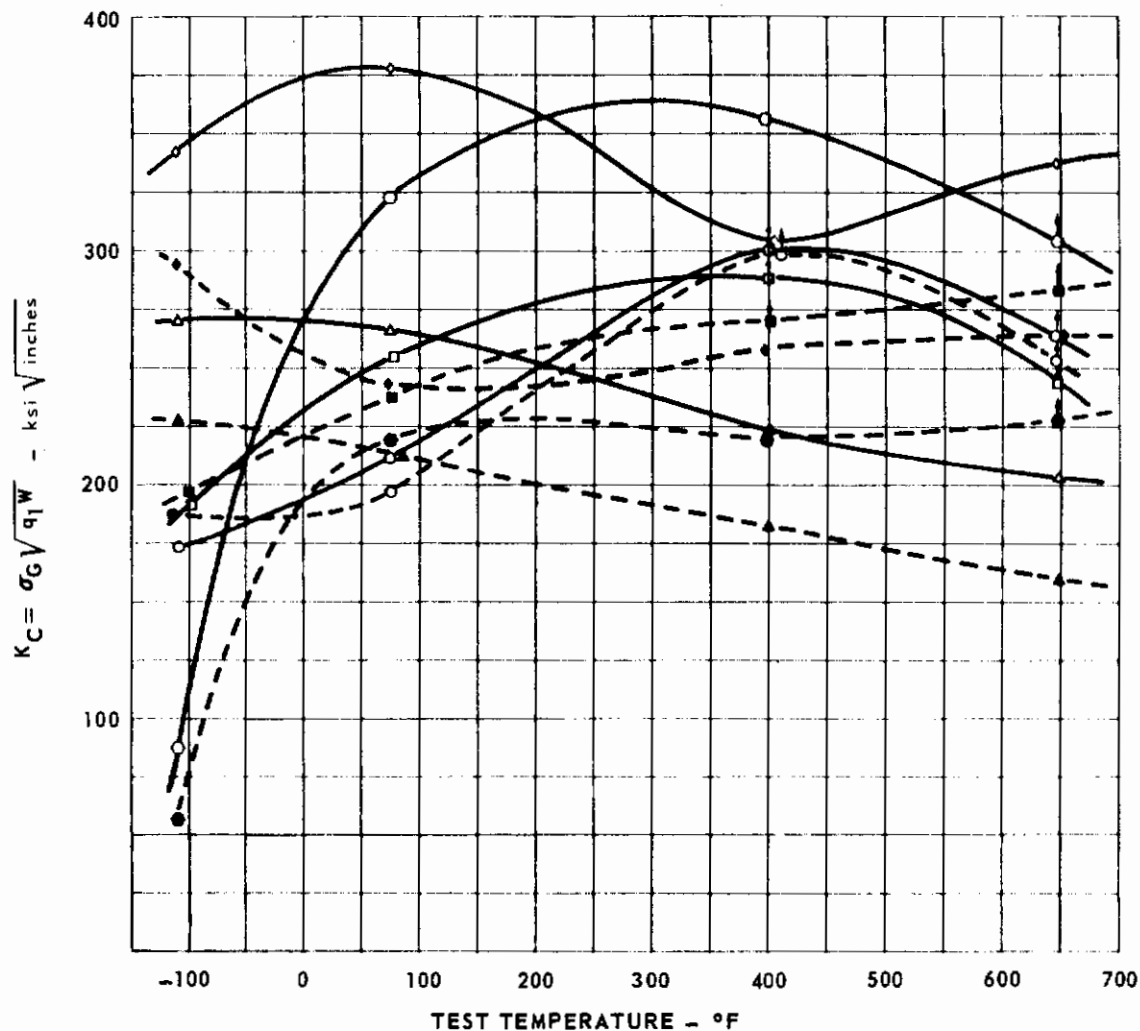
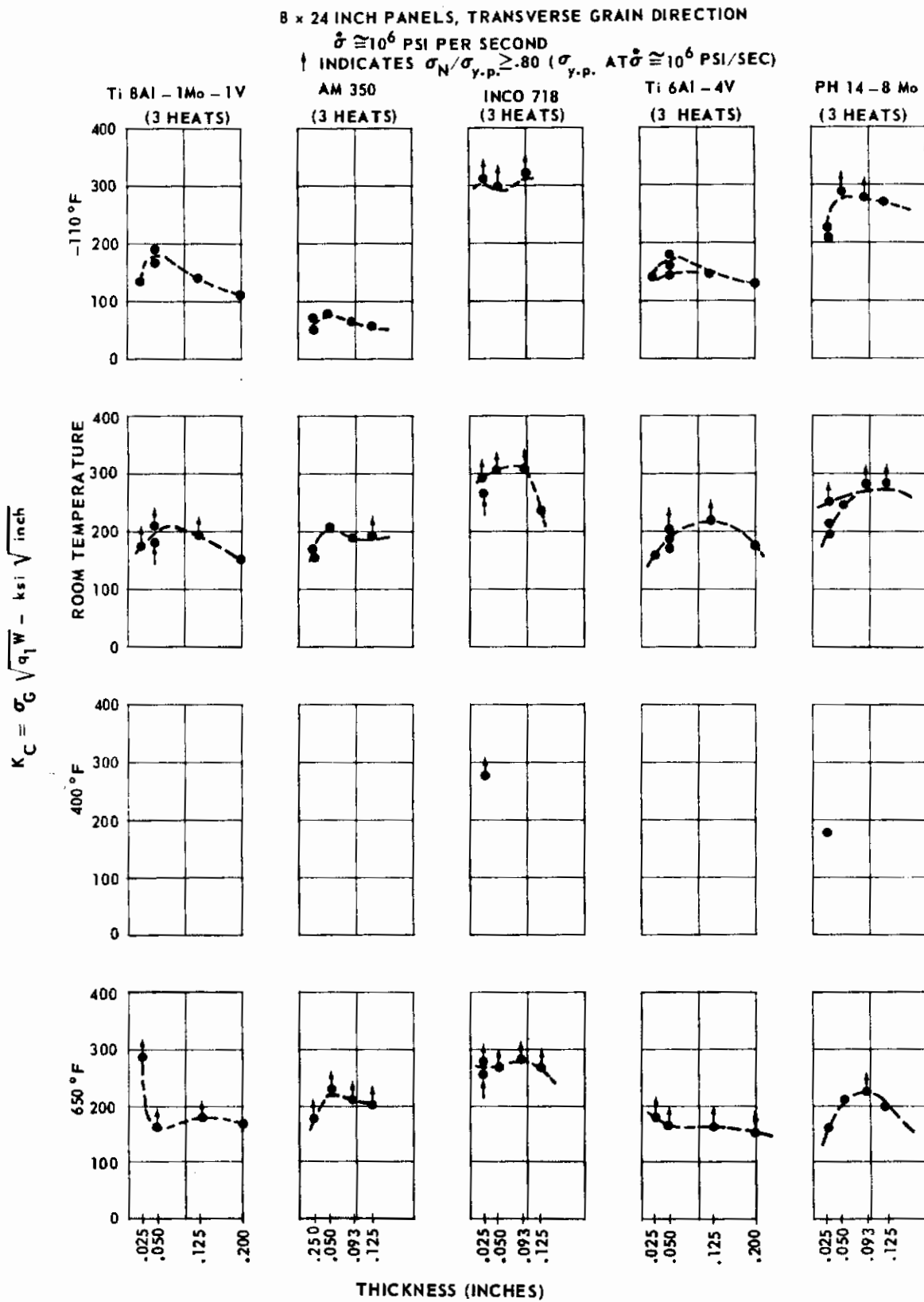


FIG. 241 VARIATION OF FRACTURE TOUGHNESS WITH TEMPERATURE FOR ALL ALLOYS.

In addition, summary graphs for each panel size are included in Figs. 242 and 243 showing the variation of K_C with thickness for each alloy and the four test temperatures. None of these data have material density included. The general trend of increasing toughness with alloy thickness is observed upon examining Fig. 243 for 24 x 72-inch panels. However, a general trend of decreasing toughness with alloy thickness is observed in examining Fig. 242 for 8 x 24-inch panels where net section yielding was the predominant factor in the thicker panels.



24 x 72 INCH PANELS, TRANSVERSE AND LONGITUDINAL GRAIN DIRECTION

$\dot{\sigma} \cong 10^6$ PSI PER SECOND

↑ INDICATES $\sigma_N / \sigma_{y.p.} \leq .80$ ($\sigma_{y.p.}$ AT $\dot{\sigma} \cong 10^6$ PSI/SEC)

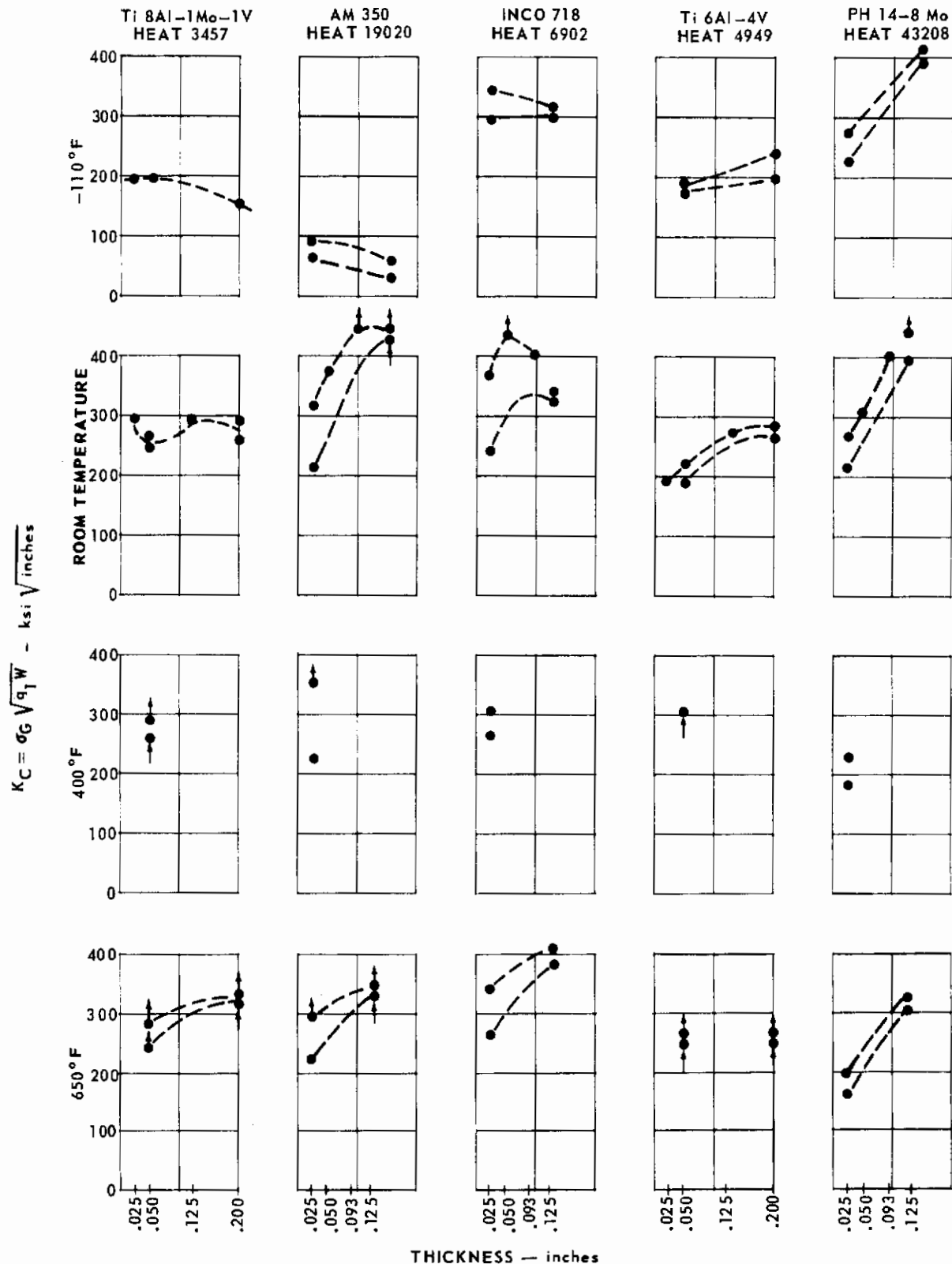


FIG. 243 ALLOY COMPARISON FOR K_C , TEMPERATURE AND THICKNESS FOR 24 x 72 INCH PANELS

Contrails

SECTION 8 CONCLUSIONS

From the fatigue crack propagation and fracture toughness test data derived during this program, the following conclusions can be drawn:

CRACK PROPAGATION TESTS

- 1) A comparison of crack propagation rates for the various sheet thicknesses shows that:
 - a) The crack propagation rate increases with increasing thickness for the Ti 8Al-1Mo-1V, Ti 6Al-4V, and Inco 718 alloys.
 - b) The crack propagation rate is not affected by sheet thickness for the AM 350 and PH 14-8Mo alloys.
- 2) By using the conservative edge of the scatter bands from the stress intensity factor-crack growth rate curves for each of the alloys for both grain directions at thicknesses of 0.025 and 0.050 inch, (see Figs. 237 and 238) it is shown that:
 - a) At a K-level of $40 \text{ ksi}\sqrt{\text{inches}}$, the Ti 6Al-4V alloy has the highest crack propagation rate followed by Ti 8Al-1Mo-1V, AM 350, PH 14-8Mo, and Inco 718 alloys, in that order.
 - b) At a K-level of $80 \text{ ksi}\sqrt{\text{inches}}$, the Ti 6Al-4V has the highest crack propagation rate followed by AM 350, Ti 8Al-1Mo-1V, PH 14-8Mo and Inco 718 alloys, in that order.
 - c) By taking the material density into consideration and making a similar comparison at a stress-intensity-factor/density ratio of $260,000 \text{ in.}^{3/2}$, the AM 350 alloy has the highest crack propagation rate followed by PH 14-8Mo, Inco 718, Ti 6Al-4V, and the Ti 8Al-1Mo-1V alloy, in that order.
- 3)
 - a) For both titanium alloys, the grain direction has no significant effect on crack propagation rates.
 - b) For the AM 350, Inco 718, and PH 14-8Mo alloys, the transverse grain direction exhibits a higher crack propagation rate than the longitudinal grain direction.
- 4) Exposure testing at 650° F for 1000 hours, at a gross stress of 25 ksi for the titanium alloys and 40 ksi for the other alloys caused:
 - a) No change in crack growth rate for the AM 350 and Inco 718 alloys.
 - b) An increase in crack growth rate for the Ti 8Al-1Mo-1V, Ti 6Al-4V, and PH 14-8Mo alloys. This increase in rate was thickness dependent with the thinnest material showing the greatest increase.

FRACTURE TESTS

- 1) A comparison over the temperature range of -110 to 650° F of the fracture test data, which includes the effect of material density (see Fig. 240) shows that:
 - a) Compared to the room temperature test results, fracture properties generally increase with increasing test temperature for Ti 8Al-1Mo-1V, Ti 6Al-4V and AM 350.
 - b) The fracture properties of Inco 718 and PH 14-8Mo are relatively unaffected by temperature.
 - c) The titanium alloys 8Al-1Mo-1V and 6Al-4V are superior over the entire test temperature range.
- 2) A comparison between longitudinal and transverse tests (see Figs. 240 and 241) shows that:
 - a) There is no consistent difference in fracture properties between the two grain directions for the Ti 8Al-1Mo-1V and Ti 6Al-4V alloys.
- 3) Fracture properties depend on thickness and the dependence is a function of both temperature and grain direction as shown in Figs. 242 and 243. In general, the longitudinal room temperature tests for all alloys show either no change, or an increase in fracture properties with increasing thickness.
- 4) Fracture properties vary with stress rate for most alloys. For both titanium alloys, these properties tend to increase with increasing stress rate. For the AM 350 material, the scatter in data obscures any trends. With the Inco 718 alloy, stress rate in general has no effect. With the PH 14-8Mo alloy, increasing stress rate causes a drop in fracture properties.
- 5) Fracture tests from material exposed under stress for 1000 hours at 650° F generally show some variation in fracture properties for all the alloys as compared to the unexposed properties. This variation is generally evident as a reduction in fracture properties with the amount of reduction dependent on thickness (see Figs. 57, 99, 140, 183, and 230).

SECTION 9 RECOMMENDATIONS

Based on the results of the tests performed in this program, the following recommendations are made:

- Continued studies toward commercial supersonic transport usage should be made with the titanium alloys 8Al-1Mo-1V and 6Al-4V for general structural sheet application and with the nickel alloy Inco 718 for specific high temperature applications.
- Increased testing emphasis should be placed on the low temperature range (-110°F to room temperature) since this is the expected region of highest structural loading for sheet material in a supersonic transport.
- Additional exposure testing of uncracked panels under conditions of stress and temperature should be carried out for periods of time longer than 1000 hours at 650°F and several temperatures below 650°F . Cyclic as well as sustained stresses should be investigated.
- Metallurgical studies should be initiated to parallel exposure testing to determine the reason for instability and possibly to develop the optimum stable heat treatment condition for each specific alloy. In addition, detailed metallurgical and fractographic studies should also be made on selected fracture panels for the present program to correlate microstructural characteristics with fracture and crack propagation behavior.
- Fracture and crack propagation testing of the candidate materials should be extended to panels simulating aircraft structure so that the limitations of the linear elastic fracture mechanics theory on simulated airframe behavior can be assessed.
- Fracture and crack propagation studies should be conducted on plate titanium alloys.

Contrails

SECTION 10 REFERENCES

1. Bently, C. W. "Notch Resistance and Fracture Toughness Characteristics of High Strength Metals," ASD-TDR-63-494, September 1963
2. Perry, D. C., "How to Select an Age-Hardening Stainless," Product Engineering, Vol. 34, No. 26, December 23, 1963
3. Griffith, A. A., "The Phenomena of Rupture and Flow in Solids," Philosophical Transactions of the Royal Society of London, Series A, Vol. 221, 1920
4. Irwin, G. R., "Fracture Dynamics," Fracturing of Metals, American Society for Metals, 1948, pp. 147-166
5. Irwin, G. R. and Kies, J. A., "Fracturing and Fracture Dynamics," Welding Journal Research Supplement, February 1952, pp. 95s-100s
6. Irwin, G. R., "Fracture," Handbuch der Physik, Vol. VI, Springer, 1958, pp. 551-590
7. Orowan, E., "Fundamentals of Brittle Behavior of Metals," Fatigue and Fracture of Metals, John Wiley and Sons, New York, 1952, p. 154
8. Irwin, G. R., "Analysis of Stresses and Strains Near the End of Crack Traversing a Plate," Journal of Applied Mechanics, Transactions of ASME, Vol. 24, No. 3, September 1957
9. Erdogan, F., Paris, P. and Sih, G., "Application of Muskhelishvili's Methods to the Analysis of Crack Tip Stress Intensity Factors for Plane Problems - Part I," Lehigh University, Institute of Research Interim Report, Fracture Mechanics Research for Boeing Airplane Company, December 9, 1960
10. Sih, G., Paris, P. and Erdogan F., "Application of Muskhelishvili's Methods to the Analysis of Crack Tip Stress Intensity Factors for Plane Problems - Part II," Lehigh University, Institute of Research Interim Report, Fracture Mechanics Research for Boeing Airplane Company, January 7, 1961
11. Williams, M. L., "On the Stress Distribution Near the Base of a Stationary Crack," Journal of Applied Mechanics, March 1957
12. Sneddon, I. N., "The Distribution of Stress in the Neighborhood of a Crack in an Elastic Solid," Proceedings of the Royal Society of London, Vol. A-187, 1946
13. Irwin, G. R., "Relation of Stresses Near a Crack to the Crack Extension Force," IXth International Congress of Applied Mechanics, University of Brussels, September 1957

14. Irwin, G. R., "Analytical Aspects of Crack Stress Field Problems," University of Illinois, Theoretical and Applied Mechanics, Report No. 213, March 1962
15. Westergaard, H. M., "Bearing Pressure and Cracks," Journal of Applied Mechanics, June 1939
16. Greenspan, M., "Axial Rigidity of Perforated Structural Members," Journal of Research of the National Bureau of Standards, Vol. 31, 1943, pp. 305-322
17. Fifth Report of a Special ASTM Committee, "Progress in Measuring Fracture Toughness and Using Fracture Mechanics," Materials Research and Standards, Vol. 4, No. 3, March 1964
18. Paris, P. C., Gomez, M. P. and Anderson, W. E., "A Rational Analytical Theory of Fatigue," The Trend in Engineering, Vol. 13, No. 1, University of Washington, January 1961
19. Anderson, W. E. and Paris, P., "Evaluation of Aircraft Material by Fracture," Metals Engineering Quarterly, ASM, Vol. 1, No. 2, May 1961
20. Donaldson, D. R. and Anderson, W. E., "Crack Propagation Behavior of Some Airframe Materials," Crack Propagation Symposium, Cranfield, England, September 1961
21. "Fracture Testing of High-Strength Sheet Materials," ASTM Committee Report, ASTM Bulletin, January 1960, p. 29
22. "Fracture Testing of High-Strength Sheet Materials," ASTM Committee Report, ASTM Bulletin, February 1960, p. 18
23. "Fracture Testing of High-Strength Sheet Materials," ASTM Committee Report, Materials Research and Standards, November 1961, p. 877
24. Cullen, T. M. and Freeman, J. W., Effect of Long Time Creep on Structural Sheet Materials, University of Michigan, Sixth Progress Report, December 1963
25. Kattus, J. R., "Tensile Properties of Aircraft-Structural Metals at Various Rates of Loading after Rapid Heating," WADC TR 38-440, Part I, May 1959
26. Morrison, J. D. and Kattus, J. R., "Tensile Properties of Aircraft-Structural Metals at Various Rates of Loading after Rapid Heating," WADC TR 55-199, Part 2, November 1956
27. Hardrath, H. F., "Crack Propagation and Final Failure," Materials Research and Standards, February 1963, p. 116

28. Boyle, R. W., "A Method for Determining Crack Growth in Notched Sheet Specimens," Materials Research and Standards, August 1962, p. 646
29. NAA Internal Report 62-1158, "Investigation of Photostress Techniques," May 1962
30. Boyle, R. W., Sullivan, A. M. and Krafft, J. M., "Determination of Plane Strain Fracture Toughness with Sharply Notched Sheets," Welding Research Supplement, p. 428s, September 1962
31. Jones, M. H., and Brown, W. F., Jr., "Acoustic Detection of Crack Initiation in Sharply Notched Specimens," Materials Research and Standards, p. 120, March 1964

Contrails

APPENDIX I
INVESTIGATION OF TECHNIQUES FOR DETECTION OF "POP-IN"

INTRODUCTION

For purposes of this investigation, "pop-in" is defined as the initial precipitous burst of crack growth (at the plane strain toughness level) which precedes the slow growth of a crack under increasing load. Previous investigators, Refs. 28 and 30, have successfully recorded pop-in using the traditional compliance gage method. Displacement between points bridging the crack is recorded as a function of applied load and is related to crack length. Using the compliance gage measurement technique, pop-in is detected as a discontinuous displacement increment at constant load. On the basis of fracture surface appearance, it is generally accepted that a crack begins in the mid-thickness region of the notch and grows forward and laterally toward the side surface in a semicircular front. This fact suggests that motion picture or other techniques that detect surface cracks can fail to sense the original internal growth and so fail to give conservative test values of pop-in. This fact was borne out in tests where motion picture records did not show surface crack growth until several bursts of crack growth had occurred. These tests are detailed under DISCUSSION. Test results demonstrated that a technique that would detect internal growth is desirable for pop-in detection. As previously noted, the compliance gage technique is the traditional or standard method for detecting pop-in. In this investigation, however, the high loading rates and test environment were such that the inertia and mechanical fragility of the compliance gage would preclude its use. The electrical resistance strain gage was selected as the most promising technique having the desired prerequisites:

- 1) Low inertia (good response)
- 2) Proven capability over the test environment range (-110°F to 650°F)
- 3) Ability to sense internal crack growth

Since an extensive background existed in the use of the compliance gage for detection of pop-in, compliance gage data was used as the standard of comparison or reference measuring system during this investigation. In addition, since Ref. 28 indicated that 0.25 inch thick, 7075-T6 plate exhibits distinct pop-in, this material was selected as the test material for evaluating the use of strain gages as a detection technique. On the basis of photoelastic studies of the strain distribution surrounding a crack, Ref. 29, it was decided that a strain gage placed approximately 0.125 inch outward from the tip of the crack would be at an optimum location for detection of initial crack growth.

DISCUSSION

A number of tests were conducted to determine the best available technique for measuring pop-in; discussions of four of the tests follow:

Test 1

The test specimen consisted of a 0.25 x 4 x 16 inch 7075-T6 aluminum specimen with a 0.72 inch fatigue-grown center notch. Load was applied over a period of several minutes with a Riehle 120,000 pound universal testing machine. Compliance gage data was supplied by an averaging extensometer, as shown in Fig. 244, and recorded in relation to machine load. Strain gages were placed 0.125 inch outboard of the crack tips and the outputs were recorded on dual X-Y recorders. Simultaneously, a motion picture camera was used to record surface crack growth. Load input to the X-Y recorders was provided by a Baldwin 50,000 pound load cell. Test data is presented in Fig. 245. Although there was no direct correlation of load versus crack length in this test, an approximate relationship of crack length versus load was obtained from the camera frame speed. This information indicated that surface crack growth did not appear until the fourth burst of crack growth (shown in Fig. 245). This test and the results of Test 2, (see Fig. 246), were the basis for the earlier statement that internal crack growth (initial pop-in) could be subsurface and consequently not detected on film. From Fig. 245, it is noted that both strain gages exhibited records similar in shape to the compliance gage data, and that bursts of crack growth are indicated at identical load levels on the strain gages and the compliance gage. This test indicated that strain gages satisfactorily detected pop-in, the precipitous burst of crack growth.

Test 2

The test specimen was a 0.25 x 8 x 24 inch, 7075-T6 aluminum sheet with a 2 inch fatigue-grown center notch. A Riehle 120,000 pound universal testing machine was used to load the specimen to failure in 118 seconds. Instrumentation consisted of a strain-gaged load link, three strain gages, compliance gage, and motion picture camera. Outputs from the strain gages and load link were recorder versus time on a CEC oscillograph. The motion picture camera photographed crack length and simultaneously recorded a digital reading of load supplied by a Datron strain indicator. The compliance gage displacement was recorded versus test machine load on an Owens-Peters X-Y recorder. The test results are presented in Fig. 246. Examination of the data shows that the pop-in steps indicated by the compliance gage occurred at slightly higher load levels than indicated by strain gages. Observed pop-in noises correlated well with the strain gage values. Again the test demonstrated that strain gages would detect pop-in - an initial abrupt burst of growth.

Test 3

This test used a 0.217 x 8 x 24 inch 6Al-4V titanium alloy specimen with a 2.07 inch fatigue-grown center crack, and it was tested in a manner similar to Test 2. The specimen was loaded to failure in 141 seconds. Unfortunately, the motion picture camera was improperly aimed during this test and only one side of the notch was photographed. The crack growth was observed to be unsymmetrical and the camera recording was of the area of greatest crack growth. The test data is presented in Fig. 247. The strain gage and compliance gage data did not indicate any pop-in (abrupt burst of growth). Only slow and continuous cracking was indicated.

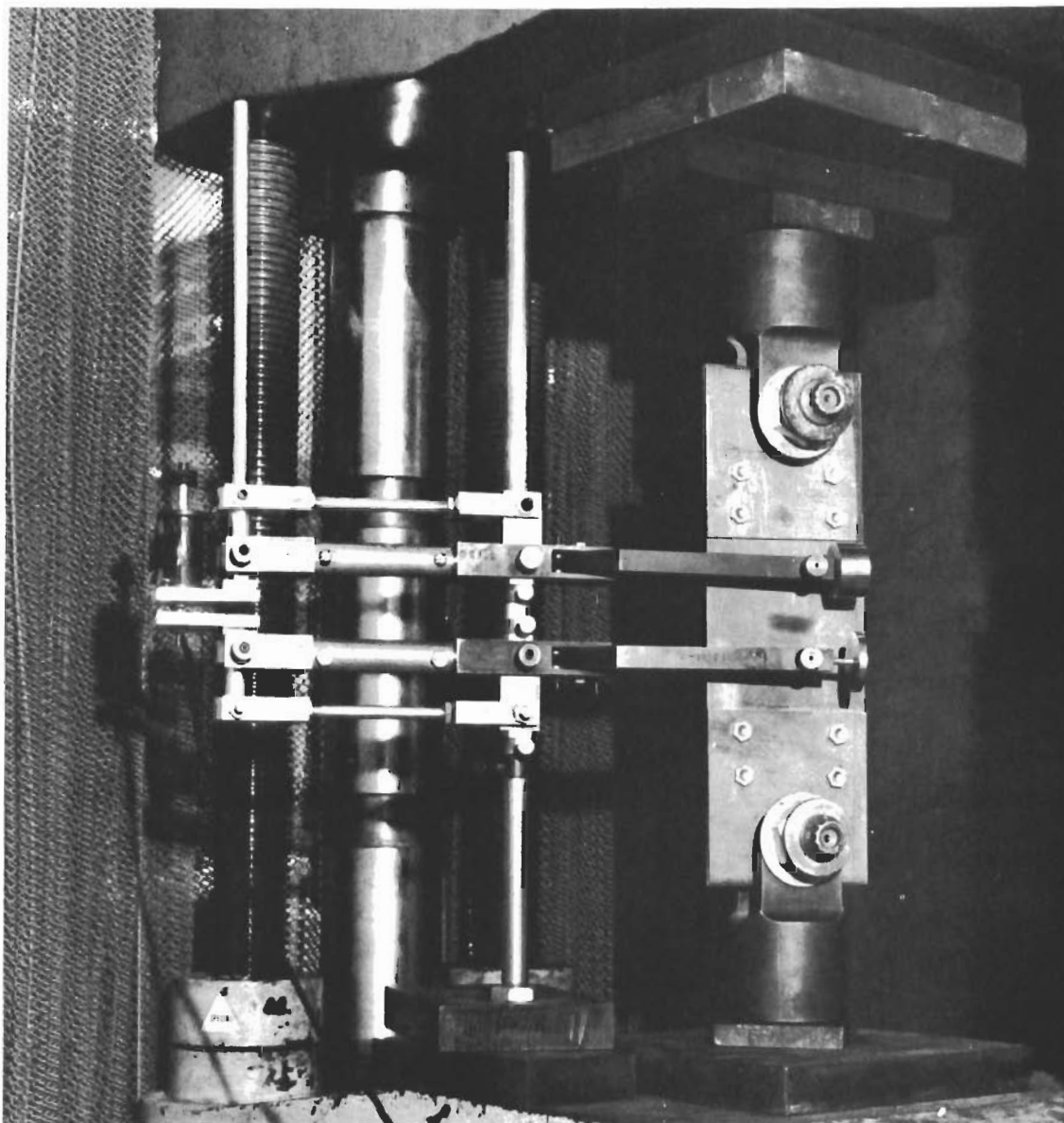


FIG. 244 TEST SETUP WITH EXTENSOMETER AND 4 x 16 INCH 7075-T 6 PANEL

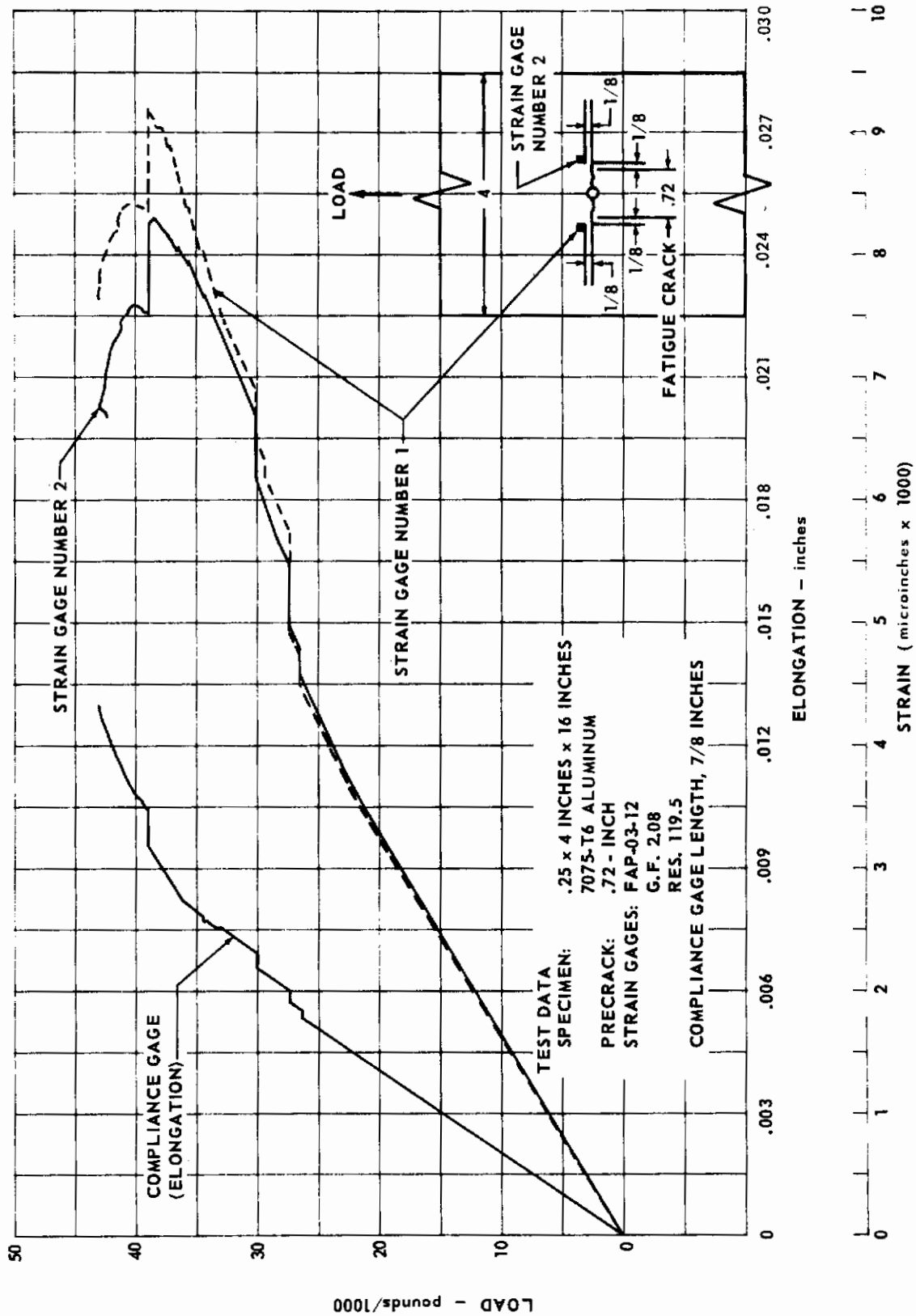


FIG. 245 COMPLIANCE AND STRAIN GAGE PLOT FOR TEST NUMBER 1

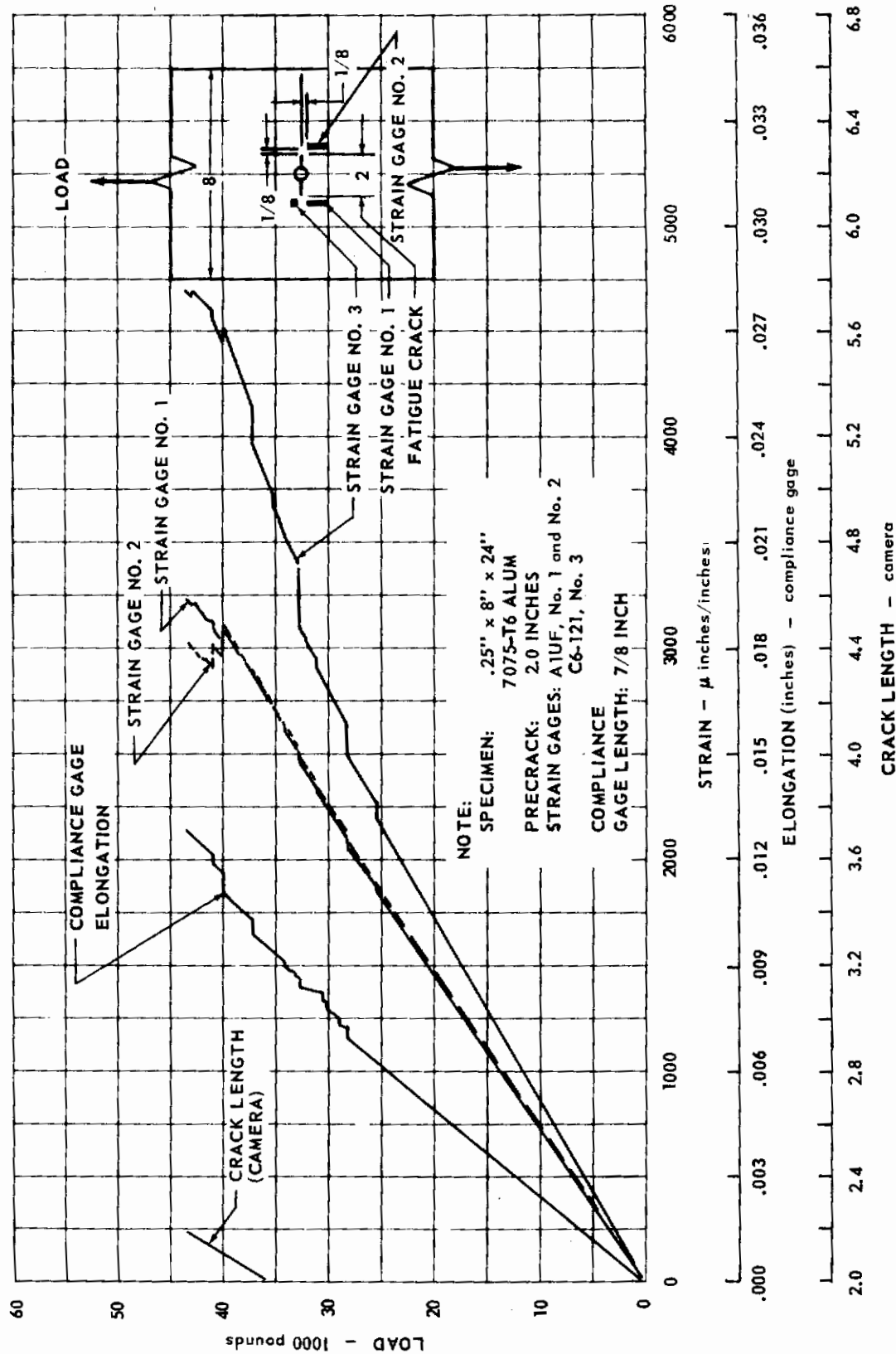


FIG. 246 COMPLIANCE AND STRAIN GAGE PLOT FOR TEST NUMBER 2

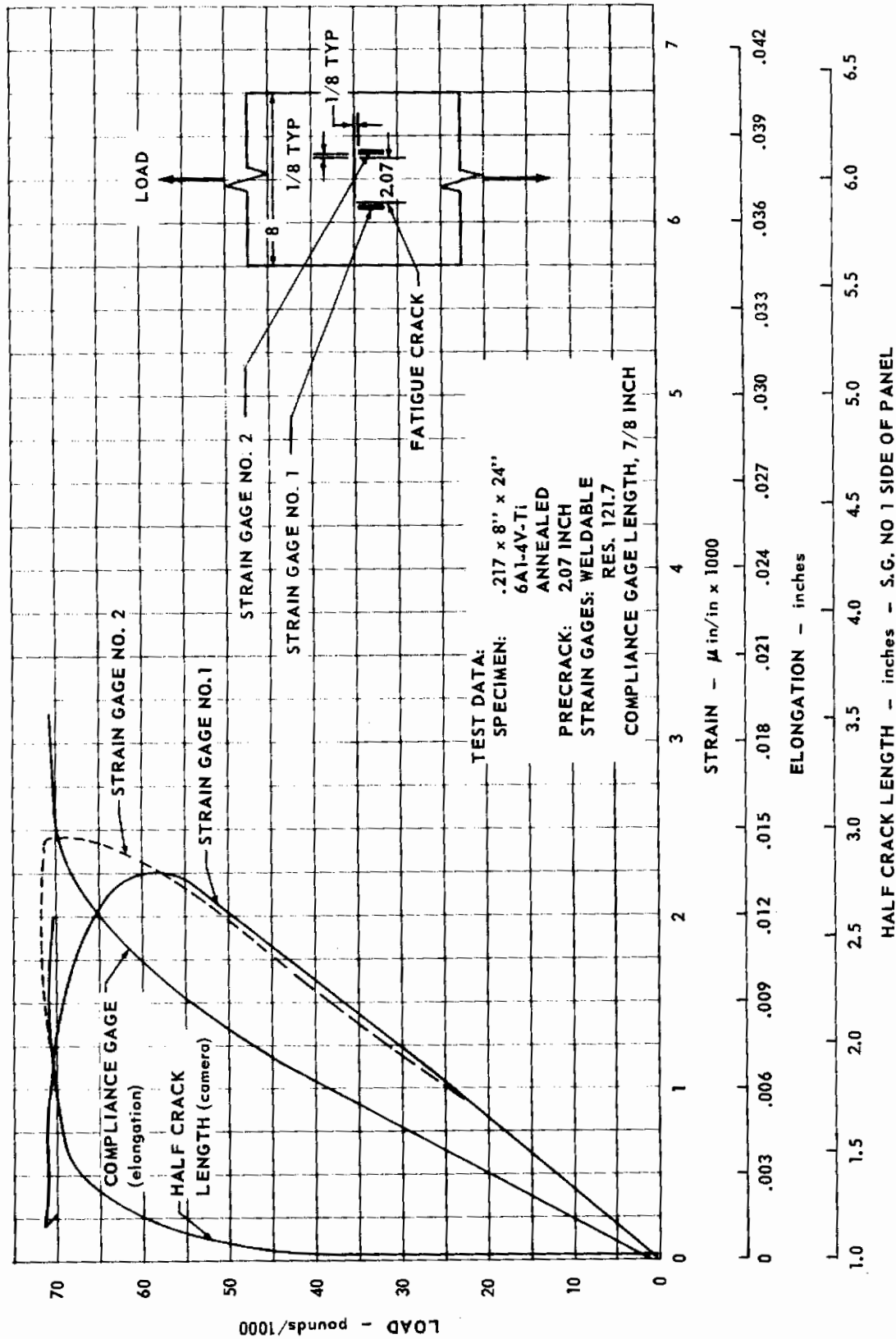


FIG. 247 COMPLIANCE AND STRAIN GAGE PLOT FOR TEST NUMBER 3

Test 4

All of the previously described tests were conducted in a Riehle 120,000 pound universal testing machine at relatively slow loading rates. It was decided to evaluate the strain gage detection technique with the same testing system planned for the 8 x 24 inch titanium and steel specimens. A 0.25 x 8 x 24 inch aluminum alloy test specimen having a 2.01 inch center fatigue crack was used.

To determine if the placement and type of strain gage would significantly affect the data, the specimen was instrumented with seven strain gages. The loading rate was approximately 5000 psi per second; outputs of the strain-gaged load link and strain gages were recorded on a CEC oscillograph. During checkout of the loading setup, the specimen was prematurely loaded and the crack grew from 2.01 to 2.5 inches. No strain gage data was recorded. Since four or five bursts of growth were obtained in the previous tests, it was decided to continue the test to see if additional bursts of growth would occur. During the ensuing test, two bursts of growth before failure were detected on the majority of the gages. Refer to Fig. 248 for gage placement and test data. It was noted that the type and placement of gage was not especially critical if the gage was within 0.188 inch of the crack tip. The only gage that was somewhat insensitive to pop-in was the gage placed 0.7 inch out from the crack tip. Motion picture coverage was included during the test with crack growth and load being simultaneously recorded on the film. Refer to Fig. 249 for test setup. The camera used was a D.B. Milliken No. 4, recording at 100 frames per second. India ink was placed in the crack to improve the photographic coverage. In this test, as previously noted, no apparent burst of surface crack growth was detected coincident with the pop-in detected by the strain gages. It is believed that the crack growth was essentially internal.

From these investigations, it was concluded that strain gages were satisfactory for detecting pop-in. Accordingly, the 8 x 24 inch titanium and steel specimens were each instrumented with two strain gages located 0.125 inch out from the tips of the center fatigue notch.

Titanium and Steel Specimens

During the ensuing tests of 8 x 24 inch titanium and steel specimens, there were no detectable pop-ins or sudden bursts of crack growth. (Refer to Fig. 250 for a typical strain output plot from a titanium specimen.) Instead, there is a gradually increasing strain rate denoting slow crack growth without pop-in. The strain data reaches a maximum and decreases as the crack tip progresses relative to the gage. No definitive relationship was observed between the strain gage output and the crack tip position.

Although it was noted in the testing reported above that pop-in occurred before surface crack growth began, in the absence of pop-in data an approximation to the upper envelope of K_{ICN} may be made by utilizing the gross stress level at which surface cracking begins in the equation

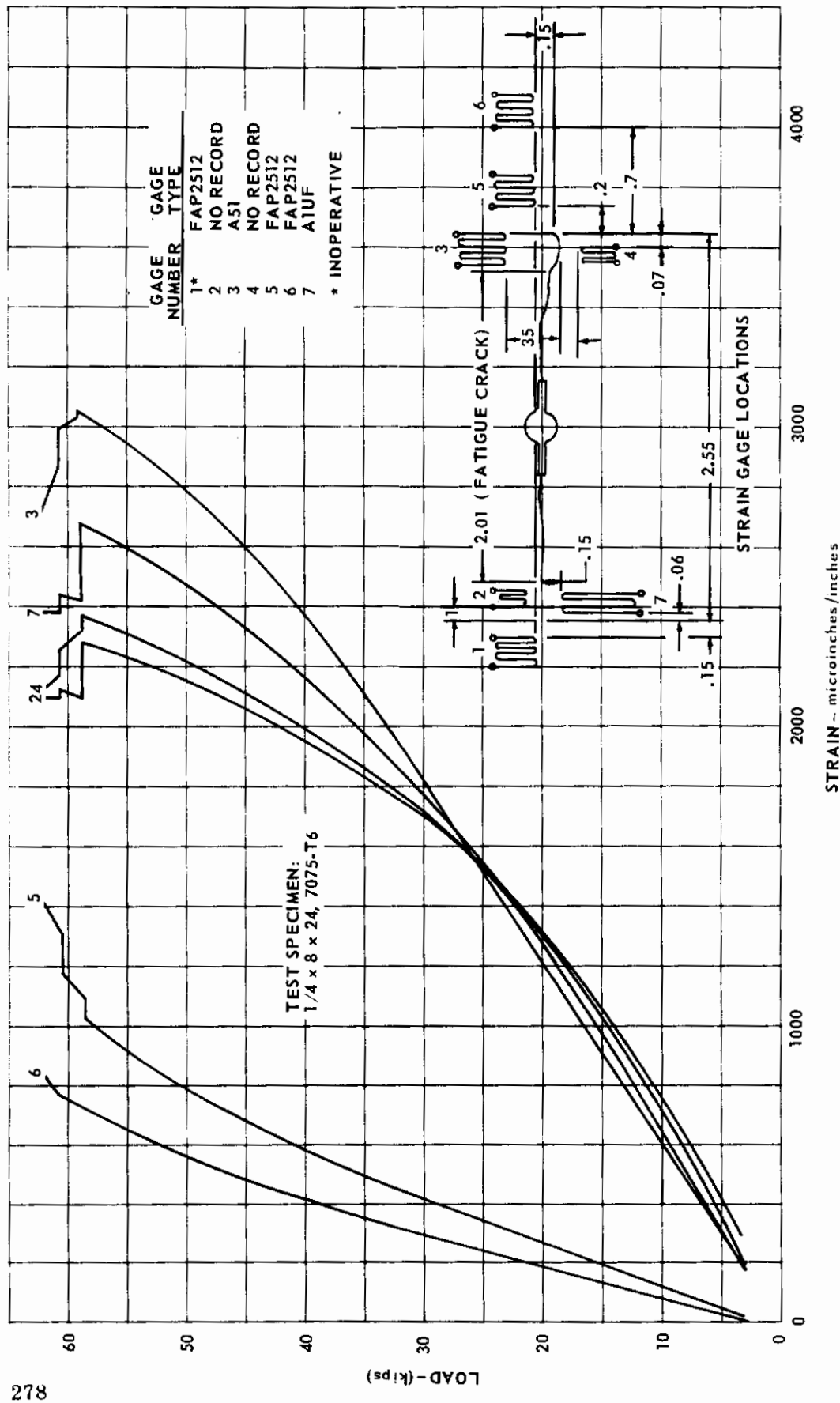


FIG. 248 COMPLIANCE AND STRAIN GAGE PLOT FOR TEST NUMBER 4

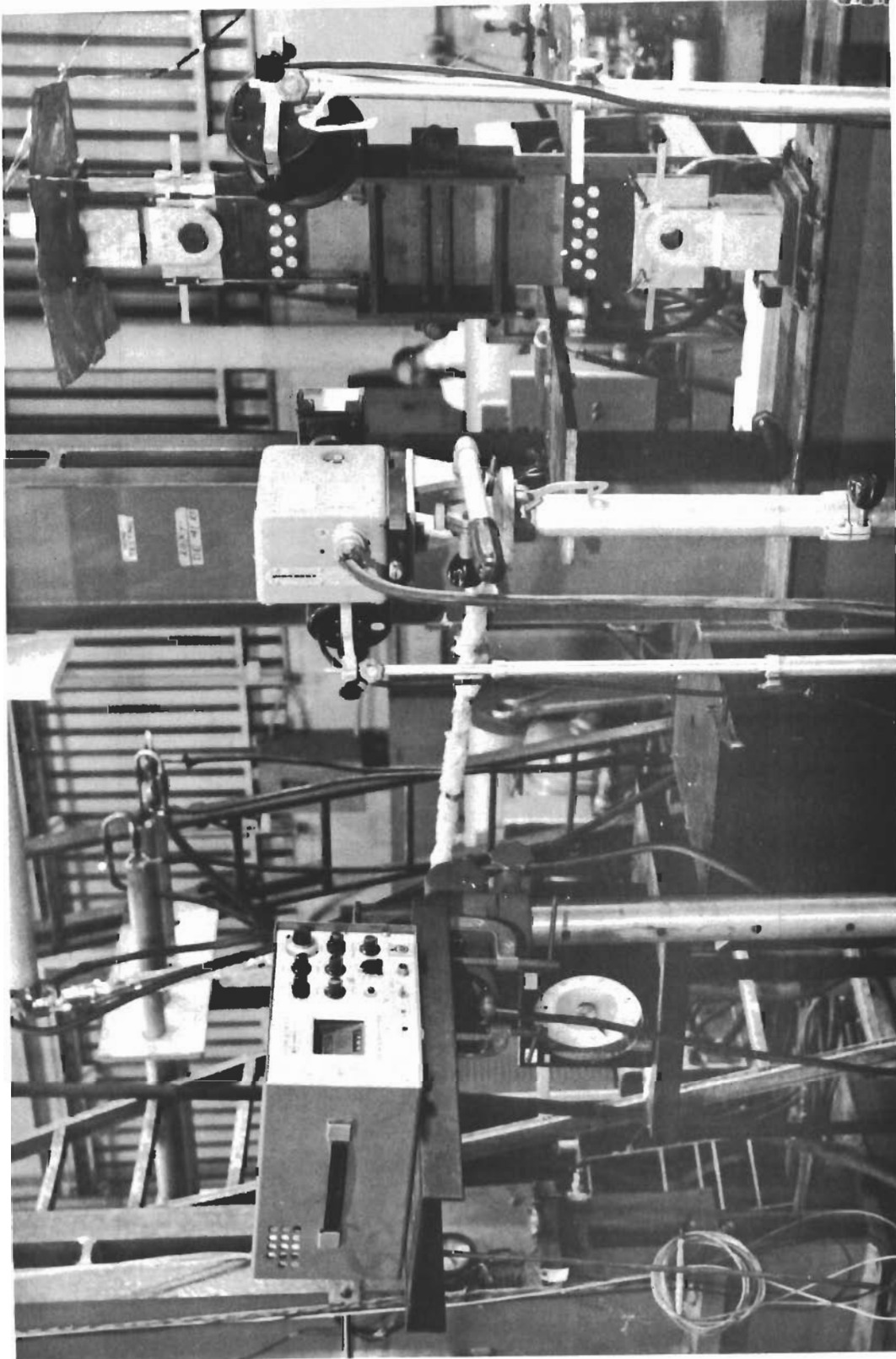


FIG. 249 TEST SETUP FOR HIGH-SPEED PHOTOGRAPHY EQUIPMENT

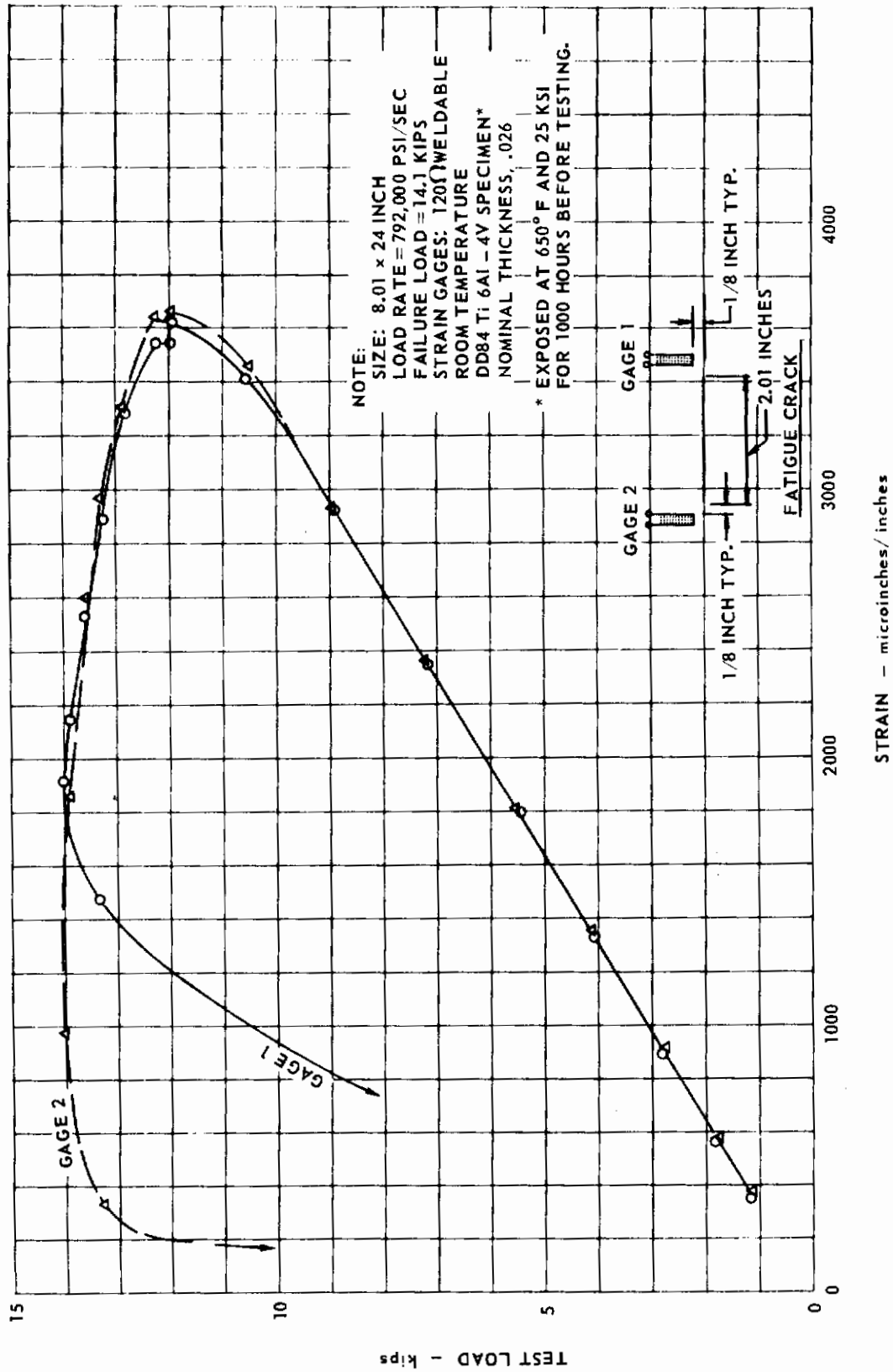


FIG. 250 TYPICAL STRAIN OUTPUT PLOT FROM A TEST OF AN 8 x 24 INCH EXHIBIT C SPECIMEN

$$K_{ICN} = \sigma_G (2b \tan \frac{\pi a_0}{2b})^{1/2}, \text{ (Reference 30)}$$

or

$$K_{ICN} = \sigma_G (\sqrt{\pi a} a)$$

The initiation of surface crack growth was recorded by the high-speed photography used to measure critical crack length on selected specimens; plots of $2a$ and P versus time are included in Appendix II.

Values of K_{ICN} computed by using the data of Appendix II are tabulated in Table 32 for the Ti 6Al-4V (mill anneal).

From a plot of K_{ICN} versus T for the Ti 6Al-4V (mill anneal) alloy in Fig. 251, the following are noted:

- 1) K_{ICN} is a function of thickness at room temperature. The 8 x 24 inch specimens tested at $\dot{\sigma} \approx 10^6$ psi/sec show the highest value for the 0.050 inch nominal thickness, then 0.025, 0.125, and finally the lowest value for the 0.200 inch nominal thickness. This same order is shown at -110°F for $\dot{\sigma} \approx 5 \times 10^3$ psi/sec, but the 0.025 inch thickness has a value higher than that for the same thickness at 650°F for $\dot{\sigma} \approx 10^6$ psi/sec.
- 2) K_{ICN} is a function of temperature. For the 8 x 24 x 0.200 inch specimens tested at $\dot{\sigma} \approx 5 \times 10^3$ psi/sec, the highest to lowest values of K_{ICN} are for 400°F , 650°F , -110°F and then R.T.
- 3) Values for the 0.050 inch nominal thickness of the 24 x 72 inch longitudinal specimens are consistent while the transverse specimens display larger scatter. Upper envelopes of K_{ICN} are approximately 130 ksi $\sqrt{\text{inches}}$ and 124 ksi $\sqrt{\text{inches}}$ respectively.

TABLE 32 VALUES OF K_{ICN} FROM INITIATION OF SLOW CRACK GROWTH REVEALED BY HIGH-SPEED PHOTOGRAPHY FOR Ti 6Al-4V

SPECIMEN NO.	HEAT NO.	ACTUAL THICKNESS inches	GRAIN DIRECTION	WIDTH inches	$\dot{\sigma}$ (psi/sec)	TEMP. °F	$K_{ICN} = \sigma_G \sqrt{\pi a_0} a$ ksi $\sqrt{\text{in}}$
DD 3	D5257	.051	L	24.07	4.96×10^3	82	137.5
DD 4	D5257	.049	L	24.06	4.92×10^3	72	137.7
DD 5	D5257	.0496	T	24.05	4.99×10^3	68	131.3
DD 6	D5257	.048	T	24.02	4.93×10^3	68	164.4
DD 19	D5257	.0495	T	8.010	6.29×10^3	-110	132.1
DD 20	D5257	.0499	T	8.004	$.96 \times 10^6$	-110	64.0
DD 22	D5256	.0515	L	24.07	4.86×10^3	71	130.8
DD 23	D5256	.052	L	24.07	4.97×10^3	72	139.6
DD 24	D5256	.054	T	24.08	4.75×10^3	74	122.2
DD 25	D5256	.0545	T	24.08	4.86×10^3	71	146.0
DD 36	D5256	.0516	T	8.012	6.14×10^3	-110	119.7
DD 38	D5256	.052	T	8.008	$.96 \times 10^6$	71	165.5
DD 42	D4949	.0513	T	8.018	$.85 \times 10^6$	650	116.4
DD 52	D4949	.025	T	8.028	$.91 \times 10^6$	650	141.4
DD 54	D4949	.025	T	8.044	$.76 \times 10^6$	70	111.6
DD 56	D4949	.1267	T	8.048	1.09×10^6	72	87.7
DD 70	D4949	.212	L	24.07	4.1×10^3	75	208.5
DD 74	D4949	.2152	T	8.010	$.99 \times 10^6$	74	75.7
DD 75	D4949	.216	T	8.040	4.6×10^3	74	58.5
DD 76	D4949	.2146	T	8.032	5.35×10^3	400	146.6
DD 77	D4949	.2133	T	8.040	5.74×10^3	650	127.6
DD 78	D4949	.2134	T	8.033	5.77×10^3	-110	82.3

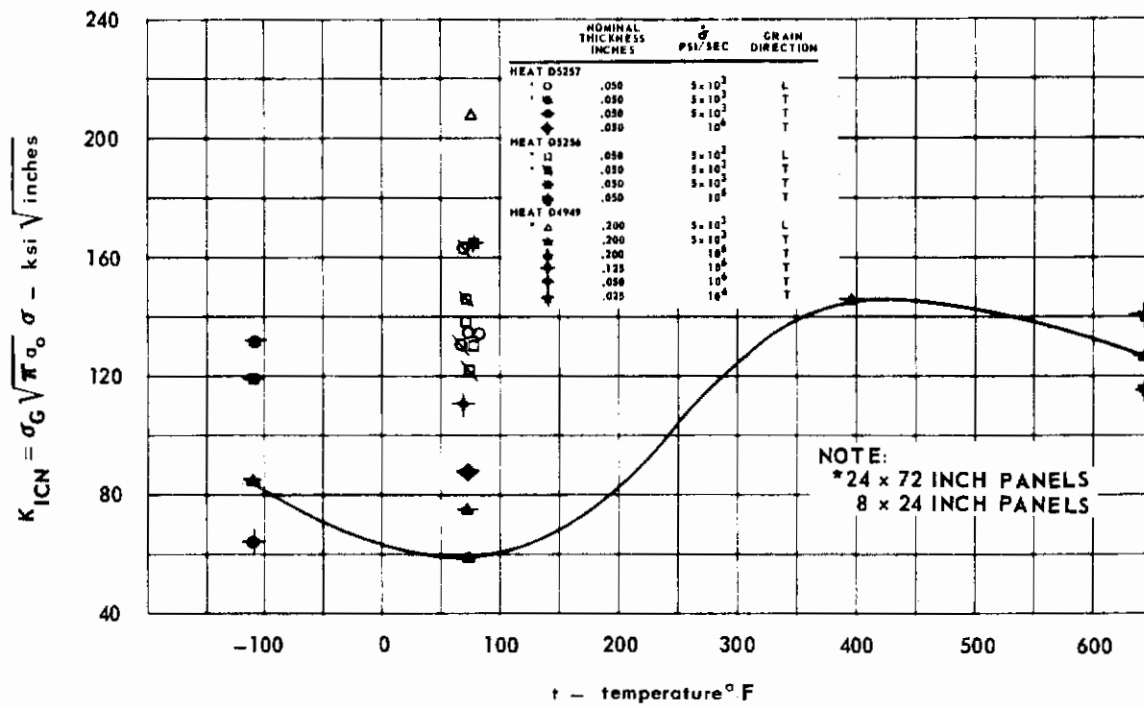


FIG. 251 PLANE-STRAIN FRACTURE TOUGHNESS BASED ON INITIATION OF SLOW CRACK GROWTH FOR Ti 6Al-4V

Contrails

APPENDIX II HIGH-SPEED PHOTOGRAPHY STUDIES

INTRODUCTION

Several methods for determination of critical crack length were considered. These methods included compliance measurement, fracture wires, electrical resistance, and motion picture photography. Among these techniques, the electrical resistance method showed the most promise but required considerable calibration plus high current for practical operation and was not sufficiently developed to be of use on this program. A decision to use motion picture photography was based upon the following:

- 1) No calibration required.
- 2) Existing photographic equipment could be utilized.
- 3) Easily adaptable to testing over a wide range of temperature and load rates.

Several specimens having $\dot{\sigma} \cong 5 \times 10^3$ psi/sec were scheduled to have the critical crack length measured, but due to a few malfunctions of photographic equipment and film development, not all of the film coverage was successful. A number of specimens having $\dot{\sigma} \cong 10^6$ psi/sec were photographed for determination of the critical crack length to make up the deficiency and a number were also photographed for extra data points.

TEST EQUIPMENT AND PROCEDURE

The camera used for test runs of $\dot{\sigma} \cong 5 \times 10^3$ psi/sec was a 16 mm. Model DBM4 Milliken. It was operated at a nominal film speed of 400 frames per second whereby a 200 foot roll of film had a run duration of approximately 20 seconds. A 36 degree shutter setting worked best. When the test run time was expected to exceed 15 seconds, the camera start was delayed so that enough film was available to capture the complete specimen separation. Kodak Plus-X film processed as a negative generally gave good results when viewed through a film reader. A high speed camera was necessary for the test runs where $\dot{\sigma} \cong 10^6$ psi/sec. Good results were obtained by utilizing a 16 mm. Magnafax camera loaded with Kodak TRI-X film. The film speed was between 1500 and 2000 frames per second and with a 100 foot roll of film the run duration was approximately 2 seconds. The film was usually processed as negative.

Occasionally the film was over exposed or there was surface reflection which caused partial improper exposure. In these cases, film readability could be improved by reprocessing the film negative to obtain a film positive.

Automatically starting the test events in the correct sequence was required for the test runs of short duration. A one switch operation started the following events in the sequence as listed:

- 1) The camera and flood lamps were switched on.
- 2) The oscillograph was turned on.
- 3) The test load ramp was started and the identifying pulse was fired (refer to Fig. 252 for Ramp Start Pulse Circuit).
- 4) The oscillograph was turned off (after specimen failure).

The load recording oscillograph was set for a paper speed of 4 inches per second for runs where $\dot{\sigma} \approx 5 \times 10^3$ psi/sec and for 64 inches per second for the runs for $\dot{\sigma} \approx 10^6$ psi/sec. Photographic illumination was obtained by using 1000 watt flood lamps. For the elevated and low temperature tests conducted within an environmental box, two parabolic reflectors using 600 watt quartz bulbs were symmetrically oriented and internally mounted. For the low temperature testing, the environmental box viewing window was a single pane of 1/4 inch plate glass. The window was kept frost free by directing hot air from a hair dryer unit at the outer surface.

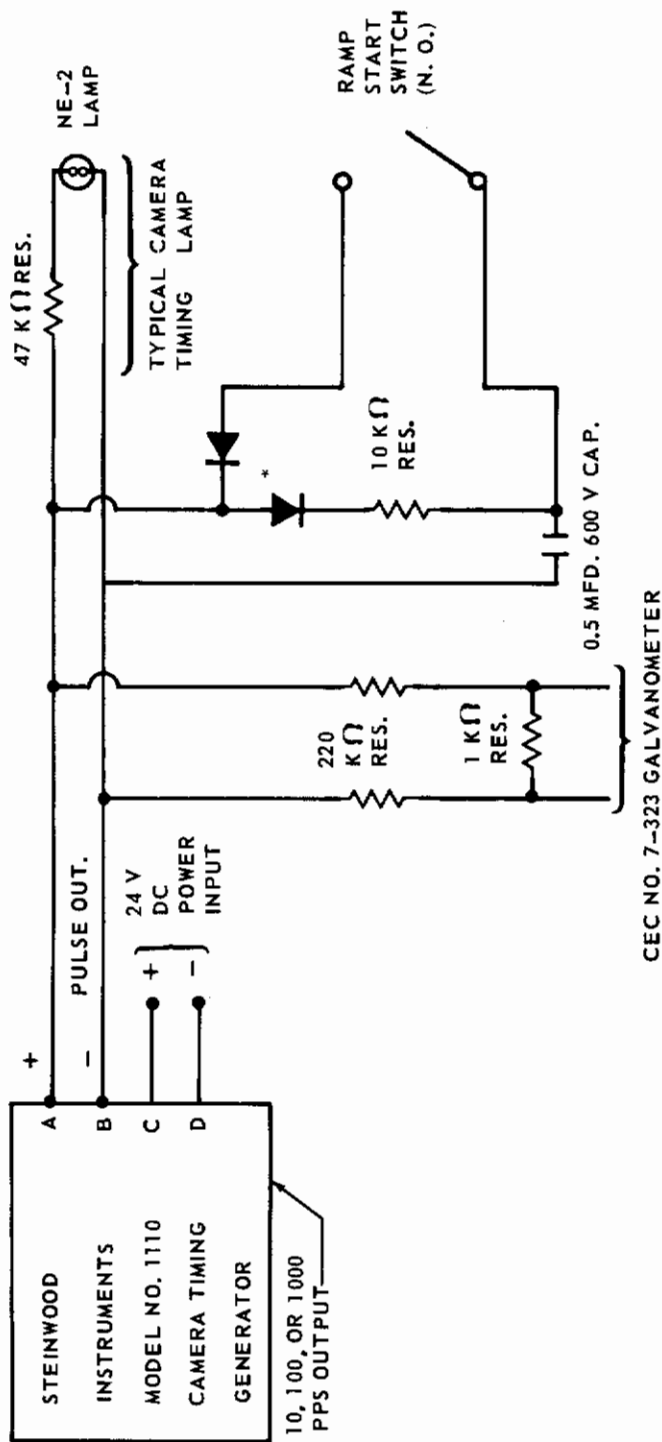
DATA REDUCTION TECHNIQUE

The film reading was done on commercial film readers. Gage marks were installed on the buckling restraint bars and placed below the crack to establish the ratio of true crack length to film projected crack length.

Crack length measurements from the projected film were recorded along with the corresponding film frame numbers. The film frame showing complete specimen separation was designated as frame zero. The frames prior to zero were assigned reading numbers (0, 1, 2, 3, etc., to the beginning). Crack length measurements from the last few hundred frames to zero were most significant in terms of rapid crack growth. The point of zero load occurring after peak load on the oscillograph trace corresponded to the first film frame showing complete specimen separation. This related crack length and load to a common time base. Timing marks, which supplied the common time base and permitted measurement of film frame rate, were placed simultaneously on the film and oscillograph paper. This was accomplished through the use of a pulse generation circuit, which is shown in Fig. 252.

The major difficulty in reading the projected film was in finding the exact location of the crack tips. This difficulty was due to factors such as:

- 1) Local surface yielding in the vicinity of the crack tip which occasionally caused a shaded area easily confused with the crack tip.
- 2) Over or under exposure of the film.
- 3) Surface reflections.
- 4) Projected crack image too small.



*"DIODES, INC." NO. D1-58 SILICON RECTIFIERS (3/4 AMP, 800 PRV.)

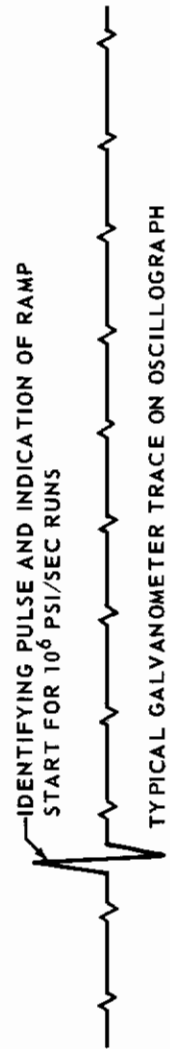


FIG. 252 TIMING AND RAMP START PULSE CIRCUITS

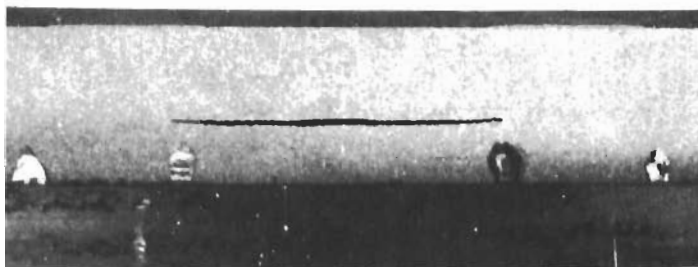
A lighting technique using polarizing screens may be a possible solution for the reduction of surface glare. Films of the 8 x 24 inch specimens were generally easier to read because of the large image size of the projected crack. A larger image size for the 24 x 72 inch specimens was obtained by reducing the film coverage from 24 to 12 inches.

Figs. 253 and 254 show a number of selected frames for a small and a large Ti 6Al-4V (mill anneal) specimen, respectively. Frames shown are enlarged prints of 16 mm. film, and are representative of both slow and rapid crack growth, complete specimen separation is also shown. The large amount of specimen compliance and the blunt shape of the crack were observed only in films of elevated temperature titanium specimens.

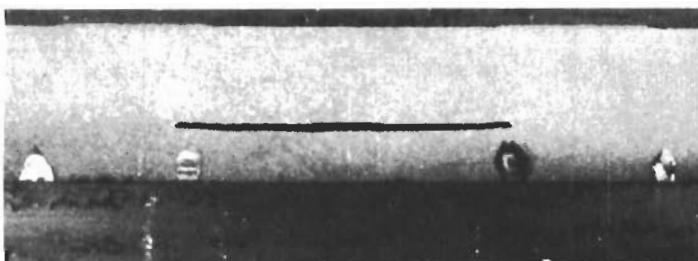
TEST RESULTS

Graphs of crack length and load versus time (film frames) are shown in Figs. 255 through 301. Critical crack length has been defined as the crack length at maximum load; this definition provides conservative fracture toughness values, because computations of K_C beyond the maximum load will yield larger K_C values.

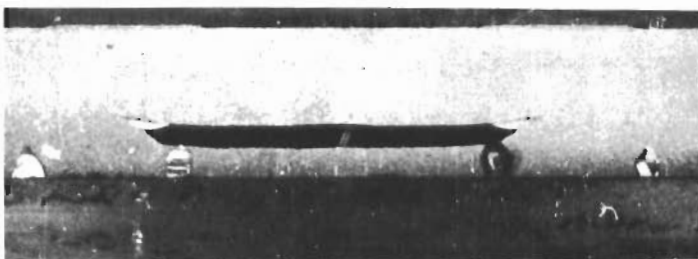
Specimen data as well as values of K_C computed from the critical crack lengths obtained by high-speed photography are contained in Table 33 for information. In general, the K_C values are higher than the corresponding K_{CN} values.



800 FRAMES BEFORE SEPARATION,
 $2a = 2.14$ INCHES,
 LOAD = 120.3 KIPS,
 START OF SLOW CRACK GROWTH.



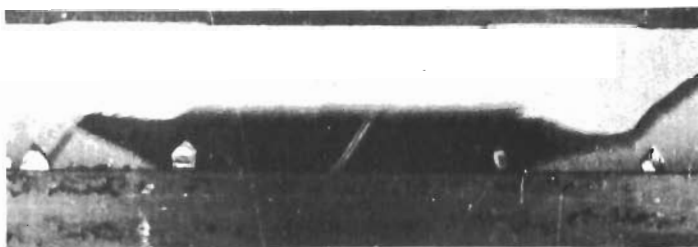
365 FRAMES BEFORE SEPARATION,
 $2a = 2.25$ INCHES,
 LOAD = 133 KIPS,
 APPROACHING FRAME
 175 WHERE
 $2a_{CR} \approx 2.35$ INCHES AND
 ULTIMATE LOAD = 137 KIPS



40 FRAMES BEFORE SEPARATION,
 $2a = 2.72$ INCHES,
 LOAD = 133.4 KIPS,
 PAST $2a_{CR}$ AND LOAD
 IS FALLING



1 FRAME BEFORE SEPARATION,
 $2a = 3.63$ INCHES,
 LOAD RAPIDLY APPROACHING
 ZERO,
 APPROXIMATELY .34 INCHES
 COMPLIANCE



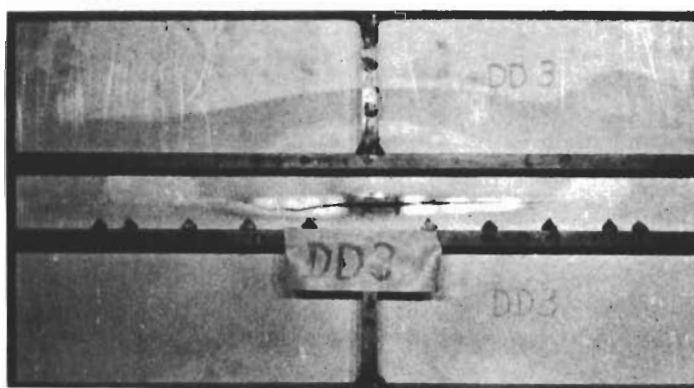
COMPLETE SEPARATION,
 LOAD = ZERO.

NOTE: Specimen DD77, $t = .21$ inch, $\dot{\sigma} = 5.74 \times 10^6$ psi/second, 650° F,
 Film Speed = 360 frames/second.

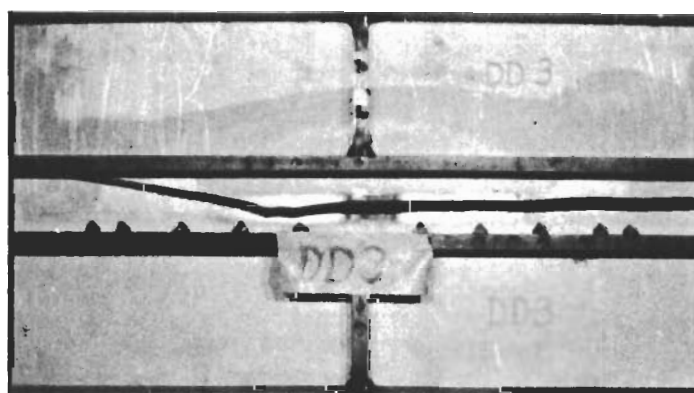
FIG.253 VARIOUS FRAMES SHOWING CRACK GROWTH OF 8 x 24 INCH Ti 6Al - 4V SPECIMEN



(A) APPROACHING CRITICAL CRACK LENGTH



(B) ONE FRAME BEFORE SEPARATION
(PAST $2a_{CR} \cong 1.23$ INCH)



(C) COMPLETE SPECIMEN SEPARATION

NOTE: Specimen DD3, $t = .049$ inch, $\dot{\sigma} = 5 \times 10^3$ psi/second, Room Temperature,
Film Speed = 360 frames/second Nominal

FIG.254 VARIOUS FRAMES SHOWING CRACK GROWTH OF 24 x 72 INCH Ti 6Al - 4V SPECIMEN

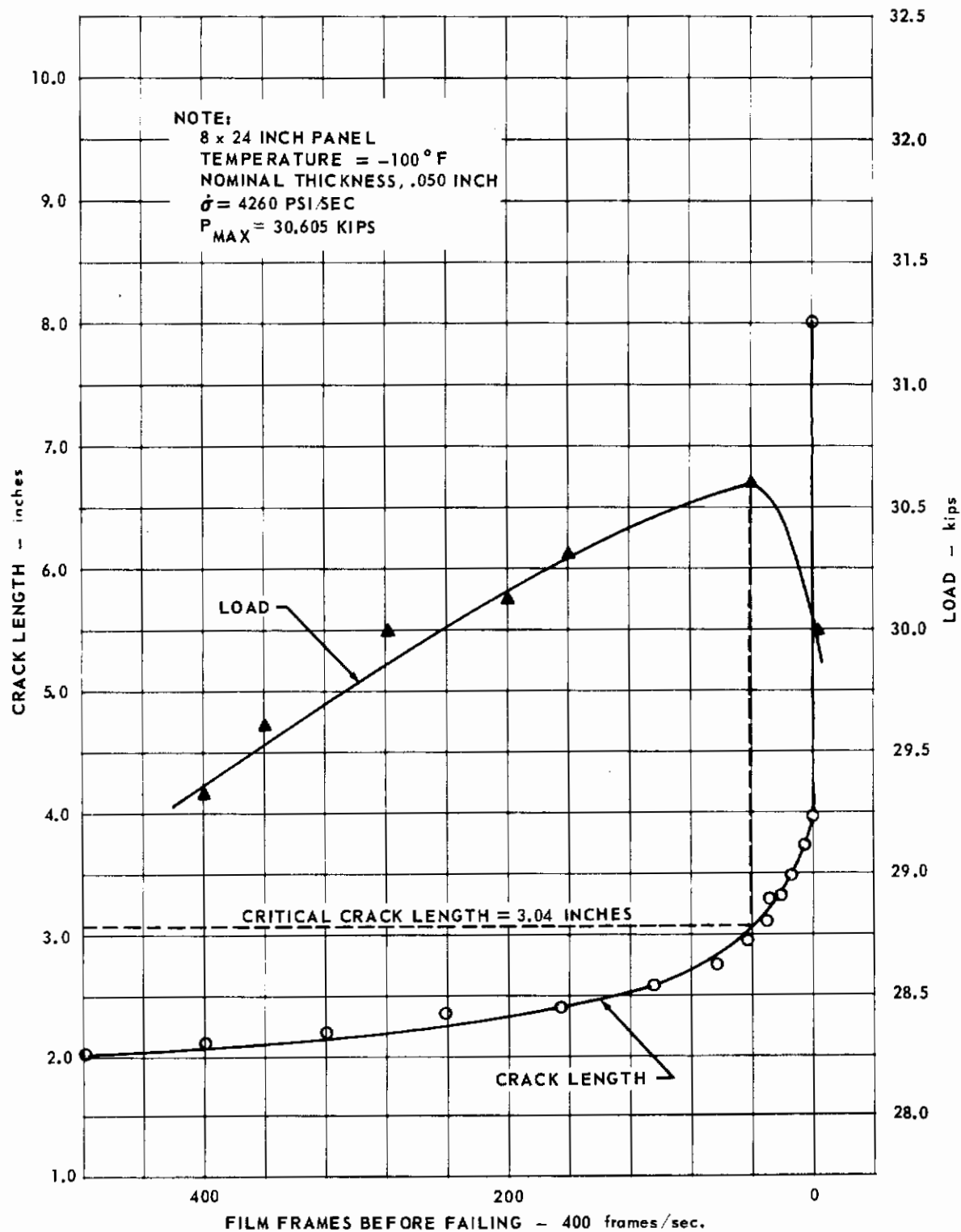


FIG. 255 STATIC CRACK GROWTH FOR Ti 8Al-1Mo-1V SPECIMEN DA19

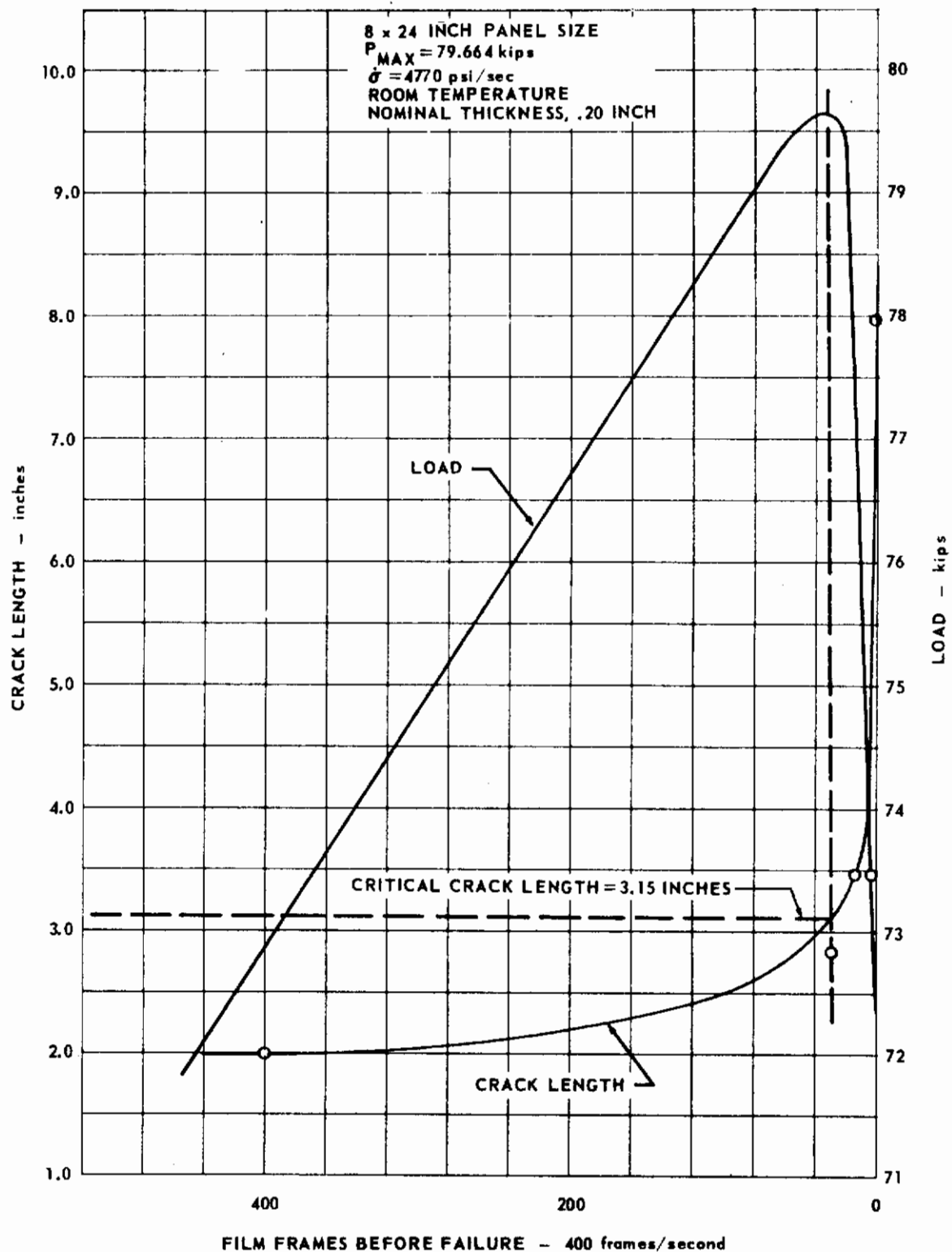


FIG. 256 STATIC CRACK GROWTH FOR Ti 8Al - 1Mo - 1V SPECIMEN DA75

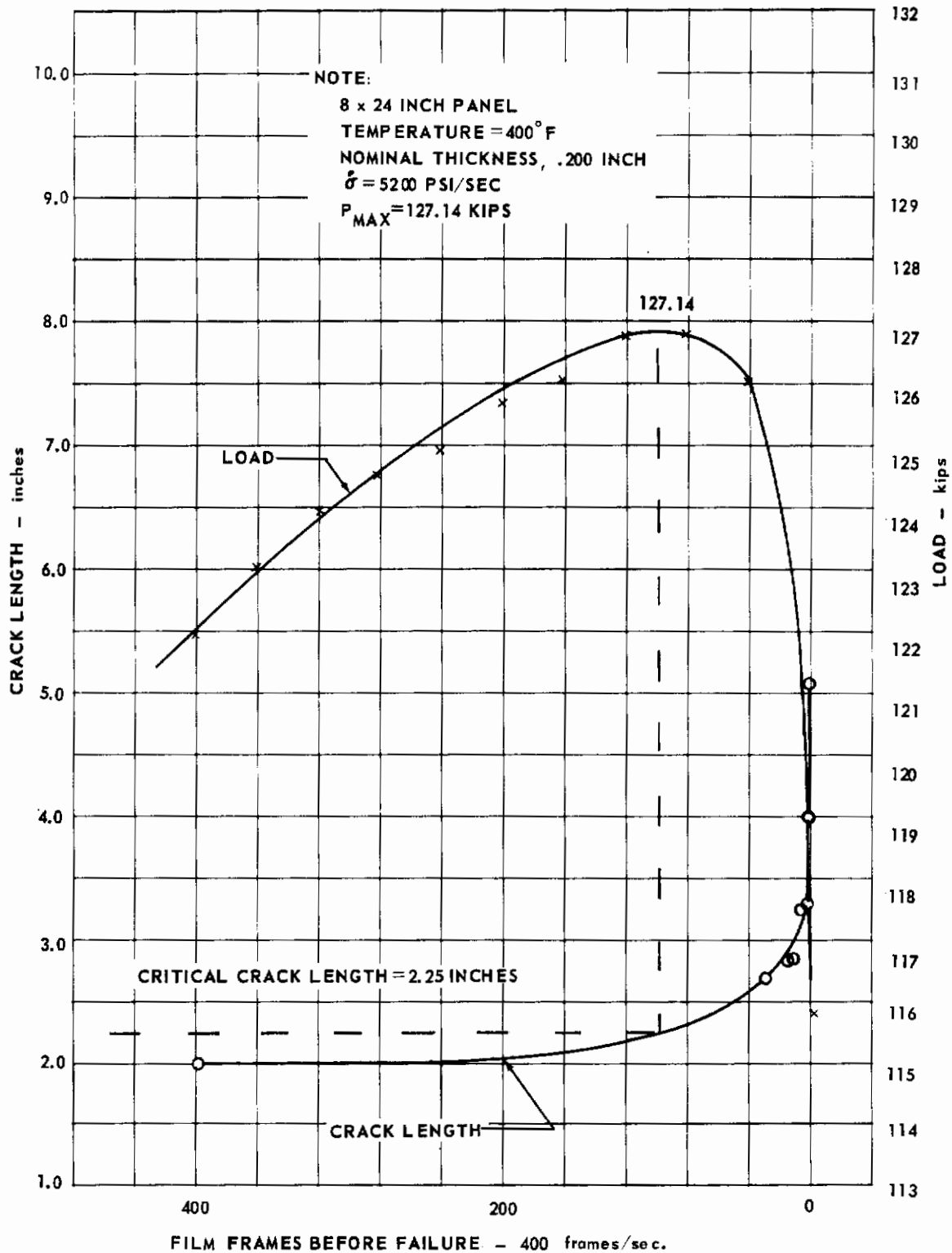


FIG. 257 STATIC CRACK GROWTH FOR Ti 8Al-1Mo-1V SPECIMEN DA76

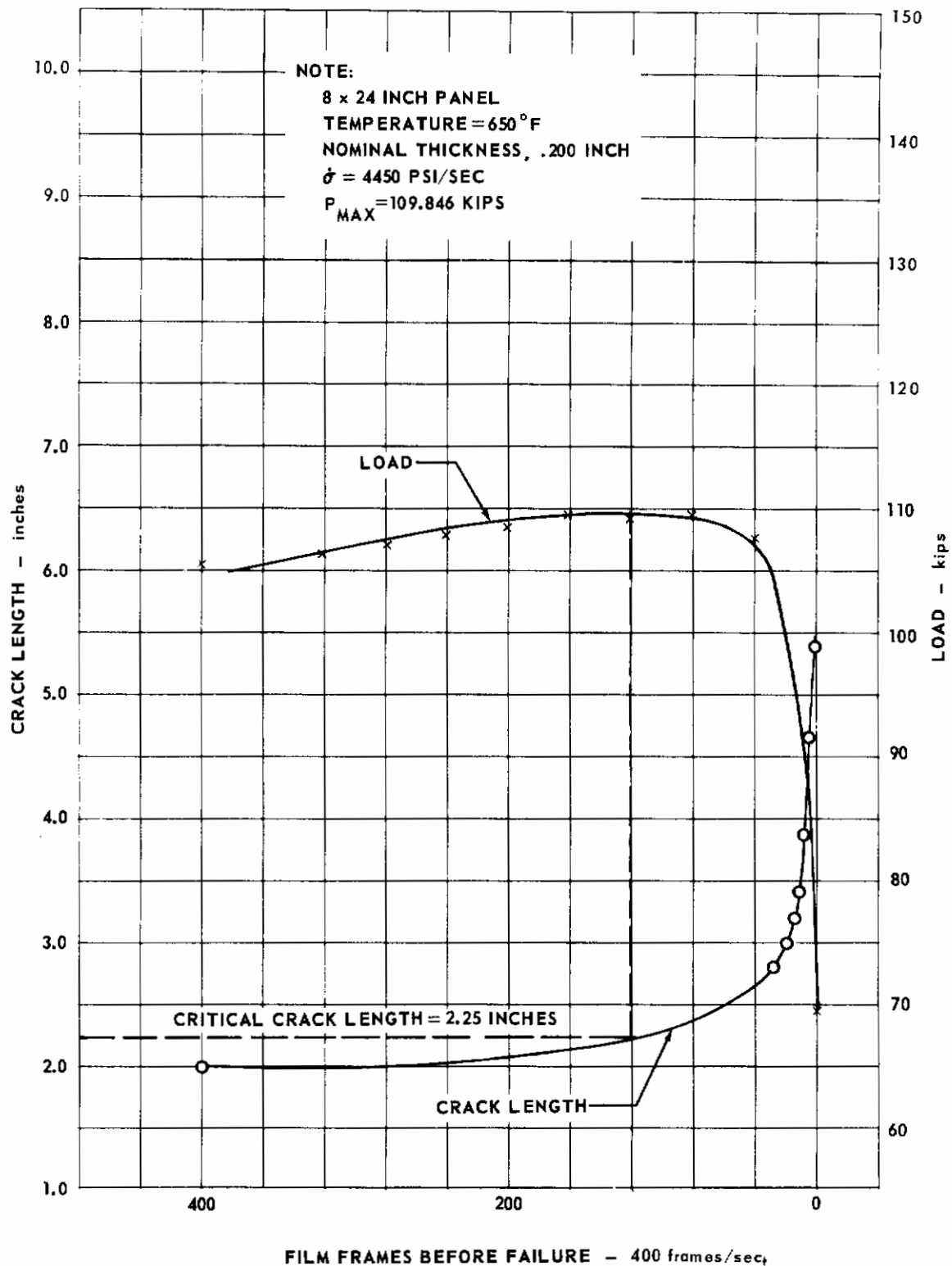


FIG. 258 STATIC CRACK GROWTH FOR Ti 8Al-1Mo-1V SPECIMEN DA77

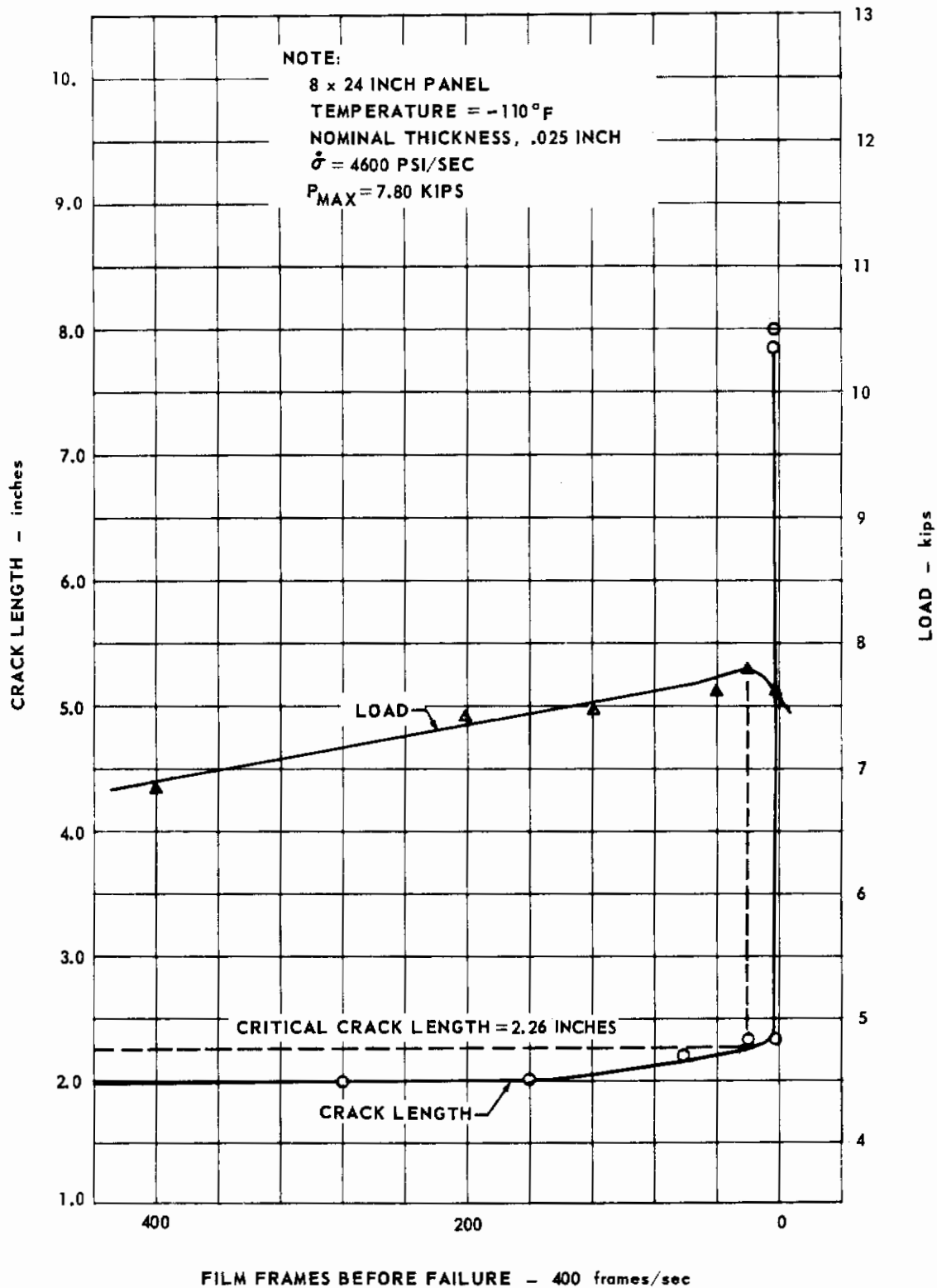


FIG. 259 STATIC CRACK GROWTH FOR AM 350 SPECIMEN DB19

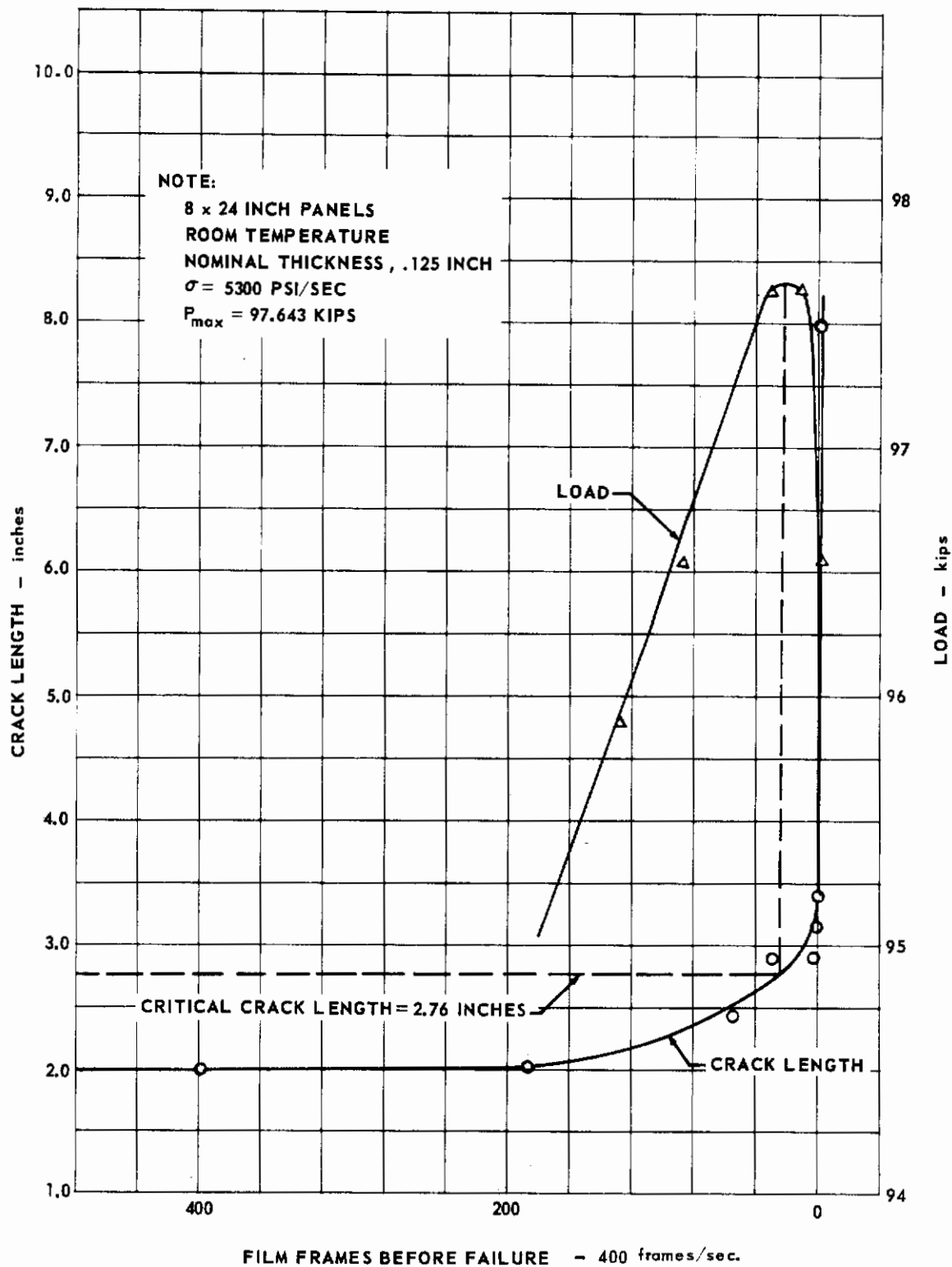


FIG. 260 STATIC CRACK GROWTH FOR AM 350 SPECIMEN DB75

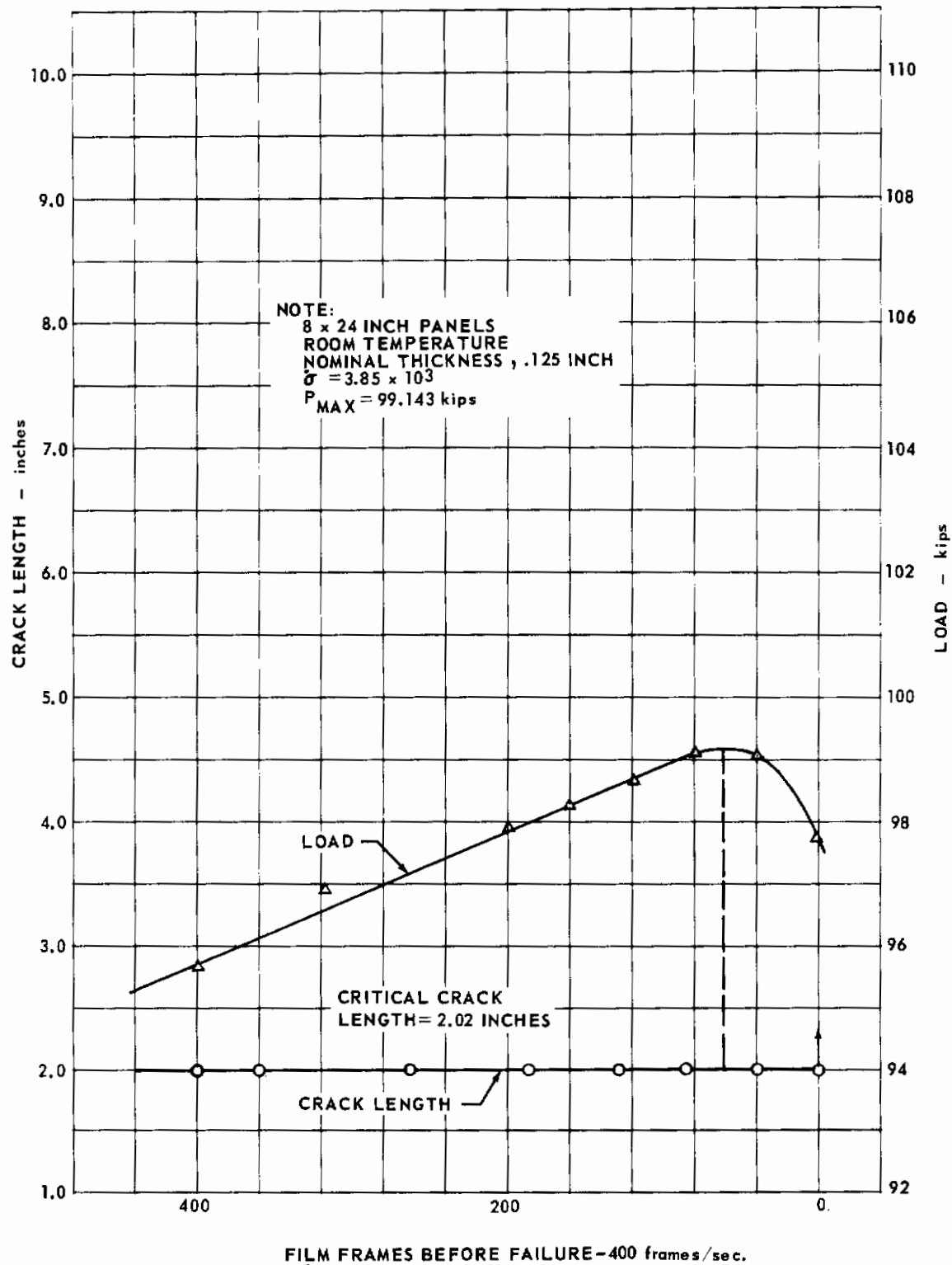


FIG. 261 STATIC CRACK GROWTH FOR AM 350 SPECIMEN DB76

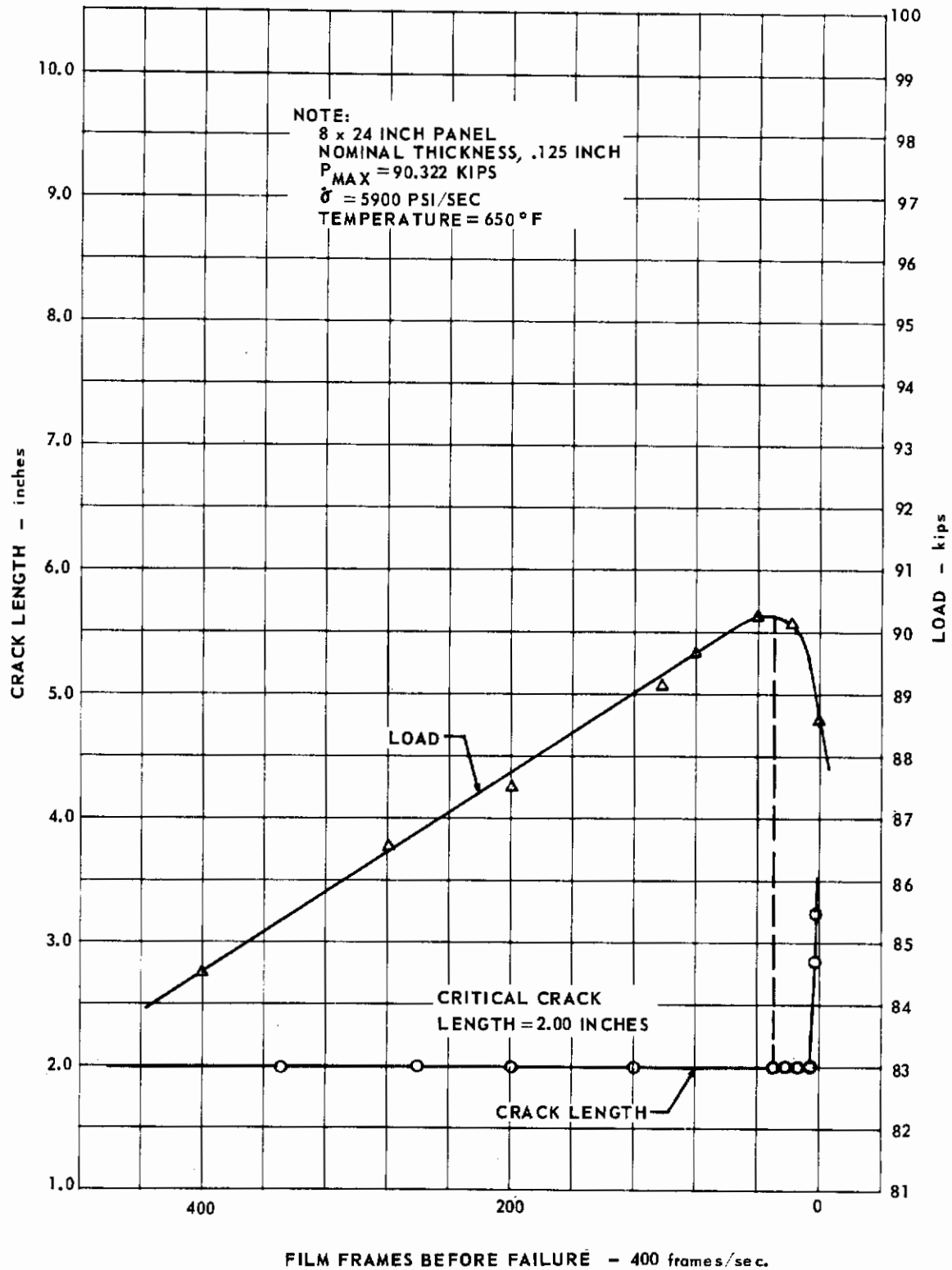


FIG. 262 STATIC CRACK GROWTH FOR AM 350 SPECIMEN DB77

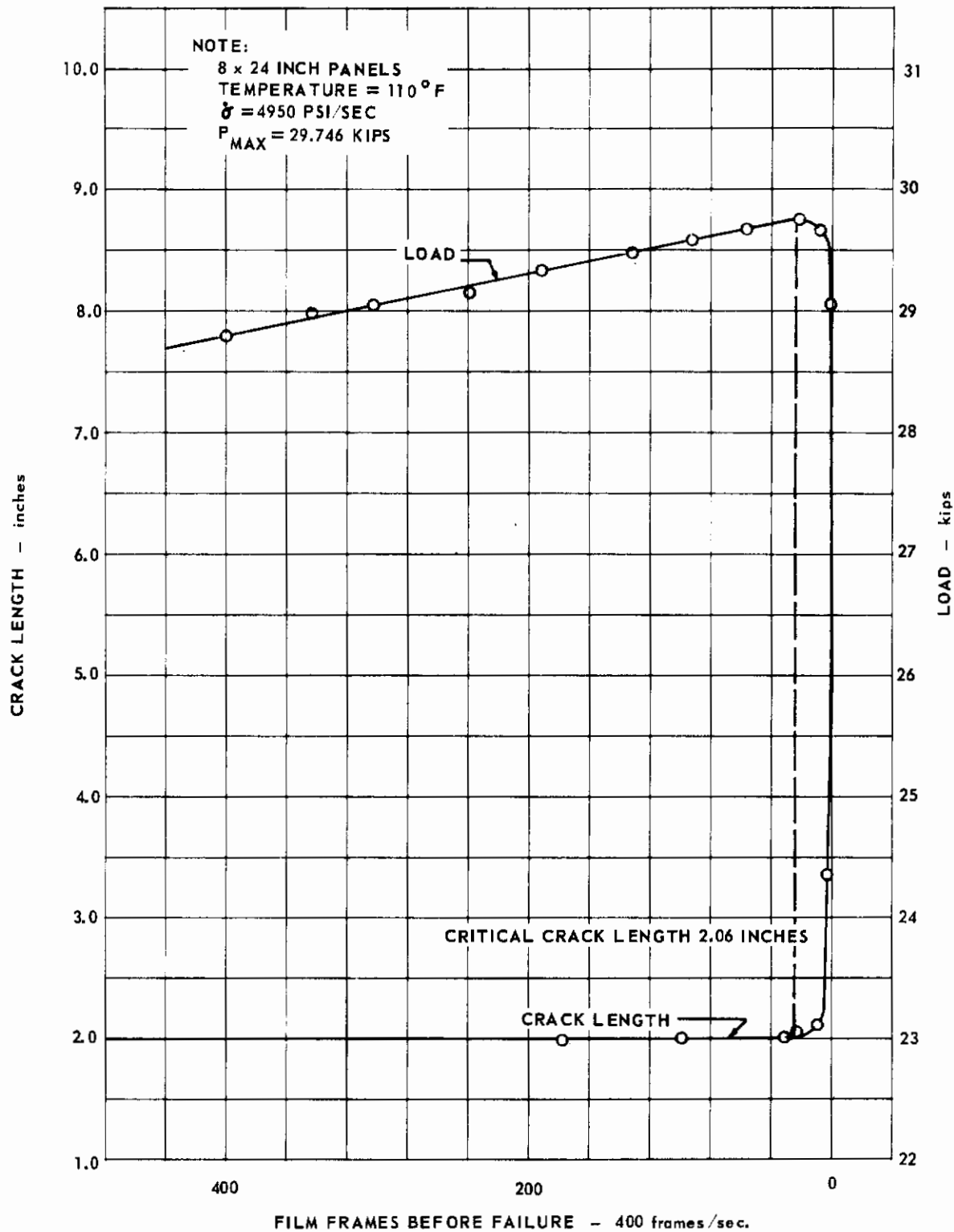


FIG. 263 STATIC CRACK GROWTH FOR INCO 718 SPECIMEN DC19

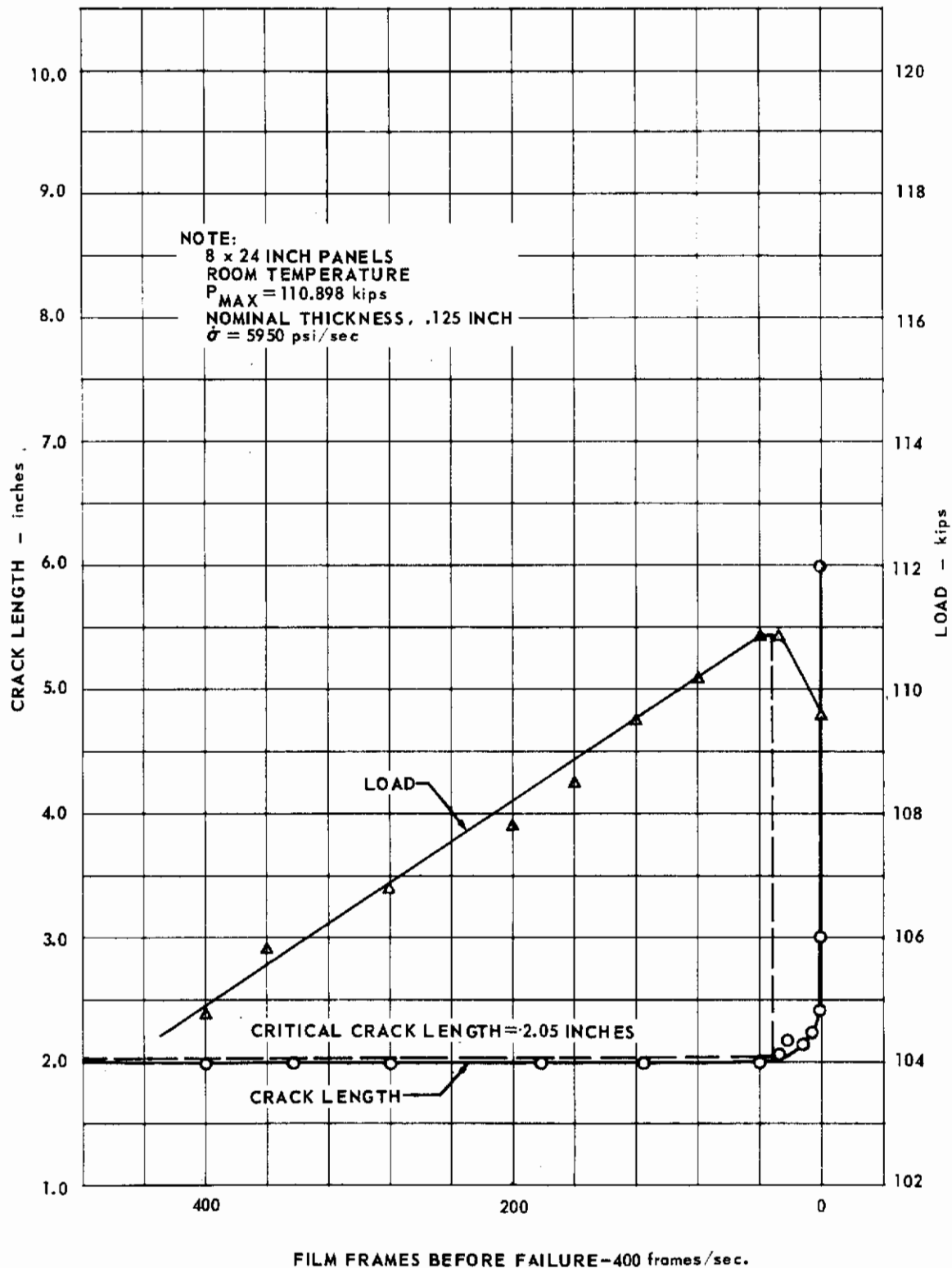


FIG. 264 STATIC CRACK GROWTH FOR INCO 718 SPECIMEN DC75

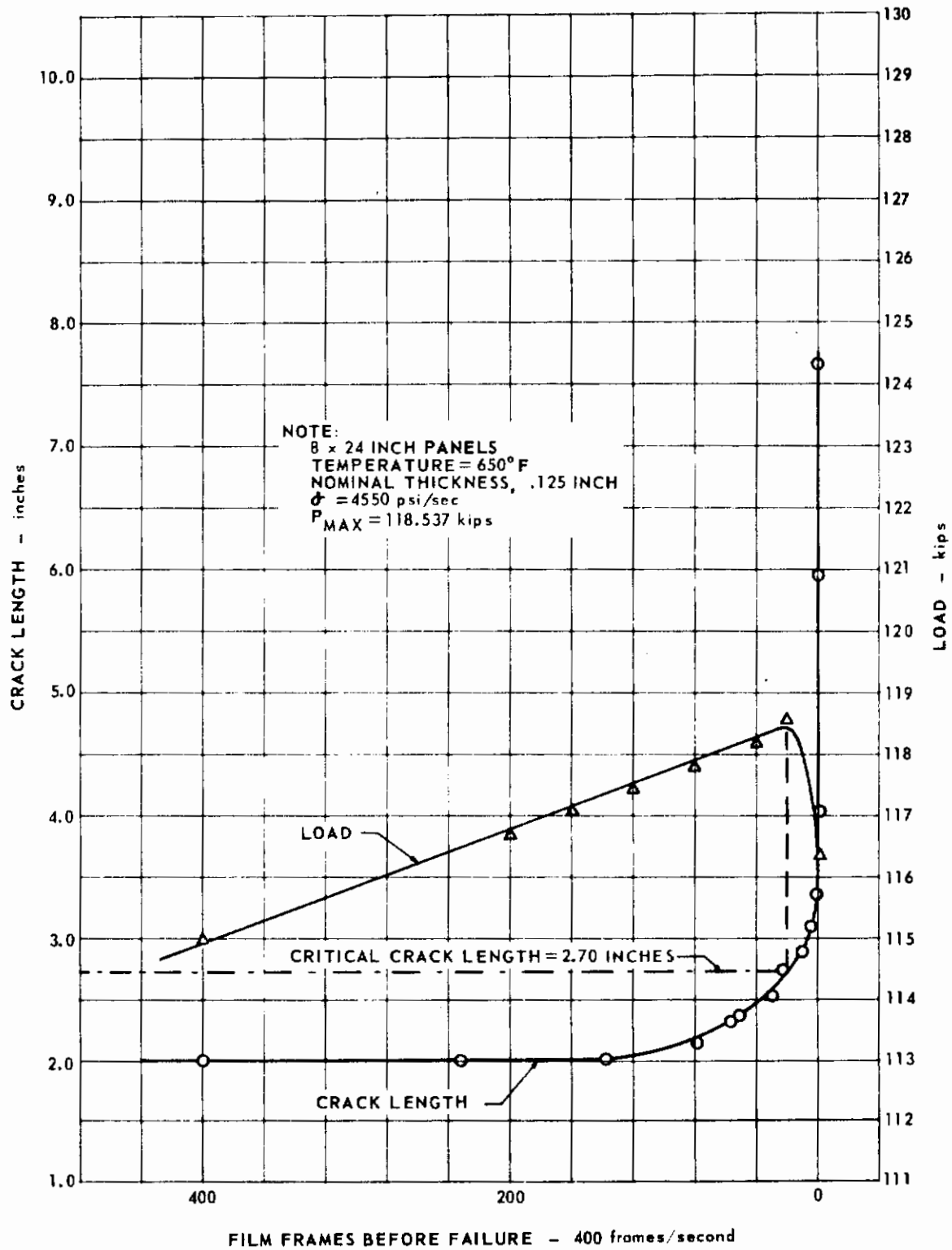


FIG. 265 STATIC CRACK GROWTH FOR INCO 718 SPECIMEN DC77

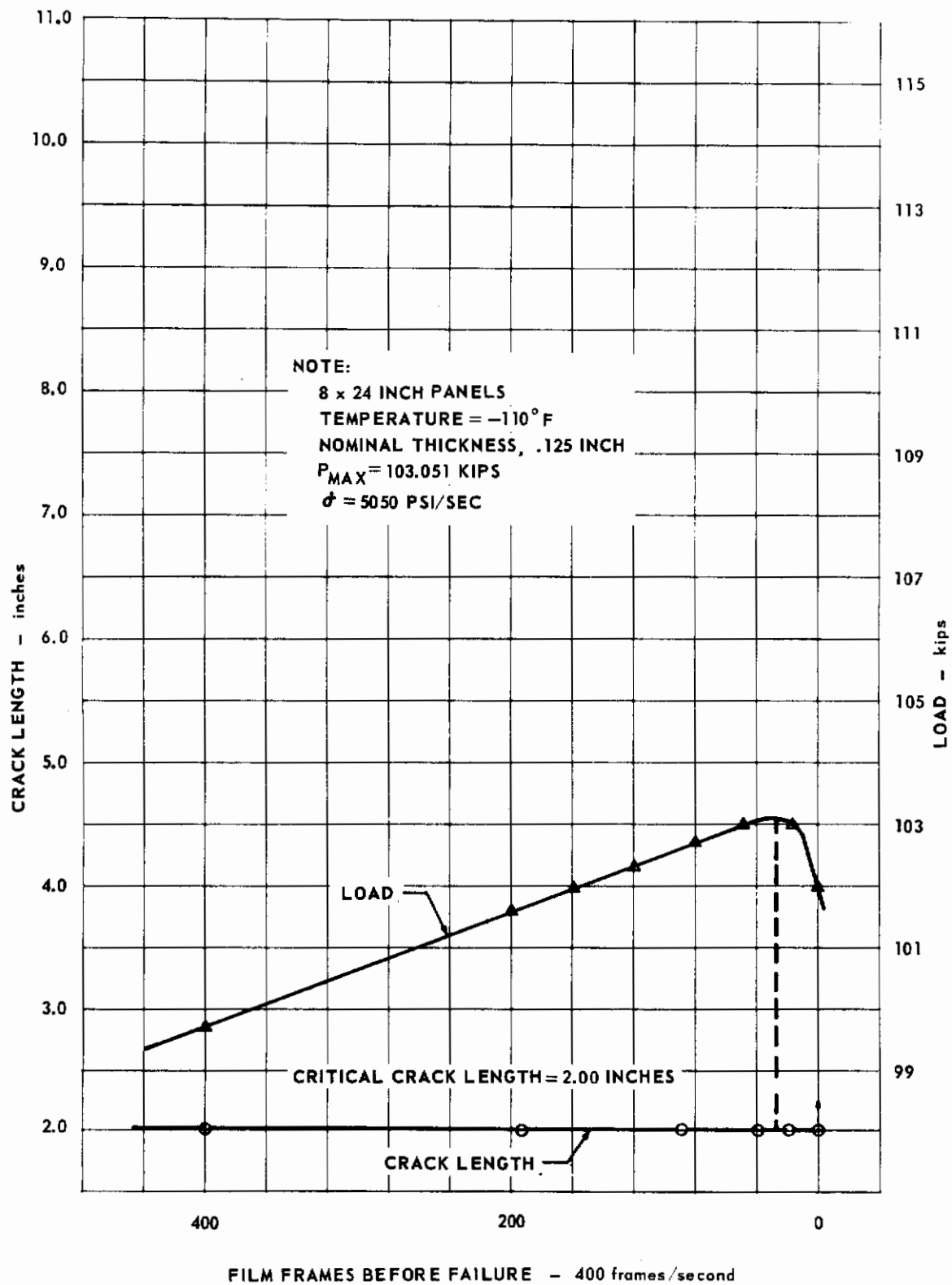


FIG. 266 STATIC CRACK GROWTH FOR INCO 718 SPECIMEN DC78

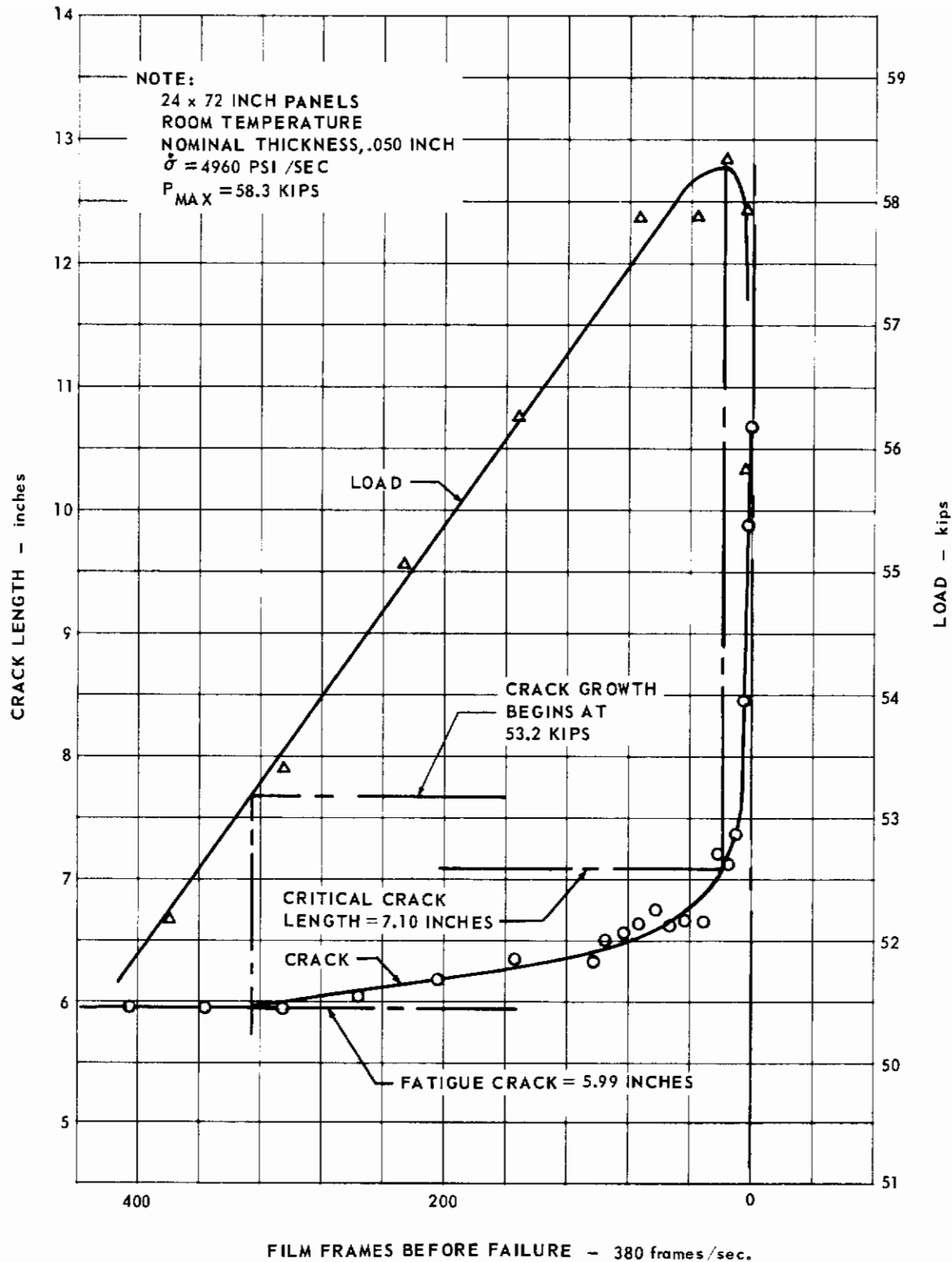


FIG. 267 STATIC CRACK GROWTH FOR Ti 6Al-4V SPECIMEN DD3

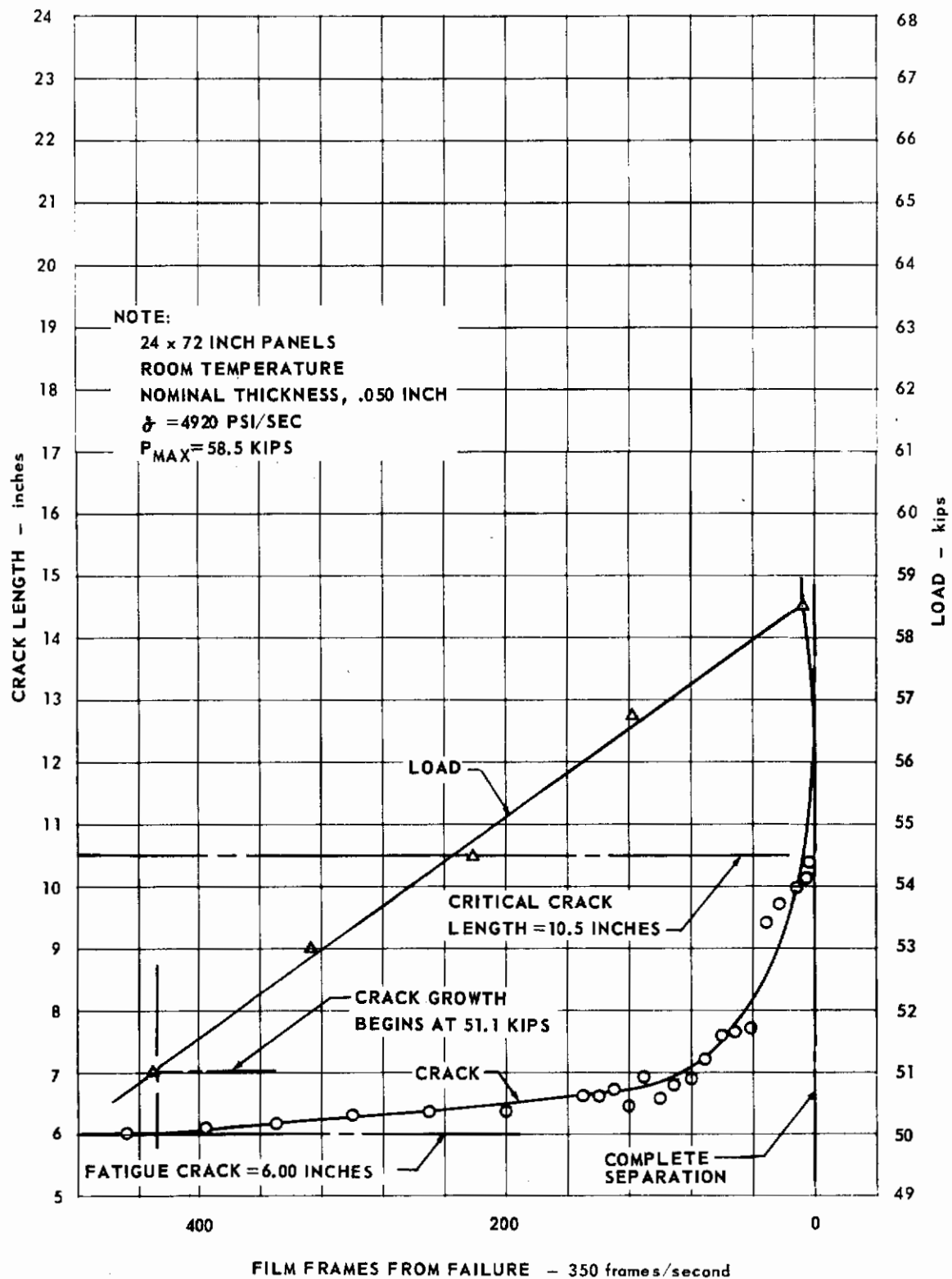


FIG. 268 STATIC CRACK GROWTH FOR TI 6Al-4V SPECIMEN DD4

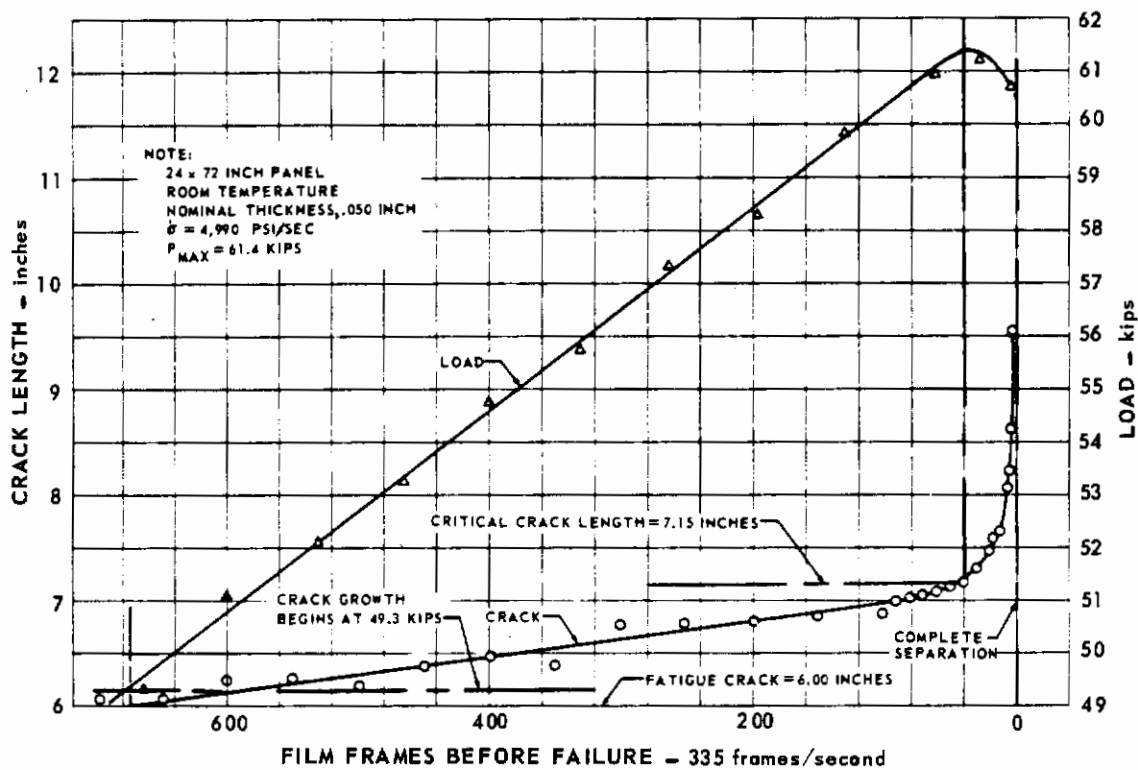


FIG. 269 STATIC CRACK GROWTH FOR Ti 6Al-4V SPECIMEN DD5

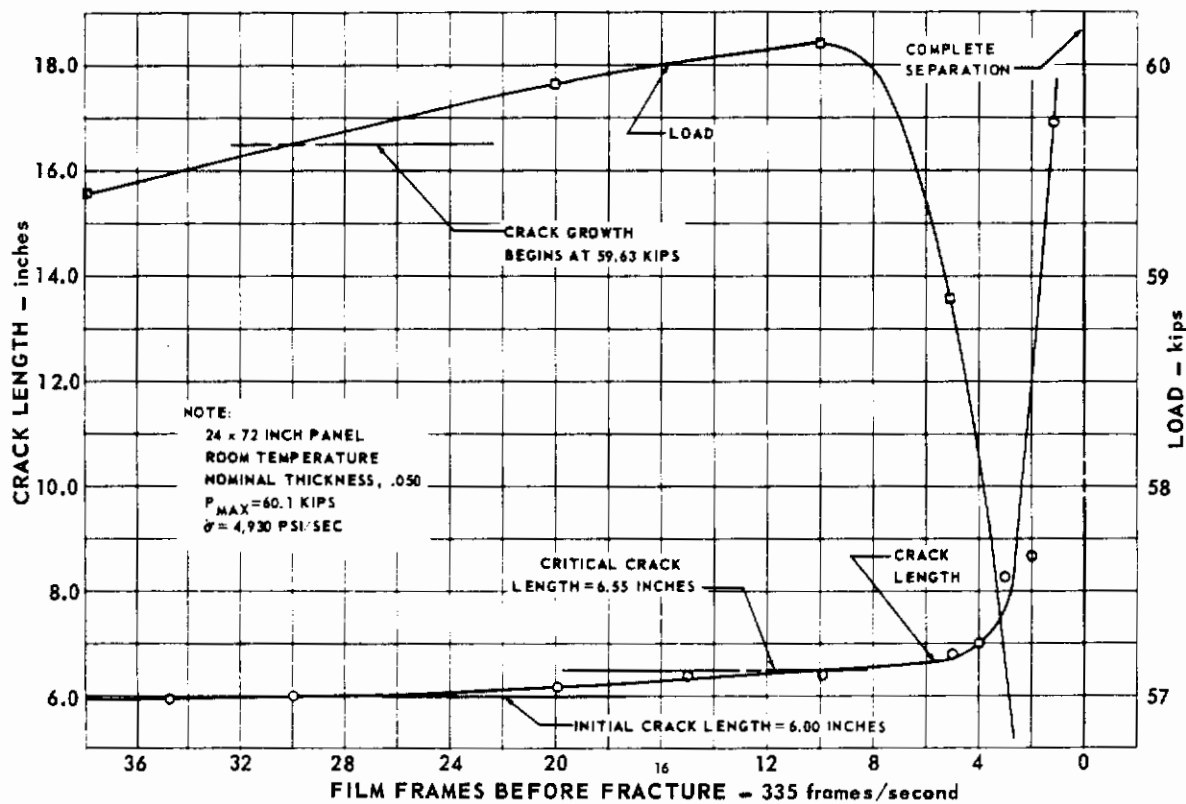


FIG. 270 STATIC CRACK GROWTH FOR Ti 6Al-4V SPECIMEN DD6

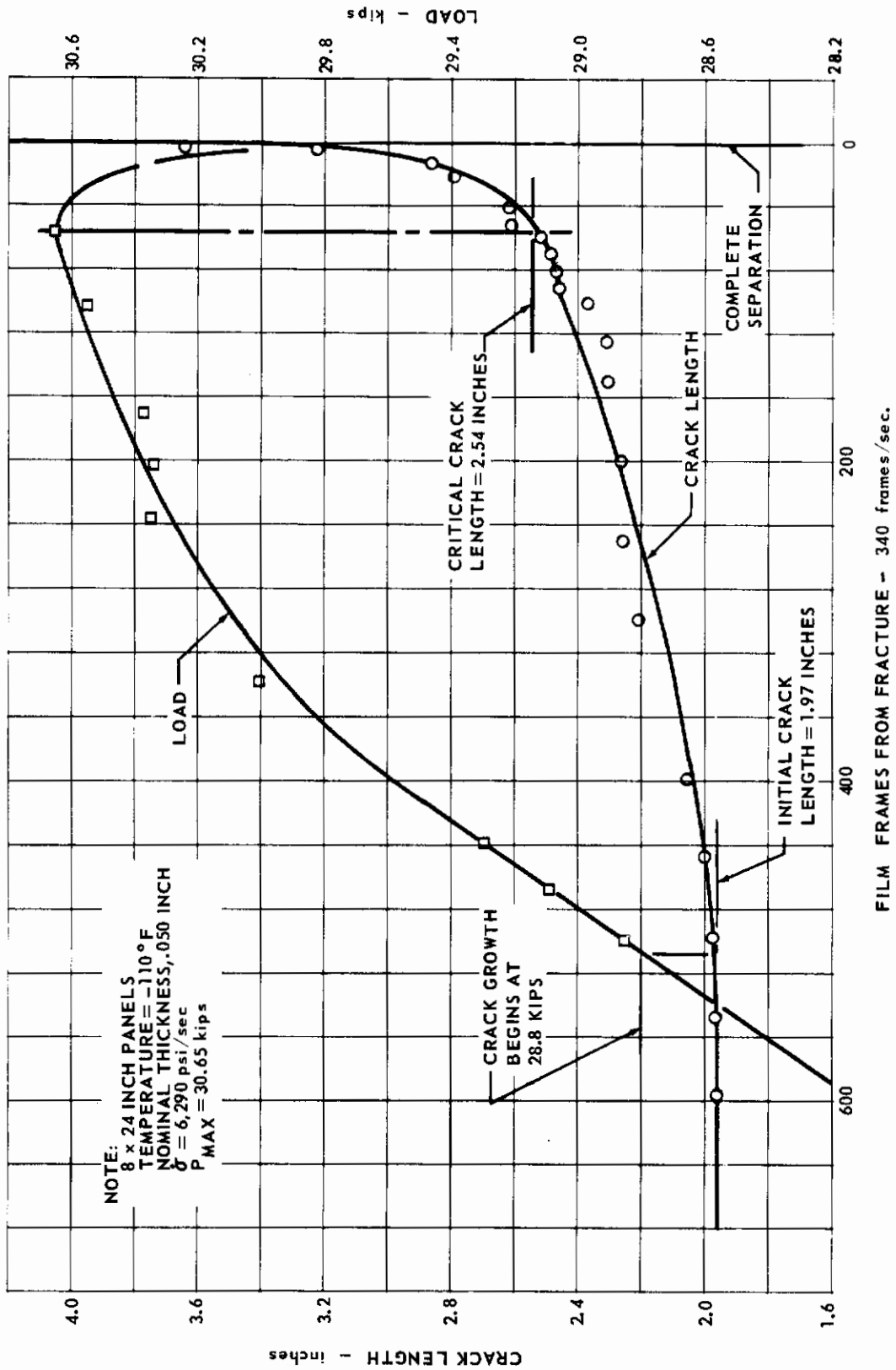


FIG. 271 STATIC CRACK GROWTH FOR Ti 6Al-4V SPECIMEN DD19

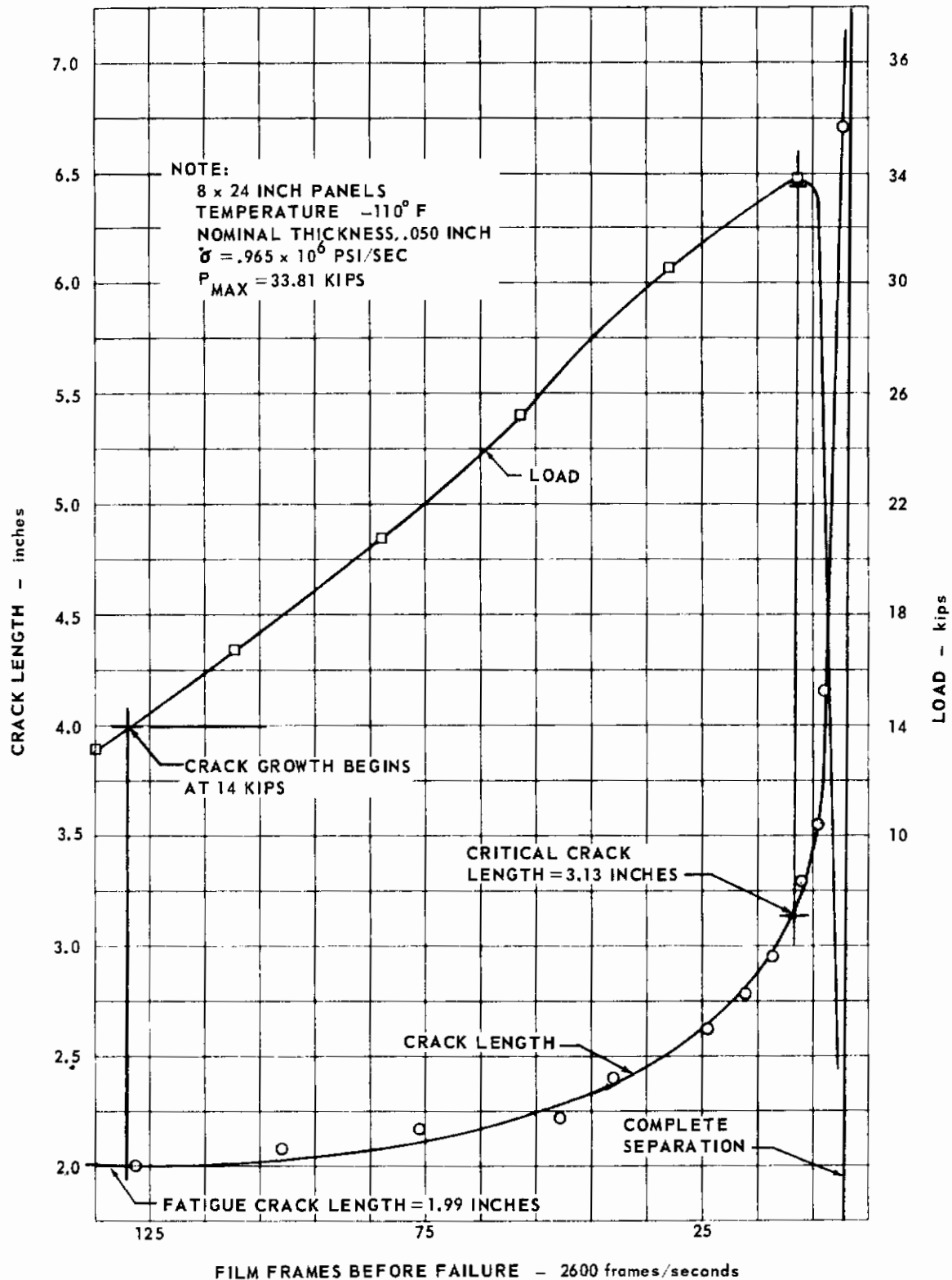


FIG. 272 STATIC CRACK GROWTH FOR Ti 6Al-4V SPECIMEN DD20

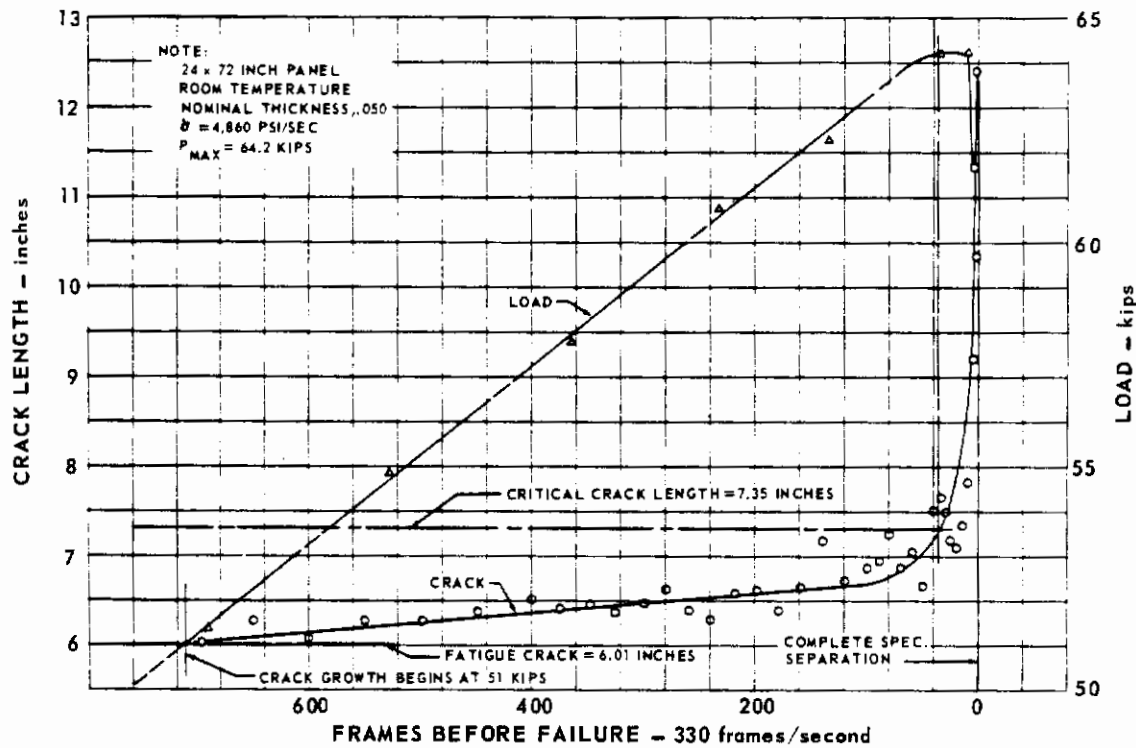


FIG. 273 STATIC CRACK GROWTH FOR Ti 6Al-4V SPECIMEN DD20

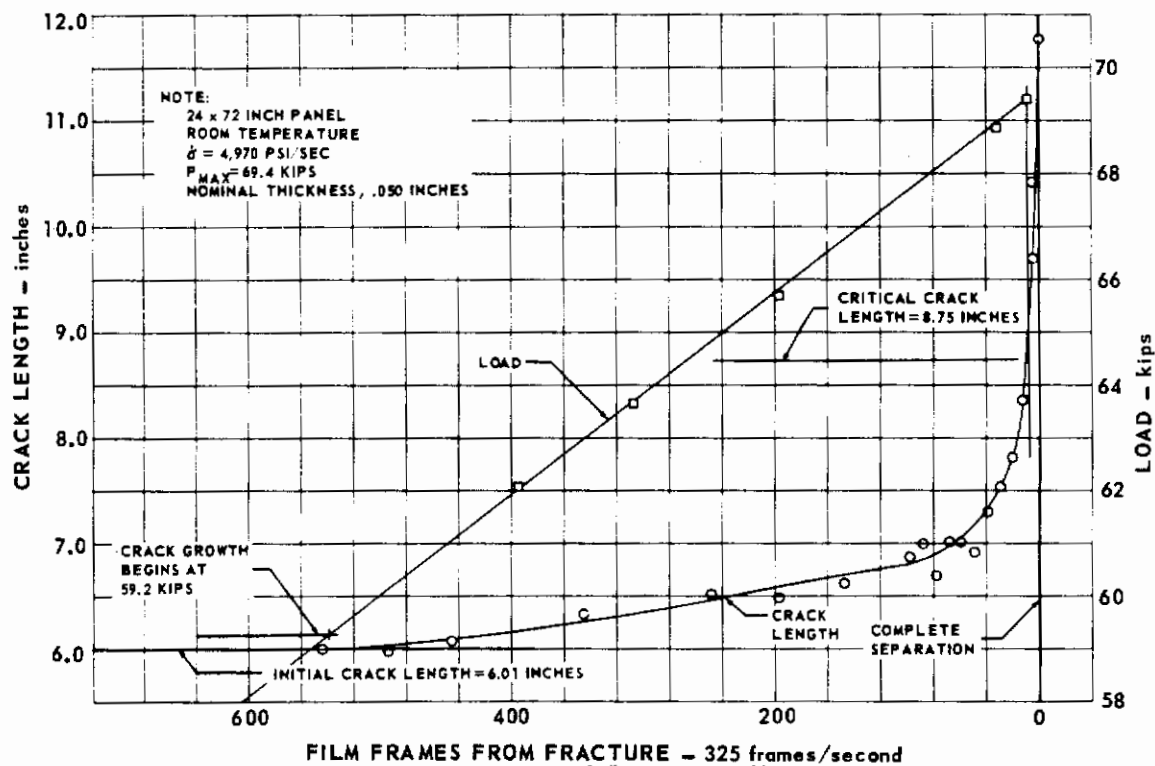


FIG. 274 STATIC CRACK GROWTH FOR Ti 6Al-4V SPECIMEN DD23

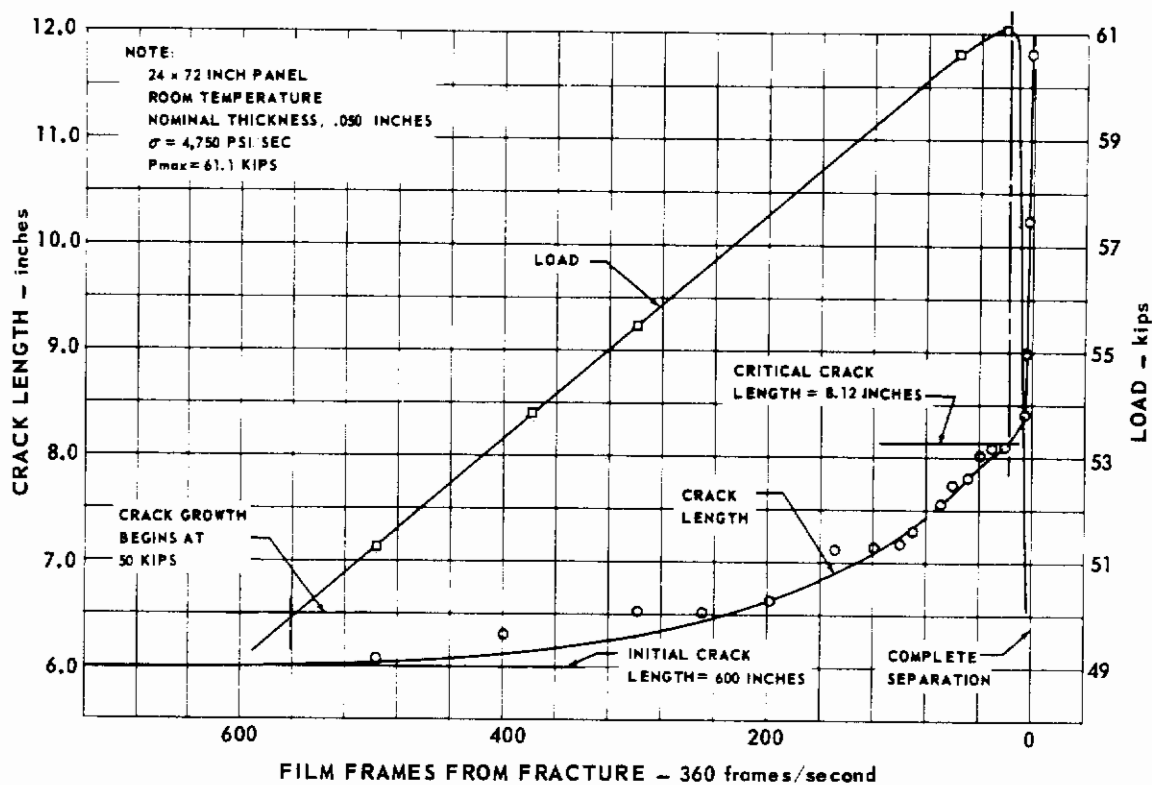


FIG. 275 STATIC CRACK GROWTH FOR Ti 6Al-4V SPECIMEN DD24

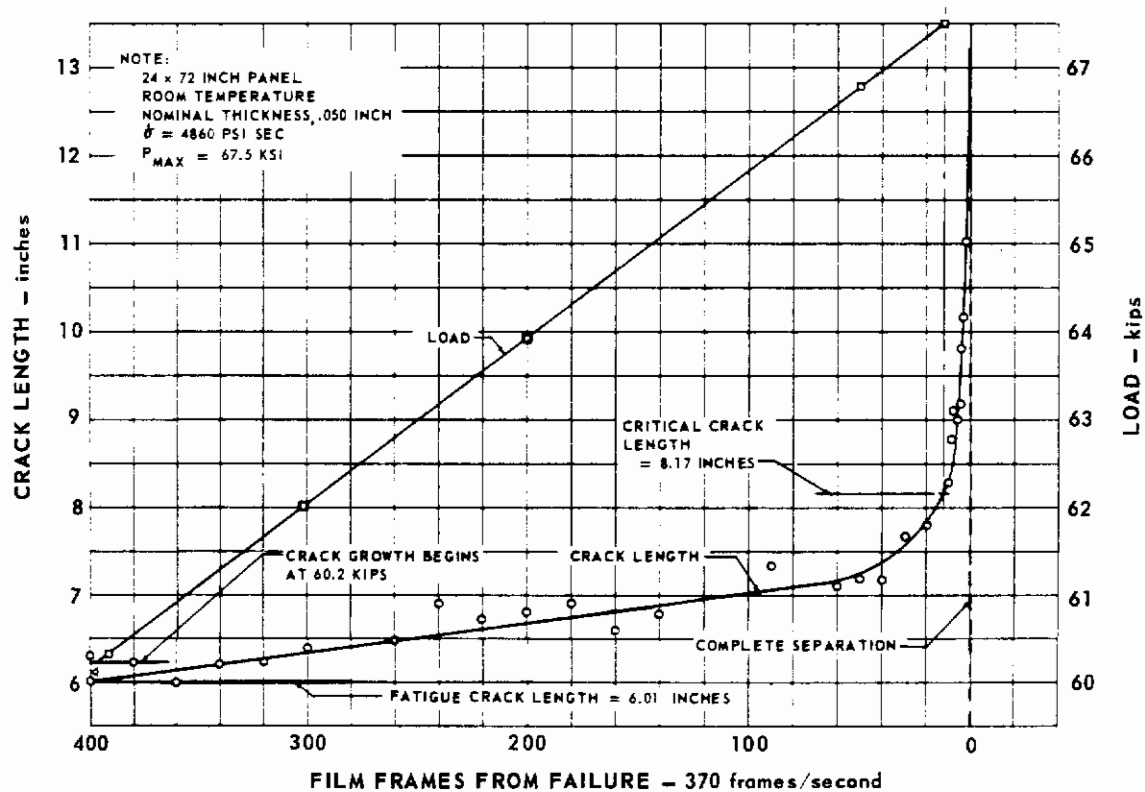


FIG. 276 STATIC CRACK GROWTH FOR Ti 6Al-4V SPECIMEN DD25

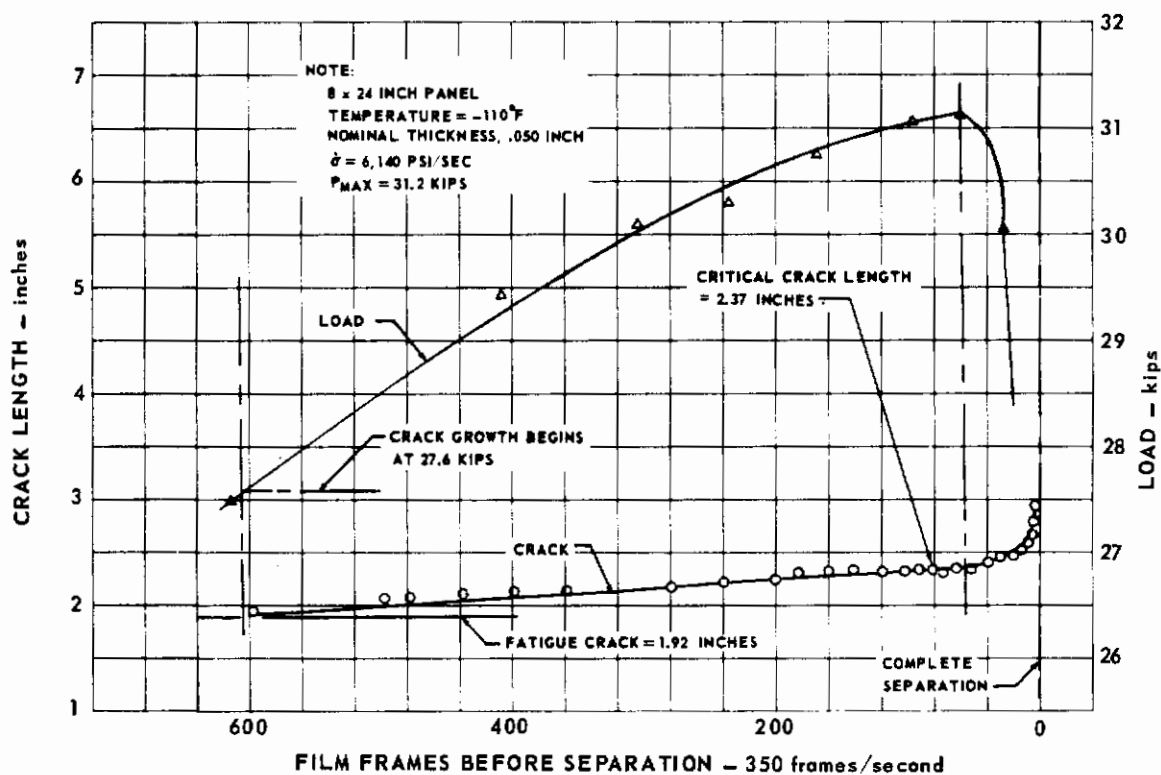


FIG. 277 STATIC CRACK GROWTH FOR Ti 6Al-4V SPECIMEN DD36

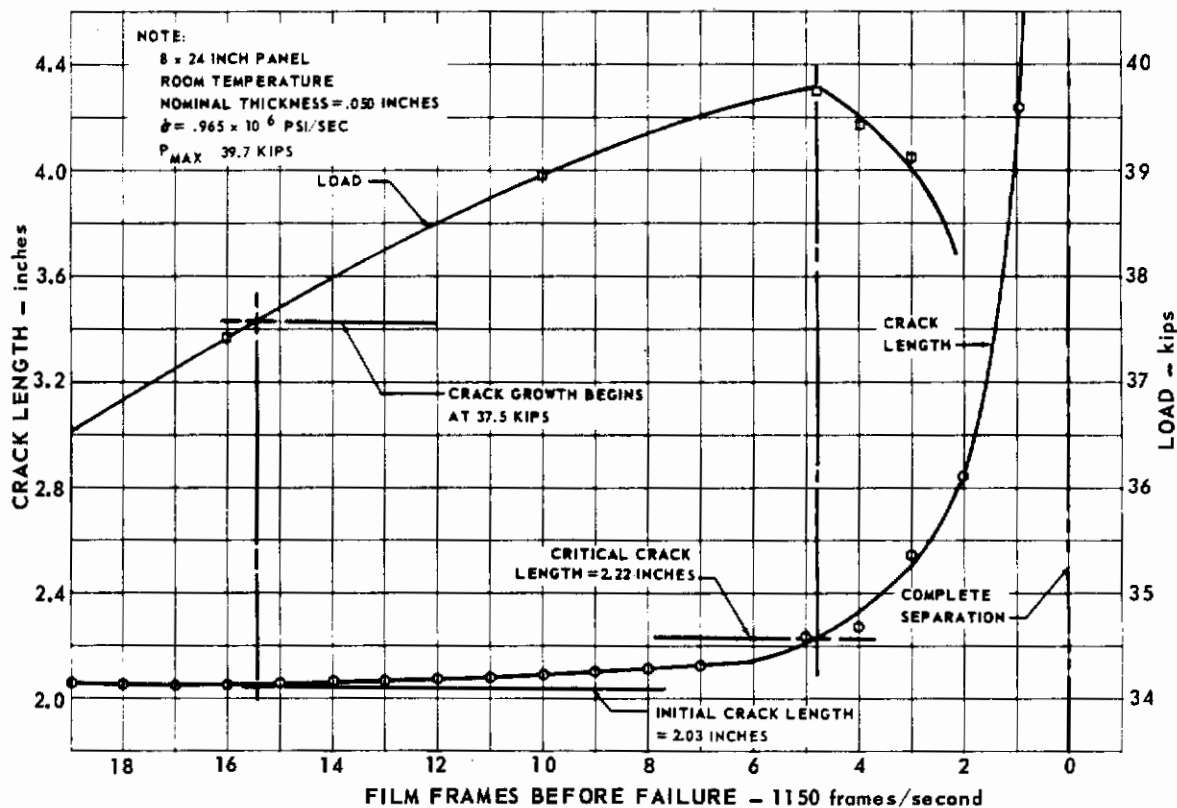


FIG. 278 STATIC CRACK GROWTH FOR Ti 6Al-4V SPECIMEN DD38

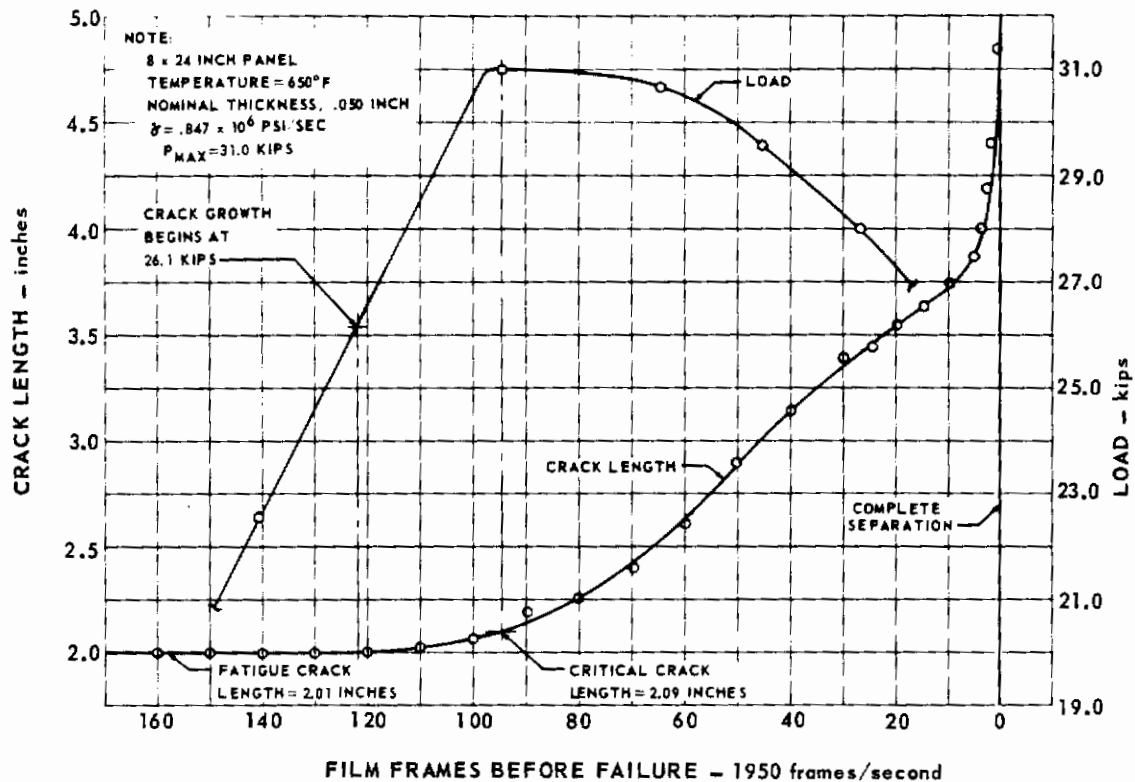


FIG. 279 STATIC CRACK GROWTH FOR Ti 6Al-4V SPECIMEN DD42

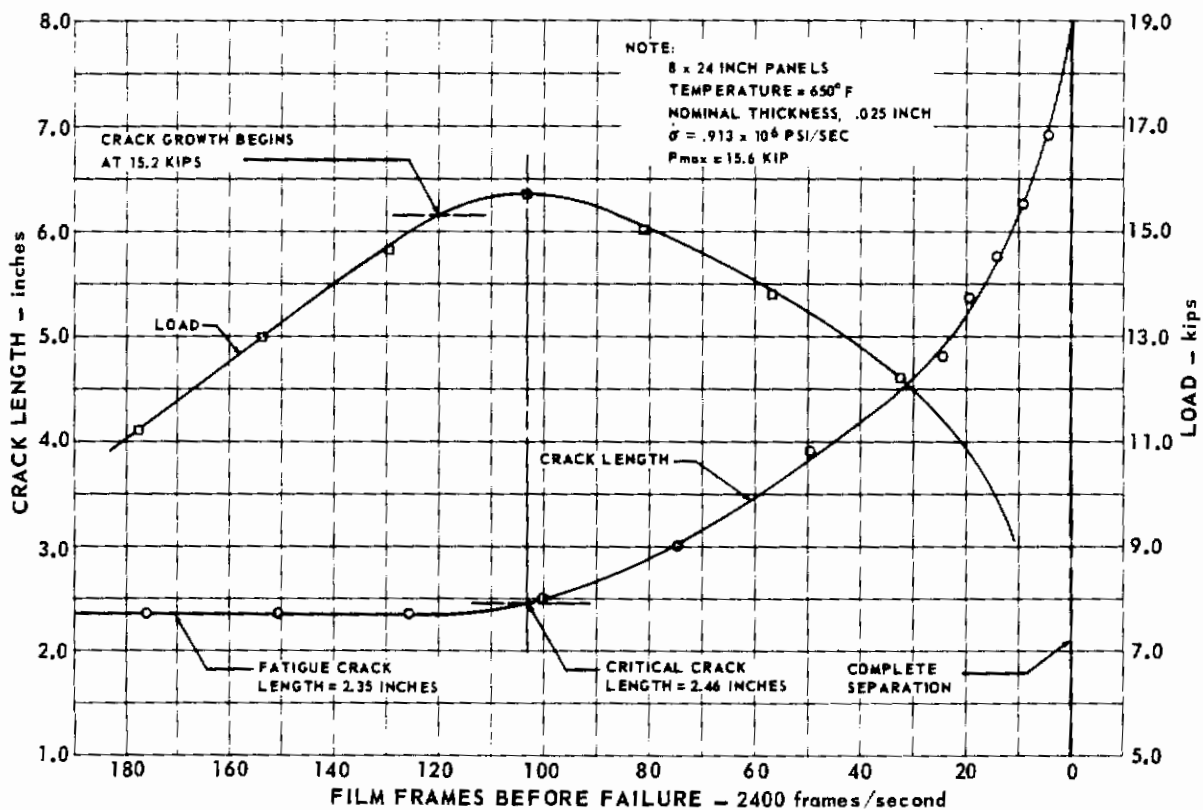


FIG. 280 STATIC CRACK GROWTH FOR Ti 6Al-4V SPECIMEN DD52

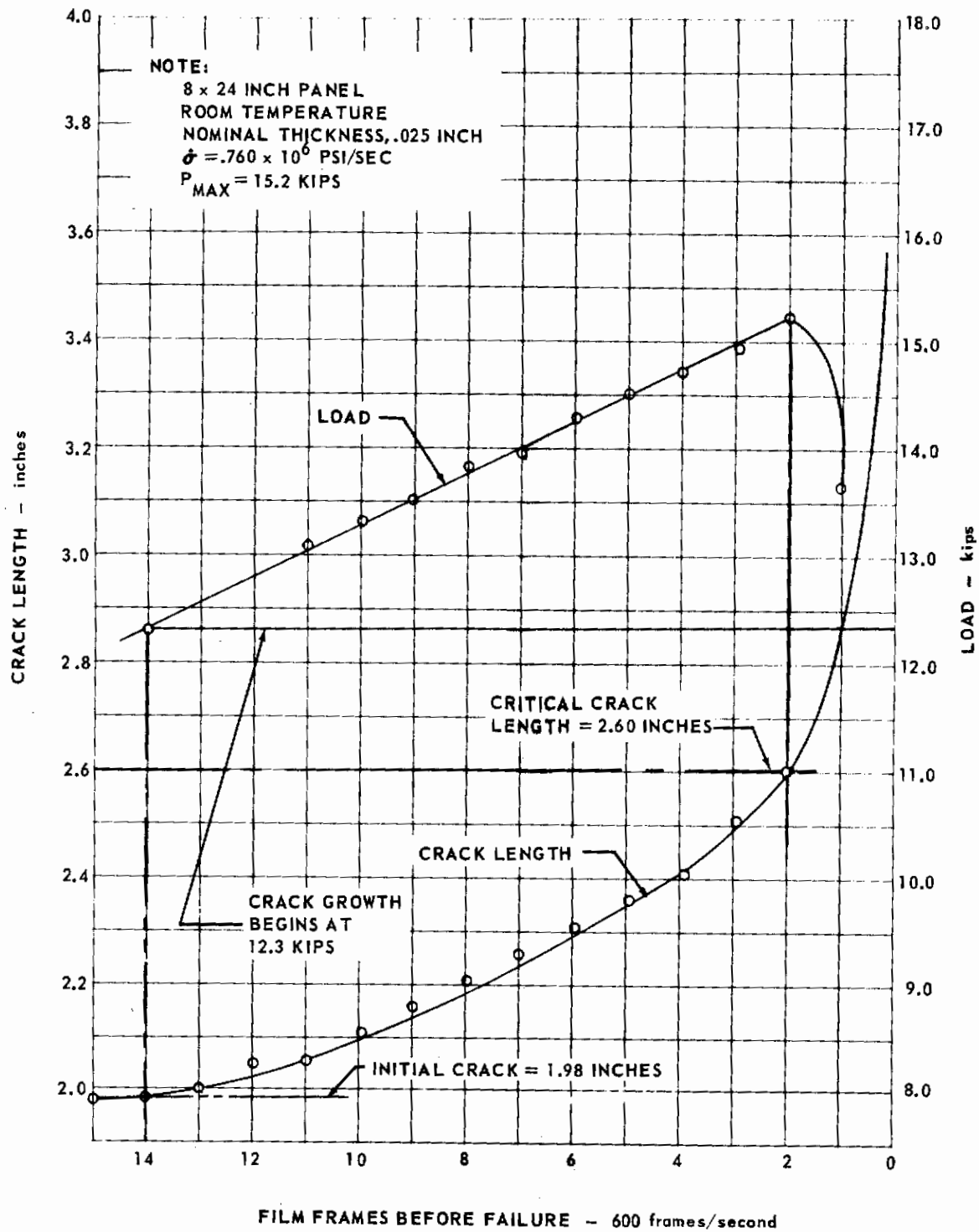


FIG. 281 STATIC CRACK GROWTH FOR Ti 6Al-4V SPECIMEN DD54

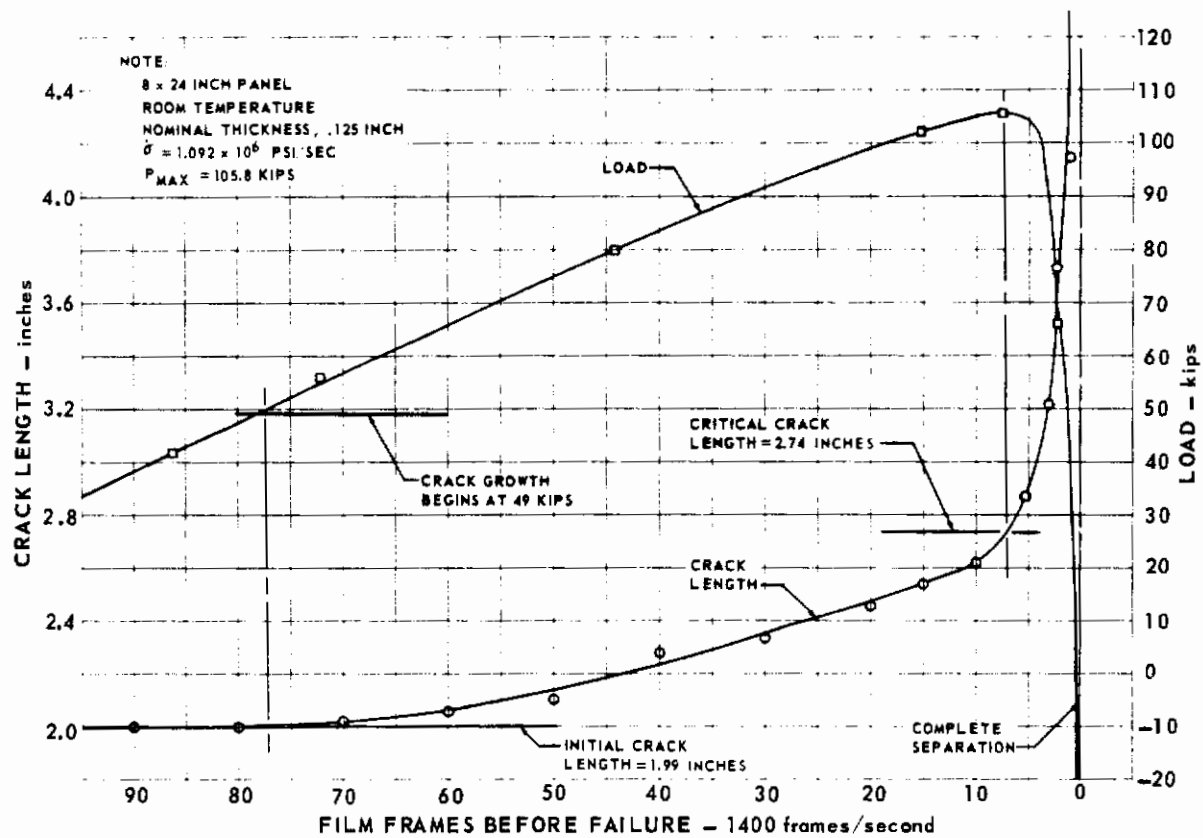


FIG. 282 STATIC CRACK GROWTH FOR Ti 6Al-4V SPECIMEN DD56

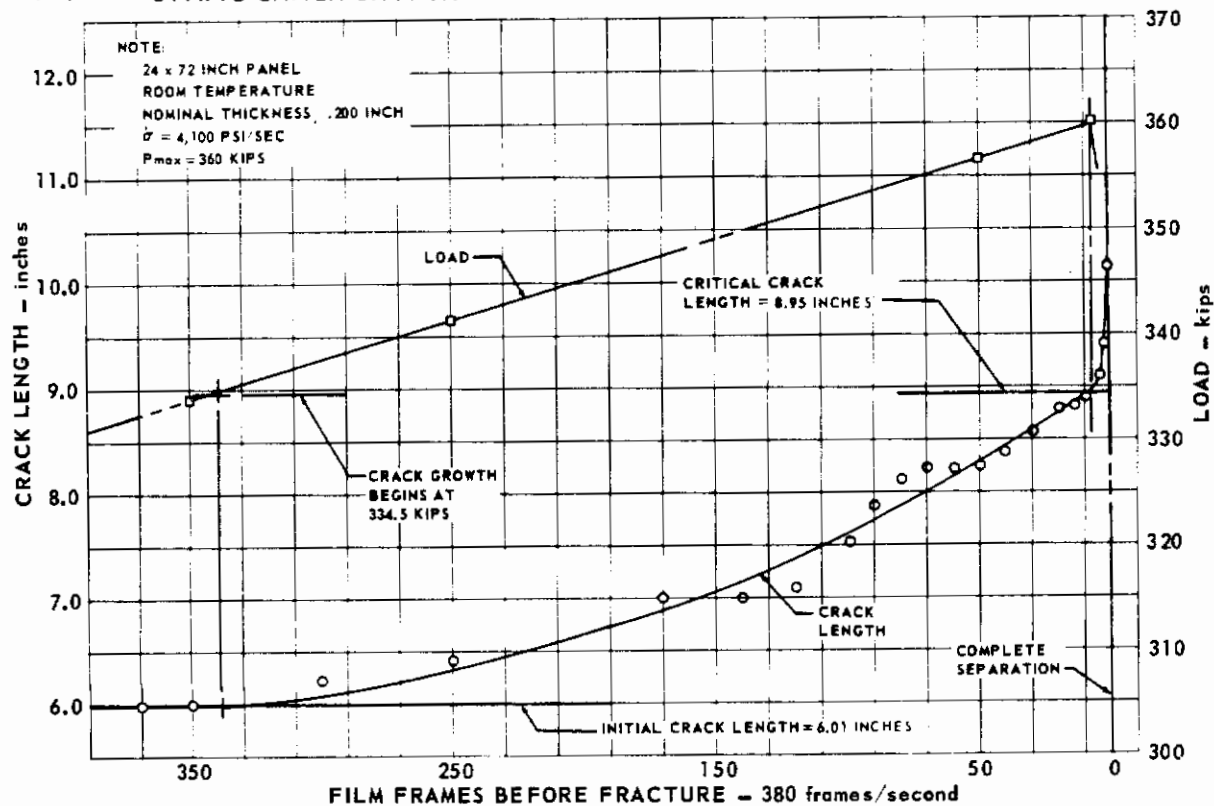


FIG. 283 STATIC CRACK GROWTH FOR Ti 6Al-4V SPECIMEN DD70

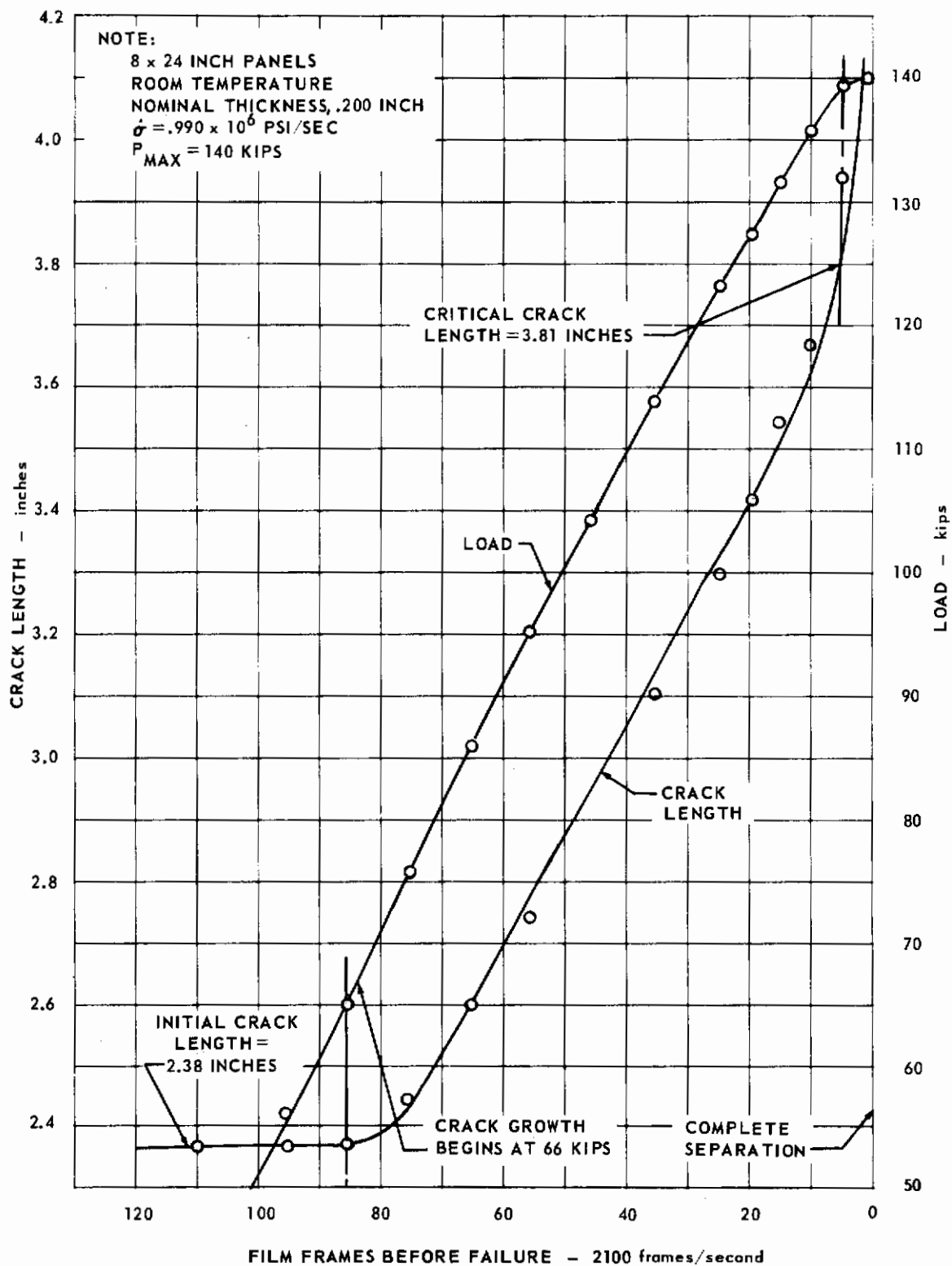


FIG. 284 STATIC CRACK GROWTH FOR Ti 6Al-4V SPECIMEN DD74

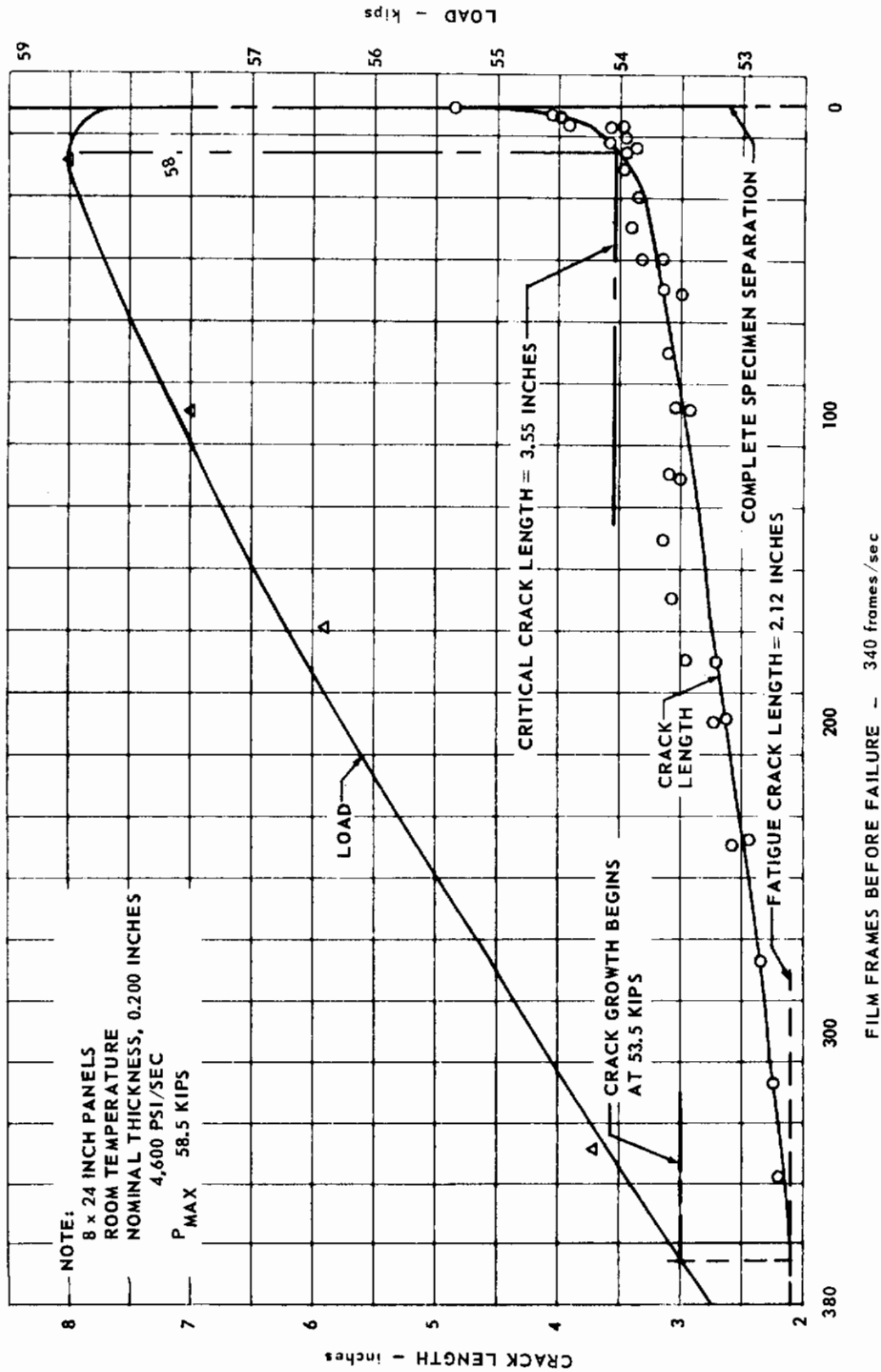


FIG. 285 STATIC CRACK GROWTH FOR Ti 6Al-4V SPECIMEN DD75

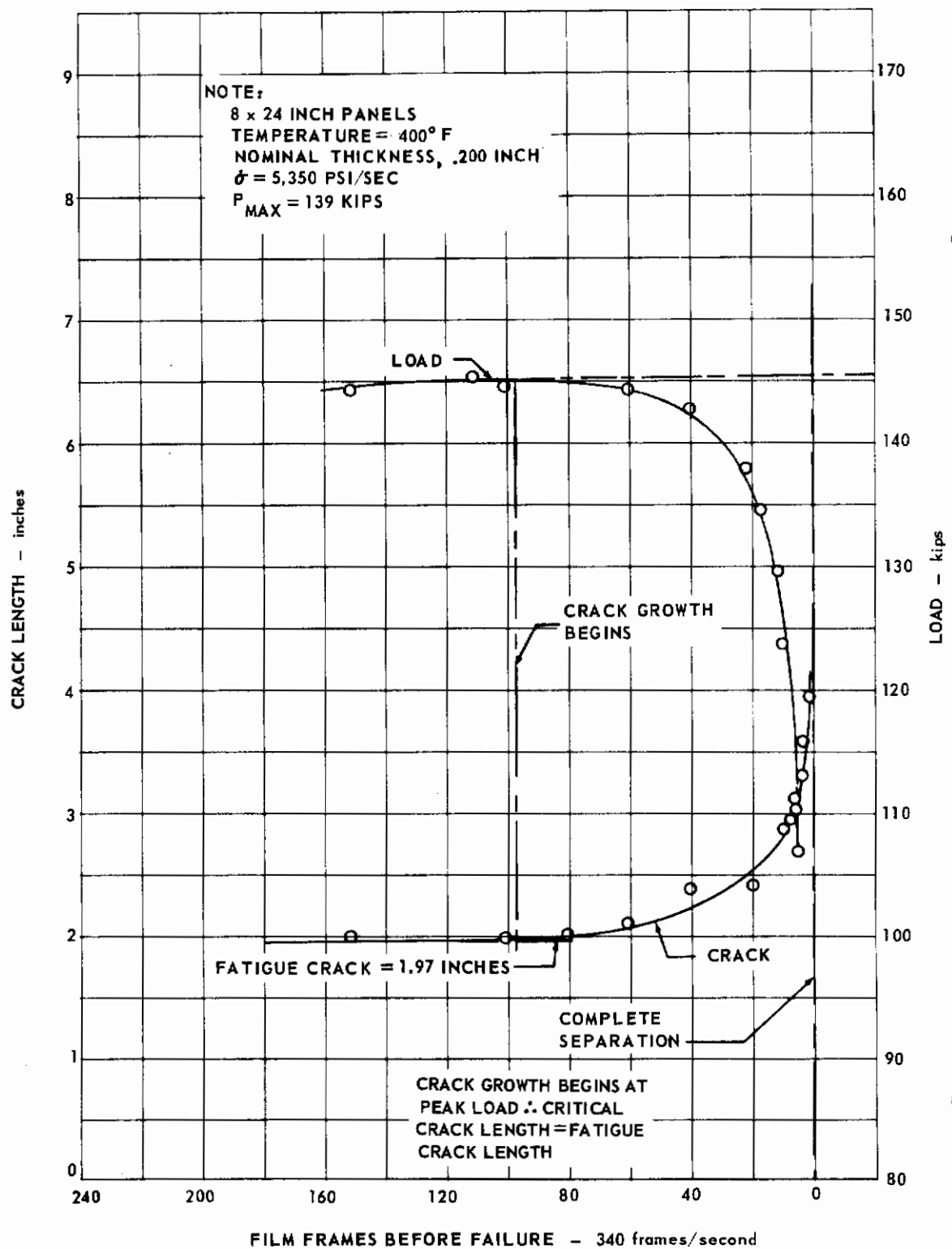


FIG. 286 STATIC CRACK GROWTH FOR Ti 6Al-4V SPECIMEN DD76

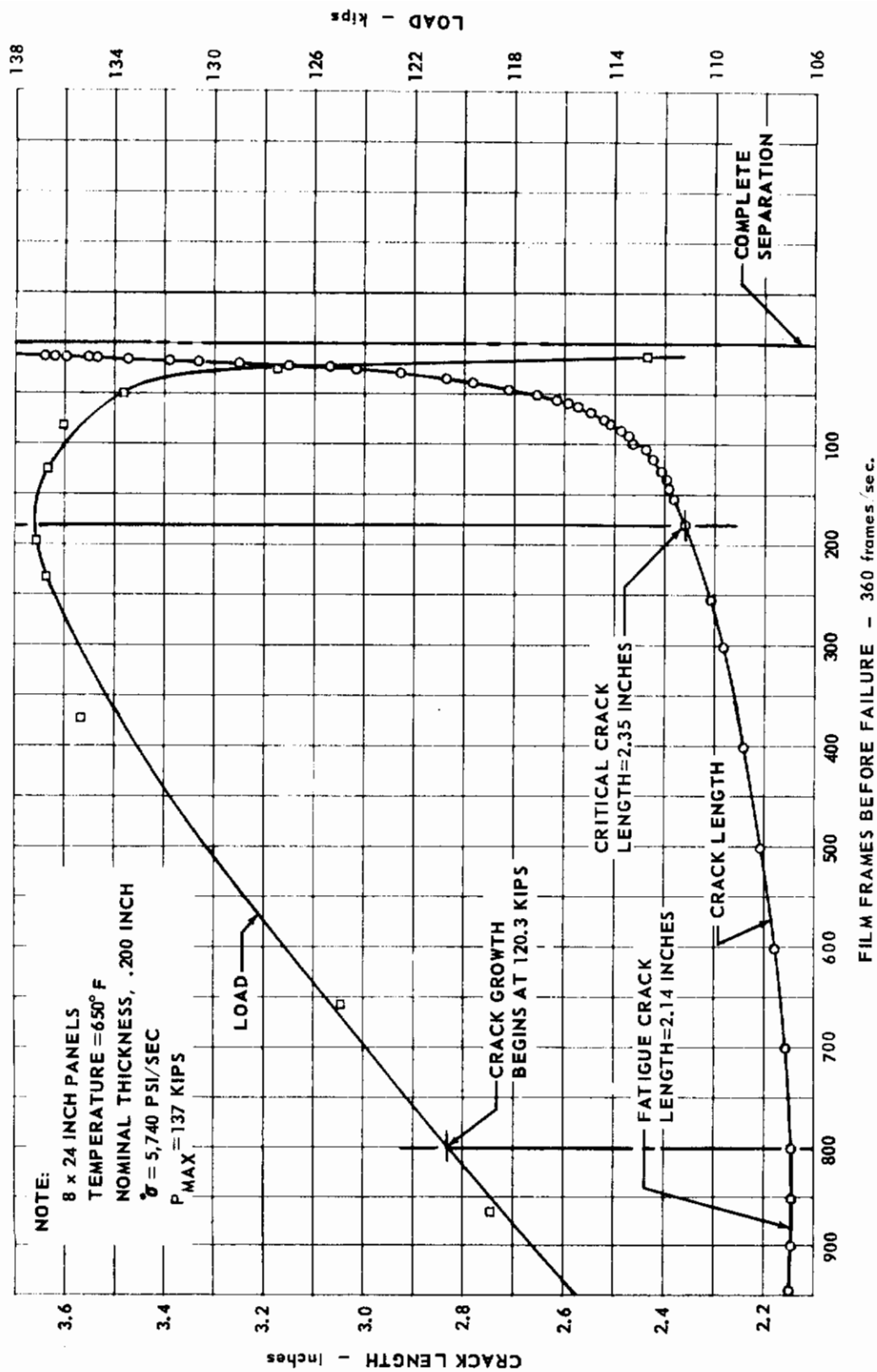


FIG. 287 STATIC CRACK GROWTH FOR Ti 6Al-4V SPECIMEN DD77

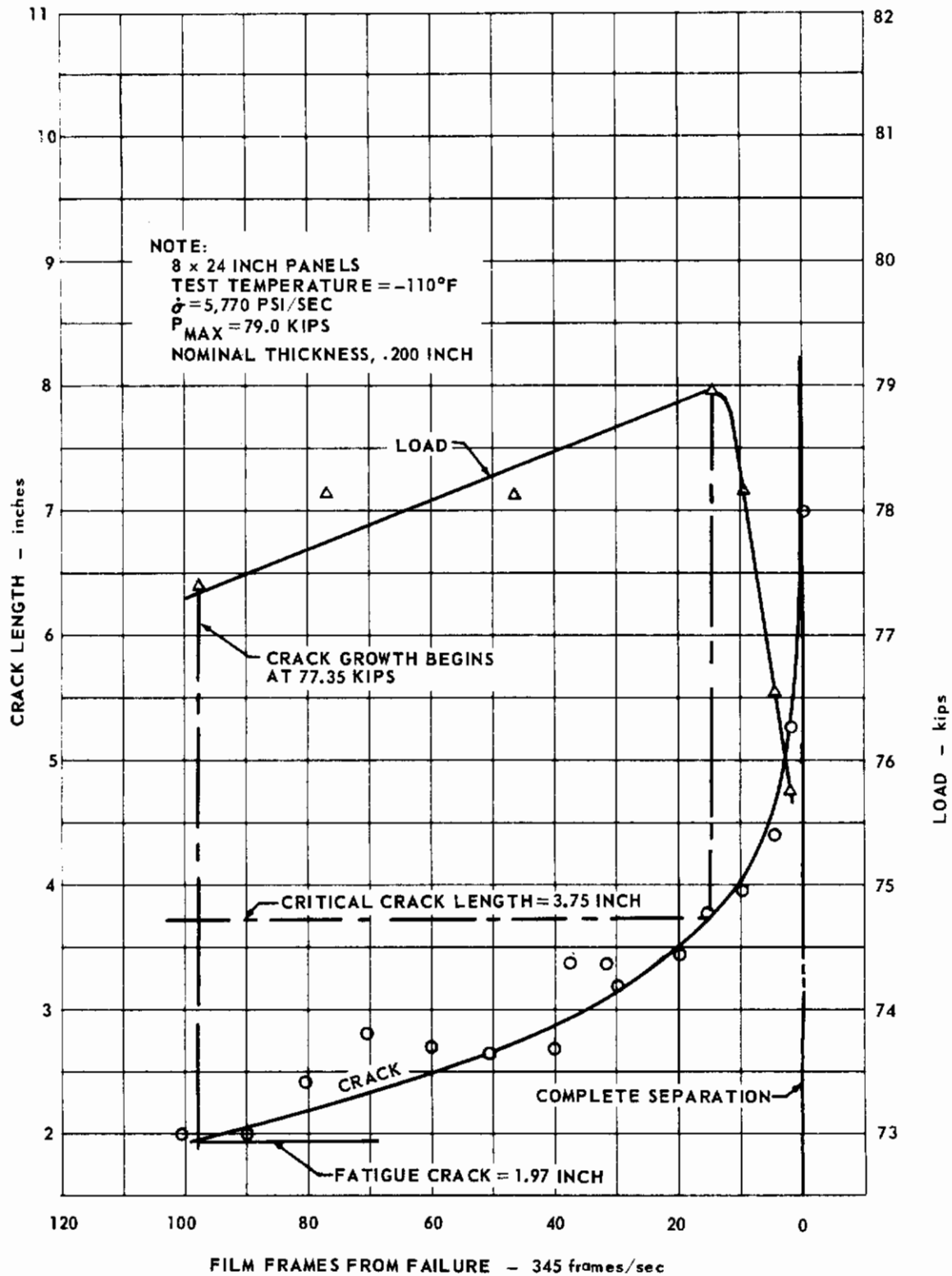


FIG. 288 STATIC CRACK GROWTH FOR Ti 6Al-4V SPECIMEN DD78

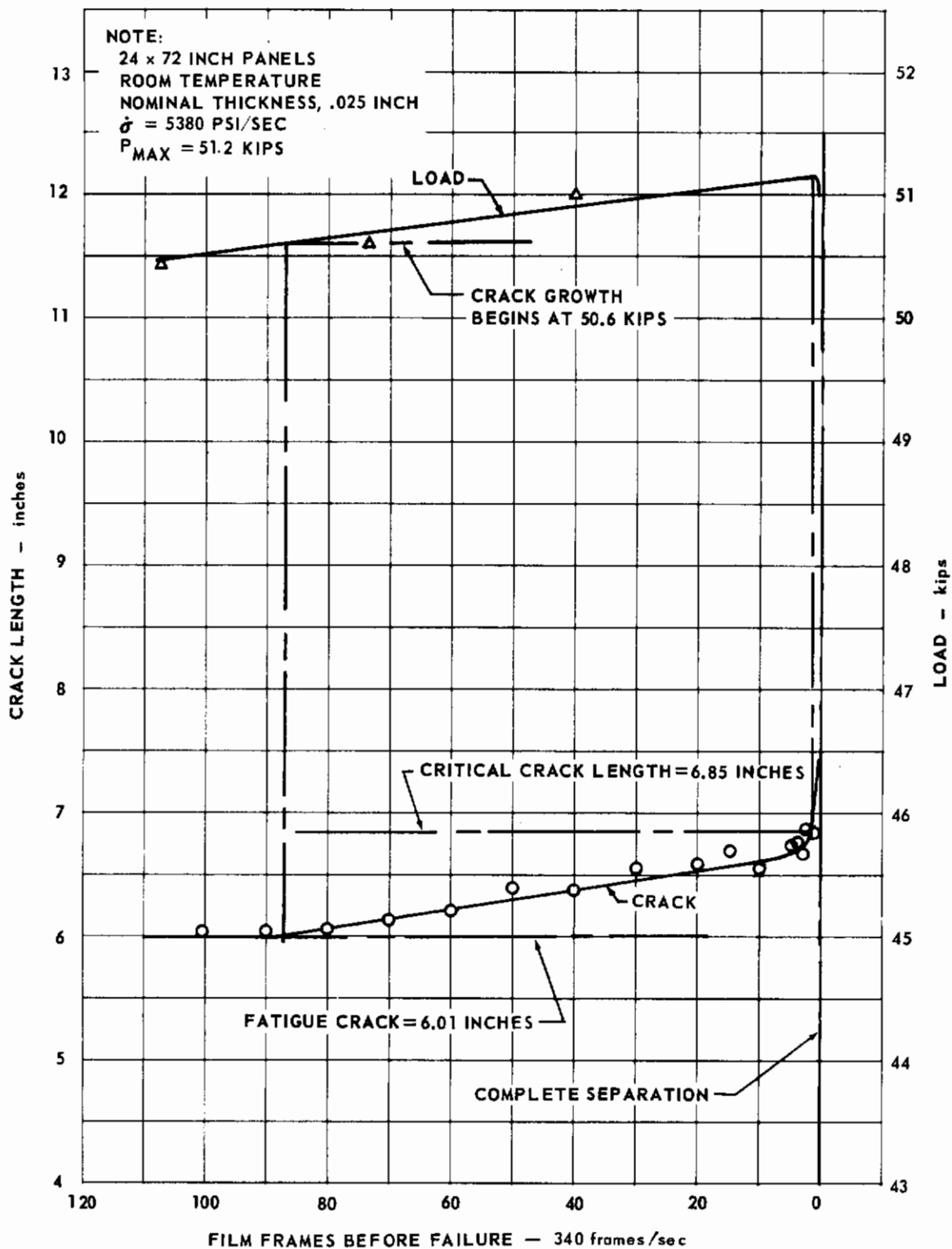


FIG. 289 STATIC CRACK GROWTH FOR PH 14-8Mo SPECIMEN DE4

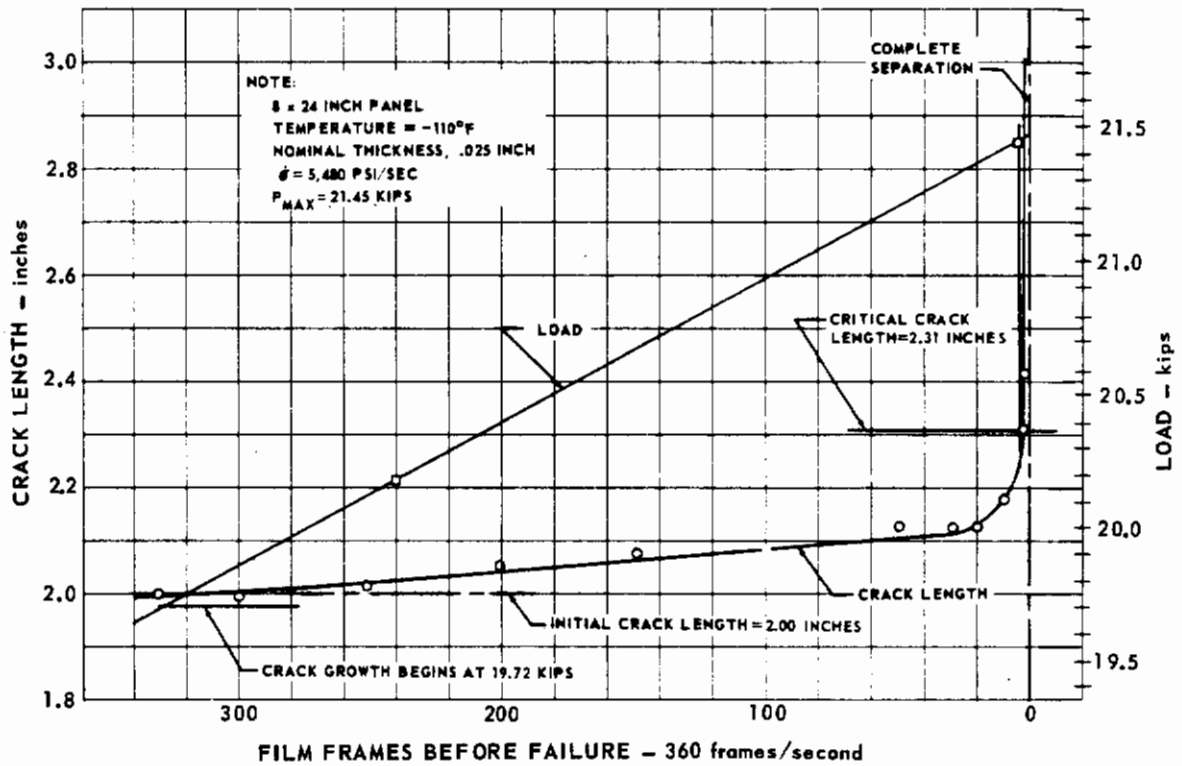


FIG. 290 STATIC CRACK GROWTH FOR PH 14-8Mo SPECIMEN DE5

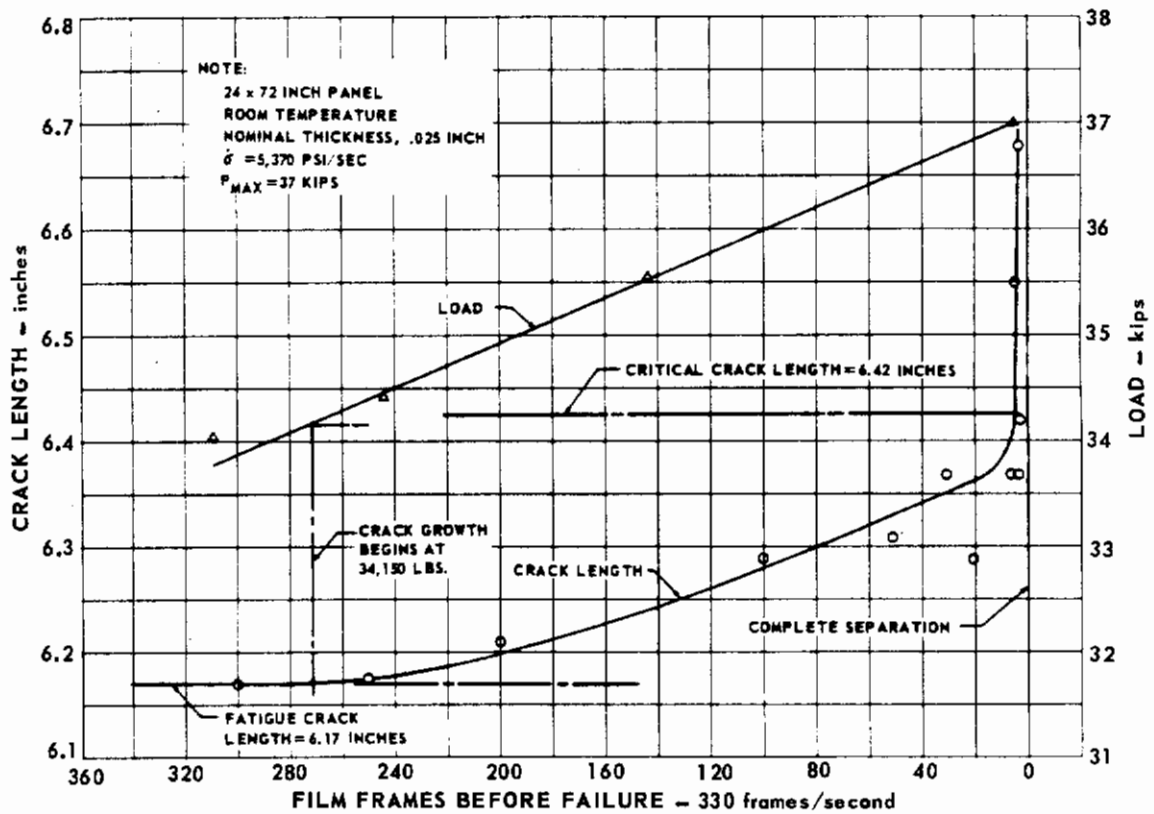


FIG. 291 STATIC CRACK GROWTH FOR PH 14-8Mo SPECIMEN DE19

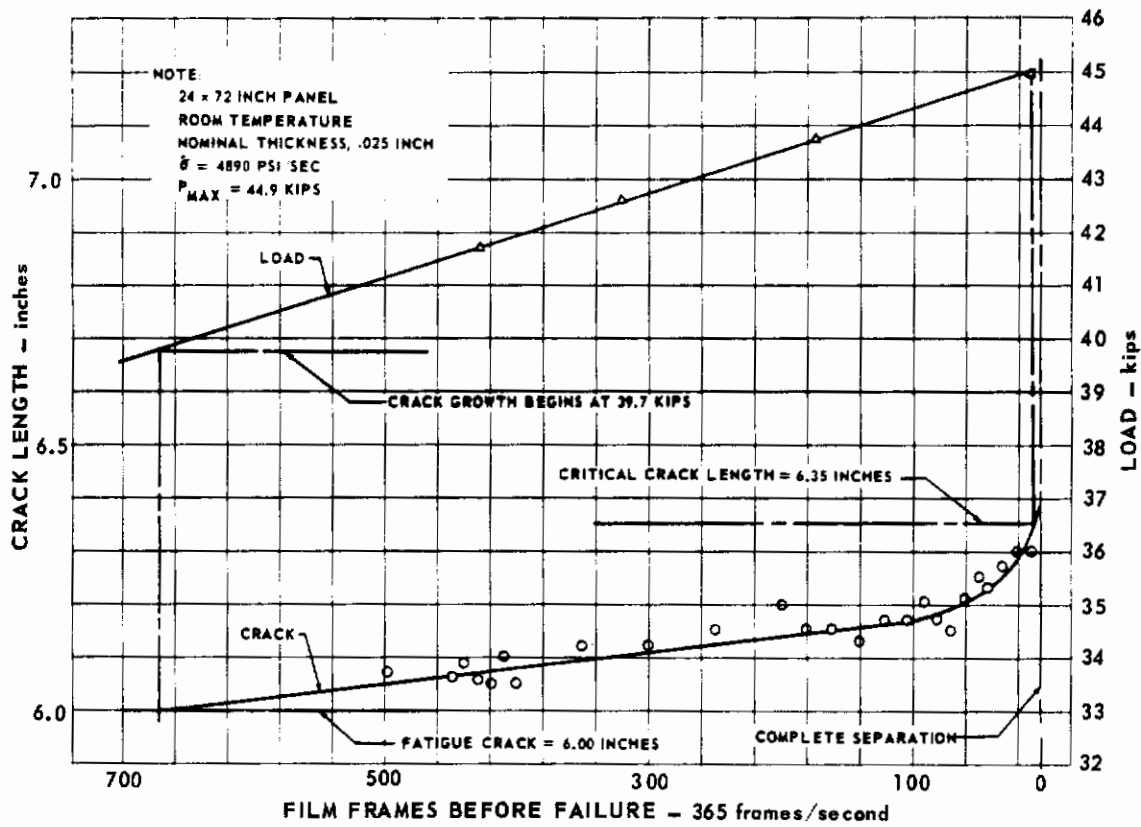


FIG. 292 STATIC CRACK GROWTH FOR PH 14-8 Mo SPECIMEN DE22

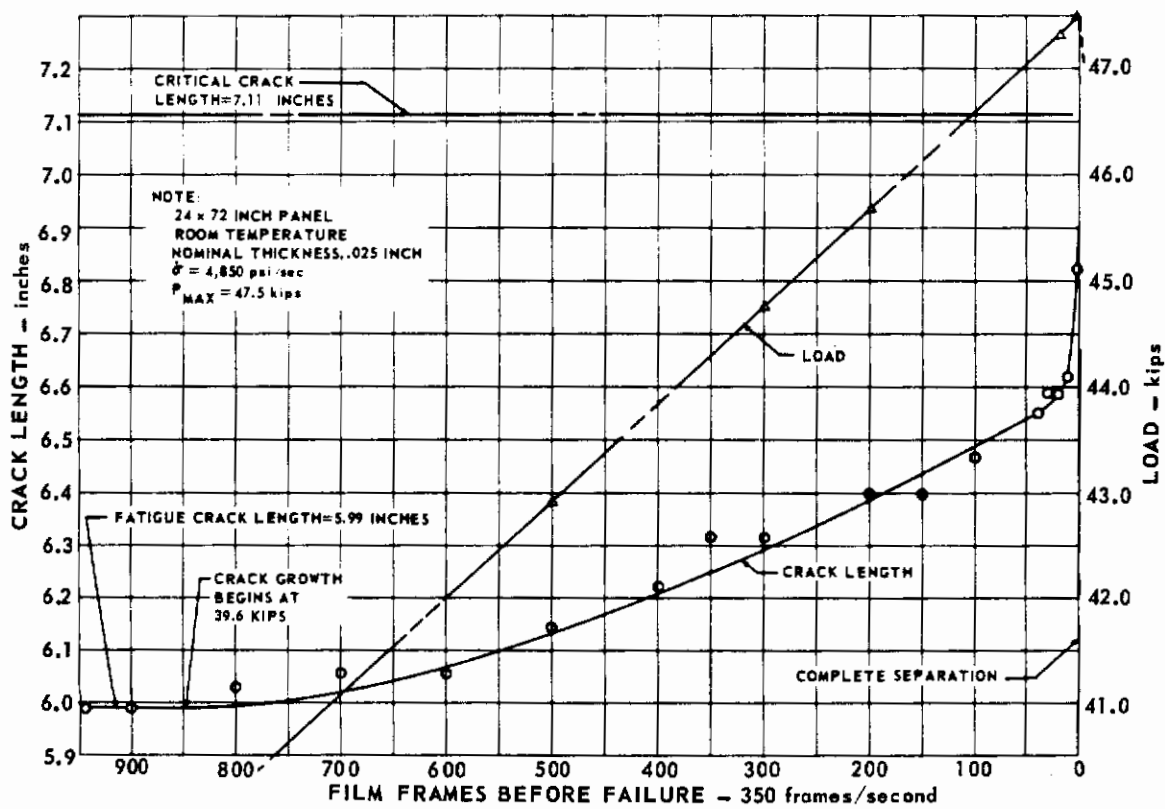


FIG. 293 STATIC CRACK GROWTH FOR PH 14-8 Mo SPECIMEN DE23

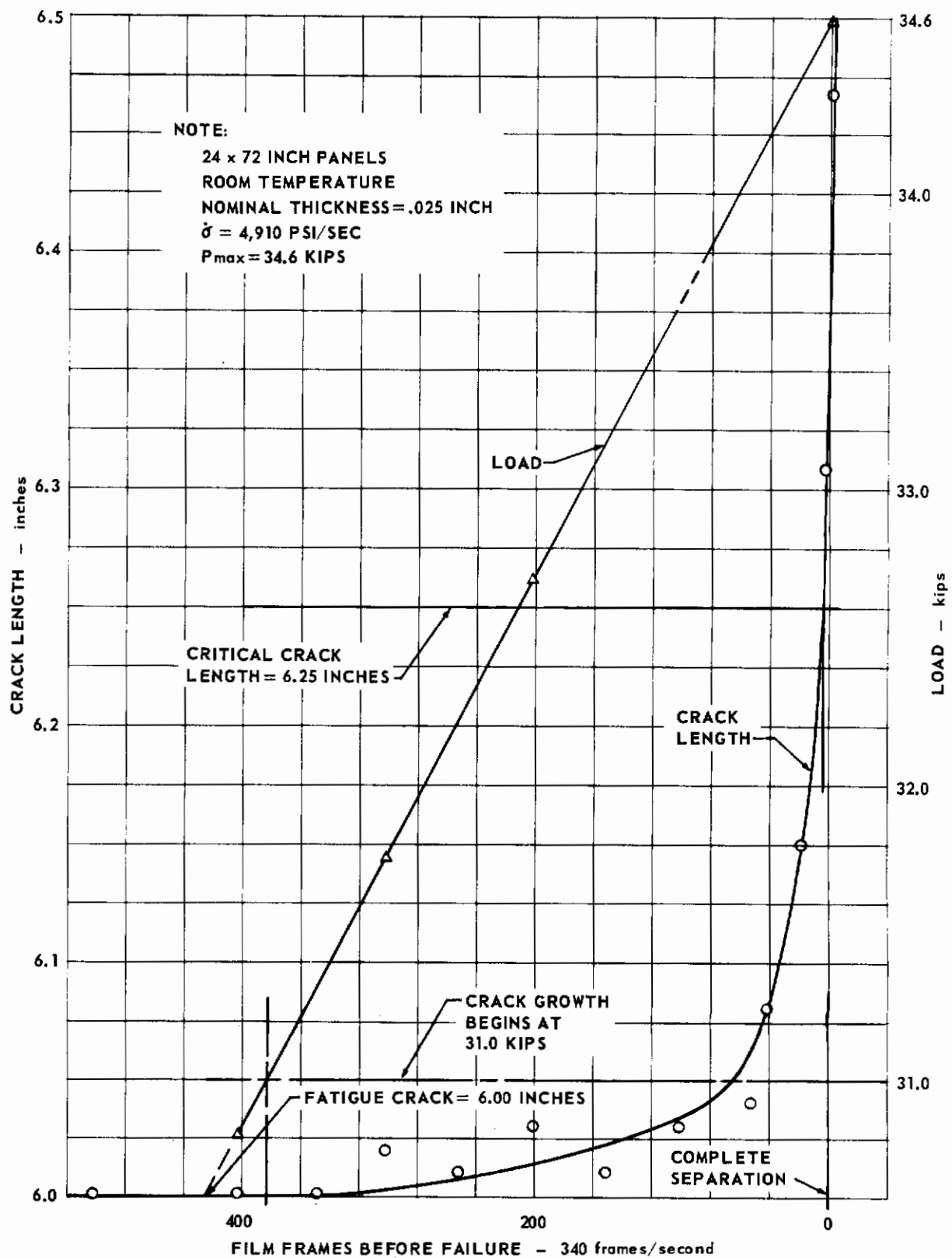


FIG. 294 STATIC CRACK GROWTH FOR PH 14-8Mo SPECIMEN DE24

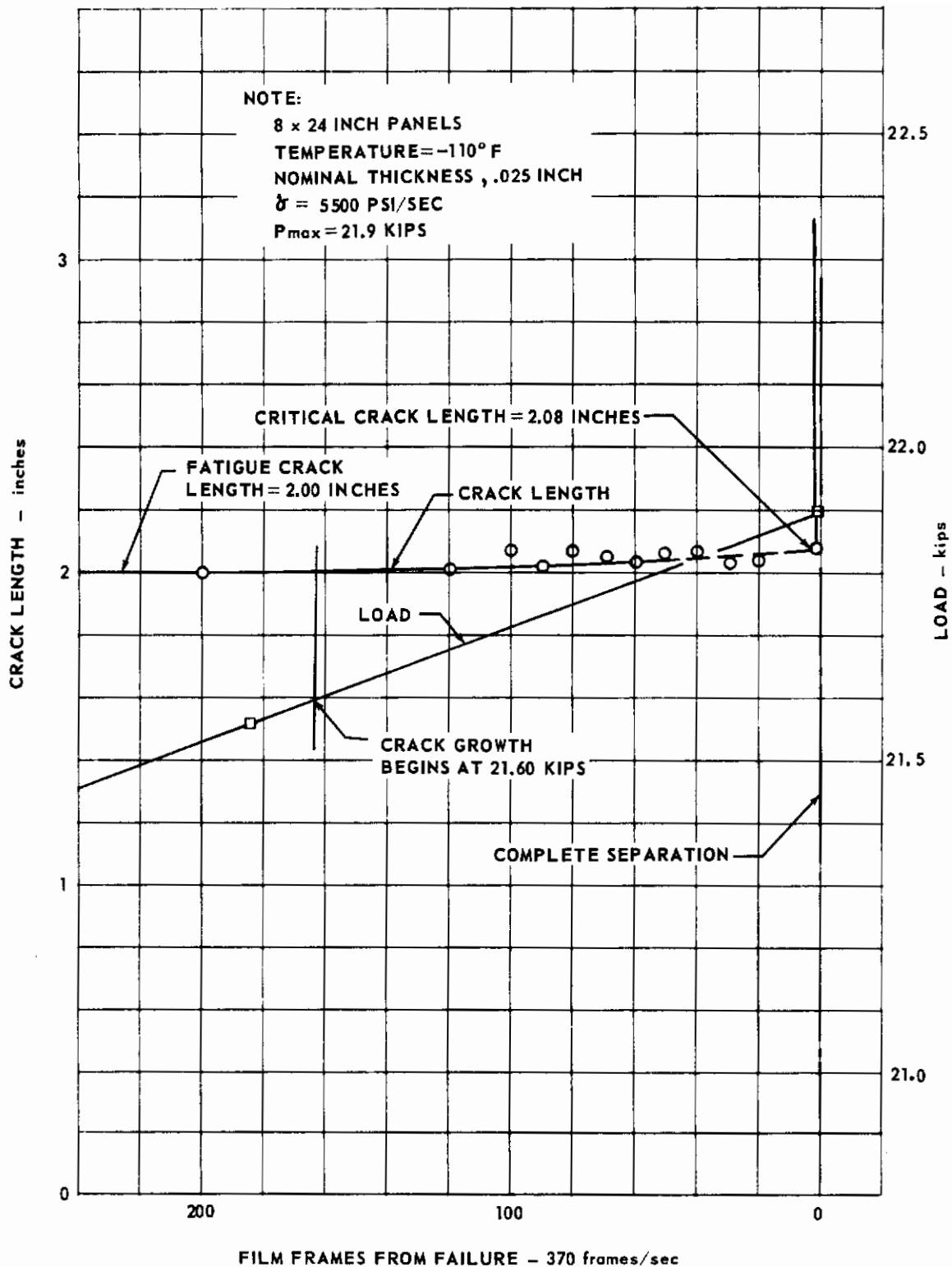
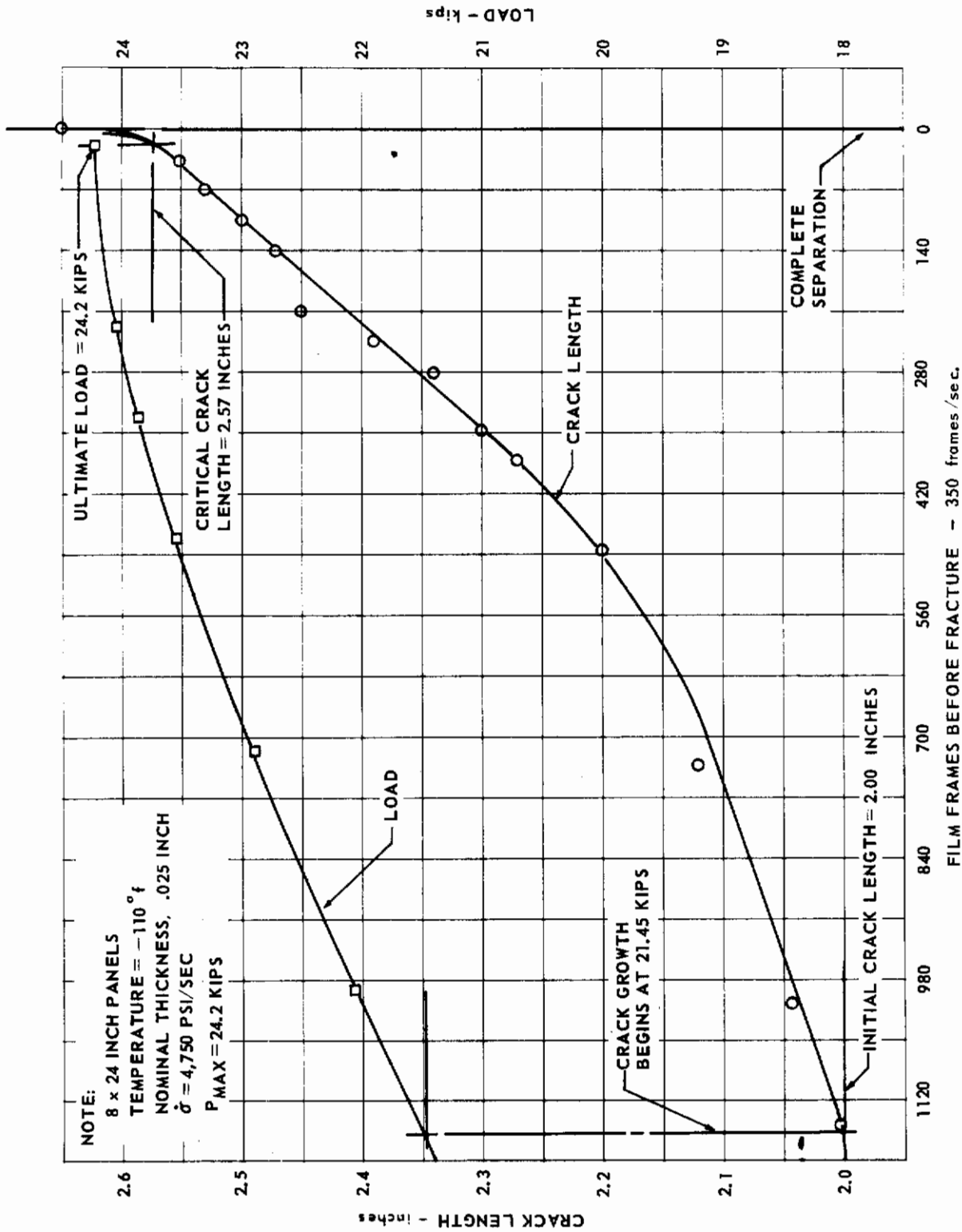


FIG. 295 STATIC CRACK GROWTH FOR PH 14-8Mo SPECIMEN DE36



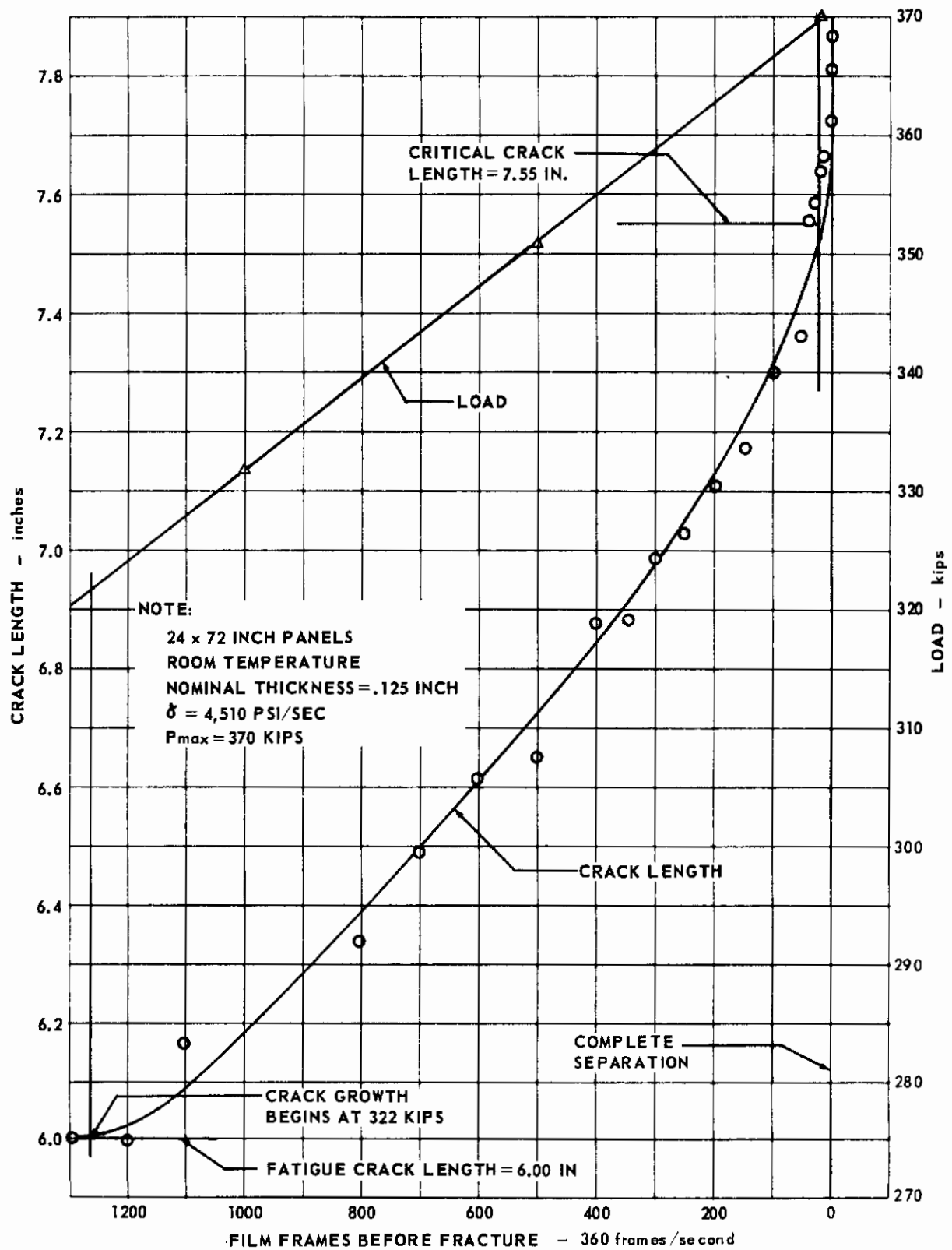


FIG. 297 STATIC CRACK GROWTH FOR PH 14-8Mo SPECIMEN DE71

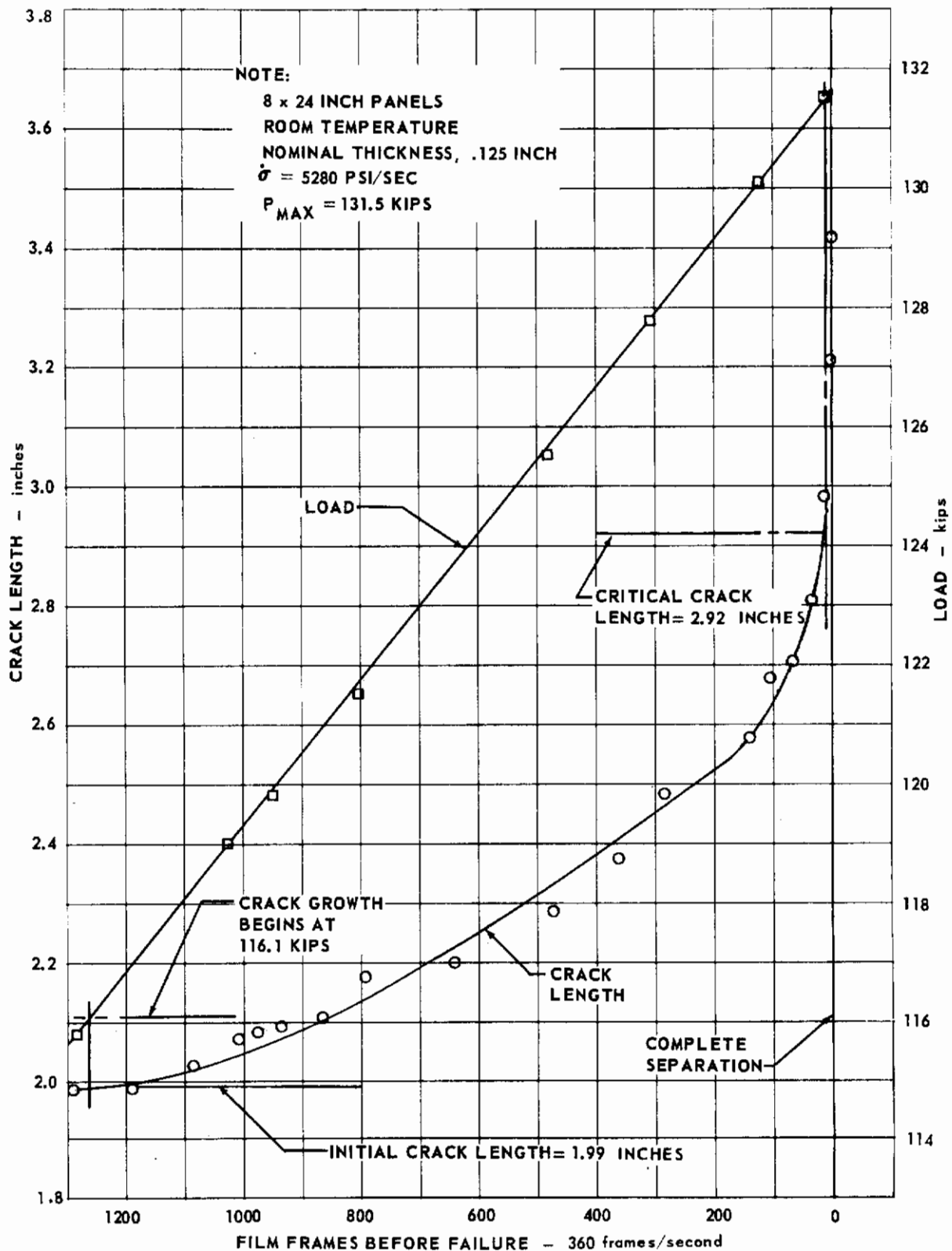


FIG. 298 STATIC CRACK GROWTH FOR PH 14-8 Mo SPECIMEN DE75

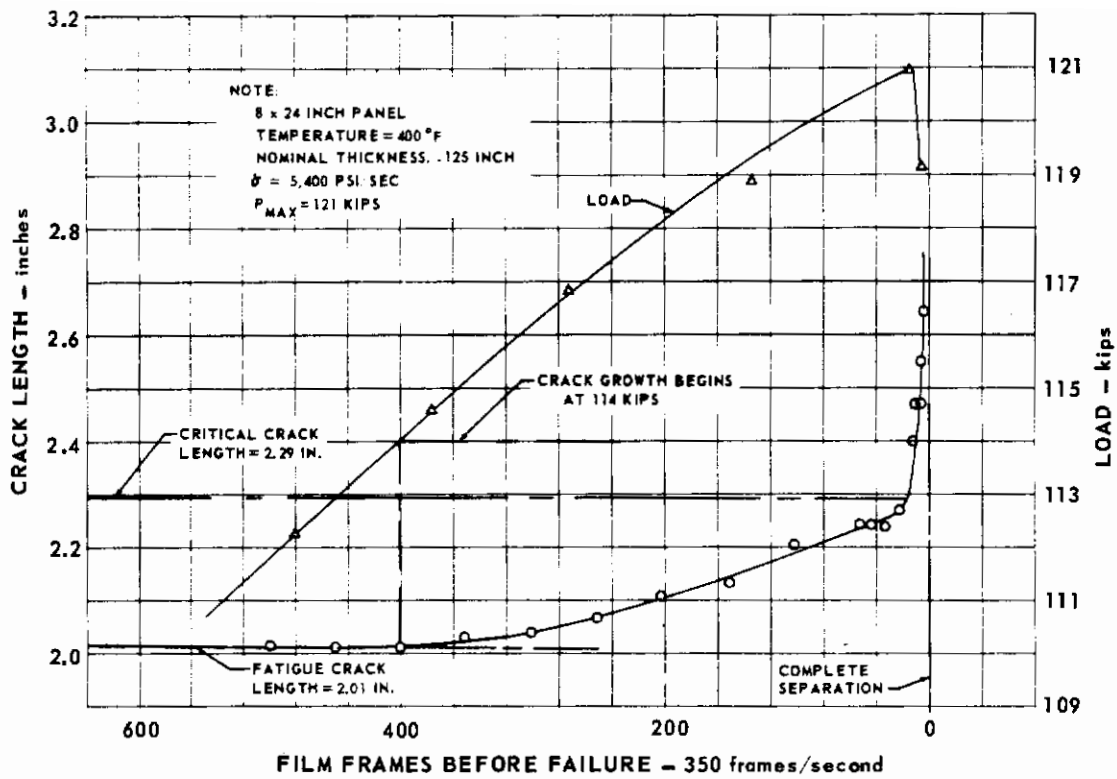


FIG. 299 STATIC CRACK GROWTH FOR PH 14-8Mo DE76

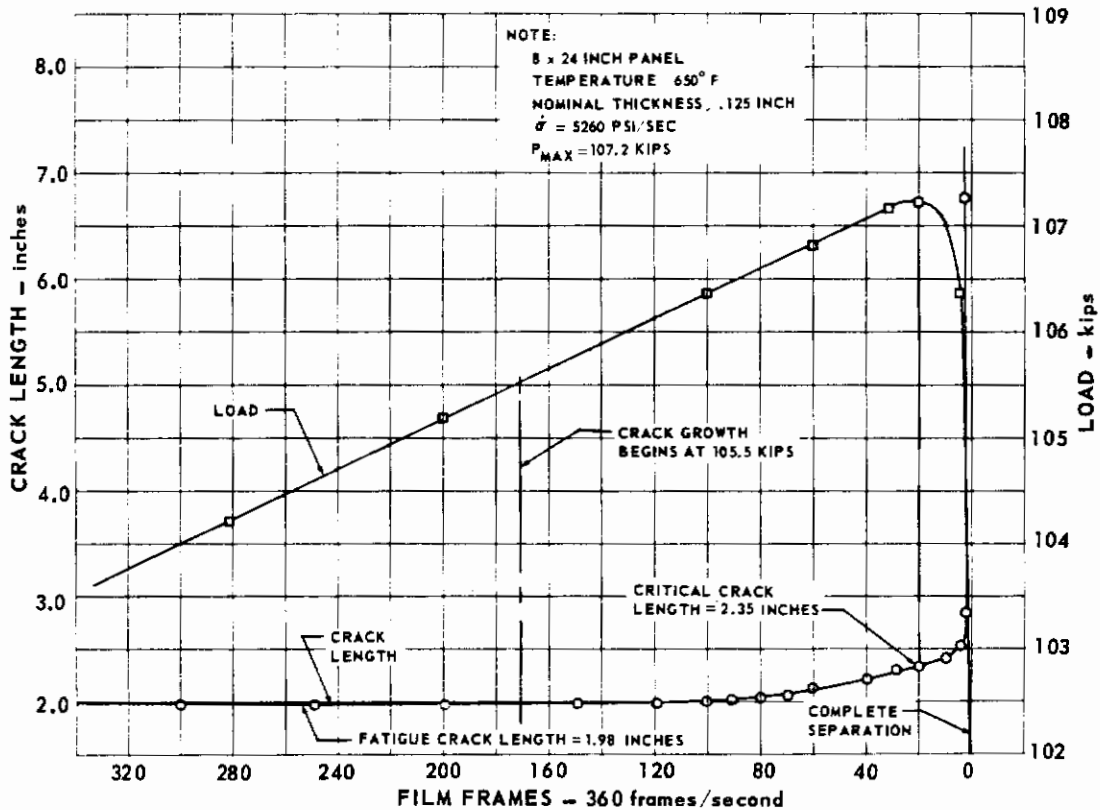


FIG. 300 STATIC CRACK GROWTH FOR PH 14-8Mo SPECIMEN DE77

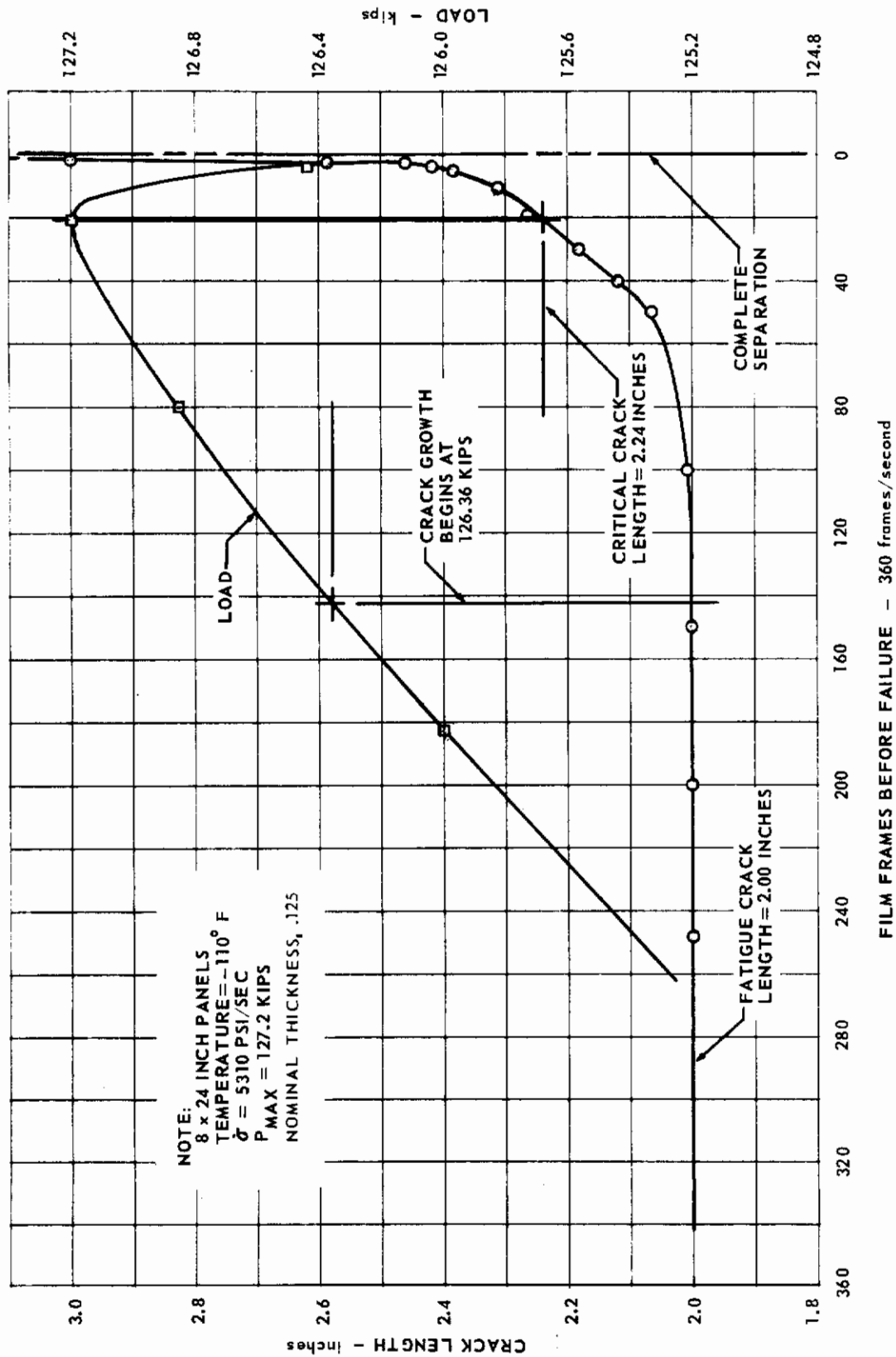


FIG. 301 STATIC CRACK GROWTH FOR PH 14-8 Mo SPECIMEN DE78

TABLE 33 SUMMARY OF FRACTURE TOUGHNESS CALCULATIONS BASED ON HIGH-SPEED PHOTOGRAPHY CRACK LENGTH MEASUREMENTS

ALLOY	SPECIMEN NO.	HEAT NO.	THICKNESS inches	GRAIN DIRECTION	WIDTH inches	\dot{a} psi/sec	TEMP. °F	a_C inches	P_{MAX} kips	$K_{IC} = \sigma_G \sqrt{\pi a_C}$ inches
Ti 8Al-1Mo-1V	DA 19	4535	.052	T	8.00	4.2×10^3	-110	1.52	30.605	171.4
	DA 75	3457	.209	T	8.00	4.77×10^3	RT	1.57	79.7	111.3
	DA 76	3457	.209	T	8.00	5.2×10^3	400	1.12	127.1	148.2
	DA 77	3457	.208	T	8.01	4.45×10^3	650	1.12	109.8	130.7
AM 350	DB 19	19207	.025	T	8.00	4.60×10^3	-110	1.13	7.80	75.8
	DB 75	19020	.128	T	8.01	3.5×10^3	68	1.38	97.6	209.5
	DB 76	19020	.129	T	8.00	3.85×10^3	400	1.01	99.1	175.5
	DB 77	19020	.129	T	8.00	5.9×10^3	650	1.00	90.3	162.0
INCO 718	DC 19	6713	.026	T	8.05	4.95×10^3	-110	1.03	29.7	262.0
	DC 75	6902	.124	T	8.01	5.95×10^3	72	1.02	110.9	205.2
	DC 77	6902	.124	T	8.01	4.55×10^3	650	1.35	118.5	219.2
	DC 78	6902	.124	T	8.01	5.05×10^3	-110	1.00	103.0	190.4
Ti 6Al-4V	DD 3	D5257	.051	L	24.07	4.96×10^3	82	3.55	58.3	166.6
	DD 4	D5257	.049	L	24.06	4.92×10^3	72	5.25	58.5	231.8
	DD 5	D5257	.0496	T	24.05	4.99×10^3	68	3.58	61.4	181.3
	DD 6	D5257	.048	T	24.02	4.93×10^3	68	3.28	60.1	174.1
	DD 19	D5257	.0495	T	8.010	6.29×10^3	-110	1.27	30.65	193.3
	DD 20	D5257	.0499	T	8.004	$.96 \times 10^6$	-110	1.56	33.81	207.3
	DD 22	D5256	.0515	L	24.07	4.86×10^3	71	3.68	64.2	185.7
	DD 23	D5256	.052	L	24.07	4.97×10^3	72	4.38	69.4	206.9
	DD 24	D5256	.054	T	24.08	4.75×10^3	74	4.06	61.1	179.5
	DD 25	D5256	.0545	T	24.08	4.86×10^3	71	4.08	67.5	196.4
	DD 36	D5256	.0516	T	8.012	6.14×10^3	-110	1.18	31.2	152.9
	DD 38	D5256	.052	T	8.008	$.96 \times 10^6$	71	1.11	39.7	183.1

TABLE 33 SUMMARY OF FRACTURE TOUGHNESS CALCULATIONS BASED ON HIGH-SPEED PHOTOGRAPHY CRACK LENGTH MEASUREMENTS (Continued)

ALLOY	SPECIMEN NO.	HEAT NO.	THICKNESS inches	GRAIN DIRECTION	WIDTH inches	$\dot{\sigma}$ psi/sec	TEMP. °F	a_c inches	P_{MAX} kips	$K_{IC} = \sigma_G \sqrt{W_{Qc} a}$ ksi $\sqrt{\text{inches}}$
Ti 6Al-4V (Continued)	DD 42	D4949	.0513	T	8.018	.85x10 ⁶	650	1.04	31.0	141.7
	DD 52	D4949	.025	T	8.028	.91x10 ⁶	650	1.23	15.6	161.1
	DD 54	D4949	.025	T	8.044	76.x10 ⁶	70	1.30	15.2	162.1
	DD 56	D4949	.1267	T	8.048	1.09x10 ⁶	72	1.37	105.8	230.1
	DD 70	D4949	.212	L	24.07	4.1 x10 ³	75	4.48	360.0	287.8
	DD 74	D4949	.2152	T	8.010	.99x10 ⁶	74	1.90	140.0	233.9
	DD 75	D4949	.216	T	8.040	4.6 x10 ³	74	1.78	58.5	91.3
	DD 76	D4949	.2146	T	8.032	5.35x10 ³	400	.98	145.5	146.6
	DD 77	D4949	.2133	T	8.040	5.74x10 ³	650	1.18	137.0	161.0
	DD 78	D4949	.2134	T	8.033	5.77 x10 ³	-110	1.88	79.0	131.4
PH 14-8 Mo	DE 4	43208	.025	L	24.04	5.38x10 ³	70	3.42	51.2	291.4
	DE 5	43208	.025	T	24.05	5.37x10 ³	76	3.21	37.0	203.3
	DE 19	43208	.0247	T	7.987	5.48x10 ³	-110	1.16	21.45	217.0
	DE 22	33570	.024	L	24.02	4.89x10 ³	75	3.18	44.9	255.5
	DE 23	33570	.024	L	24.03	4.85x10 ³	71	3.56	47.5	289.1
	DE 24	33570	.024	T	24.01	4.91x10 ³	78	3.12	34.6	195.1
	DE 36	33570	.024	T	8.00	5.5 x10 ³	-110	1.04	21.9	214.1
	DE 39	33347	.0252	T	7.993	4.75x10 ³	-110	1.28	24.2	256.1
	DE 71	33570	.119	L	24.06	4.5 x10 ³	74	3.78	370.0	470.5
	DE 75	33347	.124	T	8.00	5.28x10 ³	70	1.46	131.5	307.2
	DE 76	33347	.124	T	8.01	5.4 x10 ³	400	1.14	121.0	241.9
	DE 77	33347	.124	T	8.00	5.26x10 ³	650	1.18	107.2	217.6
	DE 78	33347	.124	T	8.00	5.31x10 ³	-110	1.12	127.2	250.9

APPENDIX III

FRACTURE SURFACE MEASUREMENTS

Table 34 contains post-fracture surface measurements made from the 24 x 72-inch panels of each of the five alloys. Measurements were made of the final surface fatigue crack length existing prior to fracture testing. In addition, a similar measurement was made of the final fatigue crack length for the mid-thickness point of each panel. The difference between the surface crack dimension and the internal crack dimension gives some indication of the shape of the fatigue crack tip.

It is possible that a continued effort toward documentation of the distinguishing features from surfaces of fractured panels may result in an increased understanding of the fracture process. The shape of the fatigue crack tip may indicate the material thickness where a transition from the plane stress to plane strain fracture mode exists during fatigue cycling. There is also a possibility that noting other fracture surface characteristics may aid in understanding the "pop-in" phenomenon. Fig. 61 in Section 6, for example shows several static fracture "rings" present on the fatigue portion of the fracture surface. If all such markings were recorded for all of the panels and a correlation attempted with the appropriate crack length and stress level, some consistent trends might be noted. Such a study is beyond the scope of the present project.

The basic surface and internal final crack dimensions are included here so that interested individuals may make use of the information to supplement the fracture test results. In addition to the fatigue crack measurements, measurements were also made of the extent of the triangular plane strain fracture areas which often exist at the extremities of the fatigue crack tip. It is possible that the presence and extent of this zone may indicate some consistent material behavior pattern.

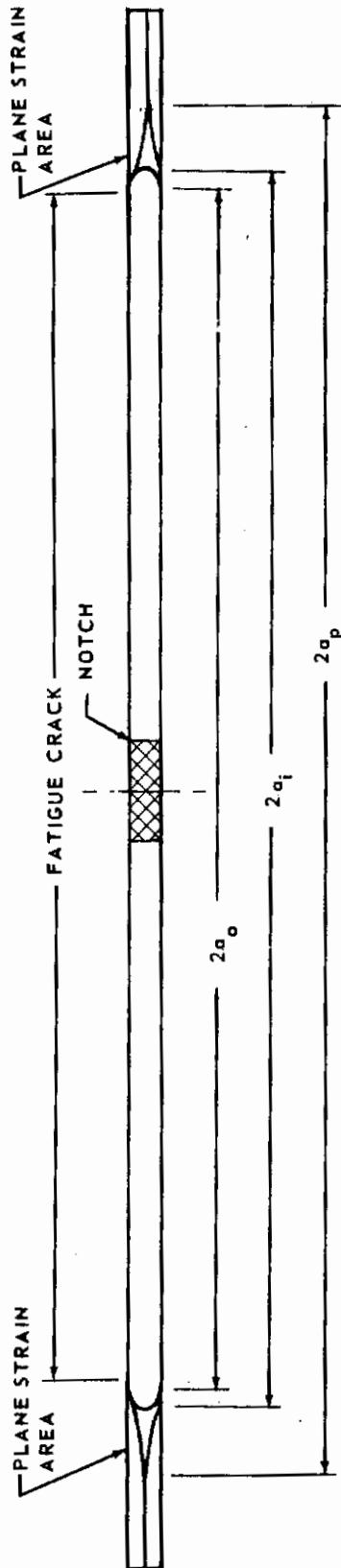


TABLE 34 POST FRACTURE CRACK LENGTH MEASUREMENTS FOR 24 X 72-INCH PANELS FOR ALL ALLOYS

SPEC. NO.	Ti 8Al-1Mo-1V			AM 350			INCO 718			Ti 6Al-4V			PH 14-8Mo		
	2a_o	2a_i	2a_p	2a_o	2a_i	2a_p	2a_o	2a_i	2a_p	2a_o	2a_i	2a_p	2a_o	2a_i	2a_p
1	3.00	3.01	3.06	3.00	3.00	—	3.00	3.01	3.05	3.00	3.00	3.06	3.00	3.00	—
2	3.00	3.01	3.07	3.00	3.01	—	3.01	3.01	—	3.00	3.01	3.07	3.00	3.63	—
3	6.00	6.01	6.08	6.00	6.00	—	6.00	6.00	—	5.99	6.07	—	6.02	6.04	6.06
4	6.00	5.99	6.05	6.00	6.00	—	6.00	6.00	—	6.00	6.02	6.08	6.01	6.02	6.03
5	6.00	6.08	6.21	6.68	6.68	—	6.00	6.00	—	6.00	6.04	6.14	6.17	6.15	—
6	6.01	6.07	6.26	6.00	6.03	—	6.00	6.01	—	6.00	6.02	6.10	6.00	6.01	—
7	6.00	6.01	6.10	6.00	6.00	—	6.00	—	—	5.99	6.01	6.07	5.99	6.02	—
8	6.00	6.04	6.10	6.00	6.00	—	6.00	6.01	—	6.00	6.02	—	5.99	6.00	6.02
9	6.00	6.03	6.10	6.00	6.00	—	6.00	6.00	—	6.00	6.04	6.12	5.99	6.00	6.02
10	6.00	6.00	6.07	6.00	6.00	—	6.00	6.01	6.02	6.00	6.03	6.11	6.00	5.98	6.00
11	6.00	6.07	6.17	6.00	6.00	—	6.00	6.01	—	6.00	6.03	6.13	6.00	6.10	—
12	6.00	6.07	6.21	6.00	6.00	—	6.00	6.01	—	6.00	6.02	6.12	6.00	6.01	6.03

TABLE 34 POST FRACTURE CRACK LENGTH MEASUREMENTS FOR 24 x 72 INCH PANELS FOR ALL ALLOYS (continued)

SPEC. NO.	Ti 8Al-1Mo-1V			AM 350			INCO 718			Ti 6Al-4V			PH 14-8Mo		
	2 σ_o	2 σ_i	2 σ_p	2 σ_o	2 σ_i	2 σ_p	2 σ_o	2 σ_i	2 σ_p	2 σ_o	2 σ_i	2 σ_p	2 σ_o	2 σ_i	2 σ_p
13	6.00	6.05	6.14	6.00	6.00	—	6.00	6.00	—	14.00	—	—	6.01	6.02	—
14	6.00	6.01	6.04	6.00	6.00	—	6.00	6.00	—	6.00	6.01	6.05	6.00	6.02	—
15	10.00	10.01	10.05	10.00	10.00	—	10.00	10.00	—	10.01	10.01	10.13	10.00	10.00	—
16	10.00	10.02	10.09	10.00	10.01	—	10.00	10.00	—	10.00	10.02	10.10	10.02	10.04	—
22	6.00	6.01	6.08	6.00	6.00	—	6.00	6.01	—	6.01	6.03	6.13	6.00	6.02	—
23	6.00	6.01	6.07	—	—	—	6.00	—	—	6.01	6.02	6.10	5.99	6.00	—
24	6.00	6.06	6.16	—	—	—	6.00	6.00	—	6.00	6.03	6.13	6.00	6.04	—
25	6.00	6.07	6.20	6.00	6.00	—	6.04	6.04	—	6.01	6.02	6.10	6.00	6.00	—
26	6.00	6.01	6.12	6.00	6.00	—	6.00	—	—	6.00	6.03	6.11	6.00	6.10	6.12
27	6.00	6.01	6.11	—	—	—	6.00	6.01	6.09	5.99	6.02	—	6.00	6.00	—
28	6.00	6.09	6.18	6.00	6.00	—	6.00	6.00	6.03	6.00	6.03	6.10	5.99	6.03	—
29	6.00	6.04	6.13	6.00	6.05	—	6.00	6.02	—	6.00	6.03	6.08	6.00	6.01	—
30	6.00	6.07	6.15	6.04	6.04	—	6.00	6.01	—	6.00	6.05	6.11	6.01	—	—
31	6.00	6.08	6.18	6.00	6.03	—	6.00	6.00	—	6.01	6.02	6.12	6.00	6.02	—
32	6.00	6.01	6.07	6.00	6.00	—	6.00	6.01	—	6.00	6.03	6.13	6.00	—	—
33	6.00	6.01	6.06	6.00	6.00	—	6.00	6.00	—	6.00	6.02	6.10	6.00	6.02	—
43	—	—	—	—	—	—	6.00	6.01	—	6.00	6.03	6.33	6.00	6.01	6.09
44	6.00	6.06	6.31	—	—	—	6.00	6.01	—	6.01	6.04	6.18	6.02	6.09	6.16
45	—	—	—	6.04	6.04	—	6.00	6.00	—	7.16	—	—	6.00	6.01	6.07
46	6.00	6.05	6.17	—	—	—	6.00	6.00	—	6.00	6.04	6.10	6.01	6.05	6.11
47	—	—	—	6.00	6.00	—	6.00	6.03	—	6.01	6.03	6.09	6.02	6.11	6.17
48	6.00	6.05	6.09	—	—	—	6.02	6.03	—	6.00	6.00	6.06	6.00	6.00	6.06
49	6.00	6.02	6.07	6.00	6.00	—	6.00	6.01	—	6.00	6.03	6.11	6.00	6.03	6.07
50	6.00	6.05	6.08	—	—	—	6.00	6.01	6.04	6.01	6.05	6.15	6.04	6.06	6.10
51	6.00	5.98	6.05	6.00	6.00	—	6.00	6.02	—	6.00	6.02	6.06	6.00	6.03	6.09
58	6.00	6.04	6.20	6.04	6.14	6.27	6.00	—	—	6.04	6.05	6.15	6.00	6.00	6.16

TABLE 34 POST FRACTURE CRACK LENGTH MEASUREMENTS FOR 24 x 72 INCH PANELS FOR ALL ALLOYS (continued)

SPEC. NO.	Ti 8Al-1Mo-1V			AM 350			INCO 718			Ti 6Al-4V			PH 14-8Mo		
	2 σ_o	2 σ_i	2 σ_p	2 σ_o	2 σ_i	2 σ_p	2 σ_o	2 σ_i	2 σ_p	2 σ_o	2 σ_i	2 σ_p	2 σ_o	2 σ_i	2 σ_p
59	3.00	3.16	3.85	3.02	3.09	—	3.02	—	—	3.01	3.03	3.48	3.00	3.02	3.22
60	3.00	3.10	3.30	3.00	3.04	3.17	3.00	3.02	3.15	2.99	3.18	—	3.00	3.07	3.20
61	6.03	6.17	8.70	6.00	6.02	6.63	6.00	6.02	—	6.00	6.04	6.34	6.00	6.04	6.18
62	6.02	6.11	7.10	6.00	6.01	6.31	6.00	6.02	—	6.00	6.10	6.60	6.00	6.02	6.12
63	6.00	6.14	6.28	6.00	6.03	—	6.00	6.02	6.10	6.00	6.10	—	6.00	6.02	6.14
64	6.00	6.11	6.17	6.00	—	—	6.00	6.00	6.10	6.00	6.18	—	6.01	6.08	—
65	10.05	10.25	11.00	10.02	10.05	—	10.00	10.00	—	10.00	10.20	10.74	10.00	10.00	10.10
66	10.00	10.25	10.48	10.00	10.04	10.11	10.00	10.00	10.22	10.00	10.14	10.30	10.01	10.08	—
67	6.00	6.17	—	6.00	6.04	—	6.00	—	—	6.01	6.07	6.97	6.01	6.04	6.20
68	6.00	6.02	—	6.01	6.04	—	6.00	6.03	—	6.00	6.20	6.65	6.00	6.06	6.25
70	6.00	6.19	—	6.00	6.04	—	6.00	6.01	—	6.01	6.14	6.57	6.00	6.06	6.28
71	—	—	—	6.00	6.04	—	6.00	6.03	6.10	6.01	6.07	6.65	—	—	—
72	6.00	6.16	7.11	6.00	6.04	—	6.01	6.03	—	6.01	6.06	6.41	6.00	6.05	6.15
73	—	—	—	6.00	6.07	—	6.00	6.02	—	6.01	6.40	6.80	6.00	6.04	—